

# ***Isotope and geochemical techniques applied to geothermal investigations***

*Proceedings of the final Research Co-ordination Meeting  
on the Application of Isotope and Geochemical Techniques to  
Geothermal Exploration in the Middle East, Asia,  
the Pacific and Africa  
held in Dumaguete City, Philippines, 12–15 October 1993*



INTERNATIONAL ATOMIC ENERGY AGENCY **IAEA**

The IAEA does not normally maintain stocks of reports in this series.  
However, microfiche copies of these reports can be obtained from

INIS Clearinghouse  
International Atomic Energy Agency  
Wagramerstrasse 5  
P.O. Box 100  
A-1400 Vienna, Austria

Orders should be accompanied by prepayment of Austrian Schillings 100,—  
in the form of a cheque or in the form of IAEA microfiche service coupons  
which may be ordered separately from the INIS Clearinghouse.

The originating Section of this document in the IAEA was:

Isotope Hydrology Section  
International Atomic Energy Agency  
Wagramerstrasse 5  
P.O. Box 100  
A-1400 Vienna, Austria

ISOTOPE AND GEOCHEMICAL TECHNIQUES APPLIED TO  
GEOTHERMAL INVESTIGATIONS  
IAEA, VIENNA, 1995  
IAEA-TECDOC-788  
ISSN 1011-4289

Printed by the IAEA in Austria  
February 1995

## FOREWORD

This publication is a compilation of the scientific papers presented at the final Research Co-ordination Meeting held in Dumaguete City, Philippines, from 12 to 15 October 1993, which brought the Co-ordinated Research Programme (CRP) on the Application of Isotope and Geochemical Techniques to Geothermal Exploration in the Middle East, Asia, the Pacific and Africa (1990–1993) to a successful conclusion.

The CRP was initiated during the Seminar on Isotope Techniques in Geothermal Exploration, held in Izmir, Turkey, in November 1989. Eight research contracts and three research agreements were awarded to the following Member States: China, Iceland, India, Indonesia, Italy, Republic of Korea, New Zealand, Pakistan, Philippines, Turkey and Viet Nam. In most of these countries, geothermal energy is an important resource for electrical and non-electrical uses.

The results of the isotopic investigations were presented at the final Research Co-ordination Meeting (RCM) which was organized by the IAEA in co-operation with the Philippine National Oil Company–Energy Development Corporation. Preliminary results were reported at the first RCM held in Beijing, China, in co-operation with the Beijing Research Institute for Uranium Geology.

This CRP enabled a preliminary geochemical investigation of the general potential for geothermal energy resource development in the region. With the application of isotope techniques, much was gained in the understanding of the hydrology of the areas which are inputs to development strategies. The skills for isotope data interpretation have also been improved through interaction among the participants.

The IAEA recognizes the valuable collaboration of the participants in the CRP and their significant contribution to the success of the programme. This TECDOC has also benefitted from a review by the experts who participated in the CRP. The IAEA is grateful to S. Arnórsson, W. Giggenbach and C. Panichi for upgrading the quality of the papers by their dedicated reviews and constructive comments. It is expected that the results presented in this publication will serve as valuable references for the exploration and development of geothermal energy resources, as well as for other related scientific investigations concerned with water resources and follow-up work.



## **EDITORIAL NOTE**

*In preparing this document for press, staff of the IAEA have made up the pages from the original manuscripts as submitted by the authors. The views expressed do not necessarily reflect those of the governments of the nominating Member States or of the nominating organizations.*

*Throughout the text names of Member States are retained as they were when the text was compiled.*

*The use of particular designations of countries or territories does not imply any judgement by the publisher, the IAEA, as to the legal status of such countries or territories, of their authorities and institutions or of the delimitation of their boundaries.*

*The mention of names of specific companies or products (whether or not indicated as registered) does not imply any intention to infringe proprietary rights, nor should it be construed as an endorsement or recommendation on the part of the IAEA.*

*The authors are responsible for having obtained the necessary permission for the IAEA to reproduce, translate or use material from sources already protected by copyrights.*

## CONTENTS

Introduction . . . . .	7
Application of isotope and geochemical techniques to geothermal exploration in Southeast China — A review . . . . .	9
<i>Wang Ji-Yang, Pang Zhong-He</i>	
Processes controlling the chemical composition of natural waters in the Hreppar-Land area in southern Iceland . . . . .	21
<i>S. Arnórsson, A. Andrésdóttir</i>	
Processes influencing $\delta^2\text{H}$ , $\delta^{18}\text{O}$ , B and Cl distribution in cold and thermal waters in the NW-Peninsula and in the Southern Lowlands, Iceland . . . . .	45
<i>S. Arnórsson, A.E. Sveinbjörnsdóttir, A. Andrésdóttir</i>	
Geochemical and isotope studies of the geothermal areas of central and northern India . . . . .	63
<i>S.V. Navada, A.R. Nair, Suman Sharma, U.P. Kulkarni</i>	
Isotope study in geothermal fields in Java Island . . . . .	83
<i>Zainal Abidin, Wandowo</i>	
The use of gas chemistry and isotope geothermometry to study the effects of exploitation and reinjection on the fluids at Larderello, Italy . . . . .	93
<i>C. Panichi, P. Noto, L. Belluci, G. Scandiffio, F. Baccarin, M. Valenti</i>	
Environmental isotope-aided studies on geothermal water in the Republic of Korea . . . .	113
<i>J.S. Ahn, Y.K. Koh</i>	
Isotopic and chemical studies of geothermal waters of northern areas of Pakistan . . . . .	127
<i>S. Dildar Hussain, M. Ahmad, R. Gonfiantini, W. Akram, M.I. Sajjad, M.A. Tasneem</i>	
Applications of stable isotopes in geothermal exploration in the Philippines — A review . . . . .	149
<i>J.Y. Gerardo, R.R. Alvis-Isidro, D.R. Sanchez, V.C. Clemente, R. Gonfiantini</i>	
Geochemical and isotopic investigation of Biliran geothermal discharges, Philippines . . .	169
<i>M.N. Ramos-Candelaria, J.R. Ruaya, A.S.J. Baltasar</i>	
Chemical and isotopic studies of fluids in the Bacon-Manito geothermal field, Philippines . . . . .	185
<i>J.R. Ruaya, M.M. Buenviaje, R.P. Solis, R. Gonfiantini</i>	
Isotopic and chemical composition of waters and gases from the east coast accretionary prism, New Zealand . . . . .	209
<i>W.F. Giggenbach, M.K. Stewart, Y. Sano, R.L. Goguel, G.L. Lyon</i>	
Isotope and geochemical survey of geothermal systems of Yozgat Province in Central Anatolia — Turkey . . . . .	232
<i>Ş. Şimşek</i>	
Preliminary geochemical and isotopic study of the south Trungbo geothermal area in central Vietnam . . . . .	249
<i>Nguyen Trac Viet, Nguyen Kien Chinh, Huynh Long, Nguyen Dieu Minh, Phan Thanh Tong</i>	
Participants Directly Involved in the Co-ordinated Research Programme . . . . .	269

## INTRODUCTION

In the last ten years, geothermal energy has emerged as an alternative source of energy for electrical and non-electrical uses. In 1992, about 21 countries were producing electricity from geothermal resources. In some of these countries geothermal energy contributed up to 40% of the national power requirement. In others, it is being widely used in agriculture, aquaculture, air conditioning, kiln and fruit drying, pulp and paper industry, greenhouses and food processing.

Exploration of geothermal resources requires geoscientific investigations to produce a conceptual hydrogeochemical model which is a basis for drilling and development. As most of the resource is situated in a complex geochemical environment and development is initially capital intensive, exploration activities demand in-depth data collection and interpretation to understand the characteristics, origin and movement of fluids.

The Co-ordinated Research Programme (CRP) on the Application of Isotope and Geochemical Techniques to Geothermal Exploration in the Middle East, Asia, the Pacific and Africa aimed at integrating isotope techniques with traditional geochemical and hydrological methods in understanding the characteristics of geothermal systems. It involved isotopic and chemical surveys of hot to cold springs, wells and rivers in exploration areas as well as in exploited reservoirs where problems such as return of injected wastewaters are experienced.

The CRP covered the high enthalpy geothermal systems in China, Indonesia, the Philippines and Turkey, where the energy is used mainly for electrical power generation; as well as the low enthalpy geothermal systems for non-electrical uses in countries such as the Republic of Korea, India, Pakistan and Viet Nam, which are starting with their geothermal exploration programme. National and international institutes that are capable of isotope measurements were also included in the CRP. Additionally, Iceland, Italy and New Zealand, where high enthalpy geothermal systems are in advanced stages of development, expertise is highly developed and much scientific experience has been gained in geothermics, also participated. Although important geothermal resources are also developed in African countries, no counterparts were identified at the time of the implementation of the programme.

The CRP gathered various kinds of expertise and involved institutions studying geothermal systems having different characteristics. It has demonstrated the strength of isotope techniques complemented by chemistry at assessing the hydrologic characteristics of the geothermal areas. The CRP also promoted the development of skills for interpretation, which at its initiation was only starting among some investigators, as more work was done and as a result of interaction with more experienced scientists. This is demonstrated by the papers herein included. The CRP, thus, has shown to be an efficient mechanism to transfer scientific capabilities between more experienced scientists and those who are starting in the same endeavour.

The other important output of this CRP is a better understanding of the nature of magmatic waters that mix with meteoric waters in geothermal systems, first introduced in the CRP for Latin America on the Use of Isotope and Geochemical Techniques in Geothermal Exploration by W. Giggenbach. It identified the processes governing thermal waters. It also emphasized the importance of isotopic enrichment due to mixing, as opposed to effects of evaporation, in postulating regions of higher heat flow during the exploration stage. More data have been generated in certain areas to enable the calculation of appropriate local meteoric water lines as well as to identify recharge areas. In addition, the effects of injection on the chemical and isotopic composition of geothermal waters were studied.

In the course of the investigations, it was commonly recognized that the use of isotope techniques in geothermal development is required for:

- the understanding of the origin and distribution of acid fluids in high temperature geothermal systems;
- monitoring of reinjection fluids; and
- isotope geothermometry.

Although initially considered, the use of  $^{34}\text{S}$  and  $^{14}\text{C}$  was not emphasized during this CRP because priority was given to the understanding of the hydrology of geothermal systems, which stable isotopes can provide. Sulphur and carbon isotopes will be applied in geothermometry applications and to further delineate the origin of certain extraneous fluids, such as acidic waters. These concerns are proposed to be the subject of a new CRP.

# APPLICATION OF ISOTOPE AND GEOCHEMICAL TECHNIQUES TO GEOTHERMAL EXPLORATION IN SOUTHEAST CHINA — A REVIEW

WANG Ji-Yang, PANG Zhong-He  
Laboratory for Geothermics, Institute of Geology,  
Academia Sinica,  
Beijing, China

**Abstract** - Hot springs that are widely distributed in the SE coastal area of China and there have been a subject of dispute on their genesis and origin. Since mid 80's, with the support of the IAEA Research Contracts, isotope and geochemical techniques have been systematically applied to the geothermal systems in the region. The techniques have proven to be very useful and effective in geothermal exploration.  $^2\text{H}$  and  $^{18}\text{O}$  have been employed to study the origin and recharge of the systems, while  $^3\text{H}$  and  $^{14}\text{C}$  have been used to determine the age of the geothermal fluids. Fluid/mineral equilibrium modelling is also useful for the calibration and use of conventional chemical geothermometers and makes reservoir temperature prediction more reliable. Different geothermal systems from Fujian, Guangdong and Hainan Provinces were selected for the study. Results show that the geothermal systems in the study area all belong to the low-medium temperature geothermal systems of convective type, which essentially differs from high temperature geothermal systems with magmatic heat sources underneath.

## 1. INTRODUCTION

Hot springs are widely distributed at the southeast coast of China, including Fujian, Guangdong and Hainan Provinces (Fig. 1). It was postulated that these are the surface manifestations of high temperature geothermal systems with magmatic heat sources. The

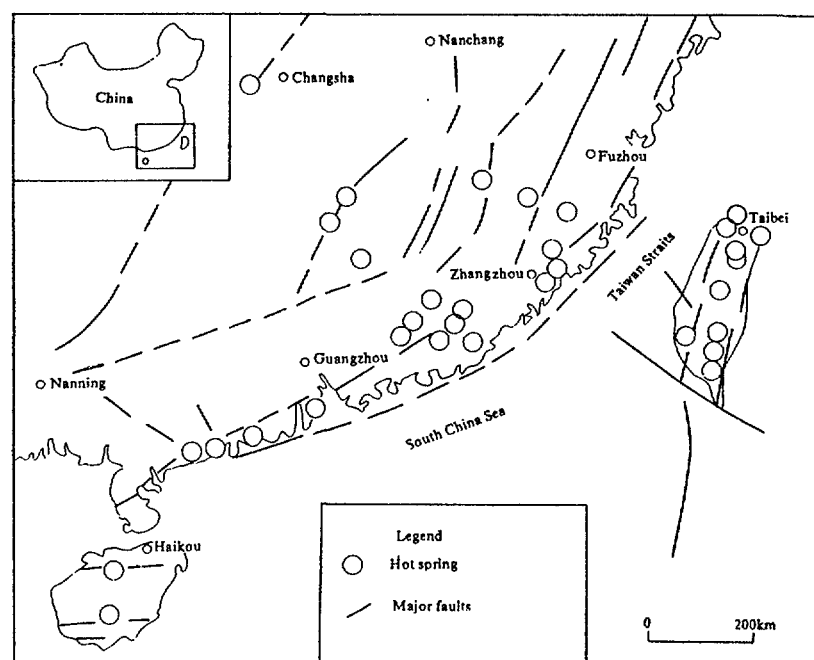


FIG. 1. Map of hot springs with emerging temperature higher than 80°C in SE China.

occurrence of the geysers induced by drilling in Zhangzhou area, the high salinity and the Cl-Na type of the geothermal fluids have been regarded as the evidences of high subsurface temperature. It is obvious that detailed investigation of the systems is necessary and urgent. Thus, since 1985, the authors have carried out multi-disciplinary investigations on the chemistry and isotopic composition of thermal waters [1]. This aimed to understand the genesis, origin and age of the thermal fluids; the recharge areas for the systems; the chemical characteristics and the dominant controlling factors or processes; the state of the chemical equilibrium of the fluids with the reservoir country rocks and the range of reservoir temperatures. This involved the use of major and trace elements, oxygen, hydrogen and carbon isotopes. It also included a computer modelling of the fluid/mineral equilibrium.

During the last several years, the following activities were carried-out: 1) Sampling of thermal waters in the Zhangzhou Basin and its surroundings for isotope and chemical determination; and 2) Sampling of gases for chemical analyses in the same area. The investigation using isotope and geochemical techniques were extended to the geothermal areas of Fujian, Hainan and Guangdong Provinces.

## 2. TECHNIQUES APPLIED

### 2.1. Chemical analyses

All the water samples were analyzed for their chemical compositions, partly on the Dionex (USA) 20201 Ion Chromatography and partly by conventional chemical methods.

### 2.2. Gas analyses

Water samples were also collected for dissolved gas analyses. The samples were stored in tightly sealed 10-liter glass bottles. They were analyzed soon after collection on the gas chromatograph in the Gas Analysis Laboratory of the Institute of Geology, State Seismological Bureau of China in Beijing.

### 2.3. Isotope Analyses

Samples of both thermal and non-thermal natural waters were collected for  $^{18}\text{O}$ ,  $^2\text{H}$  and  $^3\text{H}$  determinations. They were collected in air-tight glass bottles of 50 ml (for  $^2\text{H}$  and  $^{18}\text{O}$ ) and 500 ml (for  $^3\text{H}$ ) in volume.  $^2\text{H}$  and  $^{18}\text{O}$  were determined on MAT 251 mass spectrometer (West Germany) while  $^3\text{H}$  was analyzed on QANTLEX Liquid Scintillation Counter (Australia).  $^{14}\text{C}$  was also used in some instances as a dating tool. C is collected through precipitation method.

### 2.4. Fluid-mineral equilibrium modelling

Fluid/mineral equilibrium modelling has been developed quite rapidly these years and is now used more and more widely in geothermal studies [2, 3]. The fundamentals of the approach as presented by Reed and Spycher is as follows: Using the activities of aqueous component species calculated for homogeneous equilibrium at a series of temperatures, it is possible to compute the degree of super- or under- saturation of the aqueous phase with minerals at each temperature. This is expressed for mineral  $k$  in terms of  $\log (Q/K)_k$ :

$$\log (Q/K)_k = \log \prod a_{i,k}^{v_{i,k}} - \log K_k$$

where  $Q$  is the calculated ion activity product;  $K$  is the equilibrium constant for mineral  $k$ ;  $a_{i,k}$  is the activity; and  $v_{i,k}$  is the stoichiometric coefficient of component species  $i$  in the equilibrium mass action expression for mineral  $k$ , written with the mineral on the left side.

Therefore, the  $\log(Q/K)$  value for each mineral provides a measure of the proximity of the aqueous solution to equilibrium with the mineral. The numerical value of  $\log(Q/K)$  is greater than zero for super-saturated minerals and less than zero for under-saturated minerals.

The increasing and improved thermodynamic data for various species in aqueous solutions and the established numerical methods mentioned above have made it possible to calculate the  $\log(Q/K)$  value for many minerals using analytical values for the chemical components of geothermal fluids.

If an aqueous solution is in equilibrium with respect to a certain mineral assemblage, the temperature at which the components reach equilibrium can be identified. The convergence of  $\log(Q/K)$  curves for the equilibrium assemblage to zero at the temperature of equilibration establishes a basis not only for the judgement of the equilibrium situation of a geothermal system but also for geothermometry.

## 2.5. Chemical geothermometry

Chemical geothermometry is an efficient and reliable method for estimating the reservoir temperature of geothermal systems. To date, over twenty chemical geothermometers have been proposed by different authors. These are widely used in the exploration of geothermal resources.

However, most of the geothermometers are empirical and involve many assumptions. Different temperatures can be given by using different ones with the same set of geochemical data. A particular geothermometer may be suitable to one place but not another. This deficiency prevents geothermometers from more effective application and sometimes causes considerable problems [4].

Therefore, an attempt was made by the authors to combine the conventional geothermometers with the chemical equilibrium modelling. Hence, the applicability of the conventional geothermometers in different conditions can be verified. After this calibration, the selected geothermometers may then be applied to other geothermal systems by using a reference geothermal system. This aim has been achieved for the Southeast China Geothermal Belt.

All the conventional geothermometers proposed by different authors include the same assumptions as follows: 1. Solvents are sufficient for water-rock exchange; 2. Fluid-mineral equilibrium is attained in the study system; and 3. The equilibrium state is not changed as the thermal water flows to the surface. However, the conventional geothermometers themselves alone can not be used inversely to prove these pre-conditions. Moreover, because of the differences in the mineral phases that are in contact with the reservoir fluid, different versions of the same geothermometer may be significantly different in the coefficients used in their equations. Therefore, they may yield very different results. Taking the Na-K geothermometer as an example, since the coefficients in the equations of different geothermometers are calibrated to different sets of data, the different Na/K geothermometer equations give very different temperatures by as much as 50-70 °C for the same ratio and/or the same water sample, [5, 6]. All of the other cation geothermometers, including the Na-K-Mg-Ca

ge indicators proposed by Giggenbach [7], bear the same problem [4]. For the silica geothermometers, on the other hand, although based on relatively solid experimental data, the identification of the appropriate silica mineral phase is essential to obtain correct results because the temperature difference may reach as great as 100 °C if an unrealistic phase is assumed [5]. For the above reasons, calibration is a necessary step before a geothermometer can be used with confidence.

The main purpose of calibration is to verify if a particular geothermometer meets the conditions mentioned above. Therefore, the major tasks of calibration are: 1. To determine the equilibrium situation of the selected system; 2. To identify the equilibrium mineral assemblage; 3. To find out the equilibrium temperature as calculated; and 4. To determine the suitable geothermometer equations.

To achieve this aim, representative geothermal systems should be selected. The geological settings and geochemical environments are identical to the target area where the calibrated geothermometers will be used. In practice, the requirements of a reference geothermal system is as follows: 1. Sufficient data to prove that the system is representative in the study area of the geothermo-geological setting; 2. Measured reservoir temperature (or the bottom-hole temperature measured from deep drill-holes) of the system; 3. A complete set of analytical data of the fluids; and preferably, 4. Information on the hydrothermal alteration minerals.

The geothermal system selected for calibration should be in equilibrium and the calculated temperature should be the same as (or very close to) the measured reservoir temperature. If this is obtained, it means that equilibrium exists at that reservoir temperature. By comparing the temperatures given by the conventional geothermometers with the measured reservoir temperature it is easy to know which geothermometer gives a more reliable result.

It is strongly suggested that modelling be combined with mineral alteration studies so that more information could be obtained about the realistic equilibrium in the reference system. This, therefore, will provide an even more solid ground for the calibration and application of the chemical geothermometers.

### 3. RESULTS AND INTERPRETATIONS

#### 3.1. Origin of the thermal fluids and recharge of the systems

A local meteoric water line was determined based on the data of different types of meteoric waters including rainwater, river water and shallow groundwaters from the study area [8] (Fig. 2). The line is found to be identical to that of the global meteoric line. Waters represented by the diluted thermal waters plot in the very close proximity to the meteoric line, which implies their meteoric origin (Fig. 3). According to the “elevation effect” principle, the elevation of the recharge areas for the hot spring show that the recharge area of the systems studied usually varies from 800 to 1000 meters, higher than that of the discharge areas. In most cases, recharge areas are at the periphery of the groundwater basins. With reference to the modelling by mass and heat transport as well as conservation in the systems [9, 10], it is concluded that these hot spring systems are formed by the deep circulation of groundwater within the basins due to forced convection induced by topography [11, 13].



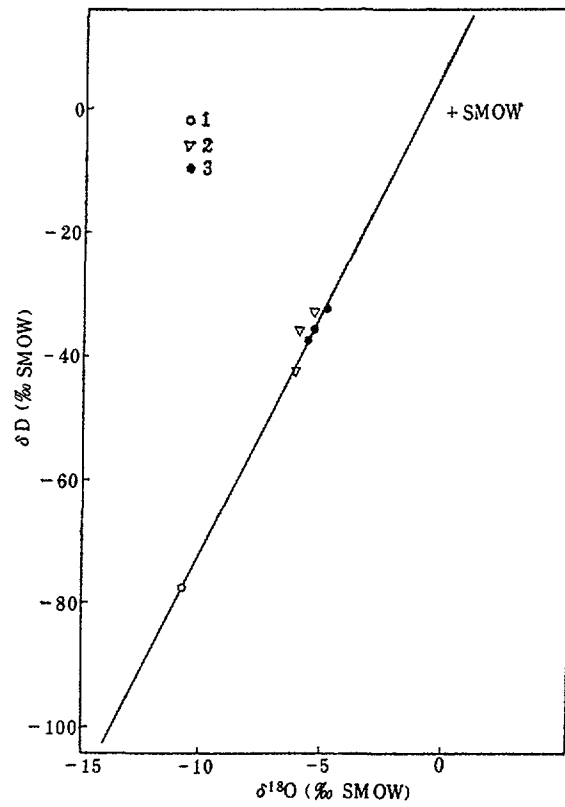


FIG. 2. Meteoric water line for the non-thermal natural waters in Zhangzhou area ( $D = 8.02 \delta^{18}\text{O} + 9.11$ ,  $n = 7$ ,  $r = 0.99$ ); 1. rain water; 2. spring water; 3. river water.

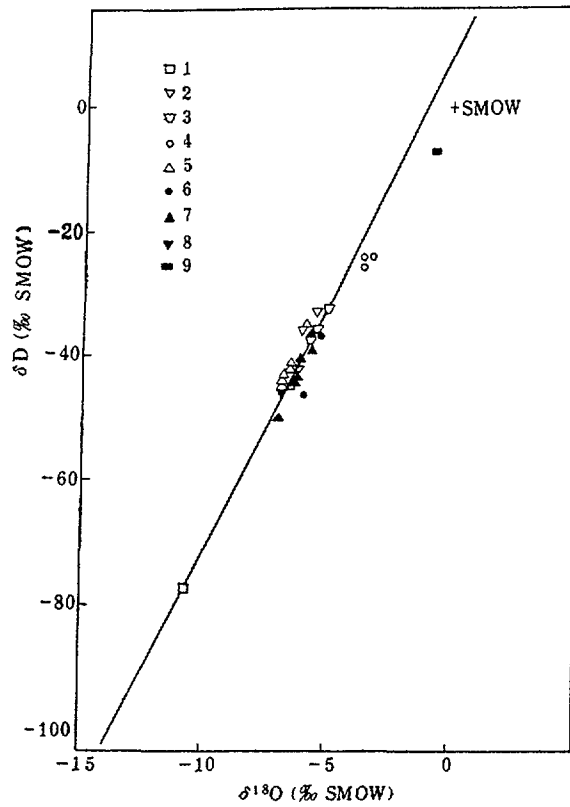


FIG. 3. Comparison of isotope compositions of the thermal waters and the non-thermal meteoric waters. 1. Rain water; 2. Spring water; 3. River water; 4. Water from Quaternary formation; 5. Water from bedrocks; 6. Thermal water from Quaternary formation; 7. Thermal water from bedrocks; 8. Hot spring water; 9. Sea water.

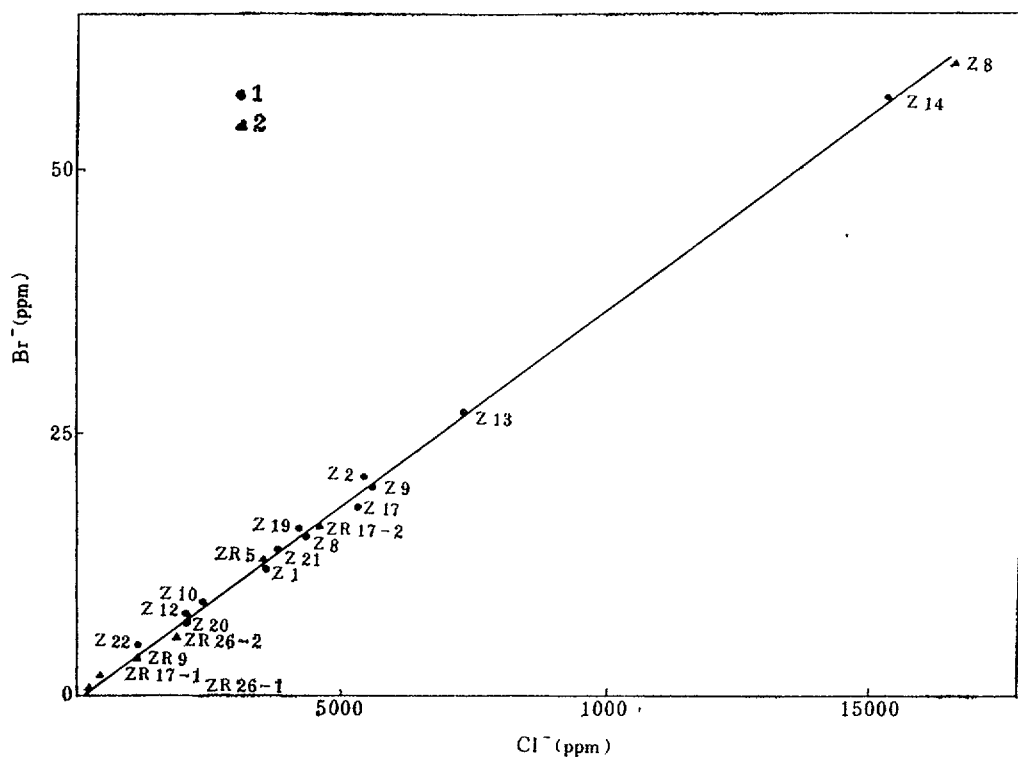


FIG. 4. Linear relation between Cl and Br in thermal waters, from Zhangzhou basin and surroundings.  
1. Thermal water; 2. Sea water.

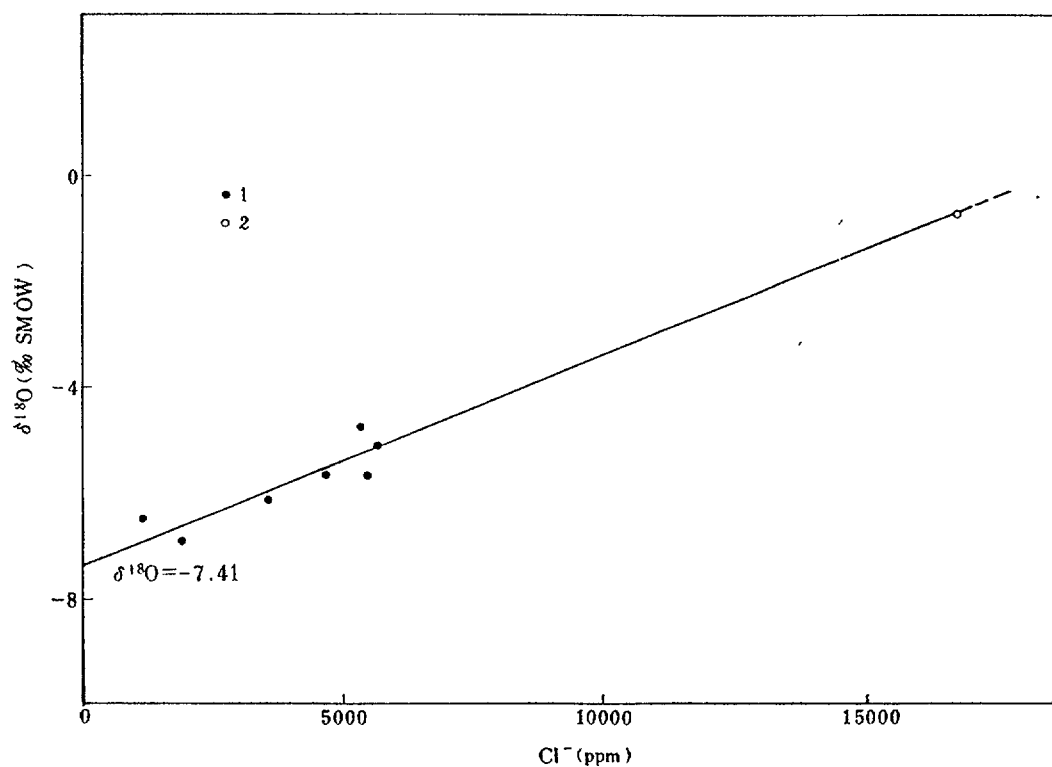


FIG. 5. Linear relation between Cl and  $^{18}\text{O}$  in thermal waters from Zhangzhou basin and surroundings.  
1. Thermal water; 2. Sea water.

### 3.2. Processes governing the fluid compositions

Most of the hot spring waters are dilute water. However, thermal waters from some geothermal systems close to the seashore are saline water. The total dissolved solids in these waters may be as high as 10 to 12 g/L. Mixing of the recharging meteoric water with sea water is evidenced by the close correlation of the Cl concentration with Br contents (Fig. 4). This is also supported by the close linear correlation between chloride concentrations and the  $^{18}\text{O}$  [14] (Fig. 5).

The Zhangzhou-Xiamen geothermal zone was selected as the sampling area for a detailed investigation on this sea water mixing processes. Samples at increasing distance from the sea shore and with different salinities were collected for chemical and isotopic analyses. The sea water in most of the geothermal systems seems to be connate water that entered the systems during high sea level period, which appeared, for SE China, 6,000-7,000 years ago. The dilute waters from other systems have chemical features derived from the dissolution of the granitic country rocks. A knowledge of the mixing processes has deepened the understanding of the genesis and origin of the systems. For instance, at the Zhangzhou Geothermal Field, it is found that two mixing phases took place in the system. Phase 1 is the mixing of meteoric water with the connate sea water at depth. Phase 2 is the mixing between the ascending saline water with the dilute groundwater in the shallow aquifers near the surface.

### 3.3. Thermal water age dating

The age (residence time) of the geothermal fluid is defined as the time since it was last isolated from the atmosphere. Radioactive isotopes  $^3\text{H}$  and  $^{14}\text{C}$  were used for age dating of geothermal water and other natural waters in the study areas [15]. Geothermal parent waters are  $^3\text{H}$  free. The presence of  $^3\text{H}$  in the thermal water is an indicator of dilution by the young shallow groundwater. It was found to be quite effective for investigating the relationship between different natural water types. However, it seems not to be a good dating method because the age of geothermal waters is far beyond the limit (about 1000 years) of  $^3\text{H}$ . Instead the thermal water from Nanjin hot spring to the west of Zhangzhou Basin was dated using  $^{14}\text{C}$ . The results indicate 1,755  $\pm$  360 years old. However,  $^{14}\text{C}$  dating failed to apply to saline water because of its low C content.

## 4. GEOTHERMAL RESOURCES POTENTIAL ASSESSMENT

For the assessment of the potential of the resources, reservoir temperature is of significant importance. In this study, conventional chemical geothermometers along with calibration, were applied to estimate the reservoir temperatures.

The Nanjin hot spring system, which has the same geological and geochemical background as the target area, is selected for the calibration of conventional geothermometers. The reservoir rock is granodiorite overlain by Quaternary sediments which are about 20 meters thick. The total natural flow rate of hot water from the hot springs is greater than 20 litres per second. The highest temperature measured, which may be regarded as the reservoir temperature of the hot springs, is 78 °C at the surface and 90 °C at the bottom of a 628 meter deep hole.

The modelling work for this geothermal system was presented by Pang & Armannsson [3]. The log (Q/K) diagram for a water sample from the spring with the highest temperature

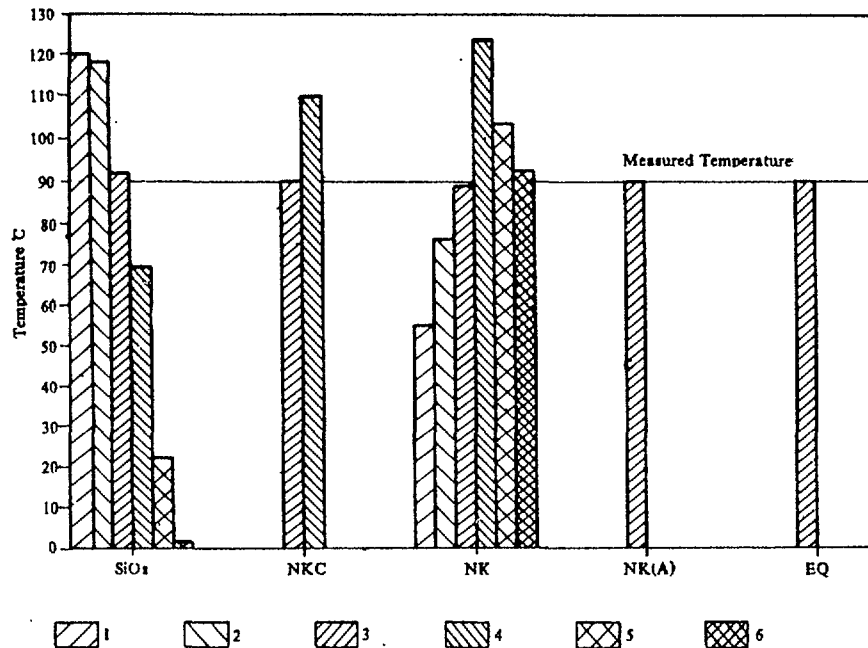


FIG. 6. Comparison of reservoir temperatures predicted by using different geothermometry methods and by fluid-mineral equilibrium calculations to the measured bottom-hole temperature for Nanjin hot spring in the Southeast China Geothermal Belt. SiO<sub>2</sub>: Silica geothermometer temperatures; NKC: Na-K-Ca geothermometer temperatures; NK: Na-K geothermometer temperatures; NK(A): mean temperature given by the six Na-K geothermometers; EQ: equilibrium temperature from the fluid-mineral equilibrium calculations. Legends numbers 1 to 6 represent different geothermometer equations of the same geothermometer. For silica geothermometers, 1: Quartz-nsl, 2: Quartz-msl, 3: Chalcedony, 4:  $\alpha$ -Cristobalite, 5:  $\beta$ -Cristobalite, 6: Amorphous silica; For Na-K-Ca geothermometers, 1: Na-K-Ca ( $\beta = 4/3$ ), 2: Na-K-Ca ( $\beta = 1/3$ ); For Na-K geothermometers, 1: Truesdell (1976), 2: Tonani (1980), 3: Arnorsson (1983), 4: Giggenbach (1988), 5: Fournier (1983), 6: Nieva (1987). The measured reservoir temperature for tyunhis system is indicated by the horizontal bar in the diagram and its value is 90°C.

in the area shows that the saturation curves of five minerals converge to the same temperature. These minerals are: Ca-montmorillonite and Mg-montmorillonite, chalcedony, fluorite, and calcite, representing a steady mineral assemblage in the reservoir. These minerals are often found in the drillholes of the area and its surroundings. The temperatures obtained by the equilibrium calculations are in good agreement with the bottom-hole temperature measured in the deepest hole of the area. Both the calculated and the measured temperatures are 90 °C.

Moreover, the reservoir temperature estimated by using different geothermometers such as Na-K-Ca ( $\beta=4/3$ ), Chalcedony [16], and Na-K [17, 18] are in good accordance with the measured temperatures, as is shown in (Fig. 6). But Quartz, Na-K-Ca ( $\beta=1/3$ ) and some other Na-K geothermometers indicate higher temperatures, implying that there may exist a deeper reservoir with a higher temperature.

The results indicate that, in this particular condition, among the six silica geothermometers, chalcedony controls the solubility of silica. For the cation geothermometers, the Na-K-Ca geothermometer can yield correct results. Some other cation geothermometers may also be applicable to low temperature environments but evidently not better than the Na-K-Ca and chalcedony geothermometers.

TABLE I. BASIC CHARACTERISTICS AND RESOURCES OF HOTSPRINGS  
IN HAINAN PROVINCE

No.	Location	Geology	Tectonics	Topography	Q(l/s)	T <sub>s</sub> (°C)	Chem. Type	T <sub>c</sub> (°C)
1	Wenchang	Granite	NE fault	Riverside	3.69	73.5	Cl-Na	137
2	Qionghai	Schist	NE fault	Riverside	0.75	75.0	Cl-NaCa	119
3	" "	Granite	NE fault	Terrace	3.31	48.0	HCO <sub>3</sub> -Na	?
4	" "	"	" "	"	0.30	58.0	"	?
5	Wanning	"	" "	Valley	0.49	34.0	HCO <sub>3</sub> Cl-Na	?
6	" "	Granite	" "	Riverside	2.40	63.0	HCO <sub>3</sub> -Na	116
7	" "	"	?	Hill	0.78	35.0	ClSO <sub>4</sub> -NaCaMg	?
8	Ningshui	"	E-W	Stream	14.14	77.0	ClHCO <sub>3</sub> -Na	?
9	Baoting	Quartzite	one fault	"	?	54.0	?	?
10	Baoting	Quartzite	two faults	Hill	4.65	84.0	HCO <sub>3</sub> -Na	122
11	Ningshui	Granite	one fault	"	2.02	68.0	Cl-NaCa	110
12	Ningshui	Granite	one fault	"	4.65	72.0	Cl-Na	122
13	Yaxian	Granodiorite	" "	Plain	0.24	47.0	"	107
14	" "	Granite	" "	"	2.78	63.0	"	?
15	" "	"	" "	Valley	4.65	78.0	HCO <sub>3</sub> SO <sub>4</sub> -Na	114
16	" "	"	" "	Plain	0.30	45.0	"	90
17	Dongfang	Migmatite	" "	Hill	0.30	38.0	HCO <sub>3</sub> -Na	97
18	" "	Shale	" "	"	0.78	49.0	"	101
19	" "	Granite	?	Plain	7.73	78.0	Cl-Na	127
20	" "	Migmatite	one fault	Hill	1.50	51.5	HCO <sub>3</sub> -Na	110
21	" "	Granite	?	Plain	2.02	51.0	"	122
22	Changjiang	"	NE fault	Stream	1.82	47.0	HCO <sub>3</sub> SO <sub>4</sub> -Na	97
23	Baisha	"	" "	Hill	0.74	38.0	HCO <sub>3</sub> -Na	93
24	" "	"	?	"	0.45	41.0	?	?
25	" "	Schist	?	Stream	3.46	40.0	HCO <sub>3</sub> -NaCa	81
26	Qiongzong	Granite	Three f.	"	0.60	34.5	?	?
27	Danxian	Quartzite	NW fault	Valley	4.00	55.0	HCO <sub>3</sub> -NaCa	?
28	" "	Granite	" "	"	3.92	83.0	HCO <sub>3</sub> -Na	107
29	" "	"	" "	Stream	0.40	59.0	"	81
30	Chengmai	"	one fault	Valley	4.46	57.0	"	101
31	" "	"	" "	Hill	0.45	70.0	?	?
32	" "	"	NE fault	Terrace	2.54	39.5	HCO <sub>3</sub> -Na	55

Notes: T<sub>s</sub> = surface temperature; T<sub>c</sub> = chalcedony temperature; ? = no data.

Similar estimations were made for many geothermal systems of southeast China. In the geothermal systems of the Zhangpu-Yunxiao areas in southern Fujian Province [19], chalcedony and Na-K-Ca geothermometers show quite a good agreement in the reservoir temperature estimations (80-100 °C) while most of the Na-K geothermometers tend to give higher temperature predictions (120-140 °C). In Hainan Province, the reservoir temperature was calculated using silica geothermometer (Table I and Fig. 7), and the result appears to have a similar trend.

There are many saline hot water systems in the coastal areas of SE China. The high salinity comes from the mixing with seawater. Applicability of conventional geothermometers to this type of systems is different from the fresh water systems. For these, modelling exhibits that there is no overall equilibrium. All cation geothermometers failed to apply. However, the influence of the salinity on the silica geothermometers may be neglected, so they are still applicable. In the Zhangzhou Geothermal Field, considering the mixing process of deep saline thermal water with shallow cold groundwater, the reservoir temperature obtained by using the chalcedony geothermometer is 140°C [20].

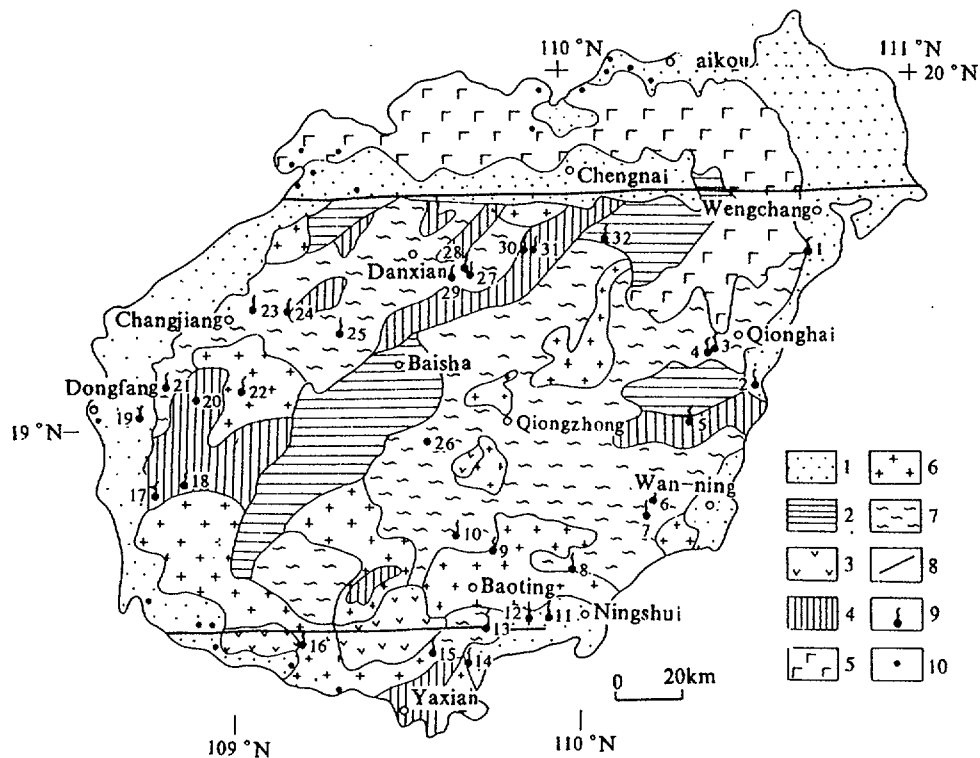


FIG. 7. Map of Hainan Island showing the locations of the major geothermal manifestations and their geological settings.

## 5. CONCLUSIONS

Geochemical and isotopic methods have been found to be very effective for the geothermal exploration and potential assessment of the low-medium temperature geothermal resources in the coastal area of SE China. It can be concluded from these studies that the hot springs are fed by low-medium temperature geothermal systems formed by the deep circulation of meteoric water [21]. The reservoir temperatures of these hot spring systems range from 100 °C to 1 °C and may not exceed 140 °C within the depth of interest. Since the sea water in the saline water systems is most likely to be connate water, the salinity tend to drop with the long-term exploitation.

**Acknowledgements** - *This investigation was carried out within the framework of the International Atomic Energy Agency Coordinated Research Programme for Africa, Asia and the Middle East on the Application of Isotope and Geochemical Techniques in Geothermal Exploration. It has been supported financially by the National Natural Science Foundation (NNSF) of China, (Project 49000034) and with partial support from IAEA Research Contract (4850/RB, 1988-1990). The support of IAEA in various means has played an important role in the achievements of the study. The authors want to express their sincere appreciation to the efforts made by the IAEA and the NNSF of China.*

## References

- [1] Wang, J., Pang, Z., Xiong, L., Fan, Z., Jiang, Z. and Zhuang, Q., 1989, in: *Advances in Geoscience* (Wang, S., ed.), China Ocean Press, 409-417.
- [2] Reed, M. and Spycher, 1984, Calculation of pH and mineral equilibria in hydrothermal waters with application to geothermometry and studies of boiling and dilution, *Geochim. Cosmochim. Acta*, 48, 1479-1492.
- [3] Pang, Z. and Armmannson, H., 1989, Modeling chemical equilibrium in hydrothermal systems: with examples from Iceland and China, in: *Water-Rock Interaction* (Miles ed.), Balkema, Rotterdam, pp 541-545.
- [4] Fournier, R., 1990, The interpretation of Na-K-Mg relations in geothermal waters, *GRC TRANSACTIONS*, Vol. 14, Part II, 1421-1425.
- [5] Pang, Z., 1992a,, Calibration of chemical geothermometers and their application to the southeast China geothermal belt, *Scientia Geologica Sinica*, 1, 237-248.
- [6] Pang, Z., 1992b, Theretical calibration of chemical geothermometers and its application to the granitic geothermal areas of SE China, *Water-Rock Interaction*, Kharaka & Maest (eds.), Balkema, Rotterdam, 1463-1466.
- [7] Giggenbach, W., 1988, Geothermal solute equilibria, derivation of Na-K-Mg-Ca geoindicators, *Geochim. Cosmochim. Acta*, 52, 2749-2765.
- [8] Pang, Z. and Wang, J., 1990a, Oxygen and hydrogen isotope study on Zhangzhou Basin hydrothermal system, southeast of China, *GRC TRANSACTIONS*, Vol. 14, Part II, 945-951.
- [9] Hu, S., 1989, Reservoir modeling of Zhangzhou low temperature fracture zone system, Fujian, China, Geothermal Institute Project Report 89.10, University of Aukland, New Zealand, pp.31.
- [10] Hochstein, M. P., Yang, Z. and Ehara, S., 1990, The Fuzhou geothermal system (P.R.China): modeling study of a low temperature fracture zone system, *Geothermics*, 19.
- [11] Wang J., Pang Z., Xiong L., Jiang Z., Zhuang Q. and Chen S., 1990, The Zhangzhou Geothermal System: a genesis model, *Proceedings of "1990 Beijing International Symposium on New and Renewable Energy Resources"*, Academic Press.
- [12] Wang J., Pang Z., Xiong L., Jiang Z., Zhuang Q. and Chen S., 1990, The Zhangzhou Hydrothermal System: a conceptual model for its genesis, *New Energy Sources*, 11, 41-43, in Chinese.
- [13] Wang J., Pang Z., Xiong L., Jiang Z., Zhuang Q. and Chen S., 1991, Genesis model of Zhangzhou Hydrothermal System, *Proceedings of 3rd National Geothermal Conference*, Beijing Science and Technology Press, Beijing, 116-122.

- [14] Pang, Z., Fan, Z. and Wang, J., 1990b, Isotopic evidence for the genesis and seawater involvement of geothermal water in Zhangzhou basin, *Geochimica*, 4, 296-302, in Chinese with an English abstract.
- [15] Pang, Z., Fan, Z. and Wang, J., 1990c, Study on Tritium of the Zhangzhou basin hydrothermal system, *Scientia Geologica Sinica*, 4, 385-393, in Chinese with an English abstract.
- [16] Fournier, R., 1989, Lectures on geochemical interpretation of hydrothermal waters, *Report of the UNU Geothermal Training Programme in Iceland*, No.10, pp 73.
- [17] Arnorsson, S., Gunnlaugsson, E. and Svavarsson, H., 1983, The chemistry of geothermal waters in Iceland II. Mineral equilibria and independent variables controlling water compositions, *Geochim. Coschim. Acta*, 47, 547-566.
- [18] Nieva, D. and Nieva, R., 1987, Developments in geothermal energy in Mexico, part 12 - A cation composition geothermometer for prosecution of geothermal resources, in: *Heat Recovery Systems and CHP*, 7, 243-258.
- [19] Pang Z., 1991, Calibration of chemical geothermometers based on fluid-mineral equilibrium calculations with application to the hot spring areas in the south of Fujian Province, China, submitted to: *GRC (U.S. Geothermal Resources Council) TRANSACTIONS*.
- [20] Pang, Z., Fan, Z. and Wang, J., 1990d, Calculation of the reservoir temperature of Zhangzhou Geothermal Field using a SiO<sub>2</sub> mixing model, *Chinese Science Bulletin*, 35(16), 1360-1363.
- [21] Wang J., Xiong L., Pang, Z., Hu, S. and Chen, M., 1993, Nature of the geothermal systems in southeast China, in: *Resources Engineering Environmental System and Economic Development Strategy in Coastal Areas of China* (Zhang, S., ed.), China Seismology Press, Beijing, 231-238.



# PROCESSES CONTROLLING THE CHEMICAL COMPOSITION OF NATURAL WATERS IN THE HREPPAR-LAND AREA IN SOUTHERN ICELAND

S. ARNÓRSSON, A. ANDRÉSDÓTTIR

Science Institute, University of Iceland,  
Reykjavik, Iceland

**Abstract** - *This contribution describes the processes controlling the chemical and isotopic composition of cold and geothermal waters (5-150 °C) in the Hreppar-Land area in southern Iceland. The area is located in Quaternary formations, mostly basaltic in composition. The chemical composition of surface- and cold groundwaters are controlled by the salt content of the precipitation, rock dissolution and organic CO<sub>2</sub> from the soil. The dissolved solids content of the geothermal waters is higher than that of the cold waters and it increases with temperature. The cause is increased rock dissolution. The pH of the cold waters is 6.5-7.5. It rises sharply to as much as 10 in the warm waters but falls again in hotter waters. At temperatures as low as 10-20 °C rock dissolution and pH increase has progressed sufficiently to cause the water to precipitate some secondary minerals. These minerals act as sinks for the various elements they incorporate. Aqueous cation-proton activity ratios and aqueous acid concentrations indicate that equilibrium with secondary minerals is rather closely approached for the following elements to temperatures as low as 40-50 °C: Na, K, Ca, Mg, Fe, Al, Si, C, F and sulphide sulphur, but not for sulphate sulphur. The minerals involved include calcite, chalcedony, smectite, low-albite, K-feldspar, an unknown Fe-bearing mineral, a zeolite, possibly heulandite and, in the case of sulphide bearing hot waters, pyrrhotite. The Cl-B relationships in the waters are considered to indicate that the geothermal water represents local precipitation. Yet, the  $\delta^{2}\text{H}$  values of these waters tend to be lower than that of local waters. This difference is not considered to reflect a distant recharge area to the geothermal systems on higher ground inland but due to the presence of a small component of "ice-age water" in the geothermal water that entered the bedrock during the deglaciation period, even earlier, when the  $\delta^{2}\text{H}$  of meteoric water in Iceland was much lower than that of today's precipitation.*

## 1. INTRODUCTION

The chemical and isotopic composition of geothermal waters has been used extensively in the exploration for and the assessment of the production characteristics of geothermal resources including prediction of subsurface temperatures from the chemical and isotopic composition of thermal springs and the location of recharge areas to the geothermal systems, thus obtaining information on regional groundwater movement [1]. Application of chemical and isotope geothermometers to predict subsurface temperatures is based on the assumption of specific mineral-solution or solute-solute equilibria in the geothermal reservoir and insignificant reactions in the upflow that would otherwise modify the composition of the water between the reservoir and the surface. Use of the stable isotopes of deuterium and oxygen has generally been based on the assumption that one can use the isotopic composition of today's precipitation to locate the recharge areas to geothermal systems. This assumption is not valid, of course, if the geothermal waters represent precipitation that fell when climatic conditions were significantly different from those today. Interpretation of chemical and isotopic data with respect to subsurface temperatures and groundwater flow in geothermal systems involves largely substantiating or disproving the validity of the assumptions involved.

In the present contribution the chemistry of natural waters in the Hreppar-Land area in southern Iceland is described and interpreted with respect to the processes affecting their chemistry. The waters include surface waters, cold groundwaters from springs, and thermal waters from springs and wells. This area constitutes one of the so-called low-temperature geothermal fields in Iceland with subsurface temperature exceeding slightly 150 °C assessment of the processes affecting the water chemistry helps evaluating conditions of mineral-solution equilibrium/disequilibrium and is, therefore, useful for geothermometry interpretation. Correlation of the chemistry of the mobile elements Cl and B with  $\delta^2\text{H}$  and  $\delta^{18}\text{O}$  helps interpretation of the isotopic data.

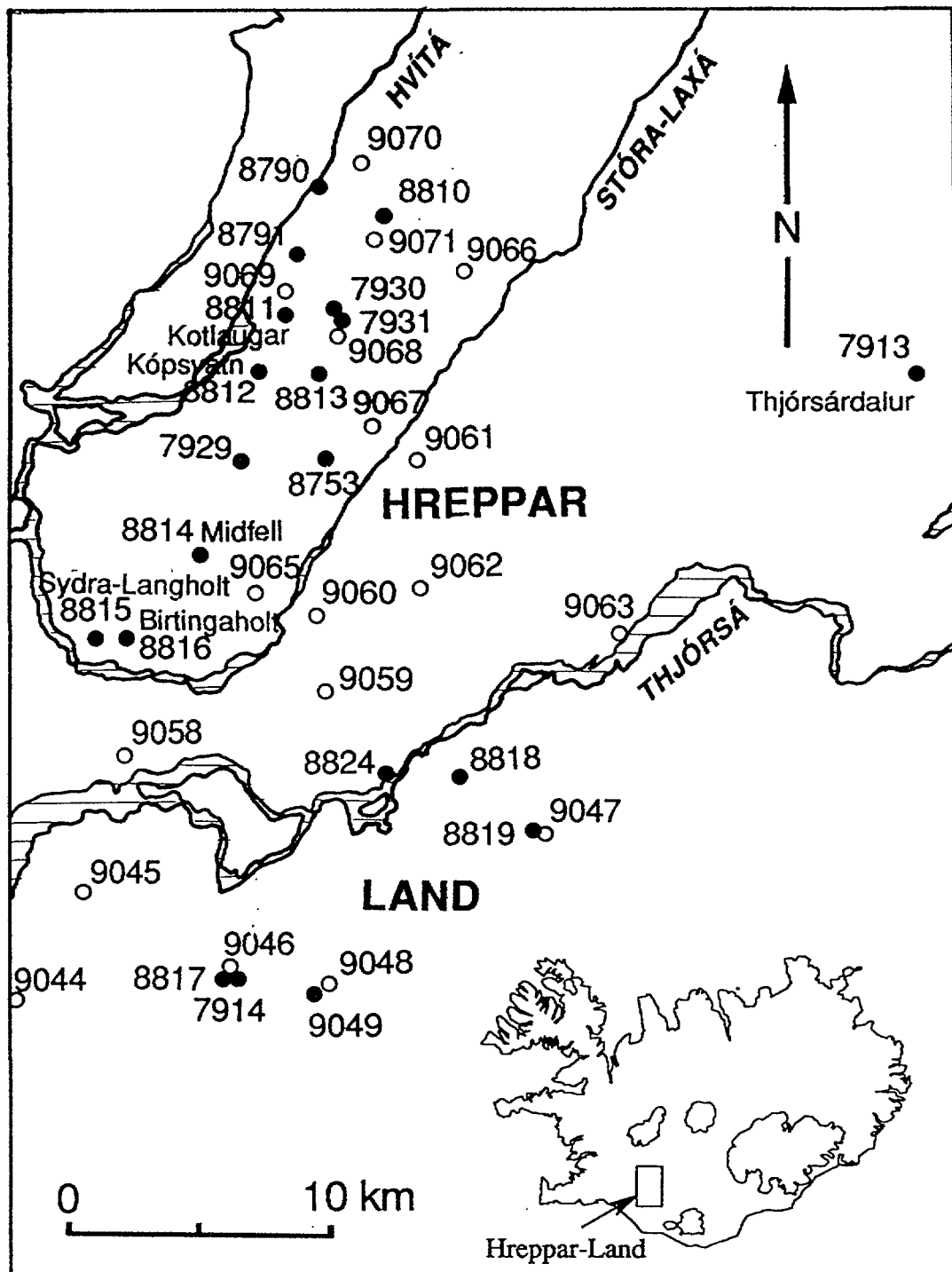


Fig. 1. Map of the Hreppar-Land area showing sample locations.

## 2. GEOLOGICAL FEATURES

The Hreppar-Land area is located in Quaternary formations in southern Iceland (Fig. 1). The bedrock consists mostly of Early Quaternary basaltic hyaloclastites formed during subglacial volcanic eruptions and of interglacial basalt lavas. In the western part of the area the lavas dip 2-8° towards northwest under the westernmore active volcanic belt in South-Iceland but in the easternmore part of the area close to the easternmore active volcanic belt in South-Iceland the strata are near horizontal. Sometimes the hyaloclastites have been reworked forming sedimentary layers between lavas but they also occur as drowned hills enveloped and overlayed by a sequence of basalt lavas with sedimentary intercalations. Two extinct central volcanic complexes occur within the area, at Stóra-Laxá and in Thjórsárdalur (Fig. 1). Silicic volcanics are associated with these complexes as well as intrusive granophyres, dolerites and gabbros at Stóra-Laxá [2].

Non-tilted interglacial lavas lie unconformably upon the Early Quaternary formations in parts of the area. These lavas which form prominent hills flowed when the main features of the present landscape had developed. They are fresh whereas the underlying bedrock is zeolitised. The zeolites, the formation of which is temperature dependent, suggests that some 500-700 m of the Early Quaternary formations had been removed by erosion before the non-tilted lavas were emplaced [3].

Warm and hot springs occur at many sites in the Hreppar-Land area and drillholes have been sunk at many of these sites and outside them to recover geothermal water (Fig. 1). Temperatures range from just above ambient to a little above 150°. The springs are often seen to be associated with NE-SW striking faults.

## 3. WATER COMPOSITIONS

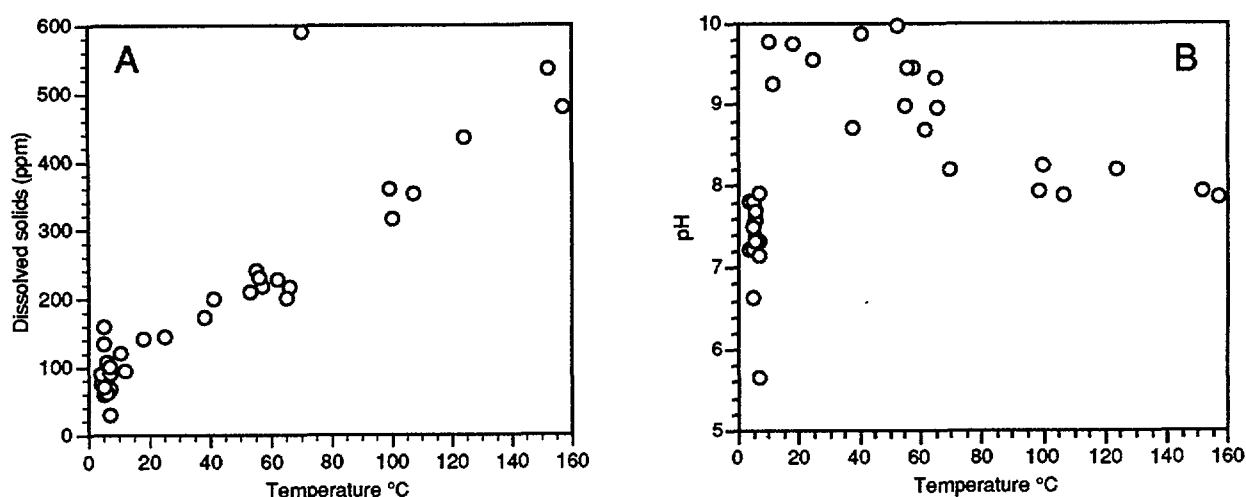
The major element composition of cold and thermal waters in the Hreppar-Land area is given in Table 1. The waters include streams, cold water springs as well as geothermal waters from springs and drillholes covering temperatures from less than 20 °C to a little over 150°C. One sample (no. 9067) is from a small lake and one (no. 9058) from a pond forming in peat soil after a heavy rainfall one night and collected the following morning. This sample was, therefore, expected to be closest to rainwater in composition.

The dissolved solids content of stream waters and cold springs lies in the range of 62-160 ppm. Geothermal waters are higher in dissolved solids, the value increasing with temperature (Fig. 2A). In the cold waters the most abundant component is silica, but the main cation is sodium and the main anions chloride and bicarbonate. Potassium, calcium, magnesium and iron generally constitute a significant proportion of the dissolved substances in these waters. The relative amount of silica is slightly higher in the thermal waters than in the cold waters. Sodium is the main cation and relatively considerably more abundant than in the cold waters. On the other hand calcium, iron and magnesium, particularly the latter two, are depleted in the geothermal waters in comparison with the cold waters and so is potassium in the warm waters but hotter waters possess similar or higher potassium concentrations than the cold waters. Aluminium and fluoride are low in the cold waters but increase in concentration with rising temperature. Sulphate and bicarbonate are the main anions in the geothermal waters although chloride is often only a little less abundant.

TABLE 1. MAJOR ELEMENT AND ISOTOPE COMPOSITION OF NATURAL WATERS IN THE HREPPAR-LAND AREA IN SOUTHERN ICELAND. CONCENTRATIONS IN PPM.

Location	Sample no.	Temp. °C	pHFC	SiO <sub>2</sub>	B	Na	K	Ca	Mg	Fe	Al	CO <sub>2</sub>	SO <sub>4</sub>	H <sub>2</sub> S	Cl	F	δD	δ18O
Þjórsárdalur s	7913	70	9.00/20	58.0	0.60	115.6	3.24	52.90	0.075	0.029	0.160	5.9	302.30	0.54	49.4	4.610	-93.6	
Hjálaleslaugar s	7914	41	10.33/20	82.1	0.17	63.3	1.61	1.82	0.030	0.004	0.050	18.8	29.50	<0.01	20.2	1.430		
Vaðmálhver s	7929	107	7.86/107	151.0	0.37	78.3	2.68	1.93	0.069	0.010	0.270	49.9	57.90	1.42	24.7	1.480		
Reykjahló w1	7930	152	7.90/152	248.5	0.64	100.5	6.10	1.26	0.050	0.007	0.410	57.5	69.50	4.20	40.9	1.830		
Reykjahló s	7931	157	7.81/157	223.9	0.67	102.3	6.70	1.22	0.057	0.005	0.270	59.8	66.00	3.82	35.9	1.760		
Hrunalaug s	8753	38	8.93/24	60.9	0.12	40.3	1.17	4.16	0.120		0.016	27.8	29.80	<0.01	17.0	0.610	-64.8	-9.25
Hvítárdalur s	8790	18	9.68/20	53.1	0.0096	41.4	1.01	1.09	0.027		0.024	39.1	6.09	<0.01	11.4	0.560	-62.9	-9.10
Skiphólt s	8791	25	9.62/20	60.6	0.018	39.3	1.88	1.64	0.046		0.051	38.6	4.88	<0.01	9.8	0.480	-61.2	-8.80
Jata s	8810	12	9.17/15	28.4	0.0026	20.7	0.98	3.44	0.485			26.5	8.41	<0.01	13.7	0.190	-60.8	-8.82
Kotlaugar w1	8811	124	8.17/124	158.8	0.48	113.7	3.40	0.93	0.006			53.3	81.10	3.21	38.8	2.260	-82.0	-10.25
Kópavann w1	8812	99	8.84/22	128.1	0.25	86.1	2.71	2.62	0.015			53.3	62.60	0.75	37.3	1.630	-76.8	-10.21
Reykjadalur w1	8813	100	9.24/22	121.0	0.32	79.0	2.02	1.69	0.002			48.0	52.20	1.69	24.8	1.250	-72.0	-9.54
Mitðell w1	8814	62	9.27/23	72.5	0.14	63.5	0.87	2.58	0.026			30.9	43.90	0.75	21.6	1.020	-70.5	-9.72
Sýra-Laugholt w1	8815	66	9.63/23	63.4	0.18	62.4	0.91	2.45	0.005			24.0	46.40	0.60	23.5	1.180	-70.5	-9.72
Birningabolt w1	8816	55	9.48/24	76.4	0.20	64.5	1.47	2.77	0.057			25.8	47.30	0.64	29.0	1.180	-70.4	-9.56
Hjálales w1	8817	53	10.56/25	80.7	0.15	68.8	0.67	1.62	0.016			17.0	27.60	<0.01	17.6	1.370	-70.7	-10.02
Hvannur w1	8818	57	9.99/26	78.1	0.15	65.4	1.28	1.75	0.012			19.8	42.50	<0.01	14.1	1.080	-67.4	-9.70
Stóri-Klofi w1	8819	56	10.05/24	68.5	0.12	64.3	0.47	3.81	0.020			8.4	68.90	<0.01	18.1	1.220	-79.5	-11.22
Þýðarárholt w1	8824	65	10.07/23	73.2	0.12	59.3	0.80	2.06	0.002			16.0	38.90	0.04	14.0	1.430	-67.7	-9.72
Gíslholt r	9044	4	7.64/22	22.2	0.0022	9.3	0.80	6.76	4.33	0.150	0.006	24.4	2.13		13.1	0.077	-56.4	-8.06
Stream by Kaldhárholtalekur r	9045	5	6.50/22	46.5	0.0044	12.1	1.10	12.10	8.80	11.90	0.038	88.7	5.44		12.6	0.158	-58.4	-8.41
Hjálales r	9046	5	7.38/22	31.3	0.0080	19.9	1.60	14.60	7.14	1.72	0.013	61.4	4.63		12.7	0.205	-55.9	-8.12
Klofalekur s	9047	6	7.57/22	22.1	0.019	17.9	1.20	6.46	2.61	0.024	0.009	29.1	9.59		9.1	0.397	-73.8	-10.36
Krókur s	9048	5	7.66/22	24.6	0.012	16.9	1.20	6.85	2.99	0.007	0.008	28.4	7.83		12.1	0.366	-67.3	-9.59
Krókur w1	9049	11	9.55/22	21.3	0.019	44.9	0.30	4.36	0.12	0.022	0.043	42.0	6.90		13.2	0.338	-59.6	-8.59
Sandalekur pool	9058	7	5.55/20	1.9	0.0059	4.2	2.81	1.35	1.18	0.061	0.033	10.1	2.01		9.7	0.018	-54.3	-7.69
Geldingabolt r	9059	6	7.25/20	21.1	0.0026	10.3	1.34	11.60	6.22	0.106	0.004	51.8	3.45		12.5	0.103	-55.2	-7.72
Fosgjá by Hlíð r	9060	6	7.49/20	27.3	0.0020	8.5	1.20	7.86	4.22	0.131	0.004	35.2	2.26		11.1	0.097	-56.5	-8.58
Laxárdalur r	9061	6	7.16/20	21.9	0.0025	7.4	0.80	4.79	2.09	0.017	0.003	19.5	2.15		11.3	0.095	-59.8	-8.77
Mástunga r	9062	6	7.45/20	30.2	0.0035	10.3	1.20	11.60	5.15	0.138	0.008	44.6	7.31		11.1	0.125	-60.2	-8.68
Hagafjall r	9063	6	7.56/20	24.6	0.0031	9.1	0.80	7.38	2.66	0.016	0.012	30.3	2.46		9.7	0.141	-60.2	-8.68
Smíðahlíð s	9065	4	7.09/20	26.0	0.0029	9.1	1.00	8.54	3.93	0.008	0.008	35.3	2.91		14.1	0.111	-60.5	-8.62
Stream by Kaldbakur r	9066	5	7.09/20	21.3	0.0026	6.4	0.80	4.93	2.00	0.002	0.004	19.6	2.22		8.6	0.116	-61.5	-8.86
Lake by Þvennypyna	9067	7	7.20/20	16.9	0.0025	8.3	0.86	6.68	2.83	0.195	0.008	26.4	1.97		11.9	0.109	-59.4	-8.19
Reykjadalalekur r	9068	7	7.77/20	28.2	0.010	10.5	1.20	8.02	3.65	0.090	0.008	37.7	3.38		9.8	0.141	-61.8	-8.75
Stream by Kotlaugar r	9069	7	7.03/20	27.2	0.0060	11.0	1.70	9.29	4.83	0.501	0.007	48.4	2.90		11.0	0.124	-60.1	-8.62
Haukholt r	9070	6	7.20/20	22.8	0.0019	7.5	1.00	4.19	1.72	0.054	0.005	19.9	1.59		8.9	0.111	-62.6	-8.95
Jata r	9071	5	7.36/20	22.8	0.0022	7.6	0.90	6.28	2.70	0.192	0.009	29.6	1.80		8.2	0.109	-61.4	-8.89

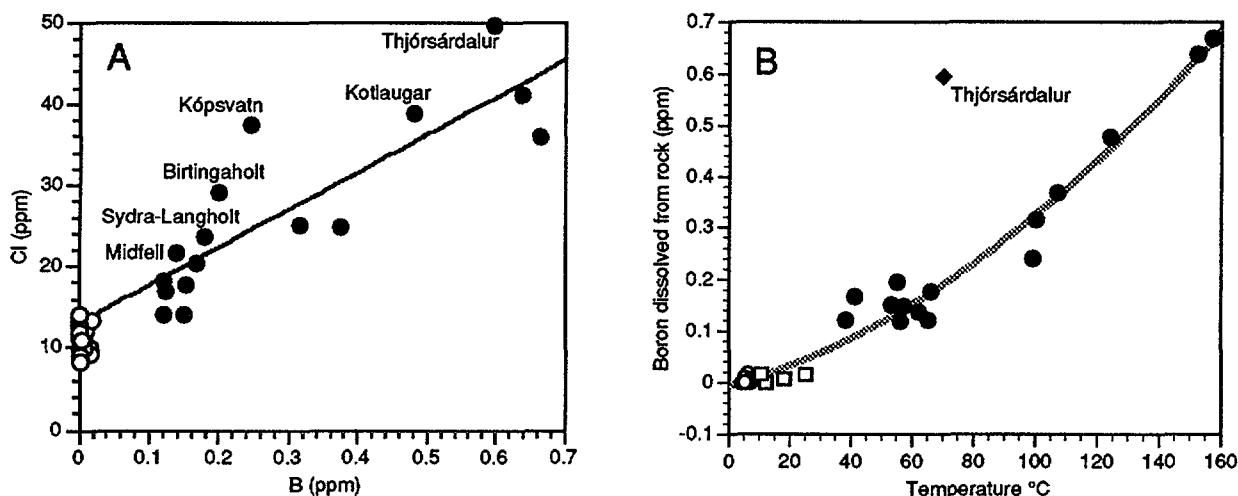
s = spring, r = stream, w = well with well number. H<sub>2</sub>S was not determined in the cold waters.



**Fig. 2.** Relationship between temperature and (A) the dissolved solids content and (B) the pH of natural waters in the Hreppar-Land area.

The pH of the surface waters lie between 6.5 and 7.6 and most of them are a little above 7 (Table 1). Warm waters have, on the other hand, significantly higher pH, up to 10, but with increasing temperature the pH falls again (Fig. 2B). The pattern of total carbonate variation with temperature is a mirror image of that of pH.

The chloride content of the cold waters lies in the range 8.2-14.1 ppm (Table 1) whereas in the geothermal waters the range is 11.4-49.4 ppm (Fig. 3A). Generally speaking chloride concentrations are positively related to temperature as are boron concentrations (Fig. 3B). In the cold waters Cl/B ratios are similar to those of seawater (4350) or somewhat lower. With increasing temperature these ratios become progressively lower and in the hottest waters they are some 50-60.

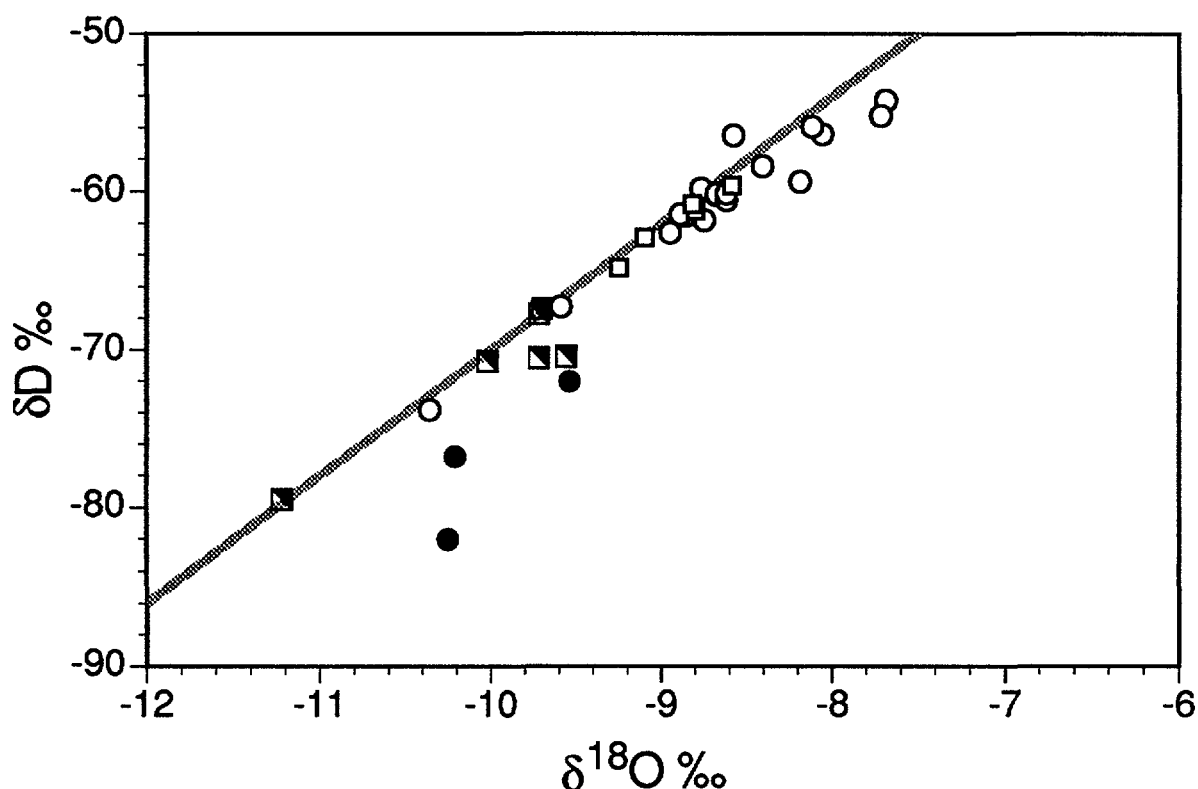


**Fig. 3.** (A) Chlorine-boron and (B) boron-temperature relationships in natural waters in the Hreppar-Land area. Circles denote cold groundwaters and surface waters and dots thermal waters. In Fig. 3B squares indicate slightly thermal waters (<30°C) and the filled diamond the geothermal water in Thjórsárdalur which is associated with silicic volcanics. Other waters are associated with basaltic rocks. The line in Fig. 3A was obtained by a linear regression through the data points. It has a slope of 50.6 (the Cl/B rock ratio) and an intercept with the Y-axis of 11.3 ppm Cl. The curve in Fig. 3B is a second order polynomial ( $B \text{ (ppm)} = 1.680 \times 10^{-5}t^2 + 1.628 \times 10^{-3}t - 6.247 \times 10^{-3}$ , where  $t$  is in °C) describing well the boron-temperature relationship. Data points for which local names are given are discussed specifically in text.

Hydrogen sulphide is not present in the cold and warm waters. It is detectable in some waters in the range 50-60 °C. Above this temperature there is a clear, approximately linear increase in H<sub>2</sub>S concentrations with temperature, some 0.4 ppm for every 10 °C

The geothermal water in Thjórsárdalur, which is located within an extinct central volcano (sample no. 7913 in Table 1), is anomalous compared to other such waters in the Hreppar-Land area, particularly in respect to low silica concentrations and high calcium, sulphate and fluoride. The hot water at Thjórsárdalur is associated with silicic volcanics. This association accounts for the elevated fluoride concentrations but not for the unusually high calcium and sulphate, whether comparison is made between geothermal waters associated with basalts in the area or with such waters issuing from silicic volcanics in other areas in Iceland. One may speculate that anhydrite is present as a hydrothermal mineral of a fossil high-temperature geothermal system within the central volcano and that its dissolution explains the anomalous calcium and sulphate concentrations. Indeed the water is just anhydrite saturated. In the discussion that follows the characteristics of the Thjórsárdalur water will not be specifically discussed but emphasis will be made of the chemical characteristics of the remaining waters which are associated with basaltic rocks.

The water sample collected from a pool in vegetated soil by Sandlækur (sample no. 9058 in Table 1) represents rainwater with very short residence time with the soil. The pool formed during heavy rainfall one night and was sampled the following morning. Indeed the pH of the water is practically the same as that of pure rain water and the silica concentration is very low. The ratio of Na to Cl is also similar to that of seawater but the ratios of other major elements (K, Ca, Mg, Al, Fe, SO<sub>4</sub> and F) to Cl, as well as B, are considerably higher



**Fig. 4.** Relationship between  $\delta D$  and  $\delta^{18}O$  in cold and thermal waters from the Hreppar-Land area. Circles denote cold waters, open squares water <40°C, half filled squares 41-80°C waters and dots waters >80°C. The line represents the meteoric line:  $\delta D = 8\delta^{18}O + 10$ .

than in seawater indicating some reaction with the soil that must have occurred within a period of few hours.

The overall compositional change associated with the evolution of geothermal waters from their parent cold waters involve an increase in the dissolved solids content caused by an increase in the concentrations of Si, Na, SO<sub>4</sub>, Cl, F, B and Al. At the same time a decrease in Ca, Mg and Fe occurs. K and CO<sub>2</sub> also tend to undergo a decrease from cold to warm waters but they show an increase in the hot waters.

The deuterium content of natural waters in the Hreppar-Land area lie in the range -55 to -94‰ (Fig. 4). All the cold and warm (<40 °C) waters, except two, possess δ<sup>2</sup>H values between -54 and -65‰. The two exceptions include the spring forming the source of the stream of Klofalækur (no. 9047) and a spring at Krókur (no. 9048) where the values are -74 and -67‰, respectively. These two springs are close to the eastern volcanic belt in South-Iceland and emerge from below very permeable post-glacial lava fields (Fig. 1). Groundwater flow through the lavas from a distant source inland is hydrologically probable, so the water in these springs is most likely not local.

Hot waters in the area have lower δ<sup>2</sup>H-values than the cold waters, or in the range -67 to -94‰. Precipitation today with δ<sup>2</sup>H values in this range falls in the area to the north of Hreppar-Land as far inland as the top of the Hofjökull ice-cap in central Iceland [4].

The hottest waters in the area show a significant oxygen shift from the meteoric line whereas the cold waters plot close to that line (Fig. 4).

#### 4. MOBILE ELEMENTS

Chloride and boron are considered to act as essentially mobile elements in the Icelandic surface- and groundwater environment [5]. This implies that they do not enter to any extent secondary minerals forming as a result of weathering and hydrothermal alteration processes. Their aqueous concentrations are controlled by their sources of supply which, in the case of the Hreppar-Land area, includes seawater spray and aerosols (the atmosphere), the rock being dissolved, and apparently a slight marine groundwater component for some of the geothermal waters [6].

It has been shown [5] that the fraction of Cl and B in natural waters in Iceland derived from the marine source (seawater spray and aerosols + marine groundwater) can be estimated from the following equations provided the Cl/B ratio of the rock with which the water interacts is known.

$$B_m = \frac{Cl_w - rB_w}{4350 - r} \quad (1)$$

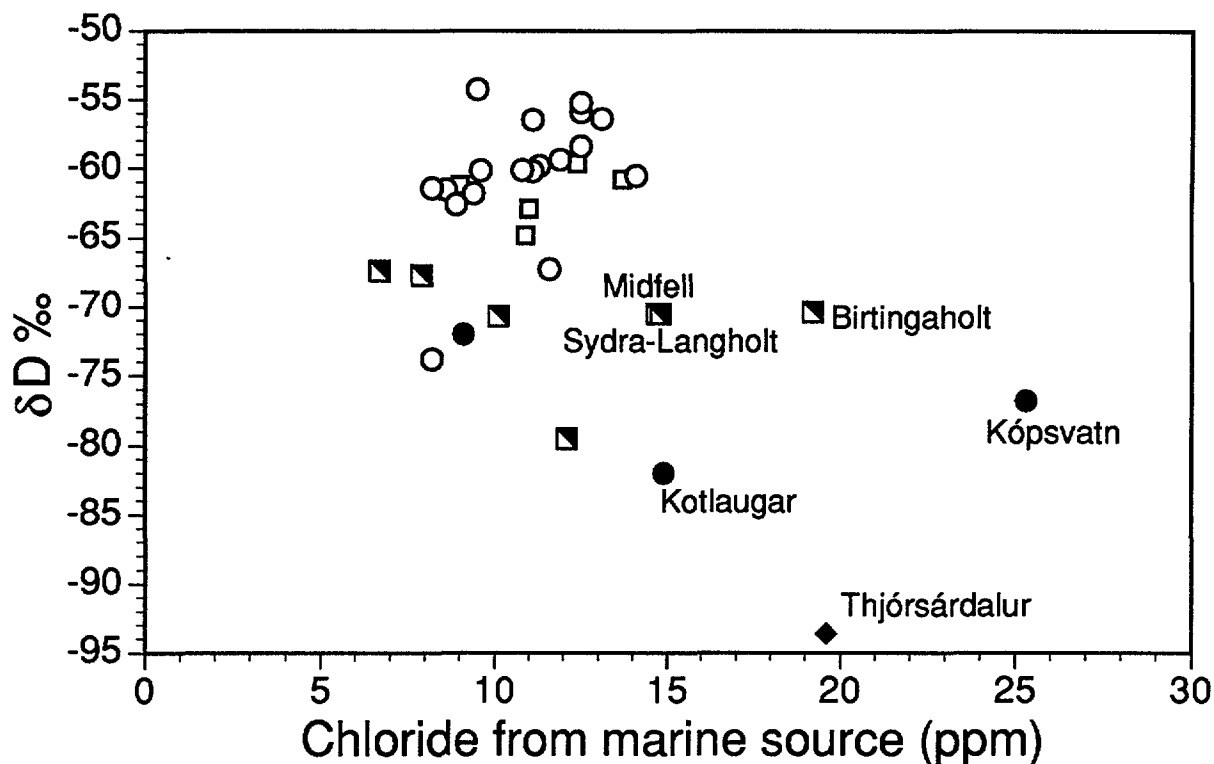
and

$$Cl_m = \frac{Cl_w - rB_w}{1 - \frac{r}{4350}} \quad (2)$$

The subscript m indicates the marine source,  $Cl_w$  and  $B_w$  represent Cl and B water sample concentrations in ppm,  $r$  is the mass ratio of Cl/B in the rock and 4350 [15] stands for the Cl/B mass ratio in seawater, i.e.  $Cl_m / B_m = 4350$ . The estimation is quite accurate, i.e. not sensitive to estimated Cl/B rock ratios, for aqueous Cl/B ratios ( $Cl_w / B_w$ ) greater than about 500.

In tholeiitic basalts in Iceland Cl/B ratios are generally in the range 80-120. They are lower in alkali-olivine basalts, as low as about 50 [5]. The distribution of data points in Fig. 3A may be used to infer about the ratio in which Cl and B are released from the rock to the water. The cluster of data points in this figure with the lowest B concentrations and about 7-15 ppm Cl (circles) correspond to the cold and slightly thermal (<300 °C) waters. Their Cl/B ratios are relatively close to that of seawater indicating that the source of supply of these elements is essentially atmospheric. Geothermal waters (dots) have higher Cl and B concentrations and lower Cl/B ratios. A line obtained by regression through the geothermal water data points has a slope of close to 50. This suggests that Cl and B are dissolved from the rock in that ratio which corresponds well with that in alkali-olivine basalts in Iceland according to [5]. Unfortunately petrochemical data on the basalts from the Hreppar-Land area are very limited so it is not known whether the basaltic rocks associated with the geothermal systems are tholeiitic or alkaline in composition.

Using a ratio of 50 for Cl/B rock dissolution in equation (2) above yields, with several exceptions, a concentration for the marine Cl component in the geothermal waters in the Hreppar-Land area in the range of 6.3-13.7 ppm (Fig. 5). The exceptions include waters from



**Fig. 5.** Relationship between  $\delta D$  and Cl derived from marine source in cold and thermal waters from the Hreppar-Land area. Symbols have the same signature as in Fig. 4. Data points for which local names are given are discussed specifically in text.



Thjórsárdalur, Kotlaugar, Kópssvatn, Birtingarholt, Sydra-Langholt and Midfell (see Fig. 1 for location). These waters, which are a little higher in marine Cl than other waters in the area, are marginal to the area. The cold waters possess marine Cl concentrations in a range 8.2-14.1 ppm (Fig. 5). The cold waters represent local precipitation and since the geothermal waters generally contain Cl from a marine source in the same range it is concluded that these waters also represent local precipitation. The more elevated marine Cl concentrations are attributed to a small component of marine groundwater in the geothermal water. At the end of the last glaciation and in early post-glacial times the southern and western margins of the Hreppar-Land area were transgressed by the sea [7]. At that time seawater is likely to have filtered into the bedrock to form marine groundwater or groundwater which is a mixture of seawater and freshwater.

## 5. $\delta^2\text{H}$ - $\delta^{18}\text{O}$ AND $\delta^2\text{H}$ - Cl RELATIONSHIPS

Both cold and thermal waters of the Hreppar-Land area fall relatively close to the meteoric line (Fig. 4). However, the hottest waters show a significant oxygen shift of as much as 2 ‰. The cold and warm waters seem, on the whole, to plot a little on the positive side of the meteoric line. This is in line with the general  $\delta^2\text{H}$  -  $\delta^{18}\text{O}$  relationship observed for surface waters in Iceland. The data plot close to a line intersecting the meteoric line at  $\delta^2\text{H}$ -values of about -64 a slope of 6.44 [8].

It is observed in many geothermal fields in Iceland that the  $\delta^2\text{H}$ -values of the geothermal waters are lower (more negative) than those of local cold waters [4]. This is also the case in the Hreppar-Land area. The difference in  $\delta^2\text{H}$ -values between local cold waters and the geothermal waters has generally been taken to indicate that the recharge areas to the geothermal systems lie on higher ground farther inland [9] but it is well known how the deuterium content of precipitation in Iceland decreases away from the coast due to altitude and inland effects [4].

Like  $\delta^2\text{H}$ , the Cl content of precipitation in Iceland decreases from coastal areas inland [6, 10]. The cause is decreasing amount of seawater spray and aerosols in the atmosphere with height and distance from the ocean, i.e. the source area of these particles.

As discussed in the previous section the concentrations of Cl from a marine source in the geothermal and local cold waters in the Hreppar-Land area lie in the same range (Fig. 5). This is taken to indicate that the source of supply of the geothermal waters is essentially local precipitation, an interpretation which hydrologically does not match with the conventional interpretation of the  $\delta^2\text{H}$  data described above. The following hydrological model for the geothermal systems in the Hreppar-Land area is consistent with both the Cl and  $\delta^2\text{H}$  data: The groundwater of the geothermal systems is derived from two and sometimes three sources of supply. The dominant source is relatively recent local precipitation, i.e. precipitation with the same  $\delta^2\text{H}$  as today's precipitation. Another source includes "old groundwater" with low  $\delta^2\text{H}$ -values that entered the bedrock during the deglaciation period, even earlier, when climatic conditions differed much from those today and when the  $\delta^2\text{H}$  of the meteoric water was much more negative, probably by as much as 50. A third component, marine groundwater is present in waters marginal to the area. At the end of the last glaciation the southern and western periphery of the Hreppar-Land area was submerged. At this time seawater is likely to have filtered into the bedrock. Since then, this marine groundwater has been gradually replaced by fresh water of meteoric origin but apparently this replacement is still not complete.

The general conceptual model for low-temperature geothermal activity in Iceland favours that geothermal systems develop by groundwater convection in recent, permeable fractures in otherwise much more impermeable bedrock [11, 12]. Water replacement is relatively rapid in the fractures but slow in the bedrock outside. The groundwater in the bedrock is postulated to be relatively light isotopically due to the presence of an "ice-age" water component and sometimes saline due to the presence of a marine groundwater component. Seepage of this water into the fractures where it mixes with local convecting water causes the geothermal water to be isotopically light relative to today's local precipitation and sometimes a little high in Cl due to supply from the marine groundwater source.

## 6. DISSOLUTION PROCESSES

Comparison between the data in Table 1 and the calculated concentrations of Cl derived from a marine source shows that a relatively small part of the aqueous Cl concentrations, except in the hottest waters, comes from the dissolving rock. This is not so for B. Only a minor part of this element in the Hreppar-Land geothermal waters, even if only slightly thermal, is derived from a marine source. The percentage,  $B_p$ , of boron dissolved from the rock may be evaluated from the following equation:

$$B_p = \frac{r}{1 + r} \times 100 \quad (3)$$

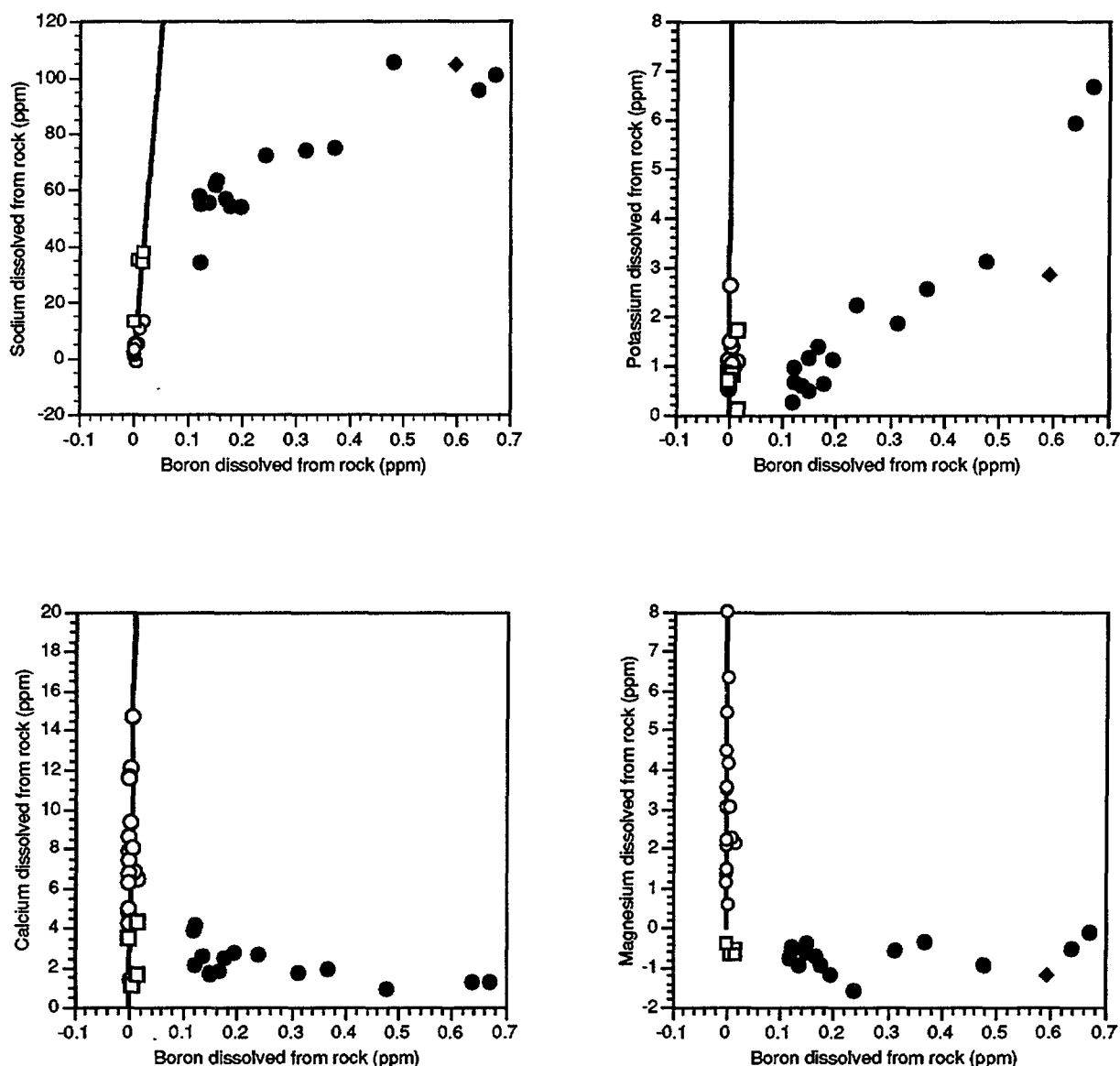
where

$$r = \frac{r_m - r_w}{r_w - r_r} \quad (4)$$

$r_m$  represents the Cl/B ratio in seawater = 4350 [15] and  $r_w$  and  $r_r$  the same ratio in a water sample and the rock, respectively. Taking  $r_r$  to be equal to 50, which appears appropriate for the Hreppar-Land waters, as discussed in section 4 above, one can see from equation (3) that for aqueous Cl/B ratios of 500 and less over about 90% of the aqueous B comes from the rock and less than about 10% from the marine source. All waters with temperatures in excess of 20° for which data are presented in Table 1 possess Cl/B ratios of less than about 500. It may, therefore, be concluded that aqueous concentrations of the mobile element boron can be quite accurately used as an indicator of the amount of rock dissolved by the Hreppar-Land waters.

The calculated net amounts (= total amount dissolved minus what has been precipitated) of the major elements (Na, K, Ca, Mg, Si, C, SO<sub>4</sub> and F) in the Hreppar-Land waters dissolved from the rock have been plotted in Figs. 6 and 7 against the calculated amount of B dissolved from the rock. The solid line in each figure corresponds to the respective element/boron ratio in the basaltic rock. The concentration of marine derived boron,  $B_m$ , was estimated for each sample with the aid of equation (1). Subtraction of this value from the analysed B concentration in each sample gives the amount of B in the samples derived from the rock. The amount of the marine contribution of other elements was obtained from the same equation but using the appropriate seawater Cl/element ratio.

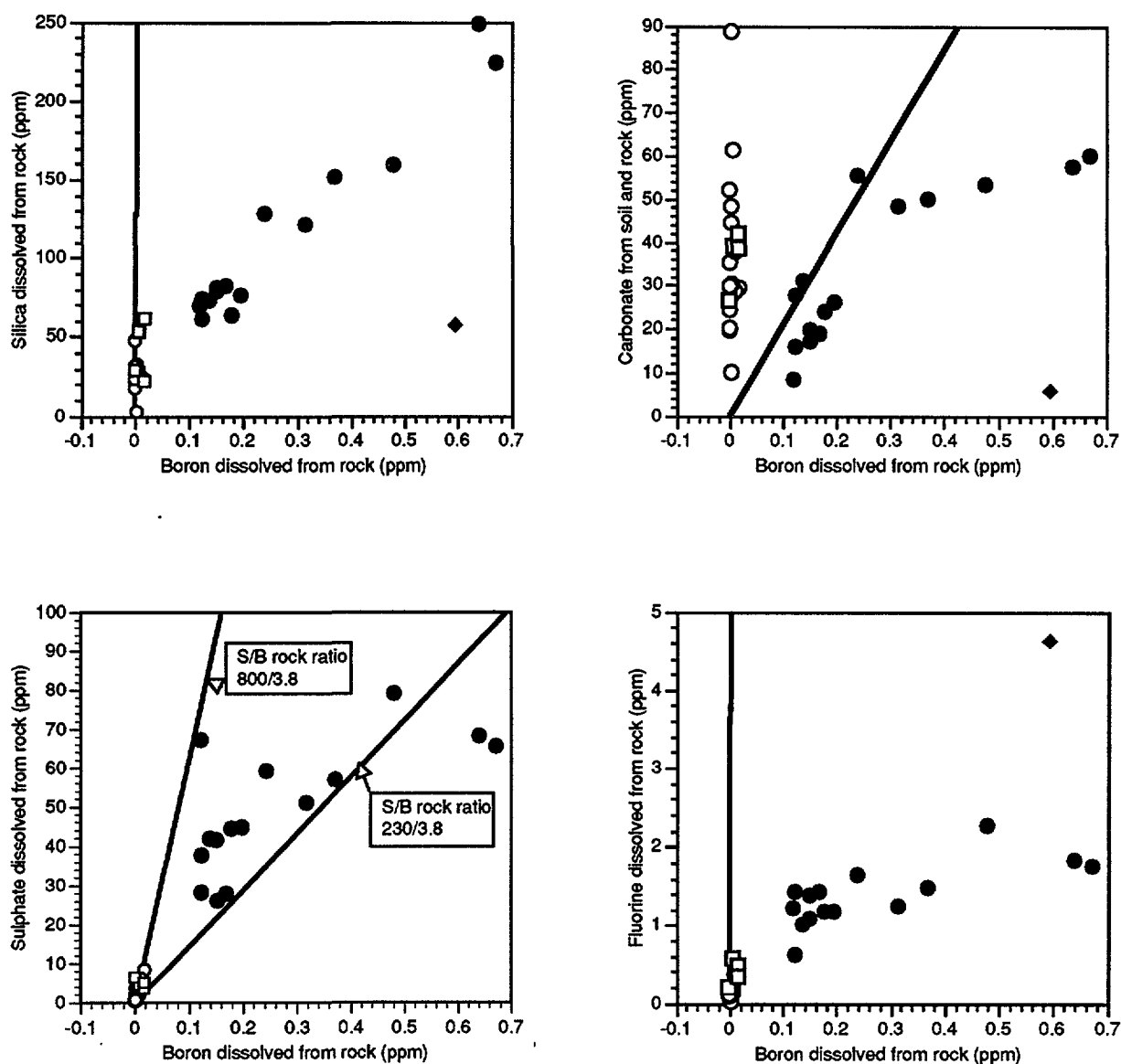
The data on cold and slightly thermal waters, displayed in Fig. 6 and 7, suggest that rock dissolution is near stoichiometric for all the major elements at these low temperatures



**Fig. 6.** Relationship between the amount of boron and the net amounts of the major cations (Na, K, Ca and Mg) in natural waters of the Hreppar-Land area dissolved from the rock and soil (=total amount dissolved minus what has been precipitated). The lines on each diagram correspond to stoichiometric dissolution of the respective elements. In order to derive these lines the following elemental concentrations were assumed in the rock: B = 3.8 ppm,  $\text{Na}_2\text{O}$  = 3.0%,  $\text{K}_2\text{O}$  = 0.8%,  $\text{CaO}$  = 10.0% and  $\text{MgO}$  = 6.5%. These numbers are representative of those in alkaline basalts in Iceland and are based on data in [13] except for B which is based on [5]. The value for Ca in the Thjórsárdalur water, which is very high (52.9 ppm) was omitted from the respective plot. Symbols have the same signature as in Fig. 3B.

except for Ca, Mg and carbonate. There is an excess carbonate in these waters relative to stoichiometric C/B dissolution from the basaltic rock. The reason is no doubt supply of carbonate from an organic source, the soil. Ca and Mg are depleted in the warm waters relative to cold waters suggesting their precipitation from solution to form weathering minerals, most likely smectites.

The geothermal waters with temperatures above about 40°C (dots in Figs. 6 and 7) are depleted in all the major aqueous components, except sulphate, relative to boron assuming



**Fig. 7.** Relationship between the amount of boron and the net amounts of aqueous silica, total carbonate, sulphate and fluoride in natural waters of the Hreppar-Land area dissolved from the rock and soil (=total amount dissolved minus what has been precipitated). The lines on each diagram correspond to stoichiometric dissolution of the respective elements. In order to derive these lines the following elemental concentrations were assumed in the rock: B = 3.8 ppm, SiO<sub>2</sub> = 48.0%, CO<sub>2</sub> = 800 ppm, S = 800 and 230 ppm, and F = 600 ppm. Data on SiO<sub>2</sub> and F are from [13], B from [5], S from [14] and C estimated from data presented in [15]. The higher number (800 ppm) for S corresponds to the sulphur content of undegassed basalts whereas the lower value is close the average S concentration in Icelandic basalts. The value for SO<sub>4</sub> in the Thjórsárdalur water, which is very high (302.3 ppm) was omitted from the respective plot. Symbols have the same signature as in Fig. 3B.

stoichiometric rock dissolution. The cause is considered to be precipitation of these components from solution to form hydrothermal minerals. For the major cations departure from the stoichiometric line is smallest for Na suggesting that this element possesses the highest mobility. It is worth observing that the values for Mg are all negative in waters above about 40°C. This implies that some of the Mg derived from the atmospheric source is incorporated into hydrothermal minerals. In other words the hydrothermal alteration of the basaltic rock is accompanied by incorporation of Mg derived from a marine source transported to the site via the atmosphere. Data for Fe and Al have not been plotted but they are comparable to those of Ca shown in Fig. 6, i.e. most of what is dissolved from the rock enters alteration minerals, even at ambient temperature.

As can be seen from Fig. 7 silica is, like Na, relatively mobile in the geothermal waters compared to the other major elements. Carbonate has minimum mobility in warm waters (40-60°C) and despite a large organic source for C from the cold water environment the aqueous carbonate/boron ratio (C/B) in waters above some 100 °C is significantly lower than that dictated by stoichiometric C/B dissolution. It is clear from Fig. 7 that a significant amount of carbon incorporated into the basaltic rock during hydrothermal alteration at low temperatures must come from an organic source.

A significant sink is not observed for SO<sub>4</sub> (Fig. 7) so this component probably acts as mobile in the Hreppar-Land waters. Indeed all the waters in the area, except for that in Thjórsárdalur (not plotted in Fig. 7), are significantly undersaturated with respect to anhydrite, the only hydrothermal mineral expected to take up SO<sub>4</sub>. The sulphur content of basalts in Iceland is quite variable due to degassing during cooling whether the basalt forms lavas or small intrusions [14]. Undegassed basaltic glass contains about 800 ppm S but the average of Icelandic basalts is about 230 ppm [14]. The steeper line for SO<sub>4</sub> in Fig. 7 corresponds to stoichiometric S/B dissolution for ungasged basalt but the line with the shallower slope to basalt of average S composition.

As deduced from the work of [16] one would expect some of the sulphur in basalt to occur as sulphide and some as sulphate. The SO<sub>4</sub> replaces SiO<sub>4</sub>-tetrahedra in the plagioclases [16]. Apparently, most of the sulphur dissolved from the basalts by the geothermal waters is on the sulphate form or that oxidation of dissolved sulphide sulphur is practically complete except for the hottest waters, which contain aqueous sulphide in appreciable concentrations (Table 1).

Although fluoride bearing minerals are not known to form as hydrothermal alteration products in basalts, it is apparent from Fig. 7 that the larger part of the F released from the basalt by the geothermal waters is removed from solution. It is considered that the fluoride enters the structures of some hydroxyl-bearing hydrothermal minerals such as smectite where F<sup>-</sup> replaces OH<sup>-</sup>. This type of exchange reaction is considered to control F<sup>-</sup> mobility.

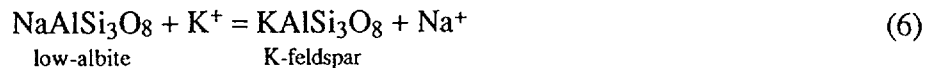
## 7. MINERAL-SOLUTION EQUILIBRIA

It is common, when constructing mineral stability diagrams, to write reactions involving Al-bearing silicates in such a way as to eliminate aqueous aluminum. Equilibrium constants represented by mineral stability lines on such diagrams are usually expressed in terms of specific cation activity ratios, but sometimes also involving the activity of aqueous silica as a variable.

Reactions involving minerals and aqueous species may also be written in such a way that the equilibrium constant is simply represented by a neutral aqueous species or a cation ratio. Two simple examples are provided by equilibria involving (a) aqueous silica and quartz and (b) sodium and potassium ions and low-albite and K-feldspar:



and



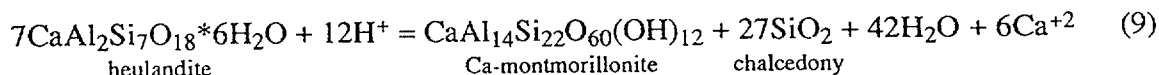
where

$$K_{\text{quartz}} = \frac{a_{\text{H}_4\text{SiO}_4^0}}{a_{\text{quartz}} a_{\text{H}_2\text{O}}^2} = a_{\text{H}_4\text{SiO}_4^0} \quad (7)$$

in the case of pure quartz and pure  $\text{H}_2\text{O}$ , but the activity of pure phases is unity. For pure feldspars the equilibrium constant is

$$K_{\text{feld}} = \frac{a_{\text{Na}^+} a_{\text{K-feld}}}{a_{\text{K}^+} a_{\text{low-alb}}} = \frac{a_{\text{Na}^+}}{a_{\text{K}^+}} \quad (8)$$

If two hydroxyl-bearing minerals are involved in a solution equilibrium, the equilibrium constant can be expressed in terms of a cation-proton activity ratio such as



where the equilibrium constant, K is

$$K = \frac{a_{\text{Ca}^{+2}}^6}{a_{\text{H}^+}^{12}} \quad (10)$$

in the case of equilibrium between aqueous solution and the mineral buffer: heulandite + Ca-montmorillonite + chalcedony.

Table 2 shows dissolution reactions for hydrothermal minerals frequently found in basaltic rocks of active low-temperature geothermal systems in Iceland, but the Hreppar-Land

TABLE 2. DISSOLUTION REACTIONS FOR SOME COMMON HYDROTHERMAL MINERALS.

Mineral	Equilibrium constant	Dissolution reaction
Chalcedony	$K_{\text{cha}}$	$\text{SiO}_2 + 2\text{H}_2\text{O} = \text{H}_4\text{SiO}_4^0$
Low-albite	$K_{\text{alb}}$	$\text{NaAlSi}_3\text{O}_8 + 8\text{H}_2\text{O} = \text{Na}^+ + \text{Al}(\text{OH})_4^- + 3\text{H}_4\text{SiO}_4^0$
Adularia	$K_{\text{adu}}$	$\text{KAlSi}_3\text{O}_8 + 8\text{H}_2\text{O} = \text{K}^+ + \text{Al}(\text{OH})_4^- + 3\text{H}_4\text{SiO}_4^0$
Calcite	$K_{\text{cal}}$	$\text{CaCO}_3 + 2\text{H}^+ = \text{Ca}^{+2} + \text{H}_2\text{CO}_3^0$
Pyrrhotite	$K_{\text{pyh}}$	$\text{FeS} + 2\text{H}^+ = \text{Fe}^{+2} + \text{H}_2\text{S}^0$
Mg-montmor.	$K_{\text{Mg-mont}}$	$\text{MgAl}_4\text{Si}_{22}\text{O}_{60}(\text{OH})_{12} + 60\text{H}_2\text{O} + 12\text{OH}^- = \text{Mg}^{+2} + 14\text{Al}(\text{OH})_4^- + 22\text{H}_4\text{SiO}_4^0$
Ca-montmor.	$K_{\text{Ca-mont}}$	$\text{CaAl}_4\text{Si}_{22}\text{O}_{60}(\text{OH})_{12} + 60\text{H}_2\text{O} + 12\text{OH}^- = \text{Ca}^{+2} + 14\text{Al}(\text{OH})_4^- + 22\text{H}_4\text{SiO}_4^0$
"FeO" <sup>a</sup>	$K_{\text{FeO}}$	$\text{"FeO"} + 2\text{H}^+ = \text{Fe}^{+2} + \text{H}_2\text{O}$
Heulandite	$K_{\text{heu}}$	$\text{CaAl}_2\text{Si}_7\text{O}_{18} + 6\text{H}_2\text{O} + 12\text{H}^+ = \text{Ca}^{+2} + 2\text{Al}(\text{OH})_4^- + 7\text{H}_4\text{SiO}_4^0$

<sup>a</sup>It is not known which mineral may control aqueous ferrous iron ion activity. "FeO" represents the ferrous iron oxide component in an unknown oxide or silicate mineral.

TABLE 3. MINERAL BUFFERS LIKELY TO CONTROL AQUOEUS IONIC RATIOS AND WEAK ACID ACTIVITIES IN GEOTHERMAL WATERS IN THE HREPPAR-LAND AREA.

Mineral buffer	
1 $\text{cha} + 2\text{H}_2\text{O} = \text{H}_4\text{SiO}_4^0$	$K_{\text{cha}} = \frac{a_{\text{H}_4\text{SiO}_4^0}}{a_{\text{cha}} a_{\text{H}_2\text{O}}^2} = a_{\text{H}_4\text{SiO}_4^0} \times k_k$
2 $7\text{heu} + 12\text{H}^+ = \text{Ca-mont} + 27\text{cha} + 42\text{H}_2\text{O} + 6\text{Ca}^{+2}$	$K_A = \frac{a_{\text{Ca}^{+2}}^{0.5}}{a_{\text{H}^+}} \times \left( \frac{a_{\text{Ca-mont}} a_{\text{cha}}^{27} a_{\text{H}_2\text{O}}^{42}}{a_{\text{heu}}^7} \right)^{1/12} = \frac{a_{\text{Ca}^{+2}}^{0.5}}{a_{\text{H}^+}} \times k_l = \left( \frac{K_{\text{heu}}^7}{K_{\text{Ca-mont}} K_{\text{H}_2\text{O}}^{12} K_{\text{cha}}^{27}} \right)^{1/12}$
3 $\text{cal} + 2\text{H}^+ = \text{Ca}^{+2} + \text{H}_2\text{CO}_3^0$	$K_{\text{cal}} = \frac{a_{\text{Ca}^{+2}}}{a_{\text{H}^+}^2} \times a_{\text{H}_2\text{CO}_3^0} = \frac{K_A^2}{k_l^2} \times a_{\text{H}_2\text{CO}_3^0}$
4 $\text{heu} + 12 \text{alb} + 12\text{H}^+ = \text{Ca-mont} + 21\text{cha} + 6\text{H}_2\text{O} + 12\text{Na}^+$	$K_B = \frac{a_{\text{Na}^+}}{a_{\text{H}^+}} \times \left( \frac{a_{\text{Ca-mont}} a_{\text{cha}}^{7/4} a_{\text{H}_2\text{O}}^6}{a_{\text{alb}}^{12} a_{\text{heu}}} \right)^{1/12} = \frac{a_{\text{Na}^+}}{a_{\text{H}^+}} \times k_m = \left( \frac{K_{\text{alb}}^{12} K_{\text{heu}}}{K_{\text{H}_2\text{O}}^{12} K_{\text{cha}}^{21} K_{\text{Ca-mont}}} \right)^{1/12}$
5 $\text{heu} + 12 \text{micr} + 12\text{H}^+ = \text{Ca-mont} + 21\text{cha} + 6\text{H}_2\text{O} + 12\text{K}^+$	$K_C = \frac{a_{\text{K}^+}}{a_{\text{H}^+}} \times \left( \frac{a_{\text{Ca-mont}} a_{\text{cha}}^{7/4} a_{\text{H}_2\text{O}}^6}{a_{\text{micr}}^{12} a_{\text{heu}}} \right)^{1/12} = \frac{a_{\text{K}^+}}{a_{\text{H}^+}} \times k_n = \left( \frac{K_{\text{micr}}^{12} K_{\text{heu}}}{K_{\text{H}_2\text{O}}^{12} K_{\text{cha}}^{21} K_{\text{Ca-mont}}} \right)^{1/12}$
6 $6\text{Mg-mont} + 7\text{heu} + 12\text{H}^+ = 7\text{Ca-mont} + 27\text{cha} + 42\text{H}_2\text{O} + 6\text{Mg}^{+2}$	$K_D = \frac{a_{\text{Mg}^{+2}}^{0.5}}{a_{\text{H}^+}} \times \left( \frac{a_{\text{Ca-mont}}^{27} a_{\text{cha}}^{42} a_{\text{H}_2\text{O}}^{42}}{a_{\text{Mg-mont}}^6 a_{\text{heu}}^7} \right)^{1/12} = \frac{a_{\text{Mg}^{+2}}^{0.5}}{a_{\text{H}^+}} \times k_o = \left( \frac{K_{\text{Mg-mont}}^6 K_{\text{heu}}^7}{K_{\text{Ca-mont}}^7 K_{\text{cha}}^{27} K_{\text{H}_2\text{O}}^{12}} \right)^{1/12}$
7 $\text{Ca-mont} + 18\text{H}_2\text{O} + 12\text{OH}^- = \text{heu} + 15\text{cha} + 12\text{Al}(\text{OH})_4^-$	$K_E = \frac{a_{\text{Al}(\text{OH})_4^-}}{a_{\text{OH}^-}} \times \left( \frac{a_{\text{heu}} a_{\text{cha}}^{15}}{a_{\text{Ca-mont}} a_{\text{H}_2\text{O}}^{18}} \right)^{1/12} = \frac{a_{\text{Al}(\text{OH})_4^-}}{a_{\text{OH}^-}} \times k_p = \left( \frac{K_{\text{Ca-mont}}}{K_{\text{heu}} K_{\text{cha}}^{15}} \right)^{1/12}$
8 $"\text{FeO}" + 2\text{H}^+ = \text{Fe}^{+2} + \text{H}_2\text{O}$	$K_{\text{FeO}} = \frac{a_{\text{Fe}^{+2}}^{0.5}}{a_{\text{H}^+}} \times \left( \frac{a_{\text{H}_2\text{O}}}{a_{\text{FeO}}} \right) = \frac{a_{\text{Fe}^{+2}}^{0.5}}{a_{\text{H}^+}} \times k_q$
9 $\text{pyh} + 2\text{H}^+ = \text{Fe}^{+2} + \text{H}_2\text{S}^0$	$K_{\text{pyh}} = \frac{a_{\text{Fe}^{+2}}}{a_{\text{H}^+}^2} \times a_{\text{H}_2\text{S}^0} = \frac{K_{\text{FeO}}^2}{k_q^2} \times a_{\text{H}_2\text{S}^0}$

alb = low-albite, cal = calcite, Ca-mont = Ca-monmorillonite, cha = chalcedony, heu = heulandite, micr = microcline, Mg-mont = Mg-monmorillonite, pyh = pyrrhotite. "FeO" represents ferrous iron component in an unknown oxide or silicate. The equilibrium constants for each mineral buffer are symbolised by  $K_A$  to  $K_E$  or, when appropriate, by a dissolution equilibrium constant defined in Table 2. The terms on the far right show how the mineral dissolution constants relate to the mineral buffer equilibrium constants.  $K_{\text{H}_2\text{O}}$  represents the dissociation constant for water.  $k_k$  to  $k_q$  are constants for any specific mineral and water compositions.

area belongs to this type of geothermal system. In Table 3 individual mineral dissolution reactions have been combined in such a way that equilibrium constants for mineral buffers and aqueous solution are always equal to a specific cation/proton activity ratio or a neutral aqueous species concentration for specific mineral activities, i.e. mineral compositions. To demonstrate this further consider the reaction in Table 3 involving calcite. We have



The equilibrium constant,  $K_{\text{cal}}$  for the reaction above is given by

$$K_{\text{cal}} = \frac{a_{\text{Ca}^{+2}}}{a_{\text{H}^+}^2} \times a_{\text{H}_2\text{CO}_3^0} \quad (12)$$

It can be seen from the second reaction in Table 3 involving heulandite, Ca-montmorillonite and chalcedony that

$$\frac{a_{\text{Ca}^{+2}}}{a_{\text{H}^+}^2} = \frac{K_A^2}{k_1} \quad (13)$$

where  $K_A$  is an equilibrium constant for reaction 2 in Table 3 equal to

$$K_A = \left( \frac{K_{\text{heu}}^7}{K_{\text{Ca-mont}} K_{\text{H}_2\text{O}}^{12} K_{\text{cha}}^{27}} \right)^{1/12} \quad (14)$$

and

$$k_1 = \left( \frac{a_{\text{Ca-mont}} a_{\text{cha}}^{27} a_{\text{H}_2\text{O}}^{42}}{a_{\text{heu}}^7} \right)^{1/12} \quad (15)$$

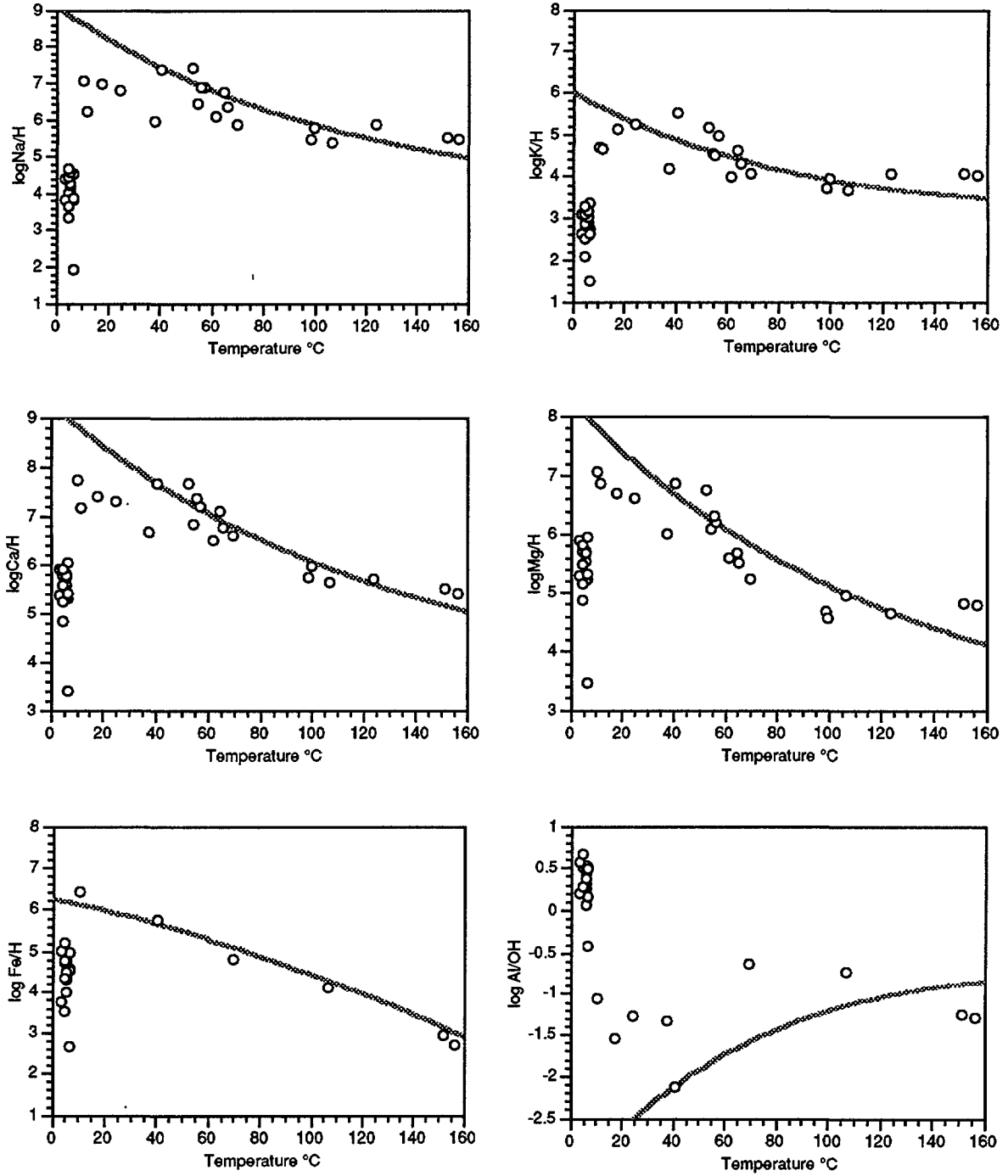
For specific mineral compositions  $k_1$  is equal to a constant. The values of the mineral dissolution equilibrium constants  $K_{\text{heu}}$ ,  $K_{\text{Ca-mont}}$  and  $K_{\text{cha}}$  are defined in Table 2.  $K_{\text{H}_2\text{O}}$  represents the dissociation constant of water.

It has been demonstrated [17] that cation/proton activity ratios and undissociated acid concentrations in Icelandic geothermal waters are uniquely defined by temperatures to temperatures as low as 60 °C. This is considered to reflect conditions of mineral-solution equilibrium for all the cations and acids involved [17].

Figs. 8 and 9 show the major cation/proton activity ratios and acid concentrations for natural waters in the Hreppar-Land area. The respective activity ratios and concentrations were calculated from the data in Table 1 with the aid of the aqueous speciation program described by [18]. The curves on the diagrams in Figs. 8 and 9 correspond to equilibrium conditions according to [17].

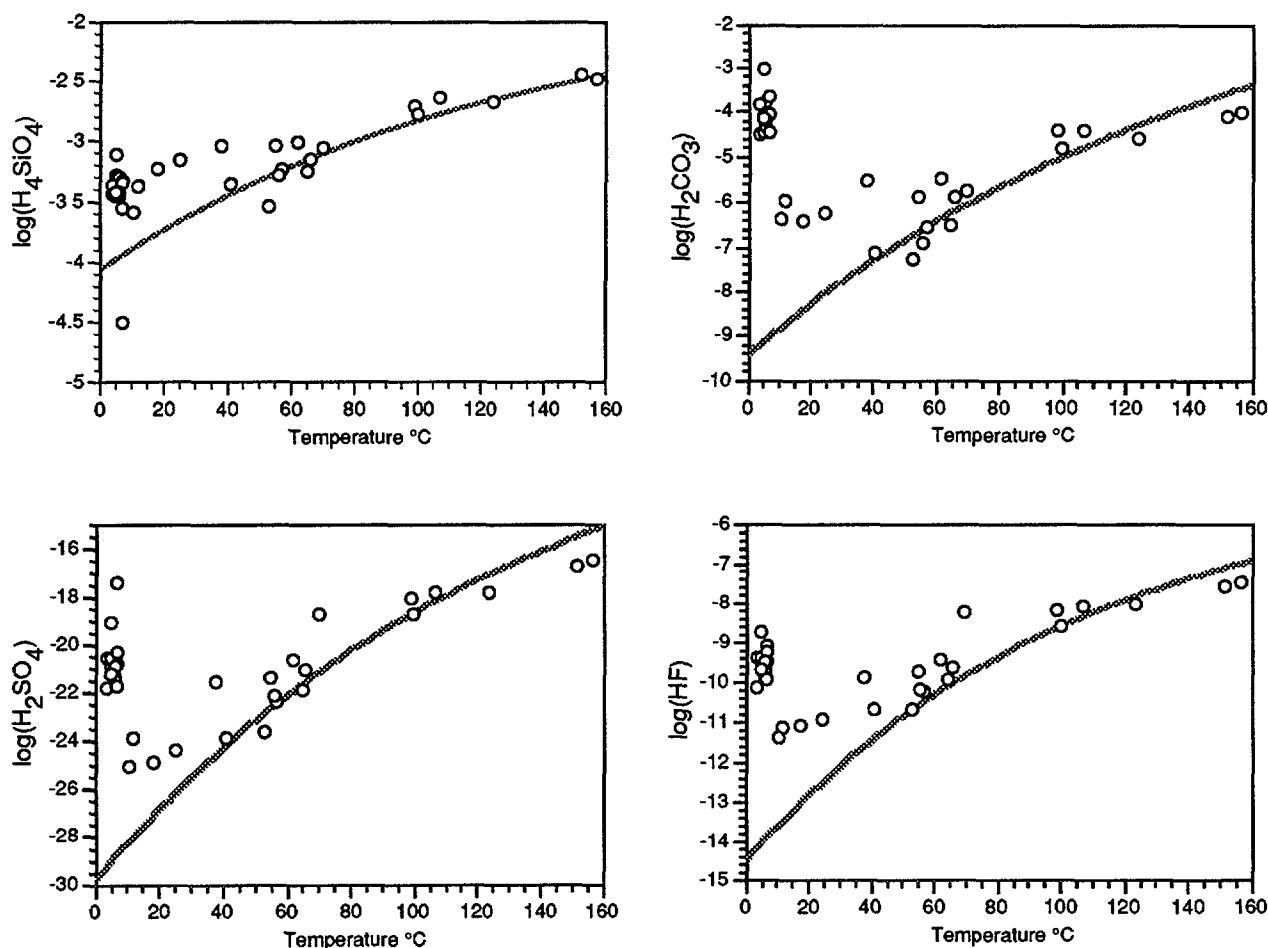
It is seen from Fig. 8 that cation/proton activity ratios in the cold waters are considerably lower than the equilibrium values which can be attributed to both low pH and low cation concentrations of these waters. At temperatures in the range of about 40 °C and higher the data points for the Hreppar-Land area plot, on the other hand, close to the equilibrium line suggesting that mineral-solution equilibrium is relatively closely approached for all the major cation forming elements to temperatures as low as 40 °C.





**Fig. 8.** Cation-proton activity ratios of natural waters from the Hreppar-Land area.

$\text{Na}/\text{H} = a_{\text{Na}^+}/a_{\text{H}^+}$ ,  $\text{K}/\text{H} = a_{\text{K}^+}/a_{\text{H}^+}$ ,  $\text{Ca}/\text{H} = a_{\text{Ca}^{+2}}^{0.5}/a_{\text{H}^+}$ ,  $\text{Mg}/\text{H} = a_{\text{Mg}^{+2}}^{0.5}/a_{\text{H}^+}$ ,  $\text{Fe}/\text{H} = a_{\text{Fe}^{+2}}^{0.5}/a_{\text{H}^+}$  and  $\text{Al}/\text{OH} = a_{\text{Al}(\text{OH})_4^-}/a_{\text{OH}^-}$ . Observe that  $\text{Al}/\text{OH} = \text{Al}/\text{H} \cdot K_{\text{H}_2\text{O}}^3 / K_{\text{Al}(\text{OH})_4^-}$  where  $\text{Al}/\text{H} = a_{\text{Al}^{+3}}/a_{\text{H}^+}$  and  $K_{\text{H}_2\text{O}}$  and  $K_{\text{Al}(\text{OH})_4^-}$  represent the equilibrium constants for the following reactions, respectively:  $\text{H}_2\text{O} = \text{H}^+ + \text{OH}^-$  and  $\text{Al}(\text{OH})_4^- = \text{Al}^{+3} + 4\text{OH}^-$ .



**Fig. 9.** Concentrations of acids in natural waters from the Hreppar-Land area the conjugate anions of which form major aqueous species ( $\text{H}_3\text{SiO}_4^-$ ,  $\text{HCO}_3^-$ ,  $\text{SO}_4^{2-}$  and  $\text{F}^-$ )

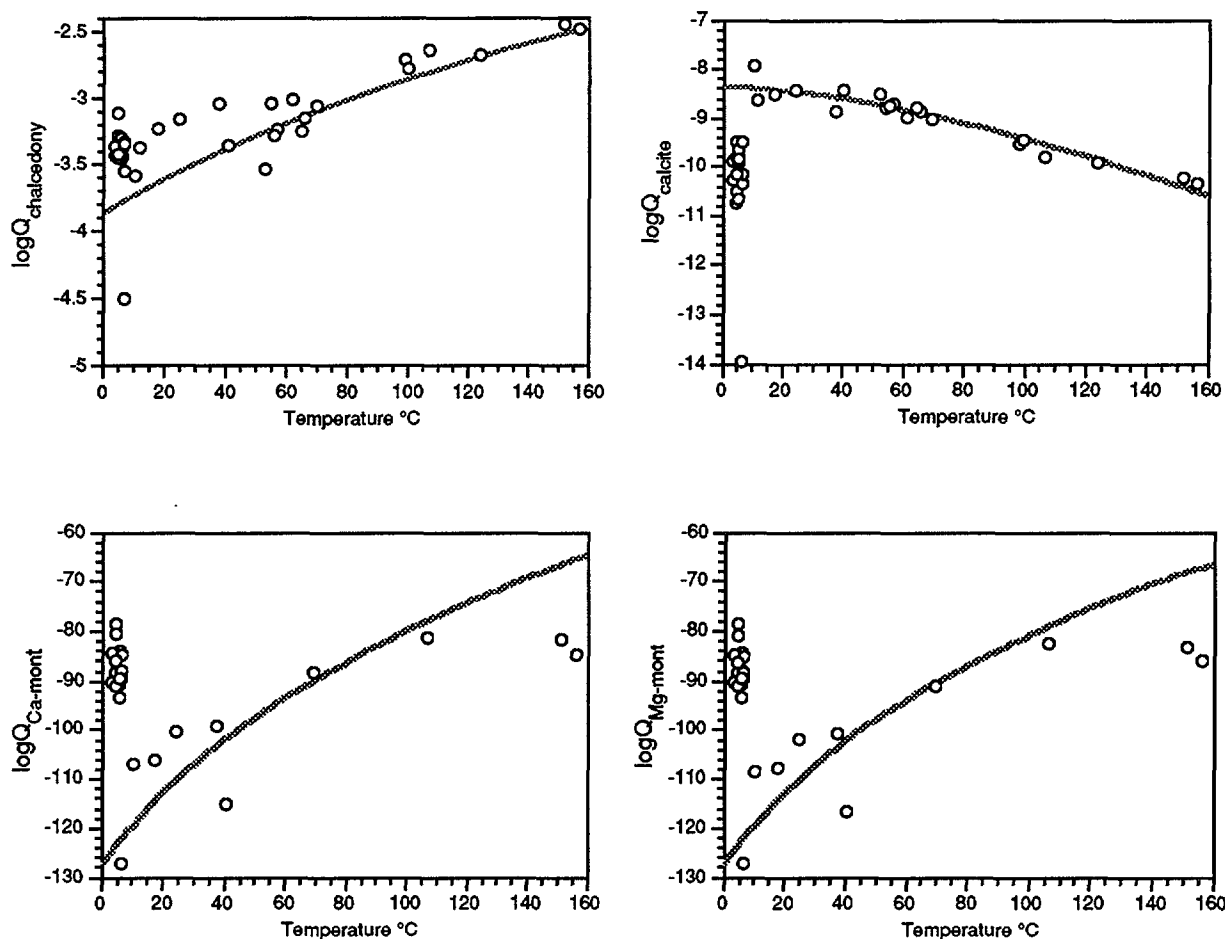
The acid concentrations in the cold waters are higher than the equilibrium values, which can again be attributed to the relatively low pH of these waters in relation to the geothermal waters. As is the case with the cations, equilibrium appears to be closely approached at temperatures of about 40°C and higher.

The fact that all major aqueous components approach equilibrium at about the same temperature suggests that one variable dominates the change of the water-rock system towards chemical equilibrium. This variable is considered to be pH. Hydrothermal alteration and weathering processes involve essentially hydrogen ion metasomatism, the rock takes up protons from the water and, at the same time, releases other cations. This proton uptake causes water pH to increase and changes the solution simultaneously towards saturation with secondary minerals.

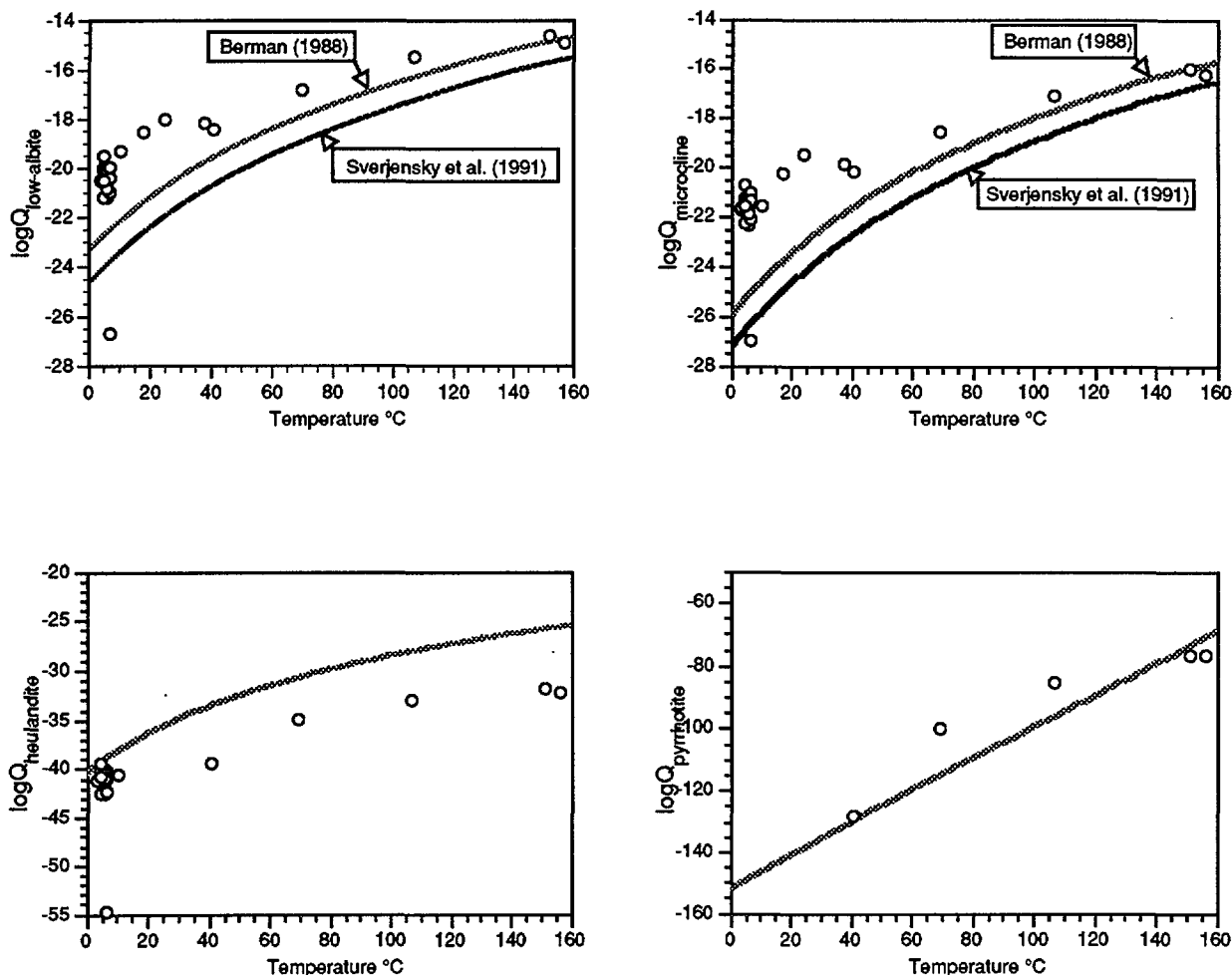
The curves in Figs. 8 and 9 do not provide information on which minerals are involved in equilibrium with the solution because they are based on geochemical data from selected drillholes in Iceland. Using the aqueous speciation program of [18] the state of saturation of the minerals listed in Table 2 was calculated (Figs. 10 and 11).

Cold waters are supersaturated with respect to chalcedony but the degree of supersaturation decreases with rising temperature and at some 50 °C and higher temperatures the waters are close to saturation (Fig. 10). The situation is similar for Ca- and Mg-montmorillonite (Fig. 10) and for low-albite and microcline (Fig. 11). On the other hand cold waters are calcite undersaturated but waters above about 10 °C are all quite close to saturation (Fig. 10). Waters with detectable H<sub>2</sub>S are all close to equilibrium with pyrrhotite (Fig. 11). Cold and hot waters are somewhat undersaturated with respect to heulandite (Fig. 11) but probably not significantly in view of the uncertainty in the chemical thermodynamic data on heulandite solubility.

The aqueous speciation program used for the present study [18] does not calculate aqueous Fe<sup>+2</sup>/Fe<sup>+3</sup> ratios in waters with no detectable H<sub>2</sub>S. When H<sub>2</sub>S is zero analysed total iron is taken by the program to be on the ferrous form. This limitation of the program does not permit the study of the state of the saturation of most of the Hreppar-Land waters with respect to ferric minerals since most of the waters do not contain detectable H<sub>2</sub>S. It is, however, evident from the ferrous ion proton ratio in Fig. 8 that some mineral buffer controls aqueous iron activities.



**Fig. 10.** The state of saturation of natural waters in the Hreppar-Land area with respect to chalcedony, calcite and Ca- and Mg-montmorillonite. The data on chalcedony solubility are from [19], but solubility data on calcite and the montmorillonites were taken from [18] and [20], respectively.



**Fig. 11.** The state of saturation of natural waters in the Hreppar-Land area with respect to low-albite, microcline, heulandite and pyrrhotite. The thermodynamic data on the feldspars used to draw the respective equilibrium curves are from [21] and [22] as indicated. The solubility data on pyrrhotite were taken from [18] but those on heulandite were calculated for the present study from calorimetric enthalpy data at 25°C from [23] and heat capacity and volume data from [24]. Data on aqueous species required to compute the solubility constant for the feldspars and heulandite were taken from [25] and [26].

The data on the state of mineral saturation shown in Figs. 10 and 11 are consistent with the results depicted in Figs. 8 and 9 that waters with temperatures greater than about 40°C are close to mineral-solution equilibrium.

It is of interest to note that the cold waters are supersaturated with respect to some of the minerals with which the geothermal waters are just saturated. This suggests that the kinetics of precipitation of these hydrothermal minerals is important in the approach to equilibrium, not just their stability. Apparently, precipitation kinetics is too slow at the lowest temperatures to compensate with the dissolution of the primary rock minerals and steady state conditions are attained at some supersaturation when mass transfer by dissolution on one hand and precipitation on the other are in balance.

## 8. CONCLUSIONS

The Cl and B in surface- and cold groundwaters of the Hreppar-Land area are essentially derived from a marine source, atmospheric seawater spray and aerosols. The calculated concentrations of Cl derived from the marine source in the geothermal waters are generally similar to those of the cold waters indicating that the geothermal waters represent local precipitation. A few geothermal waters marginal to the field possess slightly elevated Cl concentrations from the marine source relative to the local precipitation. This is considered to be due to the presence of a small marine groundwater component in these waters. This marine groundwater is considered to have entered the bedrock during the deglaciation period when the larger part of the Southern Lowlands in Iceland was transgressed by the sea.

The deuterium content of geothermal waters in the Hreppar-Land area is lower than that of the local streams, which represent local precipitation, the difference increasing with increasing temperature. The reason for this is not considered to be that the geothermal systems have a distant recharge area on higher ground farther inland, as has generally been accepted, where the  $\delta^2\text{H}$  of today's precipitation is lower than that in the Hreppar-Land area. The cause of the lower  $\delta^2\text{H}$  is considered to be due to the presence of an "ice-age water" component in the geothermal water, water that entered the bedrock during the deglaciation period, along with some seawater that was isotopically much lighter than today's precipitation. This interpretation of the  $\delta^2\text{H}$  data implies that deuterium is not always usable as a tracer to locate the recharge areas to geothermal systems.

The  $\delta^2\text{H}$ - $\delta^{18}\text{O}$  relationship of the natural waters in the Hreppar-Land area reveals a significant oxygen shift from the meteoric line for the hottest waters, up to 2‰.

The relationship between aqueous B concentrations and that of other major elements in the cold waters of the Hreppar-Land area suggests that stoichiometric dissolution governs the chemical composition of these waters together with a supply of organic  $\text{CO}_2$  from the soil as well as the initial composition of the parent precipitation. The same applies to all major elements in the warm ( $< 30^\circ\text{C}$ ) waters except for Ca, Mg and Fe. These elements are depleted in these waters relative to the mobile B suggesting that they are removed from solution through the precipitation of some secondary minerals. In geothermal waters of higher temperature all major elements, except  $\text{SO}_4$  and, of course, Cl, are depleted relative to boron due to their uptake into secondary minerals.

At temperatures in excess of about  $40^\circ\text{C}$  the geothermal waters appear to have closely approached mineral-solution equilibrium for all the major aqueous components (Si, Na, K, Ca, Mg, Fe, Al, C, sulphide-S and F) except Cl and sulphate-S.

## References

- [1] D'AMORE, F. (Co-ordinator), Application of Geochemistry in Geothermal Reservoir Development, UNITAR-UNDP publ., Rome (1991) 408 pp.
- [2] FRIDLEIFSSON, I. B., The Stóra-Laxá igneous complex, S. Iceland. Unpubl. B.Sc. thesis, Univ. St. Andrews, Scotland (1970) 70 pp.
- [3] SAEMUNDSSON, K., Interglacial lava flows in the lowlands of southern Iceland and the problem of two-tiered columnar jointing, *Jökull* **20** (1970) 62-77.

- [4] ÁRNASON, B., Groundwater systems in Iceland traced by deuterium, *Societas Scientiarum Islandica* **42** (1976) 236 pp.
- [5] ARNÓRSSON, S. et al., Processes controlling the distribution of B and Cl in natural waters in Iceland, in preparation.
- [6] ARNÓRSSON, S. et al., The distribution of Cl B,  $\delta^2\text{H}$  and  $\delta^{18}\text{O}$  in natural waters in the Southern Lowlands of Iceland, *Geofluids '93 Contributions to an International Conference on fluid evolution, migration and interaction in rocks*, British Gas (1993) 313-318.
- [7] EINARSSON, TH., *Myndun og mótun lands*, Mál og menning, Reykjavík (1991), 299 pp. (In Icelandic).
- [8] ARNÓRSSON, S. et al., these Proceedings.
- [9] ÁRNASON, B., Hydrothermal systems in Iceland traced by deuterium, *Geothermics* **5** (1977) 125-151.
- [10] SIGURDSSON F., EINARSSON, K., Groundwater resources of Iceland - availability and demand, *Jökull* **38** (1988) 35-53.
- [11] BJÖRNSSON, A., et al., The nature of hot spring systems in Iceland, *Náttúrufræðingurinn* **60** (1990) 15-38. (In Icelandic with an English summary).
- [12] ARNÓRSSON, S., GÍSLASON, S.R., On the origin of low-temperature geothermal activity in Iceland, *Náttúrufræðingurinn* **60** (1990) 39-56. (In Icelandic with an English summary).
- [13] ÓSKARSSON, N., et al., A dynamic model of rift zone petrogenesis and the regional petrology of Iceland, *J. Petrol.* **23** (1982) 28-74.
- [14] GUNNLAUGSSON, E., The origin and distribution of sulphur in fresh and hydrothermally altered rocks in Iceland, Unpubl. Ph.D. thesis, Univ. Leeds (1977) 192 pp.
- [15] WEDEPOHL H.K. (Ed.), *Handbook of Geochemistry*, Springer-Verlag (1969).
- [16] RICKE, W., Ein Beitrag zur Geochemie des Schwefels, *Geochim. Cosmochim. Acta* **21** (1961) 35-80.
- [17] ARNÓRSSON, S. et al., The chemistry of geothermal waters in Iceland. II. Mineral equilibria and independent variables controlling water compositions, *Geochim. Cosmochim. Acta* **47** (1983) 547-566.
- [18] ARNÓRSSON, S. et al., The chemistry of geothermal waters in Iceland .I. Calculation of aqueous speciation from 0° to 370°C, *Geochim. Cosmochim. Acta* **46** (1982) 1513-1532.
- [19] FOURNIER, R.O., Chemical geothermometers and mixing models for geothermal systems, *Geothermics* **5** (1977) 41-50.

- [20] HELGESON, H. C. Thermodynamics of hydrothermal systems at elevated temperatures and pressures, *Am. Jour. Sci.* **267** (1969) 729-804.
- [21] BERMAN, R.G., Internally consistent thermodynamic data for minerals in the system:  $\text{Na}_2\text{O}-\text{K}_2\text{O}-\text{CaO}-\text{MgO}-\text{FeO}-\text{Fe}_2\text{O}_3-\text{Al}_2\text{O}_3-\text{SiO}_2-\text{TiO}_2-\text{H}_2\text{O}-\text{CO}_2$ , *J. Petrol.* **29** (1988) 445-522.
- [22] SVERJENSKY, D. A., et al., Thermodynamic assessment of hydrothermal alkali-feldspar-mica-aluminosilicate equilibria, *Geochim. Cosmochim. Acta* **55** (1991) 989-1004.
- [23] JOHNSON, G.K., et al. Thermodynamic studies of zeolites: heulandite, *Am. Min.* **70** (1985) 1065-1071.
- [24] HELGESON, H.C., et al., Summary and critique of the thermodynamic properties of the rock-forming minerals, *Am. Jour. Sci.* **278A** (1978) 1-229.
- [25] SHOCK, E.L., HELGESON, H.C., Calculation of the thermodynamic transport properties of aqueous species at high temperatures and pressures: Correlation algorithms for ionic species and equation of state predictions to 5 kb and 1000°C, *Geochim. Cosmochim. Acta* **52** (1988) 2009-2036.
- [26] SHOCK, E.L., et al., Calculation of the thermodynamic and transport properties of aqueous species at high pressures and temperatures: Standard partial molal properties of inorganic neutral species, *Geochim. Cosmochim. Acta* **53** (1989) 2157-2183.

# PROCESSES INFLUENCING $\delta^2\text{H}$ , $\delta^{18}\text{O}$ , B AND Cl DISTRIBUTION IN COLD AND THERMAL WATERS IN THE NW-PENINSULA AND IN THE SOUTHERN LOWLANDS, ICELAND

S. ARNÓRSSON, Á.E. SVEINBJÖRNSDÓTTIR, A. ANDRÉSDÓTTIR  
Science Institute, University of Iceland,  
Reykjavík, Iceland

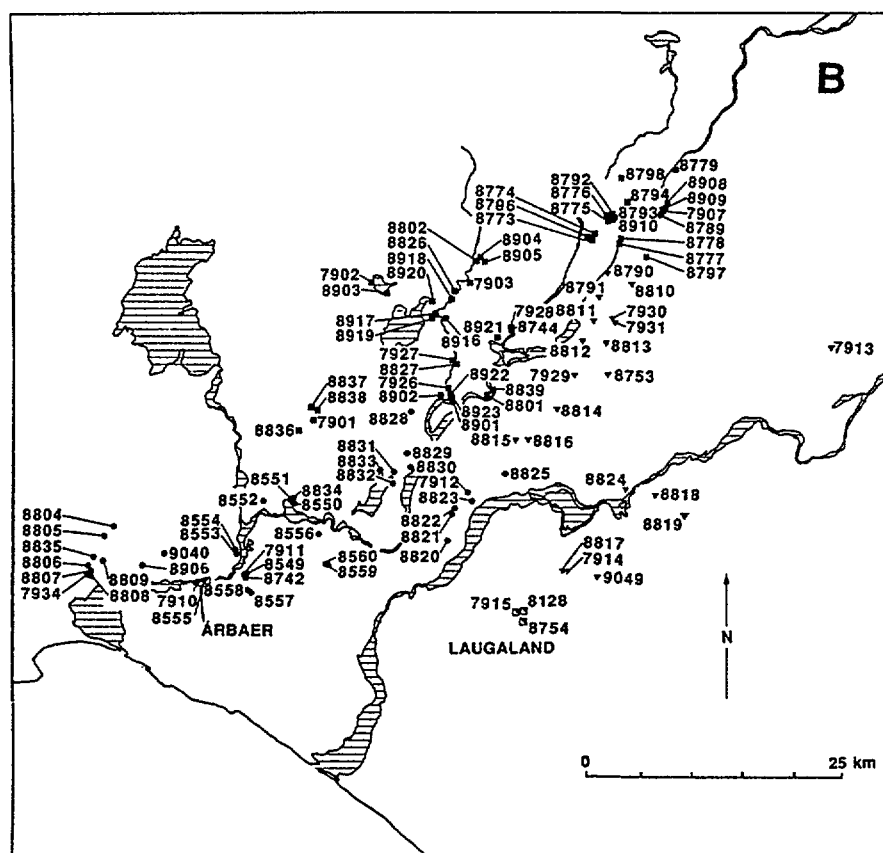
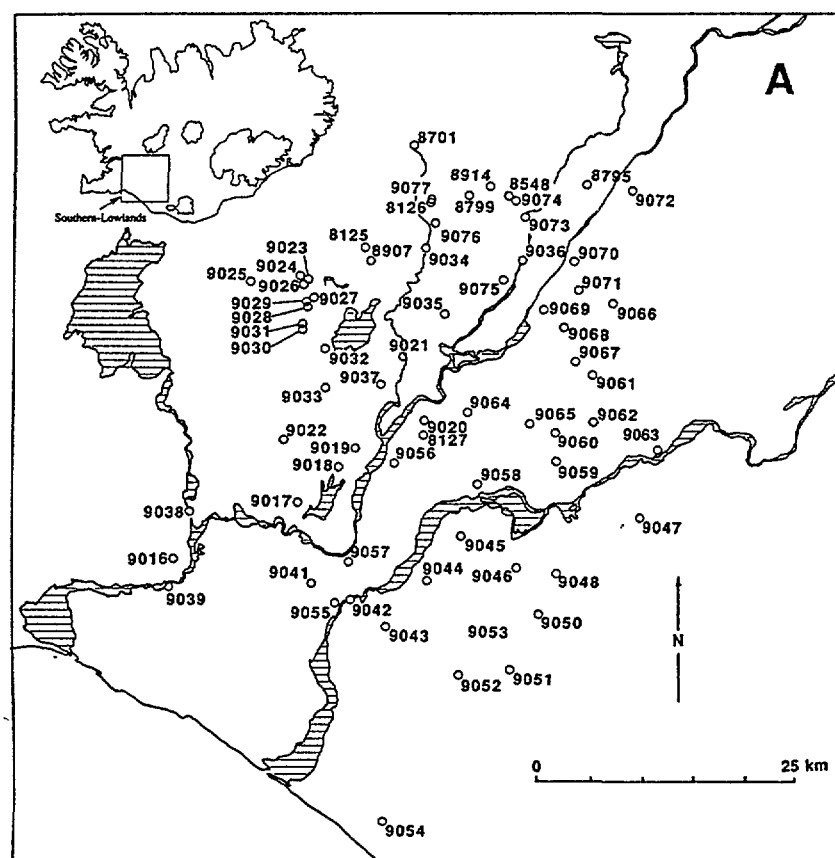
**Abstract** - Data on  $\delta^2\text{H}$  and  $\delta^{18}\text{O}$  in surface- and cold groundwaters in the NW-Peninsula and in the Southern Lowlands of Iceland plot close to a line with a somewhat shallower slope (6.44) than the meteoric line. The intercept with the  $\delta^{18}\text{O}$  axis is  $\delta^2\text{H} = -4.4\text{‰}$ . This  $\delta^2\text{H}$ - $\delta^{18}\text{O}$  relationship is considered to be representative for today's precipitation in Iceland. Geothermal waters with temperatures of less than about 50 °C show very limited, if significant, oxygen shift, whereas hotter waters do, the shift increasing with temperature of some one  $\delta^{18}\text{O}\text{‰}$  unit for every 100 °C. The distribution of Cl and B in cold and geothermal waters can be explained by supply from three sources: (1) the atmosphere, (2) the rock and soil with which the water interacts and (3) marine groundwater. The component of marine groundwater present in some of the geothermal waters in the Southern Lowlands is considered to have filtered into the bedrock during the deglaciation period (~10,000 years ago) when large parts of the area were submerged and when hydrological conditions differed from those today. In the NW-Peninsula the marine groundwater component can be accounted for by seawater infiltration into permeable fractures under present-day hydrological conditions. Cl-B relationships in the geothermal waters indicate that they represent local precipitation, as do the  $\delta^2\text{H}$  data for the NW-Peninsula. In the Southern Lowlands the  $\delta^2\text{H}$  of the geothermal waters is lower than that of local waters. This difference is not considered to reflect recharge areas to the geothermal systems on higher ground inland where today's precipitation is isotopically lighter than that in the Southern Lowlands. The cause is considered to be the presence of a component of "ice-age" water that was precipitated when the climate was significantly colder than today and, therefore, isotopically lighter. It appears that both aqueous B concentrations and the amount of oxygen isotope shift in the geothermal waters can be used to estimate the amount of rock dissolved by unit mass of these waters.

## 1. INTRODUCTION

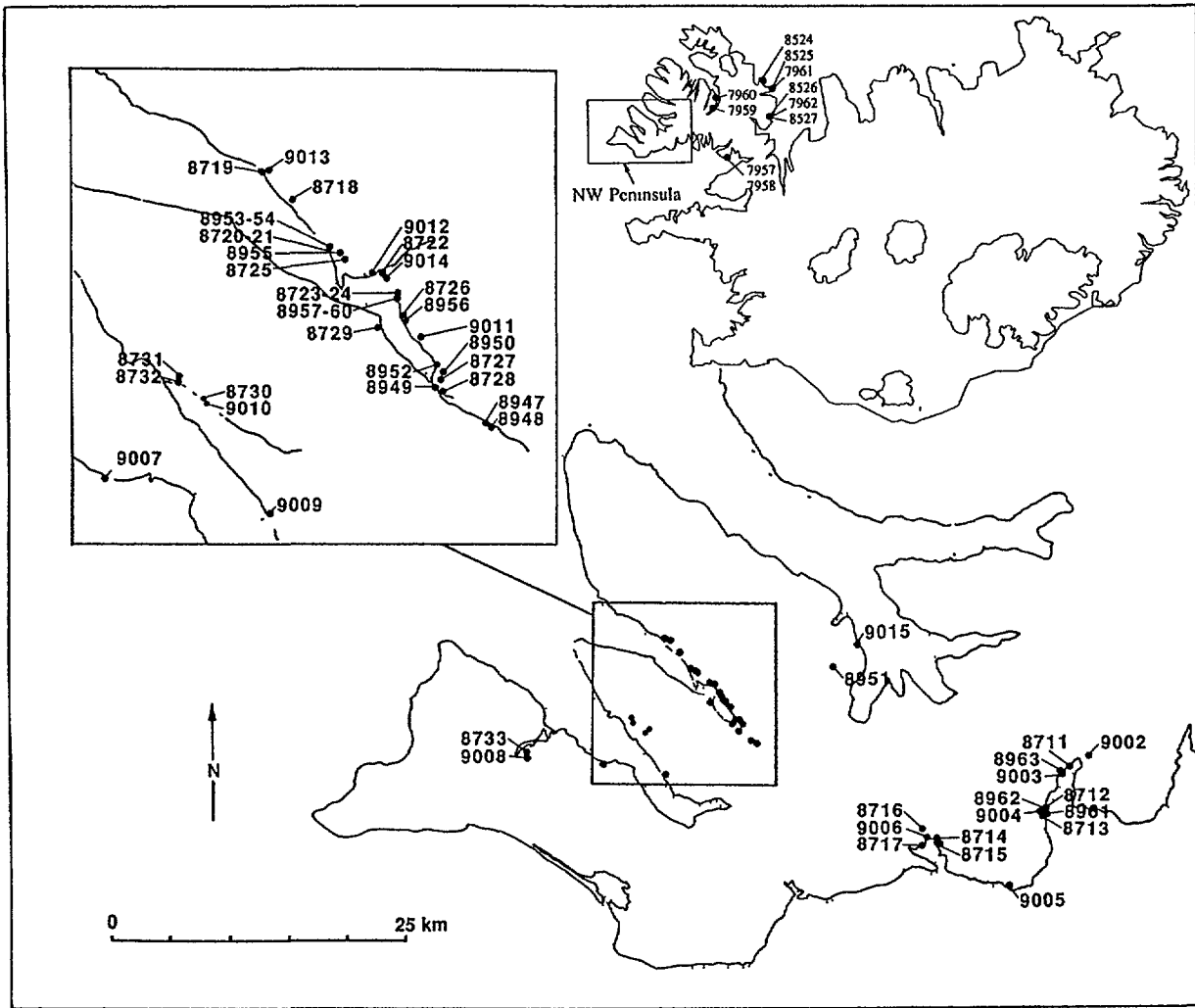
The stable isotopes of hydrogen have been used extensively as tracers to locate recharge areas to geothermal reservoirs [1-6]. The water content of all common rock types is so low that it is generally considered that isotopic exchange involving hydrogen between water and rock in the natural environment is negligible and for that reason the hydrogen isotope composition of groundwaters will not change during their passage through the ground [1, 5]. When using hydrogen isotope ratios ( $\delta^2\text{H}$ ) as tracers for groundwater movement it is generally assumed that today's precipitation has the same ratio as the precipitation represented by the geothermal water. It is, however, well known that climatic changes, especially around the deglaciation period some 10,000 years ago, were quite drastic at high latitudes so the  $\delta^2\text{H}$  of precipitation falling in any specific high latitude area at this time was quite different from that of today [1].

In this contribution data on  $\delta^2\text{H}$ ,  $\delta^{18}\text{O}$  and the mobile elements Cl and B in natural waters from two areas in Iceland, the NW-Peninsula (mostly its southwestern part) and the Southern Lowlands, are presented and interpreted with respect to the hydrology of the





**Fig. 1.** Maps of the Southern Lowlands showing sample locations for (A) cold and (B) geothermal waters.



**Fig. 2.** Map of the NW-Peninsula showing cold and thermal water sample locations.

geothermal groundwater systems in these areas. The Southern Lowlands are located in Quaternary rocks between the two active volcanic belts in South-Iceland (Fig. 1). The southwest part of the NW-Peninsula occurs in Miocene flood basalts, 10-13 My old [7] (Fig. 2). The area of the Southern Lowlands is almost all vegetated and relatively flat. On the other hand the NW-Peninsula is dissected by deep, glacially eroded valleys and fjords with 500-600 m high plateau inbetween. Except along the coast and in valleys on low ground vegetational cover is sparse.

It is shown how the isotopic data may be used in conjunction with the mobile element data to reduce the number of hydrological models with which the isotopic data alone are compatible. The data base for the present study includes altogether 96 cold water samples and 144 geothermal water samples of which 64 are from the NW-Peninsula and 176 from the Southern Lowlands (Table 1). The geothermal waters are from both hot springs and wells and range in temperature from just above ambient to a little over 150 °C. In some instances data from other areas in Iceland are also considered to substantiate various interpretations.

TABLE 1 PARTIAL ANALYSIS OF NATURAL WATERS FROM THE NW-PENINSULA AND THE SOUTHERN LOWLANDS OF ICELAND. CONCENTRATIONS IN PPM.

Sample Location No.	Temp °C	SiO <sub>2</sub>	Na	K	SO <sub>4</sub>	Diss. solids	Cl	B	Cl/B mass ratio	$\delta D\text{‰}$	$\delta^{18}\text{O}\text{‰}$	Sample Location No.	Temp °C	SiO <sub>2</sub>	Na	K	SO <sub>4</sub>	Diss. solids	Cl	B	Cl/B mass ratio	$\delta D\text{‰}$	$\delta^{18}\text{O}\text{‰}$
<i>Southern Lowlands</i>																							
7901 Klaustruhólar w 1	103	248.9	185.0	13.1	83.1	999	108.0	0.54	200			8775 Kjarnholt s	10	30.4	22.1	1.06	4.70	113	9.3	0.0061	1518	-61.1	-8.77
7902 Laugarvatn s	99	155.5	75.5	4.02	44.3	362	36.1	0.14	258			8776 Kjarnholt s	17	33.6	36.6	1.36	6.30	141	9.8	0.012	813	-61	-8.84
7903 Syðri-Reykirs	97	200.4	86.8	5.06	52.6	434	46.2	0.15	308			8777 Brúarhlöð s	11	34.8	24.0	1.26	3.95	107	9.1	0.0068	1332	-61.1	-8.96
7907 Tungufell s	22	37.5	26.0	1.66	7.2	113	8.1	0.015	540			8778 Brúarhlöð s	11	31.4	20.9	1.66	3.91	98	8.3	0.0061	1354	-62.1	-8.96
7910 Árbaer w 1	86	83.7	62.6	1.62	28.2	242	26.4	0.14	189			8779 Gullfoss s	25	67.8	39.5	1.77	13.9	168	9.1	0.034	266	-68.3	-9.75
7911 Selfoss w 9	70	62.2	160.0	4.58	53.5	583	247.0	0.13	1900			8789 Tungufell s	22	44.2	29.5	1.33	6.24	125	8.4	0.0041	2059	-64	-9.29
7912 Húsastadur w 4	70	71.8	136.0	2.88	67.6	486	172.0	0.20	860			8790 Hvítádalur s	18	53.1	41.4	1.01	6.09	186	11.4	0.0099	1152	-62.9	-9.1
7913 Þjórðarádalur s	70	58.0	116.0	3.24	302.3	593	49.4	0.60	82			8791 Skipholt s	25	60.6	39.3	1.88	4.88	157	9.8	0.018	542	-61.2	-8.8
7914 Hjalleslaugar s	41	82.1	63.3	1.61	29.5	200	20.2	0.17	119			8792 Gyðjarhólskot w 1	22	38.5	34.2	1.48	8.88	154	10.5	0.0075	1405	-62	-8.78
7915 Laugaland w 3	61	79.7	93.7	1.75	90.0	354	62.8	0.25	251			8793 Gyðjarhólskot s	18	39.3	33.9	1.59	8.75	145	10.3	0.0055	1865	-62.5	-8.92
7926 Thorlakshver s	96	112.4	76.4	2.48	57.8	332	53.7	0.27	199			8794 Gyðjarhóll s	10	28.7	19.1	1.94	3.74	110	9.4	0.0045	2098	-60.8	-8.56
7927 Spástadur w 1	76	104.0	77.6	2.29	55.5	331	48.7	0.32	152			8795 Gyðjarhóll s	7	25.7	13.5	1.21	2.24	119	8.0	0.0016	4988	-61.2	-8.86
7928 Reykholt w 1	133	179.8	110.0	5.54	72.6	483	77.7	0.35	222			8796 Kjarnholtsá s	21	62.3	50.3	2.39	6.29	196	10.4	0.0030	3460	-61.2	-8.78
7929 Veiðmálavær s	100	153.0	79.4	2.72	58.7	369	25.0	0.38	66			8797 Foss s	20	35.2	26.5	0.52	8.20	108	7.5	0.0062	1213	-62.4	-9.16
7930 Reykjaból w 1	152	252.8	102.0	6.21	70.7	536	41.6	0.65	64			8798 Kjóstadur w 1	19	41.7	33.7	0.79	6.35	164	9.7	0.017	574	-62.4	-8.99
7931 Reykjaból s	100	251.8	115.0	7.56	74.2	539	40.4	0.75	54			8799 Brúnjörn s	5	17.2	7.7	0.44	2.29	63	6.2	0.0042	1481	-62.2	-9.25
7934 Bakki w 1	134	133.6	388.0	19.6	122.5	1397	658.0	0.33	1994			8801 Laugarás s	96	94.9	82.1	1.83	56.2	308	49.9	0.21	238	-71	-9.77
8125 Ljóúar s	4	14.9	11.0	0.09	1.20	44	5.5	0.0030	1833			8802 Efir-Reykir w 23	147	188.6	102.0	5.40	35.5	744	53.6	0.14	383	-73.8	-10.2
8126 Brúnjörn s	7	18.1	7.5	0.50	1.20	64	7.5	0.0046	1630			8804 Núpar w	120	193.2	223.0	11.3	64.4	904	356.0	0.41	868	-68	-8.43
8127 Veiðmálavær s	15	21.7	11.5	0.70	4.10	95	13.1	0.0056	2339			8805 Núpar w	73	123.8	185.0	4.40	47.8	683	236.0	0.28	843	-67.1	-8.96
8128 Laugaland w 5	96	105.1	110.0	3.71	108.9	431	81.5	0.33	247			8806 Bakki w	113 <sup>a</sup>	112.4	314.0	10.7	121.5	1285	669.0	0.24	2788	-69.2	-8.92
8548 Stakksgil s	7	26.2	16.9	1.25	3.70	100	6.5	0.007	927			8807 Bakki w 2	107 <sup>a</sup>	100.3	327.0	9.42	105.4	1285	679.0	0.19	3574	-67	-8.99
8549 Selfoss w 10	84	76.7	162.0	4.67	56.4	592	247.0	0.18	1372			8808 Bakki w 1	120	114.9	395.0	17.5	122.0	1538	811.0	0.22	3686	-70.3	-9.18
8550 Vadvær w 1	69	83.4	107.0	3.60	71.8	367	78.8	0.15	525			8809 Þórðraddastadur s	96	81.7	208.0	6.22	54.3	839	403.0	0.15	2687	-64.5	-8.55
8551 Vadvær w 2	51	80.6	109.0	3.88	76.3	375	84.7	0.16	529			8810 Jata s	12	28.4	20.7	0.98	8.41	103	13.7	0.0026	5250	-60.8	-8.82
8552 Sudurkot s	33	47.3	60.3	2.33	22.9	235	64.3	0.086	748			8811 Kollaugur w 1	124 <sup>a</sup>	166.3	119.0	3.57	85.1	473	40.7	0.51	80	-82	-10.3
8553 Laugarbakkar w	53	56.2	105.0	0.93	57.3	337	104.0	0.28	371			8812 Kópavann w 1	99	128.1	86.1	2.71	62.6	377	37.3	0.25	149	-76.8	-10.2
8554 Laugarbakkar s	41	60.8	78.9	1.67	27.0	370	79.8	0.14	570			8813 Reykjadalur w 1	100	121.0	79.0	2.02	52.2	332	24.8	0.32	78	-72	-9.54
8555 Árbaer w 1	81	73.8	58.6	1.11	26.7	218	19.9	0.12	166			8814 Midfell w 1	62	72.5	63.5	0.87	43.9	238	21.6	0.14	154	-70.5	-9.72
8556 Oddagreiðshólar w 1	43	33.6	256.0	6.64	99.8	822	378.0	0.22	1718			8815 Syðra-Laugholt w 1	66	63.4	62.4	0.91	46.4	225	23.5	0.18	131	-70.5	-9.72
8557 Solvholt w 1	51	60.6	471.0	9.62	120.2	1965	1098.0	0.65	1689			8816 Birtingaholt w 1	55	76.4	64.5	1.47	47.3	249	29.0	0.20	145	-70.4	-9.56
8558 Solvholt s	35	41.0	415.0	7.98	114.6	1884	1065.0	0.50	2130			8817 Hjallesar w 1	53	80.7	68.8	0.67	27.6	216	17.6	0.15	117	-70.7	10
8559 Laugar w 1	60	54.0	167.0	2.82	89.6	540	201.0	0.19	1058			8818 Hvammur w 1	57	78.1	65.4	1.28	42.5	224	14.1	0.15	94	-67.4	-9.7
8560 Laugar s	43	57.5	166.0	2.67	85.9	541	189.0	0.22	859			8819 Stóri-Klofi w 1	56	68.5	64.3	0.47	68.9	234	18.1	0.12	151	79.5	-11.2
8701 Brúarstíkkur s	2	11.9	5.4	0.37	1.25	28	4.0	0.0019	2111	-72.3	-10.8	8820 Bleasastadur w 2	76	71.4	350.0	5.22	113.8	1065	504.0	0.32	1575	-97.6	-12
8742 Selfoss w 13	75	68.7	159.0	3.66	59.1	578	235.0	0.13	1808	-64.3	-9.43	8821 Brúnjörn w 1	61	283.0	12.4	98.2			374.0	0.28	1336	-94.2	-12
8744 Reykholt w 1	133	181.5	119.0	4.62	71.8	490	75.0	0.38	196			8822 Hlemmiskeld w 2	56	77.2	119.0	2.02	52.1	332	124.0	0.13	954	-75	-10.5
8753 Hrunalaug s	38	60.9	40.3	1.17	29.8	181	17.0	0.12	142	-64.8	-9.25	8823 Brúarholt w 1	70	74.6	156.0	2.25	66.8	502	176.0	0.18	978	-76.8	-10.6
8754 Laugaland w 4	96	106.4	97.5	1.86	67.4	346	48.8	0.25	195	-75.6	-10.5	8824 Þjórðaráholt w 1	65	73.2	59.3	0.80	38.9	206	14.0	0.12	117	-67.7	-9.72
8773 Einholt w 1	20	43.4	45.3	3.88	4.34	181	10.1	0.012	838	-60.1	-8.81	8825 Reykir w 2	70	72.3	100.0	1.36	53.6	406	156.0	0.15	1040	-68.3	-9.58
8774 Einholt r	21	40.0	39.0	1.66	5.36	148	9.8	0.0043	2286	-61.5	-8.87	8826 Bódmóðsastadur w 1	126 <sup>a</sup>	156.5	84.4	3.20	51.9	380	49.3	0.13	379	-71.5	-9.58

s = spring, r = stream, w = well with well number. a = chalcidony equilibrium temperature.

TABLE 1 continued

Sample Location No.	Temp °C	SiO <sub>2</sub>	Na	K	SO <sub>4</sub>	Diss. solids	Cl	B	C/B mass ratio	δD‰	δ <sup>18</sup> O‰	Sample Location No.	Temp °C	SiO <sub>2</sub>	Na	K	SO <sub>4</sub>	Diss. solids	Cl	B	C/B mass ratio	δD‰	δ <sup>18</sup> O‰
8827 Spóstaðir s	32	51.2	40.3	3.56	22.1	234	29.3	0.082	357	-66.4	-9.2	9027 Eyvindarunga s	6	20.0	15.4	0.55	2.60	62	5.1	0.0026	1975	-65.3	-9.51
8828 Kringla w 1	58	65.3	74.1	1.69	41.3	278	55.7	0.10	557	-70.4	-10.1	9028 Kvíslar s	4	15.9	7.9	0.46	2.05	50	5.0	0.0017	2890	-65.2	-9.5
8829 Sölheimar s	89	100.5	155.0	5.36	62.9	558	197.0	0.17	1159	-77.3	-10.6	9029 Kvíslar s	4	16.4	8.4	0.50	2.09	52	5.5	0.0021	2618	-64.8	-9.47
8830 Hamar w 1	48	58.8	220.0	5.61	68.4	751	334.0	0.13	2609	-94.4	-12	9030 Kaldagil s	4	17.3	7.9	0.53	2.07	56	6.5	0.0024	2702	-62.4	-9.17
8831 Ornstaðir w	92	120.5	139.0	3.83	49.7	580	242.0	0.11	2200	-66.8	-9.52	9031 Kaldagil s	4	17.5	7.1	0.51	2.06	56	6.1	0.0020	3009	-62.9	-9.21
8832 Varnarnes w 1	80	151.6	150.0	5.70	51.2	538	149.0	0.14	1064	-67.3	-9.42	9032 Elfr-Apavatn s	5	17.5	7.7	0.47	2.34	65	6.9	0.0024	2942	-60.4	-8.86
8833 Eyvfk w 1	75	168.5	164.0	5.19	60.0	639	111.0	0.14	793	-71.8	-10	9033 Stangarækkur r	5	16.3	7.0	0.58	2.18	59	7.7	0.0019	4148	-59.2	-8.69
8834 Varnes w 1	76	78.2	106.0	1.69	72.3	366	88.7	0.12	739	-67.2	-9.58	9034 Brúar r	6	14.6	6.8	0.45	2.20	51	6.3	0.0035	1793	-71.5	-10.4
8835 Þórðsdalsdr w 1	118	127.8	272.0	8.97	83.6	959	412.0	0.28	1471	-70.1	-9.15	9035 Hrosshagavík r	9	20.2	5.3	0.81	2.45	65	4.3	0.0016	2714	-55.7	-7.93
8836 Hæðarendi w 1	164 <sup>a</sup>	213.1	618.0	29.0	125.8	2194	278.0	0.76	366	-85.4	-8.54	9036 Tungufljót r	6	17.1	6.3	0.74	2.17	54	4.1	0.0026	1608	-64	-9.27
8837 Klausurhólar W-w	126 <sup>a</sup>	274.7	256.0	11.6	78.8	982	120.0	0.38	316	-87.1	-10.3	9037 Þórissstaðir r	9	20.2	7.9	1.19	5.29	82	6.7	0.0053	1271	-54.8	-7.93
8838 Klausurhólar E-w	140	306.2	218.0	13.1	74.0	909	122.0	0.33	370	-84.9	-10	9038 Sog r	6	11.8	8.5	0.65	2.60	55	5.9	0.0054	1097	-64.2	-9.31
8839 Audholt w 1	83	101.3	70.2	1.21	48.8	275	33.6	0.19	177	-70.6	-9.8	9039 Ölfusá r	6	14.5	7.7	0.65	3.13	57	5.1	0.0045	1143	-67.7	-9.7
8901 Reykjanes s	66	80.1	69.2	1.80	41.5	265	44.1	0.18	245	-69.4	-9.46	9040 Hvannur w 1	80	133.1	126.0	5.74	36.8	490	86.1	0.25	344	-64.9	-8.63
8902 Reykjanes s	81	86.3	98.1	2.30	51.2	360	94.3	0.18	524	-79.6	-10.9	9041 Bitra r	5	26.8	14.6	1.02	5.00	106	13.1	0.0090	1453	-56.7	-8.3
8903 Úey s	99	144.0	83.4	3.17	65.7	369	33.2	0.21	158	-71.2	-9.61	9042 Þykkvísar r	4	14.7	9.5	0.65	6.10	59	4.2	0.0077	543	-79.8	-11.3
8904 Elfr-Reyktr s	88	243.9	104.0	5.72	57.1	517	57.8	0.23	251	-71.9	-9.65	9043 Hárlaugstaðir r	5	33.1	13.1	0.94	4.25	127	14.6	0.0068	2158	-56.2	-8.09
8905 Elfr-Reyktr w	120	242.0	103.0	5.12	63.0	517	57.0	0.18	317	-72.6	-9.44	9044 Gíslholt r	4	22.2	9.3	0.75	2.13	83	13.1	0.0022	6023	-56.4	-8.06
8906 Audholt w 1	60	56.0	139.0	2.12	60.0	465	182.0	0.30	607	-66.2	-8.98	9045 Kaldarholt r	5	46.5	12.1	1.10	5.44	200	12.6	0.0044	2897	-58.4	-8.41
8907 Laugarbakkas s	4	16.6	9.9	0.26	4.00	64	9.3	0.0027	3433	-62.1	-9.18	9046 Hjalanes r	5	31.3	19.9	1.60	4.63	155	12.7	0.0080	1602	-55.9	-8.12
8908 Tungufell s	15	31.5	20.9	1.24	5.86	98	7.8	0.0039	2000	-63.5	-9.11	9047 Kíofalækkur s	6	22.1	17.9	1.22	9.59	99	9.1	0.019	478	-73.8	-10.4
8909 Tungufell s	12	31.5	19.1	1.31	7.20	111	8.8	0.0020	4375	-63.7	-9.3	9048 Krókur s	5	24.6	16.9	1.18	7.83	101	12.1	0.012	1000	-67.3	-9.59
8910 Gýgjarbólskot w	23	39.8	34.4	1.76	6.72	142	10.4	0.015	675	-61.9	-8.84	9049 Krókur w 1	11	21.3	44.9	0.33	6.90	134	13.2	0.019	688	-59.6	-8.59
8914 Fostunga s	6	24.2	11.2	0.75	8.28	81	6.8	0.0083	819	-62.5	-9.01	9050 Selgill s	8	32.3	14.6	2.68	4.55	141	15.0	0.0068	2199	-61.4	-8.77
8916 Mikholt s	28	39.5	49.7	0.93	15.1	174	17.1	0.028	615	-64.5	-9.06	9051 Árbeir s	8	31.6	16.6	1.58	3.98	151	15.1	0.0053	2876	-56.1	-8.06
8917 Mikholt s	57	122.8	74.9	1.61	46.8	326	42.8	0.14	317	-70.6	-10.1	9052 Raudilækkur r	9	34.4	16.3	1.40	5.67	165	15.4	0.0069	2241	-55.7	-7.99
8918 Mikholt s	33	113.6	68.6	1.67	31.9	342	38.0	0.13	295	-70.1	-9.91	9053 Steinslækkur r	8	33.9	17.2	1.44	10.7	160	15.2	0.011	1328	-56.9	-8.17
8919 Hagi s	29	76.5	55.0	1.72	25.2	280	23.8	0.059	403	-69	-9.42	9054 Varnskotr	10	40.2	23.4	1.98	15.5	312	24.7	0.012	2129	-54.2	-7.94
8920 Hagaes w 1	90	109.0	79.3	2.39	51.5	325	48.1	0.17	283	-70.3	-9.65	9055 Urridafoss s	5	29.1	12.2	1.28	3.74	115	14.0	0.0052	2699	-57.7	-8.53
8921 Reykjavellir s	69	129.3	90.4	3.22	46.2	409	39.3	0.27	146	-73.7	-9.75	9056 Fjall & Skeidum r	5	19.7	10.9	0.72	3.05	75	11.3	0.0030	3750	-58.7	-8.61
8922 By Þorlákshver s	73	98.7	73.5	1.77	42.1	294	46.8	0.25	187	-72.9	-10.3	9057 Skeid s	7	28.7	24.0	1.67	8.80	156	38.0	0.012	3154	-59.3	-8.47
8923 By Þorlákshver s	84	113.5	87.9	2.13	48.0	332	54.7	0.28	195	-74.9	-10.3	9058 Sandilækkur, pool	7	1.9	4.2	2.81	2.01	33	9.7	0.0059	1649	-54.3	-7.69
90016 Laugarbakkis s	5	14.9	12.6	0.46	3.19	71	11.1	0.0022	4970	-56.6	-8.36	9059 Geldingaholt r	6	21.1	10.3	1.34	3.45	118	12.5	0.0026	4808	-55.2	-7.72
90017 Hlaupandi r	9	19.1	9.4	0.68	1.20	97	10.8	0.0048	2274	-53.4	-7.45	9060 Fossgil r	6	27.3	8.5	1.15	2.26	98	11.1	0.0020	5525	-56.5	-8.58
90018 Grjófar	9	24.9	11.6	1.01	2.50	122	10.9	0.0045	2411	-57.2	-8.22	9061 Laxárdalur r	6	21.9	7.4	0.79	2.15	70	11.3	0.0025	4561	-59.8	-8.77
90019 Hveralækkur r	10	24.3	9.8	0.71	1.40	106	11.2	0.0043	2605	-55.3	-7.95	9062 Mástunga r	6	30.2	10.3	1.16	7.31	122	11.1	0.0035	3171	-60.2	-8.68
90020 Vötnufell r	10	15.3	11.5	0.86	1.44	84	9.3	0.0034	2746	-59	-8.45	9063 Hægaflall r	6	24.6	9.1	0.86	2.46	87	9.7	0.0031	3115	-60.2	-8.68
90021 Spóstaðir s	6	30.2	13.8	1.10	6.19	105	11.4	0.015	761	-64.9	-9.24	9064 Flúðir/Audsholt s	4	30.1	9.0	1.15	2.37	115	12.6	0.0035	3638	-63.1	-9.11
90022 Hóskuldslækkur r	7	23.6	11.7	0.92	6.97	95	9.3	0.0060	1570	-59.8	-8.64	9065 Smárshlíð s	4	26.0	9.1	1.00	2.91	101	14.1	0.0029	4904	-60.5	-8.62
90023 Laugarvann s	4	17.3	12.9	0.36	2.20	59	5.6	0.0022	2527	-64.7	-9.41	9066 Kaldbakur r	5	21.3	6.4	0.82	2.22	66	8.6	0.0026	3371	-61.5	-8.86
90024 Helgudalur s	4	15.5	4.7	0.43	2.01	52	6.5	0.0017	3805	-67.9	-9.73	9067 Thverspyrna, lake	7	16.9	8.3	0.86	1.97	76	11.9	0.0025	4740	-59.4	-8.19
90025 Vallalækkur r	7	15.4	8.4	0.42	1.93	49	4.4	0.0018	2519	-65.8	-9.59	9068 Reykjadalslækkur r	7	28.2	10.5	1.22	3.38	103	9.8	0.010	977	-61.8	-8.75
90026 Laugarvann r	7	16.0	5.7	0.45	2.03	56	5.4	0.0019	2862	-58.6	-8.39	9069 Kodlaugar r	7	27.2	11.0	1.69	2.90	117	11.0	0.0060	1825	-60.1	-8.62

s = spring, r = stream, w = well with well number. a = chalcidony equilibrium temperature.

TABLE 1 continued

Sample Location No.	Temp °C	SiO <sub>2</sub>	Na	K	SO <sub>4</sub>	Diss. solids	Cl	B	C/B mass ratio	$\delta D\text{‰}$	$\delta^{18}O\text{‰}$
9070 Haukholtr	6	22.8	7.5	1.00	1.59	68	8.9	0.0019	1814	-62.6	-8.95
9071 Jaa r	5	22.8	7.6	0.92	1.80	80	8.2	0.0022	3800	-61.4	-8.89
9072 Tungudalur r	4	22.6	9.3	0.89	2.47	75	7.3	0.0026	2817	-66.1	-9.41
9073 Einholtislaekur r	4	24.8	11.8	0.96	2.36	105	8.0	0.0043	1886	-62.8	-8.94
9074 Staeksa r	4	23.0	7.9	0.63	2.45	74	7.5	0.0024	3133	-60	-8.57
9075 Heiðir	4	28.4	11.9	1.71	5.24	154	18.1	0.0034	5324	-60.5	-8.51
9076 Brakka s	4	14.5	6.5	0.52	1.70	53	5.6	0.0036	1560	-65.8	-9.64
9077 Hrtla r	3	11.8	5.9	0.41	1.46	40	4.2	0.0016	2644	-73.4	-10.7
<i>NW-Peninsula</i>											
7957 Reykhoflar w 2	100	100.5	58.6	2.12	33.0	267	32.5	0.038	855		
7958 Reykhoflar s	84	106.9	55.2	2.08	31.4	251	28.8	0.027	1067		
7959 Bjarnastadir s	18	36.5	30.0	0.22	6.70	118	18.8	0.045	418		
7960 Reykjanes s	84	70.9	184.0	4.34	42.1	769	390.0	0.160	2438		
7961 Hveravik s	72	49.0	716.0	17.3	297.6	4330	2460.0	0.37	6649		
7962 Klukka s	40	33.1	26.9	0.25	6.5	102	15.6	0.016	975		
8524 Krossnes s	63	73.7	53.9	0.78	34.7	214	30.4	0.098	311		
8525 Hveravik s	76	107.9	81.7	0.64	16.2	333	93.5	0.24	398		
8526 Goddalir s	58	55.0	39.5	0.77	6.84	142	17.6	0.044	400		
8527 Svansholir s	41	38.7	33.0	0.30	5.22	113	16.9	0.063	268		
8711 Flakalundur w 1	38	24.4	23.9	0.35	8.27	88	13.4	0.015	890	-64.2	-9.53
8712 Thvera w 1	22	16.7	18.0	0.19	3.06	71	12.8	0.0077	1660	-62.9	-9.33
8713 Thvera S w 2	20	17.3	18.1	0.22	3.16	75	12.6	0.0095	1325	-63.3	-9.2
8714 Krossholt w 1	39	40.7	32.4	0.36	6.12	123	19.0	0.027	697	-62.1	-9.04
8715 Krossholt w 2	43	39.0	28.3	0.33	4.31	111	17.4	0.020	868	-61.3	-8.84
8716 Tungumtli w 1	28	26.3	21.0	0.23	3.28	93	12.7	0.0085	1496	-61.1	-9.03
8717 Os w	34	36.7	27.3	0.30	4.79	121	16.3	0.019	863	-61.7	-9.05
8718 Litli-Laugaralur w 1	44	47.4	27.8	0.45	12.5	118	15.6	0.025	614	-65.5	-9.58
8719 Stori-Laugaralur w 1	51	57.9	34.2	0.62	16.2	142	17.2	0.032	539	-66.3	-9.59
8720 Sveinseyri w 1977	25	30.2	19.9	0.54	4.16	84	15.2	0.014	1127	-64.7	-9.38
8721 Sveinseyri w 1987	20	27.6	16.2	0.63	3.83	72	14.3	0.011	1333	-65.7	-9.66
8722 Thorpid w	15	42.2	23.6	0.96	3.98	99	20.2	0.013	1617	-68.1	-9.84
8723 Undir hlidinni w	6	18.2	9.1	0.49	1.81	49	11.3	0.0037	3051	-68.3	-9.92
8724 Undir hlidinni w	5	18.6	9.6	0.48	1.81	50	11.1	0.0028	3968	-66.7	-10
8725 Takkafjofdur w	14	35.6	20.1	0.50	3.31	83	14.1	0.015	944	-64.7	-9.59
8726 Gileyrir w	14	32.5	17.8	0.57	2.37	73	14.1	0.0089	1580	-64.6	-9.47
8727 Norðurbotn E w	14	31.0	19.8	0.43	2.60	75	13.7	0.0094	1455	-63.1	-9.28
8728 Norðurbotn W w	11	20.5	16.5	0.63	2.60	62	14.2	0.0075	1891	-65	-9.42
8729 Bideyni w	11	21.8	13.7	0.30	2.40	65	18.4	0.0069	2667	-63.4	-9.32
8730 Mikidalur w	6	17.8	10.5	0.44	2.37	54	15.6	0.0042	3714	-63.8	-9
8731 Mikidalur w	19	36.6	24.9	0.45	4.58	98	20.8	0.021	997	-64.3	-9.27
8732 Mikidalur w	25	39.4	23.7	0.97	7.06	102	20.5	0.030	677	-62.7	-9.23
8733 Hnjofur w 1	6	18.2	17.4	0.41	3.54	68	22.1	0.0071	3114	-55.8	-8.09
8947 Bomsgil w A	25	30.3	95.0	0.67	5.88	157	12.4	0.0067	1851	-65.4	-9.66

s = spring, r = stream, w = well with well number. a chalcodony equilibrium temperature.

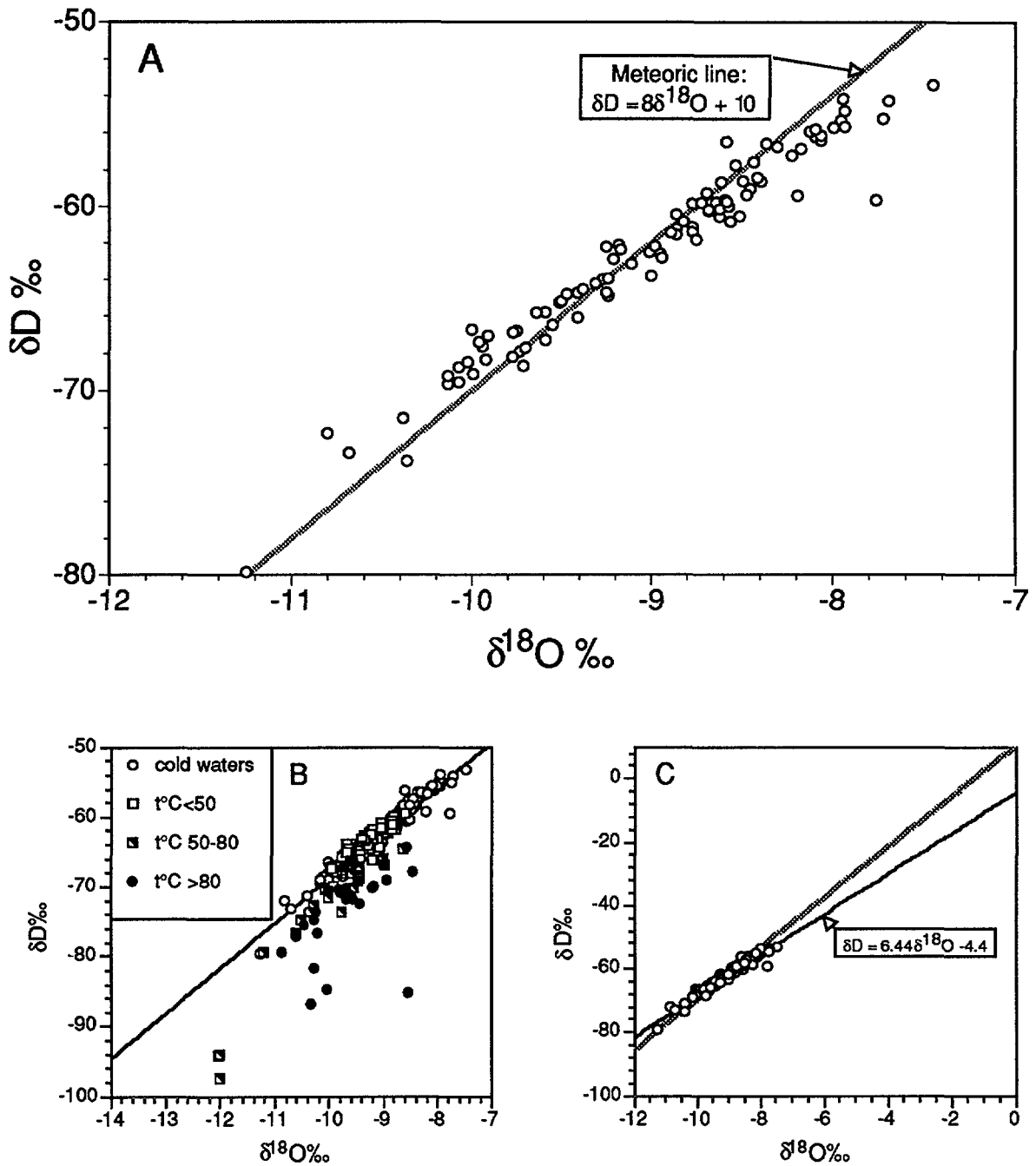
## 2. CHEMICAL CHARACTERISTICS

Geothermal waters in the NW-Peninsula and in the Southern Lowlands are, like waters from most other geothermal fields in Iceland, relatively dilute compared to geothermal waters in other parts of the world. Partial analysis is given in Table 1. The content of dissolved solids most often lies in the range of 150-500 ppm. In waters close to the coast it is, however, higher and reaches almost 2000 ppm in a few places. Cold surface- and groundwaters are lower in dissolved solids, mostly in the range 50-150 ppm. Sodium is the dominant cation in both cold and geothermal waters and silica is always an important constituent. In the dilute geothermal waters sulphate tends to be the dominant anion but chloride in the ones which are higher in dissolved solids. In cold waters chloride and bicarbonate are the main anions.

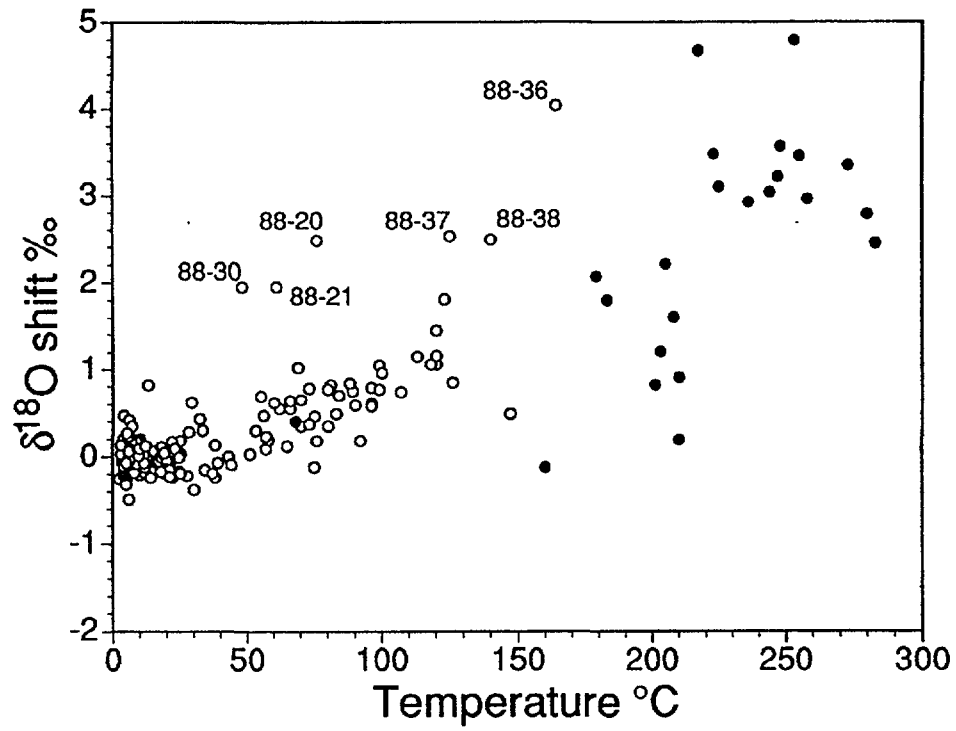
## 3. $\delta^2\text{H}$ - $\delta^{18}\text{O}$ RELATIONSHIPS

The  $\delta^2\text{H}$ -values of the cold waters in the NW-Peninsula generally lie in the range -58 to -70 ‰. In the Southern Lowlands the values are somewhat higher (less negative), or mostly in the range of -53 to -65‰ (Table 1). The data points do not plot on the meteoric line (Fig. 3A) but form a line with a somewhat shallower slope. Thus, waters with values higher than about -64‰  $\delta^2\text{H}$  (less negative) are enriched in  $\delta^{18}\text{O}$  relative to the meteoric line whereas waters with lower  $\delta^2\text{H}$ -values are depleted in  $\delta^{18}\text{O}$  relative to the meteoric line (Fig. 3A). A linear fit through the cold water data points yields a slope of 6.44 and an intercept at zero  $\delta^{18}\text{O}$  of -4.4‰  $\delta^2\text{H}$  (Fig. 3C). This distribution of the  $\delta^2\text{H}$  and  $\delta^{18}\text{O}$  values are considered to be representative for today's precipitation in Iceland. The values show that the source of the moisture for the precipitation must be at latitudes far south of Iceland [8]. The difference between the isotopic values in the Southern Lowlands and the NW-Peninsula can be accounted for by fractional condensation of the moisture as it moves northwards from its source in the south. Geothermal waters with temperatures of less than about 50 °C show very limited, if significant, oxygen shift, whereas hotter waters do, the shift increasing on the whole with temperature (Figs. 3B and 4). This shift is considered to be due to interaction of the water with the rock it dissolves. Several water samples from the Southern Lowlands show quite large oxygen shift relative to their water temperature (Fig. 4). Three of these samples are from wells drilled into a reservoir with temperatures of 130-160 °C (sample nos. 8836 to 8838 in Table 1) containing waters rich in  $\text{CO}_2$ . It is considered that the reactive  $\text{CO}_2$ -water has interacted intensively with the rock, thus causing a large oxygen shift in the water. The remaining three water samples have temperatures of 50-80 °C (sample nos. 8820, 8821 and 8830 in Table 1). As discussed below they are considered to contain a relatively large component of very old water that has, therefore, had a long time to react with the rock, thus explaining the large oxygen shift. Cold and thermal waters in the NW-Peninsula have  $\delta^2\text{H}$ -values in the same range. This is, however, not the case for the Southern Lowlands. The geothermal waters tend to be lower in  $\delta^2\text{H}$  than local cold waters, i.e. local precipitation. This difference has generally been taken to indicate that the recharge areas to the geothermal systems lie inland on higher ground [1,2] as it is well known how the  $\delta^2\text{H}$  of precipitation in Iceland decreases inland due to inland and altitude effects [1]. By the same interpretation the geothermal waters in the NW-Peninsula represent local precipitation.

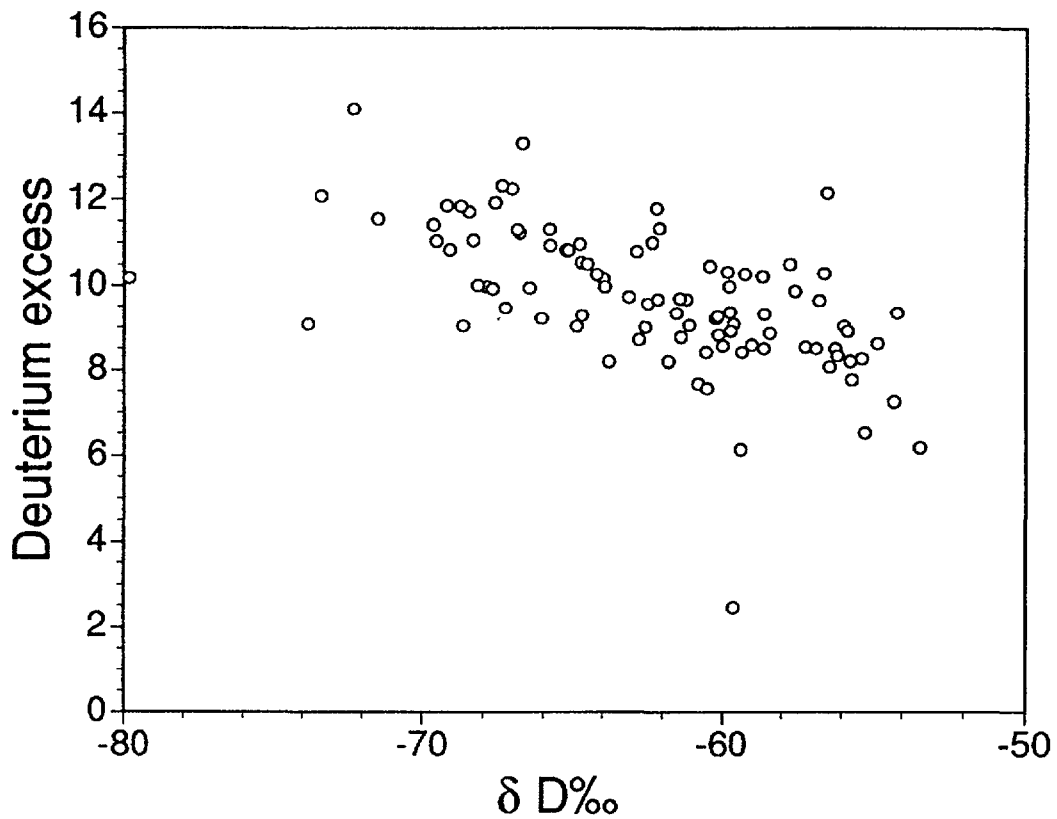
The deuterium excess (d) which is defined as the  $\delta^2\text{H}$  value of the meteoric line at  $\delta^{18}\text{O} = 0$ , i. e.  $d = \delta^2\text{H} - 8 \times \delta^{18}\text{O}$  is variable in the cold waters of the NW-Peninsula and the Southern Lowlands and it decreases distinctly with increasing  $\delta^2\text{H}$  (Fig. 5) as a result of the distribution of the data points in relation to the meteoric line. The deuterium excess is considered to be principally a function of the mean relative humidity of the air masses



**Fig. 3.** A:  $\delta D$ - $\delta^{18}O$  relationship in surface- and cold groundwaters from the NW-Peninsula and the Southern Lowlands. Part B of this figure shows the same data in addition to geothermal water data from the same areas. The line represents a regression line through the cold water data the equation for which is given in part C. The gray line in part C is the meteoric line shown in part A.



**Fig. 4.** Relationship between oxygen shift and temperature in natural waters in Iceland. The circles represent data from the NW-Peninsula and the Southern Lowlands but dots data from three high-temperature geothermal fields studied by [20].



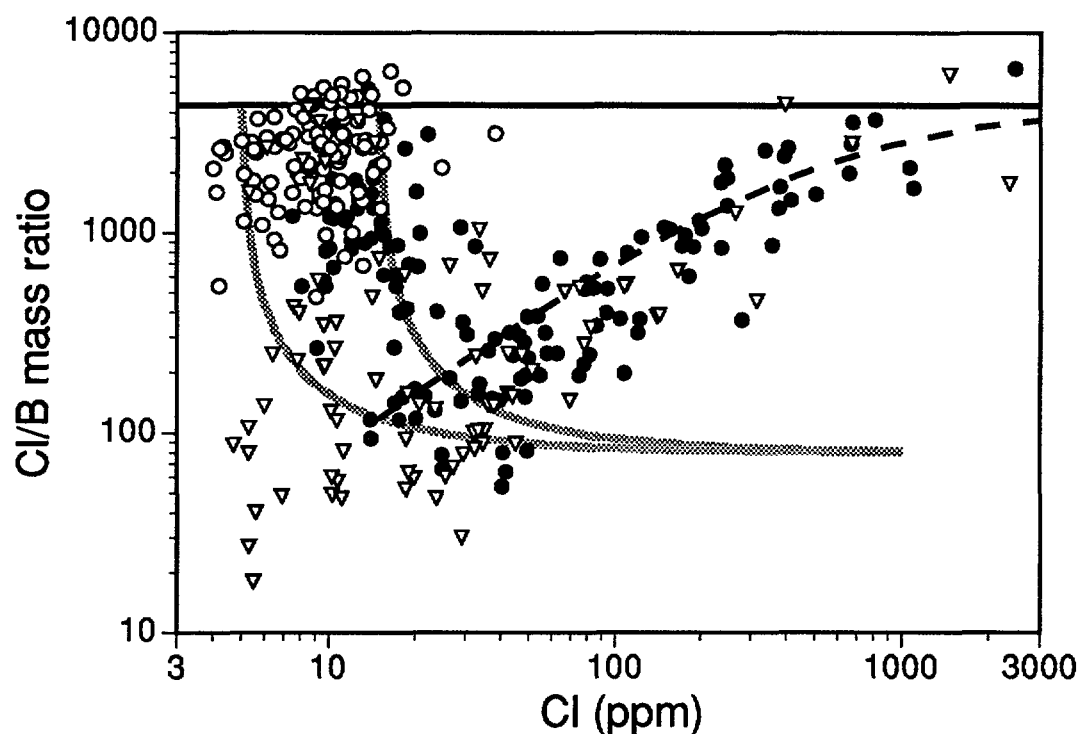
**Fig. 5.** Deuterium excess (d) in natural waters in the NW-Peninsula and the Southern Lowlands.



overlying the oceans in the source area [9]. In the eastern Mediterranean region where humidity is relatively low it is as high as +22‰ [5]. In tropical islands with conditions of high relative humidity, low deuterium excess values are observed and the slope may be less than 8 [5], just as is the case for Iceland. Although average temperatures are low in Iceland, relative humidity is high.

#### 4. Cl - B RELATIONSHIPS

The Cl concentrations of surface- and cold groundwaters in the study areas lie in the range of 5-20 ppm. The Cl/B mass ratios of these waters are similar to that of seawater (4350) [10] or somewhat lower (Fig. 6, Table 1). In the Southern Lowlands Cl concentrations decrease inland being about 20 ppm by the coast and some 7 ppm by the northern limit of the area. Farther inland in the central highlands, by the Langjökull ice-cap, Cl concentrations in surface waters are as low as 1-2 ppm [11,12]. In the NW-Peninsula no geographic variation is seen in the Cl concentrations of the cold waters. The Cl concentrations and the Cl/B ratios of the cold waters suggest that the source of supply of Cl and B in these waters is for the most part the ocean, seawater spray and aerosols brought down with the precipitation. The geothermal waters have quite variable Cl concentrations, or ranging from those of the cold waters to more than 2000 ppm. Water on low lying ground relatively close to the coast in the Southern Lowlands and coastal waters on the east side of the NW-Peninsula are highest



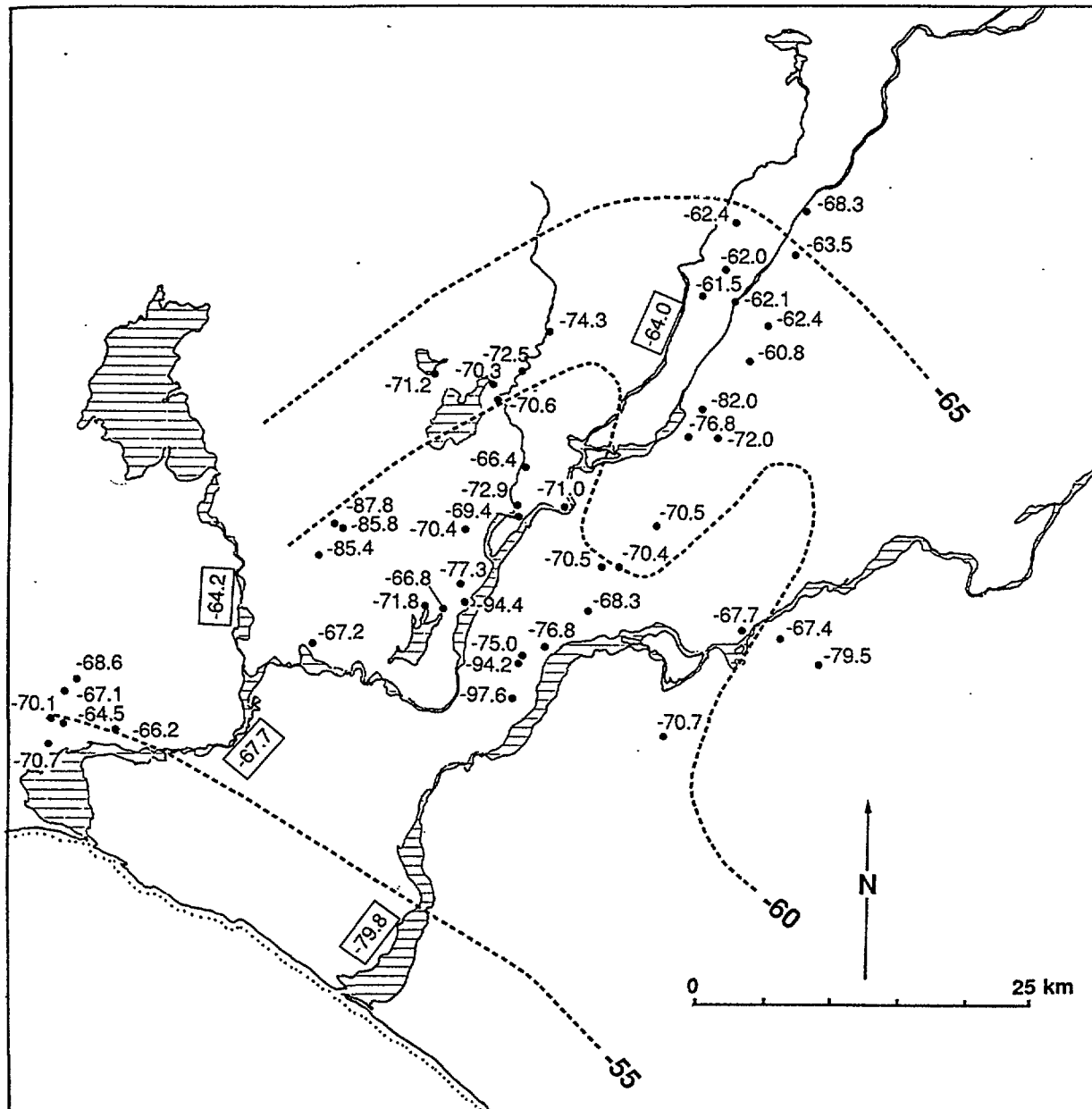
**Fig. 6.** Cl-B relationships in natural waters in Iceland. The solid horizontal line represents Cl/B mass ratio in seawater = 4350. The two gray curves represent Cl/B-Cl relationship in water with initially 5 and 15 ppm Cl and Cl/B mass ratio of 4350 which subsequently gained Cl and B by rock dissolution in the ratio of 80. The broken curve corresponds to a mixture of seawater and water containing 15 ppm Cl with a Cl/B mass ratio of 120. Circles represent cold waters from the NW-Peninsula and the Southern Lowlands and dots geothermal waters from the same areas. Triangles represent cold and geothermal waters from other low-temperature fields in Iceland.

in Cl. B concentrations range from almost 0 to 0.75 ppm. The distribution of Cl and B in the cold and geothermal waters can be explained by supply from three sources: (1) the atmosphere, i.e. seawater spray and aerosols, (2) the rock and soil with which the water interacts and (3) marine groundwater (Fig. 6). The meteoric parent water to the geothermal water will contain some Cl and B from seawater spray and aerosols, as already mentioned, and possess a Cl/B ratio similar to that of seawater. Upon reacting with the rock and gaining heat through deep convection this initial meteoric water will dissolve Cl and B from the rock, apparently stoichiometrically [13]. As a result the aqueous Cl/B ratio becomes lower because the basaltic rock possesses much lower Cl/B ratios than seawater, or in the range 50-150 [13]. As rock dissolution proceeds the aqueous Cl/B ratio will gradually approach that of the rock. The effect of rock dissolution on changes in aqueous Cl/B ratios with increasing Cl concentrations are depicted by the two gray curves in Fig. 6 for initial Cl concentrations of 5 and 15 ppm, respectively, in the parent meteoric water. In calculating these curves it was assumed that the Cl/B mass ratio of the rock was 80 and that these elements were dissolved in stoichiometric proportions. Mixing of marine groundwater with the geothermal water will cause an increase in both Cl/B ratios and Cl concentrations but affect little B concentrations unless the marine groundwater component in the geothermal water is relatively large. The broken line in Fig. 6 shows how Cl concentrations and Cl/B ratios change as water with an initial Cl/B ratio of 120 and Cl concentration of 15 ppm mixes with seawater. Since most of the data points in Fig. 6 fall between the two rock dissolution lines representing about minimum and maximum Cl in Icelandic precipitation and close to the seawater mixing line, it is concluded that it is these two processes, i.e. rock dissolution and seawater mixing, that control the distribution of Cl and B in Icelandic low-temperature geothermal waters together with the Cl and B content of the precipitation.

## 5. THE SOURCE OF THE GEOTHERMAL WATERS AND RECHARGE AREAS

The isotopic composition of the geothermal waters in the NW-Peninsula and in the Southern Lowlands show that they are for the most part meteoric in origin. Seawater mixing with this meteoric water occurs in parts of the Southern Lowlands, particularly near the coast. It also extends inland in low lying areas that were transgressed by the ocean during the deglaciation period some 10,000 years ago. In the NW-Peninsula substantial seawater component is present in geothermal waters at a few sites by the coast on the east side of the Peninsula. These sites seem to be characterized by fractures extending into the ocean along which the hot water ascends.

Direct flow of seawater into these fractures can, thus, account for the presence of the seawater component in the geothermal water in this area. This is, however, not the case for the Southern Lowlands. Hydrostatic pressure in many drilled wells in the area that issue water with a significant seawater component is higher than that of the ocean. It is not possible to have seawater flowing into these systems for distances as long as 30 km from the coast under present-day hydrological conditions. An explanation, which is acceptable to account for the marine component in these geothermal waters is that the seawater entered the bedrock during the deglaciation period when the respective sites were submerged and hydrological conditions favourable for seawater infiltration into the bedrock. In this connection it is of importance to bear in mind geohydrological data relevant to the nature of the geothermal activity in some places in the Southern Lowlands as in many other areas in Iceland. These data favour that the geothermal systems develop in fractures maintained permeable by recent earth movements in otherwise much less permeable bedrock [14, 15]. Water convection would be relatively rapid in the fractures and lead to cooling of the rock at deep levels where



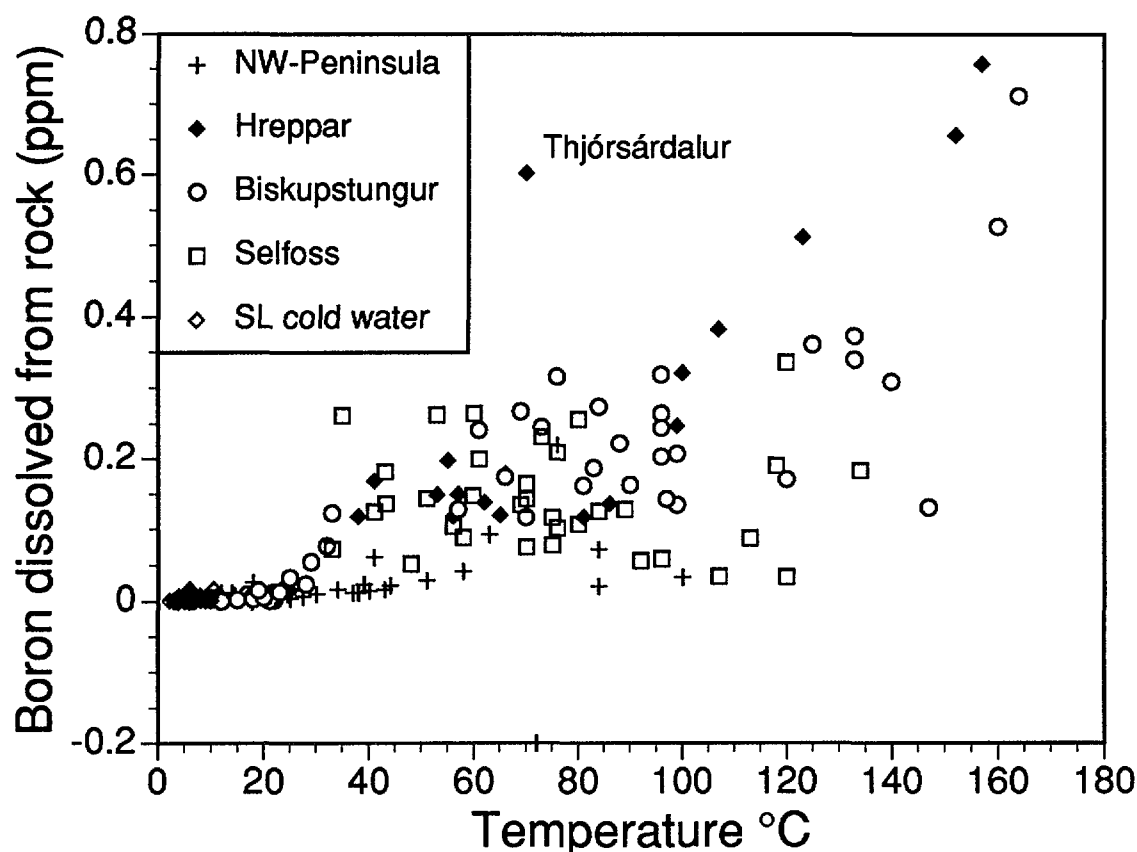
**Fig. 7.**  $\delta D$ -values in selected geothermal waters from the Southern Lowlands. Also shown are isolines for  $\delta D$  in cold waters which represent local precipitation and  $\delta D$ -values of the major rivers showing that they derive most of their water from the interior highlands.

the water warms up, but heating of the rock at shallow levels where the rising hot water cools. As a result of this, hydrostatic pressure at deep levels in the geothermal fracture would be reduced because the density of the overlying hot water column is lower than that of colder water. The pressure reduction would favour seepage of groundwater into the fracture from the surrounding bedrock. Due to the relatively low permeability of this bedrock, replacement of the groundwater would be slow, particularly in flat lying areas where the groundwater hydrologic gradient is shallow. For this reason the groundwater in the bedrock outside the fractures would be relatively old, old enough to still contain a component of seawater that infiltrated during the deglaciation period. Available data on global permeability and hydrologic gradients in Iceland substantiate this model [14].

Estimation of the amount of Cl in the geothermal waters derived from a marine source (marine groundwater and atmospheric spray and aerosols) by the method described by [16] indicates that it is similar to, or higher than in local cold waters. When higher, it is considered, as already discussed, that a component of marine groundwater is present in the geothermal water. However, when Cl concentrations in the geothermal water derived from the marine source are similar to the local cold water, it is considered that the geothermal water is solely derived from local precipitation. This result is compatible with the  $\delta^2\text{H}$  data in the NW-Peninsula but it is not compatible with the classic interpretation of the  $\delta^2\text{H}$  data of geothermal waters in the Southern Lowlands [1]. The  $\delta^2\text{H}$ -values of the geothermal waters, which are generally lower than those of local cold waters representing local precipitation, were taken to indicate that the recharge areas to the geothermal systems lie inland from the geothermal systems on higher ground. The groundwater flow from the recharge areas was considered to be driven by the hydraulic gradient. Cl concentrations of the precipitation in the inland areas where  $\delta^2\text{H}$  precipitation values are in the same range as those of the geothermal waters in the Southern Lowlands are as low as 1-3 ppm which is to be contrasted with the calculated marine Cl component in the geothermal waters of 7-15 ppm. The difference in the  $\delta^2\text{H}$  of local cold waters and in geothermal waters in the Southern Lowlands is not considered to result from distant recharge areas inland to the geothermal systems. The cause of the difference is considered to be due to the presence of a component of "ice-age" water in the geothermal water, water that corresponds to precipitation that infiltrated the bedrock during the deglaciation period, even earlier, when the climate was considerably colder than today and, as a result, the  $\delta^2\text{H}$  of the precipitation as much as 50 ‰ more negative than today [1]. Like the marine groundwater, discussed above, this "ice-age" water has in Post-glacial times being gradually replaced by younger water, but the replacement appears still to be incomplete in most of the geothermal systems.

## 6. BORON-TEMPERATURE RELATIONSHIPS

The amount of the mobile element boron in geothermal waters in Iceland can be used as a leaching indicator [13], i.e. its aqueous concentration is a measure of the amount of rock with which the water has reacted. Fig. 8 depicts the relationship between the calculated amount of B dissolved from the rock in natural waters of the NW-Peninsula and in the Southern Lowlands versus water temperature. The data from the Southern Lowlands have been subdivided into three groups, each group corresponding to each of the three main geothermal systems in the area, the Hreppar, Biskupstungur and Selfoss systems [17]. The data in Fig. 8 show that practically no B is dissolved from the rock by cold and slightly thermal ( $< 30\text{ }^\circ\text{C}$ ) waters but the amount of rock-derived B increases on the whole with temperature although the scatter of the data points is large. Closer inspection shows, however, that variations within individual areas is relatively limited at each temperature as for the Hreppar area in the Southern Lowlands and the NW-Peninsula. In the latter area, B concentration only increase a little with temperature but for Hreppar there is roughly an increase of 0.4 ppm B per  $100\text{ }^\circ\text{C}$  rise in temperature. The scatter of data points is greater for the remaining two geothermal systems in the Southern Lowlands (Biskupstungur and Selfoss). Variable relationships between temperature and aqueous B concentrations within and between geothermal systems are considered to result from either variable B content of the associated rock or variable availability of B. Tholeiitic basalts in Iceland are lower in B than alkali-olivine basalts, the average for the former being 1.2 ppm but 3.8 ppm for the latter [13]. Variations within each group of basalt lavas and minor intrusions are also considerable, most likely due to variable degassing during solidification of the magma rather than variable B content of the initial magma. In the NW-Peninsula the basalts are tholeiitic. Petrologic



**Fig. 8.** Relationship between temperature of waters from the NW-Peninsula and the Southern Lowlands and the concentration of aqueous B derived from the dissolving rock.

data from the Southern Lowlands are limited but both alkalic and tholeiitic basalts are present. The boron present in the rock is, as deduced from [18, 19] partly on a soluble form and partly within the structure of silicates. Relatively old basalts, which have undergone some alteration may have lost a large part of their soluble B. As a result waters percolating through such rocks may gain relatively little B for a certain amount of heating and rock dissolution. In waters from the Hreppar area in the Southern Lowlands B concentrations increase by about 0.4 ppm per 100°C (see Fig. 8). Taking the B content of the rock to be 3.8 ppm which represents the average value in alkali-olivine basalts in Iceland [13] the increase in B concentrations with temperature implies that the amount of rock dissolved by 100 °C water is almost 1/10 kg by every kg of water. In the NW-Peninsula the increase in aqueous B concentrations with temperature is only about 0.08 ppm for temperature increase of 100 °C (Fig. 8). Using a B concentration value for the rock of 1.2 ppm (average for tholeiitic basalt) gives a dissolved rock/water ratio of 1/15 for temperature increase of 100 °C.

## 7. RELATIONSHIP BETWEEN OXYGEN SHIFT AND WATER TEMPERATURE

Like aqueous B concentrations oxygen isotope shift in geothermal waters from the best fit line through the  $\delta^2\text{H} - \delta^{18}\text{O}$  cold water data is a measure of the amount of rock the water has reacted with. There is a general increase in the magnitude of the oxygen shift, not only for the geothermal waters of the present study areas but also of other geothermal waters in Iceland (Fig. 4). It is difficult to assess the increase in the oxygen shift with temperature due to the large scatter of the high-temperature data which are from [20] but it seems to be of the

order of one  $\delta^{18}\text{O}\text{‰}$  unit for every 100 °C, or a little higher. The amount of the shift depends not only on the amount of rock reacted but also on the initial  $\delta^{18}\text{O}$  of the meteoric parent water and on the amount of a seawater component in the geothermal water. The  $^{18}\text{O}$  values of basalts in Iceland lie in the range +3.5 to +5.7 ‰ [21]. Selecting a value of +5 ‰ and taking the initial  $\delta^{18}\text{O}$  value of the geothermal water to be -8 ‰ (corresponds to  $\delta^2\text{H}$  of -56 ‰) an oxygen shift of 1 ‰ corresponds to a ratio of 1/12 for dissolved rock/water. This ratio is in reasonable agreement with the estimated dissolved rock/water ratios derived from B data. The highest oxygen shift values in Fig. 4 of about 5 ‰ correspond to almost 1/1 dissolved rock/water ratios.

## 8. CONCLUSIONS

The source of supply of Cl and B in cold and geothermal waters from the NW-Peninsula and the Southern Lowlands of Iceland are. (1) the atmosphere, i.e. seawater spray and aerosols of marine origin; (2) the rock being dissolved by the water; and (3) marine groundwater. In cold waters, supply from the atmospheric source dominates. In geothermal waters, on the other hand, contribution from the dissolving rock is more important and accounts for practically all the aqueous B to temperatures as low as 30-40 °C. Supply from the dissolving rock increases with temperature indicating that the amount of rock that dissolves per unit mass of water is proportional to the water temperature. In some areas close to the coast there may be a significant supply of B, and especially Cl, to the geothermal water from marine groundwater. In the case of the Southern Lowlands this marine water is considered to have entered the bedrock during the deglaciation period some 10,000 years ago when the area was submerged. On the other hand it is considered that infiltration of seawater under present-day hydrological conditions accounts for the marine groundwater component in some of the geothermal waters from the NW-Peninsula. In waters not containing a significant marine groundwater component the calculated amount of Cl derived from the atmosphere in the geothermal waters is similar to the Cl concentrations in local cold groundwaters, i.e. local precipitation. This is taken to indicate that the geothermal waters represent local precipitation. This interpretation agrees with previous interpretation of  $\delta^2\text{H}$  data in the case of the NW-Peninsula, namely that the geothermal waters represent local precipitation but not with previous interpretation of such data from the Southern Lowlands. In that area the  $\delta^2\text{H}$  of the geothermal waters is lower (more negative) than that of local cold waters. It is considered that the geothermal waters in the Southern Lowlands largely represent local precipitation. The lower  $\delta^2\text{H}$ -values, as compared with the local cold waters, are accounted for the presence of an "ice-age" water component that was precipitated when the climate was considerably colder than that of today and, therefore, isotopically lighter. The relationship between aqueous B concentrations and  $\delta^{18}\text{O}$  with temperature indicate that the amount of rock dissolved by the water is roughly proportional to the water temperature and amounts to some 1/10 to 1/15 kg of rock per kg of water for every 100 °C increase in temperature.

## References

- [1] ÁRNASON, B., Groundwater systems in Iceland traced by deuterium, *Societas Scientiarum Islandica* **42** (1976) 236 pp.
- [2] ÁRNASON, B., Hydrothermal systems in Iceland traced by deuterium, *Geothermics* **5** (1977) 125-151.

- [3] HENLEY, R.W., et al., Fluid-mineral equilibria in hydrothermal systems, *Reviews in Economic Geology* **1**, Society of Economic Geologists (1984) 267 pp.
- [4] FRITZ, P., FONTES, J.C., *Handbook of Environmental Isotope Geochemistry*, Elsevier, Cambridge (1980).
- [5] NUTI, S., Isotopic techniques in geothermal studies, *Application of Geochemistry in Geothermal Reservoir Development*, UNITAR-UNDP publ., Rome (1991) 215-251.
- [6] GIGGENBACH, W.F., Isotopic composition of geothermal water and steam discharges, *Application of Geochemistry in Geothermal Reservoir Development*, UNITAR-UNDP publ., Rome (1991) 253-273.
- [7] MCDOUGALL, I., et al., Magnetostratigraphy and geochronology of northwest Iceland, *J. Geophys. Res.* **89** (1984) 7029-7060.
- [8] JOHNSEN, S., et al., The origin of Arctic precipitation under present and glacial conditions, *Tellus* **41B** (1989) 452-468.
- [9] MERLIVAT, L., JOUZEL, J., Global climatic interpretation of the deuterium-oxygen 18 relationship for precipitation, *J. Geophys. Res.*, **84** (1979) 5029-5033.
- [10] WEDEPOHL H.K. (Ed.), *Handbook of Geochemistry*, Springer-Verlag (1969).
- [11] AIRO, J., The chemistry of groundwater in the Langjökull-Thingvellir drainage area, *Nordic Volcanological Institute report*, Reykjavík (1982) 22 pp.
- [12] SIGURDSSON F., EINARSSON, K., Groundwater resources of Iceland - availability and demand, *Jökull* **38** (1988) 35-53.
- [13] ARNÓRSSON, S., ANDRÉSDÓTTIR, A., Processes controlling the distribution of B and Cl in natural waters in Iceland, in preparation.
- [14] BJÖRNSSON, A., et al., The nature of hot spring systems in Iceland, *Náttúru-fraedingurinn* **60** (1990) 15-38. (In Icelandic with an English summary).
- [15] ARNÓRSSON, S., GÍSLASON, S.R., On the origin of low-temperature geothermal activity in Iceland, *Náttúru-fraedingurinn* **60** (1990) 39-56. (In Icelandic with an English summary).
- [16] ARNÓRSSON, S., ANDRÉSDÓTTIR A., these Proceedings.
- [17] ARNÓRSSON, S., et al., The distribution of Cl, B,  $\delta D$  and  $\delta^{18}O$  in natural waters in the Southern Lowlands of Iceland, *Geofluids '93 Contributions to an International Conference on fluid evolution, migration and interaction in rocks*, British Gas (1993) 313-318.
- [18] ELLIS, A.J., MAHON, W.A.J., Natural hydrothermal systems and experimental hot water-rock interactions. Part II, *Geochim. Cosmochim. Acta* **31** (1967) 519-538.

- [19] HARDER, H., Boron content of sediments as a tool in facies analysis, *Sediment. Geol.* **4** (1970) 153.
- [20] ARNÓRSSON, S., The use of mixing models and chemical geothermometers for estimating underground temperatures in geothermal systems, *J. Volc. Geothermal Res.*, **23** (1985) 299-335.
- [21] HÉMOND, C., et al., Thorium, strontium and oxygen isotope geochemistry in recent tholeiites from Iceland: Crustal influence on mantle-derived magmas, *Earth Planet. Sci. Lett.* **87** (1988) 273-285.



# GEOCHEMICAL AND ISOTOPE STUDIES OF THE GEOTHERMAL AREAS OF CENTRAL AND NORTHERN INDIA

S.V. NAVADA, A.R. NAIR, SUMAN SHARMA, U.P. KULKARNI  
Isotope Division,  
Bhabha Atomic Research Centre,  
Bombay, India

**Abstract** - Isotope and geochemical studies were carried out in Tattapani geothermal area in Central India. The thermal activity in the area is controlled by the ENE-WSW Tattapani fault and NE-SW cross faults.  $\delta D$ ,  $\delta^{18}O$  of hot springs and hot water well samples show enrichment compared to the cold springs. Some mixing of the shallow cold waters with the hot waters is possible in some hot springs. Tritium data show that the hot waters have a residence time of over 30-40 years. Hot springs of Orissa and Bihar occur on an ENE-WSW lineament zone which is the extension of the zone where Tattapani geothermal area exist. The chemistry of hot spring samples of Bihar are similar to Tattapani geothermal waters. The hot springs of Orissa are high in sodium and chloride due to contribution from a marine source. The isotopic composition of a hot spring sample from Surajkund in Bihar is similar to thermal waters of Tattapani. The thermal water of Badrinath and Tapoban in northern India are situated at an elevation of 2000-3000 m above mean sea level in the Himalayan terrain. Thermal waters from Badrinath are of the NaCl type while those of Tapoban are of the  $Ca(HCO_3)_2$  type. Thermal waters from Tapoban and Badrinath fall near the local meteoric line and show negligible oxygen shift. From  $\delta D$  - altitude relationship the recharge area of Badrinath thermal waters is at 3200 m and those of Tapoban thermal waters at 2700 m.

## 1. GEOTHERMAL AREAS IN CENTRAL INDIA

### 1.1 Tattapani Geothermal Area

#### 1.1.1 Introduction

The Tattapani area, (Fig. 1) Surguja district Madhya Pradesh (M.P.) in Central India has one of the strongest thermal manifestations amongst the 46 known thermal areas confined within an ENE-WSW trending megatectonic zone in the Indian shield, commonly referred to as Son-Narmada-Tapti-lineament (SONATA) zone. It comprises several hot springs with moderate gas activity and silica deposits around the vents of the springs. The temperature of these springs varies from 50 °C to 98 °C and their cumulative discharge is about 60 litres per minute. The thermal activity is controlled by the ENE-WSW Tattapani fault and NE-SW cross faults. Under a Geological Survey of India (GSI) - Oil and Natural Gas Commission (ONGC) programme a number of boreholes were drilled upto 300 - 500 m depth to ensure continuous supply of thermal fluid, with temperature of 100 °C at 200 l/min for planning a binary cycle power plant of 20 KW capacity.

#### 1.1.2 Geological Setting

Two distinct lithological sequences belonging to the proterozoic and Gondwana super groups are exposed in the area [1]. Proterozoic rocks comprise grey-pink gneiss while the Gondwana super group comprises green splintery shales and sand- stones. Two major lineaments trending ENE-WSW are present in the area and can be seen on landsat imagery.

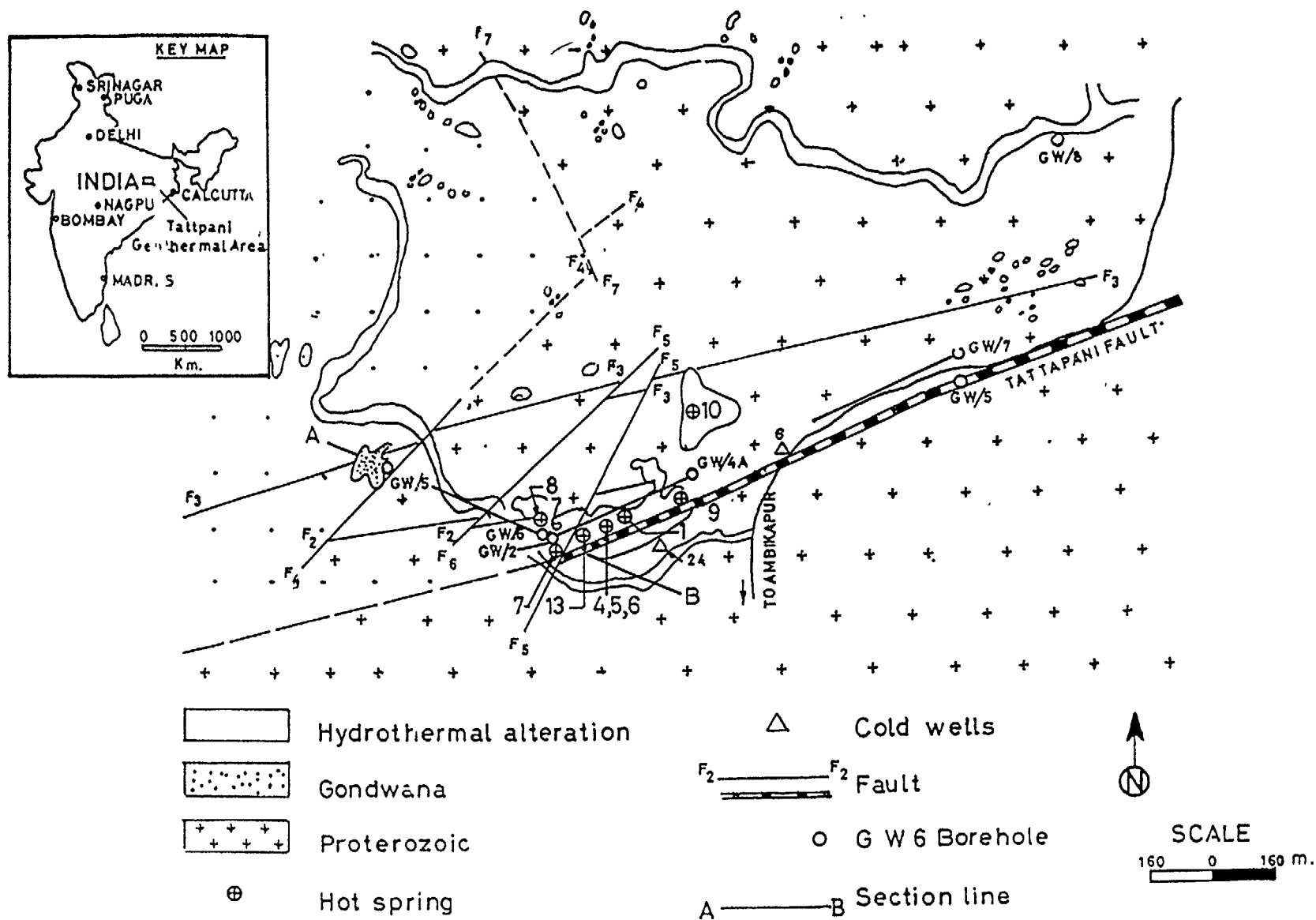


FIG. 1. The Tattapani geothermal area.

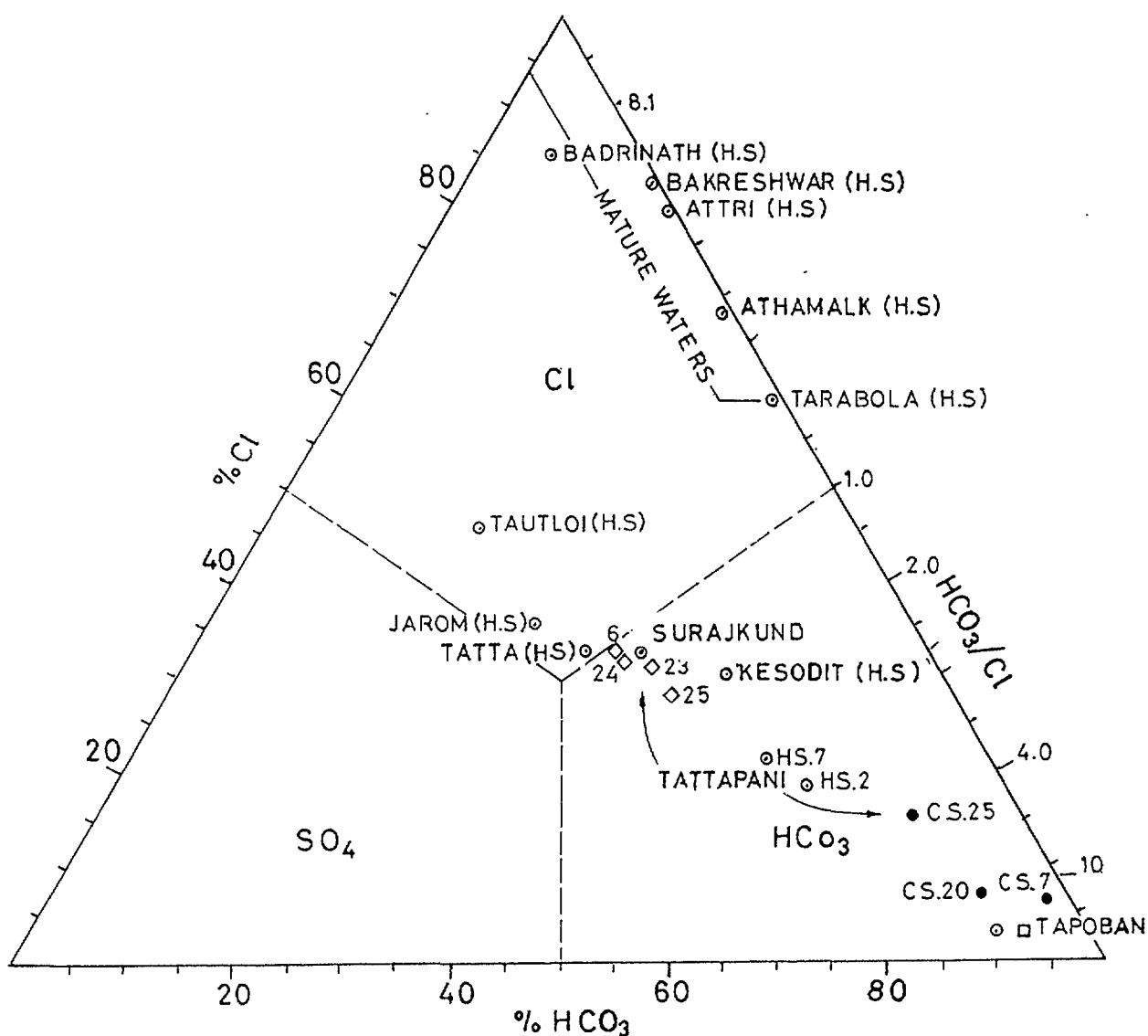


FIG. 2. Relative  $\text{Cl}$ ,  $\text{SO}_4$  and  $\text{HCO}_3$  of samples from geothermal areas in central and northern India.

Another fault with similar trend, Tattapani fault, along which the geothermal activity occurs can be seen near Tattapani village. Several cross faults have been mapped in the area. The area is tectonically active with fault bound blocks exhibiting vertical and lateral movements.

### 1.1.3 Hydrochemistry

Chemical analysis of thermal and non thermal waters from the Tattapani area has been reported by Thussu et al (1987) [2]. Two distinct types of water are recognised in the area. Type I waters is represented by cold springs and is of the  $\text{Ca-Mg-HCO}_3$  type while type-II waters is represented by dug wells and hot springs. Type II non-thermal waters is of the  $\text{NaCl}$  and  $\text{Na-Cl-SO}_4$  types while the hot waters are of the  $\text{NaHCO}_3\text{-Cl-SO}_4$  type. The relative  $\text{Cl}$ ,  $\text{SO}_4$  and  $\text{HCO}_3$ , contents of hot springs, drilled wells and cold spring samples have been presented on a triangular diagram (Fig.2). The figure shows that hot spring samples are shifted towards higher relative  $\text{HCO}_3$  values as compared to the drilled well samples. This could be due to some contribution of the cold waters to the spring discharge.

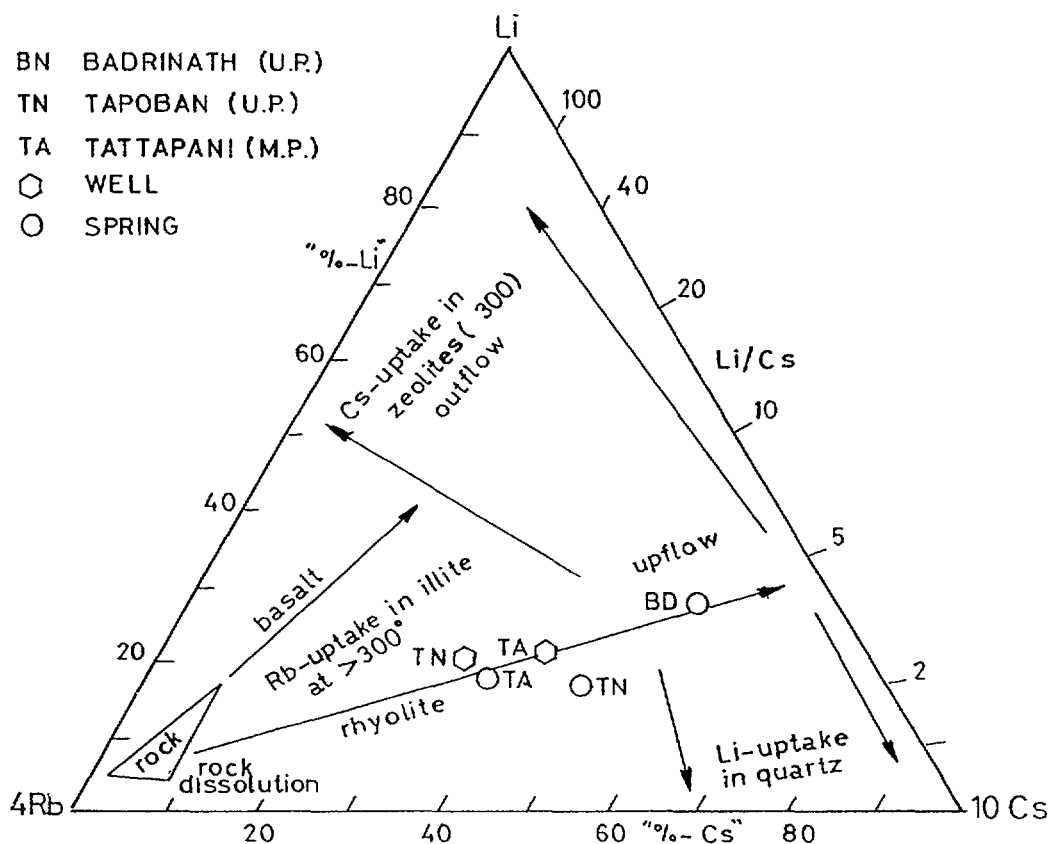


FIG. 3. Relative Li, Rb and Cs amounts in thermal waters of Tattapani, Tapoban and Badrinath.

Relative Li, Rb, and Cs contents in thermal water discharges of Tattapani are shown in Fig. 3. The points for the well discharge and the hot spring plot near to each other with low Li/Cs similar to rhyolite.

#### 1.1.4 Geothermometry

Subsurface temperatures were calculated using various chemical geothermometers. Silica thermometry, although useful for low discharge and non boiling springs, may not give the correct base temperature for these springs as silica precipitate around their spouts. However, it could give minimum possible base temperatures. The reservoir temperatures computed using chalcedony and the K-Mg geothermometers are given in Table 1.

Table 1. Reservoir temperature and computed chalcedony and K-Mg geothermometry temperatures.

Hot spring/hot water drillhole	Temp.(°C) measured	Temperature (°C) computed	
		chalcedony[3]	K -Mg [4]
HS-7	98	122	122
TAT-6	100	120	126
TAT-24	100	113	132

Thus the temperature of the reservoir computed is 120 - 130 °C.

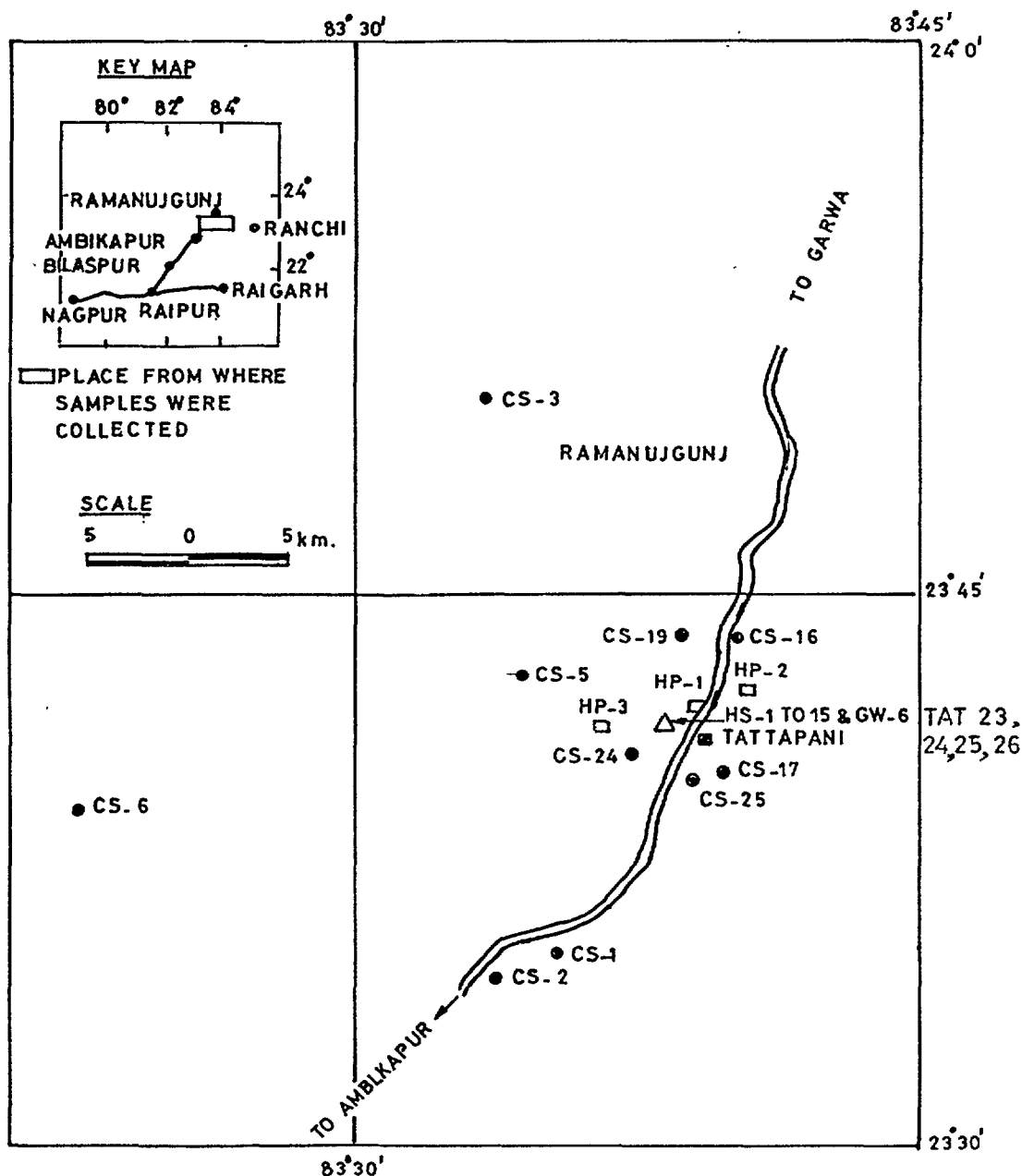


FIG. 4. Location map of water samples from Tattapani hot spring area.

#### 1.1.5 Isotope study

Samples from hot springs, hot water from drilled wells and cold springs were collected and analysed for  $\delta D$  and  $\delta^{18}O$ . Location of the sample points is shown in Fig. 4. A few samples were analysed for tritium.

#### $\delta D$ and $\delta^{18}O$ results

$\delta D$  -  $\delta^{18}O$  plot is shown in Fig. 5. It can be seen that cold spring waters fall on the meteoric line. The hot springs and the hot water well samples are enriched in both  $\delta D$  and  $\delta^{18}O$  and fall slightly off the meteoric line. Since the permeability of the rock is low, the hot springs have low discharge. Their temperature is around boiling point. It is likely that the

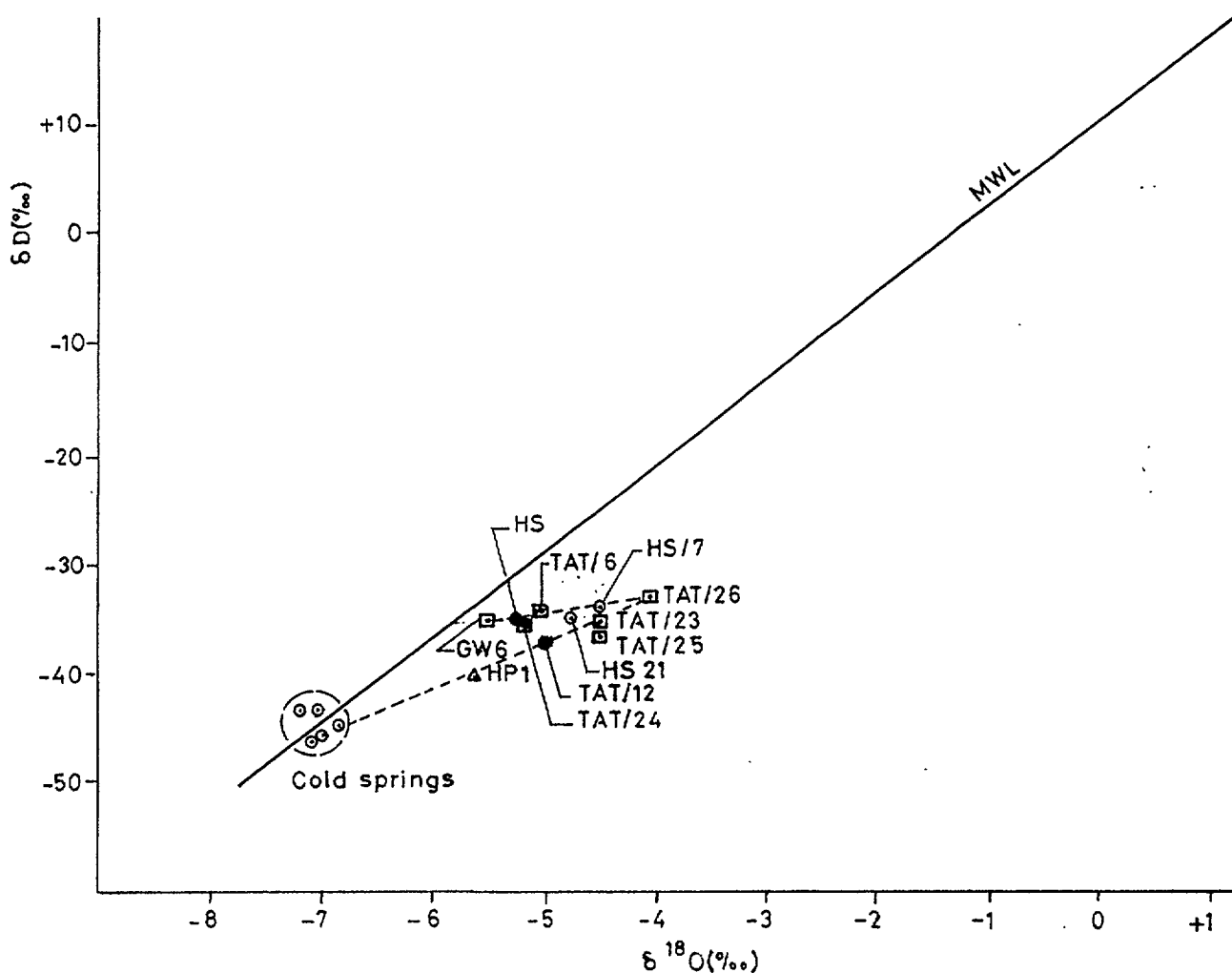


FIG. 5.  $\delta D$ - $\delta^{18}O$  plot, Tattapani.

hot water has lost some steam by boiling in the upflow. Boiling of hot water is indicated by the presence of calcite in the hydrothermally altered material associated with present day thermal regime. Hence some subsurface as well surface steam loss has lead to the observed isotopic composition.

The drill hole water sample from TAT/6 has been obtained from a depth of 165 to 215 m. The temperature of the steam water mixture flowing from the borehole is 105 °C while the sample was collected at 79 C. On  $\delta D$  -  $\delta^{18}O$  plot the TAT/6 sample falls near the meteoric line. Other drilled well waters, TAT/12, TAT/23, TAT/24 and TAT/25 have isotopic composition similar to the hot springs. TAT/26 drilled well sample has maximum oxygen-18 shift possibly due to some water rock interaction. The hot spring and hot water drilled well samples fall on a line which intersect the meteoric line at  $^{18}O = -6 \%$  and  $D = -37 \%$  which is considered to be the isotopic composition of the recharging waters for the hot waters. The cold springs are more depleted compared to these hot waters showing that they have a different source. Hand pump sample (HP-1) has a temperature of 45 °C. It is located on the channel bringing hot water laterally to the east of from the main thermal area. On the  $\delta D$  -  $\delta^{18}O$  plot, it has intermediate composition between the hot and cold waters. In Fig. 6  $\delta D$  values are plotted against water temperature. Here it is seen that samples from HP-1, CS-23, HS-2, HS-10 etc. fall on mixing line between the cold waters and hot spring samples HS7, HS8 etc.

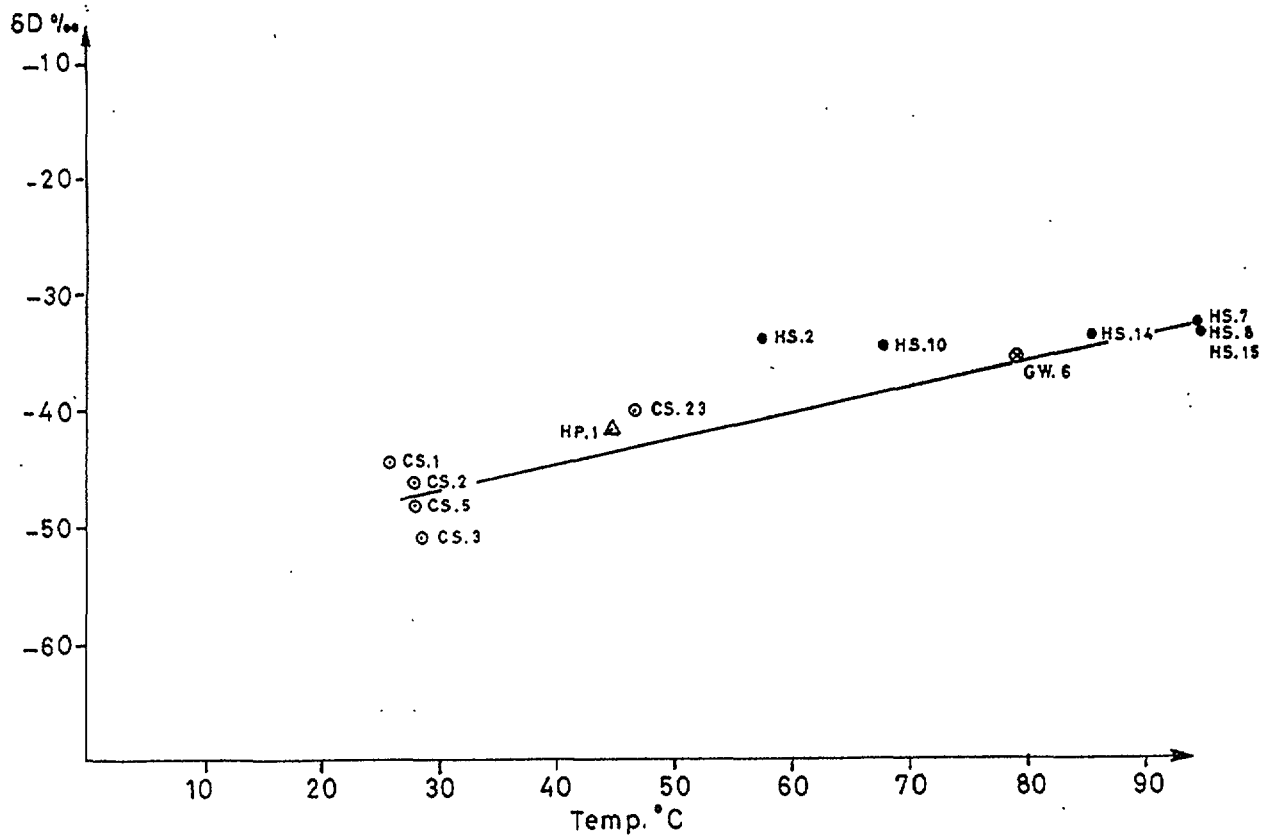


FIG. 6.  $\delta D$  vs temperature, Tattapani.

The distribution of  $\delta^{18}O$  (Fig.7) of the hot spring and borehole water show that the isotope values are lowest in the vicinity of hot springs HS-7 and HS-8. The contours along the axis of HS-7, GW-6 and HS-8 indicates a control by cross fault F5. The hot water possibly flows upward through cross fault F5 and it enters the present thermally active area near HS7. It dissipates laterally both eastward and westward and discharges through various crossfaults F1, F2 and F5 [5].

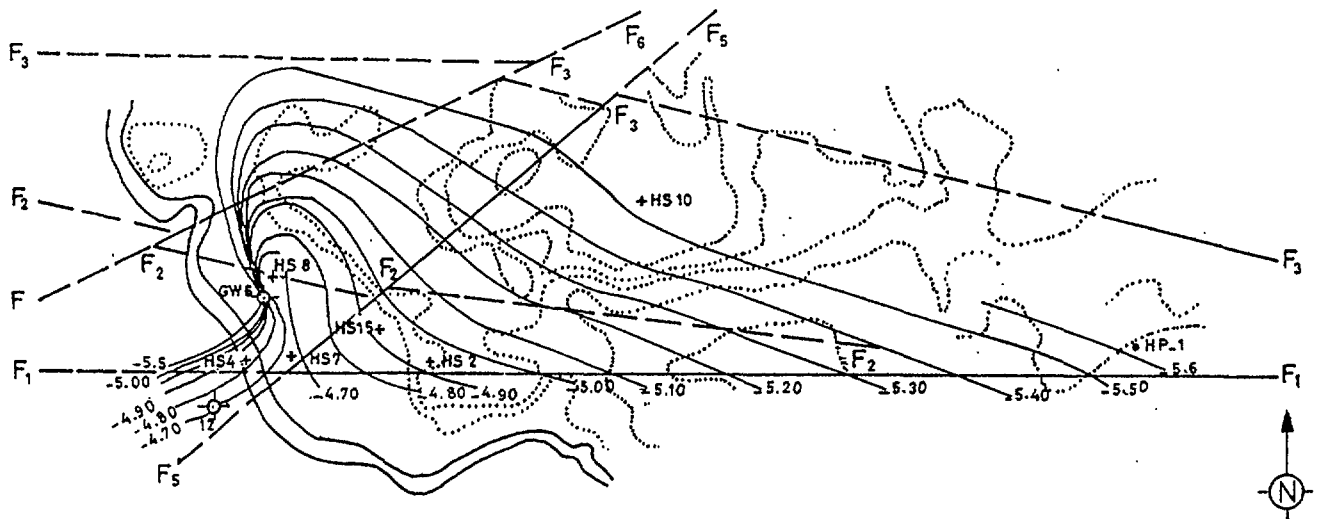


FIG. 7. Oxygen-18 compositions of Tattapani hot springs and bore holes.

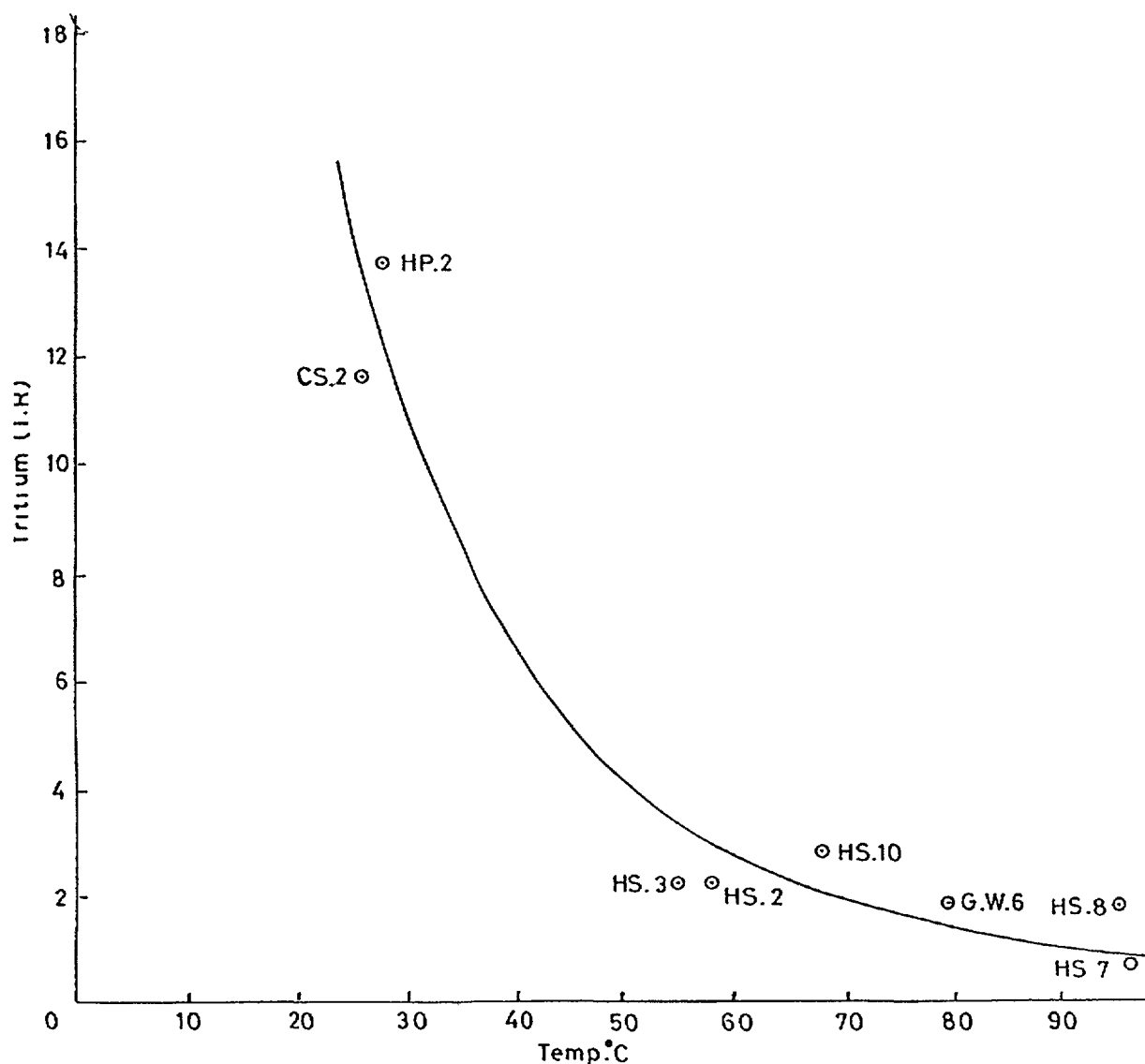


FIG. 8. Tritium content vs temperature of water samples from Tattapani geothermal area.

### *Tritium Results*

The plot of tritium contents versus temperature of the samples is presented in Fig. 8. Cold spring CS2 and hand pump shallow well sample HP-2 have tritium content in the range of 11-14 TU. The tritium content of modern precipitation was about 10 -15 TU. Hence cold springs are being recharged by modern precipitation. Hot spring HS7 as well as drilled well samples TAT/25 has negligible tritium ( $< 1$  TU) showing that these waters are older than 30 - 40 years. Hot spring samples HS2, HS3, HS10, and drilled well sample TAT/6 have small amounts of tritium (2 TU) showing possibly some mixing of hot waters with small amounts of cold water with higher tritium content.

### *Comparison of isotopic results obtained in 1985 and 1992*

The  $\delta D$  and  $\delta^{18}O$  and  $^3H$  values of samples collected in 1985 and 1992 are shown in Table 2.



Table 2. Comparison of D,  $^{18}\text{O}$  and  $^3\text{H}$  values for HS-7 and TAT/6 for 1985 and 1992.

Sample	Collected in	$\delta\text{D}$ % ( $\pm 1$ )	$\delta^{18}\text{O}$ % ( $\pm 0.2$ )	$^3\text{H}$ ( $\pm 0.3$ )
HS-7	1985	- 32.9	-4.7	0.6
	1992	- 34.8	-4.5	0.6
TAT/6	1985	- 35.8	-5.5	1.9
	1992	- 34.5	-5.0	2.2

The  $\delta\text{D}$ ,  $\delta^{18}\text{O}$  and  $^3\text{H}$  of HS-7 for 1985 and 1992 are similar. In the case of TAT-6 small enrichment (0.5 %) in  $\delta^{18}\text{O}$  observed.  $\delta\text{D}$  and  $^3\text{H}$  are, on the other hand, similar for the 1985 and 1992 samples.

#### 1.1.6 Discussions and conclusions

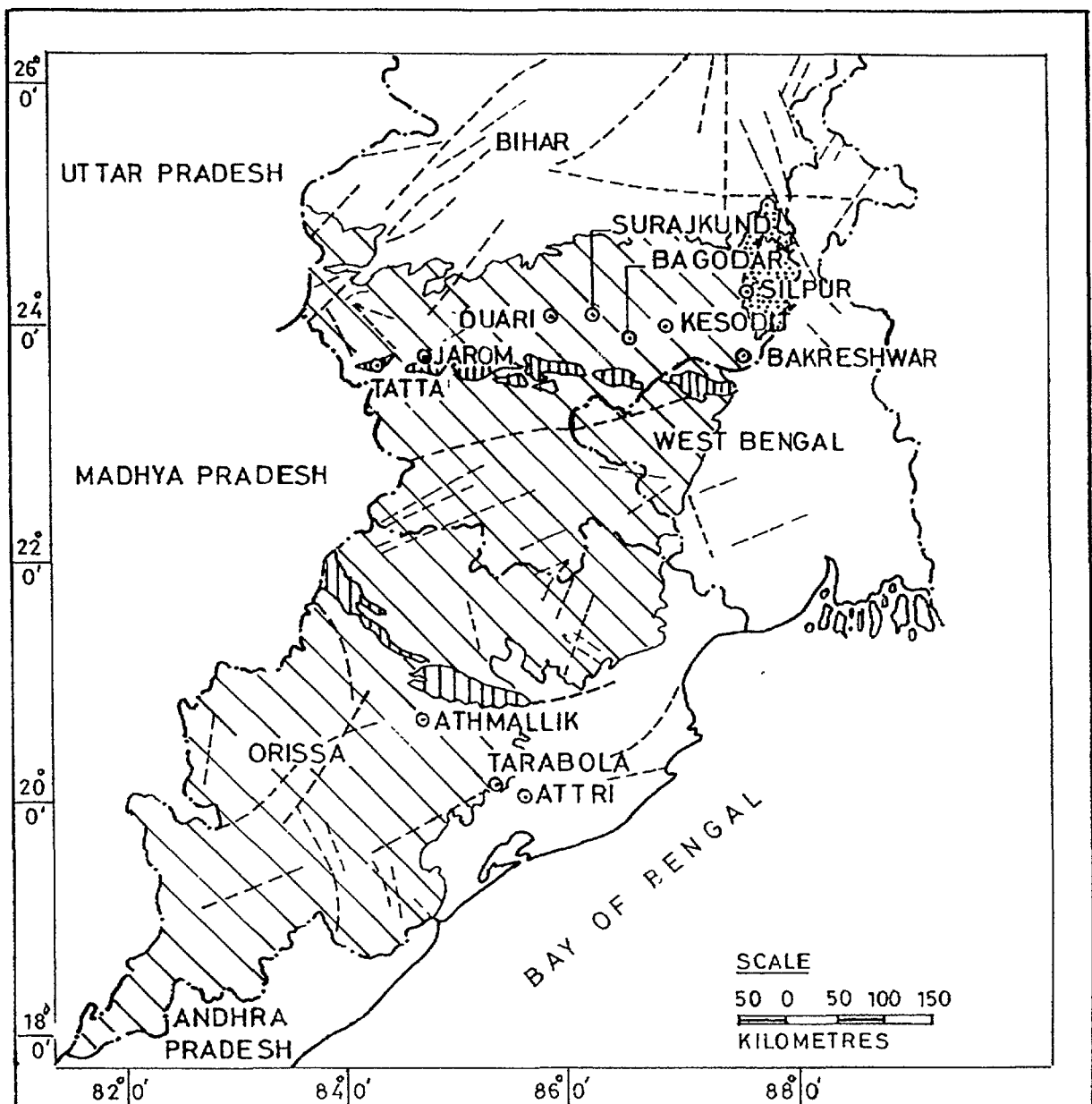
The hydrogeology, hydrochemistry and isotope results show that: i) The thermal activity in the area is controlled by the ENE, WSW striking Tattapani fault and NE-SW cross faults. ii) The hot springs have low discharge their waters are alkaline  $\text{NaHCO}_3$  - $\text{Cl-SO}_4$  type waters with silica deposits around the vents. The reservoir temperature computed from chemical geothermometer is 130 C. iii) Stable isotope results show that hot springs and hot water drilled well samples are enriched in  $\delta\text{D}$  and  $\delta^{18}\text{O}$  compared to cold spring waters. Some mixing of the shallow cold waters with the hot waters is possible in some hot springs. This is confirmed by tritium results and chemistry. Enrichment in  $\delta^{18}\text{O}$  observed in drilled well sample TAT/26 could be due to some water rock interaction. Tritium results of hot spring samples HS7 and drilled well samples TAT/12, 23, 24, 25 and 26 show that the hot waters have a residence time of over 30 - 40 years.

## 1.2 Geothermal areas in Orissa and Bihar

The geothermal areas of Orissa and Bihar occur within an ENE-WSW lineament zone which is an extension of Son-Narmada-Tapti lineament. In Orissa the hot springs are located in Attri, Tarbola and Athamalik in the Puri and Dhenkal districts. (Fig. 9). The temperature of the hot springs ranges from 50 to 66 °C and the flow rate is 2 litres/s ec. The thermal manifestations at Tatta and Jarom in Bihar occur close to the hot spring belt of Surguja district of M.P. The temperature of the hot springs vary from 50 to 65 °C. The Surajkund hot springs have a temperature range of 47 C to 88 °C with a cumulative discharge of about 4.1 litres/second.

### 1.2.1 Geology

The thermal manifestations of Attri, Tarabola and Athamallik are located withing the Eastern Ghat province represented by granites, charnockites and kondalite suit of rocks. Tarabola hot springs occur very close to the intersection of two major lineaments of which one is trending NE-SW and extending from Tattapani to Tarabola and the other trending NW-SE and extending from Athamalik to south of Attri. The Athamallik hot spring is located very close to the Mahanadi river at the contact between the Archeans and Gondwana rocks and occurs at the intersection of two major fractures trending NW-SE and NNE-SSW.



#### INDEX




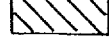
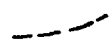
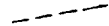
-  ALLUVIUM (QUATERNARY)
-  RAJMAHAL TRAPS (JURASSIC CRETACEOUS)
-  GONDWANAS (PALAEOZOIC/MESOZOIC)
-  CRYSTALLINES METAMORPHICS AND SEDIMENTARIES (ARCHAEOAN/PROTEROZOIC)
-  MEGALINEAMENT
-  INTERMEDIATE/MINOR LINEAMENT

FIG. 9. Thermal springs of Bihar, Orissa and West Bengal.

The thermal manifestation at Tatta and Jarom occur in ENE-WSW trending belt. The Tatta hot springs is located within a fault zone across the rocks of Barakar formation. The Jarom hot spring is located at the intersection of three fractures trending ENE-WSW, N-S

### 1.2.2. Geochemistry

The chemistry of thermal waters in Orissa is characterised by very low sulphate but high sodium and chloride contents (Na-Cl type water). High Na and Cl could be due to marine influence and negligible  $\text{SO}_4$  due to bacterial reduction of  $\text{SO}_4$  but  $\text{H}_2\text{S}$  smell is found in some of these springs. In the relative Cl,  $\text{SO}_4$ ,  $\text{HCO}_3$ , plot (Fig.4) the hot spring samples fall close to the Cl corner. The chemistry of thermal waters of Bihar (Tatta, Jarom, Surajkund etc.) are of the Na- $\text{HCO}_3$ -Cl- $\text{SO}_4$  type, or similar to the thermal waters of the Tattapani geothermal area. On the Cl,  $\text{SO}_4$ ,  $\text{HCO}_3$  plot the hot springs samples fall near those of hot water drilled well samples of Tattapani area. Surajkund hot springs have high F content (20 ppm).

### 1.2.3 Gas chemistry

The results of the gas analysis in moles % of the samples collected from hot springs in Orissa are given in Table 3.

Table 3. Gas analysis (moles %) of hot springs in Orissa

	Attri	Tarabola	Athamallik
$\text{H}_2$	-	-	-
He	1.46	0.06	0.35
$\text{N}_2$	32.05	7.85	22.85
$\text{CH}_4$	4.15	4.79	0.05
$\text{CO}_2$	61.40	86.79	76.36
$\text{H}_2\text{S}$	0.94	0.48	0.37
$\text{NH}_3$	0.01	0.02	0.02
CO	-	-	-

From the table it is evident that  $\text{CO}_2$  and  $\text{N}_2$  are the main gas constituents. He is present up to 1.46 % in Attri spring. The hot springs in Bihar are high in He, 3.9 % at Surajkund.

### 1.2.4 Geothermometry

Using the silica and potassium - magnesium geothermometer the reservoir temperature has been computed and the results are given in Table 4.

Table 4. Geothermometry temperatures of hot spring in Bihar and Orissa

Location	Measured temperature, °C	Temperature computed, °C chalcedony <sup>[3]</sup>	Temperature computed, °C K-Mg <sup>[4]</sup>
Tatta	65	97	98
Jarom	57	135	112
Surajkund	88	122	122
Attri	57	107	103
Tarabola	66	94	94
Athamallik	59	107	-

Thus the reservoir temperature range from 100 °C - 135 °C for Tatta, Jarom, Surajkund group of springs and from 95 °C- 110 °C for Attri, Tarabola, Athamallik group of springs.

#### 1.2.5 Isotope study: Orissa hot spring locality

Samples from hot springs, cold springs, hand pumped shallow wells and borewells were sampled in April 1991 and analysed for  $^2\text{H}$  and  $^{18}\text{O}$ . The results obtained are presented as  $\delta\text{D}$  -  $\delta^{18}\text{O}$  and  $\delta^{18}\text{O}$  - Cl plots (Figs. 10 & 11). From the  $\delta\text{D}$  -  $\delta^{18}\text{O}$  plot it can be seen that the composition of the hot springs from Athri and Kesodit are generally enriched in the heavy isotopes compared to the cold springs. This may be due to evaporation effect. However, the thermal and non-thermal waters from Athamallik show similar  $\delta\text{D}$  and  $\delta^{18}\text{O}$  values. The hot springs fall near the meteoric line showing that they are of meteoric origin.

In the  $\delta^{18}\text{O}$  - Cl plot the thermal and non thermal-waters show some correlation in the case of Attri samples. These samples are located near the coast and their salinity is due to supply from marine groundwaters. In the Athamallik samples even though the thermal waters have higher chloride compared to non- thermal waters, there is no change in the  $\delta^{18}\text{O}$  content. Athamallik is located away from the coast and Cl in these waters could be derived from the rock with which the water interacts.

All the hot spring samples in Bihar fall near the meteoric line consistent with their meteoric origin. Except for hot springs from Surajkund and Kesodit the other hot springs from Tatta, Jarom, Duari and Bagodar have  $\delta\text{D}$  and  $\delta^{18}\text{O}$  values similar to non-thermal waters. (Fig. 12). Hot spring samples from Surajkund and Kesodit are slightly enriched compared to non-thermal waters possibly due to evaporation.

#### 1.2.6 Discussion and conclusions

The hot springs of Orissa and Bihar occur in the ENE-WSW lineament zone which is an extension of the zone running through Tatapani. The chemistry of hot spring samples of Bihar are similar to Tatapani geothermal waters. The hot springs of Orissa are high in Na and Cl due to supply from a marine source. The  $\delta^{18}\text{O}$  of Attri thermal and non-thermal waters correlate with chloride showing some sea water contribution. In Athamallik which is away from the coast the high Cl content of hot springs is explained by rock leaching. The isotopic composition of the hot spring sample from Surajkund is similar to the hot springs of Tattapani.

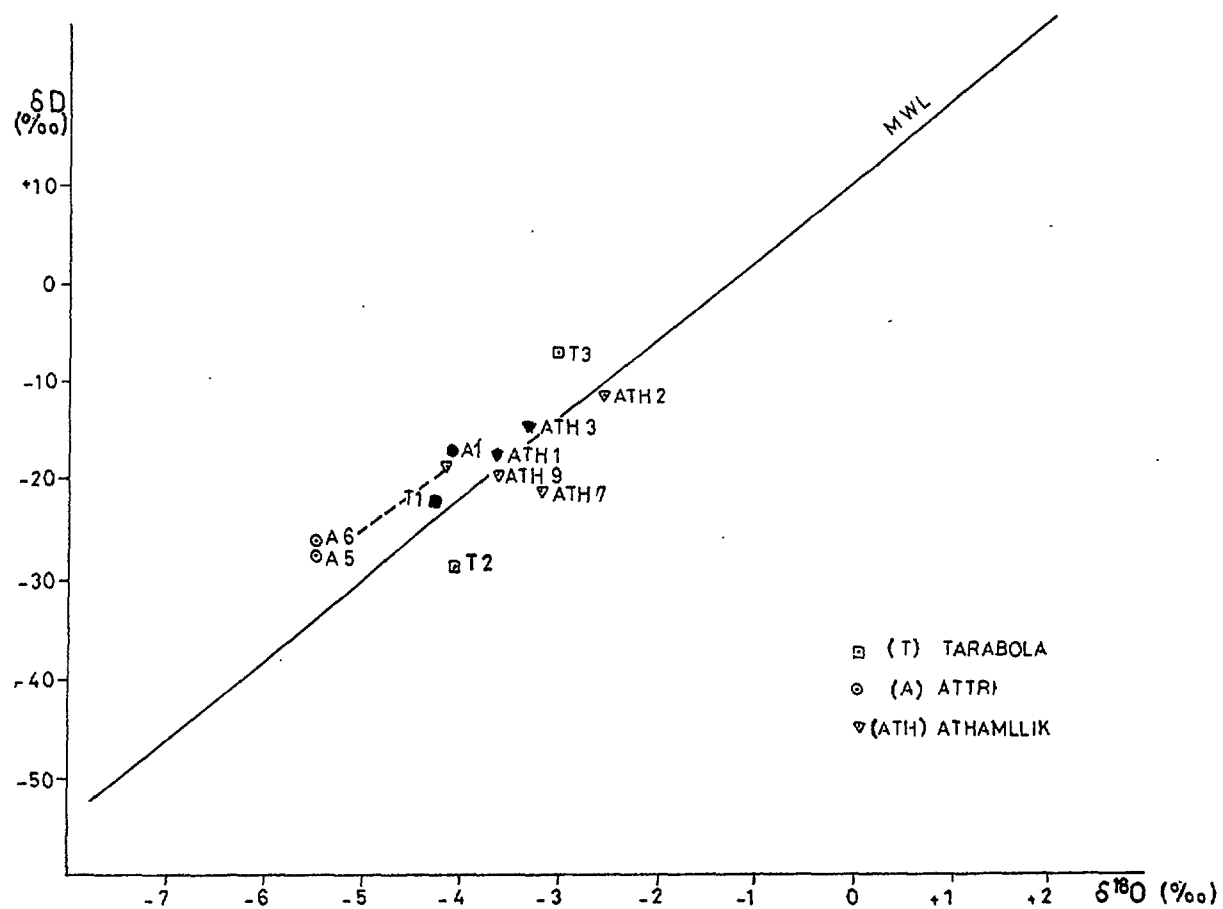


FIG. 10.  $\delta D$ - $\delta^{18}O$  plot of samples from hot spring localities in Orissa.

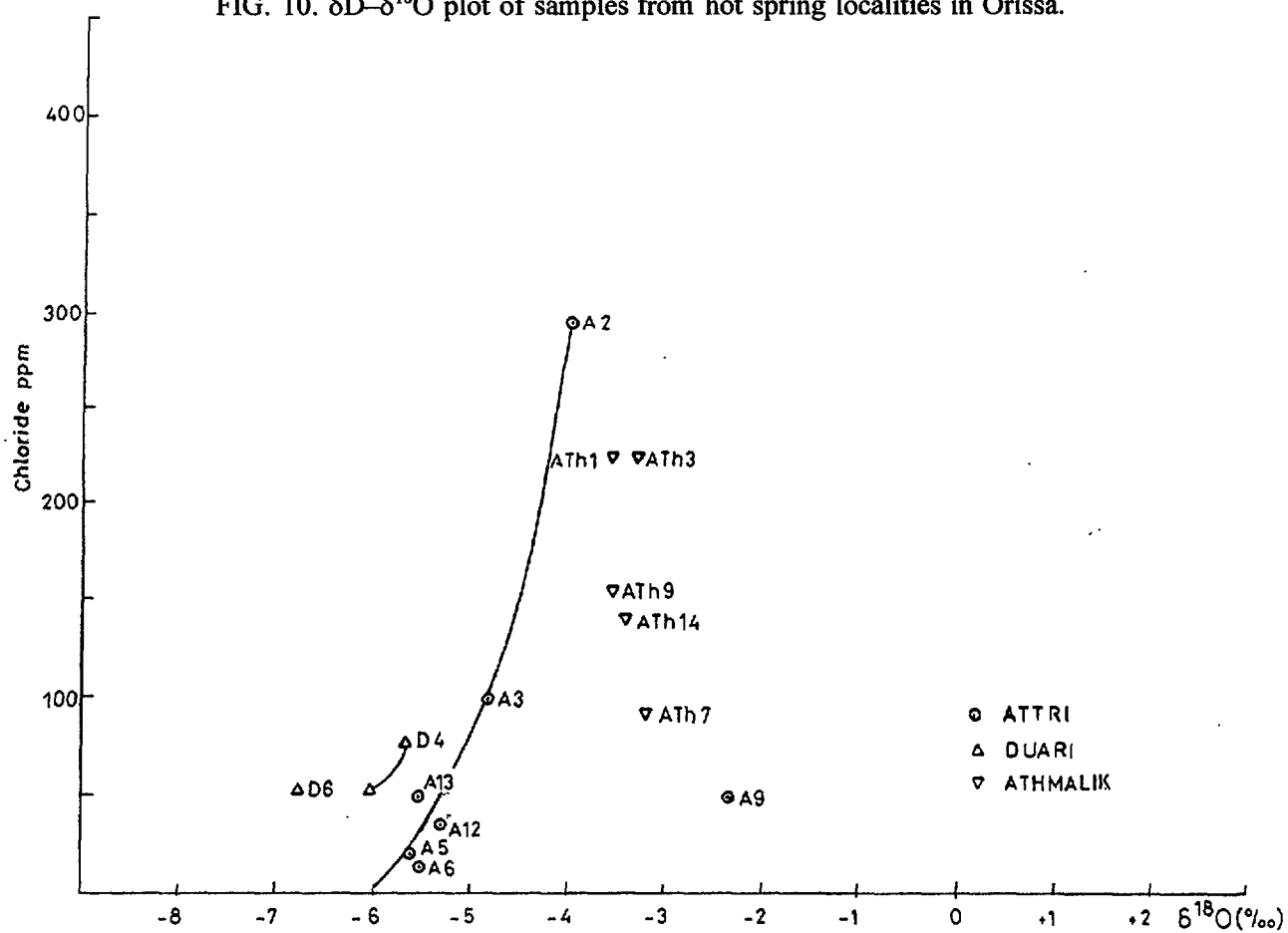


FIG. 11.  $\delta^{18}O$ - $Cl^-$  relationship of hot springs and TW waters from Orissa.

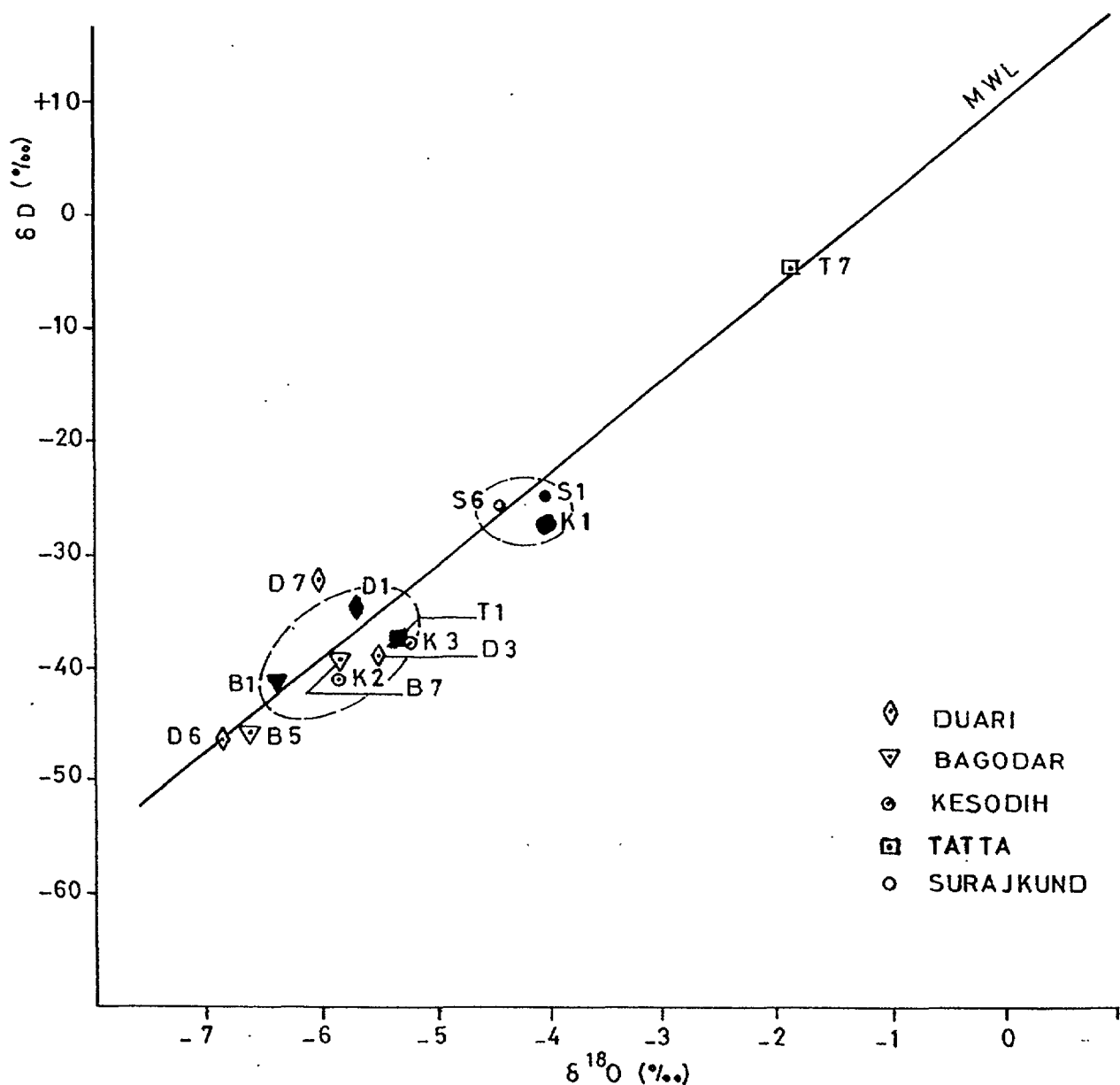


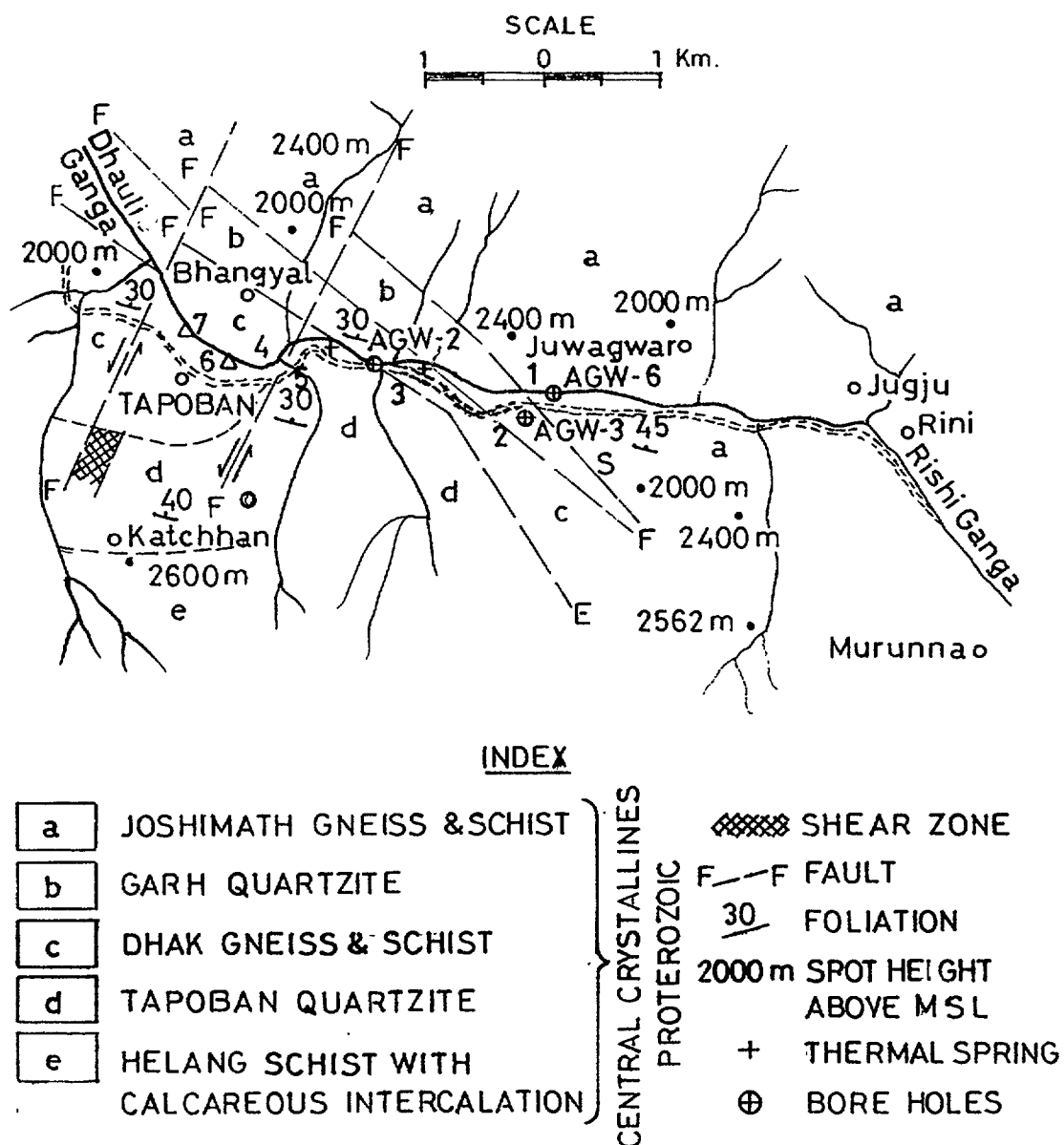
FIG. 12.  $\delta D$ - $\delta^{18}O$  plot, Bihar.

## 2. GEOTHERMAL AREAS IN NORTHERN INDIA

### 2.1 Thermal springs in the Alaknanda valley, Uttar Pradesh, Northern India

#### 2.2.1 Introduction

Thermal springs of Badrinath in Alaknanda valley and Tapoban in the Dauliganga valley are located at an elevation of 2000 - 3000 m above mean sea level, in the Himalayan terrain. The Badrinath hot springs are located at a higher elevation compared to the Tapoban hot springs. There are a dozen thermal springs clustered around 4 localities in the Tapoban area. The rocks in the Tapoban and Badrinath areas belong to the Central Crystallines. The thermal springs in Tapoban emerge in the Tapoban quartzite members. The quartzite and the underlying schist of the Helang formation form the shallow reservoir in the area [6]. The



- 1 AGW- 6 BORE HOLE (HOT)
- 2 AGW- 3        "      (HOT)
- 3 AGW- 2        "      (HOT)
- 4 HOT SPRING ON THE LEFT BANK OF TAPOBAN NALA
- 5 TAPOBAN NALA
- 6 COLD SPRING NEAR OLD SCHOOL
- 7 COLD SPRING 100 M. AWAY BHANGYAL BRIDGE

FIG. 13. Tapoban geothermal area, district Chamoli, Uttar Pradesh.

maximum temperature of the hot springs is 65 °C. Three exploratory bore holes (Fig. 13) were drilled by the Geological Survey of India (AGW-2, AGW-3, AGW-6) and from AGW-3 thermal water discharges at 13 litres/sec at a temperature of 90 °C. Mid tertiary granite is known to occur in deeper zones (~500 m) and hence the possibility of still younger phases of acid magmatism, not yet exposed by erosion, cannot be ruled out. Such acid magmatic bodies may be contributing heat to the geothermal system.

### 2.2.2 Major ion chemistry

The hot spring and hot water well samples of Tapoban are of the  $\text{Ca}(\text{HCO}_3)_2$  type, whereas the Badrinath hot springs are  $\text{NaCl}$  type waters. On the relative  $\text{Cl}$ ,  $\text{HCO}_3$ ,  $\text{SO}_4$  plot (Fig.4) the Tapoban thermal waters fall near the  $\text{HCO}_3$  corner whereas the Badrinath hot springs fall near the chloride corner. The drilled well thermal water sample from AGW-3 (Tapoban) has a higher  $\text{HCO}_3$  content than the hot spring in the area.

### 2.2.3 Minor and trace ions

Relative  $\text{Li}$ ,  $\text{Rb}$ ,  $\text{Cs}$  concentrations for the Tapoban and Badrinath thermal waters has been plotted in Fig. 5. The  $\text{Li}/\text{Cs}$  ratios for Tapoban and Badrinath spring discharges are similar. There is a small increase in the  $\text{Li}/\text{Cs}$  of hot water drilled well sample compared to spring sample of Tapoban.

Relative  $\text{Cl}$ ,  $\text{Li}$  and  $\text{B}$  contents in thermal water of Badrinath and Tapoban show that Badrinath hot springs fall near the chloride corner with low  $\text{B}/\text{Cl}$  ratio (Fig.14). The Tapoban thermal waters fall nearer the  $\text{B}$  corner with higher  $\text{B}/\text{Cl}$  ratio probably due to presence of shales in the reservoir, but such rocks are known to be relatively rich in  $\text{B}$ .

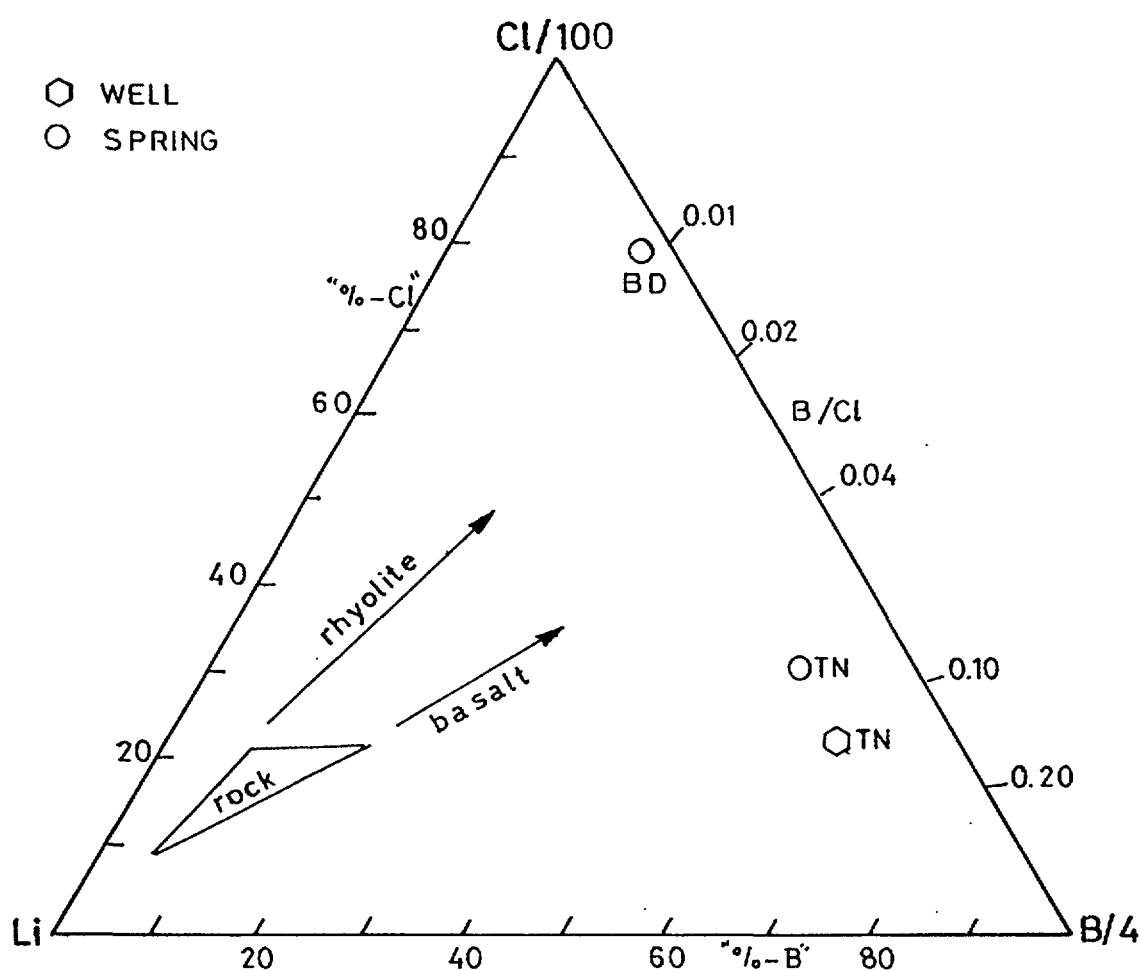


FIG. 14. Relative  $\text{Cl}$ ,  $\text{Li}$  and  $\text{B}$  contents in thermal waters from Tapoban (TN) and Badrinath (BD).



#### 2.2.4 Gas chemistry

The results of the chemical analysis of gas samples collected from Badrinath and Tapoban hot springs [7] are as follows:

Table 5. Gas Analysis (moles %) of Badrinath and Tapoban Hot springs

	H <sub>2</sub>	He	O <sub>2</sub>	N <sub>2</sub>	CH <sub>4</sub>	NH <sub>3</sub>	CO <sub>2</sub>
Tapoban H.S.	tr	0.09	2.43	18.96	tr	tr	78.52
Badrinath H.S.	tr	0.01	tr	tr	tr	tr	99.99

The results show that CO<sub>2</sub> is the main gas component in the above areas.

#### 2.2.5 Geothermometry

The reservoir temperature of Tapoban and Badrinath systems have been computed using the silica geothermometer. The results are presented in Table 6.

Table 6. Reservoir temperature of Tapoban and Badrinath system

	Temperature measured °C	Temperature computed °C Chalcedony[3]
Tapoban H.S.	59	88
Tapoban Borewell	90	99
Badrinath H.S.	55	120

Thus the reservoir temperature for Tapoban geothermal water is 100°C and for Badrinath geothermal waters is 120°C.

#### 2.2.6 Isotope study

The  $\delta D$  and  $\delta^{18}O$  results have been plotted in Fig (15). The  $\delta D$ ,  $\delta^{18}O$  values of the cold springs surface waters etc. were used to obtain the local meteoric water line. The regression line of the local meteoric water line had an equation of  $\delta D = 7.7 \delta^{18}O + 13.0$  ( $r^2 = 0.94$ ,  $n=7$ ). The hot spring and the hot water drilled well samples fall approximately on the local meteoric line showing no oxygen-18 shift.

The hot water well sample AGW-6 has a similar isotopic value as AGW-3. Hence lower temperature of discharge from AGW-6 may be due to cooling by conduction rather than due to mixing of near surface water.

The  $\delta D$  and  $\delta^{18}O$  values of the hot spring and the hot water borewell samples of Tapoban and Badrinath are low compared to the cold springs. They indicate a higher altitude of recharge for the hot springs compared to the cold springs. The altitudes of recharge of thermal waters have been estimated using D-altitude plot for the Himalayas. The D - altitude plot was constructed from snow samples collected from different altitudes in the Himalayan

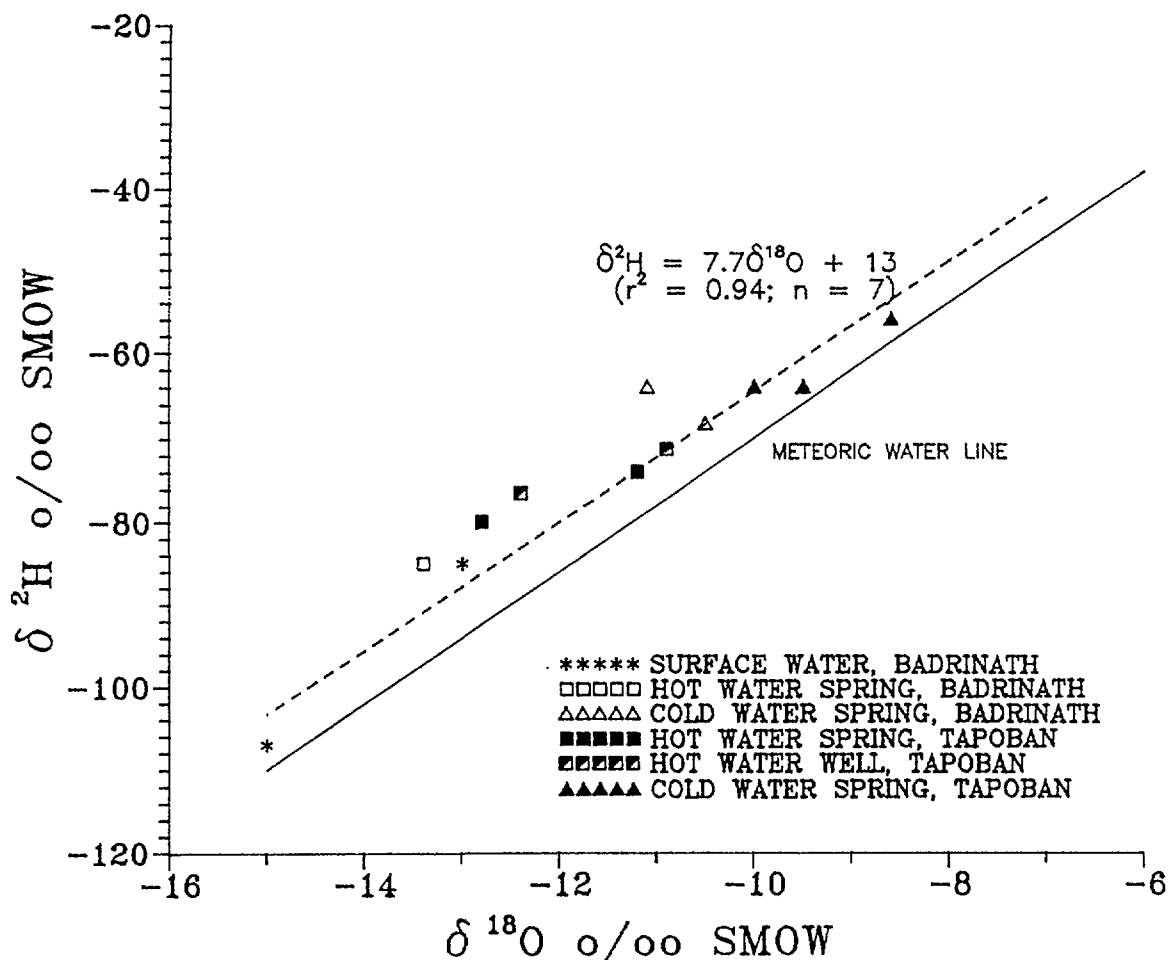


FIG. 15.  $\delta^2\text{H}$ - $\delta^{18}\text{O}$  graph of samples, Badrinath and Tapoban geothermal areas.

ranges in Himachal Pradesh and Ladakh (J & K) [5]. The hot spring and hot water borewell in Tapoban have a maximum altitude of recharge of 2700 m while the altitude of recharge for the hot spring in Badrinath is 3200 m.

The tritium values of the hot spring and hot water borewell samples in Tapoban are in the range of 21-27 TU which are higher than the values of cold springs 19 - 23 TU. The AGW-3, hot water borewell sample (temp. 91 °C) shows the highest tritium value of 27.4 TU. The tritium level of Badrinath hot spring is 7.7 TU. The present level of tritium in New Delhi which is the nearest station on the IAEA/WMO network is about 5 TU. Hence the high  $^3\text{H}$  levels observed in hot springs/hot water wells and cold spring samples show the presence of bomb tritium. The tritium value of the Himalayan stream and rivers are 20 TU and they get contributions from snow melt which has bomb tritium. Using a piston flow model and tritium out put for New Delhi the residence time of the Tapoban hot waters is about 20 years.

#### 2.2.7 Discussion and conclusions

The thermal waters from Badrinath are of the NaCl type while those from Tapoban are of the  $\text{Ca}(\text{HCO}_3)_2$  type. Gas samples from both Badrinath and Tapoban hot springs have high  $\text{CO}_2$ . Samples of carbonates deposited by artesian thermal waters flowing from boreholes AGW-2, AGW-3 and AGW-6 in Tapoban show  $\delta^{13}\text{C}$  between 1.3 to 4.3 ‰ with

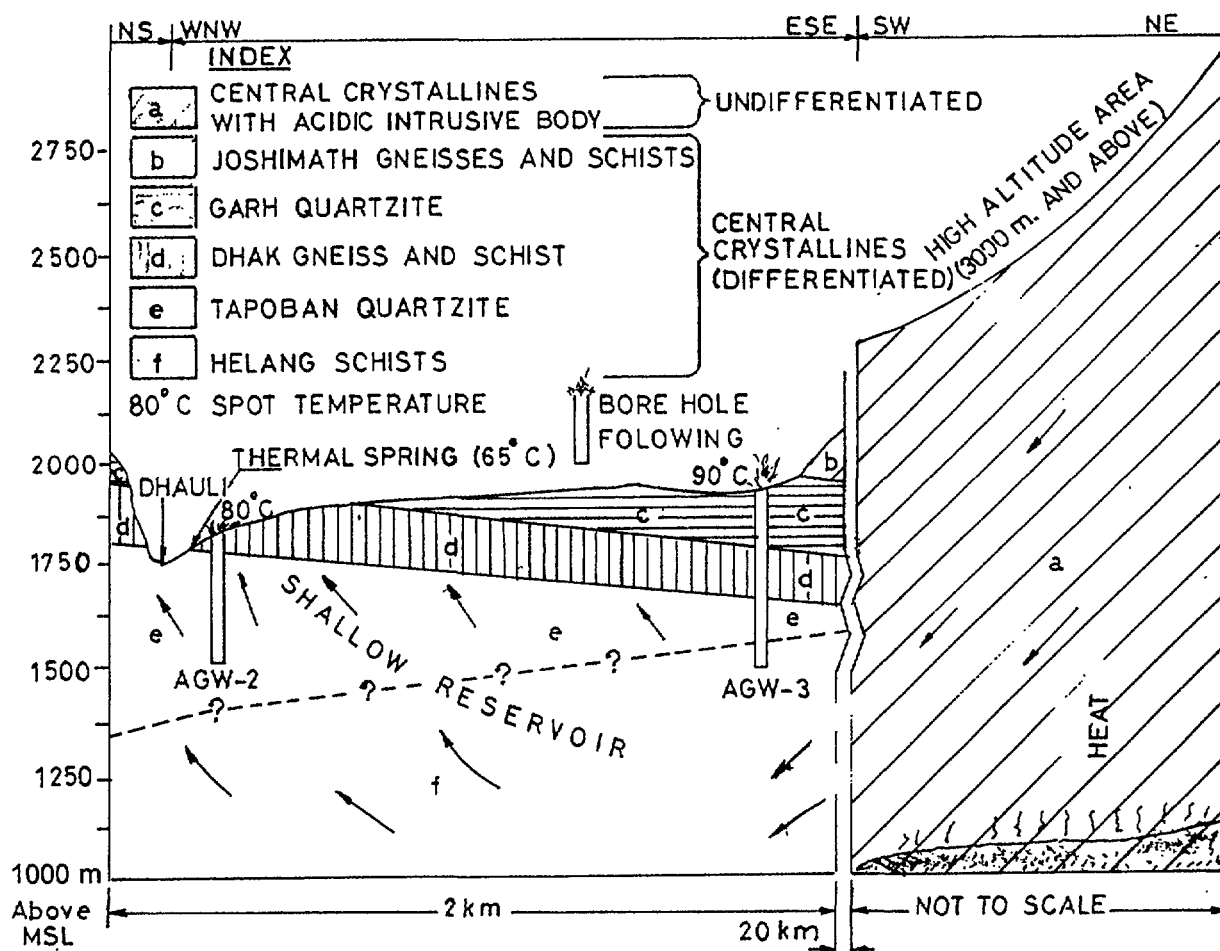


FIG. 16. Model of Tapoban geothermal system, district Chamoli, Uttar Pradesh.

respect to PDB suggesting that the  $\text{CO}_2$  in the fluids has come through dissolution of marine carbonate rocks. Thermal waters from Tapoban and Badrinath fall near the local meteoric line showing negligible oxygen -18 shift. Hot spring and hot water well samples of Tapoban and Badrinath are more depleted in  $\delta\text{D}$  and  $\delta^{18}\text{O}$  than the cold springs in the area showing that the thermal water have higher altitude of recharge compared to the non-thermal waters. Fig. 16 show the model of Tapoban geothermal system [5]. The model visualises recharging waters from elevations  $> 3000$  m getting heated from two sources viz. the geothermal gradient and from cooling acid magmatic intrusives at depths.

**Acknowledgement** - Acknowledgements are due to Mr. U.L. Pitale, Director, GSI, Geothermal Division (Central Region) for work in Tattapani and Mr. S.C. Sharma, Director, GSI, Geothermal Division (Northern Region) for studies in Badrinath and Tapoban areas. We thank our colleagues Mr. U.K. Sinha and Mr. T.B. Joseph for the tritium measurements. The present investigation was carried out within the framework of the IAEA Coordinated Research Programme for Africa, Asia and the Middle East on the Application of Isotope and Geochemical techniques in geothermal exploration.

## References

- [1] SHANKAR R., THUSSU, J.L., PRASAD, J.M., Geothermal studies at Tattapani Hot spring area, Surguja district Central India, *Geothermics* 16 (1987) 61 - 76
- [2] THUSSU, J.L., PRASAD J.M, SAXENA, R.K., GYAN PRAKASH, MUTHURAMAN, K., Geothermal energy resource potential of Tattapani Hot spring belt, District Surguja, Madhya Pradesh, *Records of GSI* 115 (1987) 30 - 55.
- [3] TRUESDELL A.H., "Stable isotopes in hydrothermal systems" *Fluid Mineral Equilibrium in hydrothermal systems - Reviews in Economic Geology Vol. 1* (Robertson, J.M. Ed.) The Economic Geology Publishing Co. USA (1984) 129 - 141
- [4] GIGGENBACH W.F., GONFIANTINI R., JANGI B.L., TRUESDELL A.H., Isotopic and chemical composition of Parbati valley Geothermal discharges, North-West Himalaya, India, *Geothermis* 12 (1983) 199-222.
- [5] NAVADA S.V., RAO, S.M., Isotope studies of some geothermal waters in India, *Isotopen praxis* 27 (1991) 153 - 163.
- [6] GEOLOGICAL SURVEY OF INDIA, Geothermal Atlas of India, Special publication 19, (1991) 38 - 45.
- [7] SINGH J.R., Chemistry of geothermal gases: Collection, Analysis and some Indian case studies, *Indian Minerals*, 43, (1989) 7 - 18.

# ISOTOPE STUDY IN GEOTHERMAL FIELDS IN JAVA ISLAND

ZAINAL ABIDIN, WANDOWO

Centre for Application of Isotope and Radiation,  
National Atomic Energy Agency,  
Jakarta, Indonesia

**Abstract** - Study in two geothermal fields, Dieng and Kamojang, in Java island by utilizing isotope technique has been carried out. Isotopic data of wells, springs and other geothermal manifestations providing informations on the recharge area of precipitation contributed to geothermal resources, flow paths and origin of geothermal fluids. The data of oxygen shift has also provided information on the characteristic the fields.

## 1. INTRODUCTION

The development of geothermal energy is subject to the availability of geothermal resources. The geothermal resources in Indonesian archipelago spread from the top of Sumatera island going down to Java and the smaller islands at the eastern part and then lining to Sulawesi island. This line is indicated by volcanic apparata, with some young volcanoes that form active volcanic belt. Tectonic movements in the past were usually followed by inner and intensive external volcanism, causing the ascent of magma to shallow depths. Most of geothermal area in Java located in the active volcanic belt in the system related to shallow hot intrusive bodies. With abundant precipitation falling in this area, have created ideal conditions for the development of geothermal energy.

The geothermal potential all over Indonesia has been assessed at about 16,000 MW, where 7,800 MW is originated from Java island. However, the utilization of geothermal energy for electric power generation in Indonesia is still very low. At present there are only two electric power generators in Indonesia, located in Kamojang ( 142 MW ) and in Dieng (2 MW) (Fig. 1). Together they contribute 1.4 % of the total demand for energy in Indonesia. In line with the programme for developing geothermal energy, intensive studies have been carried out, especially in those two areas, to update the existing data of geothermal resources.

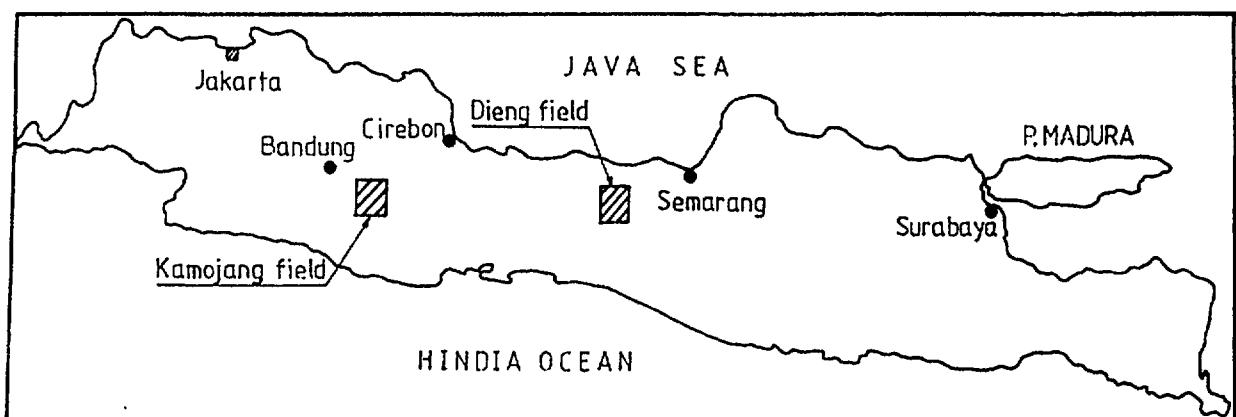


FIG. 1. Location of the geothermal field of study.

## 2. SAMPLING AND ANALYSIS

### 2.1. Sample collection

Water samples from geothermal manifestations (fumarole, hot springs, heated pools), well head, cold springs and precipitation were collected from studied geothermal areas. Samples for stable isotope analysis were collected in a 20 ml glass vial, capped tightly to prevent it from evaporation process, especially when the samples were taken from a hot spring. Sample from well head was collected through a gauge valve connected to a cooling apparatus to condense the steam and avoid any evaporation effect. The temperature of condensed steam was maintained below 20°C by regulating the valve opening or the flowrate of cooling water.

Samples from precipitation were collected by trapping rainwater into a stainless steel cylinder which was filled with paraffin oil. To measure the amount of precipitation, a graduated flask was set near this cylinder. In Kamojang and Dieng area, precipitation was collected at four locations with different altitude as follows :

AREA	LOCATIONS	ALTITUDES (m)
Kamojang	Ciparai	700
	Ibun	1,000
	Kamojang	1,485
	Crater	1,630
Dieng	Kalianget	800
	Jengkol	1,200
	Tieng	1,600
	Pawuhan	2,000

### 2.2. Analysis

For oxygen-18, samples were prepared by equilibrating with reference CO<sub>2</sub> gas for about 18 hours according to the Epstein and Mayeda method. For deuterium, a small amount of sample was treated with activated zink (BDH) in a vacuum flask heated to 450°C during 45 minutes. Analytical error for oxygen-18 was 0.15‰ and for deuterium was 2‰.

## 3. RESULTS AND DISCUSSIONS

Data of stable isotope content of meteoric water collected every month at different altitudes in Kamojang and Dieng were used as reference for local meteoric water line. The value of weighted means of oxygen-18 and deuterium at each sampling locations are shown in Table I.

Correlation of oxygen-18 and deuterium of meteoric water represent the local meteoric water line of Java island. The correlation is:

$$\delta D = 7.9 \delta^{18} O + 16.0 \quad (r = 0.98).$$

Correlation of deuterium content in precipitation and altitudes, H, can be represented as:

$$\delta D = -1.9 \times 10^{-2} H - 22.1 \quad (r=0.87)$$

This correlation suggests that for every 100 m increase of altitude the deuterium content will decrease 1.9 ‰ .

TABLE I. ISOTOPE COMPOSITION OF PRECIPITATION AT DIFFERENT LOCATIONS

Location	Altitude (m)	$\delta D$ (‰)	$\delta^{18}O$ (‰)	Precipitation (mm)
Ciparay	700	-41.7	-7.2	432
Ibum	1,000	-49.7	-8.2	925
Kamojang	1,485	-50.3	-8.3	869
Crater	1,630	-51.6	-8.5	874
Kalianget	800	-36.8	-6.8	1,870
Jemgkol	1,200	-40.3	-7.3	1,555
Tieng	1,600	-51.5	-8.5	1,650
Pawuhan	2,000	-62.6	-10.1	1,560

### 3.1. Dieng Geothermal Field

The Dieng geothermal field is located at Dieng plain about 2,000 m above sea level. It is formed by a young andesitic volcanic product within the area of mount Perahu. Surface manifestations are indicated by mofetes, fumaroles, hot springs and lakes which are probably formed by hydrothermal eruption. The hot springs are scattered along Northwest - Southeast cross section, between Bitingan and Gunung Seroja. At present there are already 20 wells with depths between 600 to 2,400 m along this cross section. The well Dieng II has been exploited to generate electric power of 2 MW capacity.

Data of stable isotope of hot prings and wells are presented in Table II. Heavy isotope contents of wells III, VI and IX, are relatively depleted. This is probably due to the mixing with ground water or interaction with  $CO_2$  gas in the well casing. The isotope composition of the wells with depth from 1,600 m to 1,800 m (well VIII and well XIII) tend to be more enrich. This suggests that there is a process of boiling or evaporation in those depths. The average deuterium content of the deep wells V, X and XI is nearly similar, namely  $-52.0 \text{ ‰} \pm 1$ , however their oxygen-18 are significantly different, namely  $-5.3 \text{ ‰}$ ,  $+1.1 \text{ ‰}$  and  $-6.4 \text{ ‰}$  respectively ( Fig. 2 ). The value of oxygen shift of the well X ( $9.8 \text{ ‰}$ ) at the North West part is higher than that in the wells V and XI ( $2.3 \text{ ‰}$ ), located at South East. This suggest that water rock interaction is more intensive in the North West than in the South East. The difference of this value probably is also due to the difference in the flow paths of fluids circulation. The difference of the value of oxygen shift also corresponds to the chloride content in each well, where the chloride content in well X is 7,175 ppm while in well XI is 1,054 ppm.

The mixing process is also shown in Fig. 3, explaining the correlation of chloride vs. deuterium. From this figure it is shown that there is a mixing between deep fluids and ground water. The close similarity of deuterium content in hot springs and in deep fluids suggest that the recharge elevation of these sources are at the same area namely between 1,600 to 1,800 m above sea level.

TABLE II. STABLE ISOTOPE COMPOSITION OF SPRINGS AND WELLS OF DIENG FIELD

Sample	Elev. (m)	Depth (m)	Temp. (° C)	$\delta$ D (‰)	$\delta$ <sup>18</sup> O (‰)	Cl (ppm)
DNG 1	820	-	41	-51.2	-8.5	367
DNG 2	830	-	41	-52.6	-8.4	373
DNG 3	750	-	55	-54.4	-8.4	315
DNG 4	900	-	52	-51.7	-8.5	200
DNG 5	1,625	-	52	-51.6	-8.3	398
DNG 6	1,650	-	52	-51.9	-8.1	278
DNG 7*	2,000	-	87	-23.2	+2.5	1.3
DNG 9	1,800	-	56	-56.2	-8.1	33
DNG 10	1,760	-	54	-54.2	-8.1	19
DNG 11	1,725	-	53	-52.6	-7.8	48
DNG 12	2,000	-	18	-59.2	-9.4	1
DNG 13	1,060	-	43	-42.5	-7.0	455
DNG 15*	2,100	-	83	-21.7	-1.0	57
DNG 19	1,260	-	57	-51.0	-8.3	138
DNG 22	970	-	57	-51.2	-8.1	218
Well III		850	-	-46.4	-13.1	821
Well V		2,050	-	-53.0	-5.3	700
Well VI		650	-	-52.2	-9.2	1,064
Well VIII		1,800	-	-38.6	-2.1	2,040
Well IX		750	-	-57.0	-8.9	195
Well X		1,900	-	-51.7	+1.1	7,175
Well XI		2,370	-	-51.3	-6.4	1,054
Well XIII	-	1,600	-	-26.0	-4.8	123

### 3.2. Kamojang Geothermal Field

Kamojang geothermal field is situated over an area of 14 km<sup>2</sup>, in the East-West trending Rakutak - Guntur volcanic chain. The area is composed of undifferentiated deposits and pyroxene andesite. There are about 30 wells producing dry steam and they are exploited for electric power generation, while the other three wells are used for reinjection of steam condensate. All the wells are located within the boundary of low resistivity zone and their depth is in the range from 600 to 2,100 m. The average temperature of the reservoir is 243°C. The purpose of the isotope study in Kamojang geothermal field is to know the origin and hydrological processes of the fluids.



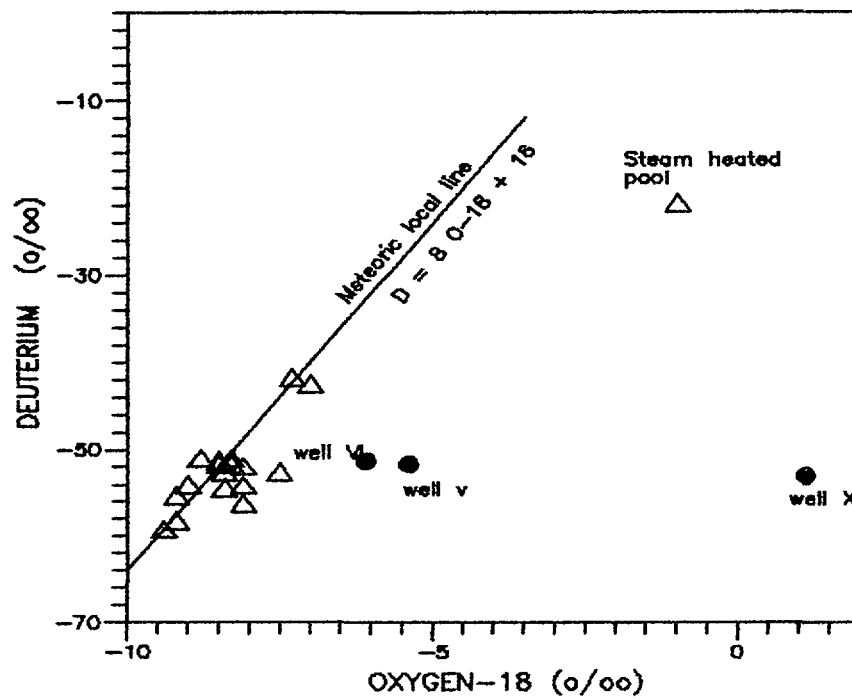


FIG. 2. Oxygen-18 vs deuterium, Dieng geothermal field, central Java.

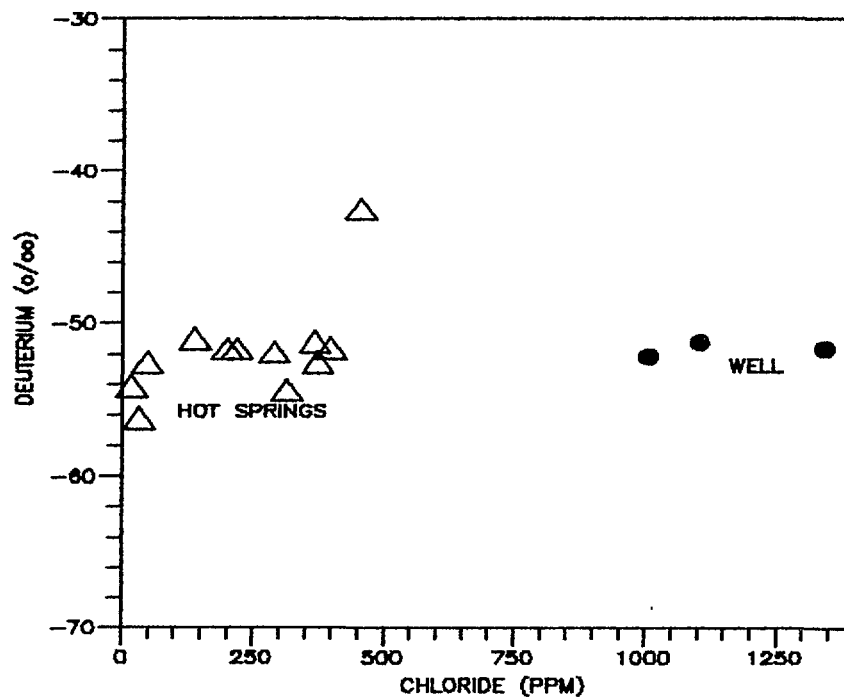


FIG. 3. Chloride vs deuterium, Dieng geothermal field, central Java.

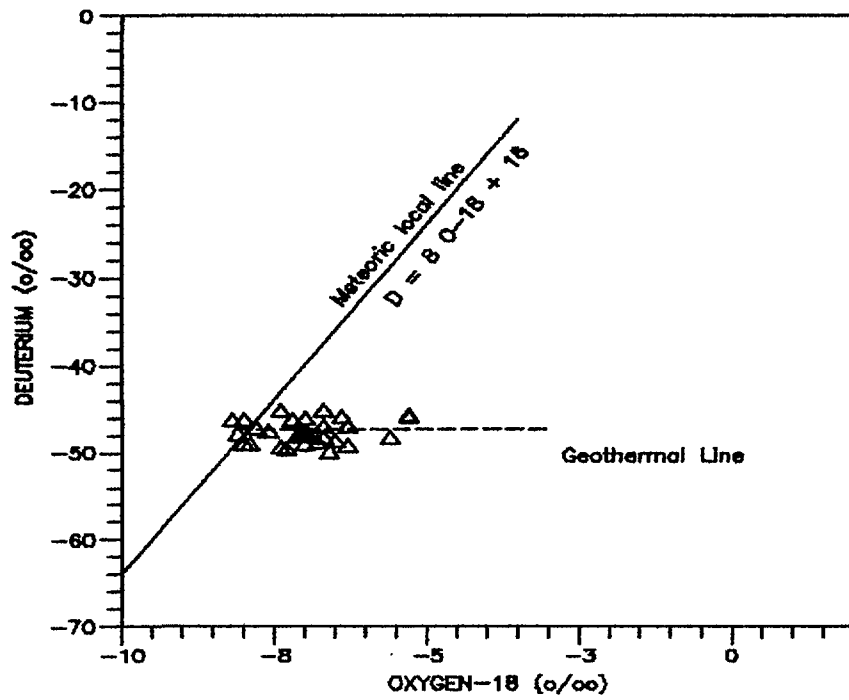


FIG. 4. Oxygen-18 vs deuterium, Kamojang geothermal field, west Java.

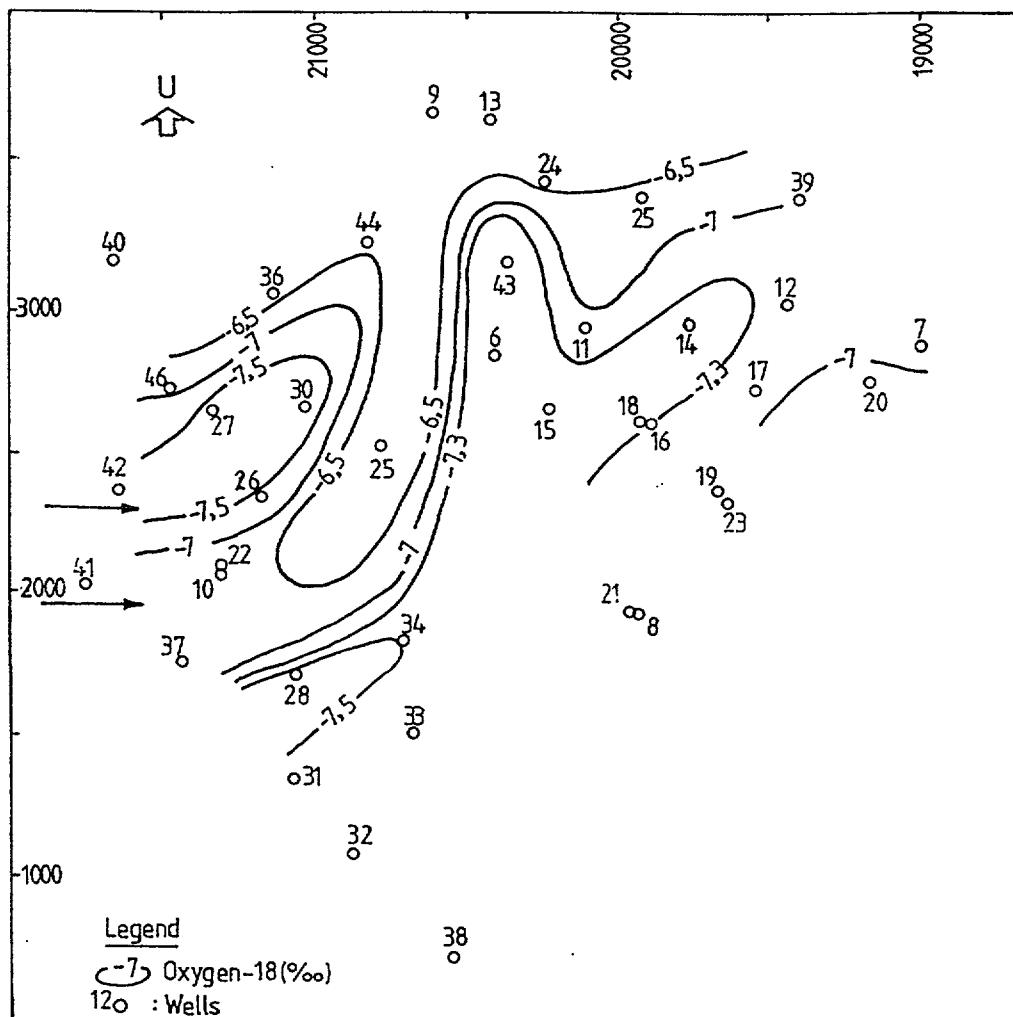


FIG. 5. Distribution of oxygen-18, Kamojang geothermal field.

TABLE III. STABLE ISOTOPE COMPOSITION OF WELLS OF KAMOJANG FIELD

Sample	$\delta D$ (‰)	$\delta^{18}O$ (‰)
KMJ 7	-45.2	-8.4
KMJ 11	-45.3	-6.8
KMJ 12	-46.1	-7.0
KMJ 13	-42.5	-12.3
KMJ 14	-46.1	-6.9
KMJ 17	-46.4	-7.0
KMJ 18	-42.7	-7.1
KMJ 20	-49.0	-6.8
KMJ 22	-46.4	-5.8
KMJ 24	-44.3	-6.4
KMJ 25	-44.5	-6.7
KMJ 26	-47.0	-7.2
KMJ 27	-48.2	-7.6
KMJ 28	-47.6	-7.4
KMJ 30	-44.9	-7.7
KMJ 31	-48.9	-7.1
KMJ 34	-47.9	-7.5
KMJ 35	-43.9	-11.6
KMJ 36	-45.5	-6.5
KMJ 37	-46.2	-7.6
KMJ 38	-46.2	-7.0
KMJ 39	-44.7	-7.0
KMJ 41	-46.5	-6.2
KMJ 42	-49.0	-15.0
KMJ 43	-43.2	-8.1
KMJ 44	-46.8	-6.1
KMJ 45	-44.3	-7.0
KMJ 46	-45.6	-9.8

The average value of deuterium content of the wells is  $-46.8 \pm 2$  ‰. It corresponds to the variation of deuterium in precipitation at altitudes 1,200 to 1,700 m. The variation of oxygen-18 is from  $-8.3$  ‰ until  $-5.3$  ‰ (Fig. 4). The geothermal line intercepts the local meteoric water line at the point where the value of oxygen-18 is  $-8$  ‰ and deuterium is  $-45.8 \pm 1.7$  ‰. This composition represents the composition of precipitation infiltrating into the ground as an input for geothermal fluids. The oxygen shift that is due to water-rock interaction is from 0 to  $2.7$  ‰. The oxygen-18 content of wells at the Western part of the field ( KMJ 27, 28, 30, and 42 ) are around  $-8$  ‰, it means that the oxygen shift is 0. While the wells at North-East and South-West ( KMJ 11, 12, 14, 17, 18, 45, 38, and 31 ) their oxygen shift is around 1, and the wells at the North ( KMJ 24, 25, 39, 36, 46, 44 and 51 ) their oxygen shift is around 1.5. The longest oxygen shift is found at KMJ 41 and 35. Since the type of rock throughout the production area is relatively similar, the difference in oxygen shift is due to the difference in the path of its circulation. The flow direction of the geothermal fluids is indicated by distribution of oxygen-18 of the wells in Kamojang area. In the Western part the flow is from West to East, while in the production area the fluids flow from South West to North East ( Fig. 5 ). This circulation informs that there is a mixing between meteoric water with original steam at the reservoir boundary and keeping a depletion of oxygen-18 at the production wells.

At the Western region the flow velocity is higher than at the Eastern region. This phenomenon is supported by the fact that the oxygen shift of wells in the Northern region is higher than those in the Southern region. The slower velocity in the Northern region is also probably due to the higher value of permeability of rock in that region.

#### 4. SUMMARY

1. The isotope study in Dieng field has provided informations of the circulation of geothermal fluids. The data on the deuterium content of the reservoirs indicate that the fluids originated from precipitation infiltrating at 1,600 - 1,800 m. The difference of the value of positive oxygen shift at South East area ( $2.3$  ‰) and at North East area ( $9.8$  ‰) is probably due to the difference of the path of circulation.

2. The geothermal fluids originated from precipitation infiltrating at elevations of 1,200 - 1,500 m. The fluids flow from South West to North East. Since the value of oxygen-18 at the South West area is more depleted than at the North East area, this indicate that there is an interaction of deep fluids with meteoric water at the boundary. The oxygen shift is relatively very small, namely  $2.3$  ‰.

**Acknowledgement** - *The authors are grateful to Dr. R. Gonfiantini who has supported the Centre for Application of Isotope and Radiation, BATAN in the upgrading laboratory facilities for doing activities in geothermal research and providing valuable consultations to the Staff members of Hydrology Laboratory at BATAN. We also would like to thank to Dr. C. Panichi for his constructive comments on this work. Appreciation is also addressed to Mrs. Nazly Hilmy, Director of the Centre for Application of Isotope and Radiation BATAN, who has put the programmes of isotope hydrology as one of the priority to be developed. And last but not least, to colleagues in Isotope Hydrology Laboratory of CAIR BATAN, we are grateful for their time to time help and cooperation.*

## References

- [1] FRITZ,P.,FONTES,C.H.,Handbook of Environmental Isotope Geochemistry, Elsevier Scientific Pub. Corp, 1 (1981)
- [2] VAN BEMMELEN,R.W.,The Geology of indonesia, Vol IA, Government Printing Office , The Hague, (1949)
- [3] PINANTUN,M.," Geothermal Development of Indonesia", Geothermics, 17, 2/3, (1988),415-420
- [4] VINCENT,T.RADJA., "Indonesia Geothermal Development in the National Energy Scenario, Development Program to the year 2000", Geothermics, 15, 5/6,(1988), 600.
- [5] MUZIEL,A., "Geothermal Energy Potensial Related top Active Volcanic in Indonesia", Geothermic, 15, 5/6, (1986), 601-607
- [6] FAUZI, A., Mineralogy and Fluid Composition at Dieng Geothermal Field, Indonesia, Master Thesis, Victoria University, Wellington (1987)
- [7] GIGGENBACH, W.F., "The Isotopic Composition of waters from the El Tatio Geothermal Field, Northern Chile", Geochim. Cosmochim. Acta, 42, (1987),979
- [8] FOURNIER, R. O., SAREG, M.L., "Chemical and Isotopic Prediction of Aquifer Temperatures in the Geothermal System at Long Valley California", J.of Volcanology and Geothermal Research, 5, (1979), 1-16

# THE USE OF GAS CHEMISTRY AND ISOTOPE GEOTHERMOMETRY TO STUDY THE EFFECTS OF EXPLOITATION AND REINJECTION ON THE FLUIDS AT LARDERELLO, ITALY

C. PANICHI, P. NOTO, L. BELLUCCI  
CNR-International Institute for Geothermal Researches

G. SCANDIFFIO, F. BACCARIN, M. VALENTI  
ENEL-VD Geothermal Activity

Pisa, Italy

**Abstract** - *Isotopic and chemical analyses of the steam and gas from producing wells since exploration until 1992, were used to define the effects of the exploitation and reinjection of waste fluids. Maps showing zonations of the isotopic composition of the steam and chemical concentrations of the gas mixtures in the Larderello geothermal system are derived independently. Inspection of the maps obtained before and after reinjection reveals good discrimination between the natural inflow of meteoric water subsequent to exploitation and of man-made recharge using waste fluids. Chemical variations of Ar appear to be a valuable tool for evaluating a recovery factor of reinjected water. Isotopic variations in  $H_2$ ,  $CH_4$  and  $CO_2$  are used to describe disequilibrium conditions between gas components induced by the establishment of a liquid plume at the production zone of the reservoir.*

## 1. INTRODUCTION

The Larderello field in southern Tuscany produces superheated steam from a vapor-dominated reservoir. In order to obtain valuable information from a reinjection study of vapor-dominated systems, one must use a methodology most suited to the type of the fluid being produced, i.e. gas and steam. Tracers are, in this respect, of considerable importance as they can provide information on the processes occurring in the reservoir and on their evolution with time. The isotopic composition of the condensate leaving the cooling towers at the power plants was successfully used as a "natural" tracer during the monitoring for reinjection tests at Larderello [1, 2 and 3].

The close correlation between the  $^2H$  and  $^{18}O$  in steam and of gas/steam ratios in the fluid indicate that mixing occurs at depth between reinjected fluids and the deep geothermal fluids. This is accompanied by the formation of a liquid plume undergoes different degrees of evaporation [3].

Variations of isotopic temperatures, derived from H and C isotopic exchanges between gas molecules such as  $CO_2$ ,  $CH_4$ ,  $H_2$  and  $H_2O$  before and after reinjection at Larderello, were interpreted by Bolognesi et al. [4] to be a consequence of the development of the liquid phase in the producing steam reservoir.

Before reinjection (late 1979), several authors have shown that the chemical and isotopic compositions of the water vapor and associated gases can be related to the physical and chemical processes in the reservoir as well as to the widening of the field, i.e., from the exploitation. The variations of the isotopic and chemical composition of fluids are also associated with the emergence of some areas in the field [5, 6, 7 and 8] and with time since drilling of individual wells [9].

The most conspicuous geochemical patterns observed in the Larderello area are the strong increases or decreases from the centre to the edges of  $^{18}\text{O}$  and  $^3\text{H}$  in the steam phase. The  $^{18}\text{O}$  patterns were considered [5] to be a result of exploitation-induced marginal recharge by less-exchanged  $^{18}\text{O}$ -poor water. This hypothesis is supported by the presence of significant amounts of  $^3\text{H}$  in steam from wells near the areas where the reservoir complex crops out (Castelnuovo, Monterotondo, Lago and Lagoni Rossi ); and by hydrological balances that indicate substantial recharge to the Larderello system.

Compositional variations with geographic location are interpreted by D'Amore and Truesdell [10] as resulting from a pre-exploitation lateral steam flow from central boiling (or inflow) zone towards the edges of the system. This 'three sources' conceptual model prepared by D'Amore and Truesdell suggests that changes in the chemistry of steam with time is the result of production from a deeper source: an upper condensation layer, a central two-phase liquid-vapor zone and a deep brine.

In each of the quoted papers, the compositional variations have been interpreted to be due to reservoir processes. These include lateral-cold water recharge, condensation of steam, and vaporisation of liquid water. However, the interpretation may be affected by the lack of information regarding the history of the exploitation of the field and the approximations that are introduced when the locations of each wells in the field are disregarded. Indeed, exploitation originated from zones where the reservoir is close to the surface and proceeded toward the deeper zones. This implies that certain zones are heavily exploited with many old, closely spaced wells while the recently developed zones have few, widely spaced wells. In the former, the reservoir is at shallow depths and may have contained steam having originally a different composition to steam from the deeper, newly developed zones.

In this paper a first attempt is made to distinguish the original differences from those induced by exploitation and successively by reinjection processes.

## 2. BRIEF HISTORY OF THE INDUSTRIAL DEVELOPMENT OF THE FIELD

The first geothermal well, only a few meters deep, was drilled in the geothermal field of Larderello in 1832. It was only in 1926 did wells reach the top of the reservoir composed of the carbonate formation. In the initial exploitation phase, a large amount of steam was produced by these wells even though the drilled area was very small and already partly drained by many shallow wells.

Between 1926 and 1940, 136 wells (82% productive wells) were drilled in an area less than  $4\text{ km}^2$  the same area which had been exploited for more than a century. Steam output gradually increased and reached 1500 t/h at the end of this period.

Between 1940 and 1950, the exploited area almost doubled, increasing to about  $7\text{ km}^2$ . Sixty-nine new wells were drilled at greater distances from each other in comparison with the previous period. The total steam production reached 2200 t/h, in spite of the decrease in the older production zones.

Since 1950, with new drilling techniques and extensive research, the exploited area was greatly extended, covering about  $180\text{ km}^2$  at the end of the 70's. Outside the early exploration zones corresponding to the high structures of the carbonate reservoir, the new wells found less favourable permeability. The well' success rate decreased rapidly, but wider

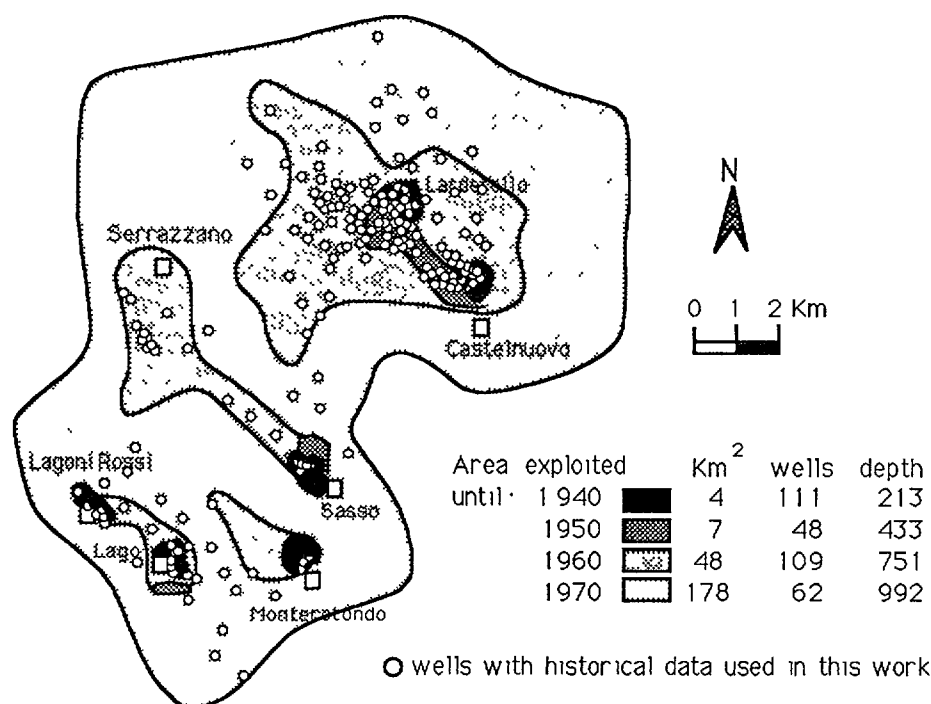


Figure 1. Cartoon representing the main features of the development of the Larderello geothermal field from 1926 to 1979

spacing between the them ( 1 well/km<sup>2</sup> ) enabled to reach a stable steam output of 3000 t/h in the early 60's.

Since 1970, when the drilling of the development wells was completed, the activities were reduced to delineating the boundary of the productive area. Only 60 wells, over a new area of 27 km<sup>2</sup>, were drilled between 1970 and 1990, mostly at the field's borders where the carbonate reservoir is absent or only slightly permeable. The success rate was particularly low in this period (37%). Data quoted above are given in detail in Figure 1.

The first water levels measured in the Larderello wells have a pressure of about 30 bars. The distribution of pressure at the top of the reservoir in 1943 shows values lower than 10 bars in the most exploited zones in Larderello and Castelnuovo. Since deep wells have not then be drilled, the pressure trend could not be reconstructed in relation to depth. However, high values in the nearby structurally low zones suggested poor vertical drainage.

Pressure distribution in 1952, immediately before the first systematic shut-in pressure well measurements were made, reveals an extension of areas with pressure lower than 10 bars. Intense drainage effects are visible in the pressure distribution with depth.

The first important reconstruction of pressure trends at the top of the reservoir in the entire geothermal field was made in 1966. Areas at Larderello and Castelnuovo for which the increase in pressure is lower than 10 bars joined together. Those in the other exploitation areas (Serrazzano, Lago, Lagoni Rossi , Monterotondo and Sasso) are still limited due to the reservoir's lower permeability which reduces interferences among wells. Zones with pressures higher than 35 bars are situated in the northeastern and western boundaries of the field and cannot be exploited due to low reservoir permeability.



The pressure decreased in the Larderello-Castelnuovo area to keep steam output at constant levels. This consequence was very significant since 50% of total steam was produced by the Larderello area and the power plants represented 50% of total installed power. A 24 MW unit of the Larderello was stopped in 1972 to try to reduce the pressure drop. Consequently, an average increase of 0.31 bars (with a 127 t/h decrease in steam flow) and a stable production were obtained.

### 3. CHEMISTRY OF GAS MIXTURES

Gas chemical analyses from the whole geothermal area and for the entire period of production was used to draw the  $X_{H_2O} - X_{CO_2} - X_i$ , where  $X_i$  refers to  $H_2$ ,  $H_2S$ ,  $CH_4$ ,  $N_2$ ,  $NH_3$ ,  $H_3BO_3$ , and  $Cl$  molar fractions, making use of the most appropriate scale factors. The aim is to examine the compositional differences of the fluid with the location of the wells and to verify the temporal variations in pressure.

The following discussion will examine only the diagrams with  $H_2$  and  $CH_4$  as minor components. As far as  $H_2S$  is concerned the diagrams are nearly identical to those with  $H_2$ . Those with  $N_2$  is very compressed towards the 100%  $CO_2$ -100%  $H_2O$  axis and do not seem to introduce diagnostic elements of any great importance.

#### 3.1. Definition of the "reference cores"

Figure 2 shows  $X_{H_2O} - X_{CO_2} - X_{H_2}$  and  $X_{H_2O} - X_{CO_2} - X_{CH_4}$  diagrams for all the fluids sampled before 1979. Points are very scattered and occupy over 60% of the plots with a common distribution between two straight lines. These lines define an internal triangle containing the  $H_2O$  and  $CO_2$  corners. The limits of the chemical variations are represented by the values  $\log X_{H_2O} / X_{H_2} = \log X_{H_2O} / X_{CH_4} = 3.2$  and  $\log X_{CO_2} / X_{H_2} = \log X_{CO_2} / X_{CH_4} = 18$ .

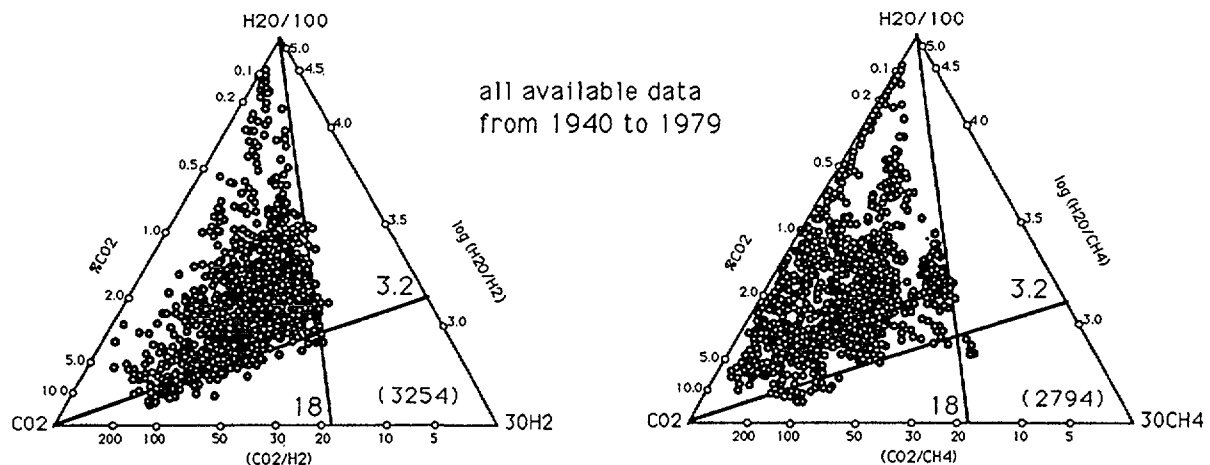


Figure 2. Relative concentrations of  $H_2O - CO_2 - H_2$  and  $H_2O - CO_2 - CH_4$  components expressed in mmol/mol on the total fluid. Samples derived from different sub-units of the field are distinguishable. The number of records used is reported in brackets.

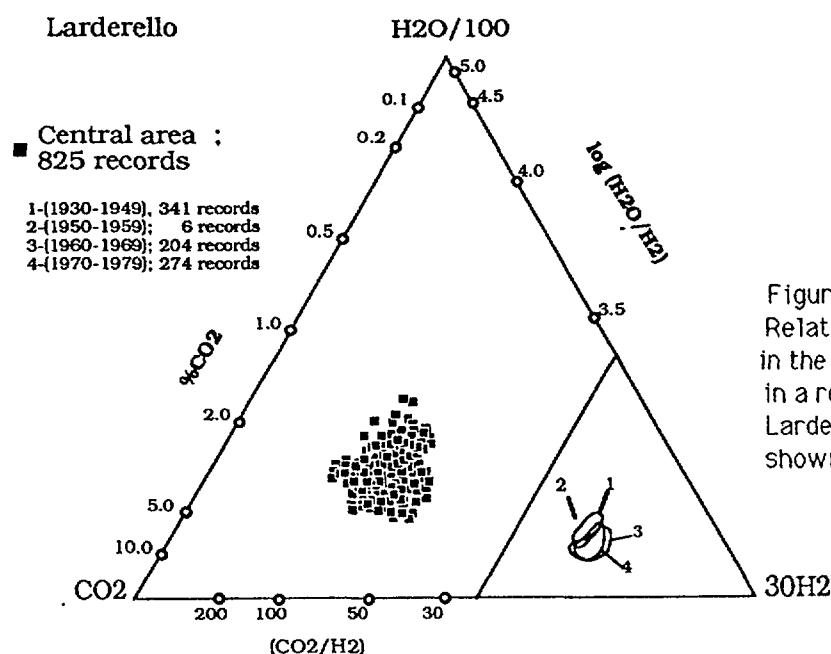


Figure 3.  
Relative concentrations of H<sub>2</sub>O-CO<sub>2</sub>-H<sub>2</sub> in the fluid from selected wells located in a restricted area of the sub-unit of Larderello. The variations in time are shown in left corner.

Considering the trends in time of the individual wells in greater detail, the variations in the CO<sub>2</sub>/CH<sub>4</sub> ratios for some of them are over 10 times. While the percentage of CO<sub>2</sub> over 25 times were observed. Very little scattering around an average value was found for the others. For example, data of the 'central' Larderello area show oscillations lower than 50% around the average values of the two parameters, namely  $2.0 \pm 1.0$  and  $50 \pm 25$  for the CO<sub>2</sub> and CO<sub>2</sub>/H<sub>2</sub>O ratios respectively (Fig. 3).

Because H<sub>2</sub>S, CH<sub>4</sub>, N<sub>2</sub>, NH<sub>3</sub> and H<sub>3</sub>BO<sub>3</sub> show the same pattern, the wells which maintained very similar chemical characteristics in the course of their production history were then isolated in the different sub-units of the geothermal field.

The calculated average chemical compositions of fluid components for the 'central' areas of each sub-unit are reported in Table 1.

Table 1. Fluid compositions of the main sub-units of the Larderello geothermal field for the period 1940-1979. The values, expressed in mmol/mol of total fluid, are calculated as an average of the analyses of the fluids delivered by wells characterised by 'stable' chemical composition.

Molar	Larderello	C.Nuovo	Lago	L.Rossi	M.Rotondo	Sasso	Serrazzano
XH <sub>2</sub> O	973.348	974.690	982.948	985.603	990.253	986.611	985.174
XCO <sub>2</sub>	18.992	23.817	15.282	13.012	8.519	12.186	13.423
XH <sub>2</sub>	.412	.288	.584	.531	.329	.334	.448
XH <sub>2</sub> S	.428	.430	.463	.363	.234	3.15	.386
XCH <sub>4</sub>	.312	.260	.370	.214	.371	.248	.223
XN <sub>2</sub>	.181	.161	.110	.085	.095	.085	.072
XNH <sub>3</sub>	.212	.227	.107	.118	.107	1.67	.212
XH <sub>3</sub> BO <sub>3</sub>	.115	.127	.136	.074	.092	.054	.062

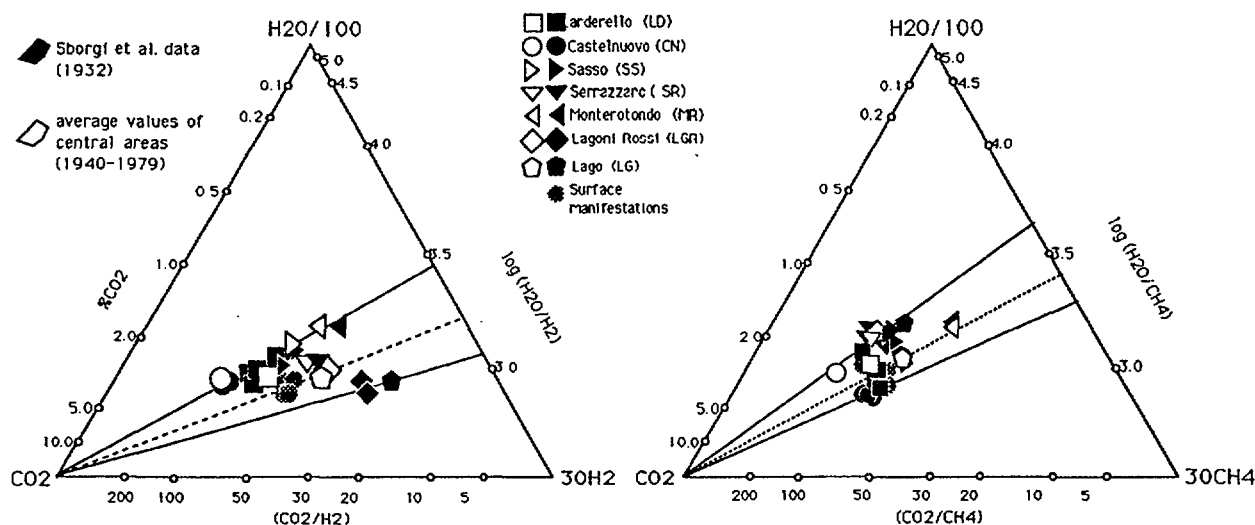


Figure 4. Relative concentrations of H<sub>2</sub>O-CO<sub>2</sub>-H<sub>2</sub> and H<sub>2</sub>O-CO<sub>2</sub>-CH<sub>4</sub> components related to the 'reference cores', surface manifestations existing before drilling, and first shallow drillholes (i.e. 'initial conditions').

Using the data from Table 1, the relative variations of H<sub>2</sub> and C<sub>4</sub> with respect to H<sub>2</sub>O and CO<sub>2</sub> are plotted in the triangular diagrams (Fig. 4). The average composition calculated for each area (open symbols) occupy distinct positions in the plots, confirming the existence of compositional differences in the chemistry of the main gas components of the fluids emerging in different areas of the Larderello field. These areas will be indicated as 'reference core' of the different sub-units.

It is important to emphasize that most of the selected wells correspond to those drilled (between 1930 and 1940) near the old surface natural manifestations, which have now almost disappeared. Chemical analyses of gas samples collected both from wells and surface manifestations during and before 1930 are available from Sborgi, et al. [12]. These data are plotted in Fig. 4 (black symbols) and compared with the average values of the sub-units. A clear overlap between calculated and observed values both for H<sub>2</sub> and CH<sub>4</sub> are observed.

Over half of Sborgi data came from wells with average depths of about 200 m in the early 1930s. Other data included shallow wells dating back to the century or even to manifestations existing in the pre-industrial period. Some of these represent steam jets sampled in 1895 and 1911 which died down in the late 20s due to interference with the wells later drilled in the area. They were considered as precious initial reference, more so since, in addition to the main constituents of the gas mixtures, their He and Ar contents were determined.

It should be stressed that the steam production of the whole field in the 1920s do not exceed the few hundreds tons/hour, most of it from natural manifestations. With the drilling, in the early 1930s, the steam production at Larderello area alone exceeded 700 t/h (380 of which produced by the wells 'Soff.1' and 'Soff.2'), while for the whole field it was around 1150 t/h. This very sizeable increase in production led to the radical depletion of the natural manifestations, which practically no longer existed by the end of the decade.

From the foregoing, it is evident that, though based on limited data, the Sborgi data may be considered the 'initial conditions' of the field. The relative position of the different productive areas of the boraciferous region (Fig. 4) constitutes a well-documented 'reference core' for each sub-units.

Two relevant exceptions are shown by the graphs of Fig. 4 where a depletion of the  $H_2$  and  $CH_4$  contents in the gas mixtures emerge during the initial conditions in the Lago-Lagoni Rossi and Larderello-Castelnuovo sub-units.

This fact suggests the existence of different behaviours of the fluids in the northern areas of the field with respect to the southern ones. It also represents a little uncertainty on the definition of the 'reference cores'. So, figures from Table 1 are fundamental for the analyses of Figure 3, that is, for the interpretation of the temporal and geographical evolution of the fluids of the whole field.

One important consequence of the nearly perfect overlap between 'initial conditions' and the 'reference cores' is that the fluid from wells in the vicinity of the manifestations remained practically stable during the exploitation history of the field. The incompleteness of certain historical series of data, such those in the southern areas, is however not an irremediable inconvenience.

### **3.2. Variation of the gas chemistry as function of the expansion of the exploited areas**

Starting from the values of the 'reference core' for each sub-units, we are going to analyse the variations observed in the gas compositions of the new wells until the pre-reinjection period (1979).

Figures 5 and 6 show the relative concentrations of  $H_2O$ - $CO_2$ - $H_2$ - $CH_4$  of gases sampled from wells drilled in the outlying zones of Larderello. The diagrams display the areas where homogeneous sets of points assume a quite different position from those belonging to the reference cores, and areas showing a more stable gas contents.

The variations occur both for  $CH_4$  and  $H_2$  of the same sub-units; Larderello, Castelnuovo and Lago show the largest ones, while Monterotondo, Serrazzano and Sasso appear to be unstable in time. Lagoni Rossi describes a particular trend.

Two main processes seem to be responsible for the distribution of data points in Figs. 5 and 6 : i) an addition of gas (mainly  $CO_2$ ) to the system may result to a shift toward the  $CO_2$  corner starting from the  $CO_2 / H_2$  and  $CO_2 / CH_4$  ratios of about 40 and 80 which are the values assumed for the reference core. The values reach a maximum of about 200 and 800 respectively; ii) an addition of water to the system may account for the trend which describe the strong depletion of %  $CO_2$  in the gas mixture with respect to the reference gas of the area. In the case of  $CH_4$ , the decrease in  $CO_2$  is often coupled with a strong decrease in  $CH_4$ , thereby reaching lowest values of 900 in the  $CO_2 / CH_4$  ratio.

#### **3.2.1 Larderello sub-unit**

The above processes occur in different zones of the Larderello area. Wells located northeast and northwest of the reference area are affected by the addition of  $CO_2$ , while wells drilled in southern and south-eastern area are affected by the addition of water.

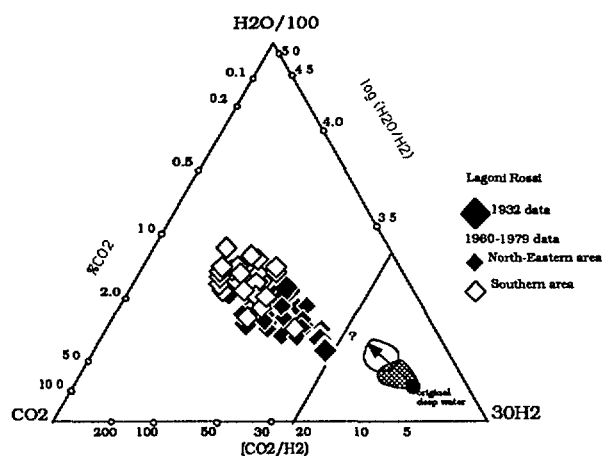
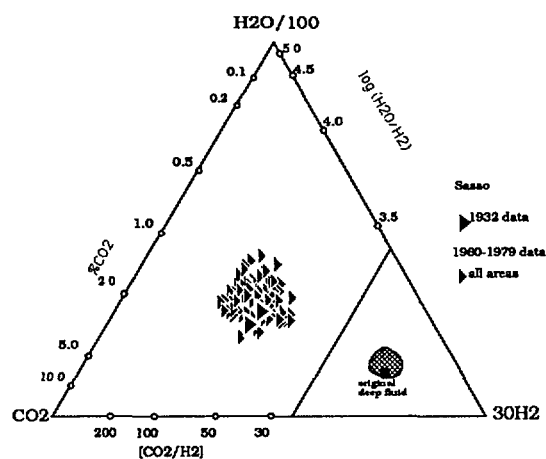
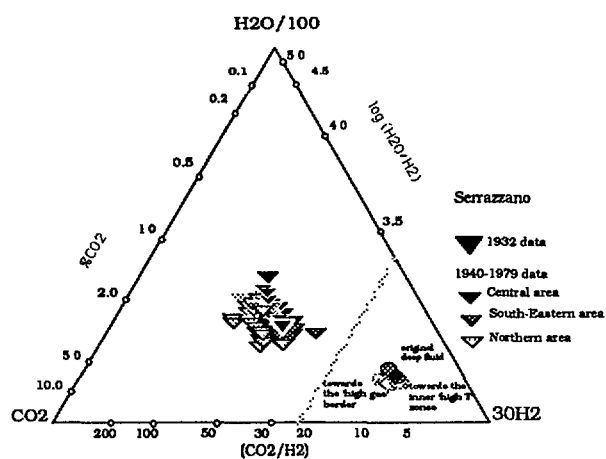
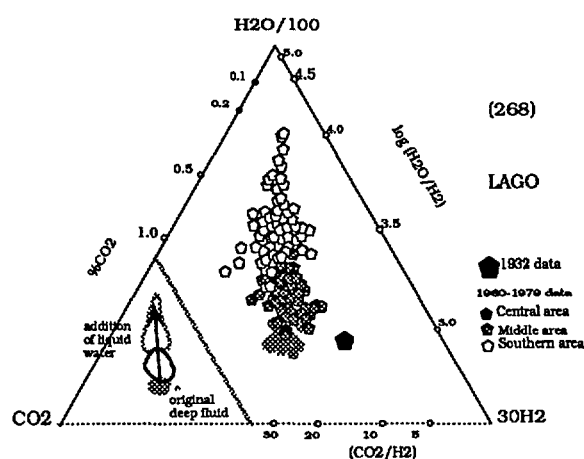
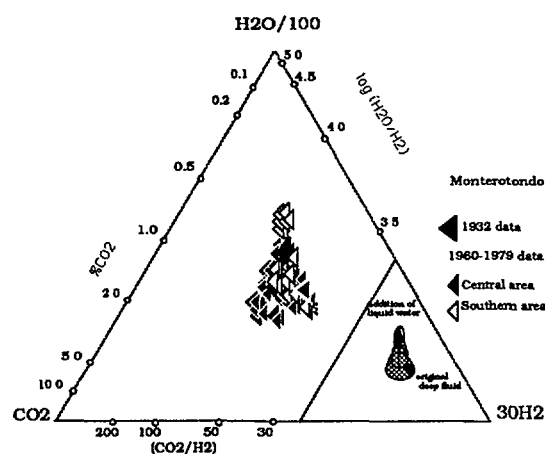
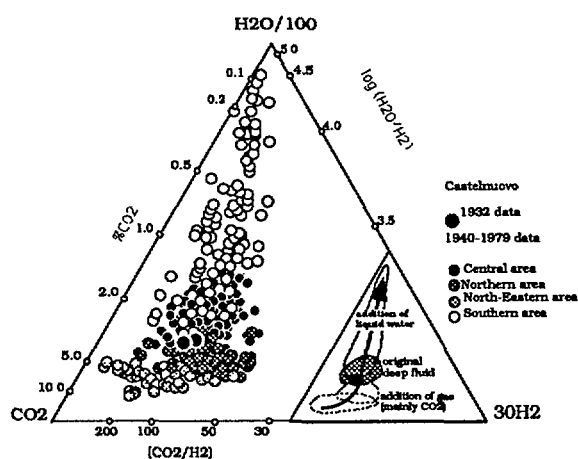
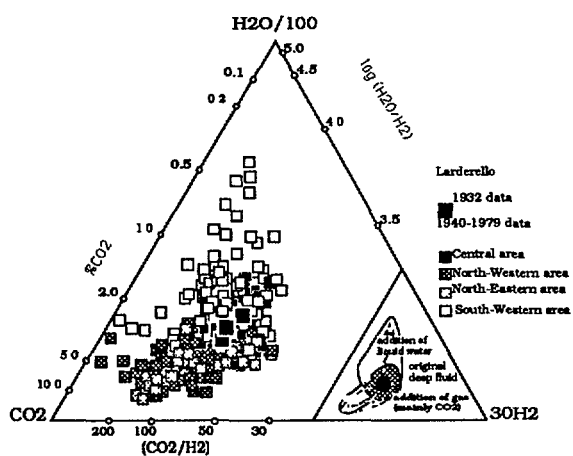


Figure 5.  
Relative concentrations of H<sub>2</sub>O-CO<sub>2</sub>-H<sub>2</sub> components for the fluids emerging in the seven sub-ts of the Larderello geothermal field.

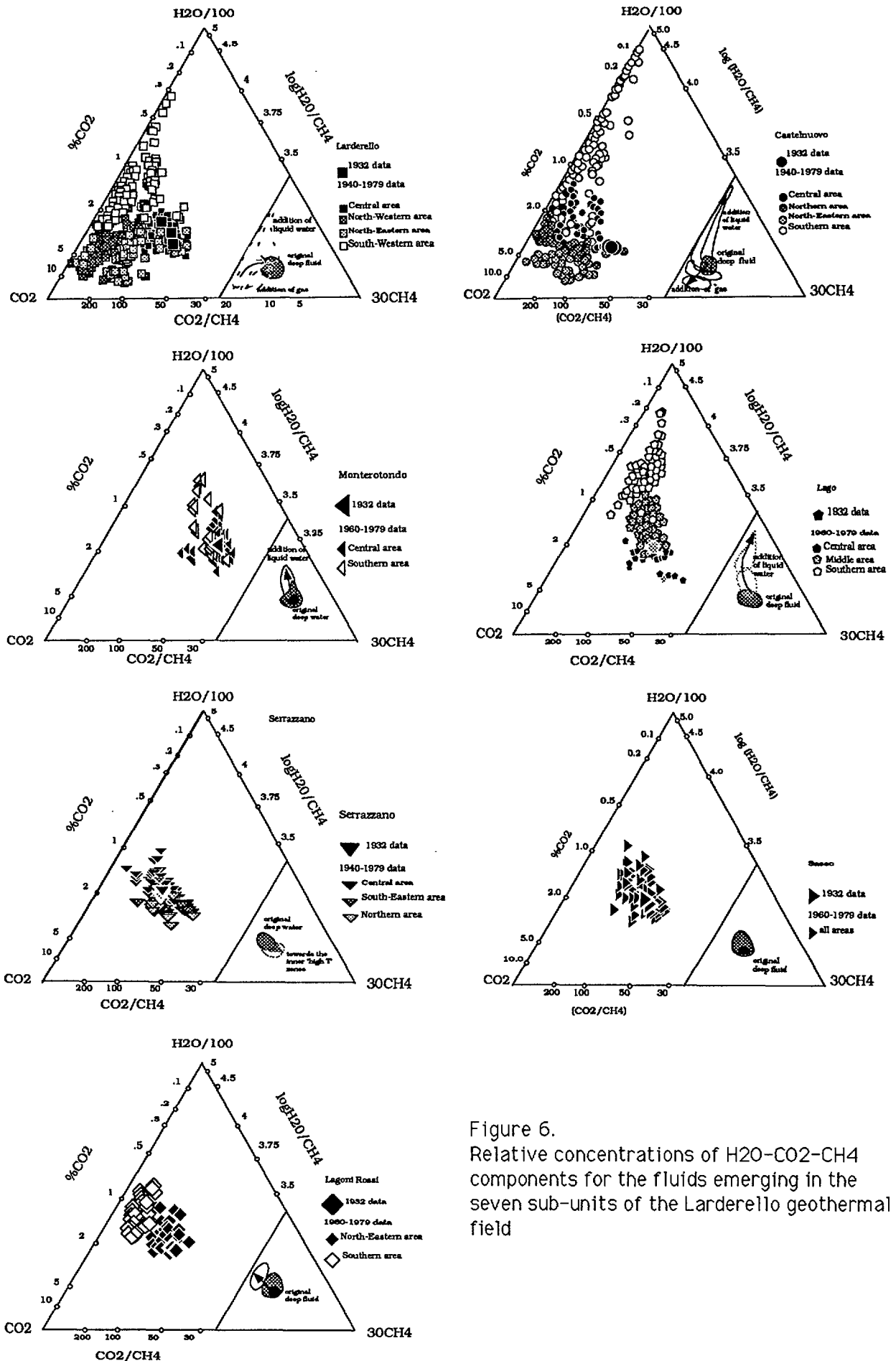


Figure 6.  
Relative concentrations of H<sub>2</sub>O-CO<sub>2</sub>-CH<sub>4</sub> components for the fluids emerging in the seven sub-units of the Larderello geothermal field

The NW and NE zones are represented in the Figures 5 and 6 with different symbols even if they follow the same pattern when the  $H_2$  component is concerned. However, some differences appear to be relevant when  $CH_4$  is considered.

Hence, the Larderello area can be represented as a complex of three to four zones. The northernmost zones display a stable  $H_2$  and  $CH_4$  content, but more  $CO_2$  (up to 5 times) than in the central, reference core zone. The other zones, including the wells drilled to the south, is basically characterised by a decrease in the gas/steam ratio.

### 3.2.2 Castelnovo sub-unit

There has been a more complex history in Castelnovo than in Larderello. Until the mid-1960s, all the old wells, also drilled in a limited area near the manifestations, maintained a nearly constant composition. After this date, substantial modifications were observed in the wells drilled in the southernmost zone. At the same time, new wells, generally located in the north north-eastern areas with respect to the reference core, produce fluids with gas components different from those of the central area.

The observed trends are reported in Figures 5 and 6 both for their  $H_2$  and  $CH_4$  contents as compared to the  $H_2O$  and  $CO_2$  concentrations. The variations are practically identical to those described for gases from the Larderello sub-unit area.

To sum up, four zones are recognisable in the Castelnovo area. The first, which is considered as a reference core, is the central zone. It was once larger, to include, before 1960, the wells further south, which from that time on can be differentiated as separated units. The third zone is made up by the wells to the northeast, and the fourth by those located to the north. The fluids produced here can be considered a mixture between those present in the central core and those of the north-eastern zone.

### 3.2.3 Lago sub-unit

Triangular diagrams again show the  $H_2$  and  $CH_4$  variations with respect to the major components (Figs. 5 and 6). Three sets of data have been identified. The first corresponds to an internal zone defined as the reference core. The other two outlying zones are located further south. For the whole field, the  $H_2O$ - $CO_2$ - $H_2$  plot shows the greatest separation between the position of the wells belonging to the reference cores and the historical data of 1932, the latter being characterised by a higher  $H_2$  content.

The possible hypotheses to explain this difference are the following:

- The historical data for Lago refer to wells with a limited flow rates ( at the time, less than 7 t/h) located in the southern zone which, in 1963, had undergone a considerable evolution. The period the variations began cannot be documented due to lack of previous data.
- The wells which, owing to their unchanged characteristics from 1963 till the present (reference core) are located further north and were drilled at least 25 years after the wells for which historical data were collected.

In conclusion, despite these limitations, the only process affecting the reference core and two peripheral zones in the Lago area is that of  $H_2O$  incursion. While the  $CO_2 / H_2$  ratio remain approximately constant ( $R = 25$ ), the relative concentration of  $CH_4$  with respect to  $CO_2$  increases from  $R = 30$  to  $R = 500$ .

Similar results have also been found for the areas of Monterotondo, Lagoni Rossi and, to a lesser degree, Sasso and Serrazzano.

### 3.3 Main features of the whole productive field

Two main mechanisms appear to be responsible for the large deviations from the reference values in the productive wells nearby the "reference cores". They are :i) the inflow of meteoric waters in the southern peripheral zones, and ii) addition of "external" CO<sub>2</sub> to the original gas mixtures emerging in the "reference core" areas.

Productive wells may be grouped according to the chemical analyses of the total fluids as sketched in Figure 7.

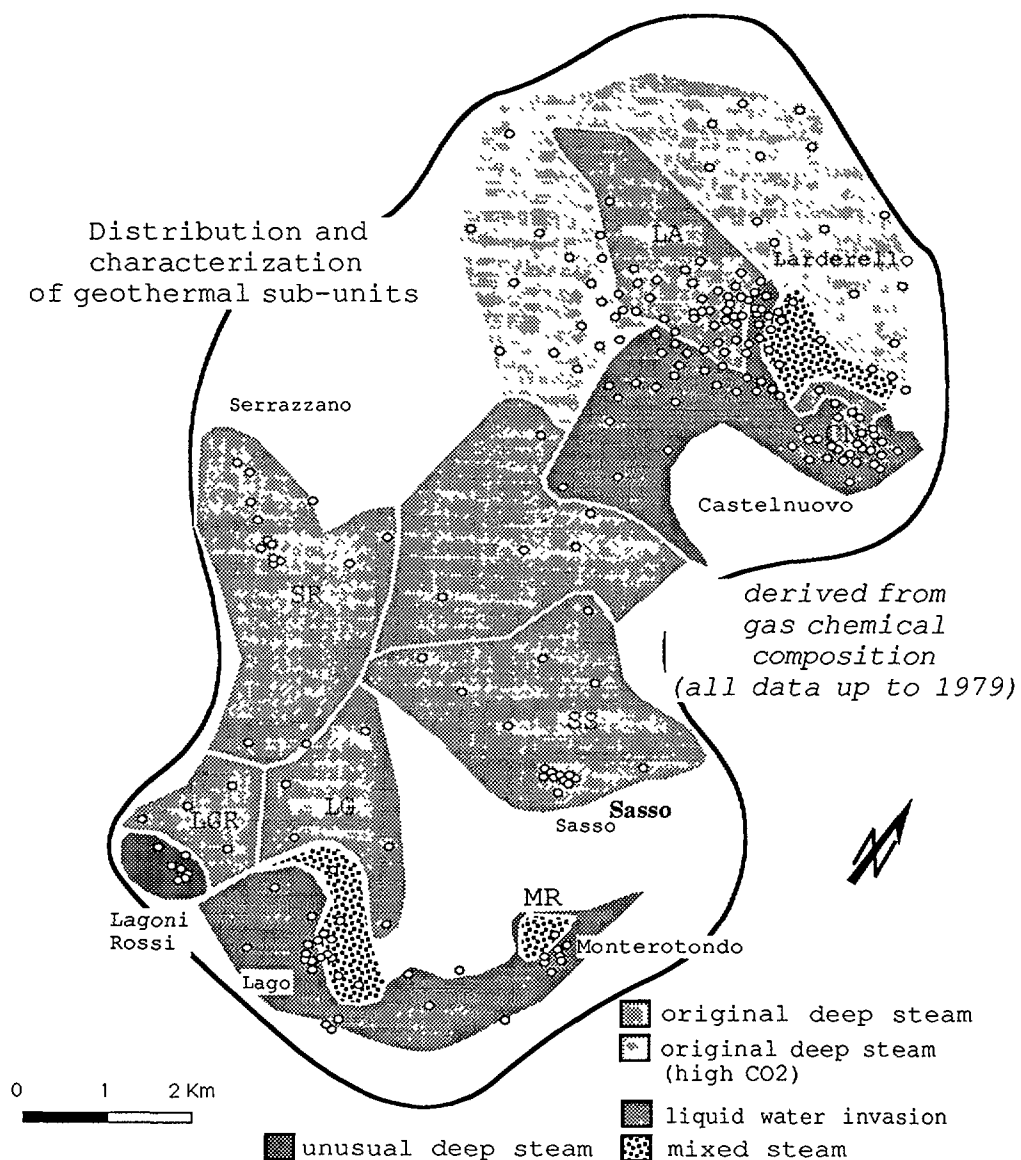


Figure 7. Zonation of the Larderello geothermal field derived from chemical analyses of the fluids delivered by productive wells from exploitation to the beginning of the reinjection (1979).



The two different mixing processes produce opposite effects on the gas contents of the fluids in the different zones. In fact, the inflow of recent cold waters results to a dilution of the gas content of the deep fluids, because the former are gas depleted with respect to the latter ones. On the contrary, addition of CO<sub>2</sub> to the deep system tends to increase strongly the amount of the gaseous phase. From the isotopic point of view, both mechanisms appear to introduce isotopic targets. The steam derived by recent waters is depleted by about 3‰ with respect to the inner fluids, as reported by Panichi et al. [5]. The CO<sub>2</sub> produced by wells with higher gas contents is depleted in <sup>13</sup>C by more than 3‰ with respect to the deep CO<sub>2</sub>.

#### 4. CHEMICAL AND ISOTOPIC EFFECTS OF REINJECTION

D'Amore et al. [3] show the effects on stable isotopes and gas contents of the steam produced in wells nearly the reinjection site in Larderello. Data referring to productive wells of the inner part of the field, where additional processes such as infiltration of local cold water or lateral steam condensation are little or absent are reported by Bolognesi et al. (1990).

In general,  $\delta D$ ,  $\delta^{18}O$ , gas/steam ratio and CO<sub>2</sub> contents may be successfully used in order to evaluate the amount of the reinjected water recovered by each productive well. The correlation between gas and stable isotope contents appears to persist for any proportion in the deep and reinjected components. Whereas the isotopic composition of the steam is clearly affected by mixing with reinjected waters in the vicinity of the reinjection sites only, the isotopic composition of gas appears to be modified over much wider zones [4].

D'Amore et al. [3] reported small variations in the concentrations of the H<sub>2</sub> and H<sub>2</sub>S components during the 1979-1982 reinjection tests. This suggests that the variations of the other gas components may be used for the evaluation of the processes occurring in the productive reservoir after reinjection.

##### 4.1. Chemical and isotopic variations of the gas components

Figure 8 shows the compositional variations between H<sub>2</sub>O-CO<sub>2</sub>-N<sub>2</sub> and H<sub>2</sub>O-CO<sub>2</sub>-H<sub>2</sub> species of the gas discharged by four wells located at different distances from reinjection sites.

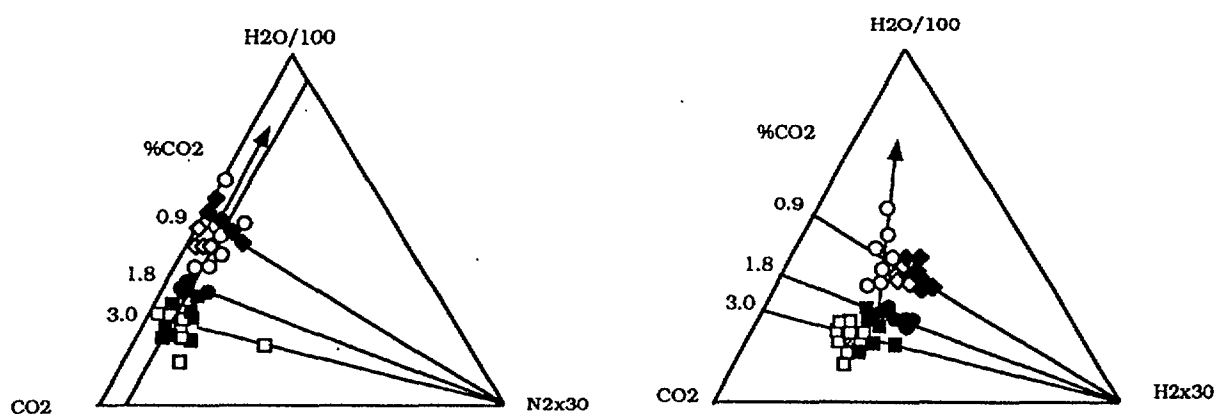


Figure 8. Relative concentrations of H<sub>2</sub>O, CO<sub>2</sub>, N<sub>2</sub> and H<sub>2</sub> (mmol/mol of total fluid) observed in three selected wells before (full symbols) and after (open symbols).

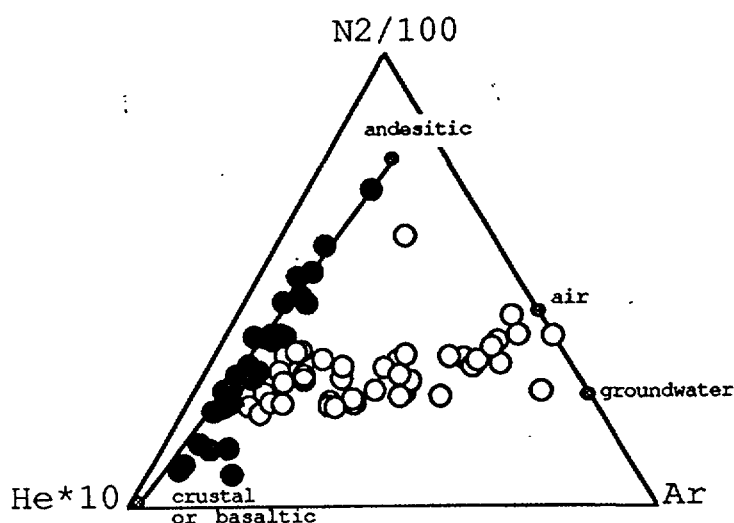


Figure 9. Relative concentrations (mmol/mol on water free basis) of N<sub>2</sub>, He and Ar components before (full symbols) and after (empty symbols) reinjection. Composition crustal and magmatic fluids together with N<sub>2</sub>/Ar ratios for the atmosphere and air saturated ground-waters are reported for comparison.

The variations observed for CH<sub>4</sub> and H<sub>2</sub>S components are similar to those observed for N<sub>2</sub> and H<sub>2</sub> respectively. The comparison between samples collected before and after-reinjection (full and empty symbols) indicates that only well No.137 is strongly affected by the injected water. The distribution of the data (Fig. 8) can be explained by a mixing between a deep component with a CO<sub>2</sub> content of about 1.8 % and injected gas-depleted water. In the case of the other three wells the composition of H<sub>2</sub> hardly changed.

H<sub>2</sub> variations imply that dilution effects of reinjected water are still evident even if the gas/steam ratios are not sensibly affected. On the other hand, the distribution of N<sub>2</sub> suggests that reinjected water contributes largely to define the content of N<sub>2</sub> in the geothermal fluid. Well No. 137 trends, in fact, towards the point where the N<sub>2</sub> / H<sub>2</sub>O ratio corresponds to that of the air saturated groundwater at 20°C.

The contribution of meteoric gases to the fluids discharged after reinjection is well documented by Figure 9, where the relative contents of N<sub>2</sub>, He and Ar components are reported for gas mixtures collected before and after-reinjection.

Injected and/or infiltrated waters previously equilibrated with the atmosphere introduce in the deep reservoir  $2.5 \times 10^4$  mmol/mol of Ar. This amount is very similar to the average content of this component in the fluid produced during the period 1930-1965 ( $1.6 \times 10^4$ ). However the two endmembers differ in the N<sub>2</sub> contents. The N<sub>2</sub>/Ar ratios are between 38 and 84 (values for the air and for the saturated underground-water, respectively), while in the original fluid this ratio is about 800. The radiogenic He is present in the deep fluid with a concentration of about  $4 \times 10^{-4}$  mmol/mol, but is completely absent in the secondary steam produced by reinjected waters.

The observed trend in Figure 9 seems to be the result of a simple mixing between deep components and the meteoric ones, introduced by waste fluids. Empty circles refer to gas emerging everywhere in the Larderello geothermal system, while full circles represent the situation recorded in the inner part of the field. In general, we can see that pre-reinjection data are able to define a mixing process between an almost pure magmatic component and a crustal one. Post-reinjection data reveal Ar as a very sensitive gas for evaluating the amount of the reinjected water in a single well. The usefulness of this tracer will be of the same order as the isotopic composition of the steam and the gas/steam ratio. Because the distribution coefficients of gases are high in the liquid/vapor transitions, gas concentrations in the produced steam are highly sensitive to the fraction of the injected water which evaporates nearby the productive zone.

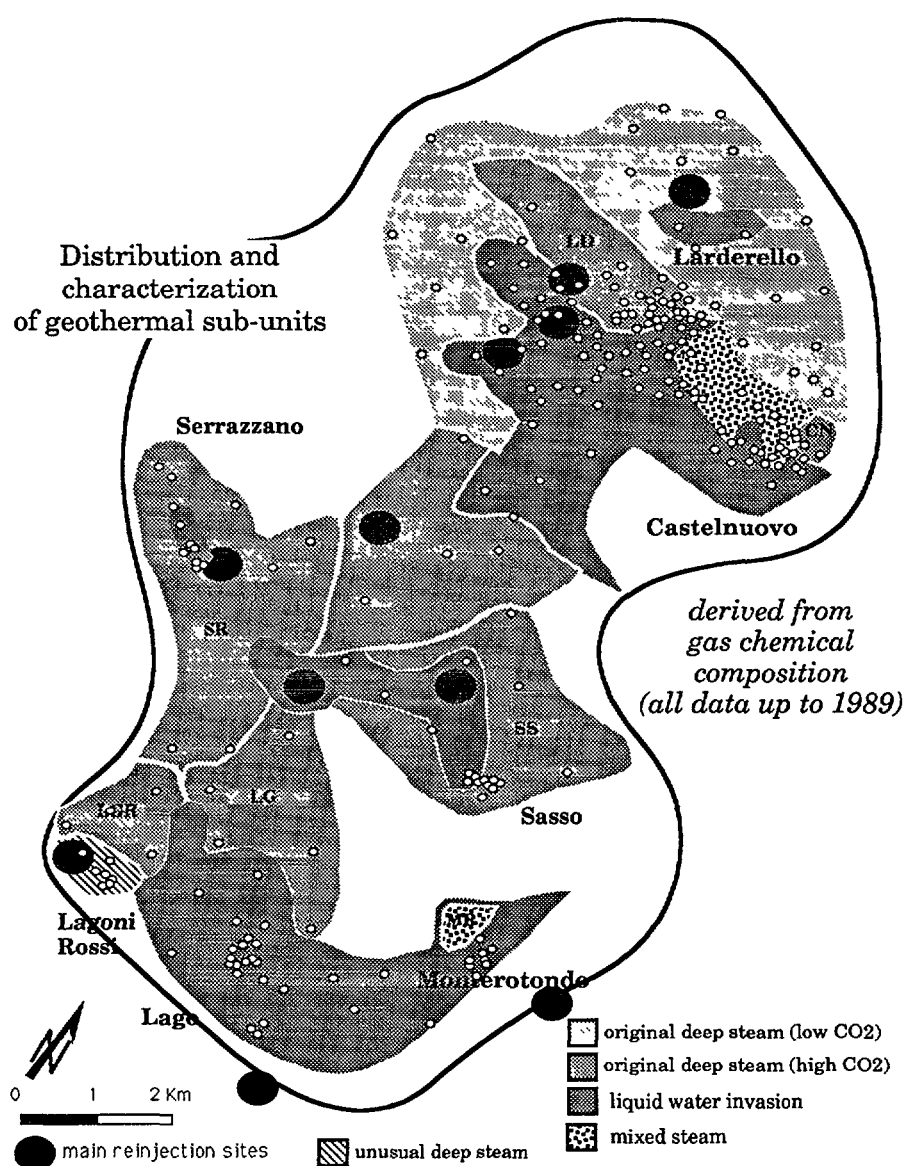


Figure 10. Zonation of the Larderello geothermal field derived from chemical analyses of the fluids delivered by the productive wells after reinjection. Reinjection sites used in the period from 1979 to 1989 are indicated.

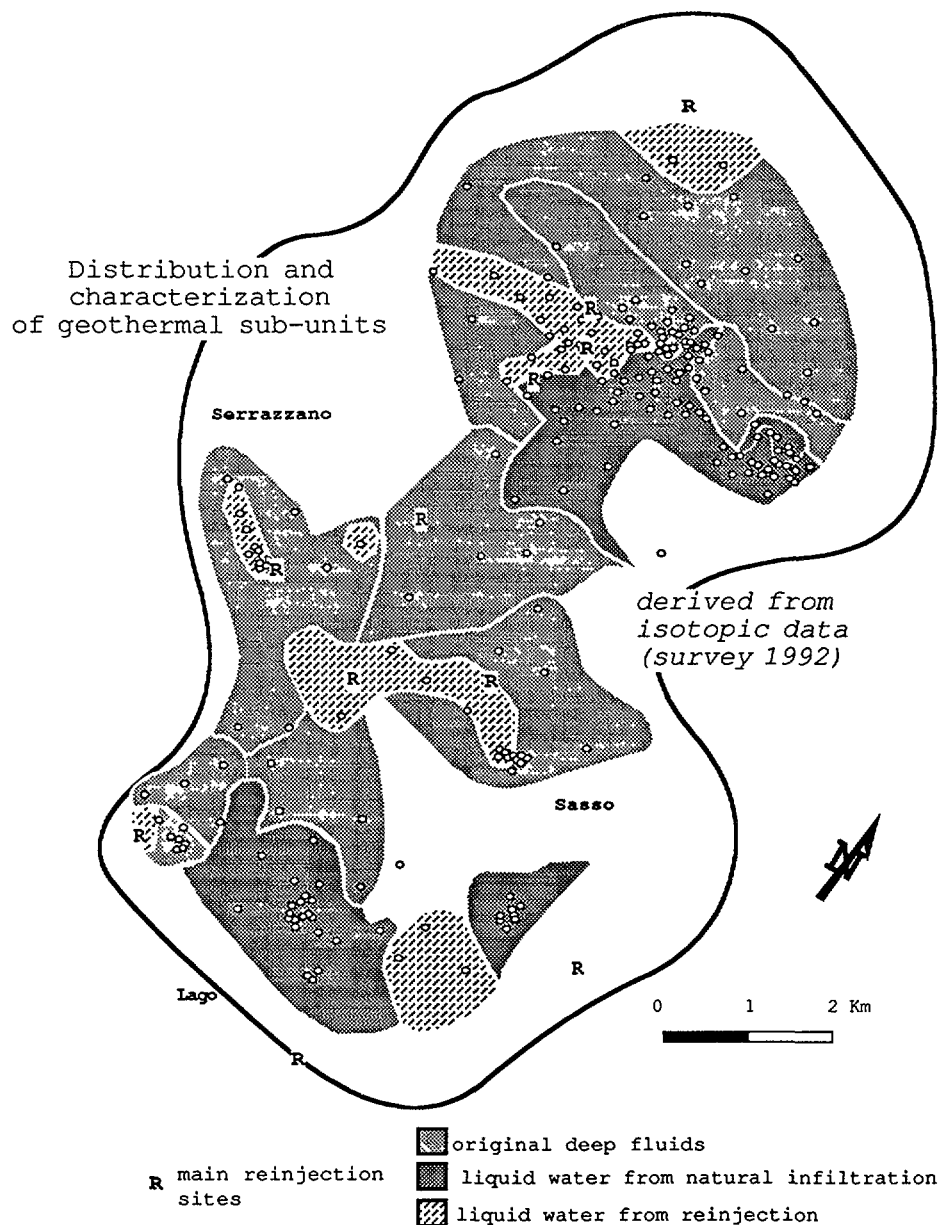


Figure 11. Zonation of the Larderello geothermal field derived from the isotopic analyses of the steam produced during reinjection.

In evaluating recovery coefficients (i.e. of the amount of the reinjected water which is recovered from the productive wells near the injection sites), probably the relative concentrations of Ar, He and N<sub>2</sub> (or CO<sub>2</sub>) may represent a tool which reflect 'immediately' the variations occurring in the reinjection sites. On the other hand, the use of stable isotopic composition of the steam delivered at the surface may give 'smoothed' results because the secondary vapour (from injected waters) consists of an admixture of the new evaporation fronts and steam from residual liquid plumes.

A picture of the state of the field in 1988 was obtained from the trends in the H<sub>2</sub>O-CO<sub>2</sub>-H<sub>2</sub> and H<sub>2</sub>O-CO<sub>2</sub>-CH<sub>4</sub> diagrams for all the wells for which analyses were performed after the start of reinjection. The reference cores, and the vapour-rich zones of the field induced by the natural inflow or artificial injection of water are distinguishable in Figure 10. These

two different contributions are generally recognisable, but cannot be discriminated on the basis of the gas chemistry. For both of them the variation consists of a substantial dilution of the original gaseous mixtures.

In August 1992, an isotopic survey was carried-out in the field to distinguish the contribution of the natural fluid relative to the injected ones. Considering the range of the isotopic variations of the vapor produced before injection ( $\delta D = -40\text{‰}$  = constant, and  $\delta^{18}O$  ranging between  $-6\text{‰}$  and  $0\text{‰}$ ), the natural recharge ( $\delta D \simeq -40\text{‰}$   $\delta^{18}O \simeq -7\text{‰}$ ) tends to modify only the  $^{18}O$  content of the steam, while the share of injected water ( $\delta D$  and  $\delta^{18}O \simeq +5\text{‰}$ ) determine the variations in both isotopes.

The congruence of  $\delta^{18}O$  and  $\delta^2H$  distribution over the entire field (Fig. 11) with the chemical data is very good. The slight differences are changes in injection wells and the different response of the two methodologies for drawing up these maps. In addition, man-made and natural recharges are well distinguished.

## 4.2 Variations in the physical conditions of the fluid at depths

A preliminary evaluation of the isotopic disequilibrium between the gaseous components of the geothermal fluid induced by reinjection was described by Bolognesi et al. [4]. Additional data on  $^{18}O$ ,  $^2H$  and  $^{14}C$  variations of the fluid discharged by 20 wells, confirm that samples after injection show a decrease in the isotopic temperatures.

Figure 12 shows that  $CH_4$  and  $CO_2$  have sufficient time to reach new isotopic equilibrium in the deep reservoir. Two distinct trends are illustrated by the  $CO_2$ - $CH_4$  geothermometer. First, injection induces production of  $CH_4$  and  $CO_2$  which simulate temperatures similar to those at the wellhead, i.e.  $40^\circ C$  lower than the values evaluated in absence of reinjection. On the contrary, the computed temperatures for the same wells show large variations from  $-20$  to  $+80^\circ C$  with respect the pre-injection data.

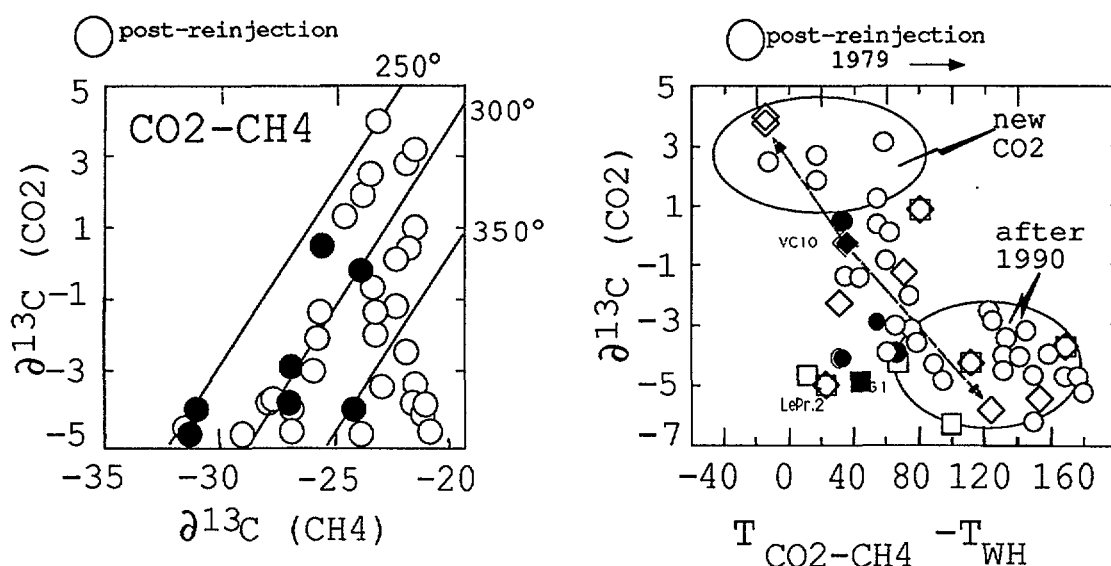


Figure 12. Relationship between  $^{13}C$  contents in  $CO_2$  and  $CH_4$  for selected wells after and before reinjection. Deviations of the isotopic temperatures from those measured at well-head are also shown.

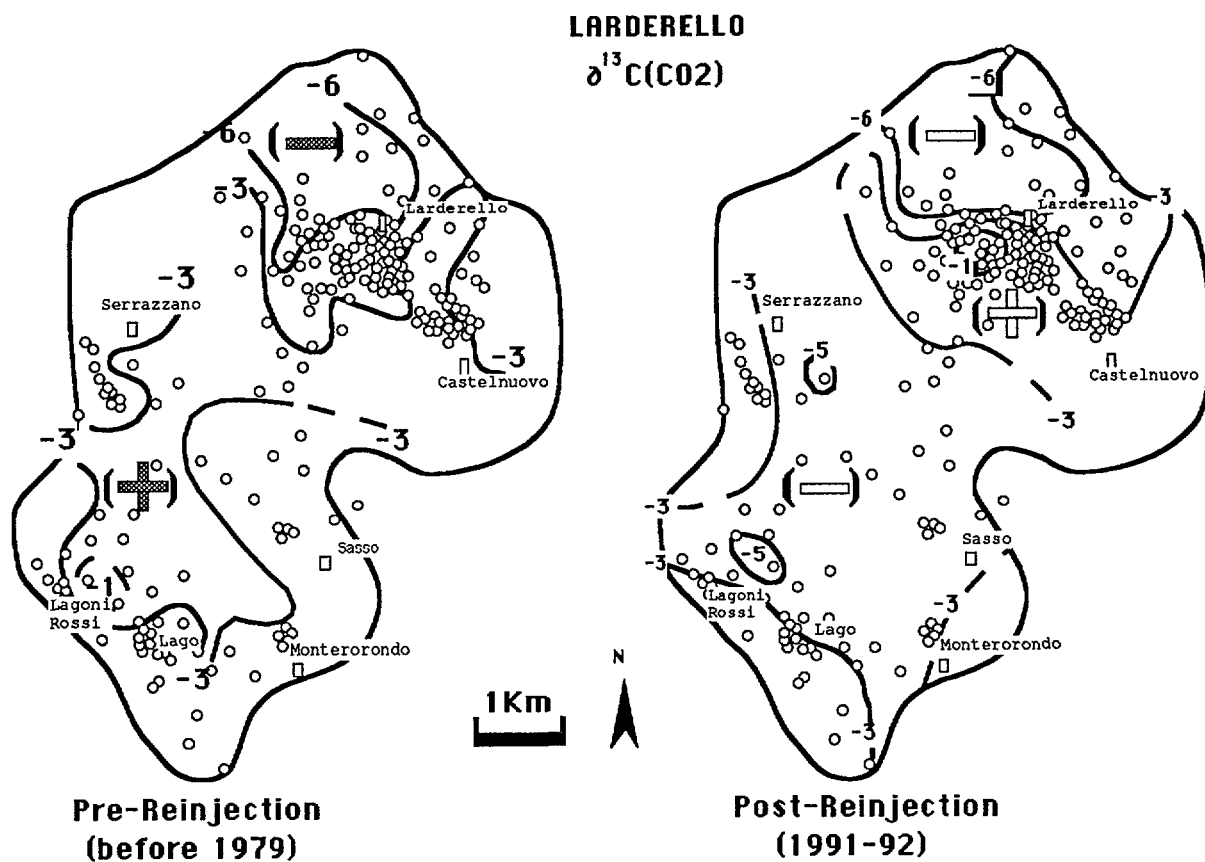


Figure 13. Distribution of  $\delta^{13}\text{C}$  contents of carbon dioxide produced by the wells before and after reinjection.

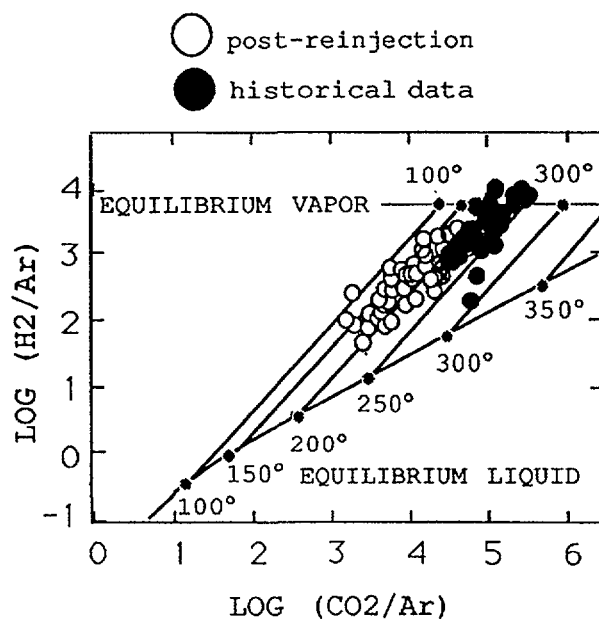


Figure 14. Evaluation of H<sub>2</sub>-Ar and CO<sub>2</sub>-AR equilibrium conditions. The concentrations are expressed in mmol/mol on water free basis.

In this case variations appear to be essentially due to significant changes in the isotopic composition of carbon dioxide.

The geographical distributions of  $\delta^{13}\text{C}$  values of  $\text{CO}_2$  in the field before and after reinjection (Fig. 13), indicate that important variations are induced by the injection of liquid water in the steam reservoir. Largest variations occur in the inner part of the field, where two distinct trends develop. In the north-eastern part, the more positive  $\delta$  values appear to be due to a newly formed  $\text{CO}_2$ , from the reaction of liquid water with limestones in that area. The central and south-western areas appear to be characterised by a very light  $\text{CO}_2$  of unknown origin. Figure 13 also shows that the peripheral areas are not yet affected by these mechanisms.

Disequilibrium conditions at depth are also supported by the relationship between  $\text{H}_2$ ,  $\text{CO}_2$ , and Ar after-reinjection period. From an original composition representing near-vapor equilibrium conditions at about 250 °C, an alignment along the 200 °C isotherm is shown in Figure 14 as a consequence of a progressive influence of the injected water on the deep component. However, evaluated chemical temperatures from Figure 14 may only be apparent, because the observed variations may be ascribed to the addition of the Ar component to the geothermal system.

In addition,  $\text{N}_2 / \text{He}$  ratio appear to be a discriminating factor for surface fluids introduced in the geothermal reservoir either from an injection process or from a natural infiltration induced by de-pressurisation of the reservoir due to the exploitation.

### References

- [1] NUTI, S. CALORE, C. AND NOTO, P. 1981. Use of environmental isotopes as natural tracers in a reinjection experiment at Larderello. Proc. 7st Stanford Geothermal Reservoir Eng. Workshop, p. 85-89.
- [2] BERTRAMI, R., CIONI, R., CORAZZA, E., D'AMORE, F., MARINI, L. (1985) Carbon monoxide in geothermal gases. Reservoir temperature calculations at Larderello (Italy). Geothermal Res. Counc. Trans. 9, 299-303.
- [3] D'AMORE, F., FANCELLI, R., PANICHI, C. (1987) Stable isotope study of reinjection processes in the Larderello geothermal field. Geochim. Cosmochim. Acta, 51, 857-867.
- [4] BOLOGNESI, L., NOTO, P. AND PANICHI, C. (1990) More mileage for the isotope gas geothermometers: the case of the Larderello geothermal field. Geothermal Res. Counc. Trans. 14/2, 857-861.
- [5] Panichi, C., Celati, R., Noto, P., Squarci, P., Taffi, L. and Tongiorgi, E. (1974) Oxygen and hydrogen isotope studies of the Larderello (Italy) geothermal system. In: Isotope Techniques in Groundwater Hydrology, 1974. IAEA, Vienna, 2, 3-28.
- [6] D'AMORE, F., CELATI, R., FERRARA, G.F., PANICHI, C. (1977) Secondary changes in the chemical and isotopic composition of the geothermal fluids in Larderello field. Geothermics, 5, 153-163.

- [7] TRUESDELL, A.H. AND NEHRING, N.L. (1978) Gases and water isotopes in a geochemical section across the Larderello, Italy geothermal field. *Pure and Applied Geophysics*, 117, 276-289.
- [8] MAZOR, E. (1978) Noble gases in a section across the vapor-dominated geothermal field of Larderello, Italy. *Pure and Applied Geophysics*, 117, 262-275.
- [9] SESTINI, G. (1970) Superheating of geothermal steam. In *Proc. U.N. Symposium on the Development and Utilisation of Geothermal Resources*, Pisa, 1970: Geothermics Spec. Issue 2, 2, 622-648.
- [10] PETRACCO, C. AND SQUARCI, P. 1975. Hydrologic balance of Larderello geothermal region. *Proc. 2nd U.N. Symposium on Development and Use of the Geothermal Energy*, San Francisco, 1975, 1, 521-530.
- [11] D'AMORE, F. AND TRUESDELL, A.H. (1979) Models for steam chemistry at Larderello and The Geysers. *Proc. Fifth Workshop Geothermal Reserv. Eng.*, Stanford, California p. 283-297.
- [12] SBORGI, U. (1934) Studi e ricerche sui gas dei soffioni borsciferi con particolare riguardo al loro contenuto in elio ed altri gas nobili. *Reale Accademia d'Italia*, 5, 667-713.



# ENVIRONMENTAL ISOTOPE-AIDED STUDIES ON GEOTHERMAL WATER IN THE REPUBLIC OF KOREA

J.S. AHN, Y.K. KOH  
Korea Atomic Energy Research Institute,  
Taejon, Republic of Korea

**Abstract** - *The typical geothermal water in the Yusung geothermal area, Korea, located in Mesozoic plutonic rocks, has been studied for its characteristics by means of analyzing its tritium, oxygen-18, deuterium and chemical composition. Cold waters, including waters of superficial origin in the same area, were also studied. Deuterium and oxygen-18 contents of thermal groundwater indicate its meteoric-water origin and show the absence of recognizable oxygen isotope ( $^{18}\text{O}$ ) shift to high oxygen-18 composition, likely due to relatively low reservoir temperature. The chemical composition of the Yusung geothermal waters shows that they are partially equilibrated and have mixed with the fresh waters in the upflow. Temperature obtained from the Na-K geothermometer is considered to be reasonably representative of reservoir temperatures. The K-Mg geothermometer re-equilibrates rapidly upon cooling and yields for that reason low temperature estimates. Reservoir temperature, according to the Na-K geothermometer, are between 103°C and 133°C. It is inferred that the source of heat is magmatic. The best permeability is considered to be fault controlled.*

## 1. INTRODUCTION

Research related to geothermal resources in Korea is still at an early stage. Geothermal areas have mostly been studied in a regional scale in terms of geological setting, lithology, and general chemical characteristics of groundwater compositions [1, 2, 3]. Therefore, studies focused on the nature and the evolution of geothermal water such as the age of geothermal water, water/rock interaction, and interaction or mixing between geothermal water and cold groundwater have been very limited. As an effort of more systematic study on geothermal water in South Korea, the Yusung geothermal area, located 150 km south of Seoul, was selected as a study site in this project. The tritium, oxygen-18, and deuterium isotopic contents of water samples taken between June 1990 and May 1993 were studied to improve the understanding of the origin of geothermal waters in this area and their chemical compositions were also studied and compared with those of environmental isotopic data to correlate their origins with geological structures in this area and to predict subsurface temperatures [4, 5].

The development of geothermal water of Yusung area for commercial purposes by modernized methods began around the early 20th century. Since then, due to the rapid increase of water demands, the depth of bore holes for pumping hot waters become deeper, around 200m up to 360m. Average pumping rate per day at present is about 6,150M/T.

## 2. SITE DESCRIPTION

The Yusung area is composed of Mesozoic plutonic rocks and dykes (Fig. 1). Metasedimentary rocks of unknown age (pre-Jurassic) envelop the Mesozoic plutonic rocks of the Yusung area [6]. The plutonic rocks are classified as schistose granite and two bodies

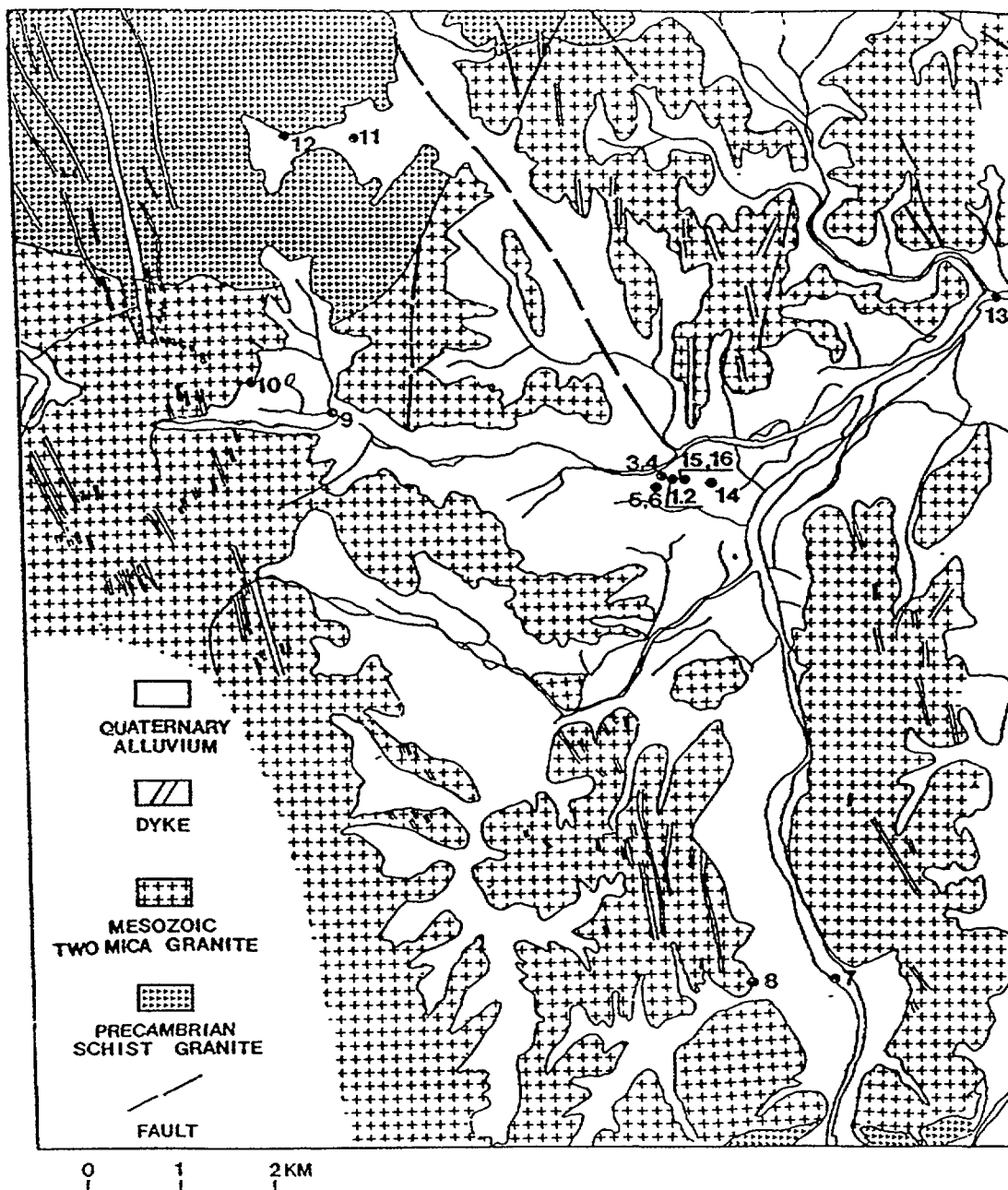


FIG. 1. Geological map of Yusung area. Sampling sites are indicated in Arabic numbers.

of mica granite which intruded the former. The dykes ubiquitously intruded the plutonic rocks throughout the area[7].

The main minerals of the schistose granite are quartz, plagioclase, microcline and biotite. Chlorite, epidote, and muscovite are secondary minerals. The two mica granites are medium to fine grained and composed of quartz, perthite, microcline, plagioclase, biotite, and muscovite with accessory minerals of zircon, rutile, apatite and magnetite. The dykes are quartz porphyry, porphyry granite and aplite. Alluvial deposits are distributed along the river valley and flood plains of major streams having a thickness of 3 to 11m.

Of special interest is patterns of the dyke and fault structures, both of which are post-Jurassic features. Most dykes have a N-S trend but faults strike N45°W.

### 3. SAMPLING AND ANALYTICAL PROCEDURES

In all 16 water sampling site were selected in the Yusung area (Fig. 1). Sampling at each site was carried out threetimes, in June 1990, July 1991 and May 1993. Water samples were categorized into three types based on the temperature and the depth of samples: hot water - temperature ranges  $33^{\circ} \sim 52^{\circ}\text{C}$  and depth of drilling is between 220 and 360m, cold water - temperature ranges  $15^{\circ} \sim 25^{\circ}\text{C}$  and depth of drilling is between 130 and 250m, and surface waters - waters from surface and subsurface (depths are less than 33m). Drilling and sampling of cold groundwaters were mostly done very adjacent to the sites of thermal waters at the same time. Therefore, the site of cold groundwaters of sample Y-1, Y-3 and Y-5 were near to these of thermal waters of sample Y-2, Y-4, and Y-6 respectively (Fig. 1).

pH, oxidation potential, and temperature were measured in situ using portable meters. Tritium contents were measured in KAERI. The contents were measured by liquid scintillation counting after the electrolytic enrichment process. Oxygen-18 and deuterium contents were analyzed in IAEA and the Centre for the Application of Isotope and Radiation in Indonesia. The major dissolved constituents were determined in IAEA by atomic absorption spectrometry, by ion chromatography and by titration (alkalinity) using standard methods. The results of stable isotopes, tritium, and chemistry are reported in Tables 1, 2, and 3, respectively.

### 4. RESULTS AND DISCUSSION

Oxygen-18 and deuterium compositions are shown in Table 1. Hot waters are weakly alkaline with pH in the range of 7.7 ~ 8.7. pH of cold waters ranges from 6.8 to 7.5. and those of surface waters are neutral to slightly acidic with a range of 5.7 ~ 7.3.

Two sets of samples were analyzed for oxygen-18 and deuterium contents.  $\delta^{18}\text{O}$  and  $\delta\text{D}$  values of hot waters range from -7.3 to -8.2 ‰ and -49.6 to -59.3 ‰, respectively. Ranges of cold waters are from -6.4 to -7.7 ‰ and -43.3 to -55.2 ‰. The oxygen-18 and deuterium contents are plotted in Fig. 2. All data are clustered along the world-wide meteoric water line ( $\delta\text{D} = 8 \delta^{18}\text{O} + 10$ ) determined by Craig [8]. The oxygen-18 and deuterium values of precipitation taken in Yusung area correspond also well to the world wide meteoric water line [9]. It is, therefore, apparent that the cold and thermal waters represent local meteoric water. The absence of oxygen shift of hot waters to a high oxygen-18 composition must be due to their relative low reservoir temperatures, which is hardly sufficient to expect an oxygen isotope exchange with the host rock.

Tritium contents are listed in Table 2 and are plotted in Figs. 3 and 4. The tritium contents of most surface waters (Y-7, Y-9, Y-10, Y-11, and Y-13) range from 5.9 to 11.8 TU except those of Y-7 sampled in August 1990. Y-8 and Y-12 show distinctively higher tritium contents than other samples. They show somewhat large variation with time (3.3 ~ 3.6 TU). Generally, tritium contents of cold waters are closer to those of surface waters than those of hot waters. Those of samples Y-3 and Y-5 vary within a range of 2.5 TU and are close to each other. The tritium content of Y-1 is lower than Y-3 and Y-5 by more than 4 TU. The tritium content of Y-15 sampled in June 1990 is very low (3.5 TU) or close to those of hot waters, but those of samples collected during other periods are very close to that of Y-1 (cold water). Hot waters are generally the lowest in tritium. Among hot waters, Y-2 and Y-4 are very uniform and lowest in tritium. Y-6 is higher than these by more than 1 TU (Fig. 4).

TABLE 1. ENVIRONMENTAL STABLE ISOTOPIC COMPOSITIONS OF VARIOUS WATER SAMPLES FROM THE YUSUNG GEOTHERMAL AREA

Sample No.	Sampling Date	Sampling Depth(m)	Water Type <sup>1)</sup>	$\delta^{18}\text{O}$ (‰)	$\delta\text{D}$ (‰)	Temp. (°C)	pH	E (mV)
Y-1	June 1990	320	C	-6.8	-45.3	22.0	7.3	8
	July 1991					22.2	7.4	-4
	April 1992			-6.9	-45.3	21.0	7.2	5
Y-2	June 1990	220	H	-7.7	-51.9	47.0	8.5	-68
	July 1991					40.8	8.4	-69
	April 1992			-7.8	-53.5	39.7	8.3	-52
Y-3	June 1990	130	C	-7.7	-55.2	15.3	6.9	31
	July 1991					15.7	7.1	13
	April 1992					16.6	6.8	30
Y-4	June 1990	350	H	-7.4	-55.7	49.0	8.5	-62
	July 1991					47.5	8.3	-68
	April 1992					45.1	8.3	-61
Y-5	June 1990	254	C	-6.4	-43.3	24.2	7.5	3
	July 1991					24.0	7.1	10
	April 1992			-7.2	-50.3	21.6	7.4	19
Y-6	June 1990	350	H	-8.2	-59.3	52.0	8.2	-42
	July 1991					44.5	8.1	-49
	April 1992			-8.2	-56.7	45.9	8.4	-40
Y-7	June 1990	0	S	-7.1	-56.1	14.5	6.9	27
	July 1991					15.0	6.9	24
	April 1992			-5.3	-34.7	15.3	7.0	32
Y-8	June 1990	3	S	-7.9	-47.5	10.5	6.0	90
	July 1991					12.5	5.9	83
	April 1992			-7.9	-53.7	11.9	5.9	94
Y-9	June 1990	0	S	-7.9	-59.1	12.4	6.5	56
	July 1991					11.5	6.6	43
	April 1992			-6.9	-46.2	12.9	6.7	51
Y-10	June 1990	8	S	-7.2	-51.3	11.2	6.0	86
	July 1991					11.9	6.1	69
	April 1992			-7.9	-55.1	12.7	6.0	88
Y-11	June 1990	0	S	-7.2	-56.5	10.9	6.9	29
	July 1991					13.1	6.7	34
	April 1992					12.7	6.8	53
Y-12	June 1990	33	S	-7.9	-50.6	12.5	6.4	62
	July 1991					12.9	6.4	50
	April 1992			-7.9	-52.8	12.9	6.5	62
Y-13	June 1990	0	S	-7.8	-53.9	14.8	6.9	29
	July 1991					16.2	7.0	19
	April 1992			-5.7	-38.0	15.6	7.3	11
Y-14	June 1990	285	H	-6.5	-50.0	42.0	7.7	-18
	July 1991					44.0	8.0	-45
	April 1992			-7.6	-50.2	33.7	7.6	-18
Y-15	June 1990	220	H	-7.7	-51.4	34.5	8.4	-55
	July 1991					33.9	7.9	-37
	April 1992			-7.4	-51.4	33.1	7.8	-28
Y-16	June 1990	300	H	-7.3	-49.6	40.2	8.7	-70
	July 1991					39.1	7.8	-31
	April 1992			-7.8	-54.3	36.3	7.8	-31

<sup>1)</sup> C = cold groundwater, H = thermal groundwater, S = surface water.

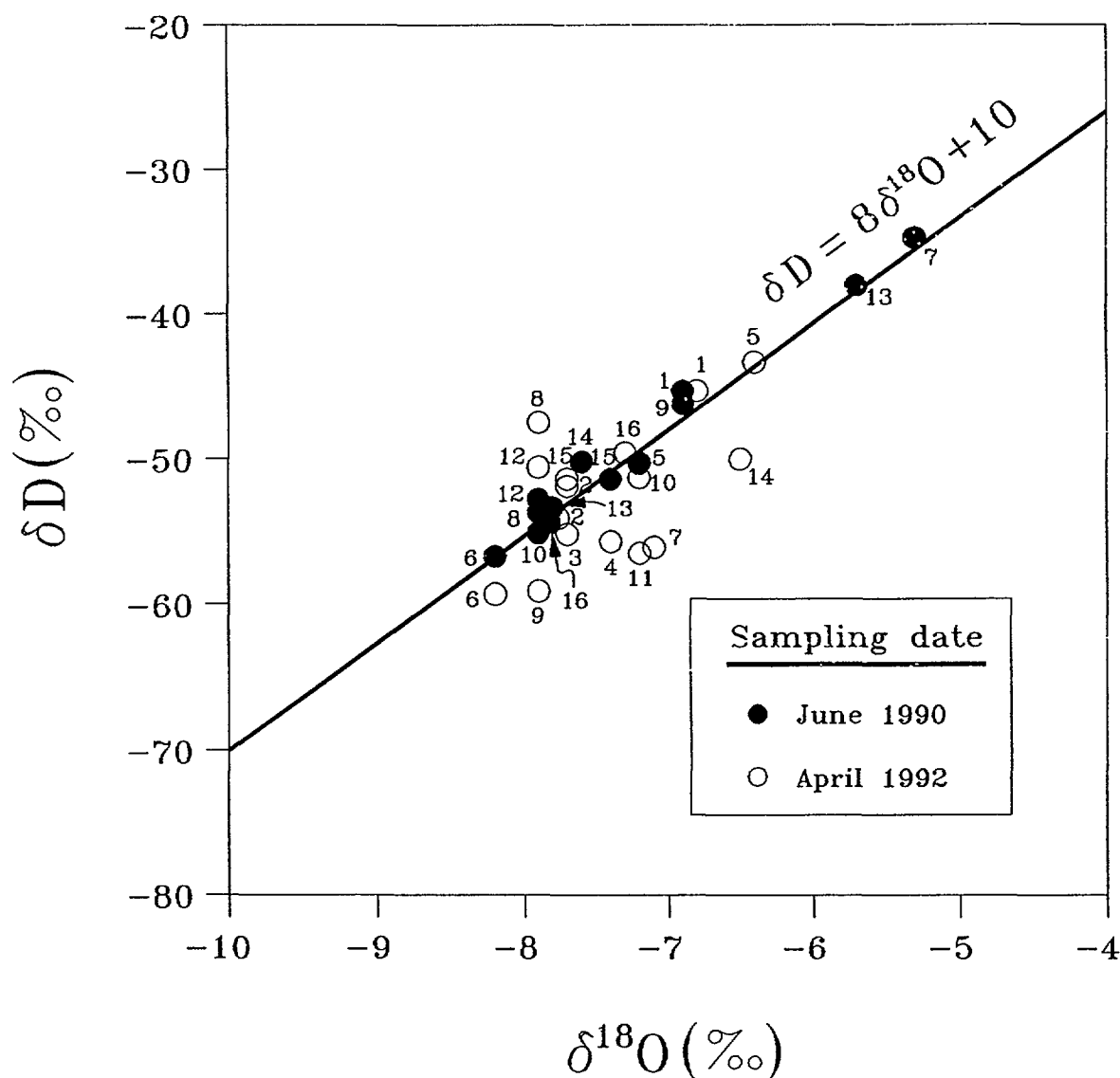


FIG. 2. Correlation between  $\delta^{18}\text{O}$  and  $\delta\text{D}$  values of various water samples from the Yusing area. See Table 1 for sample descriptions.

By reference to the tritium content of precipitation in the Taejon area, near Yusing during the past years [10], the low values of tritium of hot waters may be explained by considering them as recharged waters during pre-thermonuclear period. As an explanation of the source of geothermal water, we exclude the recent (post-thermonuclear period) meteoric waters which have recharged and circulated with the large flow rate, short flow distance, and short duration of fluid flow. However, the time elapsed since the thermonuclear period appeared in this country was too long to have significant tritiums left in meteoric waters recharged before the thermonuclear period. It is, therefore, reasonable to consider that the hot waters have mixed with cold waters in the upflow.

The chemical composition of water samples is shown in Table 3. Based on the chemical composition (low metal, low chloride and low sulphate etc.), it is considered that hot waters belong to simple spring water. The composition has been plotted in Piper's diagram in Fig. 5. The major part of the water can be classified as  $\text{Na-HCO}_3^-$  type. The

TABLE 2. TRITIUM CONTENTS (UNIT: TU) OF VARIOUS WATER SAMPLES FROM THE YUSUNG GEOTHERMAL AREA

Sample No. <sup>1)</sup>	Y-1 (C)	Y-2 (H)	Y-3 (C)	Y-4 (H)	Y-5 (C)	Y-6 (H)	Y-7 (S)	Y-8 (W)	Y-9 (S)	Y-10 (W)	Y-11 (S)	Y-12 (W)	Y-13 (S)	Y-14 (H)	Y-15 (H)	Y-16 (H)
Sampling Date																
June 1990	6.26	2.14	10.62	1.68	10.70	4.31	8.90	15.99	7.06	10.24	8.48	14.72	9.71	8.58	3.51	2.01
Aug. 1990	6.19	2.05	9.31	2.18	9.08	3.81	16.36	16.03	7.17	9.39	5.92	13.80	11.19	4.55	3.24	3.68
Apr. 1991	6.24	2.80	9.05	2.32	8.21	3.64	11.83	12.45	10.23	9.19	10.86	13.38	N.A.	7.00	6.79	4.95
July 1991	6.87	2.67	10.42	1.90	9.22	3.76	8.19	13.94	7.67	8.92	8.30	12.10	9.87	7.58	6.68	5.27
Apr. 1990	6.78	3.37	10.29	2.02	9.94	3.37	8.57	13.66	8.27	10.69	8.24	11.38	9.29	8.96	7.03	5.32
Aug. 1992	6.34	N.A.	9.94	1.89	9.61	3.95	N.A.	14.80	10.74	9.00	11.36	12.17	N.A.	8.75	6.88	5.07
May 1993	5.78	3.96	9.63	2.97	10.65	2.86	N.A.	N.A.	9.99	9.51	11.19	N.A.	N.A.	9.47	4.54	3.68

<sup>1)</sup> C = cold groundwater, H = thermal groundwater, S = surface stream water, W = surface well water  
 N.A. = not analyzed.

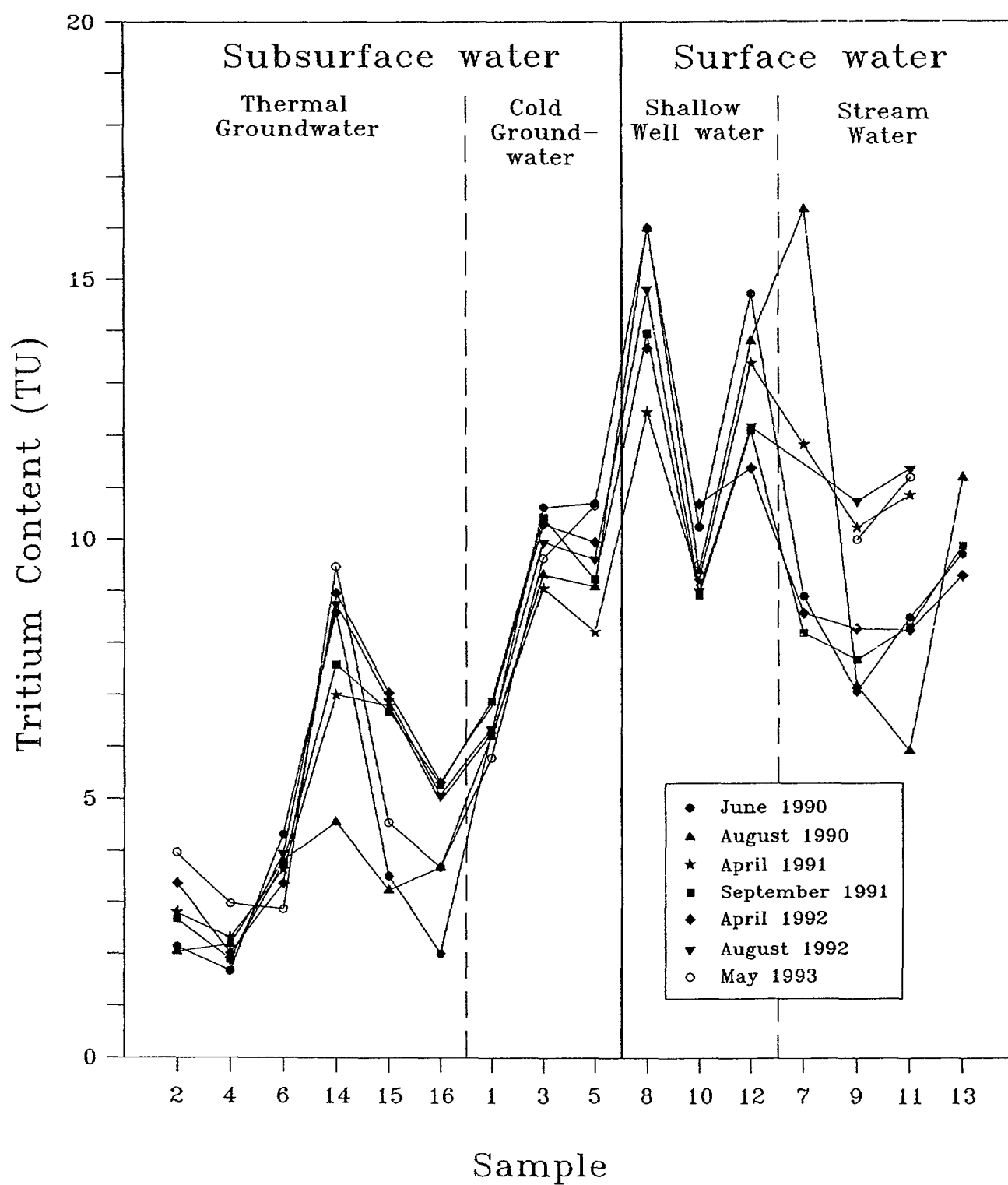


FIG. 3. Tritium contents (unit: TU) of various water samples from the Yusing geothermal area.

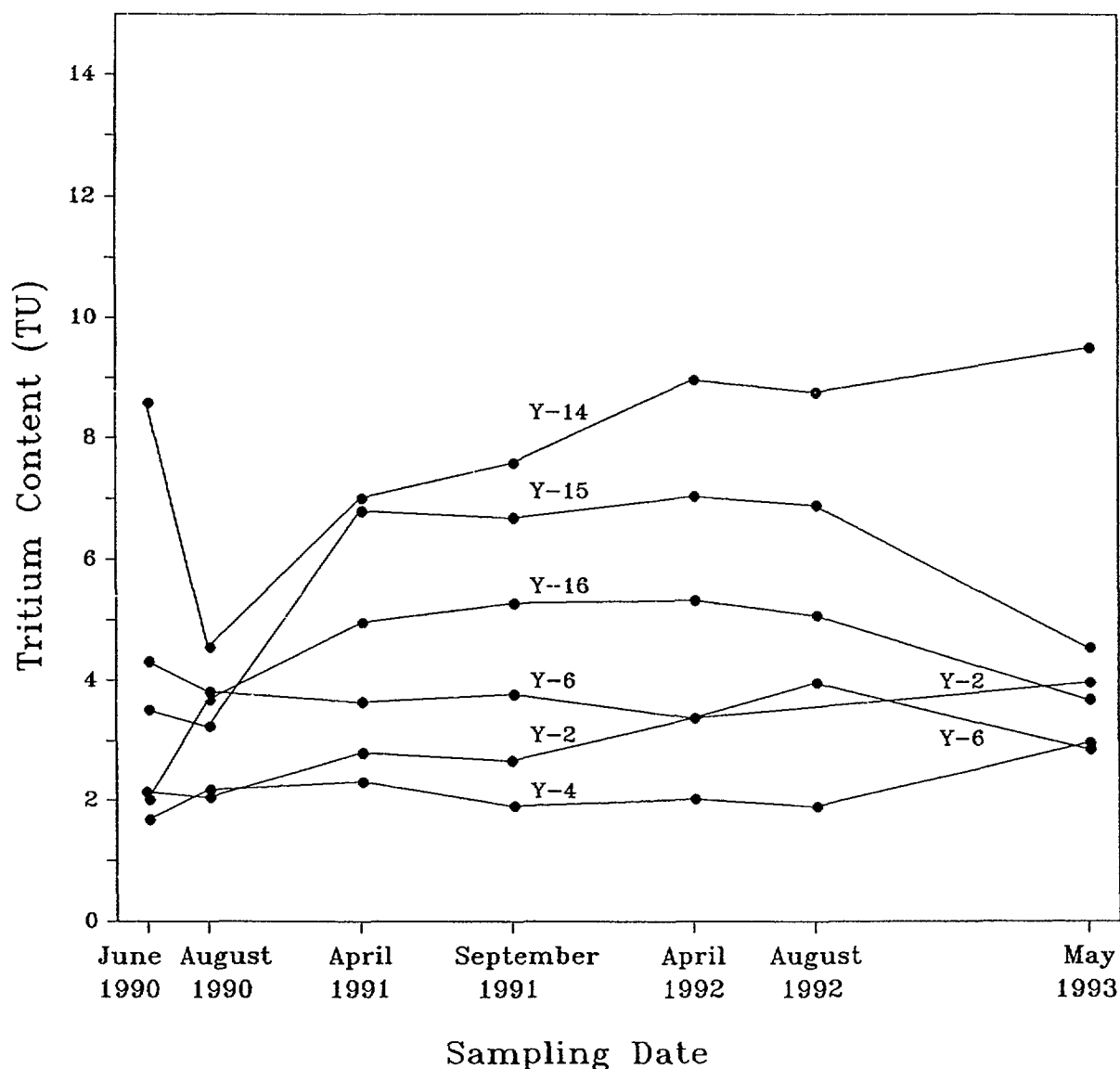


FIG. 4. Seasonal variations of tritium contents (unit: TU) of thermal groundwaters from the Yusing geothermal area.

chemical composition appears to be rather homogeneous and only cations can mark the differences between the hot and other waters. High temperature waters are mainly characterized by the abundance of Na and relative to other cations where an other water types are relatively more enriched in Ca and Mg. Y-1, Y-3, Y-5, and Y-17 water samples, grouped as cold waters by field temperature, show an intermediate chemical composition between hot waters and waters of superficial origins. It seems that cold waters are mixed with some amounts of fresh water through the geological flow channel. Tritium data also show a similar trend (Fig. 3). Moreover, both hot and cold water samples appear to be enriched in F derived from their magmatic source (Table 3).

In Fig. 6, similar to Piper's diagram used in water geochemistry, the Yusing chemical data are plotted with isothermal lines - corresponding to given K/Na (or K/Mg) ratios [9]. A geothermal fluid with a composition falling on this curve has reached equilibrium for both K-Na and K-Mg systems. But Yusing waters are plotted in the lower right region of the diagram corresponding to high Mg. All points of Yusing waters fall aligned on a straight line



TABLE 3. CHEMICAL COMPOSITIONS OF VARIOUS WATER SAMPLES (in ppm)  
FROM THE YUSUNG GEOTHERMAL AREA (May 1993)

Samp[le No. <sup>1)</sup>	EC <sup>2)</sup> ( $\mu$ S/cm)	Na <sup>+</sup>	K <sup>+</sup>	Mg <sup>2+</sup>	Ca <sup>2+</sup>	Cl <sup>-</sup>	SO <sub>4</sub> <sup>2-</sup>	HCO <sub>3</sub> <sup>-</sup>	CO <sub>3</sub> <sup>2-</sup>	NO <sub>3</sub> <sup>-</sup>	PO <sub>4</sub> <sup>-</sup>	F <sup>-</sup>
1(C)	373	56.0	0.82	1.36	23.0	25.7	28.2	133.8	n.d.	2.85	n.d.	4.0
2(H)	347	62.7	1.17	0.15	13.0	23.1	34.1	104.9	3.7	2.34	n.d.	4.3
3(C)	460	49.3	1.05	3.53	43.1	34.8	42.7	159.8	n.d.	9.18	n.d.	1.0
4(H)	267	44.3	0.68	0.25	14.4	15.0	11.7	96.7	4.3	6.49	n.d.	4.4
5(C)	579	72.7	1.11	3.97	53.2	46.3	58.7	162.9	n.d.	20.10	10.1	2.3
6(H)	285	46.7	0.84	0.33	15.5	16.3	13.9	101.9	2.9	7.96	n.d.	4.6
9(S)	182	11.6	2.83	1.70	11.0	13.0	8.6	36.8	n.d.	3.54	n.d.	0.4
10(W)	181	13.8	1.80	2.55	14.0	13.6	11.4	17.9	n.d.	39.40	n.d.	0.5
11(S)	174	8.1	1.98	1.47	11.1	9.0	7.9	38.1	n.d.	1.54	tr.	0.2
12(W)	100	10.6	0.72	0.77	7.6	10.6	1.1	32.7	n.d.	6.71	tr.	0.1
14(H)	428	78.6	1.21	0.04	13.3	28.6	64.9	105.9	2.5	2.50	n.d.	2.5
15(H)	410	73.8	1.91	0.09	15.8	29.3	48.7	118.4	2.0	1.96	n.d.	3.4
16(H)	428	71.4	1.03	0.31	21.2	30.9	49.0	13.1	n.d.	2.83	n.d.	3.7

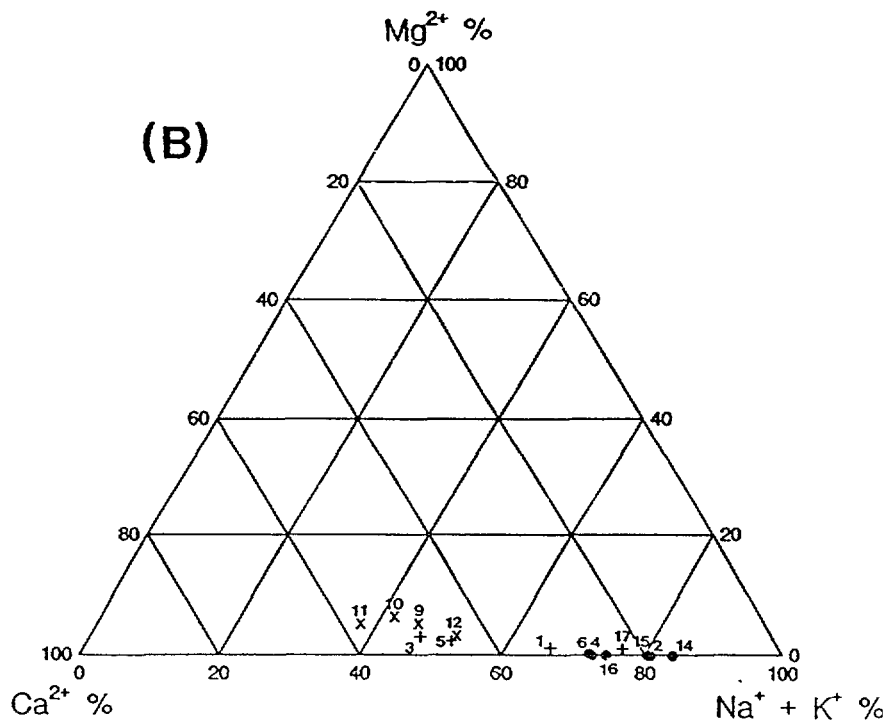
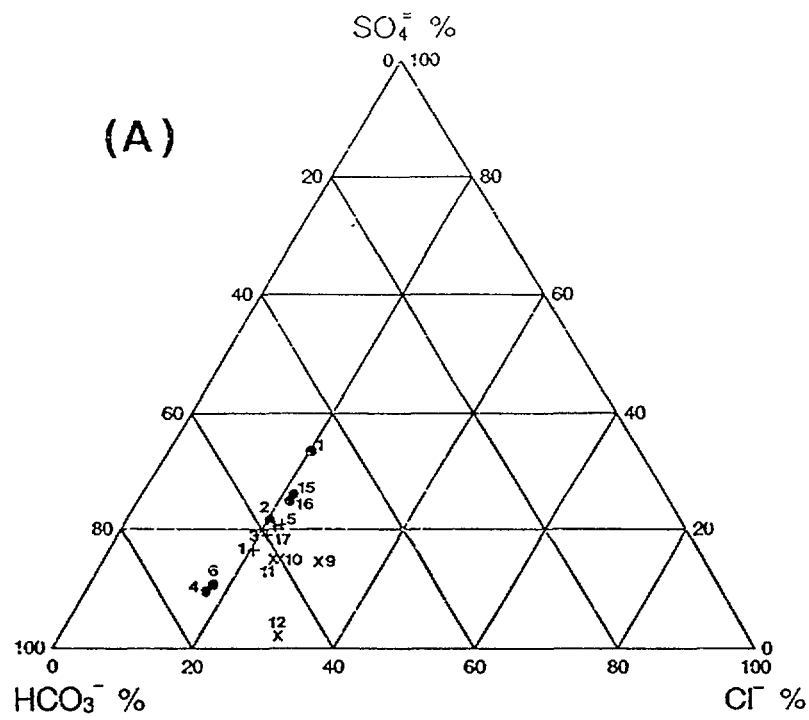
<sup>1)</sup> C = cold groundwater; H = thermal groundwater; S = surface stream water; W = surface well water.

<sup>2)</sup> EC = electrical conductivity

All data in ppm (n.d.= not detected at detection limit; tr.= trace)

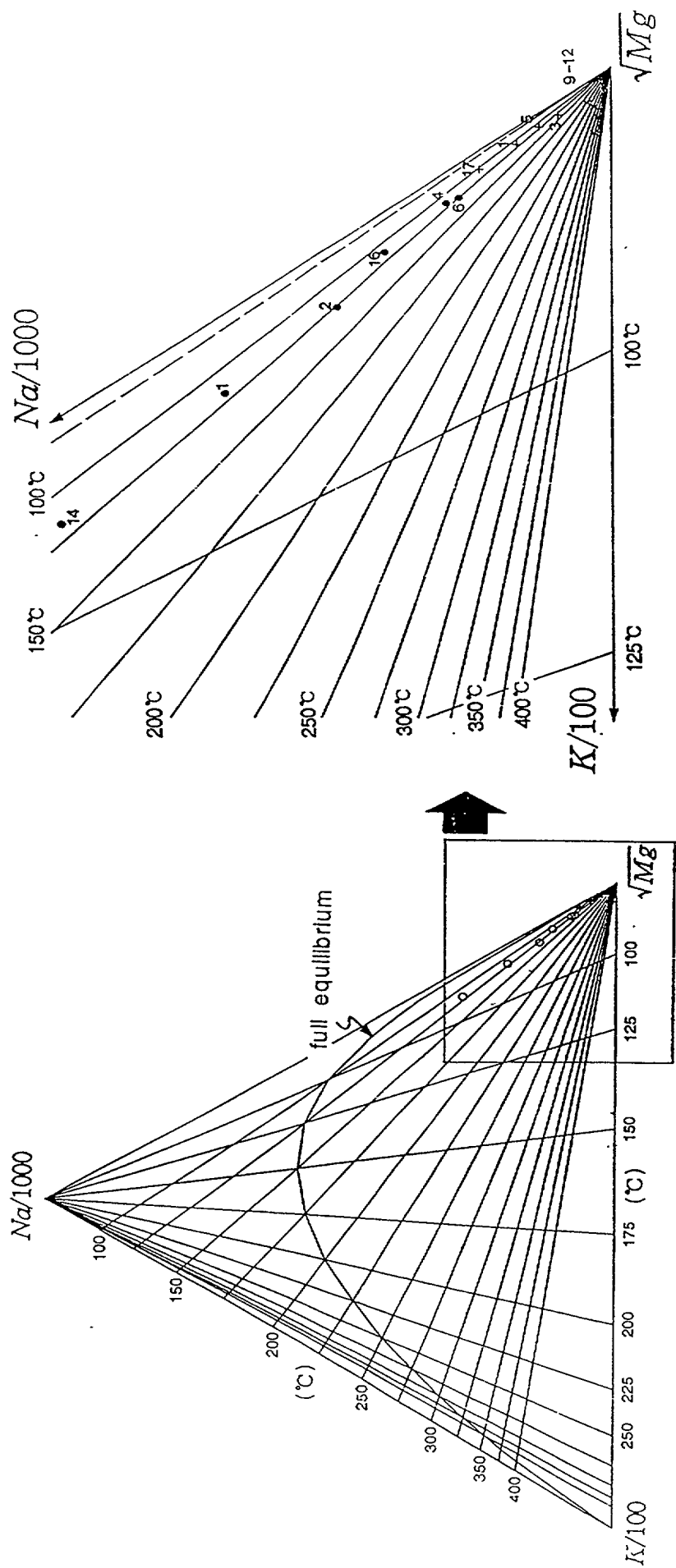
from the Mg corner of shallow waters to the farthest sample Y-14. This is an indication that they all form a single family, confirming the previous observations. The relatively position of the alignment is due mainly to Na-K and K-Mg geothermometric equations chosen by Giggenbach [11]. It is evident that in this case the two geothermometers are inconsistent. The region between this and the full equilibrium curve is occupied by geothermal waters partially equilibrated or re-equilibrated, or mixed with the fresh water.

Assuming that thermodynamic equilibrium for a given chemical reaction among the geothermal fluid components is achieved in the geothermal reservoir, it is possible to compute the fluid temperature in the reservoir. The Yusung data have been plotted in K/Na vs K/Mg geothermometer diagram in Fig. 7 [11]. The temperature indicated by the K/Mg geothermometer is between 32° and 83°C, usually lower than those in the geothermal reservoir. This shift could be explained in terms of the different re-equilibrations rates involving the considered cations during the rise of the deep fluid to the surface. In Yusung case, it is reliable to apply K/Na geothermometer for Yusung geothermal reservoir. Reservoir



• : thermal water; + : cold groundwater; × : surface water

FIG. 5. (A) Relative HCO<sub>3</sub><sup>-</sup>, Cl<sup>-</sup> and SO<sub>4</sub><sup>2-</sup> contents of water collected in 1993. (B) Relative Na<sup>+</sup> + K<sup>+</sup>, Mg<sup>2+</sup> and Ca<sup>2+</sup> contents of water collected in 1993.



• : thermal water; + : cold groundwater; × : surface water

FIG. 6. Triangle plot for Na, K and Mg (after Giggenbach, 1988).

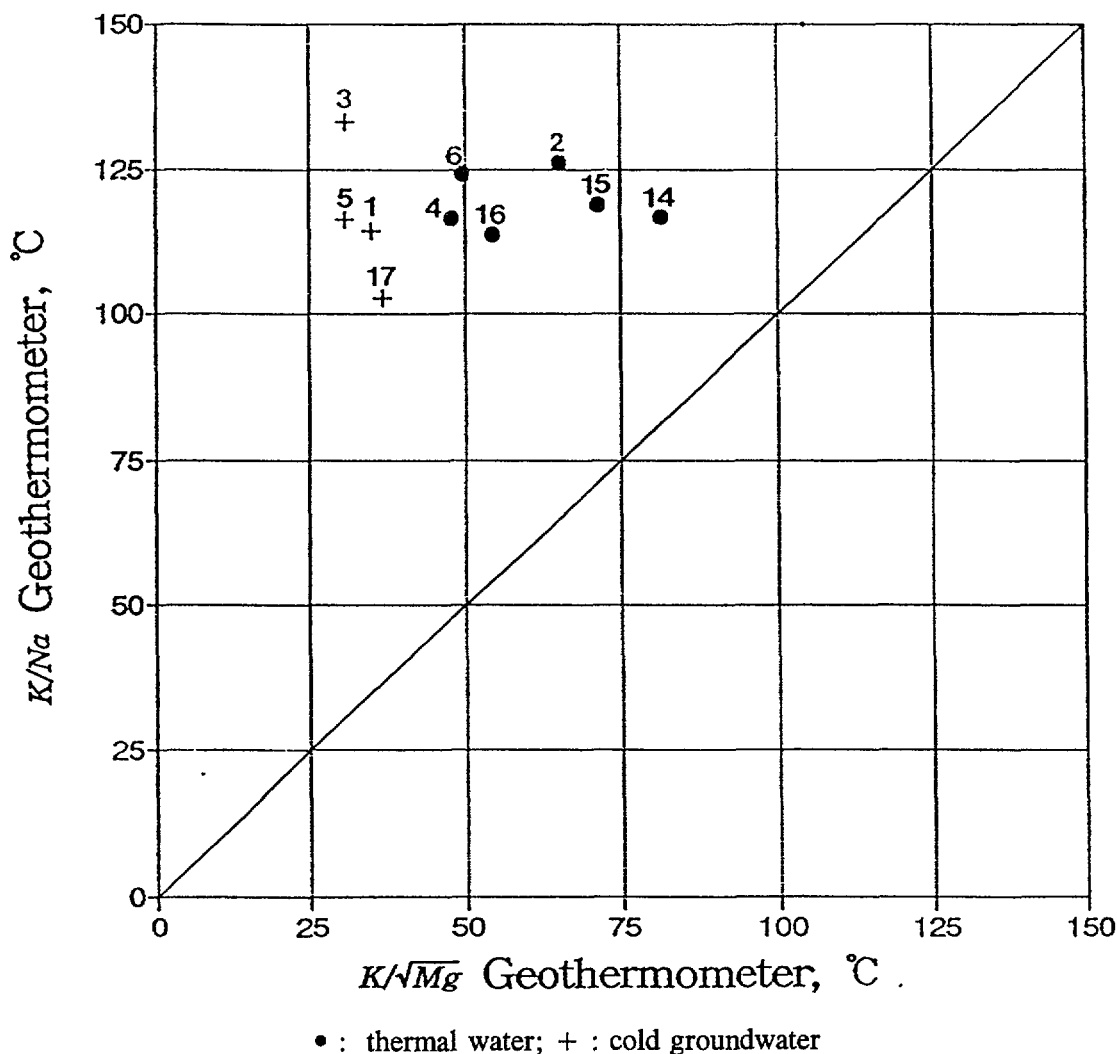


FIG. 7. Relationship between Na/K and  $K/\sqrt{Mg}$  geothermometer.

temperatures calculated from the Na-K geothermometer range from 103° to 133°C. Although temperatures measured in-situ range from 33° to 52°C, there is no specific trend for in-situ measured temperature and geothermometry temperatures.

Based on geological observation, no volcanic activity and related hydrothermal processes were identified in the area. Therefore, it is inferred that the source of heat is the normal heat flow conducted from the earth's interior to the surface of the earth. The geological features of fault and dyke systems may be closely related to the formation and the size of geothermal systems in the Yusung area. Fault systems developed along N45°W might have played a role of flow channel so that meteoric water penetrates into the heat source. Dyke systems (N-S trend) generally crossing the fault system may impede the deep groundwater movement.

## 5. CONCLUSIONS

Most hot waters seem to have been recharged before the pre-thermonuclear period. Judging from tritium values of the hot waters showing very low but not zero values, the thermal waters have mixed with cold waters in the upflow. No appreciable exchanges of

oxygen-18 between fluids and host rocks are observed. The lack of oxygen-18 isotopic shift can be explained in terms of the low temperature in the reservoir. The hot and cold waters, enriched in F<sup>-</sup>, are partially equilibrated or mixed with the fresh waters. Reservoir temperatures calculated from the Na-K geothermometer range from 103° to 133°C. It is inferred that fault systems trending N45°W play a role channelling groundwater of meteoric origin to deep levels.

**Acknowledgments** - *The present investigation was carried out within the framework of the IAEA Coordinated Research Programme for Africa, Asia and the Middle East on the Application of Isotope and Geochemical Techniques in Geothermal Explorations (Research Contract No. 6020/F). The authors deeply thank Dr. J. I. Shin, President of KAERI, whose advice and support made this work successful. Sincere thanks are also extended to Dr. R. Gonfiantini, Isotope Hydrology Section, IAEA, for providing data on the chemical composition and for scientific advice. The authors are grateful to Dr. Y. S. Kim for the his assistance and scientific advice during the experiment and the treatment of data.*

### References

- [1] YANG, M. Y., Chemical compositions of thermal springs in Korea, geology and ore deposits, Geological Survey of Korea **13** (1971) 42-49.
- [2] KIM, K. G., NAKAI, N., A study of hydrogen, oxygen, and sulfur isotope ratio of the hot springs in South Korea, *Geochem. Jour.* **15** (1981) 6-16.
- [3] JEONG, B. J., Geological characteristics and prospects of thermal springs in Korea, *Jour. Geol. Soc. Korea*, **19** 2 (1981) 63-74.
- [4] TANAKA, K. et. al., Geochemical study of Arima hot spring waters, Hyogo Japan by means of tritium and deuterium, *Geochem. Jour.* **18** (1984) 173-180.
- [5] INDEM, H., Hydrogen isotope (T.D.) study of hot spring waters from Nasu, Tochigi prefecture, *Ibid.* **19** (1985) 289-299.
- [6] PARK, H. I., LEE, J. D., CHEONG, J. G., Geological map of Yusung sheet (NJ 52-13-20) (1976).
- [7] YU, I. H., CHEONG, S. Y., KIM, Y. J., The applied geological map of the northern part of Taejon, *KIER* **2** (1982).
- [8] CRAIG, H., Isotopic variations in meteoric waters, *Sciences*, **133** (1961) 1702-1703.
- [9] AHN, J. S., A study on the groundwater flow and hydrogeochemical interaction in fractured rock masses, KAERI/NEMAC/RR-38/91 (1991).
- [10] INTERNATIONAL ATOMIC ENERGY AGENCY, Statistical treatment of environmental isotope data in precipitation, IAEA-TR-206, Vienna (1987)
- [11] GIGGENBACH, W. F., Geothermal solute equilibria. Derivation of Na-K-Mg-Ca geoindicators, *Geochim. Cosmochim. Acta*, **52** (1988) 2749-2765.

# ISOTOPIC AND CHEMICAL STUDIES OF GEOTHERMAL WATERS OF NORTHERN AREAS OF PAKISTAN

S. DILDAR HUSSAIN\*, M. AHMAD\*, R. GONFIANTINI\*\*<sup>1</sup>  
W. AKRAM\*, M.I. SAJJAD\*, M.A. TASNEEM

\* Pakistan Institute of Nuclear Science and Technology,  
Islamabad, Pakistan

\*\* Isotope Hydrology Section,  
International Atomic Energy Agency,  
Vienna

**Abstract** - Northern Areas is one of the major thermal fields of Pakistan with more than two dozen known hot springs having discharge temperature ranging from 35°C to 94°C. Isotopic and chemical techniques applied to study the geothermal fields show that thermal waters are of meteoric origin and can be classified as Na-HCO<sub>3</sub>, Na-SO<sub>4</sub> and mixed type on the basis of their chemical contents. At some places cooling of thermal waters seems to be due to steam separation whereas mixing with fresh cold water is prominent at the remaining sites. The temperatures estimated by isotopic and chemical geothermometers for the two major fields i.e. Tatta Pani and Murtazabad are 83-257°C and 65-296°C respectively.

## 1. INTRODUCTION

Northern Areas, located between the latitudes 35°20'N to 36°30'N and longitudes 74°E to 76°E approximately, is one of the major geothermal fields of Pakistan having more than two dozen known hot springs with discharge temperatures ranging from 35°C to 94°C (Fig. 1). It is characterized by steep topography and U-shaped glaciated valleys and is drained by the rivers Indus, Gilgit and Hunza while the rivers Shigar, Shyok, Ishkuman and Yasin form the major tributaries to the main streams. Some important mountain ranges of the area are Kailas, Rakaposhi, Masherbrum and Karakoram. The climate is characterized by cold winters and warm and dry summers. June-August are the hot months during which mean maximum temperature is about 30°C. Snow fall occurs during cold months of December-February when minimum temperature goes several degrees below the freezing point. Rainfall is scanty.

### 1.1. Tectonic Setting

The geotectonic development of Northern Areas of Pakistan during late-Cretaceous to Cenozoic involves three tectonic elements viz. Indo-Pakistan shield and its northern sedimentary cover (Indian Mass); the rocks deposited on the southern part of the Eurasian Mass; and Kohistan Island Arc Sequence [1].

From Archaean times, the Indian sub-continent was a part of Gondwana land which stretch of Tethyan sea existed between the Indo-Australian part of Gondwana land and Eurasian Mass. About 130 million years ago, the Indian Ocean plate departed from Gondwana land and started drifting towards Eurasia with the simultaneous consumption of

---

<sup>1</sup>Present address: Laboratoire d'Hydrologie et Géochimie Isotopique, Université de Paris Sud, F-91405 Orsay Cedex, France.

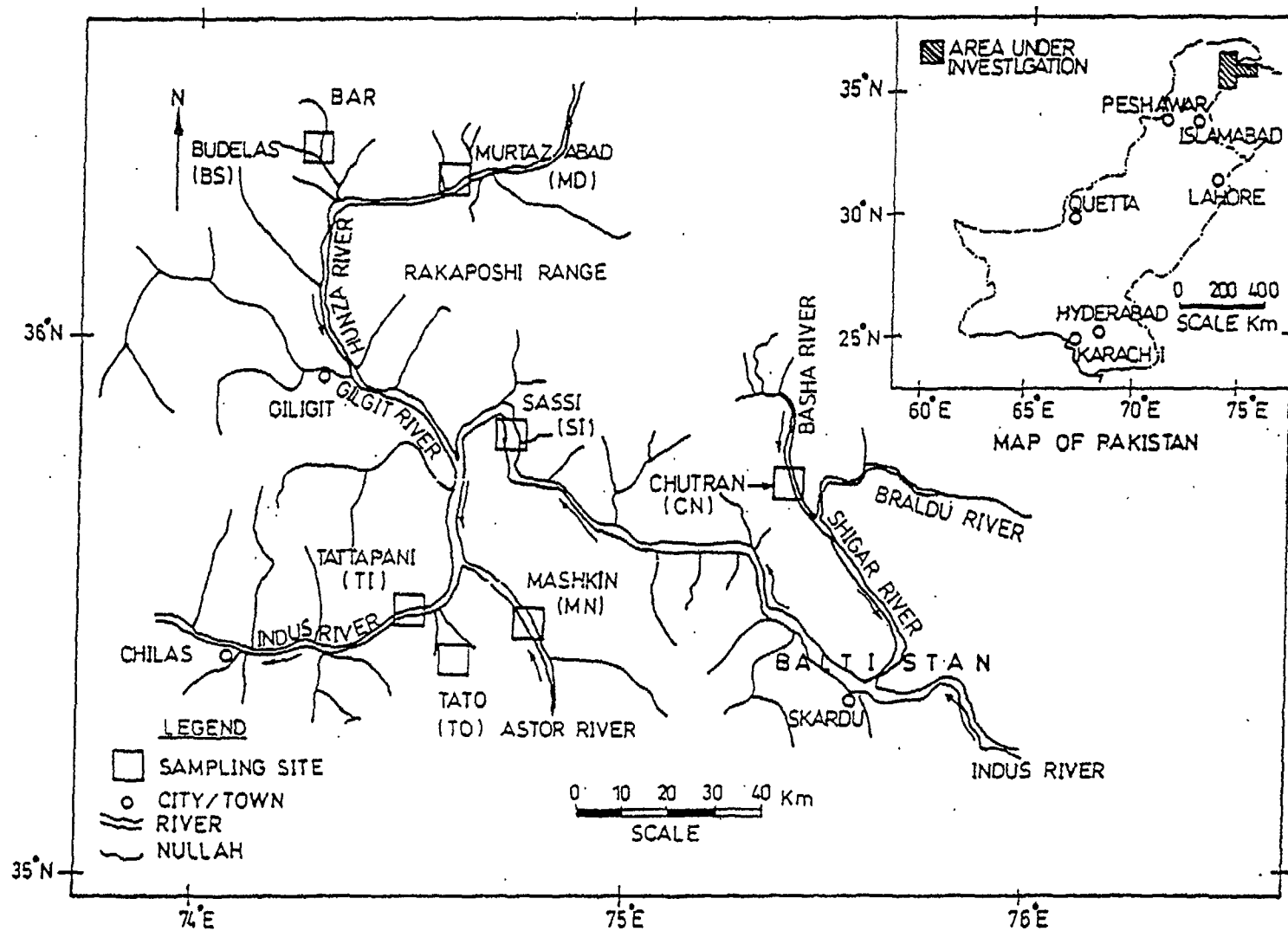


FIG. 1. Map showing the study area and sampling sites.

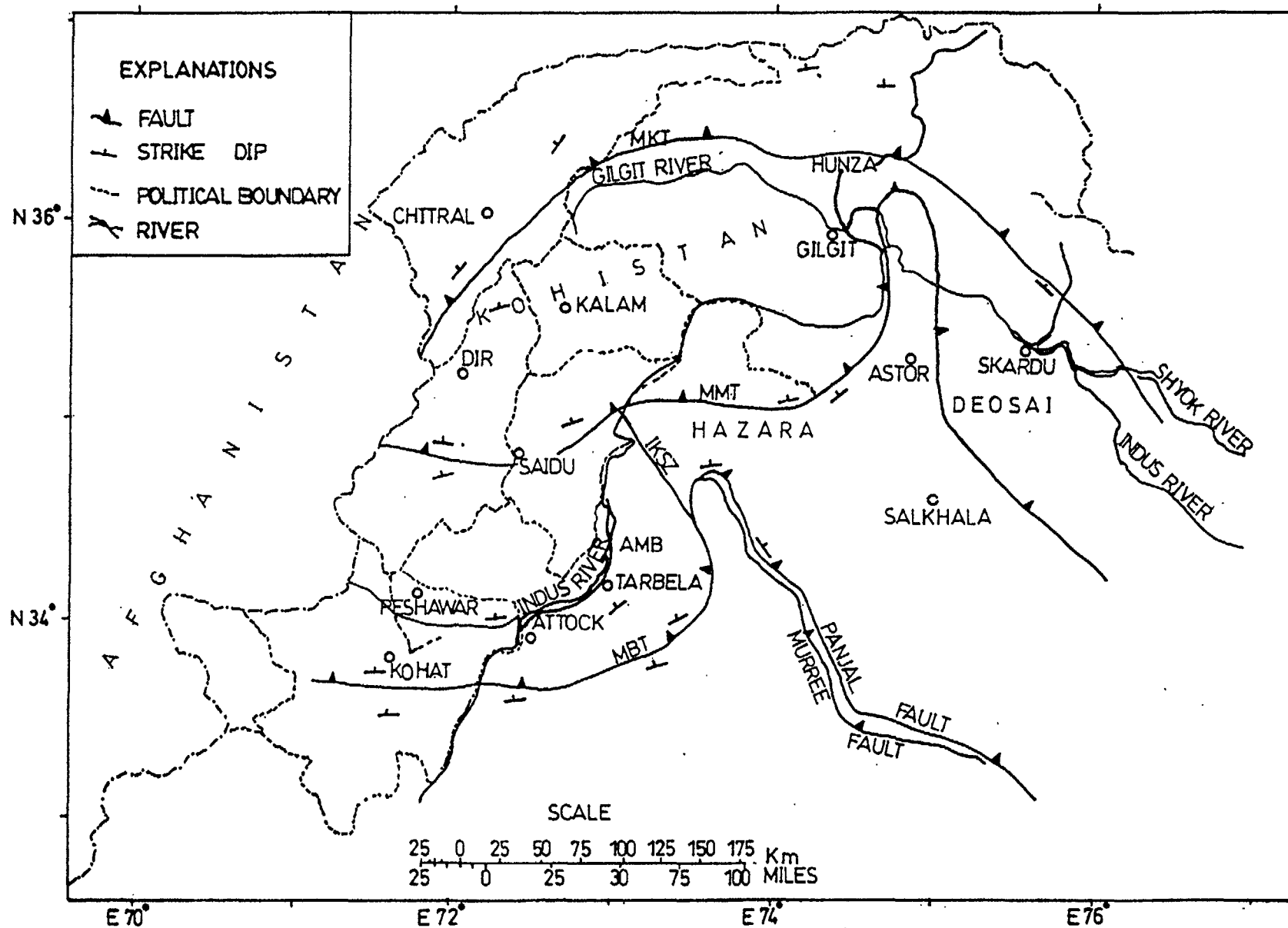


FIG. 2. Map showing major tectonic features of the northern area [2]



the Tethys Sea plate in between [2]. As a result of intra-oceanic subduction in front of the Indo-Pakistan plate, Kohistan Island Arc Sequence was produced on the north of subduction zone. The first contact of this Island Arc was with Indo-Pakistan plate which finally collided with Eurasian Mass. The Kohistan Island Arc Sequence is juxtaposed between the Indo-Pakistan plate and Eurasian plate.

A major thrust fault called Main Mantle Thrust (MMT) separates geologically the Indian Mass from the Kohistan Island Arc Sequence while another thrust fault called Main Karakoram Thrust (MKT) marks the boundary between the Kohistan Island Arc Sequence and the Eurasian Mass [3]. The thrust faults, MMT and MKT, along which geothermal manifestations under investigation lie, are still active. The heat is generated mainly due to friction along these faults [4]. The major tectonic features of Northern Areas of Pakistan are shown in Figure 2.

## **1.2. Regional Geology**

The oldest rocks of the Indian Mass are the Salkhala Series which are involved in the Nanga Parbat tectonics and constitute a substantial part of the massif. The main rock types are slate, phyllite, various types of schists, paragneisses, sandstone and quartzitic crystalline conglomerate which are intruded by the basic to acidic igneous rocks. The other rock units of the Indian Mass are Hazara Formation and Tanawal Formation (Precambrian), Abbottabad Formation and Mansehra Granite (Cambrian).

The rocks of Hazara Formation (black slates, brown phyllite, slightly metamorphosed greywackes, siltstone and limestone) and Tanawal Formation (laminated fine grained quartz schist and black slates) are believed to be deposited in deep sea basin by turbidity currents. Limestones and dolomites are the main lithologies of Abbottabad Formation while Mansehra Granite is porphyritic, foliated and tourmaline bearing in parts.

The rocks constituting the Kohistan Island Arc Sequence consist of a thick calc-alkaline plutonic, volcanic and volcano-sedimentary rocks, Jurassic-Cretaceous in age [4].

The rocks of Eurasian Mass north of Main Karakoram Thrust are late-paleozoic metasedimentary rocks, mainly flysch (limestone and shale dominant) which are considered deep sea sediments deposited by turbidity currents along the Eurasian plate margin in northern Tethys geosyncline [2].

## **1.3. Local Geology of Geothermal Sites**

Tatta Pani springs emanate from unconsolidated to semi-consolidated fluvial deposits or talus. Amphibolites fractured by the MMT constitute the hard rocks exposed around these geothermal manifestations. Tato spring emerges from semi-consolidated fluvial and moraine deposits. It lies at an altitude of about 1200 m above that of Tatta Pani springs. The hard rocks exposed around the Tato manifestation are Nanga Parbat Gneisses (Migmatite granitic gneisses) of pre-cambrian age. Mushkin spring emanates from surface soil. The rocks exposed around the spring are the Nanga Parbat Gneisses. Sassi springs emerge from quaternary deposits and the hard rocks exposed around the thermal springs largely comprise gneisses of Kohistan Island Arc Sequence.

Murtazabad springs emanate from a steep cliff which is made up of fluvial deposits largely comprising gravels. The hard rocks exposed around the manifestations are garnet staurolite schist and limesilicate marble of the Baltit Group which is assigned lower paleozoic to precambrian age. The Karakoram Granodiorite Belt is located 15 km north of the manifestations. Hakuchar springs are located on the left bank of the Hunza river towards south of Murtazabad springs and arise from fluvial deposits. The hard rocks exposed around Hakuchar springs are the same as those around Murtazabad springs. The manifestations at Murtazabad and Hakuchar lie north of the Main Karakoram Thrust. Budelas manifestations are located between the MKT and the Karakoram Granodiorite. The rocks exposed around the springs belong to the Baltit Group and comprise garnet staurolite schist. Chutran spring issues from the semi-consolidated quaternary deposits. The hard rocks exposed around the spring are limestones of Eurasian Mass [4].

## 2. METHODOLOGY

Four sets of water samples for measurement of isotopes ( $D$ ,  $^3H$ ,  $^{13}C$  and  $^{18}O$ ) and chemical ions were collected from hot springs, cold springs, rivers/streams etc. Budelas, Mushkin and Chutran sites could be approached in the first sampling only. Filtration and acidification of samples was carried out in the field if required. For analysis of  $\delta^{34}S$  and  $\delta^{18}O$ , sulphates were precipitated in the field while collecting the last three sets of samples [5]. Steam samples were collected from two hot springs (MD-19/H and TO-39/H). Steam was condensed by passing through cooling coil placed in cold water.

Physico-chemical parameters like temperature, pH and electrical conductivity were determined in the field.

Chemical analyses were carried out by using atomic absorption spectrophotometry (Na, K, Ca, Li), ICP (Mg, B, Rb), UV-visible spectrophotometry (Si,  $SO_4$ ), ion selective electrode (Cl) and titrimetry ( $HCO_3$ ).

Stable isotopes e.g.  $^{18}O$  and  $D$  contents of the water samples were determined relative to SMOW on mass spectrometers with the standard error of 0.1 ‰ and 1 ‰ respectively. The  $\delta^{18}O$  was measured by the  $CO_2$  equilibration method [6]. Water samples were reduced to hydrogen gas by zinc shots for  $\delta D$  measurement [7].  $BaSO_4$  precipitated in the field, after removing carbonates, was converted to  $CO_2$  for  $\delta^{18}O$  measurement [8]. Conversion of sulphate to  $SO_2$  for measurement of  $\delta^{34}S$  was carried out by using  $V_2O_5$  as catalyst [9].

Tritium content of the samples was determined by electrolytic enrichment and liquid scintillation counting method [10]. The standard error of measurement is of the order of  $\pm 1$  TU.

## 3. RESULTS AND DISCUSSION

Mean values of the results of chemical and isotopic analyses are given in Tables I & II.

TABLE I: RESULTS OF CHEMICAL ANALYSIS

SAMPLE	Na	K	Ca	Mg	SiO <sub>2</sub>	Li	B	Rb	Cl	TIC	SO <sub>4</sub>
TI-1/H	205	4.72	0.34	0.61	61	0.53	9.84		38	208	199
TI-2/H	195	3.72	0.27	0.05	52	0.54	9.80		38	217	221
TI-3/H	191	3.88	0.19	0.06	57	0.51	9.86	0.03	42	201	241
TI-4/H	193	4.23	0.34	0.36	59	0.53	9.75		44	201	206
TI-5/C	224	4.82	0.44	0.36					49	220	166
TI-6/H	201	3.42	0.24	0.05	57	0.65	10.10		46	211	212
TI-7/H	188	3.67	0.24	0.05	59	0.65	9.91		49	297	199
TI-8/H	200	4.93	0.24	0.05	70	0.70	10.25		44	217	198
TI-9/H	224	5.74	0.25	0.12	87	0.82	12.00		60	280	237
TI-43/H	165	2.90	0.30	0.07	63	0.53			56	267	126
MN-10/H	267	14.23	0.27	1.71					93	290	98
MN-11/C	18	9.44	7.67	2.26					2	101	64
MN-12/N	8	7.92	1.14	1.70					3	114	67
MN-13/R	13	6.20	0.98	23.44					6	105	37
BS-14/H	369	31.00	18.00	28.00					116	281	266
BS-15/C	31	9.00	27.00	16.00					21	123	210
BS-16/H	16	7.00	16.00	15.00					3	97	134
BS-17/H	67	11.00	20.00	24.00					8	83	180
BS-18/R	12	18.00	3.00	29.00					2	57	98
MD-19/H	495	35.53	N.D.	3.41	160	4.02	7.65	0.06	82	637	272
MD-21/H	410	41.88	2.53	3.15	111	2.93	5.25		45	474	276
MD-22/H	541	40.90	1.99	5.06	205	4.53	8.01	0.11	75	631	354
MD-23/H	437	39.35	5.10	21.43	154	3.46	6.60	0.09	52	567	320
MD-24/H	275	36.23	10.89	93.25	129	2.05	1.73	0.10	35	614	241
MD-25/H	254	41.00	7.99	82.00	111	1.50	2.18	0.07	47	521	203
MD-26/N	8	9.48	15.08	14.54					3	86	38
MD-27/H	194	26.53	29.37	54.00	72	0.68	0.20		20	356	244
SI-29/N	7	4.50	11.46	5.07					4	85	37
SI-30/H	246	11.50	12.31	6.12	83	0.58	2.05		23	400	231
SI-31/H	246	11.80	10.02	4.78	87	0.61	2.22		28	371	192
CN-32/H	16	7.00	17.00	20.00					5	114	70
CN-33/R	4	9.00	22.00	14.00					3	70	45
IND-34/R	8	4.81	20.87	9.74					6	105	21
GIT-35/R	5	2.70	12.30	5.24					4	83	22
HKR-36/H	216	19.45	25.95	20.10	147	1.40	3.27		28	516	217
SM-38/N	1	2.36	21.40	3.05					4	77	21
TO-39/H	270	15.57	N.D.	0.07	169	1.80	25.74		163	493	152
NP-40/SM	4	4.53	11.13	2.03					4	73	25
IND-41/R	8	5.34	15.80	3.76					5	77	26
HKR-42/N	11	5.90	22.00	0.74					7	55	44

N.B. ALL IONIC CONCENTRATIONS IN PPM

H=HOT SPRING; C=COLD SPRING N=NULLAH; R=RIVER;  
IND=INDUS RIVER; GIT=RIVER GILGIT; HKR=HAKUCHAR  
SM=SNOW MELT; NP=NANGA PARBAT

### 3.1. Physicochemical Parameters

The discharge temperature of the hot springs of Tatta Pani varies from 49°C to 73°C while that of thermal waters of Murtazabad has a range of 38 to 94°C. The two hot springs of Sassi have almost the same temperature. The two springs, one at Murtazabad (MD-19/H) and the other at Tato (TO-39/H) have relatively high discharge temperatures of 94°C and 92°C respectively.

TABLE II: RESULTS OF ISOTOPIC ANALYSIS

SAMPLE	FIELD PARAMETERS				ISOTOPE CONTENTS				
	Flow (ml/s)	TEMP (°C)	pH	EC (μS/cm)	WATER			SULPHATE	
					SO-18 (‰)	SD (‰)	TU	SO-18 (‰)	SS-34 (‰)
TI-1/H	30	63	8.19	917	-10.92	-75	0	1.11	11.44
TI-2/H	1000	73	8.34	972	-11.02	-74	0	0.97	11.82
TI-3/H	300	70	8.16	958	-11.27	-75	0	1.07	11.64
TI-4/H	30	49	8.36	896	-11.03	-74	0	0.84	11.56
TI-5/C		23	8.73	968	-9.71	-66	0		11.33
TI-6/H	400	60	8.35	941	-10.74	-74	0	2.44	11.28
TI-7/H	400	69	8.32	990	-11.14	-73	0	1.63	
TI-8/H	150	64	8.31	1003	-10.82	-73	0	2.28	11.22
TI-9/H	150	50	8.53	1016	-10.43	-73	0	3.03	
TI-43/H	500	62	7.90	927	-11.07	-76	0	0.62	
MN-10/H		50	6.96	1060	-11.40	-79	6		
MN-11/C		17	7.94	199	-11.50	-77	55		
MN-12/N		17	8.30	78	-12.10	-84	27		
MN-13/R		13	8.11	54	-12.50	-82	16		
BS-14/H		35	6.75	2220	-11.80	-87	28		
BS-15/C		20	7.00	741	-12.90	-86	23		
BS-16/H		46	7.22	438	-11.80	-80	35		
BS-17/H		38	6.62	786	-11.80	-79	26		
BS-18/R		8	8.33	168	-13.70	-93	35		13.21
MD-19/H	1200	94	8.88	3058	-12.73	-90	6	-0.26	8.42
MD-19/SC					-18.08	-118			
MD-21/H	100	80	8.11	2668	-12.14	-86	23	0.19	10.67
MD-22/H	60	68	8.44	3010	-12.60	-90	8	-2.62	9.27
MD-23/H	50	67	7.96	2605	-12.50	-87	23	1.24	5.69
MD-24/H	100	62	7.38	2220	-11.85	-80	40		
MD-25/H		38	7.75	1850	-11.62	-79	42	-1.86	
MD-26/R		3	8.18	165	-13.71	-94	39		-3.10
MD-27/H	50	41	7.13	1603	-11.63	-76	60		
SI-29/N		9	7.91	177	-11.74	-77	33		9.72
SI-30/H	100	49	7.22	1297	-10.51	-70	38	4.82	
SI-31/H	50	50	7.30	1307	-10.54	-71	38	5.80	4.61
CN-32/H		44	7.07	483	-13.20	-91	22		
CN-33/R		10	8.42	209	-15.10	-104	25		
IND-34/R		11	7.77	243	-14.51	-104	26		
GIT-35/R		12	7.82	184	-14.34	-98	31		
HKR-36/H		65	6.95	1742	-12.95	-88	27		6.23
SM-38/N		9	8.09	427	-13.30	-88	49		
TO-39/H	2000	92	8.90	1569	-10.81	-78	0		15.65
TO-39/SC					-17.83	-120			
NP-40/SM		7	8.74	141	-13.40	-92	38		
IND-41/R		13	8.20	260	-13.03	-82	30		
HKR-42/N		7	6.99	642	-11.80	-82	65		
MD-44/S					-11.33	-73			
MD-45/S					-11.84	-79			

N.B. SC=STEAM CONDENSATE; S=SNOW

OTHER ABRIVATIONS ARE THE SAME AS IN TABLE I

All the thermal waters in the area are neutral to slightly alkaline. The hot springs of Tatta Pani have pH values from 7.90 to 8.73 while those of Murtazabad have pH values in the range of 7.13 to 8.88.

The remarkable feature of the fluids emerging from thermal manifestations is their low salt contents. The maximum electrical conductivity (EC) value is 3058 μS/cm

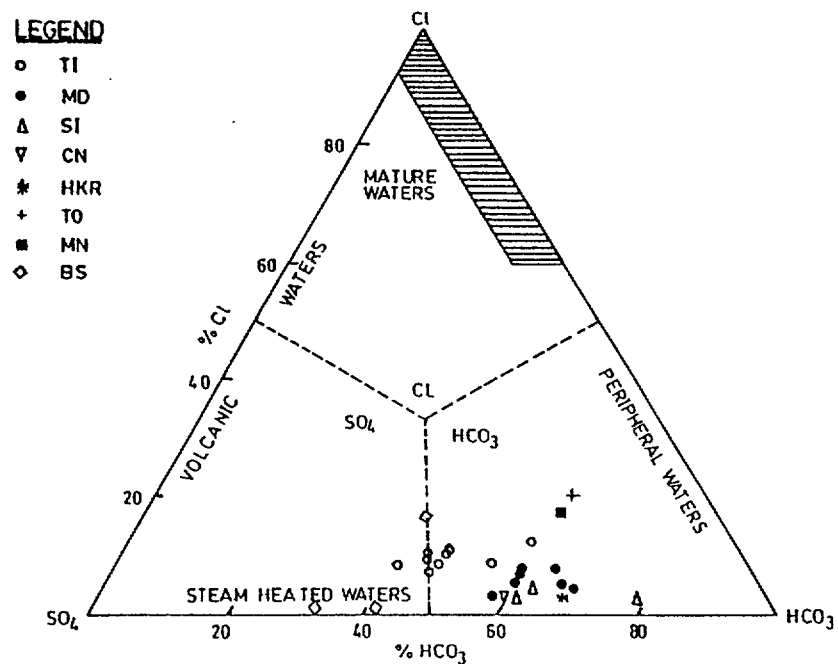


FIG. 3a. Triangular plot showing relative  $\text{Cl}$ ,  $\text{SO}_4$  and  $\text{HCO}_3$  contents.

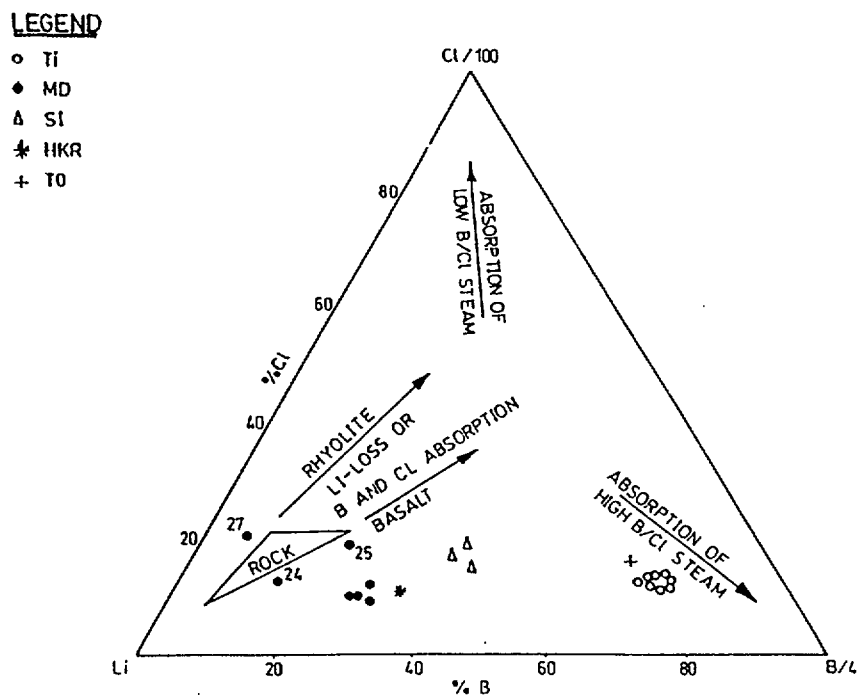


FIG. 3b. Triangular plot showing relative  $\text{Cl}$ ,  $\text{Li}$  and  $\text{B}$  contents.

(MD-19/H). The Tatta Pani hot springs have EC values in the range 896 - 1016  $\mu\text{S/cm}$  whereas Murtazabad hot waters are relatively more saline (EC: 1603 to 3058  $\mu\text{S/cm}$ ).

### 3.2. Water Chemistry

The chemistry of thermal waters (Table I) indicates that Na is the dominant cation in all the cases except the spring CN-32/H. Hence the hot waters of the study area are of sodic type. The relative anionic composition of hot waters is shown in Figure 3a from which it is obvious that waters can be classified into three types in terms of anionic dominance viz. bicarbonate type; sulphate type; and mixed type where both sulphate and bicarbonate are approximately equally abundant.

The water samples from Budelas are of sulphate type whereas the Tatta Pani hot waters show a mixed character lying on the boundary between sulphate and bicarbonate types. In all the remaining hot water samples  $\text{HCO}_3^-$  is the dominant anion. These are classified as Na- $\text{HCO}_3$  type of waters.

The geothermal waters studied have low chloride concentrations which indicate that they are simply heated immature waters (Fig. 3a).

The relative Cl, Li, and B contents of all the thermal waters are depicted in triangular plot [5] in Figure 3b. The position of all the Tatta Pani waters in this diagram suggests the absorption of high B/Cl steam after neutralization of HCl. The Murtazabad hot springs MD-24, -25, -27/H plot close to the area marked as ROCK suggesting that their composition may be controlled by rock leaching. Most of the remaining hot springs of Murtazabad area also tend to plot towards this corner in the figure.

### 3.3. Local Meteoric Water Line (LMWL)

The rains in this area are usually in traces and are not reliable for determining the LMWL. The precipitation in the area is mostly in the form of snow fall. The LMWL has been determined using the samples of snowmelt water drained by the rivers/mountain streams. The equation of LMWL comes out to be:

$$\delta\text{D} = (8 + 0.4)\delta^{18}\text{O} + (16.5 + 6) \quad (r^2 = 0.933, n=24) \quad (1)$$

### 3.4. Processes Affecting the Isotopic Composition and Chemical Concentrations of Thermal Waters During Their Rise to the Surface

There are two most important processes affecting the isotopic and chemical concentrations in geothermal waters viz. steam separation due to adiabatic expansion of thermal fluids with decreasing pressure; and dilution and mixing with waters derived from shallow sources [11]. The isotopic and chemical signatures of the geothermal fluids have been used to identify the process prevailing at different geothermal fields and are described as follows:

#### a) Tatta Pani

The tritium content of all the samples is zero which shows that thermal waters of Tatta Pani may be older than 50 years and have not mixed with fresh water. In  $\delta^{18}\text{O}$  vs  $\delta\text{D}$  plot (Fig. 4) all the sample data points lie below the local meteoric water line and their trend

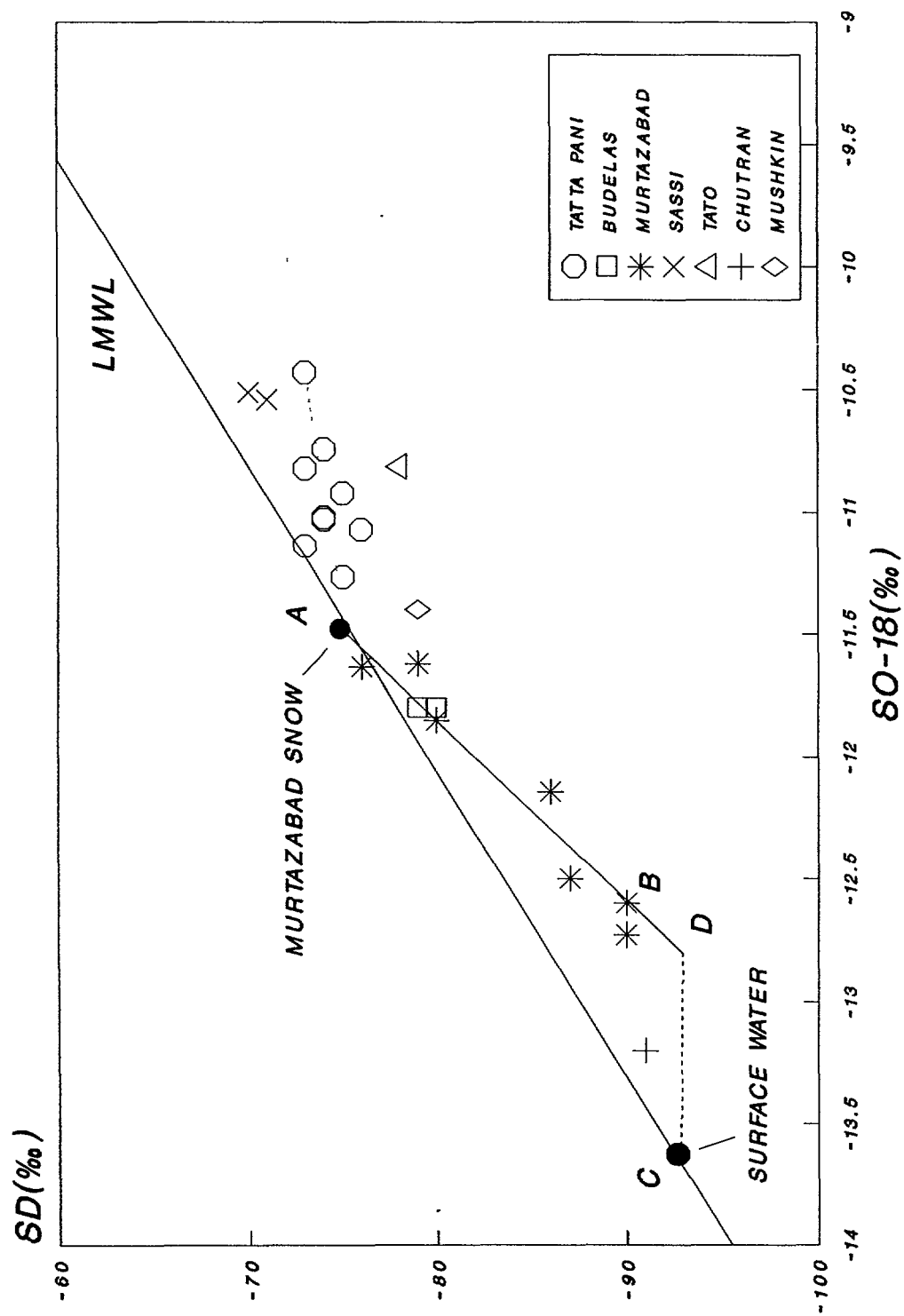


FIG. 4. Plot of  $\delta^{18}O$  vs  $\delta D$  of hot water samples.

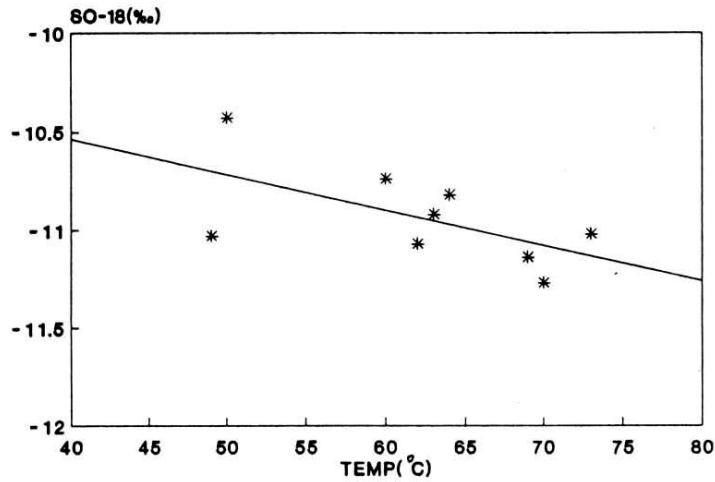


FIG. 5.  $\delta^{18}\text{O}$  vs temperature for the Tatta Pani area.

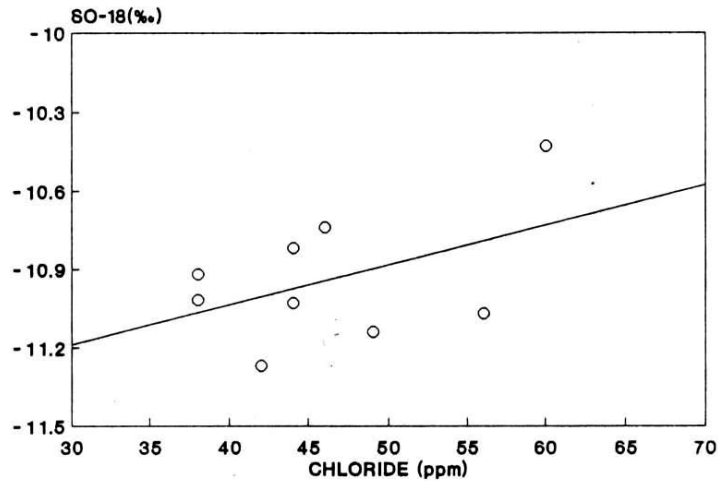


FIG. 6.  $\delta^{18}\text{O}$  vs chloride for the Tatta Pani area.

indicates that the thermal waters originate from meteoric water having  $\delta^{18}\text{O} = -11.5\text{‰}$  and  $\delta\text{D} = -76\text{‰}$  approximately and  $\delta\text{D}-\delta^{18}\text{O}$  correlation line has a slope of about 2. Such a slope could be explained by the isotopic enrichment for steam heating and non equilibrium evaporation of deep waters at elevated temperatures [12]. The slight enrichment of  $\delta^{18}\text{O}$  does not seem to be due to exchange with rocks because the temperature and  $\delta^{18}\text{O}$  of these waters are negatively correlated (Fig. 5) i.e. these waters get isotopically enriched with the lowering of temperature. This behaviour supports the idea that cooling of geothermal waters is due to evaporation/steam separation process. Cl content of water increases with the enrichment of  $\delta^{18}\text{O}$  (Fig. 6) which is also in favour of the existence of evaporation process.

Results of chemical analyses of samples do not show any significant correlation between Cl and other dissolved ions showing the absence of mixing of thermal waters with fresh water.



Assuming single step steam separation and using the following equation derived from heat balance relation, the fraction of residual water is given by:

$$F = \frac{H_{V,T(RW)} - H_{L,T(OW)}}{H_{V,T(RW)} - H_{L,T(RW)}} \quad (2)$$

Here, F is fraction of residual water, H is enthalpy and V, T, RW, L and OW in the subscripts represent vapour, temperature (°C), residual water, liquid and original water respectively. Values of calculated F are in the range of 80 to 84 %.

b) Tato

Location of this point in  $\delta^{18}\text{O}$  vs  $\delta\text{D}$  plot (Fig. 4) is way below the LMWL which may be due to evaporation/steam separation during the movement of water towards ground surface. Lack of tritium and high chloride contents show that no detectable amount of fresh water is mixing with the thermal water. Fraction of residual water after single step steam separation is 81 %. Using the following isotopic balance equation, the values of  $\delta^{18}\text{O}$  and  $\delta\text{D}$  come out to be -12.1 ‰ and -86 ‰ respectively for the thermal water before steam separation:

$$\delta_o = F_L \cdot \delta_L + F_V \cdot \delta_V \quad (3)$$

Here, F is fraction of residual water and O, L and V stand for original thermal water, liquid phase and vapour phase respectively.

c) Mushkin

Low tritium and high chloride contents show that mixing of fresh water with thermal water is less. In  $\delta^{18}\text{O}$  vs  $\delta\text{D}$  plot (Fig. 4), its position also indicates the domination of evaporation process.

d) Sassi

Thermal water emanates from talus at many points along the road. Flow rate of the springs is usually small. Two springs having considerable flow were sampled. Almost all the parameters are similar for these springs indicating that the same water is seeping at different points. The results of isotopic analyses show that these springs are enriched in  $^{18}\text{O}$  and D and their position is below LMWL (Fig. 4). Tritium contents similar to that of the fresh water indicate that the residence time of circulating water is short. The enrichment in  $^{18}\text{O}$  and D may be because of evaporation and/or mixing with relatively enriched fresh water resulting from precipitation at low altitude.

e) Murtazabad Area

The tritium concentration of thermal springs ranges from 6 to 60 TU which indicates that the emanation of different waters may be due to mixing of varying proportions of fresh water with the thermal water during its movement towards the earth surface. Both the temperature and chloride decrease with the increase of tritium content (Fig. 7). This indicates that the cooling of thermal water is mainly due to mixing with fresh water having relatively low  $\text{Cl}^-$  and high tritium contents.

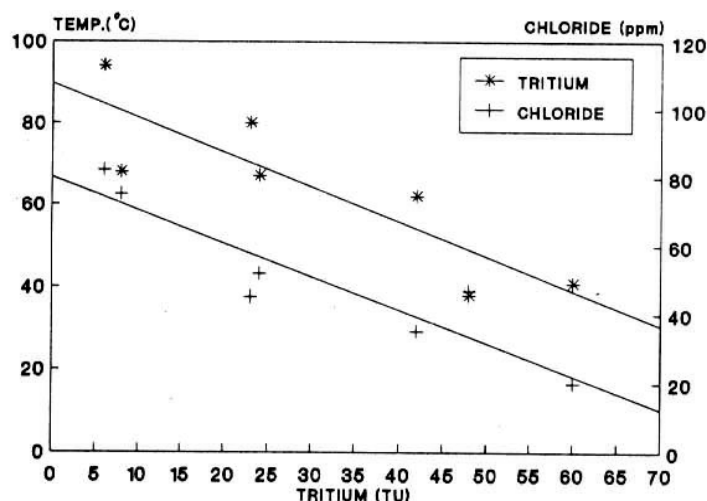


FIG. 7. Temperature and Cl vs tritium for Murtazabad.

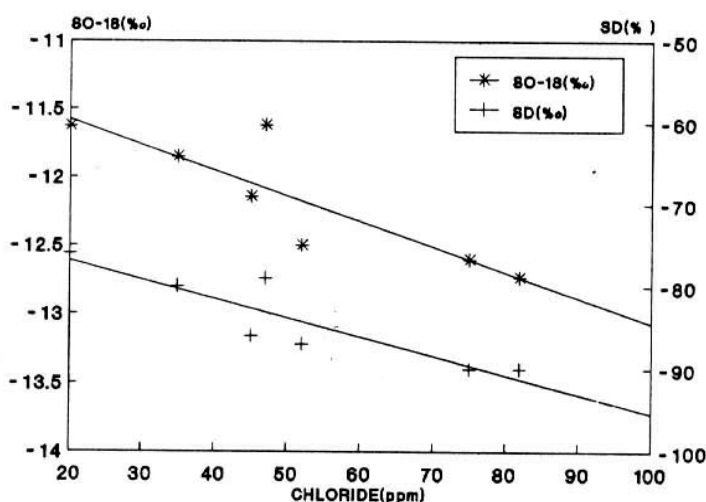


FIG. 8.  $\delta^{18}\text{O}$  and  $\delta\text{D}$  vs chloride for Murtazabad.

Plots of  $\delta^{18}\text{O}$  and  $\delta\text{D}$  against  $\text{Cl}^-$  are given in Figure 8. Had the evaporation/steam separation process been dominant, the  $\text{Cl}^-$  content would have increased with the enrichment of  $^{18}\text{O}$  and D but the observed trend is in the opposite direction. This also indicates that the thermal water is getting mixed with the shallow cold water enriched in  $^{18}\text{O}$  and D. Relationship of  $\text{Cl}^-$  with other dissolved ions (Fig. 9) shows significant positive correlation which also favours the existence of mixing process [13].

Mixing trend is clearly represented in  $\delta^{18}\text{O}$  vs  $\delta\text{D}$  plot (line AB in Fig. 4). The hottest spring sample lies at the lower end of the line AB, while the sample with minimum temperature is at the upper end. A point showing the average  $\delta^{18}\text{O}$  and  $\delta\text{D}$  values of two snow samples (No. MD-44/S and MD-45/S) collected from Murtazabad terrace is also located near the upper end of the line AB. Snow of the local area is isotopically enriched as compared to general meteoric water of the area i.e. precipitation at high altitudes

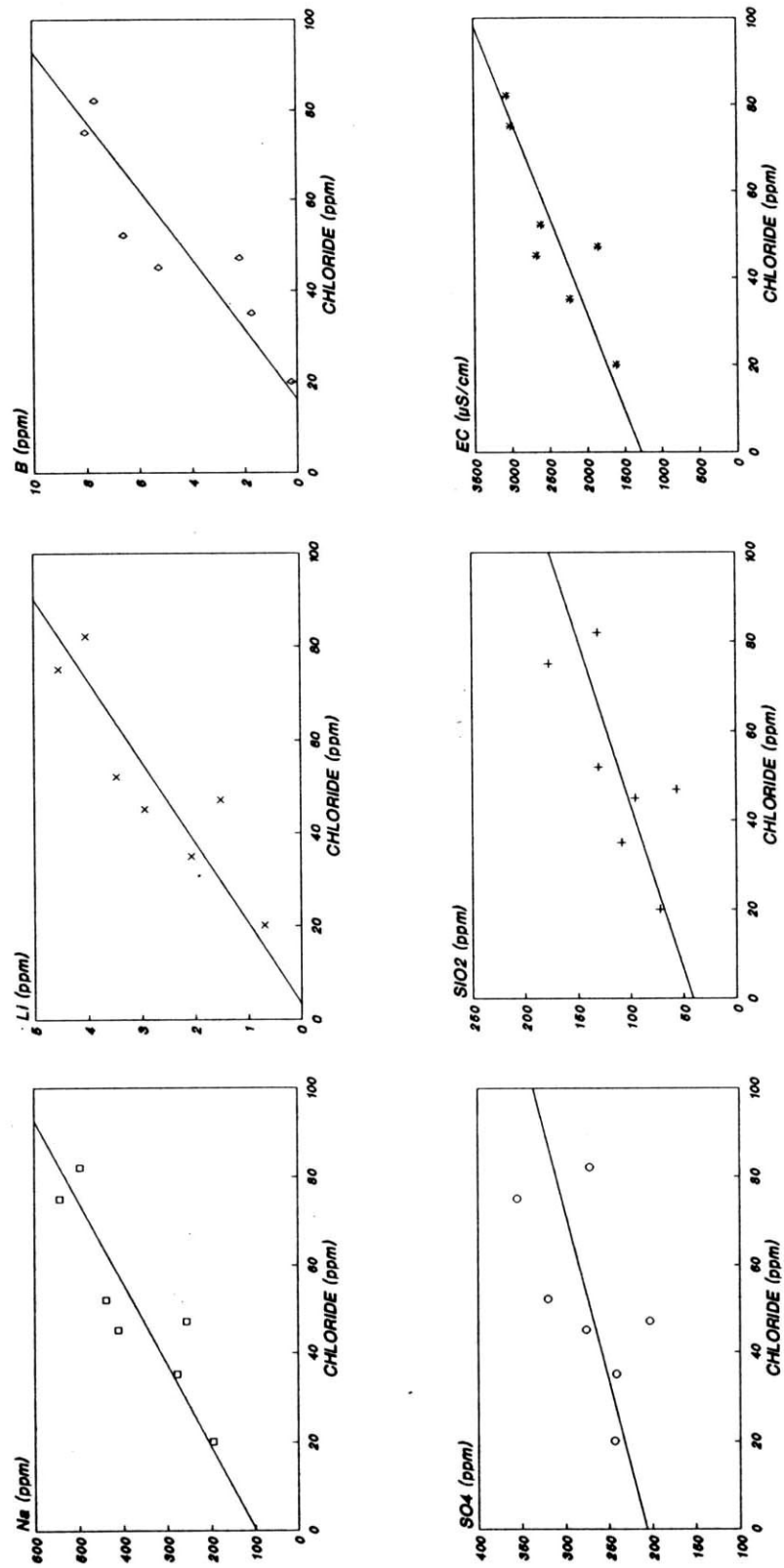


FIG. 9. Dissolved ions vs chloride of the Murtazabad area.

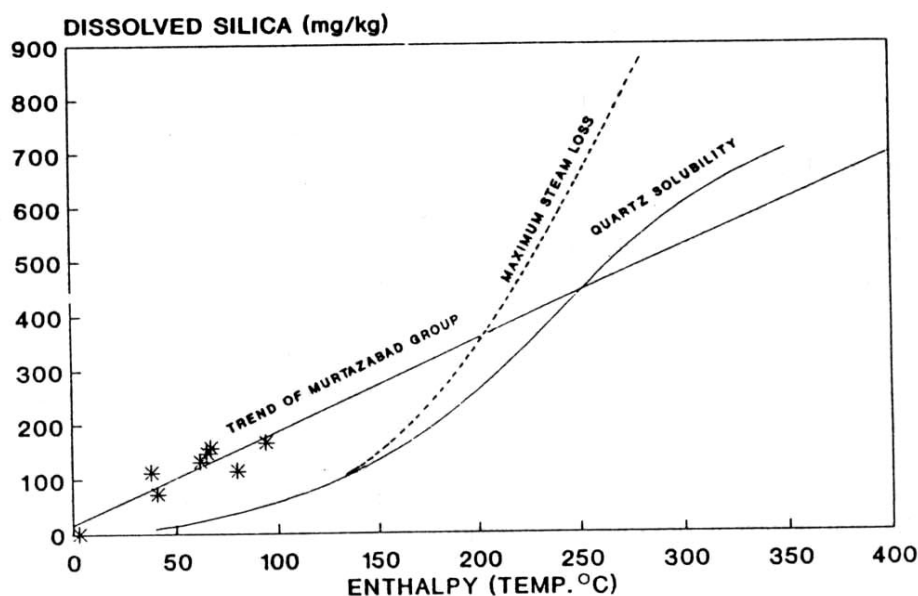


FIG. 10. Dissolved silica vs enthalpy.

drained by rivers ( $\delta^{18}\text{O} = -13.8 \text{ ‰}$ ,  $\delta\text{D} = -94 \text{ ‰}$ ). This is probably due to the fact that the area is located at a low altitude. The index of meteoric water lies to the left of the point B in Figure 4. Considering such meteoric water as the origin for this field, the  $\delta^{18}\text{O}$  shift of the hottest spring seems to be about 1‰. Tritium values decrease from 60 TU to 6 TU along the line AB. On extrapolation, this line meets the possible oxygen shift line at a point D. It can be inferred that before mixing, the thermal water had  $\delta^{18}\text{O}$  and  $\delta\text{D}$  values similar to those of the point D and tritium concentration nearly zero. The isotopic and chemical concentrations go on changing due to the mixing of shallow water resulting from local snow.

The temperature of hot water component before mixing was estimated by using dissolved silica-enthalpy graph [14] and was found to be in the range of 200-250°C (Fig. 10).

f) Budelas

One spring BS-14/H is well separated from the other two springs which are located close to each other. The stable isotopic data of BS-14/H hot spring resemble those of some of the hot springs of Murtazabad area. The two closely located springs have relatively low electrical conductivity and their position in  $\delta^{18}\text{O}$  vs  $\delta\text{D}$  plot (Fig. 4) is close to LMWL. It seems that mixing of the river water with thermal water is dominant. The location of these springs being very near to the river bank also supports this finding.

g) Chutran

High tritium, low chloride contents and its location in  $\delta^{18}\text{O}$ - $\delta\text{D}$  plot (Fig. 4) show that mixing of thermal water with fresh water takes place during its upward movement towards the ground surface.

### 3.5. Origin of Geothermal Waters

Isotopic data can well differentiate between the three possible types of origin of thermal waters i.e. magmatic origin, oceanic origin and meteoric origin. The isotopic composition of all the sampled geothermal manifestations do not show the presence of any significant amount of magmatic water which, generally, has  $\delta^{18}\text{O}$ : +6 to +9 ‰ and  $\delta\text{D}$ : -40 to -80 ‰ [15]. The possibility of oceanic origin of the encountered thermal waters is ruled out by the absence of highly enriched  $\delta^{18}\text{O}$  and high salinity values.

All the points in the  $\delta^{18}\text{O}$  vs  $\delta\text{D}$  plot (Fig. 4) seem to form two groups. The first group (Tatta Pani, Tato, Mushkin and Sassi) which belongs to MMT lies at lower altitude and is isotopically more enriched compared to the second group (Murtazabad, Budelas and Chutran) belonging to MKT. All the data points, however, lie close to the meteoric water line with little  $\delta^{18}\text{O}$  shifts due to rock interaction, evaporation or mixing processes [11]. So the origin of thermal waters is obviously meteoric.

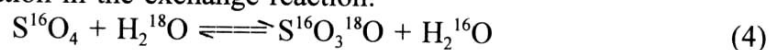
### 3.6. Source of Sulphates

In a geothermal flow system,  $\delta^{34}\text{S}$  of sulphates with a magmatic origin ranges between 0 ‰ and +2 ‰ CDT (Canyon Diablo troilite) and sulphates resulting from the dissolution of evaporites can have  $\delta^{34}\text{S}$  from +10 ‰ to +35 ‰, whereas in modern oceanic sulphates its value is about +20 ‰ [15]. The  $\delta^{34}\text{S}$  values of sulphates collected from Tatta Pani hot springs are in the range of 11.2 to 11.8 ‰ whereas those of Murtazabad area fall in the range of 4.6 to 10.7 ‰. Hot spring of Tato has  $\delta^{34}\text{S}$  value 15.7 ‰ which is the maximum in the area.

The data (Table II) show that the sulphates are neither of magmatic origin nor of modern oceanic origin. The possibility of oceanic origin ( $\delta^{18}\text{O}$ : +9.6 ‰) is further ruled out as the  $\delta^{18}\text{O}$  of sulphates is in the range of -2.6 to +5.8 ‰. Looking at  $\delta^{34}\text{S}$  values of sulphates in Tatta Pani and Tato hot springs, it appears that the principal source of sulphates is dissolution of evaporites from sedimentary rocks present in the area. For Murtazabad area, relatively low values of  $\delta^{34}\text{S}$  indicate that the major contribution of sulphates is derived from reduced sulphur compounds such as sulphide minerals and/or organic sulphides [15].

### 3.7. Isotope and Chemical Geothermometry

All the geothermal fields in the Northern Areas are water dominated. For such systems the most useful isotope geothermometer i.e. sulphate-water, is based on oxygen isotope distribution in the exchange reaction:



The reservoir temperatures have been calculated using the equation experimentally determined by Lloyd [16].

Chemical geothermometers viz. Na-K [17], K-Mg [18], Li-Mg [19], Na-K-Ca [20],  $\text{SiO}_2$  (quartz) [21], K-Ca [22] and Na-Li [23] thermometers have been applied and the calculated temperatures given in Table III. The ionic concentrations used are in ppm units except for Na-K-Ca geothermometer where they are in mole/L.

For Tatta Pani geothermal manifestations, deep reservoir temperatures calculated by sulphate-water, Na-K, Li-Mg, quartz (after adiabatic steam loss) and Na-Li geothermometers

TABLE III: TEMPERATURES ESTIMATED BY VARIOUS GEOTHERMOMETERS

SAMPLE Code	Na-K-Ca	Na-K	Na-Li	K-Ca	SI QUARTZ	SI QUARTZ*	SO4-H2O	MEAN (°C)	F (%)
TI-1/H	203	137	135	231		132	146	164	81.2
TI-2/H	197	128	141	238		129	157	165	82.5
TI-3/H	214	131	138	225		131	170	168	81.5
TI-4/H	195	135	140	238		132	159	166	78.7
TI-6/H	198	122	152	239		131	149	165	80.5
TI-7/H	200	129	158	235		132	157	168	81.3
TI-8/H	220	141	159	219		134	149	170	80.2
TI-9/H	230	143	163	212		138	130	169	78.3
TI-43/H	176	124	153	257		133		168	80.2
MN-10/H	300	187		170					
BS-14/H	171	219		237					
BS-16/H	72	386		337					
BS-17/H	98	275		310					
MD-19/H		207	240		165		163	194	
MD-21/H	277	234	226	172	143		161	202	
MD-22/H	296	211	243	167	182		163	211	
MD-23/H	240	224	237	191	163		142	199	
MD-24/H	193	256	230	214	152		185	205	
MD-25/H	211	274	206	200				223	
MD-27/H	138	259	158	262	120		114	175	
SI-30/H	130	178	129	289	127		131		
SI-31/H	137	180	132	280	130		115		
CN-32/H	71	386		340					
HKR-36/H	129	224	215	278	160		100		
TO-39/H		192	218		169			193	80.1

\* = AFTER ADIABATIC STEAM LOSS

F = FRACTION OF WATER LEFT AFTER STEAM SEPARATION

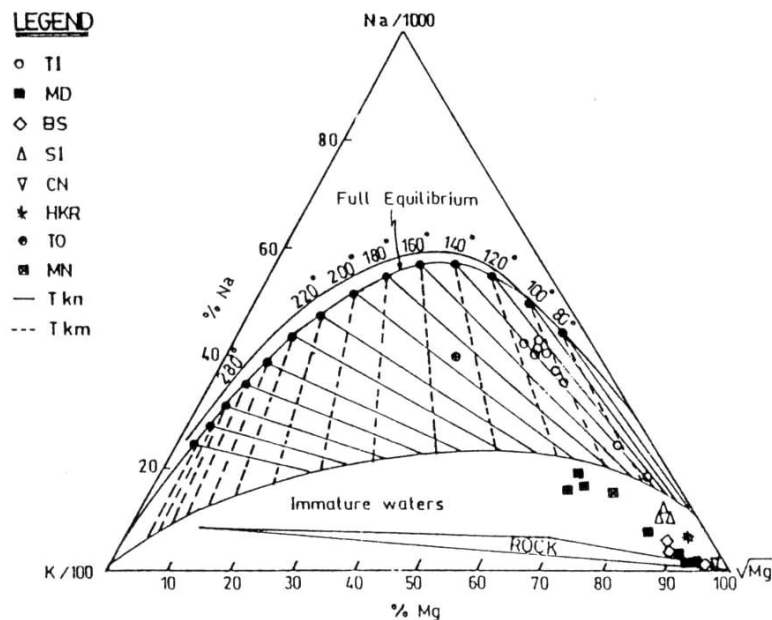


FIG. 11. Evaluation of Na-K-Mg temperatures.

are in reasonable agreement. The Na-K-Ca and K-Ca temperatures are on higher side while K-Mg temperatures are relatively low.

In Murtazabad area, sulphate-water and  $\text{SiO}_2$  (quartz) geothermometers yield similar results. The Na-K, Na-K-Ca, K-Ca and Na-Li temperatures are on higher side while K-Mg and Li-Mg temperatures are on the lower side for this area.

The same chemical geothermometer applied to the different geothermal springs in Sassi area provides close reservoir temperatures. The temperatures determined by sulphate-water, Na-K-Ca, quartz and Na-Li thermometers are in good agreement with each other. Strong variations are evident in case of Budelas and Chutran hot springs which are perhaps due to the reason that thermal waters at these sites get mixed with river water. Hence different geothermometers used for temperature calculations seem to be inappropriate for these springs [24].

### 3.8. Evaluation of Na-K-Mg-Temperatures

Evaluation of Na-K-Mg-temperatures [5] is shown in Figure 11. The position of all the data points indicates that none of the thermal systems of the study area attained full equilibrium. The Tatta Pani and Tato hot springs show partial equilibrium. The high percentage of Mg in all the remaining samples places them in the compositional area marked as Immature Waters. Murtazabad hot springs No. MD-24, -25 and -27 plot in the area marked as ROCK suggesting that their composition is controlled by rock leaching. These springs show a similar trend in Cl-Li-B triangular plot (Fig. 3b).

## 4. CONCLUSIONS

The thermal waters of Northern Areas are neutral to slightly alkaline and have low dissolved salt contents. Sodium is the dominant cation in almost all the cases. In terms of anions the hot waters of Budelas area are of sulphate type, those of Tatta Pani are of mixed character and those of the remaining areas show bicarbonate domination. Tatta Pani and Tato springs show partial equilibrium.

The thermal waters are of meteoric origin and have acquired their heat during circulation in the fault systems. Shallow fresh water does not mix with thermal waters of Tatta Pani and Tato whereas it contributes a little to the discharge of Mushkin spring. The thermal waters of the remaining areas (Murtazabad, Budelas, Sassi and Chutran) contain a significant component of fresh water incorporated in the flow system prior to discharge. The absence of tritium in Tatta Pani and Tato hot springs indicates that residence time of recharging water in the geothermal system is more than 50 years while at the remaining fields, the thermal waters appear to be young in age.

Deep reservoir temperatures estimated by different isotopic and chemical geothermometers for the two major fields i.e. Tatta Pani and Murtazabad are 83-257°C and 65-296°C, respectively. At Tatta Pani thermal manifestations, sulphate-water, Na-K, quartz (after adiabatic steam loss) and Na-Li geothermometers yield close estimates. In case of Murtazabad hot springs, sulphate-water and quartz thermometers give close results.

Most of the sites have estimated reservoir temperatures in excess of 150°C. Further exploration to assess the potential of the sites for economic production of electricity is required.

**Acknowledgments** - *The present investigation was carried out within the framework of IAEA co-ordinated research programme for Africa, Asia and the Middle East on the Application of Isotope and Geochemical Techniques in Geothermal Exploration. Sincere thanks are due to Dr. S. Arnorsson and Dr. W.F. Giggenbach for the guidance/suggestions provided during the technical discussions. The authors acknowledge the co-operation of Dr. Mukhtar Ahmad, Mr. Niaz Ahmad, Mr. Zahid Latif and Mr. Muhammad Rafique.*

### References

- [1] Powell, C.McA., A Speculative Tectonic History of Pakistan and Surroundings: Some constraints from the Indian Ocean, In: Abul Farah & Kees, DeJong (eds.), Geodynamics of Pakistan, Geological Survey of Pakistan, Quetta (1979).
- [2] Khan, K.S.A., Khan, I.H., Leghari, A.L., Khan, M.S.Z., Geology along the Karakoram Highway from Hasan Abdal to Khunjerab Pass, Geological Survey of Pakistan, Quetta (1987).
- [3] Tahirkheli, R.A., Geology of the Himalayas, Karakoram and Hindukush in Pakistan. Geol. Bull. Univ. Peshawar, Spec. Issue, Vol. III (1982).
- [4] Todaka, N., Shuja, T.A., Jamiluddin, S., Khan, N.A., Pasha, M.A. and Iqbal, M., A Preliminary Study for Geothermal Development Project in Pakistan, Geological Survey of Pakistan (1988).
- [5] Giggenbach, W.F. and Goguel, R.L., Collection and analysis of geothermal and volcanic water and gas discharges, Report No. CD 2401, Chemistry Division, DSIR, Petone, New Zealand (1989).
- [6] Epstein, S. and Mayeda, T., Variation of  $^{18}\text{O}$  content of waters from natural sources, Geochim. Cosmochim. Acta 4 (1953) 213-224.
- [7] Sajjad, M.I., Isotope Hydrology in Pakistan, Instrumentation - Methodology - Applications, Ph.D. thesis, University of the Punjab, Lahore (1989).
- [8] Nehring, N.L., Bowen, P.A. and Truesdell, A.H., Techniques for the conversion of carbon dioxide of oxygen from dissolved sulphates in thermal waters, Geothermics, Vol. 5 (1977) 63-66.
- [9] Yanagisawa, F., Sakai, H., Thermal decomposition of barium sulphate - vanadium pentoxide - silica glass mixture for preparation of sulfur dioxide in sulfur isotope ratio measurements, Analytical Chemistry, Vol. 55, No. 6 (1983) 985-987.



- [10] Cameron,J.F., Payne,B.R., Apparatus for concentration and measurement of low tritium activities, Proc. 6th Int. Conf. Radiocarbon and Tritium. Dating, CONF-650652 Chemistry, TID-4500, (1966) 454-470.
- [11] Giggenbach,W., Gonfiantini,R., Panichi,C., Geothermal Systems, In: International Atomic Energy Agency, Guidebook on Nuclear Techniques in Hydrology, Tech. Report Series No. 91, IAEA, Vienna (1983) 359-379.
- [12] Bertrami,R., Camacho,A., Stefanis,L.De, Medina,T., Zuppi, G.M., Geochemical and isotopic exploration of the geothermal area of Paipa, In: International Atomic Energy Agency, Geothermal Investigations with Isotope and Geochemical Techniques in Latin America, IAEA-TECDOC-641, IAEA, Vienna (1992) 169-199.
- [13] Mazor,E., Levitte,D., Truesdell,A.H., Healy,J. and Nissenbaum,A., Mixing models and ionic thermometers applied to warm (upto 60 °C) springs: Jordan Rift Valley, Israel, J. Hydrol., Vol. 45, (1980) 1-19.
- [14] Truesdell,A.H. and Fournier,R.O., Procedure for estimating the temperature of hot water component in a mixed water by using a plot of dissolved silica versus enthalpy, Jour. Research U.S. Geological Survey Vol. 5, No. 1 (1977)49-52.
- [15] Pearson,F.J.Jr., and Rightmire,C.T., Sulphur and oxygen isotopes in aqueous sulphur compounds, In: Fritz,P. and Fontes,J.-Ch., Handbook of Environmental Isotope Geochemistry, Vol. 1, Elsevier Scientific Publishing Company, Amsterdam-Oxford-New York (1980) 227-257.
- [16] Lloyd,R.M., Oxygen isotope behaviour in the sulphate-water system, J. Geophys. Res., Vol. 73 (1968) 6099-6110.
- [17] Giggenbach,W.F., Gonfiantini,R., Jangi,B.L. and Truesdell, A.H., Isotopic and chemical composition of Parbati valley geothermal discharges, north-west Himalaya, India, Geothermics, Vol. 12, No.2/3 (1983) 129-140.
- [18] Henley,R.W., Truesdell,A.H., Barton,P.B., Whitney,J.A, Fluid-Mineral Equilibria in Hydrothermal Systems, Reviews in Economic Geology, Vol. 1, Society of Economic Geologists, U.S.A. (1984) 31-43.
- [19] Kharaka,Y.K., Mariner,R.H., Chemical geothermometers and their application to formation waters from sedimentary basin, In: Naeser,N.D. and McCollon,T.H. (eds.), Thermal History of Sedimentary Basins, Springer-Verlag, New York (1989) 99-117.
- [20] Fournier,R.O. and Truesdell,A.H., An empirical Na-K-Ca geothermometer for natural waters, Geochimica et Cosmochimica Acta, Vol. 37 (1973) 1255-1275.
- [21] Fournier, R.O. Chemical geothermometers and mixing models for geothermal systems, Geothermics, Vol. 5(1977) 41-50.
- [22] Tonani, F., Some remarks on the application of geochemical techniques in geothermal exploration, Proc. Adv. Eur. Geoth. Res., Second Symp., Strasbourg, (1980) 428-443.

- [23] Fouillac, C. and Michard, G., Sodium/lithium ratios in water applied to geothermometry of geothermal reservoirs, *Geothermics*, vol. 10 (1981) 55-70.
- [24] Arnorsson, S., Chemical equilibria in Icelandic geothermal systems - implications for chemical geothermometry investigations, *Geothermics*, vol. 12, No. 2/3, (1980) 119-128.

# APPLICATIONS OF STABLE ISOTOPES IN GEOTHERMAL EXPLORATION IN THE PHILIPPINES — A REVIEW

J.Y. GERARDO<sup>1</sup>, R.R. ALVIS-ISIDRO, D.R. SANCHEZ, V.C. CLEMENTE  
Geothermal Division,  
Philippine National Oil Company – Energy Development Corporation,  
Makati, Metro Manila, Philippines

R. GONFIANTINI<sup>2</sup>  
Isotope Hydrology Section,  
International Atomic Energy Agency,  
Vienna

**Abstract** - A review of the isotopic data from geothermal exploration areas in the Philippines indicates that the surface thermal waters and well discharges are enriched in heavier isotopes and deviate from the local meteoric water line defined by  $\delta^2\text{H} = 8\delta^{18}\text{O} + (14 \pm 2)$ . This enrichment is commonly due to: 1) near surface evaporation; and 2) mixing between meteoric waters and isotopically enriched deep magmatic waters, a phenomenon confirmed by deep well fluids in developed Philippine geothermal systems, such as Tongonan, Palinpinon and Alto Peak. Waters that are isotopically enriched due to the latter are found to be more significant to exploration because in most cases, these are representative of fluids from hotter sources. The dominant process forming these waters can be distinguished by the relationship between stable isotopes and Cl compositions.

## 1. INTRODUCTION

The Philippines currently has a total installed generating capacity of 1,036.5 MWe from geothermal energy resources. The Philippine National Oil Company-Energy Development Corporation (PNOC-EDC) generates about 36% of these from the following geothermal fields (Fig. 1): Bacon-Manito (BacMan) I (110 MWe) and II (20 MWe) in Sorsogon in Luzon; Palinpinon I (112.5 MWe) and II (20 MWe), and the 1.5-MWe pilot plant in Southern Negros; and, Tongonan I (112.5 MWe) in Leyte.

By 1996-1997, the huge geothermal potential of Leyte (additional 640 MWe) shall be developed in line with the plan for the total interconnection of the country into a single grid. The Mindanao 1 (Mt. Apo) geothermal project (40 MWe) shall also be commissioned in 1996 to provide supply diversification in Mindanao.

Despite these, 1,595 MWe is still required to augment the energy demands in the next five years. To meet these needs, PNOC-EDC is exploring and developing 21 geothermal prospect areas, ten in Luzon, six in the Visayas and five in Mindanao, from where a total of 1090 to 2550 MWe is expected.

These programs imply greater demand for geoscientific investigations, for which isotopic techniques play an important role. Isotopic investigations have been conducted in Philippine geothermal exploration areas since 1989 under the International Atomic Energy Agency

---

<sup>1</sup>Present address: Isotope Hydrology Section, International Atomic Energy Agency, P.O. Box 100, Wagramerstrasse 5, A-1400 Vienna, Austria.

<sup>2</sup>Present address: Laboratoire d'Hydrologie et Géochimie Isotopique, Université de Paris Sud, F-91405 Orsay Cedex, France.

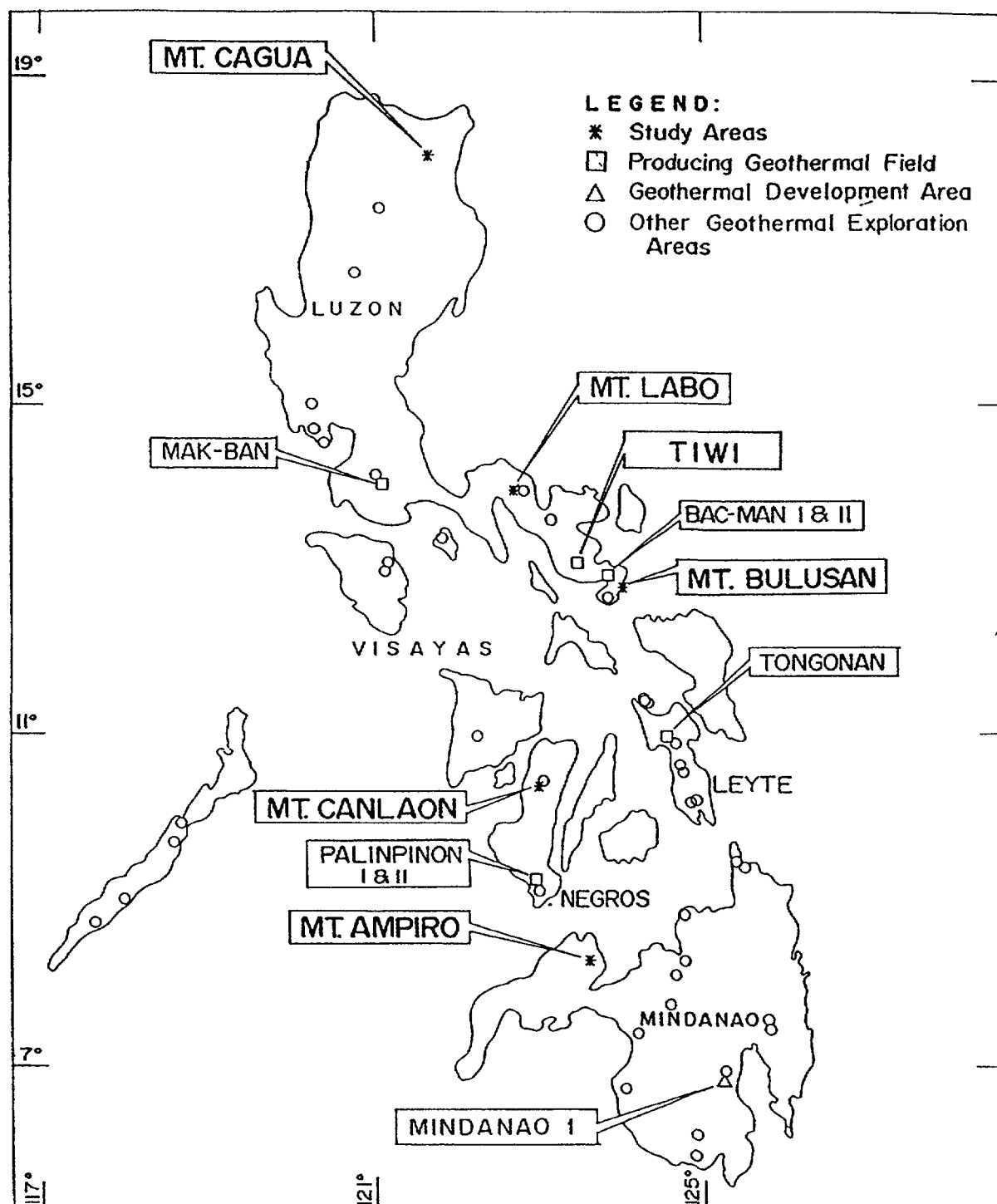


FIG. 1. Location map of Philippine geothermal areas.

(IAEA) assistance with the following objectives: a) to establish the baseline isotopic data of thermal and meteoric waters in the geothermal exploration areas; and b) to determine the hydrological characteristics of geothermal areas through the use of  $^{18}\text{O}$ ,  $^2\text{H}$  and  $^3\text{H}$ .

This paper aims to review and summarize the results of these isotopic investigations. It defines the local meteoric water line, illustrates the common phenomena affecting the thermal and non-thermal fluids in geothermal exploration areas, and identifies the possible origin of fluids. The review is focussed on Mts. Cagua, Labo and Bulusan in the island of Luzon, Mt. Canlaon in the Visayas region, and Mt. Ampiro in the island of Mindanao (Fig. 1).

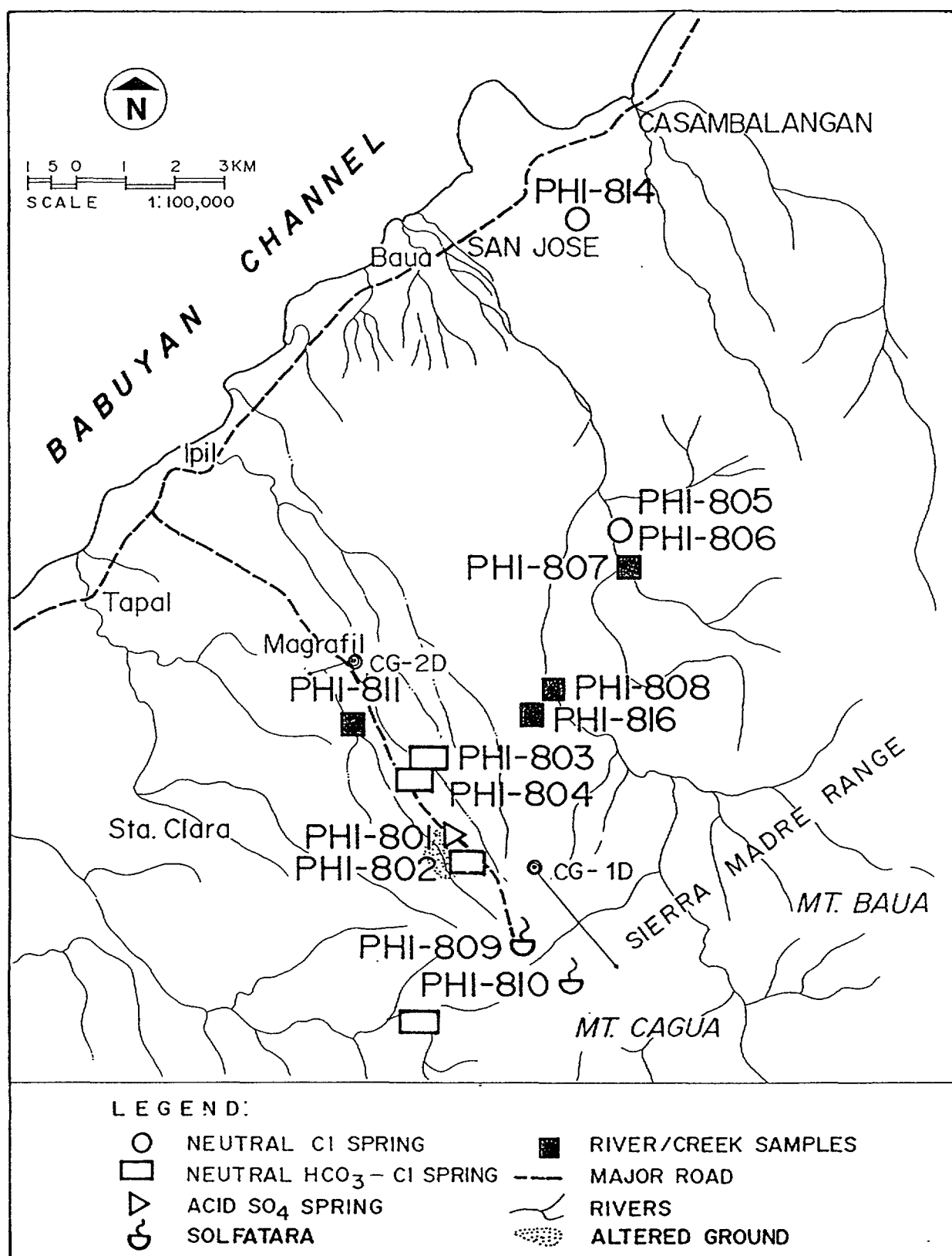


FIG. 2. Map of the Mt. Cagua geothermal project showing the sampling location of the thermal and surface meteoric waters. The well tracks of CG-1D and CG-2D are shown.

## 2. SAMPLING AND ANALYSIS

Meteoric water samples were collected at different elevations (20 to 1100 m asl) from headwaters of rivers, groundwaters tapped by wells and cold springs found in the different study areas (Figs 2-6). The thermal fluids were collected mainly from springs, geothermal wells and solfataras. Where exploratory wells were drilled, as in Mts. Labo and Cagua, samples were collected at stable conditions during discharge testing by using a Webre separator to separate the steam and liquid phases. The number of samples were, however, limited by the short duration of the tests, but are sufficient to characterize the deep geothermal fluids. The analytical results were corrected to their total discharge compositions [1, 2].

All samples were stored in polyethylene bottles and analyzed at the Isotope Hydrology Laboratory of IAEA in Vienna for  $^{18}\text{O}$ ,  $^2\text{H}$  and  $^3\text{H}$ . The corresponding chemical compositions were analyzed at the PNOC-EDC Head Office Chemical Laboratory in Manila. The isotopic results were reported in ‰ deviation from the Vienna Standard Mean Ocean Water (VSMOW) with uncertainty ranges of  $\pm 0.1$  ‰ and  $\pm 1.0$  ‰ for  $\delta^{18}\text{O}$  and  $\delta^2\text{H}$ , respectively. Tritium results were reported in tritium units (TU), where 1 TU has a ratio of  $^3\text{H}/^1\text{H} = 10^{-18}$ . The average analytical error is  $\pm 0.4$  TU.

## 3. DESCRIPTION OF THE STUDY AREAS

### 3.1 Mt. Cagua

Mt. Cagua is associated with an active magmatic hydrothermal system. It is underlain mainly by andesite lava flows, tuffs and breccias, with minor layers of basalts and sediments. The heat source is associated with microdiorites [3].

This area is characterized by a solfataras (Maasok) which discharges superheated steam at  $96^\circ\text{C}$  (Fig. 2). A neutral pH chloride-bicarbonate spring with a temperature of  $42^\circ\text{C}$  is found beneath the crater. The hydrothermal system is postulated to outflow towards the northwest.

Two wells drilled in this area, CG-1D and CG-2D, yielded a maximum measured temperature of  $340^\circ\text{C}$  at the well bottom. It is hypothesized that the system consists of a two-phase shallow liquid dominated reservoir and a deeper gas rich zone with magmatic characteristics [4].

### 3.2 Mt. Labo

Mt. Labo is an inactive Quaternary volcano. It is underlain by the Upper Miocene volcanics consisting of andesitic to dacitic lava flows, agglomerates and tuffs. This is overlain by a Pliocene sedimentary sequence. The youngest and most widespread units are the Pleistocene volcanics which are the products of the volcanism to which the hydrothermal activity is associated [5].

The geothermal system is manifested at the surface by neutral pH chloride springs (1700-2700 ppm Cl) which discharge at temperatures of  $45$ - $88^\circ\text{C}$  (Fig. 3). These are found at lower elevations (90-205 m asl) southwest of the prospect. Some acid-sulfate springs with temperatures of  $30$ - $50^\circ\text{C}$  and Cl of 130-450 ppm are found at higher elevations (565-590 m asl) at the central portion of the volcano [5].

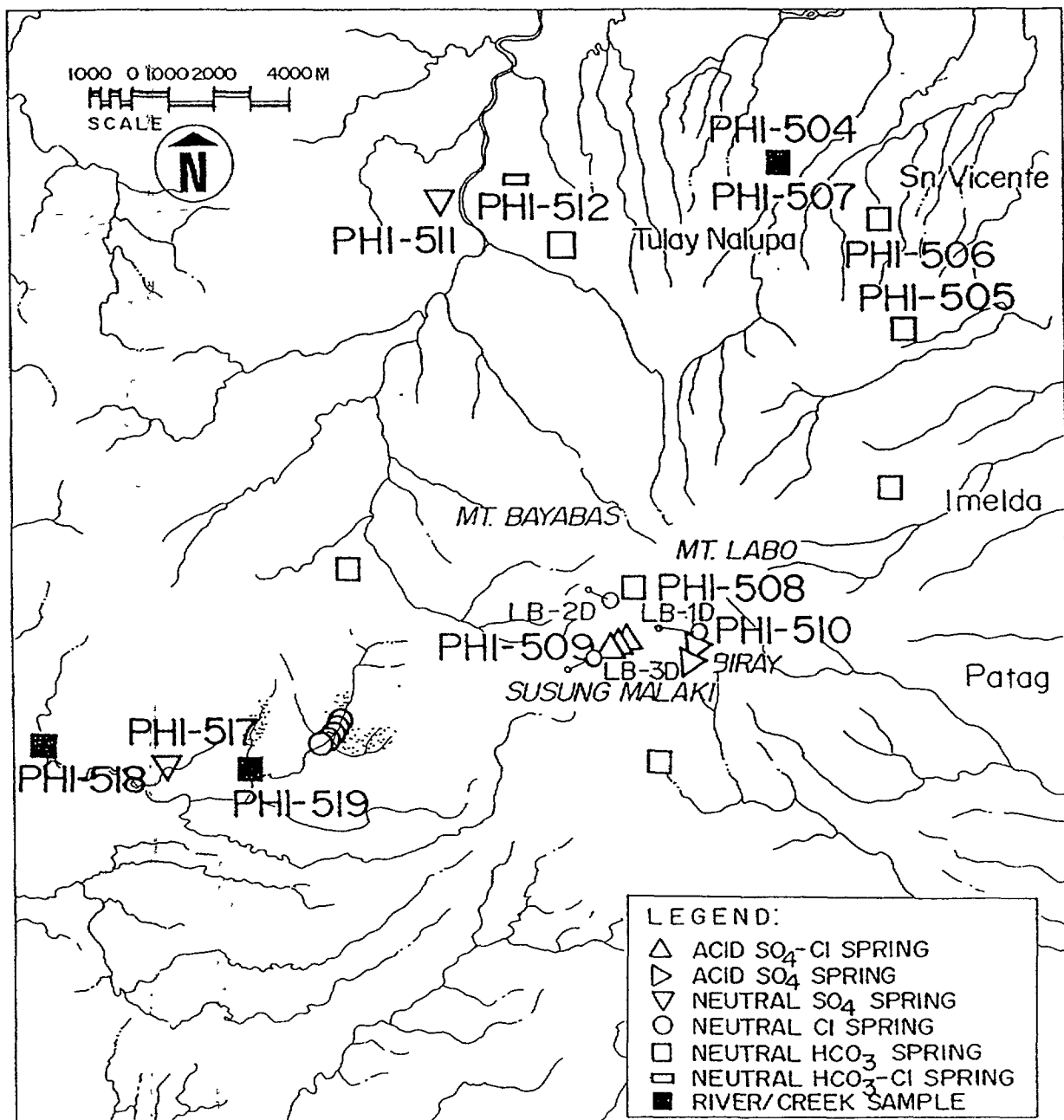


FIG. 3. Sampling location map of the Mt. Labo geothermal project. The well tracks of LB-1D, LB-2D and LB-3D are also shown.

Among the three exploration wells drilled, only two were successfully discharged. Well LB-1D, however, discharged acidic fluids (pH = 3.4) with measured temperature of 270°C at well bottom. Well LB-3D initially had a neutral pH discharge which subsequently became acidic. It has a well bottom measured temperature of 264°C [5].

### 3.3 Mt. Bulusan

Mt. Bulusan is a caldera-hosted hydrothermal system which is associated with andesitic volcanism and minor rhyolitic intrusions [6]. The thermal manifestations are confined within the caldera, mainly in the form of warm springs having temperatures up to 63°C (Fig. 4). The neutral pH chloride-bicarbonate springs are found at lower elevations (0-20 m asl) [7].

### 3.4 Mt. Canlaon

Mt. Canlaon is a volcanic complex consisting of four eruption centers. The youngest crater is characterized by minor and periodic eruptions of ashes. The hydrothermal system is associated with the oldest and extinct eruption crater at the southwest. It is underlain by Pleistocene andesite lavas that are intercalated with minor sedimentary layers [8].

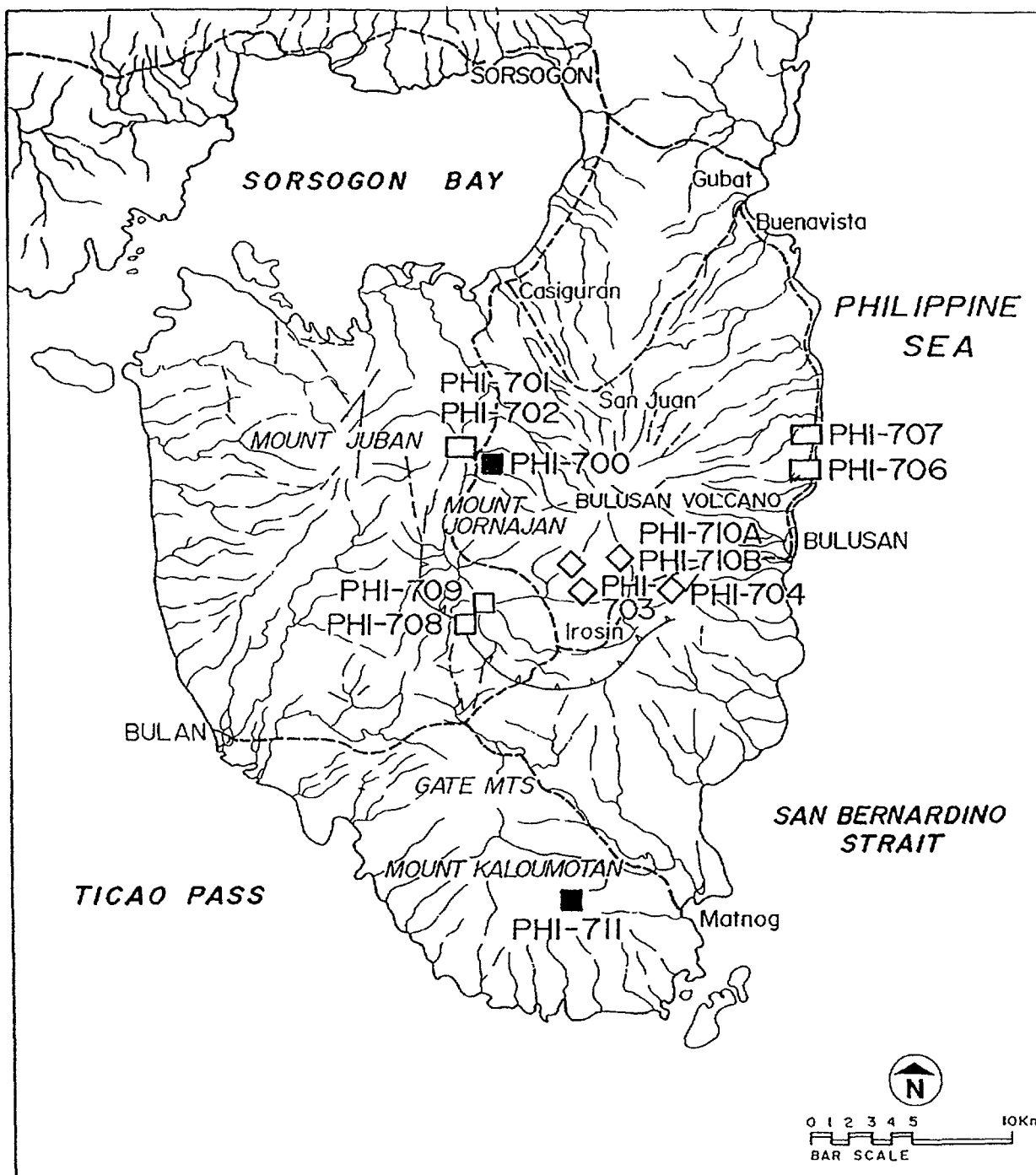


FIG. 4. Structural and sampling location map of the Mt. Bulusan geothermal prospect. The  $\text{SO}_4\text{-HCO}_3$  waters are denoted by  $\diamond$ . All other symbols used are the same as in Figs 2 and 3.



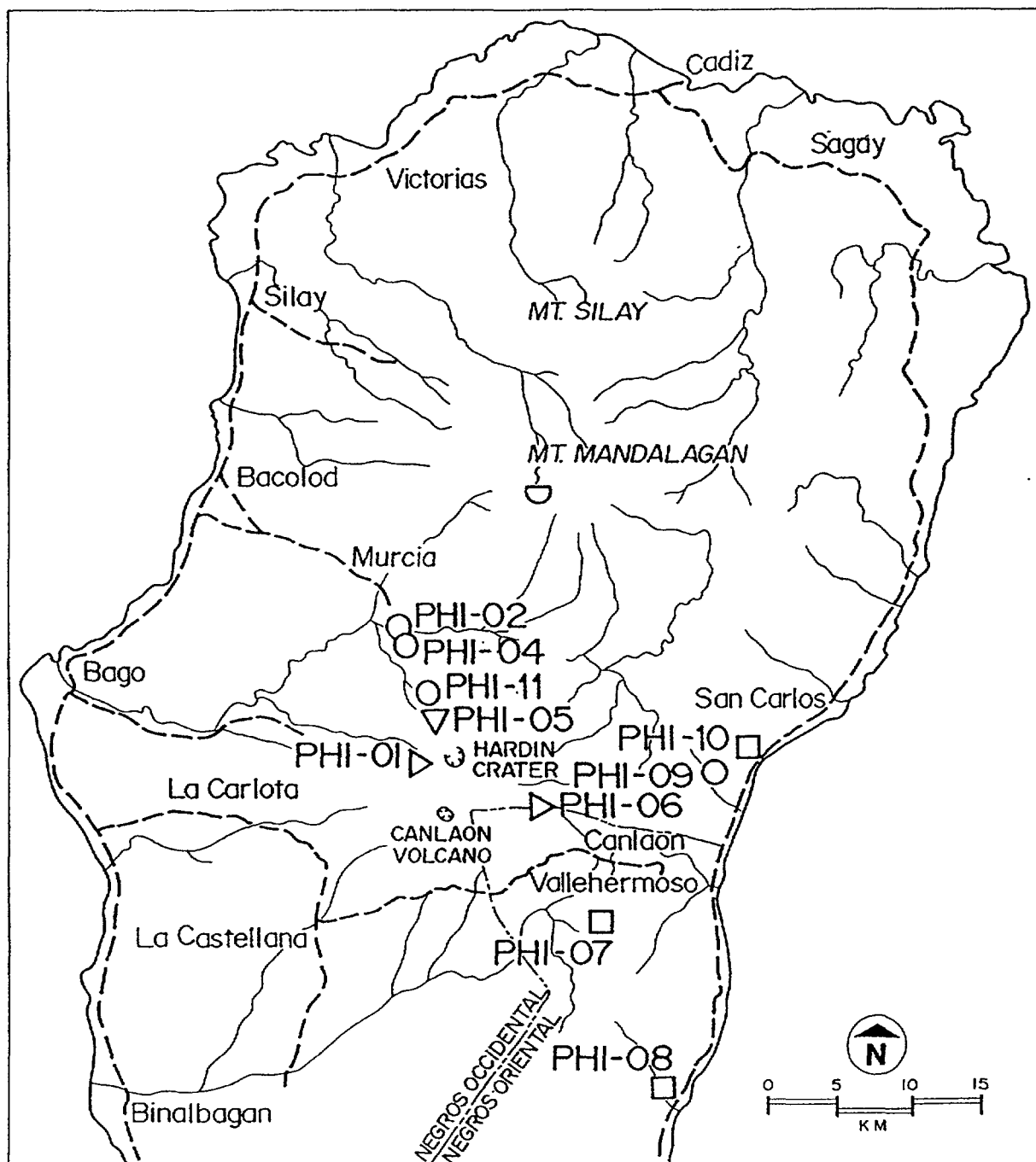


FIG. 5. Map showing the sampling location of thermal waters in Mt. Canlaon geothermal project. Symbols used are the same as in Figs 2 and 3.

The neutral pH chloride springs, which are manifestations of the outflowing geothermal fluids, are found at the northwestern slope of the volcano (Fig. 5) at an elevation of 340 m asl and with a maximum temperature of 64°C. The acid-sulfate springs are situated at higher elevations (340-870 m asl). A 265°C neutral pH chloride reservoir is postulated to upflow beneath the northwestern part of the volcanic complex [9, 10].

### 3.5 Mt. Ampiro

Mt. Ampiro, another caldera-hosted hydrothermal system, is underlain predominantly by basaltic rocks with minor andesitic units. A few thermal manifestations consisting of springs

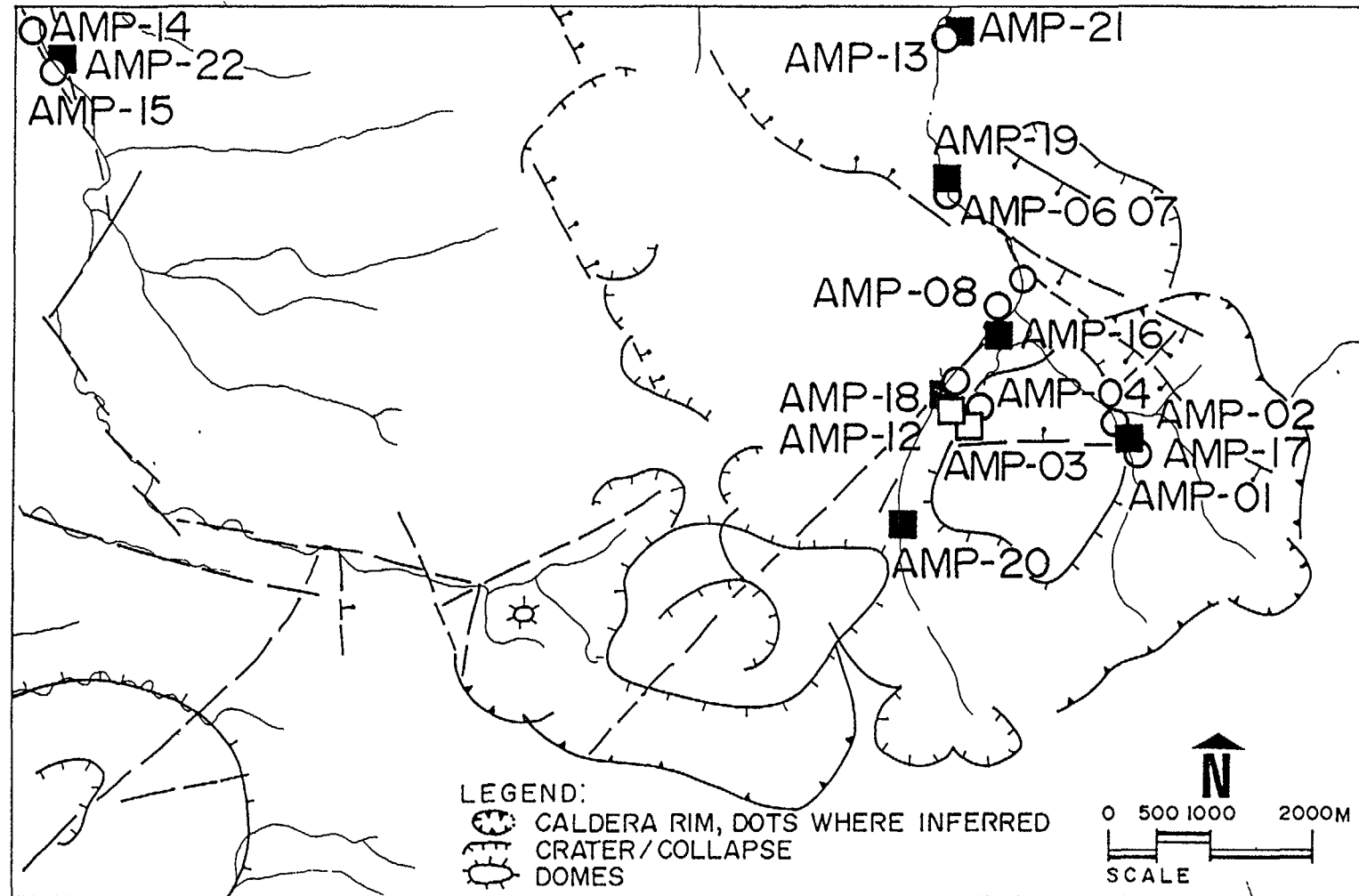


FIG. 6. Map of the Mt. Ampiro geothermal prospect showing the major structures and the sampling location of surface thermal and meteoric waters. Symbols used are the same as in Figs 2 and 3.

with maximum temperature of 53°C, are confined within the caldera (Fig. 6). The heat source of the hydrothermal system is associated with intracaldera domes [11]. A reservoir with temperature of 275°C is postulated [12].

#### 4. METEORIC WATERS

The meteoric waters collected from the study areas have a compositional range of -7.59 to -4.73 ‰ in  $\delta^{18}\text{O}$ , -44.8 to -26.8 ‰ in  $\delta^2\text{H}$  and 7 to 25 ppm in Cl (Table I). It may be noted that meteoric waters which are more enriched in the heavy stable isotopes are found in the northern part of the Philippines and the depleted ones in the south (Fig. 7). This behavior may be a reflection of the latitude effect on the isotopic composition [13].

The average deuterium excess [14],  $d$ , calculated assuming an a priori slope of 8, is 13.4 for all areas (Table I). This is consistent with the value calculated for Palinpinon ( $d = 14 \pm 2$ ) [1], for Leyte ( $d = 13.7$ ) [2] and for Bacon-Manito ( $d = 13.7$ ) [15].

TABLE I. STABLE ISOTOPIC COMPOSITION OF METEORIC WATER SAMPLES FROM THE VARIOUS STUDY AREAS

Code	Source	DATE	Elevation (m asl)	Cl (ppm)	$\delta^{18}\text{O}$ (‰)	$\delta^2\text{H}$ (‰)	Deuterium excess <sup>1</sup>	Tritium (TU)
<b>MT. CAGUA</b>								
PHI-807	Rapa Creek	16-Feb-91	60	17	-5.38	-26.8	16.3	
PHI-808	Baua River	16-Feb-91	25	18	-5.72	-30.6	15.2	
PHI-811	Tapel River	19-Feb-91	270	11	-6.48	-38.7	13.2	
PHI-812	Pad-A coldspring	19-Feb-91	700	18	-6.44	-35.8	15.7	
PHI-813	Main Dam	19-Feb-91	400	7	-6.80	-40.7	13.8	
PHI-815	Pateng River	20-Feb-91	10	14	-6.20	-35.5	14.1	
PHI-816	Bulawan River	20-Feb-91	140	25	-6.70	-39.2	14.4	
	<i>Average</i>						14.7	
<b>MT. LABO</b>								
PHI-502	Magana coldspring	10-May-90	202	8.51	-4.73	-28.2	9.6	3.0
PHI-504	CNWD 6 test well	10-May-90	120		-5.15	-28.6	12.6	
PHI-505	Alinao coldspring	11-May-90	253	8.86	-5.05	-31.0	9.4	2.7
PHI-506	Bamban coldspring	11-May-90	207	9.40	-5.51	-34.5	9.6	3.3
PHI-507	CNWD1 well	14-May-90	120	9.57	-5.24	-31.5	10.4	2.2
PHI-508	Hagdan coldspring	15-May-90	850	9.93	-5.80	-35.4	11.0	1.9
PHI-518	Layatun River	18-Jan-93			-5.60	-30.6	14.2	
PHI-519	Bakoko River	18-Jan-93			-5.41	-30.9	12.4	
	<i>Average</i>						11.1	
<b>MT. BULUSAN</b>								
PHI-700	Bacolod	07-Jun-90	20	13	-5.27	-27.5	14.7	
PHI-711	Bolocawe	08-Jun-90	20	12	-5.93	-33.7	13.7	
	<i>Average</i>						14.2	
<b>MT. AMPIRO</b>								
AMP-03	Sibucal 1	23-Nov-91	920	12	-6.63	-41.7	11.3	
AMP-16	Sabinit River	21-Jan-92	780		-6.89	-41.2	13.9	
AMP-17	Manimatay River	22-Jan-92	950		-6.72	-40.0	13.8	
AMP-18	Sabinit River	22-Jan-92	960		-6.13	-36.1	12.9	
AMP-19	Tuminawan River	22-Jan-92	750		-5.12	-28.7	12.3	
AMP-20	Upper Sabinit	23-Jan-92	1100		-7.35	-44.2	14.6	
AMP-21	Nunganga	25-Jan-92	650		-6.18	-36.2	13.2	
AMP-22	Onidos	27-Jan-92	450		-7.59	-44.6	16.1	
	<i>Average</i>						13.6	

<sup>1</sup> Deuterium excess =  $6^2\text{H} - 8^6\text{O}$  (Dansgaard, 1964)

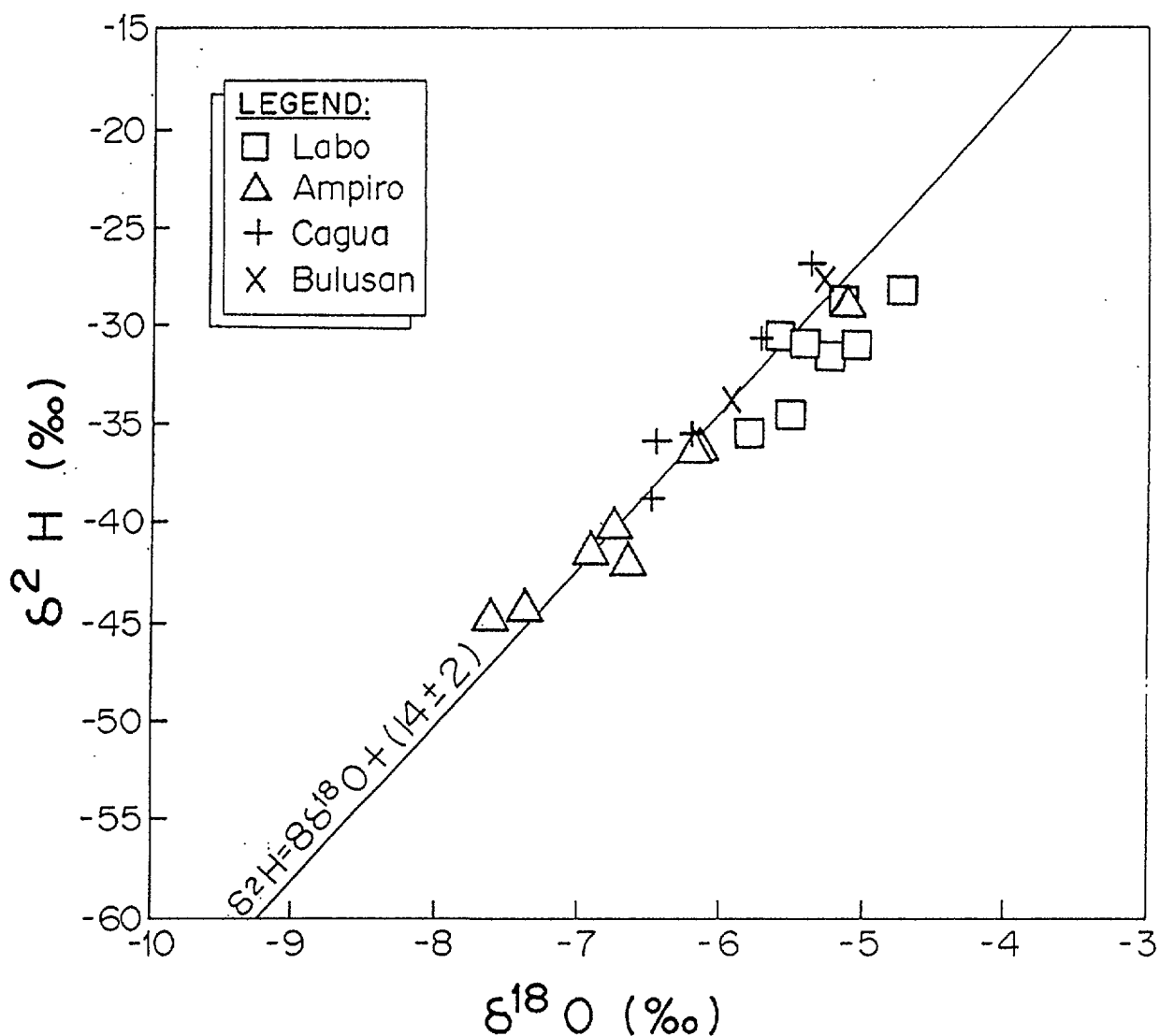


FIG. 7. Stable isotope concentrations of meteoric waters in the study areas.

The deuterium excess for Metro Manila is equal to 10, computed from the weighted means of the monthly average rainfall in Manila Station (average elevation is about 40 m asl) from 1963-76 [9, 16]. This is consistent with the global meteoric water line [17]. The differences, however, in  $d$  between the study areas and Metro Manila may be attributed to the effect of mean relative humidity of the air masses overlying the oceans [18]. It may also be due to the contribution of the ocean vapor and vapor from terrestrial evaporation and transpiration [19]. These factors were also postulated to be the causes for the larger  $d$  in Palinpinon and Leyte. Considering the similarity of  $d$  in all geothermal areas, it may be pragmatic to consider that the local meteoric water line (LMWL) has the equation  $\delta^2\text{H} = 8\delta^{18}\text{O} + (14 \pm 2)$ . Figure 7 illustrates the isotopic relationship of the meteoric waters at a correlation coefficient,  $r^2 = 0.97$ , for 25 samples.

## 5. THERMAL WATERS

### 5.1 Chemistry of thermal waters

The thermal waters are classified according to their major anion compositions as reflected on the  $\text{Cl-SO}_4\text{-HCO}_3$  triangular diagram (Fig. 8). Table II also includes a summary

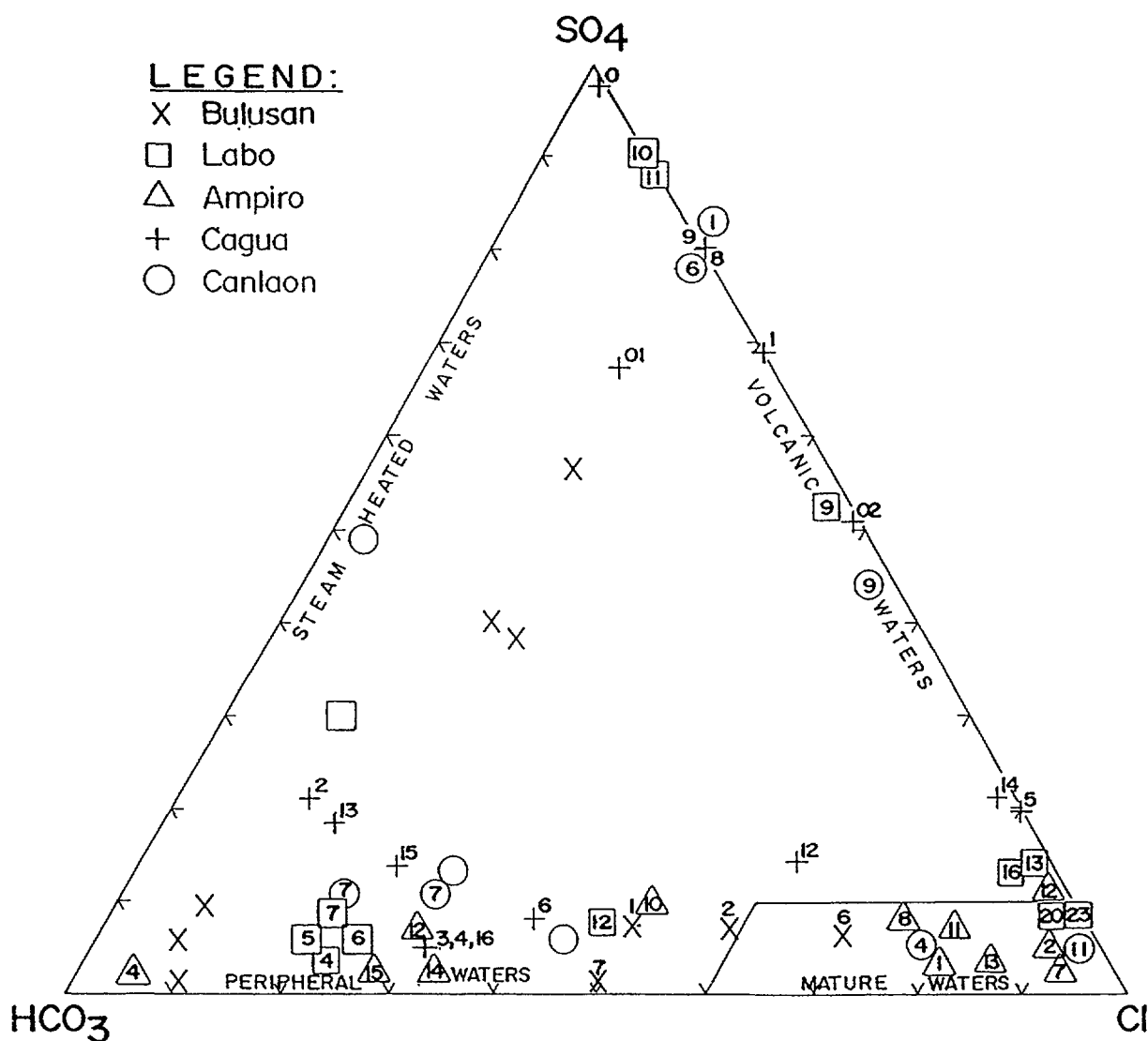


FIG. 8. Classification of thermal waters in the study areas, based on anions (Giggenbach, 1988). The numbers in the symbols correspond to the last digits of the sampling codes as presented in Table II.

of that classification. The mature neutral pH chloride waters which are the best representative of the deeper geothermal brine for all study areas, except Mt. Cagua, are indicated. Most samples are mixtures of bicarbonate, chloride-rich geothermal fluids or sulfate-rich volcanic vapors. A few samples are volcanic in nature and are mixtures of sulfate-rich vapor and mature geothermal waters.

As illustrated in the Na-K-Mg diagram [20] (Fig. 9), most of the partially equilibrated fluids are neutral pH chloride discharges from geothermal wells. In areas such as Mts. Labo and Ampiro, where more data are available, dilution trends are defined. This triangular diagram also suggests that the possible temperatures of the deep geothermal brine are about 220°C for Mt. Cagua, 230°C for Mt. Labo and 260°C for Mt. Canlaon.

TABLE II. ISOTOPIC COMPOSITION OF THERMAL WATERS IN THE VARIOUS STUDY AREAS

Code	Source	Date	Temp C	Elevation (m asl)	pH	Type of waters, by anion content	Cl (ppm)	$\delta^{18}\text{O}$ (‰)	$\delta^2\text{H}$ (‰)	Tritium (TU)
<b>MT. CAGUA</b>										
<i>Thermal springs</i>										
PHI-801	Magrafil A	15-Feb-91	32	400	3.3	SO <sub>4</sub>	11	-7.44	-46.3	
PHI-802	Magrafil B	15-Feb-91	50	400	7.5	HCO <sub>3</sub>	18	-7.10	-41.5	
PHI-803	Kabinlangan A	15-Feb-91	41	280	7.9	HCO <sub>3</sub> -Cl	198	-6.16	-38.6	
PHI-804	Kabinlangan B	15-Feb-91	48	280	7.8	HCO <sub>3</sub> -Cl	198	-6.20	-38.8	
PHI-805	Manaring A	16-Feb-91	62	25	7.9	Cl	1278	-4.50	-24.1	
PHI-806	Manaring B	16-Feb-91	58	25	8.0	Cl	1313	-4.50	-24.2	
PHI-809	Maasok Pool 1	18-Feb-91	94	760	2.2	SO <sub>4</sub> -Cl	354	12.78	9.7	
PHI-810	Maasok Pool 2	18-Feb-91	84	760	2.3	SO <sub>4</sub> -Cl	354	15.12	12.4	
PHI-814	San Jose	20-Feb-91	38	40	7.2	Cl	867	-4.70	-21.9	
<i>Well waters</i>										
PHI-800	CG-1D							1.24	-21.5	1.4
PHI-801	CG-1D							0.61	-32.8	
<b>MT. LABO</b>										
<i>Thermal springs</i>										
PHI-509	Mabahong Labo	15-May-90	50	565	2.6	SO <sub>4</sub>	484	-5.13	-33.6	2.0
PHI-510	Wala	15-May-90	19	780	3.1	SO <sub>4</sub>	11	-5.59	-34.6	2.0
PHI-511	Natuldocan	15-May-90	30	80	6.2	SO <sub>4</sub>	15	-5.06	-30.1	0.5
PHI-512	Baay	16-May-90	30	100	6.7	HCO <sub>3</sub>	320	-4.92	-29.9	1.4
PHI-517	Mukbok	18-Jan-93	38		6.0	SO <sub>4</sub>	22	-5.77	-31.6	
<i>Well waters</i>										
PHI-513	LB-1D, 1800 m bsl	01-Dec-90	119		7.8	Cl	1142	-3.69	-30.5	
PHI-514	LB-1D, 2500 m bsl	01-Dec-90	127		4.7	SO <sub>4</sub>	79	-5.55	-30.1	
PHI-515	LB-1D, 1800 m bsl	02-Sep-92	154		6.1	Cl	1547	-3.18	-28.6	
PHI-516	LB-1D, 2500 m bsl	02-Sep-92	154		6.5	SO <sub>4</sub>	1682	-2.96	-30.2	
PHI-520	LB-3D	29-Nov-92	254		4.5	Cl	4386	-1.10	-29.6	
PHI-522	LB-3D	11-Dec-92	273		4.3	Cl	4399	-0.75	-31.8	
PHI-523	LB-3D	13-Nov-92	263		6.8	Cl	3799	-1.23	-28.1	
<b>MT. BULUSAN</b>										
PHI-701	Banyo	07-Jun-90	63	20	7.9	Cl-HCO <sub>3</sub>	271	-5.05	-28.2	
PHI-702	Banyo	07-Jun-90	53	20	8.0	Cl-HCO <sub>3</sub>	532	-5.13	-30.2	
PHI-703	San Benon	07-Jun-90	55	60	8.1	HCO <sub>3</sub> -SO <sub>4</sub>	184	-5.62	-30.5	
PHI-704	Masakrot	07-Jun-90	35	285	8.2	HCO <sub>3</sub> -SO <sub>4</sub>	89	-5.55	-29.8	
PHI-706	Porog	07-Jun-90	45	0	8.0	Cl-HCO <sub>3</sub>	1845	-4.25	-26.8	
PHI-707	Buhang	08-Jun-90	46	0	7.6	Cl-HCO <sub>3</sub>	640	-4.56	-27.8	
PHI-708	Gumapia	08-Jun-90	43	35	8.5	HCO <sub>3</sub>	56	-5.58	-30.5	
PHI-709	Talistison	08-Jun-90	45	55	8.2	HCO <sub>3</sub>	52	-5.59	-31.8	
PHI-710A	Pinirincipi	08-Jun-90	45	450	8.2	SO <sub>4</sub> -HCO <sub>3</sub>	212	-5.42	-29.8	
PHI-710B	Pinirincipi	08-Jun-90	48	450	8.1	SO <sub>4</sub> -HCO <sub>3</sub>	197	-5.44	-28.0	
<b>MT. CANLAON</b>										
PHI-01	Hagdan	09-Nov-89	44	870	2.7	SO <sub>4</sub>	96	-8.88	-56.1	
PHI-02	Hda. Montilla	08-Nov-89	25	190	8.1	HCO <sub>3</sub>	140	-7.82	-49.6	
PHI-04	Hda. Paz	08-Nov-89	36	220	7.6	Cl	396	-7.62	-49.5	
PHI-05	Kinabkaban	09-Nov-89	38	920	8.0	SO <sub>4</sub>	11	-8.72	-52.7	
PHI-06	Maluyong	17-Nov-89	24	840	3.4	SO <sub>4</sub>	40	-8.42	-52.0	
PHI-07	Bucalan	17-Nov-89	52	320	7.9	HCO <sub>3</sub>	90	-7.46	-46.8	
PHI-08	Kinayan	11-Nov-89	36	20	7.7	HCO <sub>3</sub>	97	-6.54	-42.3	
PHI-09	Mabato B	11-Nov-89	64	78	7.6	Cl	200	-6.94	-43.1	
PHI-10	Hda. Florida	11-Nov-89	30	10	8.4	HCO <sub>3</sub>	186	-6.43	-41.4	
PHI-11	Aquapool	28-Jun-91	64	340	8.3	Cl	1530	-6.35	-48.1	
<b>MT. AMPIRO</b>										
AMP-01	Manimatay 1	23-Nov-91	35	950	7.6	Cl	590	-5.21	-33.5	
AMP-02	Manimatay 2	23-Nov-91	53	950	7.6	Cl	1585	-4.34	-35.2	
AMP-04	Sibucal 2	24-Nov-91	37	920	7.1	HCO <sub>3</sub>	108	-7.71	-45.8	
AMP-06	Tuminawan 1	26-Nov-91	56	750	7.5	Cl	2130	-4.26	-34.1	
AMP-07	Tuminawan 2	26-Nov-91	49	750	7.2	Cl	1975	-3.83	-31.4	
AMP-08	Lawayan 1	27-Nov-91	45	780	8.1	Cl	2260	-4.91	-36.7	
AMP-11	Sabinait 1	27-Nov-91	45	960	7.9	Cl	4240	-3.39	-36.7	
AMP-12	Sabinait 2	27-Nov-91	40	950	8.2	HCO <sub>3</sub>	350	-6.89	-43.7	
AMP-13	Nunganga	30-Nov-91	44	650	8.1	Cl	1600	-4.27	-30.1	
AMP-14	Onidos 1	06-Dec-91	28	450			1429	-6.38	-39.7	
AMP-15	Onidos 2	06-Dec-91	28	450			1007	-6.55	-42.9	

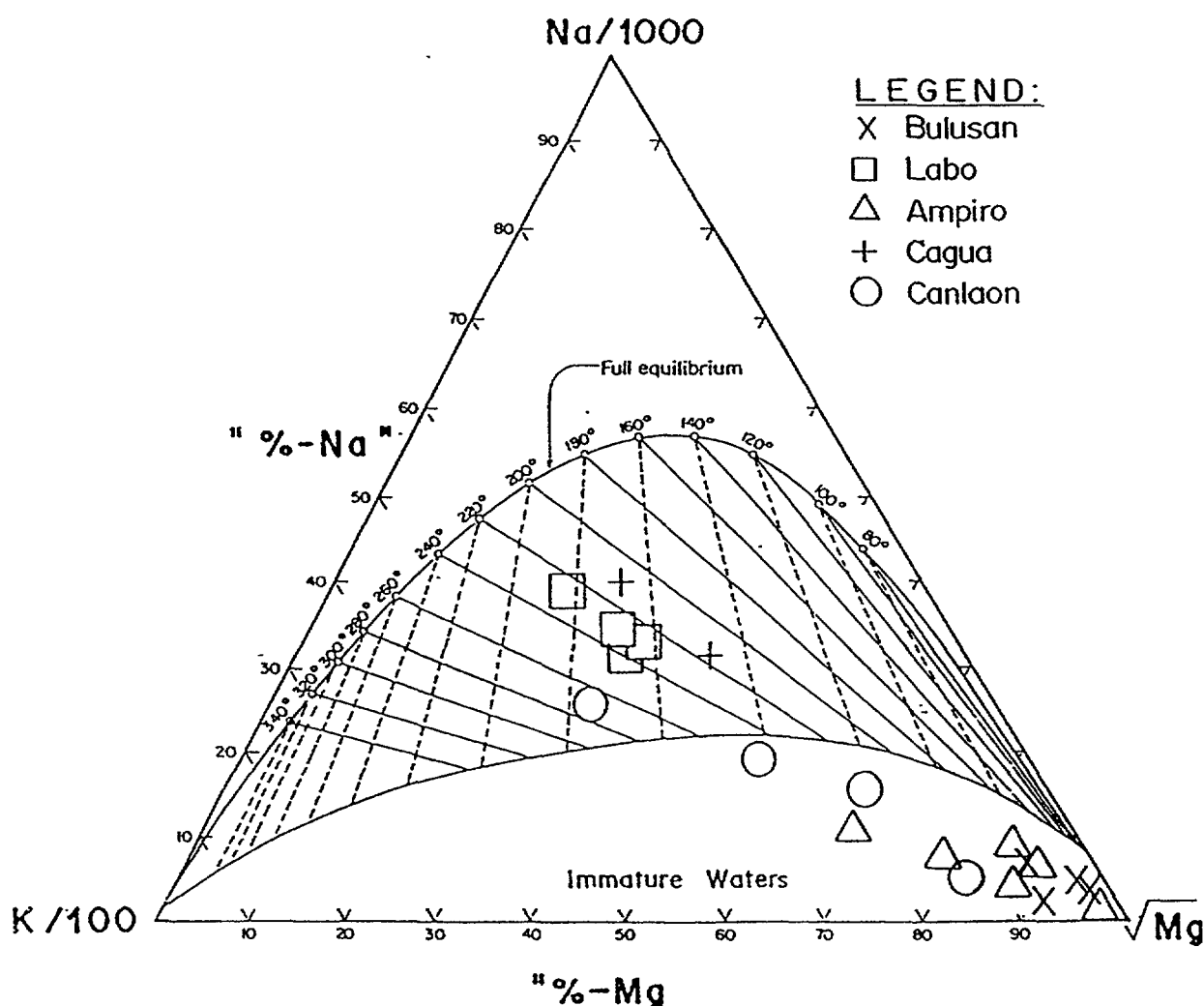


FIG. 9. Na-K-Mg diagram (Giggenbach, 1998) showing the relative maturity of the neutral pH chloride waters in the study areas, the mixing trends, and the corresponding estimated reservoir temperatures.

## 5.2 Isotopic composition of thermal waters

The isotopic composition of thermal waters in the study areas are also tabulated in Table II and plotted in Fig. 10. These waters have  $\delta^{18}\text{O}$  of -7.82 to -0.75 ‰ and  $\delta^2\text{H}$  of -50 to -28.8 ‰. They generally cluster along the LMWL but are slightly enriched both in  $^{18}\text{O}$  and  $^2\text{H}$ . The enrichment is pronounced for Mts. Labo and Cagua where samples were taken from deep geothermal wells.

The thermal waters also plot to the right of the LMWL on a slope from 1 (in Mts. Canlaon and Labo ) to 3 (in Mt. Bulusan). These lines intersect the LMWL at the isotopic composition equivalent to the composition of the local meteoric water which recharges the areas (Table III).

## 5.3 Processes affecting the isotopic compositions of thermal waters

The isotopic trends exhibited by Fig. 10 represent at least two processes, namely: a) evaporation of a thermal water having a composition similar to the local groundwater; or b)

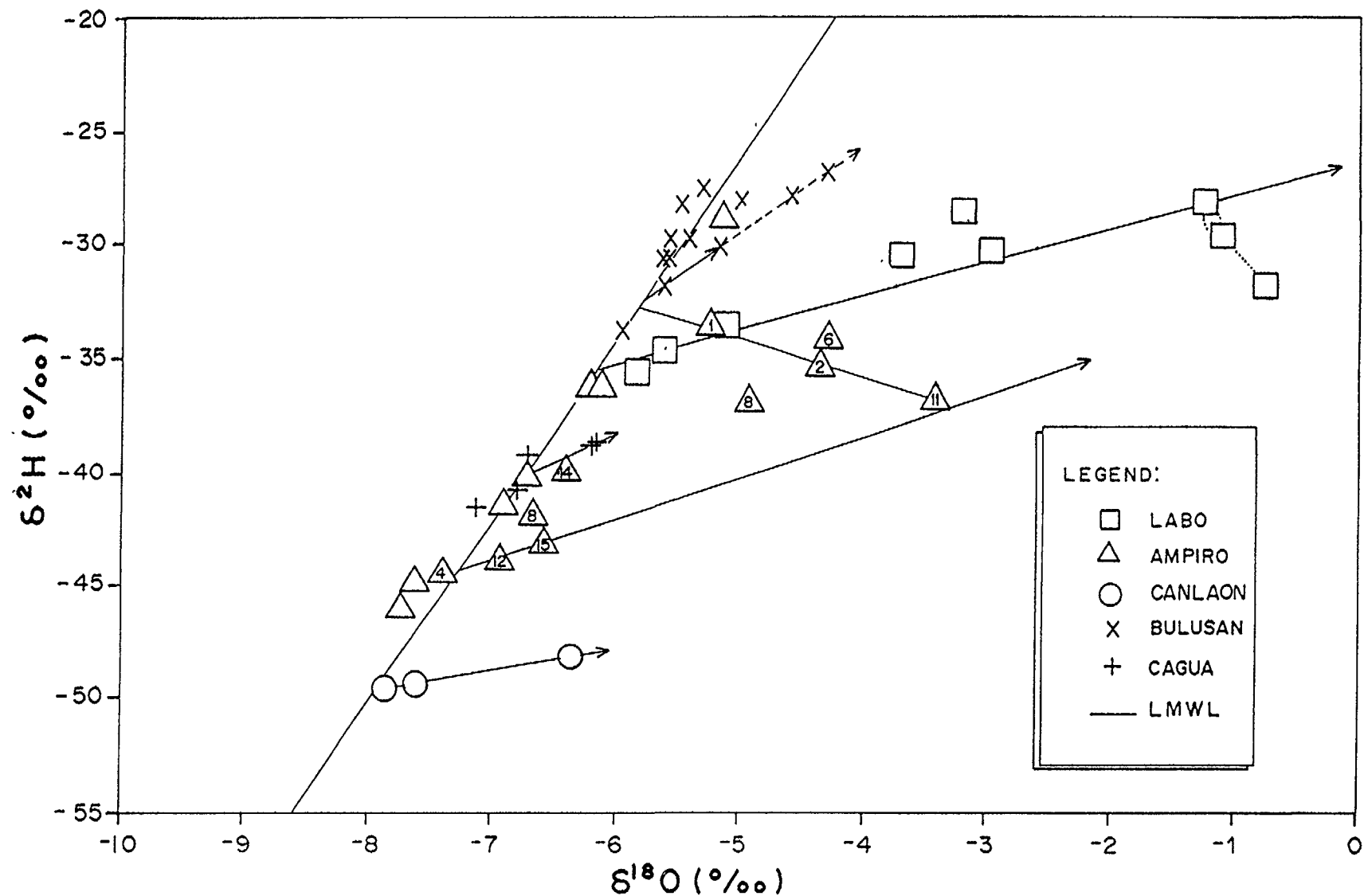


FIG. 10. Stable isotope composition of the thermal waters from the study areas. Fine lines indicate the mixing trends. Their respective intercepts with the local meteoric water line represent the isotopic concentration of the meteoric water recharge.



TABLE III. STABLE ISOTOPIC COMPOSITION OF LOCAL  
METEORIC WATER RECHARGE IN THE VARIOUS STUDY AREAS

Geothermal area	$\delta^{18}\text{O}$ (‰)	$\delta^2\text{H}$ (‰)
Mt. Cagua	-6.7	-41
Mt. Labo	-6.1	-31
Mt. Bulusan	-5.8	-33
Mt. Canlaon	-8.0	-50
Mt. Ampiro	-7.2	-44

mixing between two end members, one being an isotopically enriched deep thermal water with the other end member being groundwater. Both these processes result to the enrichment of the heavy stable isotopes. However, these two processes are distinguished by plotting  $^{18}\text{O}$  and Cl. Mixing of fluids shows a linear trend while evaporative fractionation gives a logarithmic relationship [21]. Evaporation would increase the heavy isotopic and chloride compositions depending on the temperature of fractionation and the fraction of steam removed from the water.

To illustrate, Mt. Ampiro is characterized by neutral pH chloride fluids, with AMP-11 having the largest  $^{18}\text{O}$  shift (Fig. 10) and considered the best representative of deep thermal waters. Bicarbonate-rich thermal waters also exist. The  $^{18}\text{O}$  - Cl diagram (Fig. 11) illustrates two mechanisms: 1) the logarithmic trend of bicarbonate-rich waters which show evaporation with  $^{18}\text{O}$  enrichment and no or slight increase in the chloride content; and 2) linear trend which indicates mixing with isotopically enriched fluids, with the increase in the chloride contents corresponding to an enrichment in  $^{18}\text{O}$ .

Similarly, Mt. Canlaon data points lie close to the LMWL (Fig. 10) indicating that the thermal waters are meteoric in origin. There are no indications of an active magmatic water input despite the presence of the active Canlaon volcano nearby. There also exists a mixing trend between the dilute fluids and the neutral pH chloride geothermal waters (Fig. 11). The same trend is observed for Mts. Cagua, Labo and Bulusan (Fig. 11). This illustrates that the neutral pH chloride thermal waters define a mixing line with isotopically enriched waters. The secondary waters, on the other hand, like bicarbonate and sulfate waters are logarithmically related and since these waters are produced by the adsorption of  $\text{H}_2\text{S}$ -rich vapors into the groundwater, their isotopic enrichment is due to fractionation at lower temperatures near the surface.

#### 5.4 Origin of geothermal waters

Isotopic data from exploration areas clearly show that the thermal waters are essentially a mixture of meteoric water and isotopically enriched fluids, with meteoric waters contributing a greater proportion. The effect of water-rock interaction to the enrichment of  $^{18}\text{O}$  and Cl is however, not discounted. The meteoric water component has the isotopic composition equivalent to the intercept of the  $\delta^2\text{H}$  -  $\delta^{18}\text{O}$  mixing line defined by the thermal waters with the LMWL.

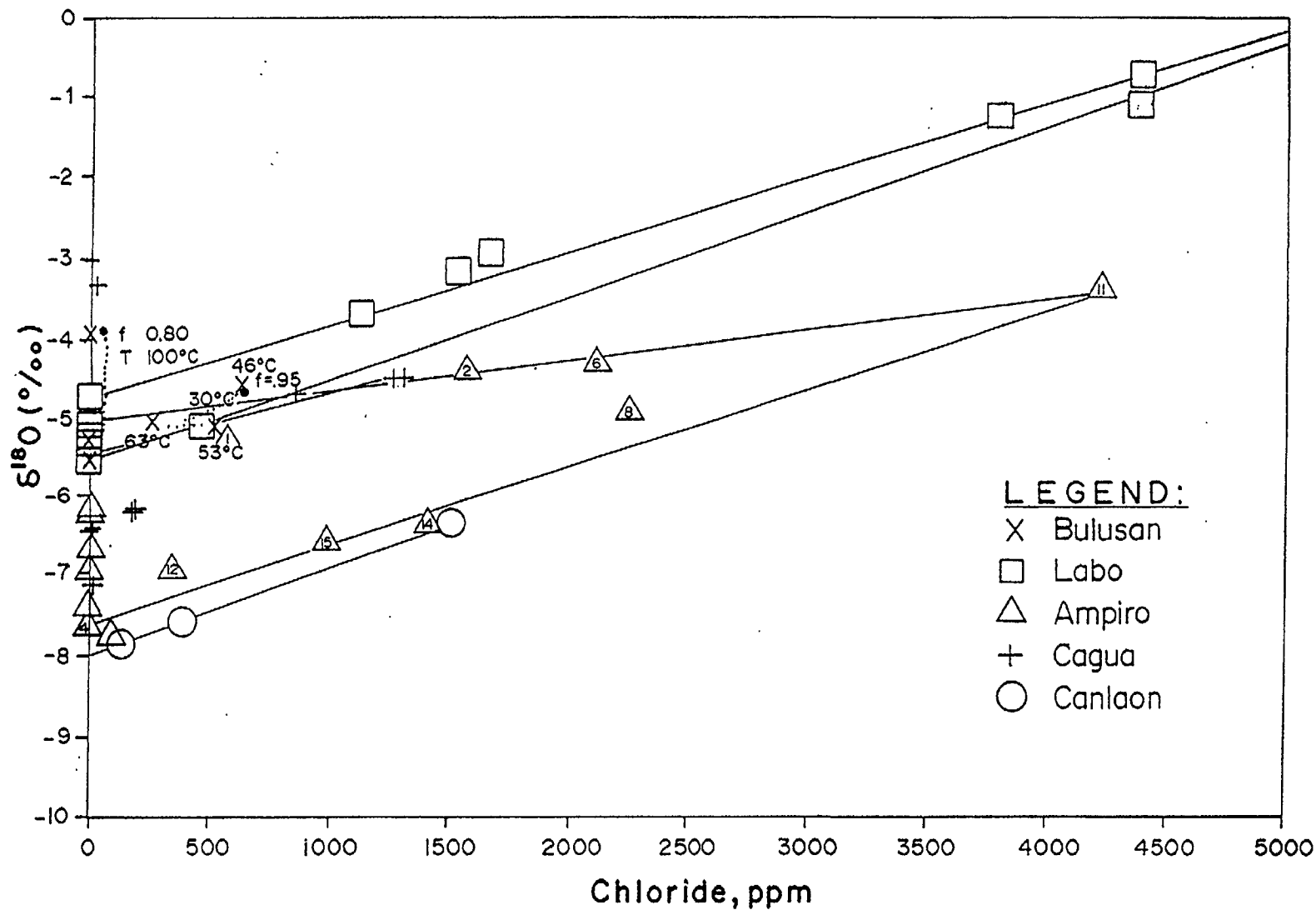


FIG. 11.  $^{18}\text{O}$ -Cl relation of geothermal waters in the study areas. A mixing trend is illustrated by fine lines which also correspond to those in Fig. 10. Evaporation trends are indicated by dots.

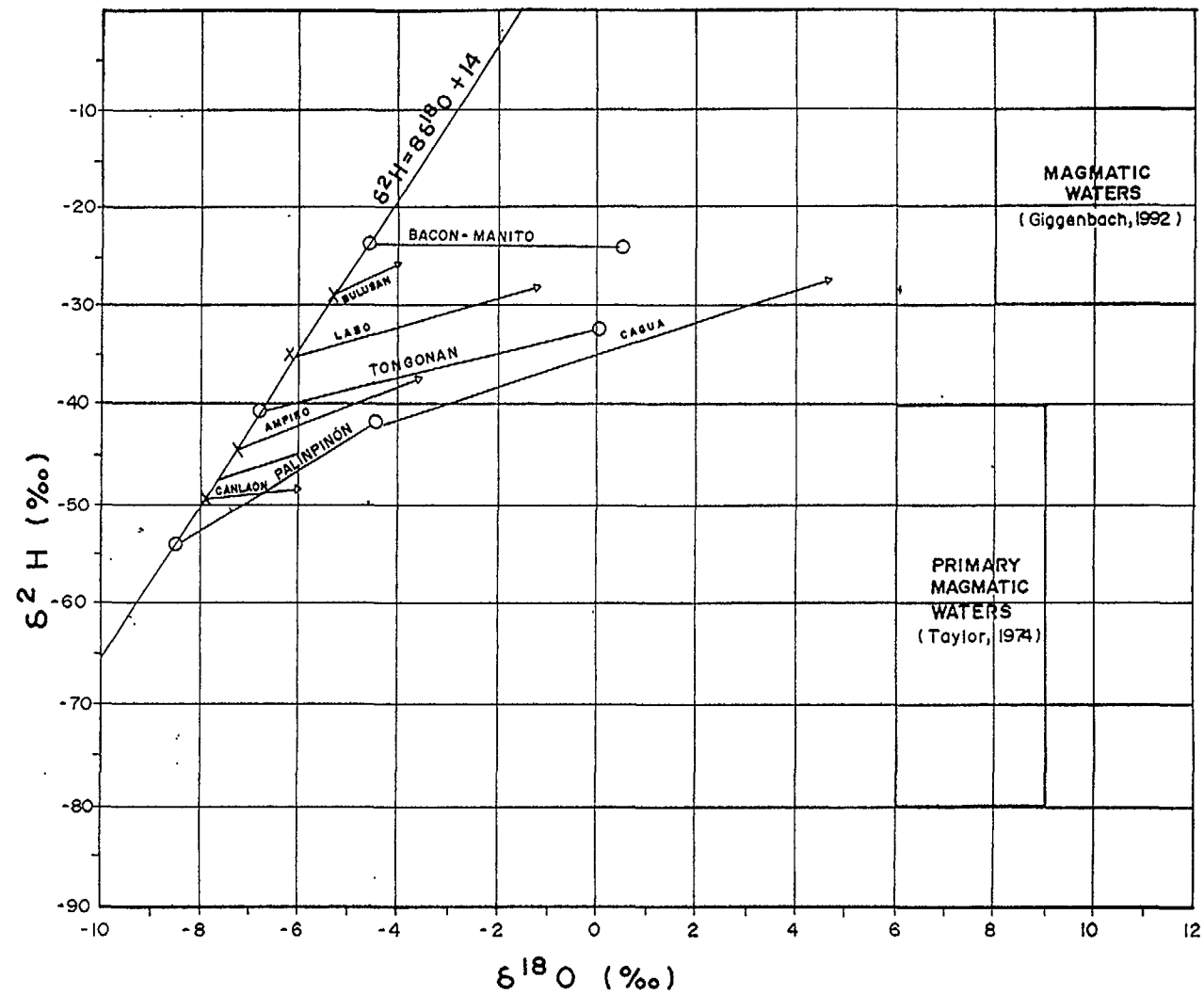


FIG. 12. Stable isotopic trends of the geothermal waters in the study areas, and in producing geothermal areas in the Philippines, with extrapolation towards the magmatic sector as defined by Giggenbach (1992). The primary magmatic water by Taylor (1974) is also illustrated for comparison. The intercepts of the mixing trends showing the recharge of meteoric waters to the geothermal system is indicated.

By extrapolating the composition of the other end-member to the waters having the most enriched composition, the values approach the composition of magmatic waters [22]. The geothermal waters, in most cases, are isotopically heavier due to mixing with isotopically heavy magmatic waters. This relationship is observed in most Philippine geothermal systems, particularly where a number of wells have been drilled, e.g. Palinpinon [1], Tongonan [2], and Alto Peak [23]. This also holds true for some Italian and Japanese high temperature systems [24-27].

## 6. CONCLUSIONS

The LMWL, as a working requirement for interpreting isotopic data, is defined by  $\delta^2\text{H} = 8\delta^{18}\text{O} + (14 \pm 2)$ . Such equation is common for all geothermal areas. However, with the availability of more data in the future, this line may be further verified.

Two processes generally influence the isotope enrichment of thermal fluids, and these are evaporation and mixing with isotopically heavier magmatic fluids. Both can be distinguished by  $^{18}\text{O}$  - Cl relationships. The enrichment of waters with heavier isotopes due to the latter is a strong indication that the fluids are geothermal in nature and, in most instances, come from a hotter source.

**Acknowledgment** - *This work was completed with IAEA assistance under Research Contract no. 6019 within the framework of the Coordinated Research Programme for the Application of Isotope and Geochemical Techniques in Geothermal Exploration in Asia, Middle East and the Pacific. The authors wish to thank Dr. Stefan Arnorsson for reviewing the manuscript.*

## References

- [1] Gerardo, J.Y., Nuti, S., D'Amore, F., Seastres, J.S. and Gonfiantini, R. (1993) Isotopic evidence for magmatic and meteoric water recharge and the processes affecting reservoir fluids in the Palinpinon geothermal system, Philippines. *Geothermics* **22** 521-533.
- [2] Alvis-Isidro, R.R., Solana, R.R., D'Amore, F., Nuti, S. and Gonfiantini, R. (1993) Hydrology of the Greater Tongonan geothermal system, Philippines, as deduced from geochemical and isotopic data. *Geothermics* **22**, 435-449.
- [3] Bayrante, L.F., Ruiz, C.C., Layugan, D.B., Apuada, N.A. and Clemente, V.C. (1989) Geoscientific exploration and evaluation of Mt. Cagua geothermal prospect, Northeastern Luzon. Unpublished. PNOC-EDC internal report. 112 pp.
- [4] Tebar, H.J., Reyes, A.G., Clemente, V.C., Vergara, M.C., Catane, J.P.L. and Sarit, A.D. (1991) Mt. Cagua resource assessment report. Unpublished. PNOC-EDC internal report. 111 pp.
- [5] Geoscientific Staff (1993). Resource assessment update on the Mt. Labo geothermal project. Unpublished. PNOC-EDC internal report. 81 pp.
- [6] Delfin, F.G., Panem, C.C. and Defant, M.J. (1993) Eruptive history and petrochemistry of the Bulusan volcanic complex: implications for the hydrothermal system and volcanic hazards of Mt. Bulusan, Philippines. *Geothermics* **22** 417-434.

- [7] Ramos, M.N. and Baltasar, A.S.J. (1991) Isotopic and chemical composition of the Mt. Bulusan geothermal discharges. Unpublished. PNOC-EDC internal report. 19 pp.
- [8] Pamatian, P.I., Salonga, N.D. and Tebar, H.J. (1992) The geology of Northern Negros geothermal prospect. Unpublished. PNOC-EDC internal report. 60 pp.
- [9] Gerardo, J.Y. (1990) Geochemistry of the Northern Negros geothermal project. Unpublished. PNOC-EDC internal report. 27 pp.
- [10] Gerardo, J.Y. (1992) A geochemical assessment of the Northern Negros geothermal project. Unpublished. PNOC-EDC internal report. 30 pp.
- [11] Pagado, E.S. and Camit, R.A. (1992) The geology of the Mt. Ampiro geothermal prospect, Misamis Occidental, Mindanao. Unpublished. PNOC-EDC internal report. 27 pp.
- [12] Clemente, V.C. (1992) Isotope chemistry of the Mt. Ampiro geothermal prospect. Unpublished. PNOC-EDC internal report. 17 pp.
- [13] Nuti, S. (1992) Isotopic techniques in geothermal studies. In *Applications of geochemistry in geothermal reservoir development* (Edited by D'Amore, F.) pp. 215-251. UNITAR/UNDP Centre on Small Energy Resources, Rome, Italy.
- [14] Dansgaard, W. (1964) Stable isotopes in precipitation. *Tellus* **16**, 436-468.
- [15] Ruaya, J.R., Buenviaje, M.M., Solis, R.P. and Gonfiantini, R. (1993) Chemical and isotopic studies of fluids in the Bacon-Manito geothermal field, Philippines (these proc.).
- [16] Environmental Management Bureau internal file on IAEA and isotopes (1990).
- [17] Craig, H. (1963) The isotopic geochemistry of water and carbon in geothermal areas. In *Nuclear Geology in Geothermal Areas* (Edited by Tongiorgi, E.) pp 17-53. CNR, Pisa, Italy.
- [18] Merlivat, L. and Jouzel, J. (1979) Global climatic interpretation of the deuterium-oxygen-18 relationship for precipitation. *J. Geophys. Res.* **84** 5029-5033.
- [19] Ingraham, N. and Matthews, R. (1990) Stable isotope study of fog: the Point Reyes Peninsula, California, U.S.A. *Chem. Geol. Isotope Geoscience Section* **80** 281-290.
- [20] Giggenbach, W.F. (1988). Geothermal solute equilibria. Derivation of the Na-K-Mg-Ca geoindicators. *Geochim. cosmochim. Acta* **52** 2749-2765.
- [21] Olafsson, J. and Riley, J.P. (1978) Geochemical studies on the thermal brine from Reykjanes (Iceland). *Chem. Geol.* **21** 2197-2237.
- [22] Giggenbach, W.F. (1992) Isotopic shifts in waters from geothermal and volcanic systems along convergent plate boundaries and their origin. *Earth Planet. Sci. Lett.* **113** 495-510.

- [23] Reyes, A.G., Giggenbach, W.F., Salera, J.R.M., Salonga, N.D. and Vergara, M. C. (1993) Petrology and geochemistry of Alto Peak, a vapor-cored hydrothermal system, Leyte Province, Philippines. *Geothermics* **22** 479-519.
- [24] Mizutani, Y., Hayashi, S. and Sugiura, T. (1986) Chemical and isotopic composition of fumarolic gases from Kuju-iwoyama, Kyushu, Japan. *Geochem. J.* **20** 273-285.
- [25] Bolognesi, L. and D'Amore, F. (1993) Isotopic variation of the hydrothermal system on Vulcano Island, Italy. *Geochim. cosmochim. Acta* **57** 2069-2082.
- [26] Seki, Y. (1991) The physical and chemical structure of the Oku-aizu geothermal system, Japan. *Geochem. J.* **25** 245-265.
- [27] Yoshida, Y. (1991) Geochemistry of the Nigorikawa geothermal system, southwest Hokkaido, Japan. *Geochem. J.* **25** 203-222.

# GEOCHEMICAL AND ISOTOPIC INVESTIGATION OF BILIRAN GEOTHERMAL DISCHARGES, PHILIPPINES

M.N. RAMOS-CANDELARIA, J.R. RUAYA, A.S.J. BALTASAR  
PNOC-Energy Development Corporation,  
Makati, Metro Manila,  
Philippines

**Abstract** - *The most impressive thermal feature on Biliran island is the Vulcan-Libtong thermal area which hosts a volcano-andesitic hydrothermal system. The chemical signatures of the original andesitic vapors are largely retained in the fluid discharge chemistry and isotope composition. The Vulcan Fault is believed to be the main conduit for the passage of acid andesitic gases from a cooling magma beneath Vulcan to the surface. Away from the Vulcan area, a neutral Cl brine has already evolved by progressive neutralization of a previously acid fluid by intensive water-rock interaction. This neutral water was encountered at depth by wells BN1 and BN2. BN3 drilled close to the Vulcan Fault discharged highly acidic fluids. The main constraint towards the development of the resource is the presence of acid andesitic volatiles at the central portion and the limited area available for exploitation by conventional techniques.*

## 1. INTRODUCTION

Several internal reports on the geochemistry of Biliran thermal features have appeared (Ferrer, 1980; Galia and Clemente, 1981; Glover, 1981; Obusan, 1980) although none of these reports have presented a clear-cut geochemical model of the hydrothermal regime existing in the island. Ruaya (1981) re-evaluated the prospect area from a chemical point of view and proposed a geochemical model of Central Biliran. With the use of solute correlations and initial studies on mineral equilibria he showed that the area close to Vulcan is a highly acidic oxidizing zone, at least at the upper levels.

At an early stage in the scientific evaluation of Central Biliran, the presence of acidic andesitic volatiles HCl, HF and SO<sub>2</sub> from a degassing magma beneath the Vulcan thermal area was already recognized. Despite, this three exploratory wells BN1, BN2 and BN3 were drilled with the assumption that acidic fluids may be confined to the Vulcan Fault, and an exploitable neutral Cl reservoir may exist away from this zone. Lawless and Gonzales (1982) summarized existing geoscientific data at that time and preliminary results of BN1 drilling. The results of the three wells drilled are reported in KRTA (1986).

This report aims to review all existing surface and well chemistry data to assess the viability of the Vulcan-Libtong geothermal resource for further development.

## 2. WATER CHEMISTRY OF SURFACE THERMAL FEATURES

Extensive water sampling has been carried out in the prospect area since 1982. Additional samples mainly for stable isotope analyses were gathered in 1992. A generalized location map of the surface thermal features and wells drilled in the area is shown in Fig. 1.

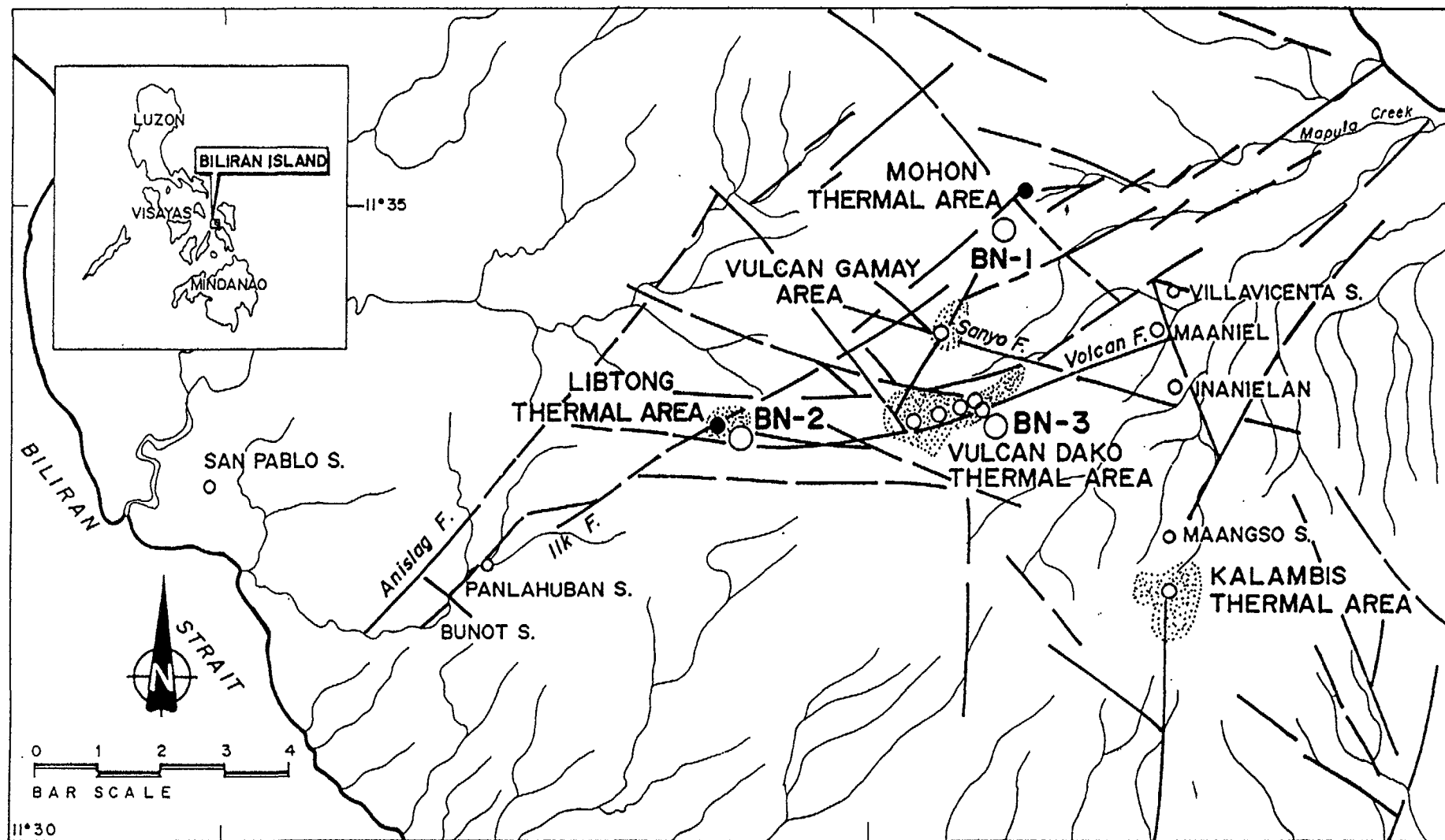


Fig. 1 Location map of all Biliran thermal features including all confirmed structures (Adapted from Pagado et al., 1993).



Table I. CENTRAL BILIRAN WATER CHEMISTRY RESULTS

SOURCE	CODE	ELEV. MASL	SAMPLE NO.	DATE	FIELD Temp.	pH	Li	Na	K	Rb	Cs	Ca in mg/kg	Mg	Fe	C1	S04	F	B	Si02	HC03	H2S	NH3	C1/B
VULCAN WS #1	V1	635	BNE-08	Apr 15, 1992	56.0	1.98	.00	33	11	.10	.00	103.0	27.0	43.80	296	1532	.12	.87	196	0	.75	0	104
VULCAN WS#2	V2	635	BNE-01	Apr 15, 1992	50.0	2.43	.10	11	4	.10	.00	39.4	5.8	5.14	82	440	.08	.87	83	0	.75	0	36
VULCAN CS#3	V3	640	BNE-02	Apr 15, 1992	28.0	3.69	.00	13	4	.10	.00	47.1	6.2	2.79	12	201	.12	.69	80	0	.75	0	5
VULCAN HS #4	V4	635	BNE-07	Apr 15, 1992	65.0	2.11	.00	60	12	.09	.00	115.0	40.2	23.80	445	1330	.28	.69	301	0	.61	0	197
VULCAN BUBBLING POOL	V8		BNE-03	Apr 18, 1992	65.0	2.03	.00	3	3	.04	.00	5.1	19.4	8.90	25	1604	.07	.69	382	0	.68	0	0
VULCAN (V6)	V6				80.0	1.40	.09	475	163	.60	.20	43.5	24.1	425.00	7651	9616	.02	89.70	371	0	0	0	284
MAANIEL	MA	450	BNE-25	Jul 21, 1992	85.0	1.78	.04	75	31	.11	.00	85.0	37.5	64.80	1569	1922	.00	8.22	154	0	0	0	49
TENEGO	T1	440	BNE-26	Jul 21, 1992	79.0	1.35	.03	76	45	.08	.00	74.9	37.5	43.70	1373	3776	.00	9.89	58	0	0	0	22
TENEGO (V8)	T2				82.0	1.70	.04	77	53	.20	.10	24.4	25.9	146.00	2419	5642	.03	19.40	373	0	0	0	1419
LIBTONG CS#2	L1	395	BNE-04	Apr 14, 1992	28.0	2.66	.00	5	3	.07	.00	7.7	3.0	.48	13	313	.00	.52	66	0	.61	0	8
LIBTONG #1	L2	395	BNE-05	Apr 14, 1992	60.0	3.01	.20	5	2	.07	.00	5.2	2.2	.84	9	171	.00	.52	61	0	.41	0	0
LIBTONG (L3)	L3				53.0	3.00	.00	12	4	.00	.00	6.1	4.8	9.60	7	2473	.00	.00	249	0	0	0	0
LIBTONG (L4)	L4				74.0	3.10	.00	7	4	.00	.00	7.2	3.2	7.30	18	543	.00	.00	127	0	0	0	0
LIBTONG (L4A)	L5				74.0	3.10	.00	10	5	.00	.00	1.9	4.7	26.80	7	1889	.00	.00	257	0	0	0	3
LIBTONG #3	L6	395	BNE-15	Jul 1, 1992	60.0	2.91	.00	8	2	.00	.00	5.6	2.6	3.88	9	321	.00	.09	58	0	0	.26	29
LIBTONG #4	L7	390	BNE-16	Jul 1, 1992	91.0	2.50	.00	8	4	.00	.00	2.5	3.0	4.08	10	665	.00	.09	127	0	0	.18	34
LIBTONG #5	L8	390	BNE-17	Jul 1, 1992	85.0	3.32	.00	8	3	.00	.00	9.2	2.6	.79	7	109	.00	.09	62	0	0	.13	1
VULCAN GAMAY	G1	490	BNE-06	Apr 18, 1992	37.0	3.14	.00	14	2	.05	.00	96.5	10.1	1.00	12	424	.05	.69	92	0	.34	0	0
VULCAN GAMAY (4)	G2				85.0	2.10	.36	255	25	.10		78.5	30.8	4.20	585	972	.56	41.00	265	0	0	0	45
VULCAN GAMAY (5)	G3				68.0	1.80	.03	9	3	.00		5.6	14.5	24.10	16	3111	.05	4.00	240	0	0	0	2
BUNOT	B1	95	BNE-27	Jul 23, 1992	52.0	7.08	.13	154	35	.02	.00	77.4	42.5	1.99	172	205	.00	2.88	167	376	0	0	14
BUNOT	B2				65.0	7.10	.14	158	38	.00	.00	72.9	47.0	.00	177	221	.00	3.70	175	0	0	0	69
VILLAVICENTA A	A1	40	BNE-12	Jun 30, 1992	41.0	7.85	.04	101	22	.02	.00	249.0	75.0	.68	201	429	.00	.78	128	493	0	.33	65
VILLAVICENTA B	A2	40	BNE-13	Jun 30, 1992	51.0	7.09	.07	143	37	.06	.00	178.0	81.4	1.87	224	413	.00	.95	154	542	0	.52	34
VILLAVICENTA (1)	A3				52.0	7.40	.09	135	43	.10	.00	93.4	74.7	.00	196	312	.17	2.00	169	0	0	0	15
VILLAVICENTA (2)	A4				50.0	7.30	.08	121	31	.10	.00	114.0	80.5	.00	240	482	.17	4.00	165	0	0	0	65
SAN PABLO	SP	0	BNE-29	Jul 25, 1992	39.0	7.22	.07	480	6	.03	.00	173.0	116.0	1.50	1036	149	.00	1.12	100	487	0	0	3511
MOHON 1	M1	230	BNE-18	Jun 30, 1992	35.0	7.43	.02	111	9	.00	.00	320.0	40.1	2.36	75	835	.00	2.94	102	246	0	2.95	1
MOHON 2	M2	220	BNE-23	Jul 12, 1992	44.0	7.00	.02	71	15	.02	.00	223.0	48.5	9.65	24	314	.00	18.20	118	674	0	0	2
MOHON	M3				46.0	7.10	.01	134	9	.00	.00	315.0	49.0	.00	101	960	.00	4.70	116	238	0	0	14
PANLAHUBAN	P1	80	BNE-19	Jul 1, 1992	48.0	7.99	.11	145	34	.05	.00	49.9	35.8	1.60	140	156	.00	2.25	159	361	0	.25	15
PANLAHUBAN	P2				42.0	7.40	.13	125	28	.00	.00	52.4	38.7	.00	121	160	.00	2.80	163	0	0	0	28
INANIELAN	IN	460	BNE-24	Jul 21, 1992	45.0	2.52	.00	41	3	.04	.00	65.0	18.8	9.00	19	414	.00	1.30	129	0	0	0	1

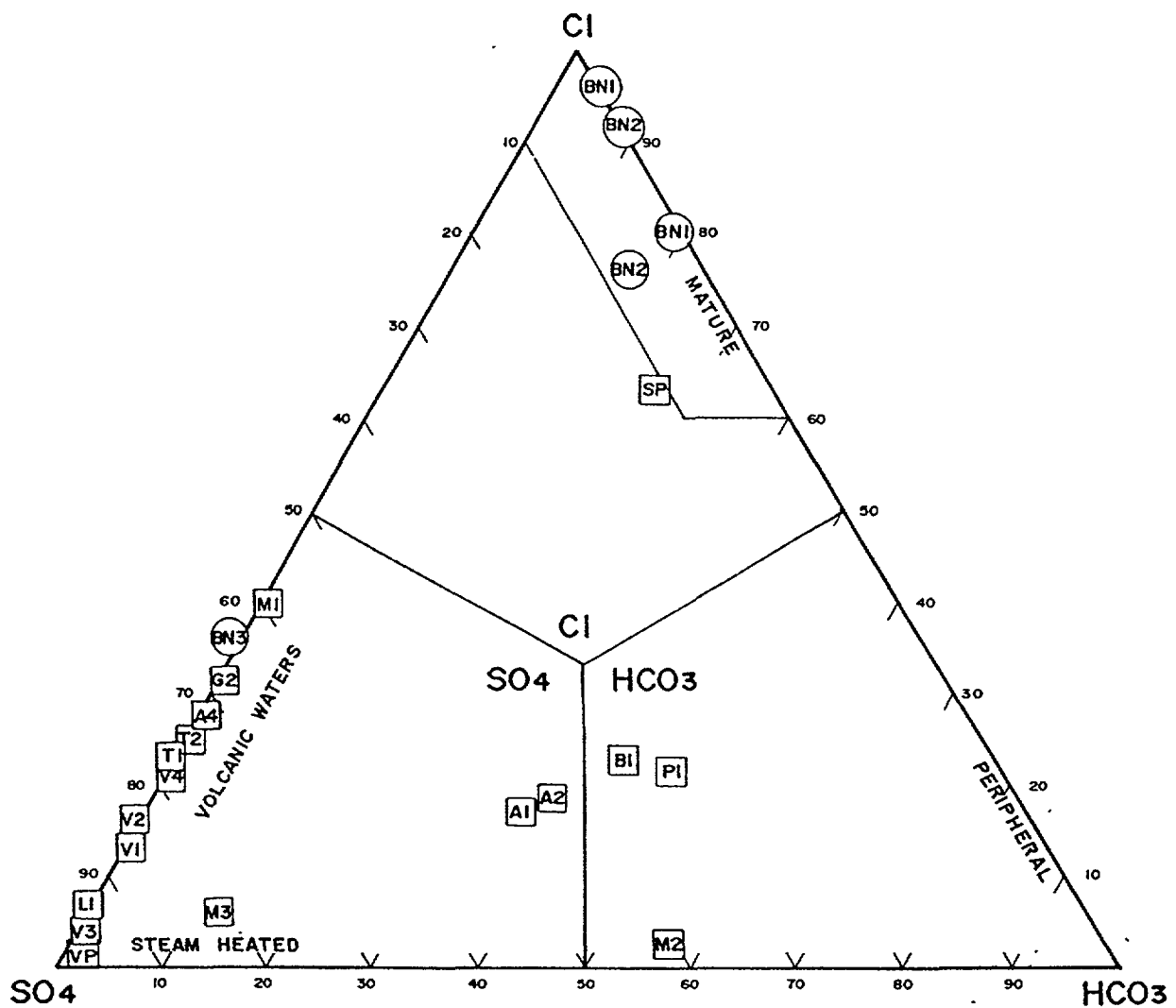


Fig. 2 Relative composition of Cl, HCO<sub>3</sub>, and SO<sub>4</sub> of central Biliran thermal waters

Table II. CATION-ANION BALANCE SHOWING IONIC IMBALANCE OR EXCESS CHLORIDE AND SULFATE

SOURCE	CODE	pH	TOTAL CATIONS [meq]	TOTAL ANIONS [meq]
VULCAN WS#2	BNE-01	2.43	3.353	11.460
VULCAN CS#3	BNE-02	3.69	3.705	4.515
VULCAN BUBBLING POOL	BNE-03	2.03	2.553	34.095
LIBTONG CS#2	BNE-04	2.66	0.950	6.878
LIBTONG#1	BNE-05	3.01	0.754	3.820
VULCAN GAMAY	BNE-06	3.14	6.394	9.158
VULCAN HS#4	BNE-07	2.11	13.298	40.242
VULCAN WS#1	BNE-08	1.98	11.505	40.245
TENEGO	BNE-26	1.35	13.682	117.343

Notes:

1. TOTAL CATIONS = Li + Na + K + Rb + Ca + Mg + Fe + Mn + NH<sub>4</sub>
2. TOTAL ANIONS = Cl + SO<sub>4</sub>

The chemical composition of the Biliran thermal waters are given in Table I. Initial classification and segregation of the thermal waters can be done using a  $\text{Cl-HCO}_3\text{-SO}_4$  plot as shown in Fig. 2. Following are the different classes of waters found in Central Biliran:

mixed waters

neutral Cl

neutral  $\text{Cl+HCO}_3$

neutral  $\text{HCO}_3\text{+SO}_4$

acid  $\text{SO}_4\text{+Cl}$

San Pablo, BN1, BN2

Panlahuban, Bunot

Villavicenta

Vulcan, Vulcan Gamay, Vulcan

Bubbling Pool, Maaniel, Tenego

Libtong, Inanielan, BN3

neutral  $\text{SO}_4\text{+Cl}$

Mohon 1

The Vulcan and Vulcan Gamay thermal areas in Central Biliran host a number of high temperature springs, bubbling pools, mudpools, fumaroles and an active solfatara with extensive altered grounds (Fig. 1). East of Vulcan Daku is a kaipohan like feature at Inanielan (Fig. 1). The Libtong thermal area is smaller (  $2\text{km}^2$  ) of less impressive features made up of bubbling hot pools, warm springs and altered grounds with steaming vents.

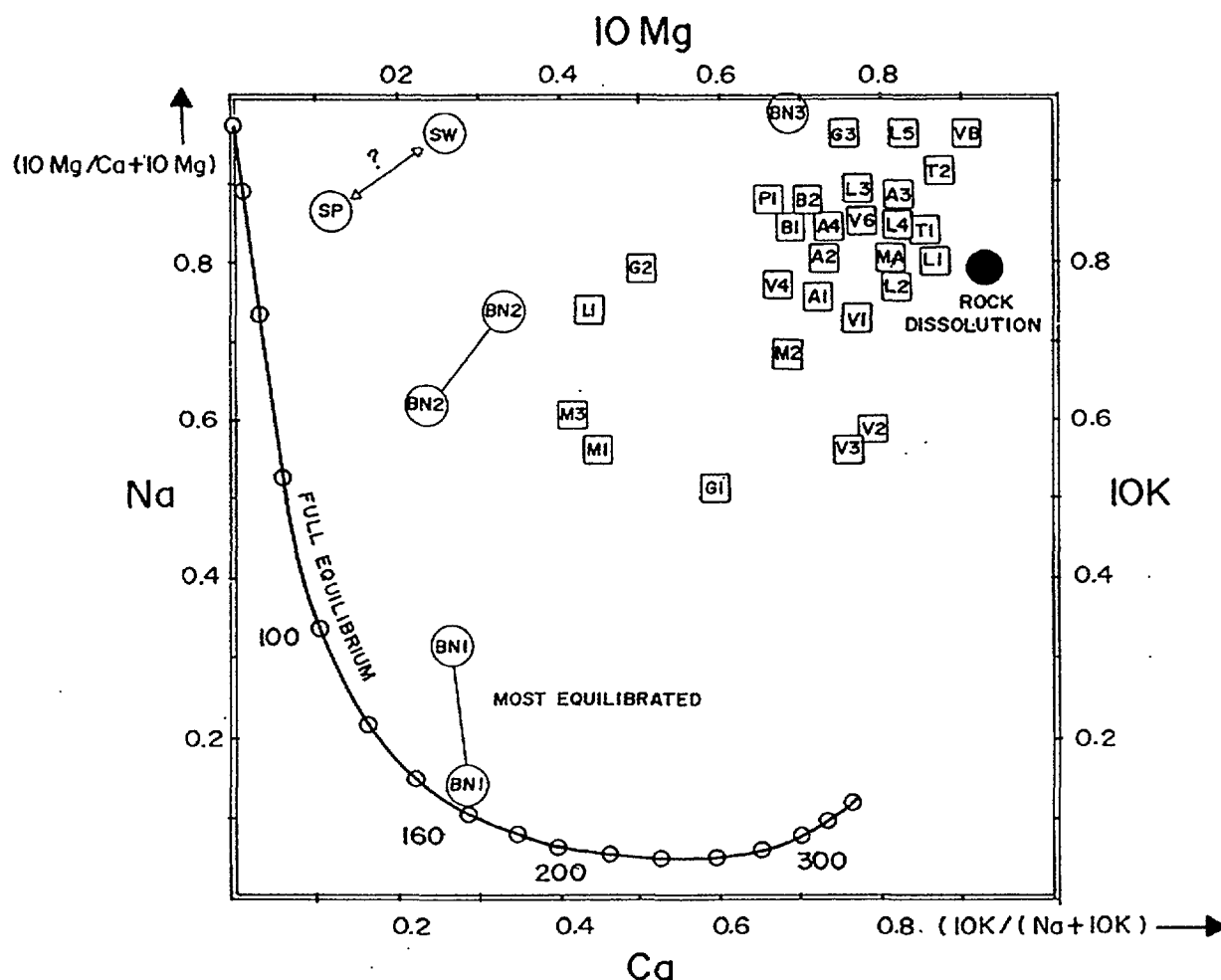


Fig. 3 Relative Na, K, Mg and Ca contents of central Biliran thermal waters

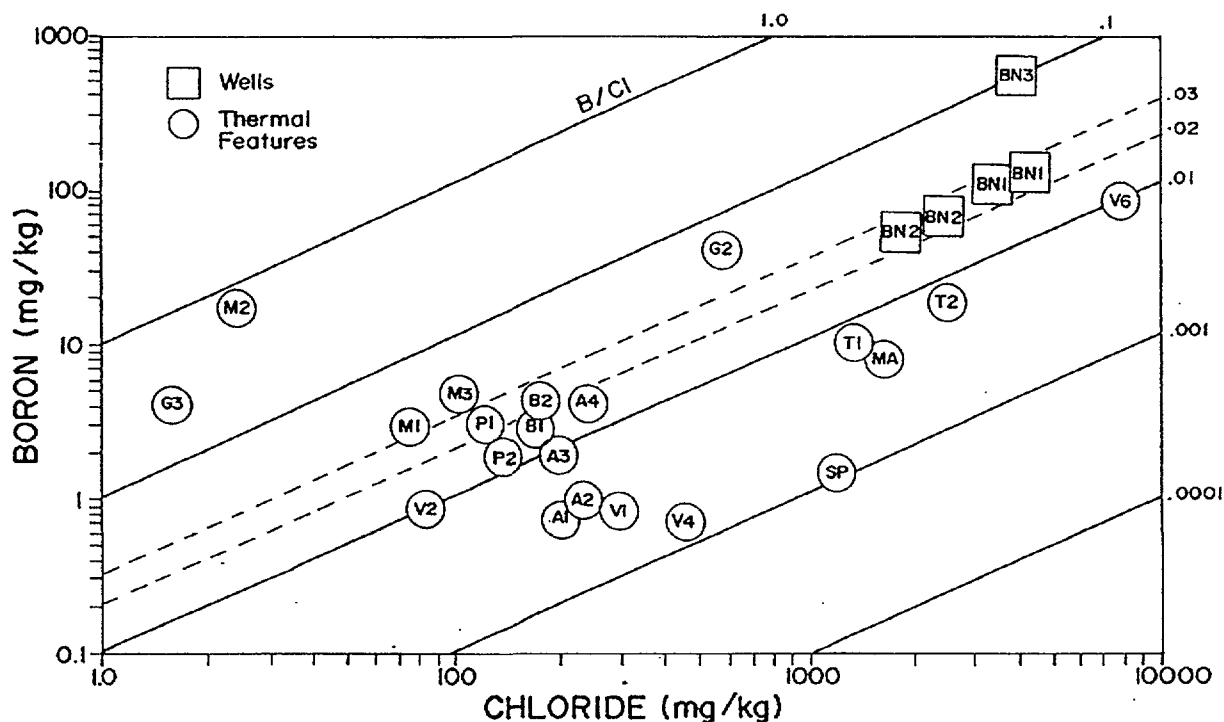


Fig. 4 Chloride and Boron relationships of Biliran thermal waters

The waters are usually mixed acid  $\text{SO}_4\text{-Cl}$  in nature. The Mapula and Kabibihan rivers which drain the Vulcan and Vulcan Gamay thermal areas, respectively also have low pH with high  $\text{SO}_4\text{-Cl}$  waters (Galia and Clemente, 1982). Water samples from Vulcan and Libtong show excess milliequivalents of Cl and  $\text{SO}_4$  in comparison to the relative abundance of major cations Na, K, Mg and Ca (Table II). The very high Cl and  $\text{SO}_4$  nature of these waters would imply that both Cl and  $\text{SO}_4$  are not transported from depth with their usual cation associates (i.e. alkalis Na and K with Cl and the alkaline earths Mg and Ca with  $\text{SO}_4$ ). All these indicate the passage of free HCl and  $\text{H}_2\text{S}$  or  $\text{SO}_2$  from depths with subsequent dissolution of HCl and oxidation of  $\text{H}_2\text{S}$  or  $\text{SO}_2$  in groundwater producing highly acidic and oxidizing waters. The low levels of primary alkali cations clearly supports the idea that these are just surface waters with condensed andesitic gases.

There are no true mature neutral Cl waters on the island except for the well waters of BN1 and BN2. A quaternary plot of Na-K-Mg-Ca (Fig. 3) clearly show that most of the thermal waters plot near rock dissolution characteristic of highly immature waters. The neutral Cl springs of San Pablo may have true geothermal signature, or possible contribution of sea water due to its nearness to the sea. Thermal waters found outside the Vulcan-Libtong thermal areas already have neutral pH and significant Cl. These include the Panlahuban, Mohon and Villavicenta warm springs. But the most equilibrated waters are the BN1 well waters. These would suggest extensive water rock interaction of the fluids entering the well.

Cl-B relationship (Fig. 4) of the Biliran samples show a wide scatter of points which may suggest that both species are carried to the springs by different mechanisms. The Vulcan, Maaniel and Tenego samples plot at the high Cl, high B end showing that these are carried from depths as volatiles. The Cl-rich springs of Mohon, Panlahuban, Bunot and Villavicenta cluster at moderate Cl and low B concentrations showing primary geothermal

brine signature. BN1 and BN2 plot at the high Cl, high B end of the diagram but with B/Cl ratios between 0.01 and 0.03 characteristic of the Cl rich springs of Villavicenta, Mohon and Bunot and Panlahuban. BN3 has a distinct B/Cl ratio of 0.1 suggestive of a different source fluid.

### 3. GAS CHEMISTRY OF THE SURFACE THERMAL FEATURES

The Biliran gas chemistry data are shown in Table III. Extensive gas sampling has been undertaken in the Libtong and Vulcan thermal area to deduce the origin of the vapors (Glover, 1981; Ferrer, 1980). Glover (1981) detected andesitic gases SO<sub>2</sub>, HCl and HF in Vulcan and Libtong.

The following observations support the existence of andesitic gases in the Vulcan and Libtong thermal areas :

- 1) high N<sub>2</sub>/Ar ratios (300-3,000) characteristic of andesitic volatiles
- 2) high CO<sub>2</sub> and H<sub>2</sub>S concentrations characteristic of high temperature systems
- 3) high gas source temperatures (T<sub>H<sub>2</sub>/Ar</sub> 300°C)

A plot of CO<sub>2</sub>-N<sub>2</sub>-Ar (Fig. 5) clearly show the predominant andesitic character of the Vulcan Dako and Vulcan Gamay vapors, while the two Libtong vapor samples show distinct mixing with air.

KRTA (1986) sampled steam condensates from Vulcan and Libtong but showing very high concentration of Cl (1177 mg/kg) only in Vulcan 3. This supports the assumption that Cl surfaces in Vulcan in the form of free HCl gas.

TABLE III. COMPOSITION OF VAPOR DISCHARGES FROM THE BILIRAN GEOTHERMAL PROSPECT

SOURCE	DATE [MM/DD/YY]	CO <sub>2</sub> X-----	H <sub>2</sub> S in mmoles/100	He	H <sub>2</sub> moles	Ar	N <sub>2</sub>	CH <sub>4</sub>	Cl* -----X [mg/kg]	CO <sub>2</sub> /H <sub>2</sub> S	N <sub>2</sub> /Ar	TH <sub>2</sub> /Ar [deg C]
VULCAN DAKO	04/15/92	7,419	431		0.601	0.012	33	0.2		17	2809	307
VULCAN DAKO	04/15/92	3,942	253		0.447	0.059	18	0.1		16	310	237
VULCAN GAMAY	04/18/92	38,170	3,584		2.558	0.049	140	1.0		11	2868	300
VULCAN GAMAY	04/18/92	34,854	3,486	0.017	0.373	0.325	107	26.9		10	329	182
LIBTONG	04/14/92	16,248	3,043		0.161	3.658	271	37.0		5	74	79
LIBTONG	04/14/92	8,548	1,267		0.052	0.109	40	20.0		7	365	151
LIBTONG	04/14/92	24,721	3,075		0	2.335	190	119.0		8	82	0
VULCAN 1	DEC, 1979	3,305	32		0.039		15	3.7		102		
VULCAN 2	DEC, 1979	7,026	164		11.43		144	4.6	56	42		
VULCAN 3	DEC, 1979	3,538	47		0.082		36	12.2	1177	76		
VULCAN 8	DEC, 1979	33,706	245		1.614		402	20.9		138		
LIBTONG 4	DEC, 1979	4,274	80		0.044		3	1.3	61	53		
LIBTONG 5	DEC, 1979	2,424	73		0.016		23	1.3		33		

Notes: 1. TH<sub>2</sub>/Ar from Giggenbach and Goguel, 1989

2. Cl - sampled from steam condensates at same location by KRTA in 1981

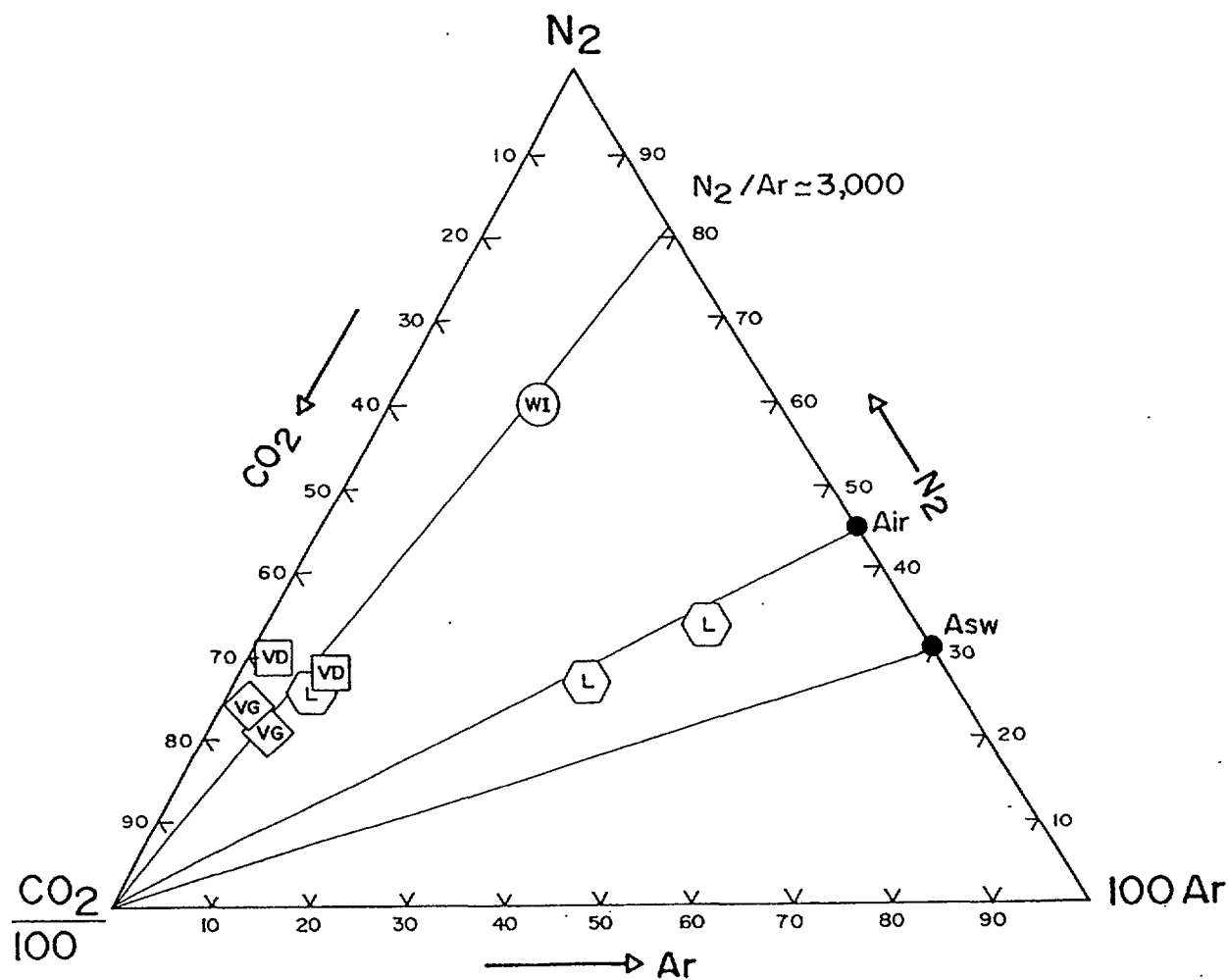


Fig. 5 Relative CO<sub>2</sub>, N<sub>2</sub> and Ar contents of Biliran vapor discharges

#### 4. STABLE ISOTOPE CHEMISTRY

Stable isotope data from the Biliran surface thermal and non-thermal features gathered in 1982 and 1992 are given in Table IV. Downhole samples from BN1 (1100m) and BN3 (1600m) including water and steam were separated samples from BN2 and BN3 are also available. The different samples will be discussed separately by year in order to avoid possible inconsistencies.

The stable isotope data for 1992 were plotted in a <sup>2</sup>H against <sup>18</sup>O diagram shown in Fig. 6. Most of the cold water samples fall close to the Leyte Meteoric Water Line (LMWL) defined by Alvis-Isidro et al (1993) to have the equation:

$$\delta^2\text{H} = 8\delta^{18}\text{O} + 13.7 \quad (1)$$

The Vulcan solfatara and Tenego thermal waters show the greatest enrichment in both <sup>2</sup>H and <sup>18</sup>O relative to the background Vulcan Gamay Creek and Vulcan cold spring. The highest <sup>18</sup>O, <sup>2</sup>H shift is shown by the steam sample from the Vulcan solfatara. A dilution line from the meteoric water line passing through these points can be drawn intersecting the andesitic water composition (Giggenbach, 1992). An andesitic water fraction of 60% for the Vulcan solfatara steam sample was computed.

TABLE IV. STABLE ISOTOPE COMPOSITION AND CHLORIDE CONTENT OF WELLS, SURFACE THERMAL AND NON-THERMAL DISCHARGES FROM THE BILIRAN GEOTHERMAL PROSPECT

SOURCE	CODE	SAMPLE NUMBER	SAMPLING DATE [MMDDYY]	OXYGEN-18 [in per mille VSMOW]	DEUTERIUM [in per mille VSMOW]	Cl [mg/kg]	H [KJ/KG]	SP [MPa]
[1992 SAMPLES, analyzed at IAEA]								
VULCAN SOLFATARA	VS	PHI-BNE00	41592	2.91	-30.6			
VULCAN 2 WARM SPRING	VW	PHI-BNE01	41592	-5.51	-33.9	82		
VULCAN COLD SPRING	VC	PHI-BNE02	41592	-6.52	-39.4	12		
VULCAN GAMAY BUBBLING POOL	VG	PHI-BNE03	41892	-4.01	-29.5	25		
LIBTONG BUBBLING POOL	LP	PHI-BNE05	41492	-6.56	-43.3	9		
VULCAN HOT SPRING	VH	PHI-BNE07	41592	-5.64	-38.9	445		
VULCAN WARM SPRING	VW	PHI-BNE08	41592	-4.14	-34.4	296		
MOHON WARM SPRING	MW	PHI-BNE23	71292	-6.44	-41.3	24		
INANIELAN WARM SPRING	IW	PHI-BNE24	72192	-5.72	-36.2	19		
MAANIEL HOT SPRING	MH	PHI-BNE25	72192	-4.83	-36.0	1569		
TENEGO WARM SPRING	TW	PHI-BNE26	72192	-2.84	-35.3	1373		
BUNOT WARM SPRING	BW	PHI-BNE27	72392	-6.90	-46.0	172		
SAN PABLO WARM SPRING	SP	PHI-BNE29	72592	-6.97	-45.3	1036		
MABAHO COLD SPRING	MC	PHI-BNE32	72992	-6.63	-37.0	8		
KALAMBIS RIVER	KR	PHI-BNE33	72892	-6.25	-35.3			
ANAS RIVER	AR	PHI-BNE34	42092	-6.76	-37.8			
VULCAN GAMAY CREEK	VR	PHI-BNE35	41892	-7.03	-40.4			
[1982 SAMPLES, analyzed at INS New Zealand]								
TENEGO	TE	V10	112582	-5.03	-36.6	1369		
TENEGO	TE	V8	112582	5.75	-13.7	2750		
VULCAN	VU	V6	112582	6.76	-0.6	1400		
PANLAHUBAN	PB		112582	-7.16	-45.8	148		
LIBTONG	LB	L4	112582	-6.10	-36.4	18		
MAPULA RIVER	MR		112582	-6.61	-38.1	5		
BN1 (DH 1100m)	BN1		011783	-3.67	-33.1	1135		
BN1 (DH 1100m)	BN1		120482	0.23	-31.3	2916		
BN2-11 (WEB/H2O)	BN2		110682	-3.67	-30.6	1498	870	.654
BN2-12 (WEB/STEAM)	BN2		110682	-42.6	-42.6		870	.654
BN3 (DH 1600m)	BN3			1.53	-24.6	1462		
BN3 (WEB/H2O)	BN3		122482	2.48	-25.7	2039	2006	0.89
BN3 (WEB/STEAM)	BN3		122482	-1.80	-34.2		2006	0.89

The San Pablo and Bunot Cl springs are lighter in  $^2\text{H}$  but slightly higher in  $^{18}\text{O}$  than the groundwaters. This may suggest deep percolation of a high altitude precipitation to deep level, being heated up and emerging as weakly mineralized thermal springs near the coast. Their stable isotope compositions negates the possibility of any seawater contribution.

A plot of the Biliran stable isotope data in 1982 is also shown in Fig. 6. The established Leyte Meteoric Water Line (Alvis-Isidro et al., 1993) is used to compare the results. The Mapula river sample which passes through the Vulcan thermal area falls on the meteoric water line. Similarly, the Libtong warm spring sample, despite its close association with a fumarole has the isotopic composition of meteoric waters.

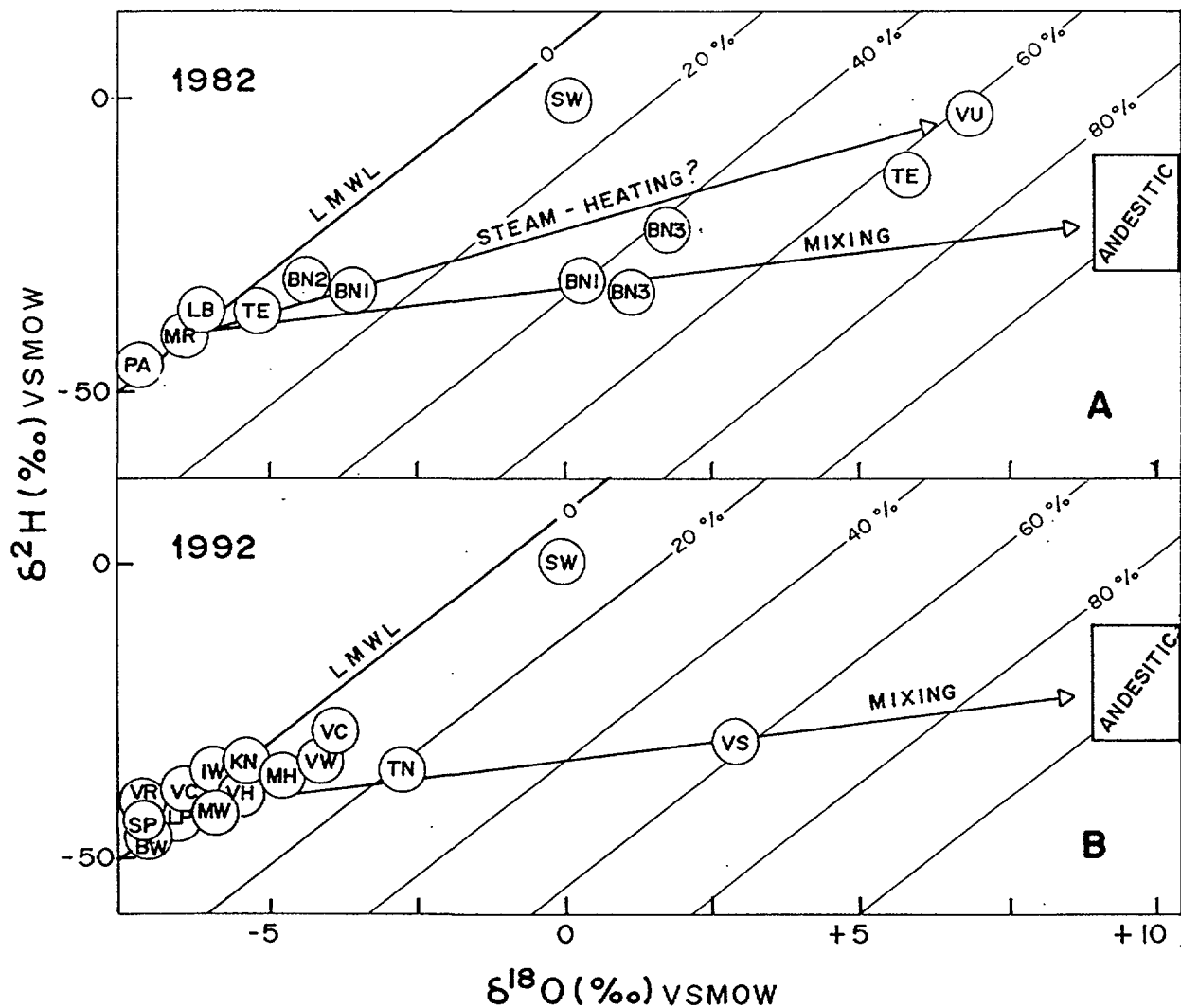


Fig. 6 Plot of  $\delta^2\text{H}$  against  $\delta^{18}\text{O}$  of Biliran isotope samples in 1982 and 1992

Two BN1 samples from 1100m or the shallow zone are available, with the earlier sample showing greater  $^{18}\text{O}$  enrichment. KRTA (1986) suggested that the observed large oxygen shift is suggestive of it being originally acidic. This is because the reaction of acid fluids with country rocks would result in greater isotopic exchange than for neutral fluids due to enhanced reaction rates. This rationale is supported by water chemistry data (See BN1 well chemistry discussions). Similarly an andesitic fluid contribution would also give rise to a large oxygen shift. The BN1 downhole samples lie close to the andesitic-meteoric water dilution line in support of this idea.

The BN2 isotope sample was taken before the well had stabilized and may reflect more meteoric waters from drilling fluids. Even with such dilution BN2 waters already show a pronounced oxygen shift and fall on the andesitic-meteoric water dilution line characteristic of geothermal waters.

The BN3 sample taken from the suspected acid horizon at 1600m shows a very large  $^{18}\text{O}$  and  $^2\text{H}$  shift indicative of the contribution of andesitic waters. In fact a dilution line from



the Mapula river sample passing close to BN3 can be drawn intersecting the andesitic water composition (Giggenbach, 1992). This line is defined by:

$$\delta^2\text{H} = 1.6 \delta^{18}\text{O} - 27.9 \quad (2)$$

BN3 has a computed andesitic water component of 40-50%, while TE or the steam sample from Tenego has 60%. It appears that the 1982 steam sample from Tenego has similar andesitic water contribution as the Vulcan steam sample in 1992. Although these are two distinct sampling points, both the Vulcan and Tenego samples were taken at steam vents close to each other (Fig. 1). It is assumed that gas compositions in this area are uniform (See Table III) and any variations are attributed to changes with time. If this assumption is valid, there is no apparent change in the contribution of andesitic water to the system in a span of ten years.

## 5. WELL CHEMISTRY

### 5.1 BN1 and BN2

Representative well chemistry data are shown in Tables V and VI. BN1 drilled 3 km. north and BN2 located 4 km west of the Vulcan thermal area encountered neutral-Cl fluids with  $T_{\text{SiO}_2}$  (Fournier and Potter, 1982) temperatures of 220°C and 210°C, respectively. This proves the existence of a moderate temperature neutral Cl resource away from the Vulcan thermal area. This contention is supported by the dominance of neutral secondary mineral assemblage in both wells (Reyes, 1983a). Both wells have a Cl/B ratio of 10, showing the homogeneity of the source fluid.

These wells are unique in that they discharged appreciable F (1-35 ppm), Fe (0.3-1 ppm) and Mg (1-10 ppm), relative to other neutral wells in the Philippines where typical concentrations of these elements are maintained at negligible quantities. Their discharge was also accompanied by elevated  $\text{SO}_4$  (100-300 ppm) levels. All these may imply neutralization of a previously acidic fluid (rich in HF and  $\text{H}_2\text{SO}_4$ ) by water-rock interaction. The absence of distinct andesitic imprints in the fluid discharges of BN1 and BN2 implies that the primary andesitic environment may be limited within the vicinity of the Vulcan thermal area.

Gas chemistry data are limited with no analysis for residual gases He and Ar, important in tracing the origins of the gas discharge. It is however believed that the gas discharge has no andesitic signature as discerned from the low registered temperatures and moderate  $\text{CO}_2$  and  $\text{H}_2\text{S}$  compositions (Table VI).

### 5.2 BN-3

BN-3 drilled closer to the Vulcan Fault discharged acid Cl- $\text{SO}_4$  waters having weirbox pH of 3.0. It reached a  $\text{Cl}_{\text{res}}$  of 2,000 mg/kg in its 15 day discharge. It had very high  $\text{SO}_4$ , Mg and Fe concentrations typical of acid fluids. Cl/B ratio of 2 shows that the BN3 discharge is very different from BN1 and BN2 waters. The discharge was accompanied by high excess enthalpy (360 -1403 kJ/kg ) and delivered enough steam to generate from 5-6 MWe. However the corrosive nature of the discharge fluid destroyed the wellhead assembly and forced subsequent shutting of the well.

TABLE V. SELECTED DISCHARGE WATER CHEMISTRY, CALCULATED RESERVOIR CONCENTRATIONS AND GEOTHERMOMETRY OF BILIRAN WELLS

WELL	DATE [YMD]	WHP [MPa]	Hd [KJ/KG]	SP [MPa]	pH	Li	Na	K	Rb	Cs	Ca IN MG/KG	Mg	Fe	Cl	F	SO4	HCO3	B	NH3	SiO2
BN1	820805	0.38	1050	0.35		2.55	2697	87	0.35	0.19	4.2	0.2	0.1	3533	21.5	98	0	110	6	404
BN1	820805	0.38	1144	0.10	8.4	2.74	2947	101	0.37	0.19	6.4	0.1	0.3	3936	23.5	122	1085	122	4	421
BN2	821201	0.94	849	0.87		1.31	1484	40	0.15	0.19	11.7	1.8	0.1	1918	0.7	261	0	56	3	347
BN2	821201	0.94	849	0.10	8.4	1.52	1700	47	0.18	0.21	13.1	2.1	0.1	2251	0.8	208	550	66	1	399
BN3	821230	0.81	1958	0.10	2.6	3.52	2187	460	1.60	0.80	1.8	33.9	489.0	3870	3.8	5394	0	593	1280	1562

WELL	DATE [YMD]	WHP [MPa]	Hd [KJ/KG]	SP [MPa]	ClRES	MgRES	SO4RES	CaRES	SiO2RES	Cl/F	Cl/Ca	Cl/SO4	Cl/B	Na/Li	Na/K	Ca/Mg	TQTZ [IN DEGREES CENTIGRADE]	TNa-K-Ca	TK/MgTK/Na	Ex H [KJ/KG]	
IN MG/KG																					
BN1	820805	0.38	1050	0.35	2936	0	81	3	336	88	951	98	10	319	53	13	220	182	191	156	107
BN1	820805	0.38	1144	0.10	3015	0	93	5	323	90	695	87	10	325	50	39	216	182	211	159	217
BN2	821201	0.94	849	0.87	1747	1.65	238	11	316	1428	185	20	10	342	63	4	215	154	124	145	0
BN2	821201	0.94	849	0.10	1745	1.65	161	10	309	1453	194	29	10	338	62	4	213	155	124	146	0
BN3	821230	0.81	1958	0.10	1892	16.58	2638	1	764	546	2431	2	2	188	8	0	340	312	146	300	360

TABLE VI. SELECTED DISCHARGE AND TOTAL DISCHARGE GAS COMPOSITION (IN MMOL/100 MOLES STEAM) OF BILIRAN WELLS

WELL	DATE [YMD]	WHP [MPa]	Hd [KJ/KG]	SP [MPa]	CO2	H2S	NH3	RG	H2	N2*	CH4	CO2	H2S	NH3	RG	N2	H2	CH4	CO2					TDAP [ deg C]
X----- AT SAMPLING PRESSURE -----XX----- AT TOTAL DISCHARGE -----X																				-----X				
																				H2S	NH3	H2	N2	CH4
BN1	820404	0.40	1101	0.40	7155	26	8.1	187.0	0.3	44	115	1662	6.1	1.88	43.4	10.2	0.1	26.7	273	882	21044	163	62	218
BN2	821201	0.94	849	0.873	11136	51	0.7	1518.2	6.1	117	97	596	2.7	0.04	81.3	6.2	0.3	5.2	218	16139	1838	96	115	255
BN3	821224	1.59	2006	0.89	1906	240	0.7		7.2	29	3	1185	149.1	0.44		18.2	4.47	1.96	8	2685	265	65	603	350

Notes: RG - Residual gas

\* - Corrected for air contamination

Downhole samples under flowing and shut conditions were taken to establish the depth of the acid fluid inflow. Flowing downhole surveys show increasing pH with depths (pH 3.9 to 5.5 from 1400 to 2300) with the highest  $\text{SO}_4$  concentration at 1600 of 2325 mg/kg at pH of 4.40. Acid alteration zone at 1628, 1676 and 1700 m composed of pyrophyllite, diaspore, anhydrite, quartz, alunite, pyrite and occasional kaolinite is coincident with minor permeable zones at 1500-1600 m and 1700-1800 m (Reyes, 1983b). It appears that acidic fluids are entering the well between 1600 and 1700 m coincident with the intersection of the Vulcan Fault..

The very high gas concentrations ( $\text{CO}_{2\text{TD}}$ ,  $\text{H}_2\text{S}_{\text{TD}}$ ,  $\text{H}_{2\text{TD}}$ ,  $\text{N}_{2\text{TD}}$ ) and the high calculated gas source temperature ( $350^\circ\text{C}$ ) (Table VI) indicate the proximity of the well to a high temperature with possible andesitic gas association. The zone north of the Vulcan Fault where acidic thermal discharges dominate, consisting of bubbling pools and fumaroles may still host acid two-phase conditions at depth.

## 6. HYDROGEOCHEMICAL MODEL

The Vulcan-Libtong thermal area is host to a volcano-andesitic geothermal system as shown in Fig. 7. Ample evidence is available to show that the surface thermal activity in Central Biliran closely resemble the geochemical model proposed by Giggenbach et al.(1990) for the volcano andesitic hydrothermal system on Nevado del Ruiz, Columbia. A high temperature vapor zone exists beneath the Vulcan Dako thermal area. In this manner the chemical signatures of the original andesitic vapors are largely retained in the fluid discharge chemistry data and isotope composition of the Vulcan and Tenego thermal discharges. These include:

1. The abundance of acid  $\text{Cl-SO}_4$  waters at high elevations having excess  $\text{Cl}$  and/or  $\text{SO}_4$  denoting the presence of free  $\text{HCl}$  and  $\text{H}_2\text{S}$  or  $\text{SO}_2$  in the discharge.
2. High gas concentrations and temperatures exceeding  $300^\circ\text{C}$ .
3. High  $\text{N}_2/\text{Ar}$  ratios (300-3,000) showing definite andesitic contribution.
4. Isotope composition of Vulcan and Tenego steam discharge giving 40-60% contribution of andesitic water.

The Vulcan Fault is believed to be the main conduit for the passage of acid andesitic gases from a cooling magma beneath Vulcan to the surface. This is based on the abundance of a wide variety of gas hydrothermal features along its trace, ranging from hot acid springs, bubbling pools, mud pools, fumaroles, gas seepages and advanced acid hydrothermal minerals (i.e. Cr, S, Al, Py, Q, K-fspar).

The heat source driving the system is probably a small magma body beneath Vulcan located at a depth of around 10 km or more, and which is interpreted to be partly molten (Pagado et al., 1993).

Away from the Vulcan and Tenego thermal areas, a neutral  $\text{Cl}$  brine has already evolved by progressive neutralization of a previously acidic fluid by intensive water- rock interaction as the fluid migrates laterally. This was encountered at depth by wells BN1 and BN2. A shallow permeable zone of well BN3 may have intersected a splay of the Vulcan

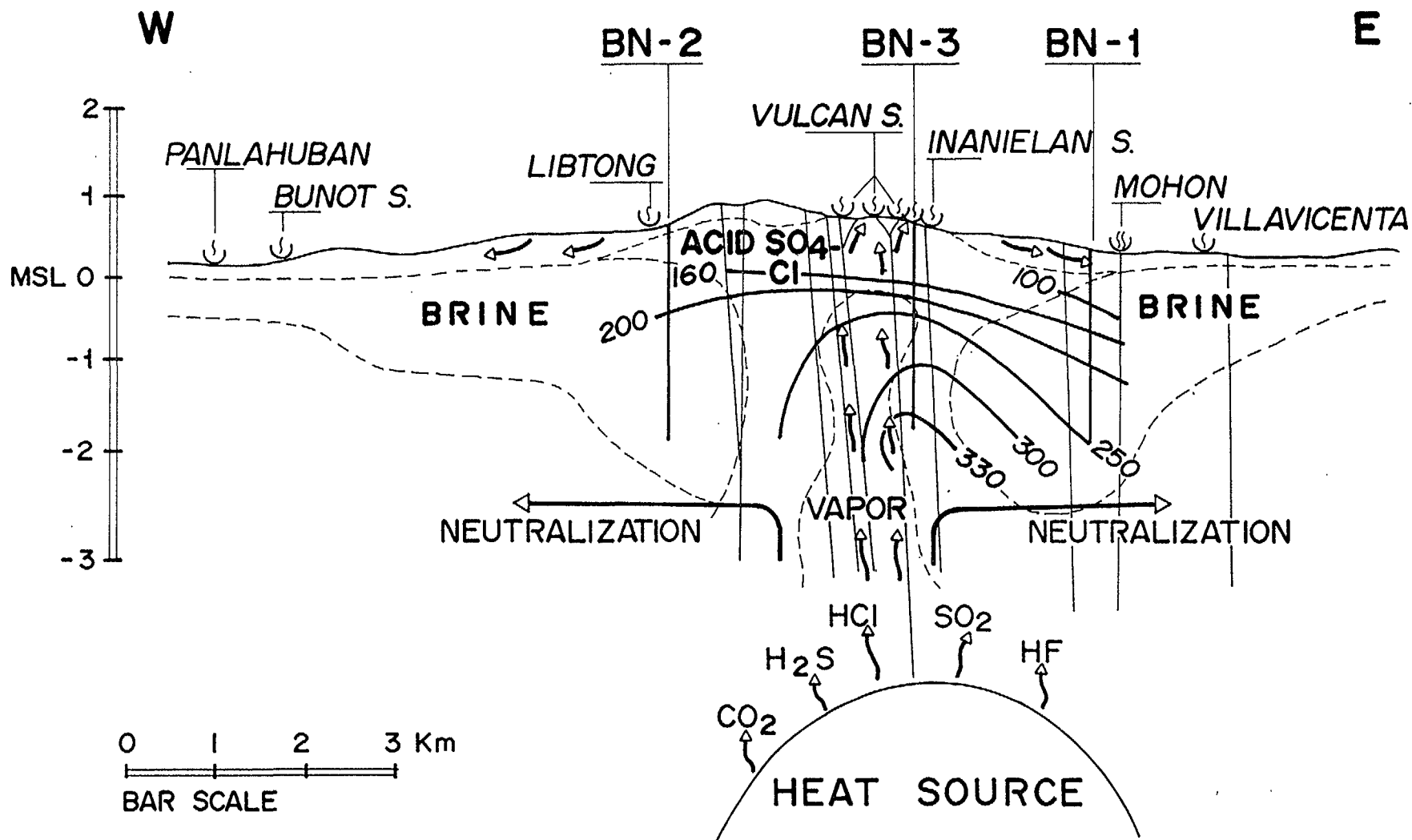


Fig. 7 Detailed conceptual hydrogeochemical model of Central Biliran showing approximate locations of the neutralized brine, the two-phase acid region fed by andesitic gases, and the measured temperature contours

Fault (Reyes, 1983b) which conducts andesitic gases giving rise to an acidic discharge at the weirbox. This is borne out by the confirmed presence of exotic minerals lazulite-scorzalite, which are strong indicators of andesitic contribution (Reyes, 1983b).

BN1 and BN2 are already in the periphery of the viable geothermal resource as attested to by moderate fluid temperatures (210-240°C). BN3 is close to the high temperature resource with source temperature of at least 300°C.

## 7. IMPLICATIONS TO DEVELOPMENT

The main constraint towards the development of the proven geothermal resource in Central Biliran is the confirmed presence of acidic andesitic volatiles in the Vulcan Dako thermal area. KRTA (1986) expressed some optimism about developing the estimated 14 to 16 km<sup>2</sup> resource area. This estimate is high because it failed to consider the sizable area affected by unproductive acidic fluids. Developments in other geothermal fields have already shown us the problems arising from the encroachment of acid fluids into the productive resource due to pressure drawdown caused by massive exploitation.

In addition, although neutral fluids were encountered in wells BN1 and BN2, these wells are considered to be in the margins of the exploitable resource based on their registered moderate subsurface temperatures. Also, these are enriched in F, SO<sub>4</sub> and Mg indicating neutralization of a previously acidic fluid with lateral migration. In this case, wells must be sited at a considerable distance from the acidic Vulcan region, increasing the chances of encountering unsuitable reservoir temperatures.

Considering the limited potentially useful resource area available (about 6 km<sup>2</sup>) and present technical limitations with regards to harnessing acidic fluids, developing the Vulcan-Libiong geothermal field is fraught with considerable risks.

But if power demand increases in the future to make this a commercially viable prospect area, any development strategy undertaken must be innovative to address the concerns with respect to acid fluid management, with suitable injection strategies to prevent acid fluid migration and maintain reservoir pressures.

***Acknowledgements** - This paper has been carried out within the framework of the IAEA Coordinated Research Programme for Asia, Africa and the Middle East on the applications of isotopes and geochemical techniques in geothermal development. The 1992 isotope samples were analyzed at the IAEA Isotope Laboratory in Vienna, Austria as part of the PNOC-IAEA Technical cooperation under Research Contract RB/6019. The 1982 samples were analyzed at the former Institute of Nuclear Sciences in New Zealand under the Economic Cooperation Program. Thanks are also extended to Dennis Sanchez for supervising the 1992 geochemical sampling at Vulcan and Libiong. We would also like to acknowledge the numerous people both foreign and local who took tremendous efforts to sample the diverse thermal features specifically the highly inaccessible. Without their contribution, we would not have obtained a clear understanding of the interesting geothermal systems found in Biliran Island.*

## References

- [1] FERRER, H.P. (1980) Preliminary evaluation of the Biliran geothermal prospect. PNOC- EDC Internal Report.
- [2] GALIA, E.J., CLEMENTE, V.C., Jr. (1981) Geochemistry of Biliran gas and water samples and their geothermal significance. PNOC-EDC Internal Report.
- [3] GLOVER, R.B. (1981) Geochemical report. DSIR mission to the Philippines.
- [4] OBUSAN, R.O. (1980) The geochemistry of the Biliran geothermal prospect, Northern Leyte. PNOC-EDC Internal Report.
- [5] RUAYA, J.R. (1981) Geochemistry of Biliran Island: Water chemistry and mineral equilibria. PNOC-EDC Internal Report.
- [6] LAWLESS, J.V., GONZALES, R.C. (1982) Geothermal geology and review of exploration, Biliran island. Proc. of Pacific Geothermal Conf. incorporating the 4<sup>th</sup> N. Z. Geothermal Workshop, Auckland, N. Z. , 114-121.
- [7] KRTA (1986) Evaluation of Biliran geothermal prospect. PNOC-EDC Internal Report.
- [8] GIGGENBACH, W.F. (1992) Isotopic shifts in waters from geothermal and volcanic systems along convergent plate boundaries and their origin. *Earth and Planetary Science Letters* **113** 495-510.
- [9] ALVIS-ISIDRO, R, SOLAÑA, R., D'AMORE, F., NUTI, S., GONFIANTINI, R. (1993) Hydrology of the Greater Tongonan geothermal system, Philippines, as deduced from geochemical and isotopic data. *Geothermics*, **22**, 5/6, 435-449.
- [10] FOURNIER, R.O., POTTER, R.W. (1982) A revised and expanded silica (quartz) geothermometer. *Getherm. Resourc. Counc. Bul.*, 3-11.
- [11] REYES, A.G. (1983a) Petrology of well Biliran-2 (BN2), Biliran Island, Leyte. PNOC-EDC Internal Report.
- [12] REYES, A.G. (1983) Petrology of well Biliran-3 (BN3), Biliran Island, Leyte. PNOC-EDC Internal Report.
- [13] GIGGENBACH, W.F., GARCIA, N.P., LANDOÑO, A.C., RODRIGUEZ, L.V., ROJAS, N.G., CALVACHE, M.L.V. (1990) The chemistry of fumarolic vapor and thermal spring discharges from the Nevado del Ruiz volcano-andesitic hydrothermal system, Colombia. IN: S. N. Williams (Editor), *Nevado del Ruiz Volcano, Colombia I. J. Volcanol. Geotherm. Res.* **42**, 13-39.
- [14] PAGADO, E.S., CAMIT, G.R.A., ROSSEL, J.B. (1993) The geology and geothermal systems of Biliran island. PNOC-EDC Internal Report.

# CHEMICAL AND ISOTOPIC STUDIES OF FLUIDS IN THE BACON-MANITO GEOTHERMAL FIELD, PHILIPPINES

J.R. RUAYA

Energy Research and Development Division,  
Philippine National Oil Company–Energy Development Corporation,  
Quezon City, Philippines

M.M. BUENVIAJE, R.P. SOLIS

Geothermal Division,  
Philippine National Oil Company–Energy Development Corporation,  
Makati, Metro Manila, Philippines

R. GONFIANTINI<sup>1</sup>

Isotope Hydrology Section,  
International Atomic Energy Agency,  
Vienna

**Abstract** - Chemical and isotopic data from springs, rainfall and wells have been used to characterize the fluids and to identify the major reservoir processes at Bacon-Manito geothermal field, Philippines. The deep reservoir fluid is postulated to be heated to about 325 °C and have 7500-8500 mg/kg chloride. Its chemical and isotopic composition is best characterized by wells OP-3D and OP-4D. Spring isotopic data show that their discharges are predominantly meteoric in origin, with a few following a simple evaporation trend. Chloride-enthalpy and chloride- $\delta^{18}\text{O}$  relations reveal that the upflowing geothermal reservoir fluid undergoes: (1) dilution with meteoric water, (2) conductive cooling as these move away, (3) mixing with steam condensate, and (4) vapor gain. Well gas chemistry points to the absence of direct magmatic contributions while it is shown that the equilibrium reaction  $\text{CH}_4 + 2\text{H}_2\text{O} = \text{CO}_2 + 4\text{H}_2$  is likely to be established. The observed positive  $^{18}\text{O}$  shifts of well waters relative to the local water meteoric line were considered to be due primarily to mixing of deeply-seated "andesitic" and meteoric waters while water-rock interaction could not be ruled out. Finally, a conceptual geochemical model of the geothermal system is proposed.

## 1. INTRODUCTION

The Bacon-Manito (Bacman) geothermal field is located at the tip of the chain of volcanic centers comprising the Bicol arc in the southwestern part of Luzon Island, Philippines. Surface scientific exploration work commenced in 1977 and culminated in the drilling of about 40 wells to date. Roughly one-half of the number, will supply steam to the 110 MWe Bacman I power plant and two additional 20 MWe power plant modules in Cawayan and Botong, collectively called Bacman II project. The Bacman I and Cawayan have power plants have been commissioned last year while Botong unit will be commissioned this year (1994).

The Bacon-Manito geothermal reservation has an approximate area of 200 km<sup>2</sup>. It is composed of several small composite cone volcanoes collectively called the Pocdol mountains. Together with other 14 Pliocene to Recent composite cones, which include the active Mayon and Bulusan volcanoes, they define a 250-km volcanic chain related to subduction of the oceanic plate along the Philippine trench.

---

<sup>1</sup>Present address: Laboratoire d'Hydrologie et G ochimie Isotopique, Universit  de Paris Sud, F-91405 Orsay Cedex, France.

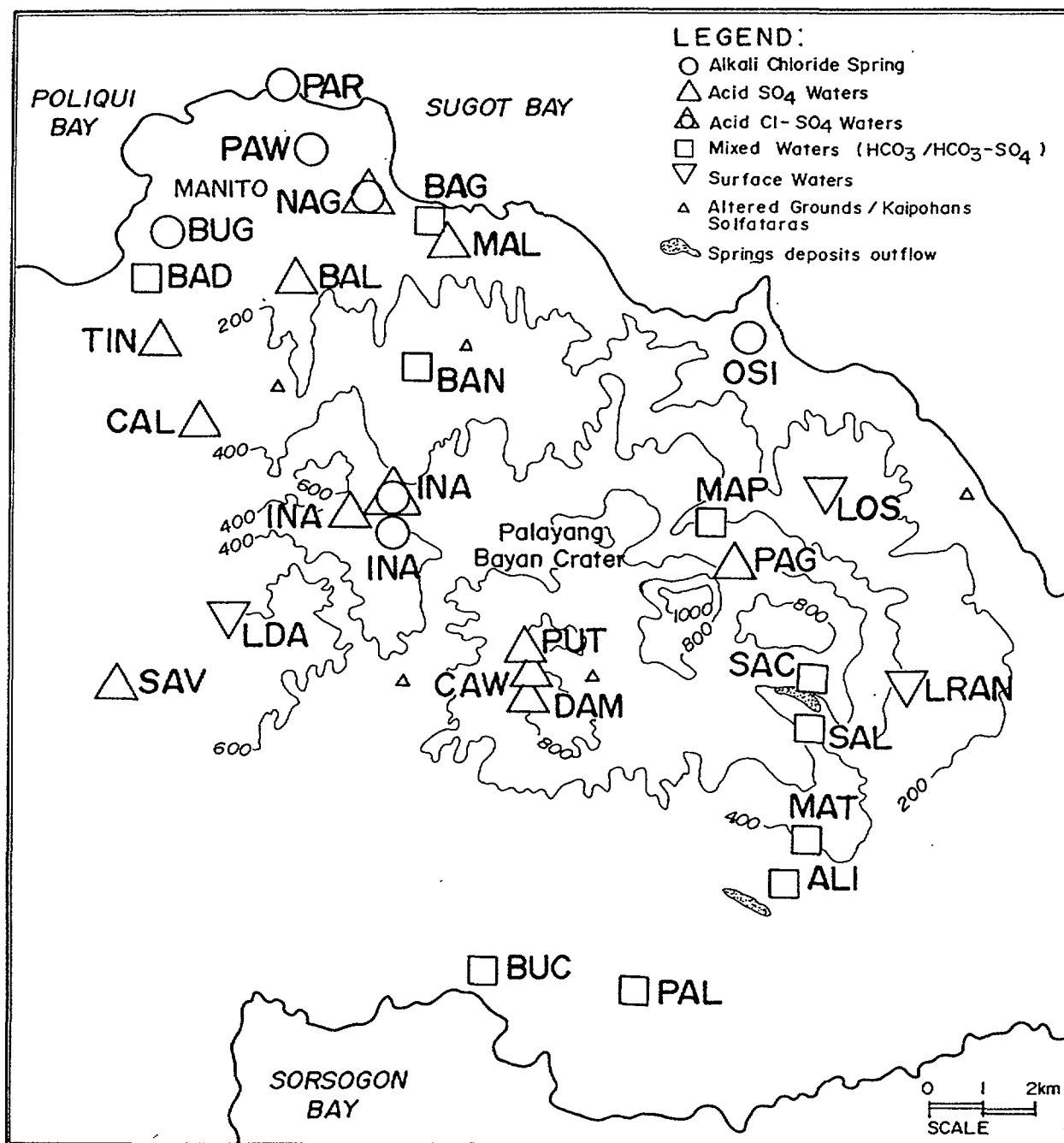


FIG. 1. Location map of the Bacon-Manito geothermal field showing the major thermal manifestations and altered grounds.

The lithology of the field is composed of the Gayong Sedimentary Formation (GSF), the Pocdol Volcanics (PV), and Cawayan Intrusive Complex (CIC). The GSF is composed primarily of calcareous sedimentary breccias. The lower PV are composed of hyaloclastites, andesites and basalts, the upper PV of fresh hornblende-bearing andesite, intensely to completely altered volcanic rock, intercalated with andesitic breccias, lavas and tuffs. The CIC includes basalt or diabase, microdiorite and plutonic dikes that intrude the GSF and PV.

Based on subsurface geology, permeability at the reservoir is mainly controlled by structures; mostly due to the intersection of faults and dike intrusions.



Extensive thermal manifestations dot the area (Figure 1). These include the Pangas (PAG) steam vents (activity has since declined upon drilling) at the highest elevation, cold gas seepages, steam heated springs and altered ground at Damoy (DAM), Cawayan (CAW), and Puting-bato (PUT) at high to intermediate elevations, warm springs at middle to lower elevations, steaming grounds and bubbling pools at Inang Maharang (INA), and Naghaso (NAG) hot lake and hot to warm springs in the lowlands, even Parong (PAR) springs located right on the seashore.

A large body of field scientific data have been amassed and are found in unpublished proprietary reports. The limited geochemical information that has filtered out deals only with specific observations on particular wells [1,2] or shows only preliminary field trends [3].

The purpose of this paper is to present the basic chemical and isotopic data from the field, and to attempt to delineate the natural fundamental physical and chemical processes occurring in the reservoir prior to large scale production.

## 2. CHEMISTRY OF FLUIDS FROM SURFACE THERMAL FEATURES

Water samples for chemical and isotopic analysis were collected from the major thermal features, some rivers and streams, and groundwater sources in 1977-1981, and again in 1990-1991. Analysis of the chemical constituents were done in the field and Manila laboratories using standard techniques, e.g. atomic absorption spectroscopy for the cations, UV-visible spectroscopy for silica and sulfate, and titration for chloride, boron and bicarbonate. Most of the analysis for  $\delta^{18}\text{O}$  and  $\delta^2\text{H}$  were performed at the IAEA while some earlier (1984-85) samples were analyzed at the former Institute of Nuclear Sciences, New Zealand. Examination of the earlier and later sets of data does not reveal significant differences. In this study, the latter set of values were used (Table I) since these include stable isotopic analysis.

The springs can be roughly divided into three groups according to the dominant anion present (Figure 2). These are (1) the steam-heated, acid sulfate waters of CAW, PUT, DAM, Tinapian (TIN), Malangto (MAL), INA and Calpi (CAL); (2) the bicarbonate to bicarbonate-sulfate springs at San Lorenzo (SAL), Balasbas (BAL), Balading (BAD), Balabagon (BAG), Alinao (ALI), Banao (BAN), Mapaniki (MAP), Malangto (MAL-1), as well as the cold springs Palhi (PAL) and Bucal-bucalan (BUC); and (3) the chloride springs at Pawa (PAW), Buang (BUG), PAR, Osiao (OSI) and acidic chloride springs of NAG. PAR and OSI are on the seashore and, PAR particularly, which is on the intertidal zone, is contaminated by seawater during high tides. To minimize the effects of possible seawater contamination, sampling for these intertidal springs were done during ebb tides.

In an attempt to obtain subsurface temperatures and some information on mineral-fluid equilibria, the data points are plotted on a Na-K-Mg diagram [4]. It can be seen in Fig. 3 that none of the natural thermal waters plot close to the full equilibrium line as defined by Giggenbach, which represents the equilibrium composition of the typical alkali chloride hot water with the most common hydrothermal mineral suite found in high temperature geothermal fields. As to be expected, all of the surface bicarbonate and acid sulfate waters plot close to the Mg apex. Only the chloride springs at Lake Naghaso (LNAG) fall into the partial equilibrium region. The other chloride springs fall within the "immature waters" area, suggesting that these waters are diluted by meteoric or non-equilibrated waters.

The highest estimates of the subsurface temperatures from the K-Mg geothermometer is only about 180 °C, but the Na-K geothermometer gave values of about 260 °C. The discrepancy in the values obtained by the two geothermometers is usually explained by the fact that the K-Mg geothermometer adjusts more rapidly to changing temperatures than the Na-K geothermometer, which retains some memory of its deeper equilibration condition.

Deep drilling aimed at power production showed that the maximum temperature estimates based on Fig. 3 are lower than the actual temperatures encountered in the hottest wells. For comparison, representative well waters are also plotted on Fig. 3 which shows that the deep water has attained full equilibrium with the rocks at temperatures above 300 °C. Wells at the periphery (OP-1RD and Pal-1RD) are also at or near equilibrium, but at lower temperatures. The highest temperature attained both from geothermometric estimates and actual downhole measurements is close to 320 °C.

### 3. STABLE ISOTOPE CHEMISTRY OF SURFACE WATERS

The  $\delta^2\text{H}$  and  $\delta^{18}\text{O}$  contents of the surface waters are shown in Table I and plotted in Figure 4. The values are measured in per mille (‰) deviations from the Vienna SMOW standard.

TABLE Ia. Chemistry and Isotopic Analysis of Surface Waters from Bacon-Manito Geothermal Field.

Source	SAMPLE CODE	Elev. m	Date yymmdd	T C	pH 25 C	Na	K	Ca	Mg	Cl	SO <sub>4</sub>	HCO <sub>3</sub>	B	SiO <sub>2</sub>	18O o/oo	2H o/oo	3H T.U
Inang Maharang	INA	285	900402	96	5.96	145	15.5	103	12.5	366	107	2	0.85	127	-0.22	-3.3	0.5
Inang Maharang	INA	285	900402												0.23	-3.0	
Pawa	PAW	10	900405	69	6.44	800	129	75	9.2	1364	46	93	6.7	174	-4.52	-25.3	nd
Buang	BUG	5	900404	45	6.36	339	42.2	97	33.9	697	60	73	1.73	76	-5.47	-39.0	nd
Parong 1	PAR-1	0	900417	98	5.19	3280	306	177	174	5545	416	nd	18.4	230	-2.50	-27.9	nd
Oslao well 1	OSW	5	900503	31	6.66	3.5	25	44	57.4	516	49	30	1.51	82	-5.13	-28.0	2.1
Oslao well 1	OSW	5	900503												-4.80	-27.0	nd
Naghaso 2	NAG-2	5	900405	69	3.01	1190	159	73	1.3	1993	56	nd	14.2	209	0.24	-10.0	nd
Naghaso 7	NAG-7	5	900405	94	3.45	1420	204	117	2	2426	87	nd	18	257	1.72	-5.0	nd
Lake Naghaso	LNAG	5	900405	65	3.80	2500	321	257	4.1	4379	82	nd	25.6	300	-1.16	-19.4	1.3
Lake Naghaso	LNAG	5	900405									nd			0.80	-14.3	nd
Inang Maharang	INA	285	900405	94	3.32	56.3	9	32.4	8.1	136	150	nd	0.97	143	2.54	-0.4	nd
Balaabas 1	BAL-1	55	900404	75	3.42	4.0	0.7	5.5	1.4	17	60	nd	0.8	20	-1.89	-32.1	nd
Balaabas 2	BAL-2	55	900404	59	5.25	6.1	2	7.1	3.5	17	41	nd	0.8	31	-2.09	-27.0	nd
Malangto 2	MAL-2	35	900405	64	2.97	15.2	1.1	7.1	3.5	22	235	nd	1.3	71	-0.90	-13.1	2.0
Malangto 2	MAL-2	35	900405									nd			-0.86	-20.4	
Damoy 3	DAM-3	660	900406	26	3.22	6.7	1.6	13.1	10	17	316	nd	0.67	73	-5.30	-26.7	
Damoy 2	DAM-2	660	900406	26	2.69	16.6	4.9	20.7	8.4	26	482	nd	0.65	146	-7.31	-27.6	3.7
Damoy 2	DAM-2	660	900406												-7.13	-26.7	
Puting Bato	PUT	450	900416	33	4.55	18	3.6	37.9	6.4	21	171	4.3	0.21	67	-5.70	-30.3	nd
Calpi	CAL	85	900416	40	5.44	46.3	4.6	61	3.9	19	266	6.7	0.17	55	-5.29	-30.7	nd
Cawayan 4	CAW-4	615	900417	29	3.43	7.7	2.4	20.1	4.1	17	113	nd	0.21	57	-5.05	-30.1	nd
Tinapian 1	TIN-1	75	900417	26	5.21	9.5	3.1	16.6	5.7	17	82	nd	3.24	82	-4.90	-33.1	nd
Mapaniki	MAP	475	900403	40	6.67	46	11.8	125	66.4	19	46	721	1.3	121	-5.54	-31.9	nd
Balading	BAD	35	900404	32	6.43	36	7.6	23.9	9.6	60	9	104	0.7	65	-5.34	-39.0	nd
Banao	BAN	125	900404	41	6.82	26.5	7	30.2	10.6	19	8	185	0.8	121	-5.54	-38.4	nd
Malangto 1	MAL-1	35	900405	95	7.14	66.2	15.2	40.6	10	21	16	31	0.43	149	-5.39	-34.1	nd
Alinao 1	ALI-1	275	900419	39	6.23	94.1	8.4	140	116	34	107	1136	0.88	147	-6.31	-36.6	nd
Salvacion 2	SAV-2	600	900504	22	5.63	6.2	1.5	5.9	2.8	19	97	5	0.16	60	-7.54	-44.6	nd
Salvacion 1	SAV-1	600	900504	22	5.34	6.7	2.2	6	3.6	23	83	1	0.22	57	-4.36	-29.5	nd
San Lorenzo 2	SAL-2	600	900502	37	6.19	37.1	10.1	163	46.1	35	251	566	0.76	136	-5.47	-29.2	nd
Balabagon	BAG	5	901116	64	6.87				66						-5.29	-29.4	
Oslao Lake	LOS	400	900403	30	6.54	2.8	0.6	2.2	0.7	17	5.3	nd	nd	nd	-2.22	-26.1	nd
Puting Bato creek	PUT-C	450	900404	28	6.50	4.8	0.7	5.7	1.6	21	8	6.1	0.22	31	-5.56	-31.1	nd
Palhi	PAL	5	900416	26	6.49	14	2.7	26.1	9.9	27	7.3	119	0.12	87	-6.37	-42.7	nd
Bucal-bucalan	BUC	5	900416	26	6.57	102	2.6	14.1	6.3	27	5.9	74	0.21	63	-6.12	-42.7	nd
Rangas Lake	LRA	800	900421	27	5.27	3.6	0.3	1.6	0.6	17	11.9	15	0.19	136	-0.28	-1.7	nd
Parong seawater	SW	0	900417	29	6.14	10000	372	80.7	1080	18940	1194	110	4.5	0.9	0.65	-1.2	

The rainwater together with the groundwater samples were linearly regressed to obtain the local water meteoric line. The lake samples were excluded since these are subject to evaporation and variable inputs. This line is defined by the equation (taking an a priori slope of 8)

$$\delta^2\text{H} = 8\delta^{18}\text{O} + 15.3 \quad (r^2 = 0.99) \quad (1)$$

The y-intercept deviates somewhat from the value of 10 of the global meteoric water line, but the observed value is quite similar to other Philippine areas [5, 6].

Most of the acid-sulfate and bicarbonate springs plot very near the meteoric water line suggesting that these are of shallow origins. A few samples are more oxygen shifted, while two samples (both from DAM) are significantly depleted in  $^{18}\text{O}$ . As to be expected, the chloride spring waters are positively oxygen-shifted relative to meteoric water.

The classical explanation for oxygen shift in chloride springs is water-rock interaction, where it is accompanied by a nearly constant corresponding values of  $\delta^2\text{H}$ . In the absence of a distinct horizontal shift, water-rock interaction may not be the only process. However, an evaporation line can be drawn through the steamheated LNAG chloride-rich lake water.

**Table 1b. Isotopic Analysis of Rain Waters.**

Source	SAMPLE CODE	Elev. m	Date yyymmdd	$^{18}\text{O}$ o/oo	$^2\text{H}$ o/oo	$^3\text{H}$ T.U.
Basecamp	R2	625	9004(11-30)	-2.56	-7.8	1.8
Basecamp	R3	625	9005(1-31)	-4.30	-20.9	1.8
Basecamp	R4	625	9006(1-30)	-9.77	-64.8	1.4
Basecamp	R4i	625	900604	-1.82	0.00	2.4
Basecamp	R5	625	9007(1-31)	-7.30	-43.9	-
Basecamp	R6	625	9008(1-30)	-9.20	-60.1	-
Basecamp	R7	625	9009(1-30)	-6.53	-38.8	-
Basecamp	R8	625	9010(1-30)	-6.71	-39.0	-
Basecamp	R9	625	9011(1-30)	-4.40	-21.6	-
Basecamp	R10	625	91(1118-1203)	-3.49	-15.0	-
Basecamp	R11	625	91(1204-0101)	-2.77	-7.2	-
Basecamp	R12	625	92(0102-0131)	-2.63	-6.5	-
Basecamp	R13	625	92(0201-0301)	-2.03	-0.8	-
Basecamp	R14	625	92(0302-0331)	-1.47	-1.9	-
Inang Maharang	R15	285	911207-920102	-2.53	-6.6	-
Inang Maharang	R16	285	92(0103-0202)	-2.54	-3.8	-
Inang Maharang	R17	285	92(0203-0229)	-1.82	1.5	-
Botong	R18	475	911212-920103	-2.86	-5.0	-
Botong	R19	475	92(0203-0301)	-2.40	-0.5	-
Botong	R20	475	92(0302-0331)	-2.24	-5.1	-
Balasbas	R21	55	911205-920101	-2.82	-7.7	-
Balasbas	R22	55	92(0103-0131)	-2.42	-3.0	-
Balasbas	R23	55	92(0201-0229)	-2.09	0.2	-
Manito	R24	5	91(1118-1204)	-3.02	-8.5	-

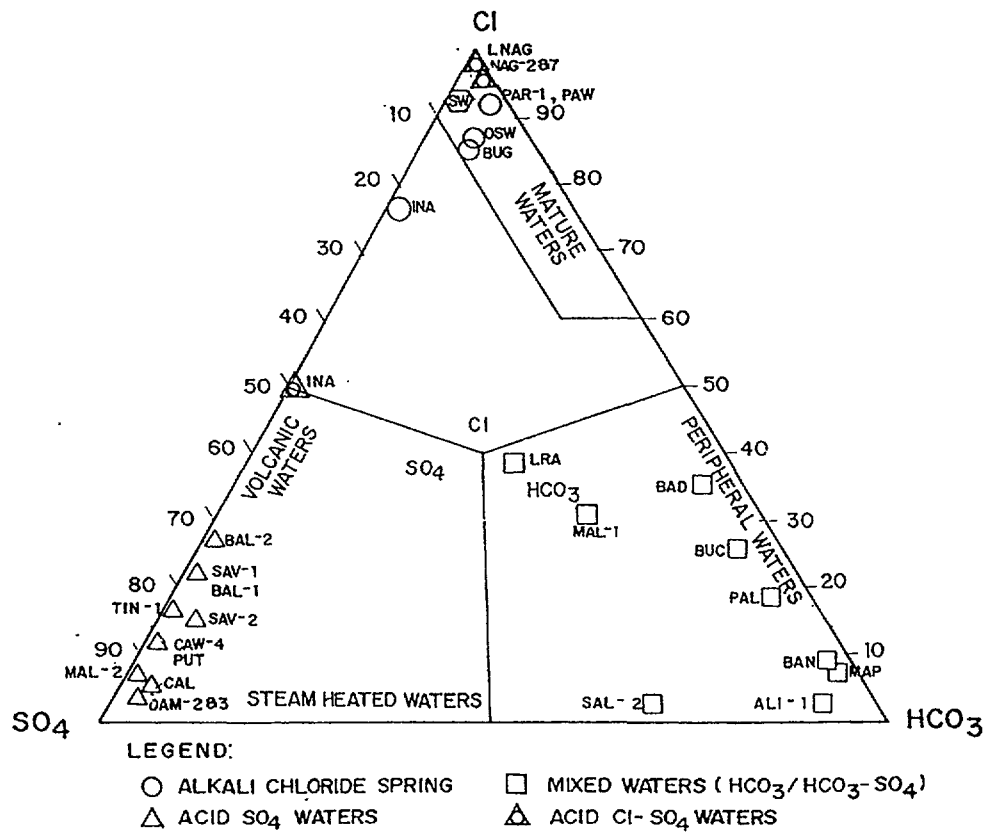


FIG. 2. Classification of thermal springs based on the major anions Cl-SO<sub>4</sub>-HCO<sub>3</sub>.

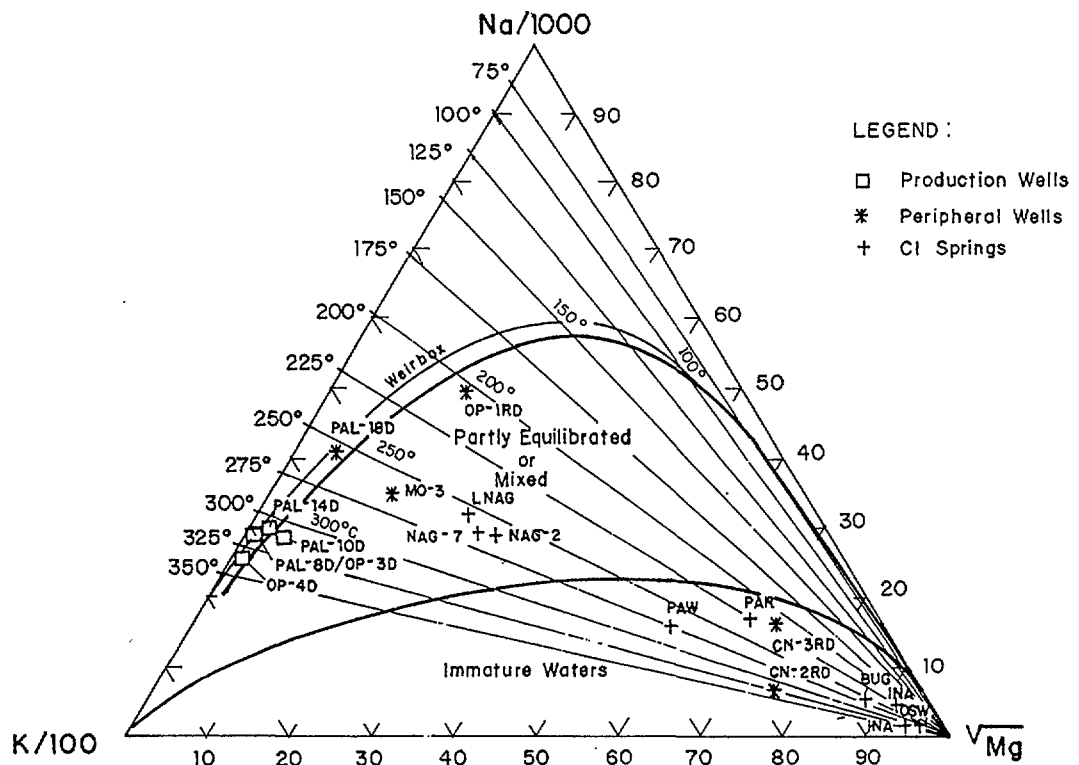


FIG. 3. Assessment of subsurface temperatures and water rock equilibrium using the Na-K-Mg diagram of Giggenbach (1988). Shown are representative well waters for comparison.

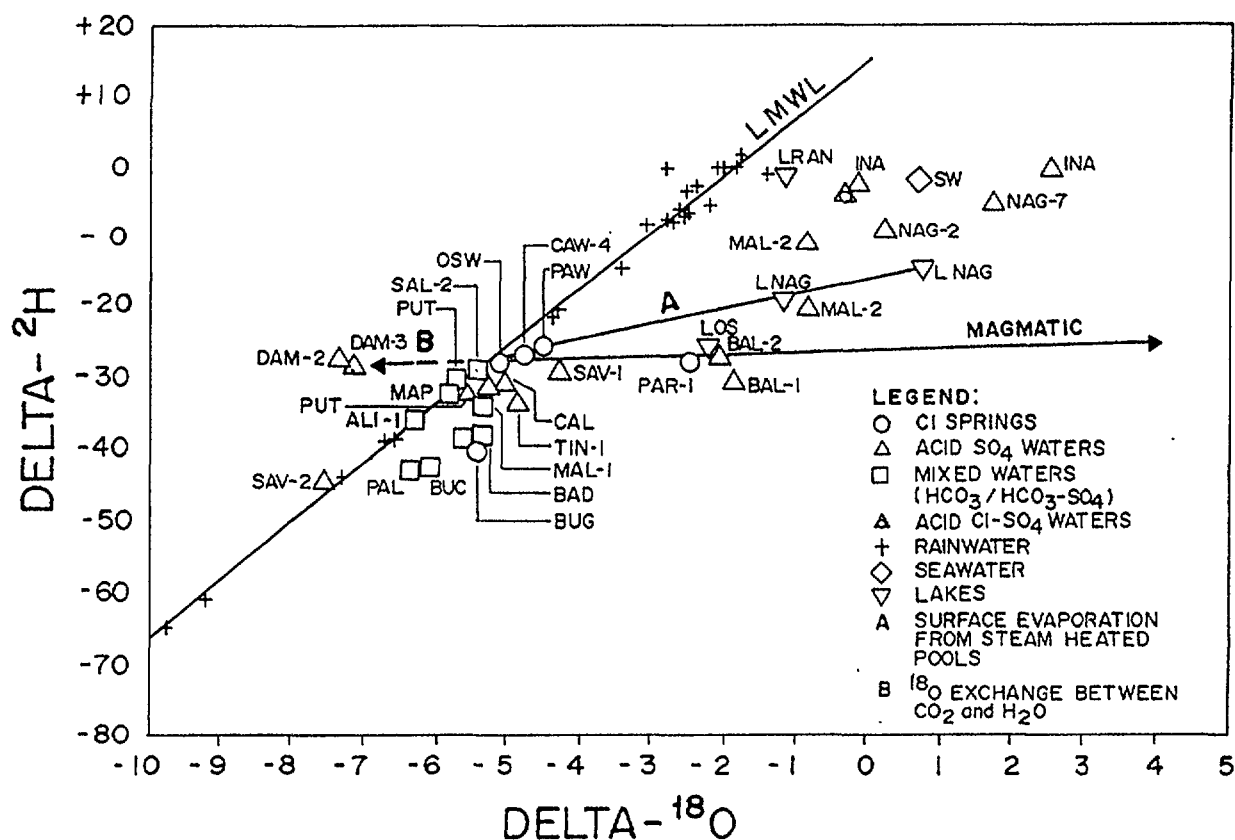


FIG. 4. A plot of  $\delta^{18}\text{O}$  versus  $\delta\text{D}$  for surface thermal and nonthermal waters at Bacon-Manito geothermal field. Hatched square represents the probable parent water. It has a salinity of  $7500 \pm 5$  °C.

The two DAM samples are prominently shifted to the left of the local meteoric water line (LMWL). The DAM manifestations are cold-bubbling pools in a highly altered argillized surface, and the predominant gas has been shown to be  $\text{CO}_2$  with minor amounts of  $\text{H}_2\text{S}$  and other gases. Cold water samples which are depleted in  $^{18}\text{O}$ , but not in  $^2\text{H}$ , are likely to have exchanged its heavier oxygen isotope with another oxygen-containing fluid, rather than with rocks. In this case, the exchange is with  $\text{CO}_2$  which is abundant in the area.

This phenomenon, apparently first observed by Ferrara et al. [7], could be more common in nature than previously thought. It has been invoked to explain similar shifts in the mineral and thermal waters in Sudety Mountains, Poland [8] and in the Valles Caldera, New Mexico, hydrothermal area [9].

#### 4. WELL WATER CHEMISTRY

Typical measured drilled depths for wells are from 2000 to 3000 m. Due to topographic constraints and to minimize surface equipment, most of the wells are deviated. During testing for output, water and gas samples are taken for analysis and interpretation. Table II lists the chemical analyses of well waters.

The hottest portion of the field is in the vicinity of wells OP-3D, OP-4D, Pal-10D, Pal-8D and Pal-14D where quartz temperatures are 300-320 °C (Fig. 5). There is a pronounced elongation of the contours towards Inang Maharang, and this could be indicative



TABLE II. Representative Separated Water Chemistry of Well Discharge Fluids from Bacon-Manito Geothermal Wells.

Well	Date yymmdd	H kJ/kg	SP MPaa	pH 25 C	Li	Na	K	Rb	Cs	Ca	Mg	Cl	SO4	HCO3	B	SiO2
										mg / kg						
Pal-1	830101	1077	0.095	7.77	6.24	4480	552	2.2	1.1	178	0.55	8225	44	32.7	35	607
			0.640	6.87	5.42	3674	477	1.9	0.5	168	0.49	6949	41	16.3	30	505
Pal-2D	830614	1499	0.095	7.28	7.87	4324	853	3.4	0.7	53	7.77	7807	86	32.9	62	886
			0.336	7.17	7.35	4112	819	3.3	0.6	71	2.43	7241	48	6.7	52	770
Pal-2D	840312	1281	0.094	4.70	5.80	3510	629	2.2	0.5	28	6.15	6298	179	1.2	49	933
			0.611	5.33	5.17	3040	554	2.0	0.4	25	5.71	5368	141	0.6	42	790
Pal-3D	830520	1255	0.095	6.68	8.01	4882	904	3.7	0.6	150	0.10	8774	22	22	50	846
			0.398	6.38	6.81	3954	744	3.1	0.5	139	0.07	7249	22	32.3	45	700
Pal-4D	831220	1308	0.094	7.53	11.10	4927	957	4.4	0.8	177	0.82	8970	24	20.7	51	891
			0.349	7.51	9.86	4136	860	4.1	0.8	153	0.91	7551	23	15.9	53	764
Pal-5D	840712	1230	0.094	7.63	6.90	4350	767	3.0	0.6	220	0.16	8066	29		33	751
			0.542	7.49	6.26	3810	666	2.7	0.5	197	0.12	7023	26		29	676
Pal-6D	840607	1547	0.094	7.29	9.64	5330	1060	3.9	0.7	170	0.30	9945	45	35.6	61	933
			0.225	7.01	8.97	4860	980	3.7	0.7	181	0.30	9076	35	40.7	56	812
Pal-7D	840807	1162	0.094	7.39	6.31	4720	903	3.3	0.6	212	0.43	8739	36	16.5	40	853
			0.832	6.38	5.52	3910	762	2.9	0.5	186	0.36	7306	28	9.2	34	722
Pal-8D	840412	1479	0.095	7.74	16.80	5950	1510	5.2	0.9	162	0.81	10930	10	46.1	136	1062
			0.619	7.16	13.90	4630	1200	4.2	0.7	126	0.16	8544	8	61	108	
Pal-9D	861126	1158	0.094	7.68	10.20	4774	955	3.9	0.9	190	0.73	9088	21	9.2	58	865
Pal-10D	851219	1407	0.980	6.66	8.94	4394	966	3.7	0.1	171	0.46	7977	23	34.2	65	807
Pal-11D	880927	1425	0.094	7.29	15.80	5408	1065	4.6	1.1	225	0.51	10270	26	42.7	92	944
			0.839	6.79	13.30	4490	891	3.9	1.0	180	0.43	8502	22	48.8	79	763
Pal-12D	880506	1353	0.094	7.57	14.30	5697	1313	5.2	0.8	137	0.26	10576	21	33.5	94	1056
			0.839	7.03	13.20	5030	1151	4.5	0.7	119	0.18	8779	18	52.5	79	822
Pal-13D	870308	1277	0.094	7.45	11.50	5554	1225	4.8	1.0	182	1.07	10224	18	14	83	1019
			0.910	6.84	9.90	4639	1025	4.1	0.8	150	0.84	8413	19	26.2	69	839
Pal-14D	890113	1334	0.094	7.52	18.70	6020	1362	6.4	1.0	138	0.24	11209	16	15.6	97	1132
			0.556	7.15	16.10	5200	1136	5.5	0.9	119	0.20	9607	13	36.6	80	914
Pal-15D	891127	1112	0.094	6.50	11.70	4700	1060	4.2	0.8	181	1.56	8669	26	8.5	78	983
Pal-15D	891214	1218	0.094	7.25	10.90	4580	1030	4.2	0.8	173	1.63	8596	26	14	70	906
OP-1R	880720	1256	0.096	7.91	7.38	4003	306	0.8	0.3	16	2.10	5689	119	830	275	687
			0.289	7.95	6.71	3635	281	0.7	0.3	20	1.09	5310	73	915	218	598
OP-2R	880818	848	0.096	8.52	2.90	3010	113	0.1	0.1	1.63	0.77	3386	241	1891	147	363
			0.413	8.06	2.60	2778	107	0.1	0.1	1.38	0.56	3034	203	1824	134	338
OP-3D	900122	1581	0.094	7.53	25.20	7960	2050	7.2	1.2	227	0.13	14547	18	115	222	1122
OP-4D	910715	1478	0.094	7.19	18.90	6370	1820	12.7	1.2	200	0.21	11810	10	48.8	165	1316
			0.484	6.46	16.30	5490	1575	11.1	1.1	170	0.17	10259	8	35.4	147	1177
OP-5D	910092	2457	0.094	6.49	22.10	6400	1710	11.7	0.8	240	0.48	12325	33	34.2	128	927
OP-6D	910316	2526	0.094	8.08	1.24	765	99	0.2	0.1	3	0.07	1218	70	293	76	1034
			0.632	7.74	0.82	505	66	0.1	0.1	2	0.35	859	49	311	49	694
Pal-1R	840928	1099	0.095	7.94	7.48	4330	618	2.5	0.6	293	0.71	8193	48	8.5	41	621
			0.702	7.41	6.60	3750	544	2.3	0.5	251	0.43	7015	38	14.6	36	533
Pal-3R	850204	1280	0.096	7.78	7.42	4610	472	1.6	0.6	281	0.98	8209	46	16.5	52	552
			0.262	7.49	7.02	4390	438	1.5	0.6	257	1.89	8156	43	33.6	48	511
Pal-4R	880318	1094	0.094	7.59	8.83	4619	700	1.7	0.7	261	0.24	8103	40	4.3	40	629
			0.480	7.28	7.87	4023	611	1.3	0.6	226	0.20	7155	35	13.4	36	542
CN-1	821119	1214	0.094	7.71	7.50	4542	921	3.9	0.7	174	0.08	8693	22	2.3	37	806
CN-2D	821007	1331	0.094	3.79	3.31	2910	275	1.2	0.4	7.5	9.18	4272	1635		24	592
CN-3D	901020	1297	0.825	7.25	10.30	4150	886	3.9	0.5	173	0.15	7672	23	9.8	41	739

of a major outflow direction towards the northwest. Steep temperature gradients are noted west of Cawayan, and to the north and northeast towards well OP-2RD. These areas could have thermal barriers, possibly due to geologic structures. The contours somewhat fanned out towards the southeast, but there is some uncertainty as to the contours towards the south due to absence of wells.

## 5. ENTHALPY-CHLORIDE RELATIONS

Figure 6 shows a plot of Cl concentrations in total fluid discharge (that is, analyzed concentrations corrected for the presence of steam) versus the measured discharge enthalpies. Also shown for comparison are the Cl springs of PAW, NAG, PAR, BBUG, the hot water lake at LNAG and the artesian well at Osiao (OSW).

Several distinct trend lines representing major reservoir processes are apparent in this diagram. The relative boiling-mixing relationships between the various wells and Cl springs have yielded a focal point representing the inferred deep parent fluid composition of about 7500 mg/kg Cl with a fluid temperature of approximately 325 °C.

By projecting back this major boiling-steam gain line from the inferred parent fluid towards the enthalpy of pure steam, a high temperature (>300 °C) fluid with the highest C is represented by OP-3D water. The representative fluid chemistry of OP-3D shows higher excess enthalpy and non-condensable gases (NCG) which supports the steam gain process involved. A secondary boiling-steam gain line again describes the high NCG and steam-dominated well discharges of OP-5D and OP-6D.

Farther down this secondary boiling-steam gain line are the end-member fluids represented by the gas-depleted waters of IM-1, MO-1 and MO-2 wells. These waters suffered boiling in the reservoir and are interpreted as residual fluids. Malangto (MO) wells were drilled in the lowlands with a distance of 10 kms from Palayang Bayan. This observation implies that the major outflow of the deep reservoir fluids is towards the lowlands in the NW through the Inang Maharang area. It can be deduced that the structures which serve as conduits of geothermal fluids toward the Manito lowlands are very permeable, hence, the presence of boiling Cl springs.

There are two dilution lines that can be deduced from this diagram. The first is that of the cold local meteoric ground water, which probably dilutes the relatively low-gas wells of Pal-7D, Pal-13D, and Pal-14D. Well Pal-14D is another least mixed hot (300 °C  $\text{TSiO}_2$ ) single-phase fluid deduced to be closest to the parent fluid in the Palayang Bayan sector. The end-member fluids of the heavily diluted waters are the Cl springs at the lowlands, i.e. BUG, and PAW. The high Cl NAG waters are diluted geothermal alkali-Cl waters which have undergone extensive surface evaporation (dotted line).

The second dilution line is deduced from the mixing of steam condensate with that of the fluid probably of well OP-3D. Some of the production wells, i.e. OP-4D, Pal-8D, Pal-10D, and Pal-11D, along this steam condensate dilution line have higher excess enthalpy and are gassy. Among all the production wells, OP-4D fluid has the highest quartz temperature of 320 °C and tapped a single water phase reservoir. It is deduced, based on its chemistry that OP-4D is located closest to the upwelling region of the field. This dilution line connects to the peripheral wells, PB-1A, Man-1 and Man-2, CN-2RD and CN-3RD, and OP-1RD, and the acid- $\text{SO}_4$  fluid discharges of wells Pal-2D and CN-2D. The diluting



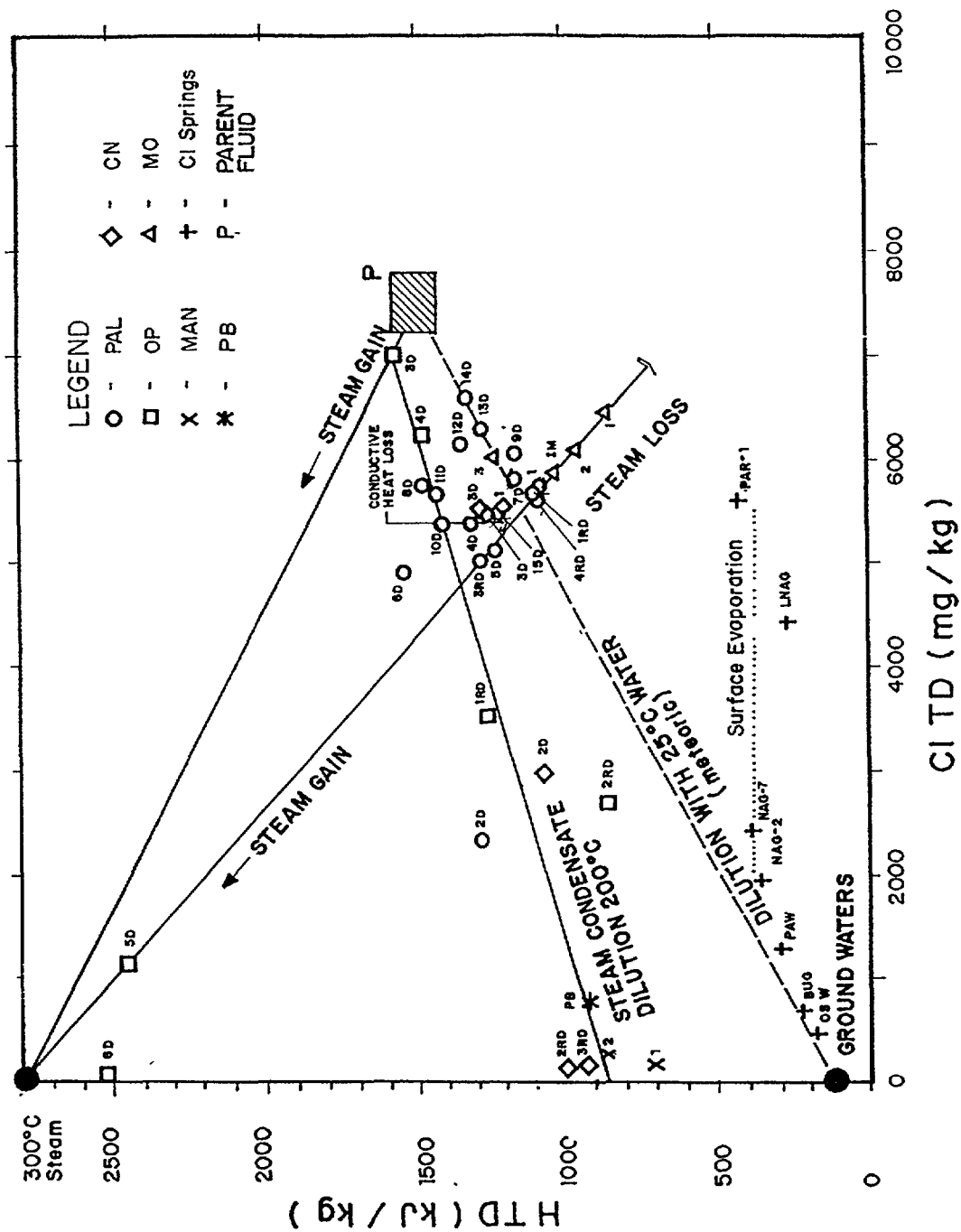


FIG. 6. Chloride-enthalpy (in total discharge) relations for the wells and springs in the Bacon-Manito geothermal field. Hatched square represents the probable parent water. It has a salinity of 7500 + 500 mg/kg Cl and a temperature of about 325 ± 5 °C.

water is likely to come from separated steam as geothermal water ascends and boils with a drop in pressure at shallower depths. Because these wells are located at the margins of the reservoir, the relatively colder temperature allow the steam to condense. The condensed steam trickles down to the CI reservoir through fractures and are simultaneously discharged with the CI waters. Steam condensate dilution is by no means rare in geothermal environments. For example, it has been noted in New Zealand fields [10] and inferred from surface data in Mt. Natib, Philippines [2].

**TABLE III. Representative Gas Chemistry of Well Discharge Fluids from Bacon-Manito Geothermal Wells.**

Well	Date yyymmdd	H kj/kg	SP MPaa	Ys	CO2 ----- mmoles / 100 moles SP	H2S	NH3	N2	CH4	Ar
Pal-1	830101	1077	0.640	0.194	750	4.62	1.80	7.80	8.6	-
Pal-2D	830614	1499	0.391	0.420	6820	61.40	1.69	-	56.6	-
Pal-2D	840312	1281	0.611	0.292	5040	47.10	-	45.50	36.9	-
Pal-3D	830520	1255	0.398	0.283	597	19.60	4.10	0.79	0.6	-
Pal-4D	831220	1308	0.349	0.337	951	20.50	-	0.70	12.7	-
Pal-5D	840712	1230	0.542	0.275	174	5.02	1.47	5.43	2.1	-
Pal-6D	840607	1547	0.225	0.468	850	7.03	2.50	3.76	6.5	-
Pal-7D	840807	1162	0.832	0.212	1020	9.40	1.80	5.96	15.3	-
Pal-8D	840412	1479	0.619	0.386	2000	24.90	4.98	0.97	3.8	-
Pal-8D	860129	1794	0.450	0.552	1720	31.00	5.00	1.16	18.1	-
Pal-9D	860802	1415	0.870	0.333	100	3.27	2.10	8.57	5.4	-
Pal-9D	861126	1158	0.430	0.255	413	15.60	4.50	1.20	3.2	0.06
Pal-10D	851219	1407	0.900	0.327	1900	42.00	7.88	1.41	22.6	0.17
Pal-11D	871031	1526	0.810	0.393	2220	28.70	6.24	5.33	29.4	-
Pal-11D	880927	1425	0.810	0.340	3190	37.70	3.63	2.06	31.6	0.12
Pal-12D	880506	1353	0.840	0.305	1070	18.90	3.91	3.13	9.6	0.03
Pal-13D	870317	1345	0.630	0.321	1060	23.60	3.49	7.87	16.1	0.15
Pal-13D	870308	1277	0.910	0.262	1010	26.70	4.41	1.49	4.6	0.04
Pal-14D	890113	1334	0.550	0.323	791	13.60	5.01	3.71	5.3	0.10
Pal-15D	891127	1112	0.460	0.229	659	22.30	4.50	2.69	1.1	-
Pal-15D	891214	1218	0.500	0.273	720	23.20	6.62	2.50	1.5	0.05
OP-1RD	880720	1256	0.130	0.337	4180	27.30	10.30	2.86	130.0	0.85
OP-2RD	880818	848	0.390	0.115	5340	15.30	1.43	0.96	43.9	0.29
OP-3D	900122	1581	0.410	0.456	2820	68.20	19.70	4.51	78.7	0.06
OP-4D	910716	1478	0.470	0.400	2190	48.80	3.04	1.50	8.8	0.03
OP-5D	910921	2457	0.230	0.883	2030	45.40	8.65	3.86	34.2	0.05
OP-6D	910316	2526	0.610	0.888	4040	113.00	13.70	5.50	104.0	0.07
Pal-1RD	840928	1099	0.700	0.195	338	4.26	2.69	1.88	2.1	-
Pal-3RD	850204	1280	0.260	0.339	767	5.61	2.52	4.40	17.9	-
Pal-4RD	880318	1094	0.480	0.218	244	3.52	1.82	-	-	-
CN-1	821119	1214	0.580	0.263	191	7.07	2.42	0.24	0.9	-
CN-2D	821007	1058	0.650	0.180	24400	89.30	-	31.20	737.0	-
CN-3D	901020	1297	0.830	0.279	2851	11.70	2.91	2.53	3.5	0.04
CN-2RD	910510	965	0.430	0.163	419	16.10	2.01	30.40	5.6	0.47
CN-3RD	910913	922	0.330	0.160	499	2.80	-	47.50	5.4	0.63
MO-1	820727	870	0.930	0.060	373	7.84	-	0.48	2.9	-
MO-2	830105	950	0.760	0.063	349	4.89	2.17	-	-	-
MO-3	840803	1225	0.160	0.338	231	5.53	0.09	9.71	1.3	-
IM-1	820227	1040	0.240	0.233	229	6.85	-	-	-	-

Many of the production wells, however, fall within the two dilution lines. This means that fluids from these wells have, to varying degrees, conductively cooled. This major trend is noted in wells Pal-3D, Pal-4D, Pal-15D, CN-1 and CN-3D, which have not suffered much dilution but rather, conductive cooling. This observation is consistent with the almost uniform Cl of about 6000 mg/kg within the central Palyang Bayan sector but with varying quartz temperatures across the field.

## 6. WELL GAS CHEMISTRY

Table III shows the gas chemical data from the wells. Gas data may be used to obtain some idea on the origin of the geothermal fluids. To determine magmatic fluid contribution, a trilinear  $\text{CO}_2$ - $\text{N}_2$ -Ar and  $\text{N}_2$ -He-Ar plots for Bacman well gases is shown in Figs. 7 and 8 [11, 12].

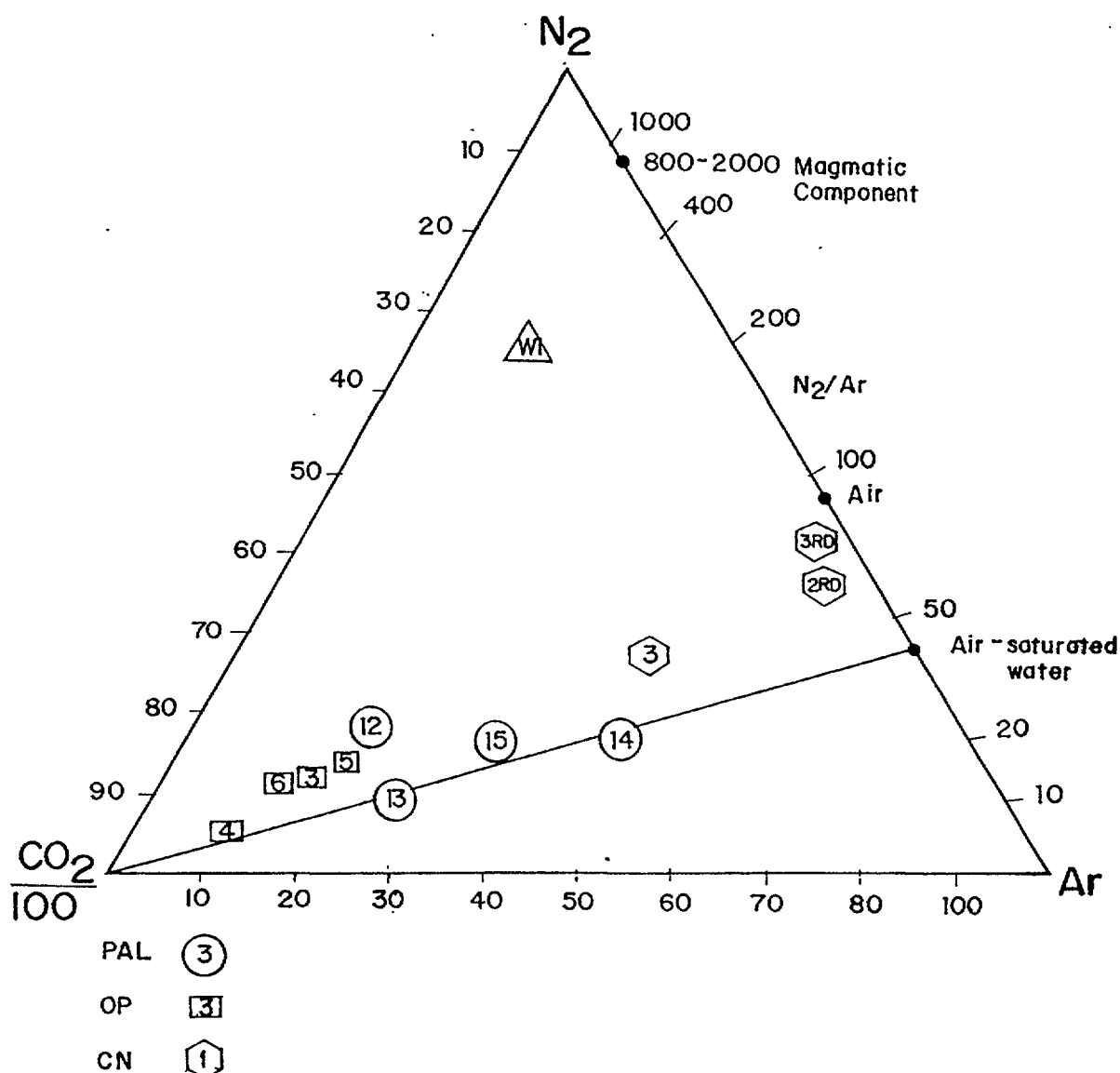


FIG. 7. A trilinear  $\text{CO}_2$ - $\text{N}_2$ -Ar plot for Bacon-Manito gas data to determine magmatic fluid contribution. Shown are the air composition and the air-saturated groundwater at the prevailing ambient conditions.

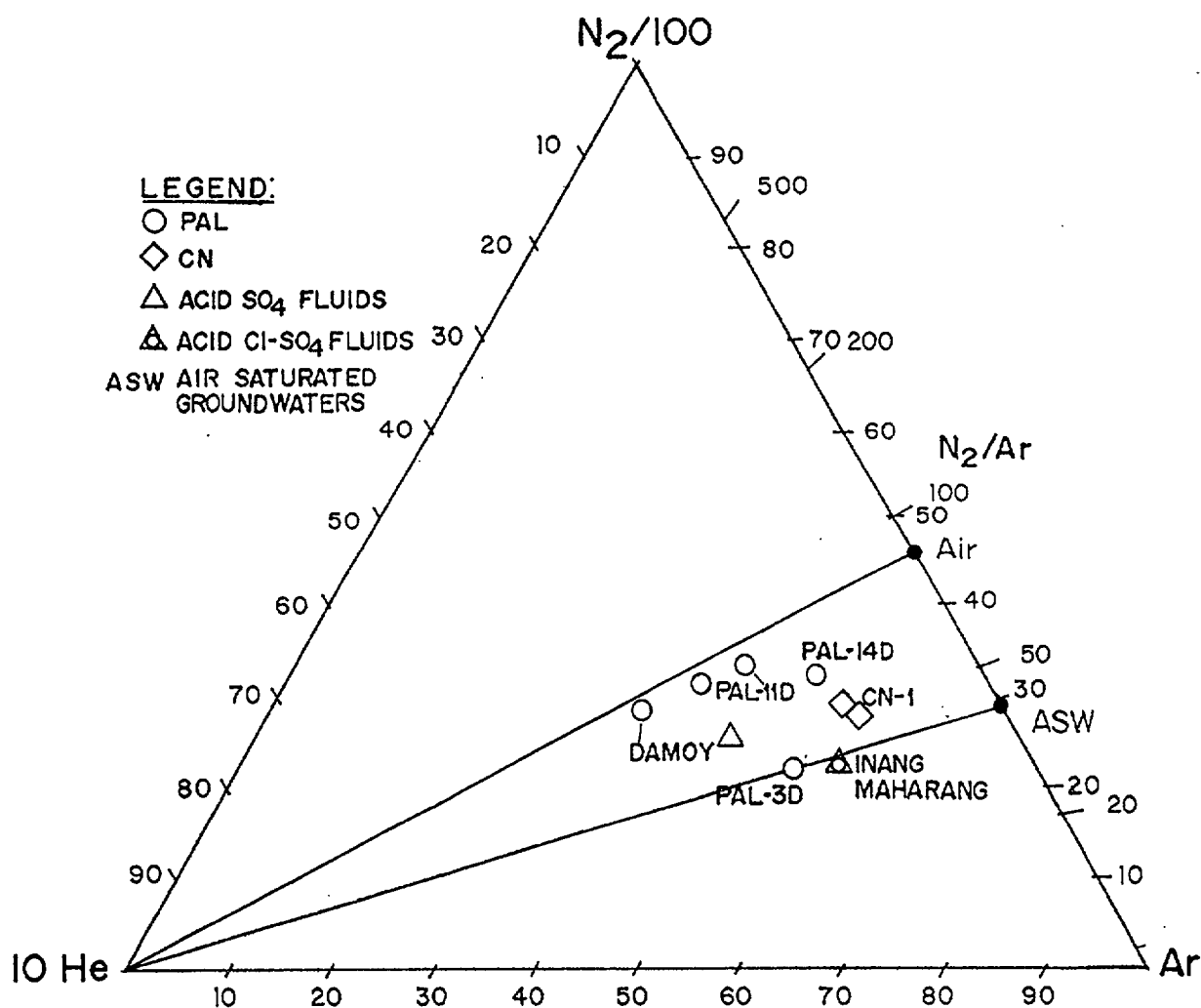


FIG. 8. Relative N<sub>2</sub>-He-Ar values for Bacon-Manito gas samples from wells and thermal areas indicating a possible "older magmatic" system (Giggenbach, pers. comm.).

It can be seen that the N<sub>2</sub>/Ar ratios are too low, or the CO<sub>2</sub>/N<sub>2</sub> are too high for most samples compared to the volcanic systems in White Island, New Zealand, the Japanese volcanoes, or Mt. Pinatubo, Philippines [11, 12, 13, 14], that a direct or active magmatic fluid contribution can be ruled out at this stage. This also means that the fluids tapped are essentially mixtures of deep geothermal fluids and varying amounts of atmospheric gases. Worth noting are the two reinjection wells at Cawayan, wells CN-2RD and CN-3RD, which plot near points representing air and air-saturated water. These wells have been deliberately drilled away from the chloride reservoir, in the cooler margins of the field. It is to be expected that atmospheric contamination is greatest here.

It seems possible that OP-4D may be tapping the hottest original liquid phase, as it has the highest CO<sub>2</sub>/N<sub>2</sub> ratio, assuming that the bulk of the N<sub>2</sub> source is the atmosphere. Indeed, at a value of 1460, it is the highest.

The CO<sub>2</sub> content of the deep original fluid which is assumed to be best represented by OP-4D discharge was estimated using the linear correlation between CO<sub>2</sub> content in total discharge and measured enthalpy at an inflow temperature between 310-320°C. A value of 2.0 wt % CO<sub>2</sub> was derived for the reservoir fluid. This is a reasonable value, considering Henry's Law on gas solubilities at 320 °C.

In Fig. 8, the Bacon-Manito geothermal system is represented by wells Pal-3D, Pal-11D, Pal-14D, CN-1 and thermal areas from DAM and INA. The geothermal system does not show any increased  $N_2/Ar$  ratios which could indicate an "older magmatic" system, with much of the earlier, high  $N_2/Ar$  "volcanic" gases driven off, but still retaining much of the "magmatic" water and heat (Giggenbach, pers. comm.).

## 7. GAS EQUILIBRIA

Geothermal processes may be delineated using gas chemistry owing to the fact that analyzed gas compositions at the surface may reflect equilibration at depth. A fluid phase gas reaction evaluated for equilibration at depth in this study is:

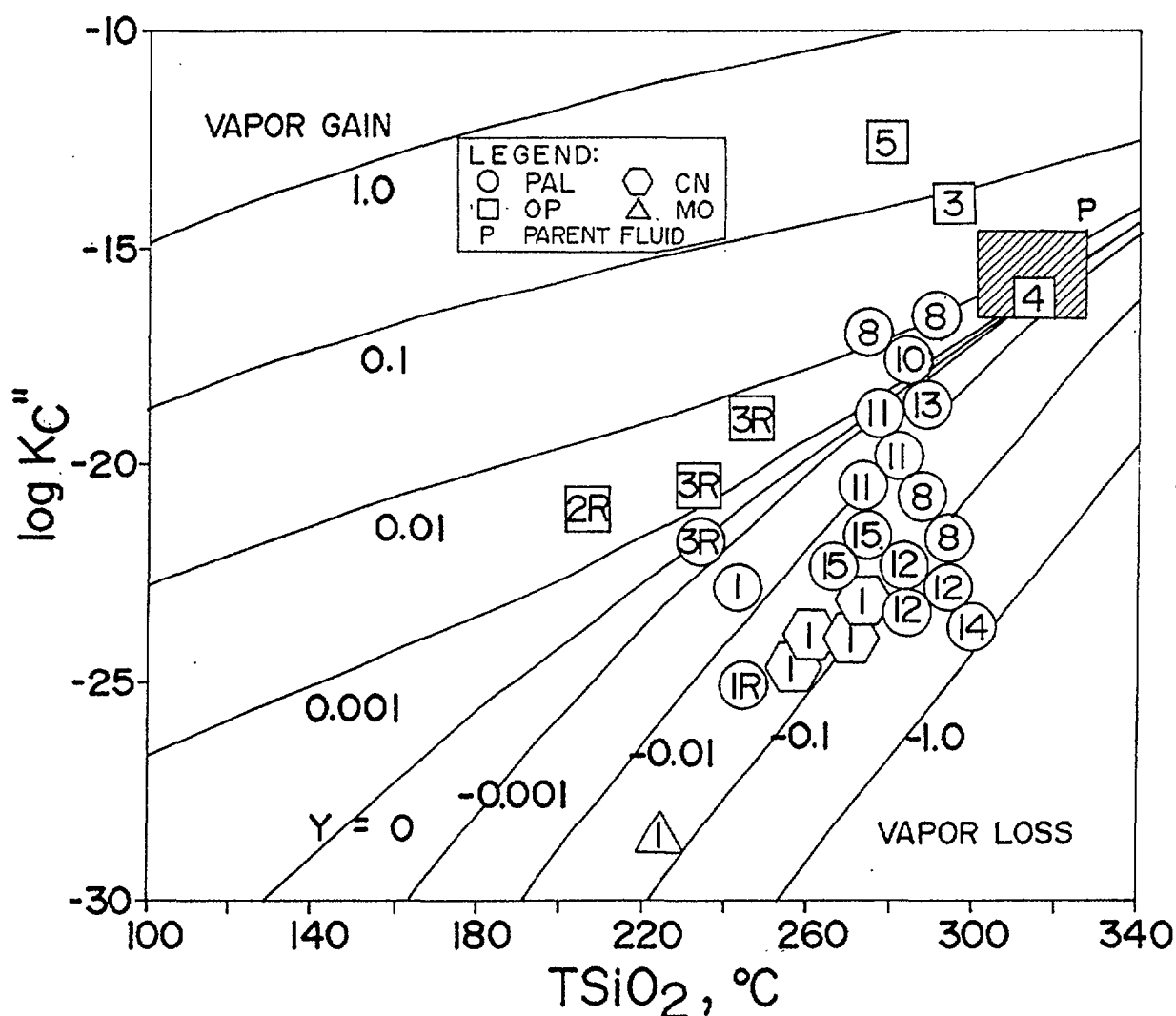


FIG. 9. A plot of the theoretical  $\log K_c''$  versus temperature at various values of vapor fraction  $y$  gained or lost. Plotted points are based on well gas data and on silica temperatures. Big hatched square represents the probable parent water. It has a temperature ranging from 310 to 325 °C and possible reservoir steam fraction ranging from -0.01 to +0.05.

Before the gases reach the surface, however, the single-phase fluid originally in equilibrium may have lost or gained vapor, owing to changes in pressures or mixing with cooler waters [15]. The effects of vapor gain or loss can be taken into account, by linking an apparent thermodynamic equilibrium constant,  $K_c$  in the above reactions with measured quantities. Theoretical values for  $\log K_c$  as a function of temperature and vapor fraction,  $y$ , which is lost or gained are shown in Fig. 9. Measured values of  $\log K_c$  for the Bacman wells are plotted for comparison.

The wells sampled can be classified into two groups according to fluid temperatures. The first group consists of those that have been drilled at the exploration stages where the reservoir has not yet been clearly defined (e.g. MO-1, IM-1, Pal-1, OP-1RD, etc.) and those that have been drilled specifically for reinjection (Pal-1RD, CN-2RD, etc.) at the periphery of the main reservoir after the main resource has been defined. This group has typical temperatures of 200 to 260 °C and the (simple) average of 240 °C is taken for gas equilibration evaluation.

The second group comprises the high temperature, mainly good producing wells with temperatures of above 260 °C to as high as 320 °C from silica geothermometer and downhole measurements at the main producing zones. The temperatures cluster at around 280-295 °C, and an approximate equilibration temperature of 290 °C is taken.

In Fig. 9, the hottest well OP-4D lies exactly on the equilibrium liquid phase at close to 320 °C. Up to the area of Pal-10D and Pal-13D, where silica temperatures are already down to 280 °C, the fluid remains on the liquid equilibrium phase. Beyond that, the fluid starts to lose vapor as it moves in the west to northwest directions towards the lowlands. Near Pal-11D, Pal-12D, Pal-14D and Pal-15D, the fluid has lost at least 10% of the fluid as vapor. By the time the fluid reaches the Cawayan area at CN-1, and at Pal-1RD (which is considered at the outflow and the area reserved for reinjection sector), it is already extensively degassed. MO-1 which is located in the lowlands several kilometers away from the production area, is also highly degassed. But the water discharged from this well turned acid, and it is not entirely clear that the deviation is real. Experience with applying the evaluation techniques to a few wells in the area which have acidic discharge (e.g., Pal-2D, CN-2D, etc.) usually do not yield reasonable values (e.g., points plot beyond the  $y = 1.0$  limit), and it could mean that the gas reactions considered (Eqs. 2 and 3) do not represent equilibrium conditions, or that  $H_2$  is added from corrosion of drillpipes.

On the other hand, the Osiao-Pangas wells, OP-3D and OP-5D (no representative gas sample from OP-6D was obtained) have gained considerable vapor, as also shown earlier in the enthalpy-Cl plot. These wells are highly two-phase, and the excess steam could come from boiling within the well and from a previously boiled off fluid which found its way through fractures to the upper portions of the well. An alternative explanation is that since these wells are found in only one sector within the fluid, these wells delineate a vapor-dominated horizon or an area of low water/rock ratio. Their quartz temperatures may not reflect their actual reservoir temperatures.

The influence of the geological formation on the chemistry of the fluids should also be considered. For example, the Cl/B ratios in Tongonan have been used to delineate fluid flow pattern and reduction in temperature across the field [16,17] owing to the gradual uptake of boron in clays as temperatures drop. However, the reverse trend occur in Bacon-Manito. There is a steep drop in Cl/B ratio from about 60-70 in Cawayan in the west to only 7 in Osiao-Pangas. At the same time, the GSF are found in shallower depths from Cawayan to Botong.

TABLE IV. Discharge Chemistry of Water and Gas Samples from Bacon-Manito Geothermal Wells.

Well	Date mmddyy	SP MPaa	H kJ/kg	pH 25 C	Na	K	Ca	Mg	Cl	SO4	HCO3	B	SiO2	CO2	H2S
Concentration in mg/kg															
MO-3	08-09-84	0.17	910	5.1	3760	532	281	3.11	7073	153		36	377	195	5
PAL-16D	03-04-92	0.28	1003	7.4	3914	456	67	0.74	6509	79	104	90	581	799	16
PAL-4D	05-05-85	0.61	1335	6.4	3750	750	149	0.27	6718	20	32	46	686	565	19
PAL-7D	07-23-84	0.96	1235	6.3	3960	750	185	0.30	7296	37	17	33	712	926	9
PAL-5D	07-20-84	0.68	1238	7.4	3660	627	204	0.09	6860	25	5.5	29	656	192	7
CN-3RD	09-13-91	0.34	922	8.6	340	25	12	2.35	241	287	104	6	589	489	11
CN-2RD	06-07-91	0.42	966	3.5	225	41	12	4.26	198	868	ND	5.0	573	441	15
PAL-9D	02-21-85	0.74	1137	5.5	3850	801	155	0.22	6913	26	37	46	687	547	17
OP-4D	06-12-91	0.45	1803	6.7	6090	1640	230	0.36	11271	14	53	155	1179	2668	59
OP-4D	06-19-91	0.40	1813	6.8	5435	1660	230	0.26	11310	12	49	158	1152	2459	62
OP-4D	08-28-91	0.43	1824	6.8	5980	1740	215	0.18	11579	13	45	163	1123	2612	66
OP-6D	02-14-91	0.36	2449	8.5	405	59	1.6		570	74	331	45	795	3847	107
OP-6D	03-12-91	0.63	2453	8.1	486	63	1.5	0.3	782	55	12	45	696	4027	112
OP-6D	08-29-91	0.36	2449	8.2	1310	250	9	0.04	2298	28	251	87	756	3570	112
OP-6D	09-04-91	0.36	2451	8.2	1600	240	9	0.07	2522	33	234	93	775	3243	107
OP-3D	08-27-91	0.34	1827	7.2	6830	1720	173	0.11	12719	15	107	197	1043	2412	59
CN-1	08-12-93	1.06	1153	6.91	3611	618	174	0.95	6609	40		30.9	655	738	14
CN-1	09-24-93	1.05	1216	7.27	3793	667	181	0.15	6786	23	3.66	30.3	675	207	7
CN-3D	10-01-93	1.35	1253	7.15	3914	801	150	0.39	6990	21	14.00	37.0	665	279	14
Pal-4D	09-23-93	0.99	1344	7.03	4260	904	167	0.95	7888	31	14.00	47.2	786	551	16
Pal-9D	08-17-93	0.96	1357	6.71					7469	51		49.0	744	638	14
Pal-10D	08-12-93	0.91	1750	7.14	4518	950	187	0.28	8124	27	39.00	70.8	856	359	8
Pal-13D	08-13-93	0.86	1334	6.52	4206	759	183	1.41	7617	28		43.4	764	624	15
Pal-14D	10-07-93	1.06	1350	6.95	4703	1170	113	0.11	8947	17	50.00	83.7	885	221	6
Pal-18D	01-11-93	0.56	1270	6.81	4720	597	174	0.21	8241	26	39.70	77.9	659	1270	10

**TABLE V. Fluid Chemistry and Isotopic Analysis in Total Discharge and Reservoir Condition of Water and Gas Samples from Bacon-Manito Geothermal Wells**

Well	Date mmddyy	TSIO2 deg.C	ExH kJ/kg	y	18O 0/00	2H 0/00	CITD mg/kg	18OT 0/00	2HTD 0/00	CO2TD mmol/100mol	H2STD	Cires mg/kg	18Ores -----0/00-----	2Hres
MO-3	08-09-84	212	3	0.19	-1.70	-19.7	5804	-2.63	-24.4	36	0.9			
PAL-16D	03-04-92	245	0	0.21	2.75	-17.5	5154	-1.86	-21.4	387	6.4			
PAL-4D	05-05-85	264	181	0.32	-0.66	-24.1	4584	-17.4	-27.8	179	5.9	4080	-1.58	-28.2
PAL-7D	07-23-84	269	56	0.24	-2.35	-18.1	5560	-3.06	-20.0	220	2.2	5338	-3.01	-20.1
PAL-5D	07-20-84	261	98	0.26	-2.49	-21.5	5051	-3.35	-24.4	51	2.0	4748	-3.26	-24.6
CN-3RD	09-13-91	247	0	0.16	-3.13	-21.2	202	-3.77	-23.9	78	1.7			
CN-2RD	06-07-91	246	0	0.18	-2.69	-21.9	162	-3.37	-24.6	80	2.6			
PAL-9D	02-21-85	272	0	0.21	-1.30	-25.6	5469	-1.97	-27.7	114	3.5			
OP-4D	06-12-91	316	366	0.55	2.43	-18.2	5126	0.42	-26.0	1489	33	7186	0.64	-26.7
OP-4D	06-19-91	313	394	0.56	2.52	-20.2	4908	0.40	-28.8	1394	36	7035	0.64	-29.6
OP-4D	08-28-91	311	417	0.54	2.37	-18.1	5002	0.36	-26.0	1489	37	7318	0.62	-22.9
OP-6D	02-14-91	273	1249	0.87	5.23	-11.6	75	1.82	-25.9	3341	93	353	2.83	-26.8
OP-6D	03-12-91	265	1294	0.85	4.98	-14.3	115	2.13	-24.1	3439	96	552	3.23	-27.0
OP-6D	08-29-91	269	1270	0.87	6.22	-12.4	304	2.81	-26.7	3101	97	1432	3.86	-29.7
OP-6D	09-04-91	271	1261	0.87	6.35	-10.1	331	2.94	-24.4	2819	93	1566	3.97	-27.4
OP-3D	08-27-91	301	477	0.57	4.04	18.9	5488	1.94	-27.2	1376	34	8318	2.26	-28.3
CN-1	08-12-93	264	0	0.19	-2.16	-22.3	5360	-2.70	-23.6	139	2.6			
CN-1	09-24-93	267	46	0.22	-2.31	-22.3	5286	-2.94	-23.8	46	1.6			
CN-3D	10-01-93	268	79	0.22	-1.54	-23.3	5461	-2.12	-24.4	61	3			
Pal-4D	09-23-93	281	103	0.29	-1.46	-22.0	5608	-2.30	-24.2	159	4.6	6011	-2.22	-25
Pal-9D	08-17-93	275	147	0.30	-1.00	-18.8	5242	-1.89	-21.1	190	4.1	5781	-1.78	-21
Pal-10D	08-12-93	289	466	0.49	+0.68	-21.2	4104	-0.785	-25.3	178	4	6004	-0.45	-26
Pal-13D	08-13-93	277	114	0.29	-1.22	-20.6	5375	-2.10	-23.2	184	4.3	5804	-2.01	-24
Pal-14D	10-07-93	294	39	0.29	0.48	-24.1	6378	-1.31	-26.1	63	1.6			
Pal-18D	01-11-93	260	136	0.29	+0.27	-19.4	5835	-0.72	-22.9	372	3	6354	-0.6	-23



## 8. STABLE ISOTOPE CHEMISTRY OF WELL FLUIDS

For a few wells, both steam and gas samples were taken for  $^{18}\text{O}$  and  $^2\text{H}$  analysis through a side tapping located at a distance of approximately ten times the pipe diameter downstream of the throttling plates of the discharge pipe using a webre separator at a measured pressure (Table IV). The isotopic analysis of the separate samples were then combined to obtain the total discharge composition, e.g.  $\delta^2\text{H}_t$  for the case of deuterium, according to

$$\delta^2\text{H}_t = (1 - y_s)\delta^2\text{H}_l + y_s\delta^2\text{H}_v \quad (3)$$

where the subscripts l and v refer to the liquid and vapor fractions respectively (Table V).

Analytical results for water samples only (i.e., the steam fraction was not analyzed) were corrected to total discharge composition assuming isotopic equilibration at the sampling condition by the relation

$$\delta^2\text{H}_t = \delta^2\text{H}_l - y_s 10^3 \ln \alpha_{2\text{H}} \quad (4)$$

where  $\alpha_{2\text{H}}$  is the fractionation constant of  $^2\text{H}$  between liquid water and steam. Analogous relations were also used for  $^{18}\text{O}$ .

Figure 10 shows a plot of  $\delta^2\text{H}$  versus  $\delta^{18}\text{O}$  for all the wells sampled together with the LMWL and the measured values for rain and groundwaters. The cold lake samples (Rangas,

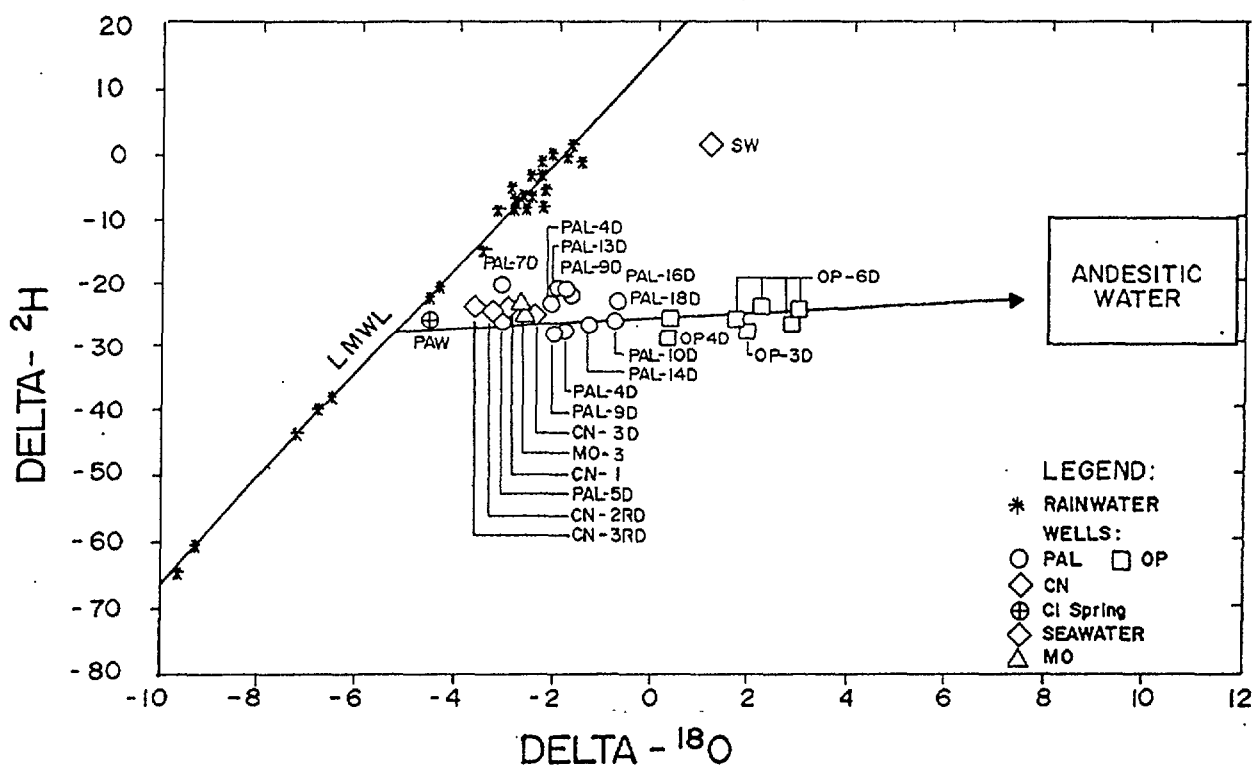
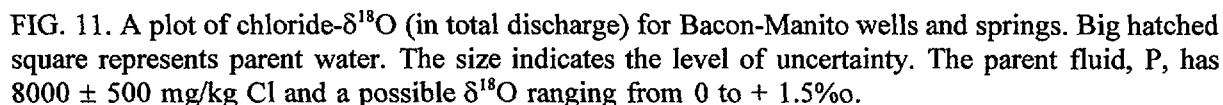


FIG. 10. A plot of  $\delta^{18}\text{O}$  versus  $\delta^2\text{H}$  for well waters at Bacon-Manito geothermal field. Line drawn through the points is a regression line. The square labelled "andesitic water" is from Giggenbach (1992). The line drawn through the rain samples (represented by asterisks,\*) is the local meteoric water line (LMWL) obtained by regression.

A regression line of well data including PAW spring gives

which is almost horizontal. The intersection of this line with the LMWL gives a tentative isotopic signature of the recharge meteoric water which is  $\delta^2\text{H} = -28\text{‰}$  and  $\delta^{18}\text{O} = -5.3\text{‰}$ . Several groups of springs located southwest and southeast in relation to the main production sector, Palayang Bayan, approximates this isotopic composition.

Other explanations have to be invoked. OP-6D, as shown earlier in the Cl-enthalpy plot, is fed by a relatively shallow and gassy horizon. Its fluids could have undergone high



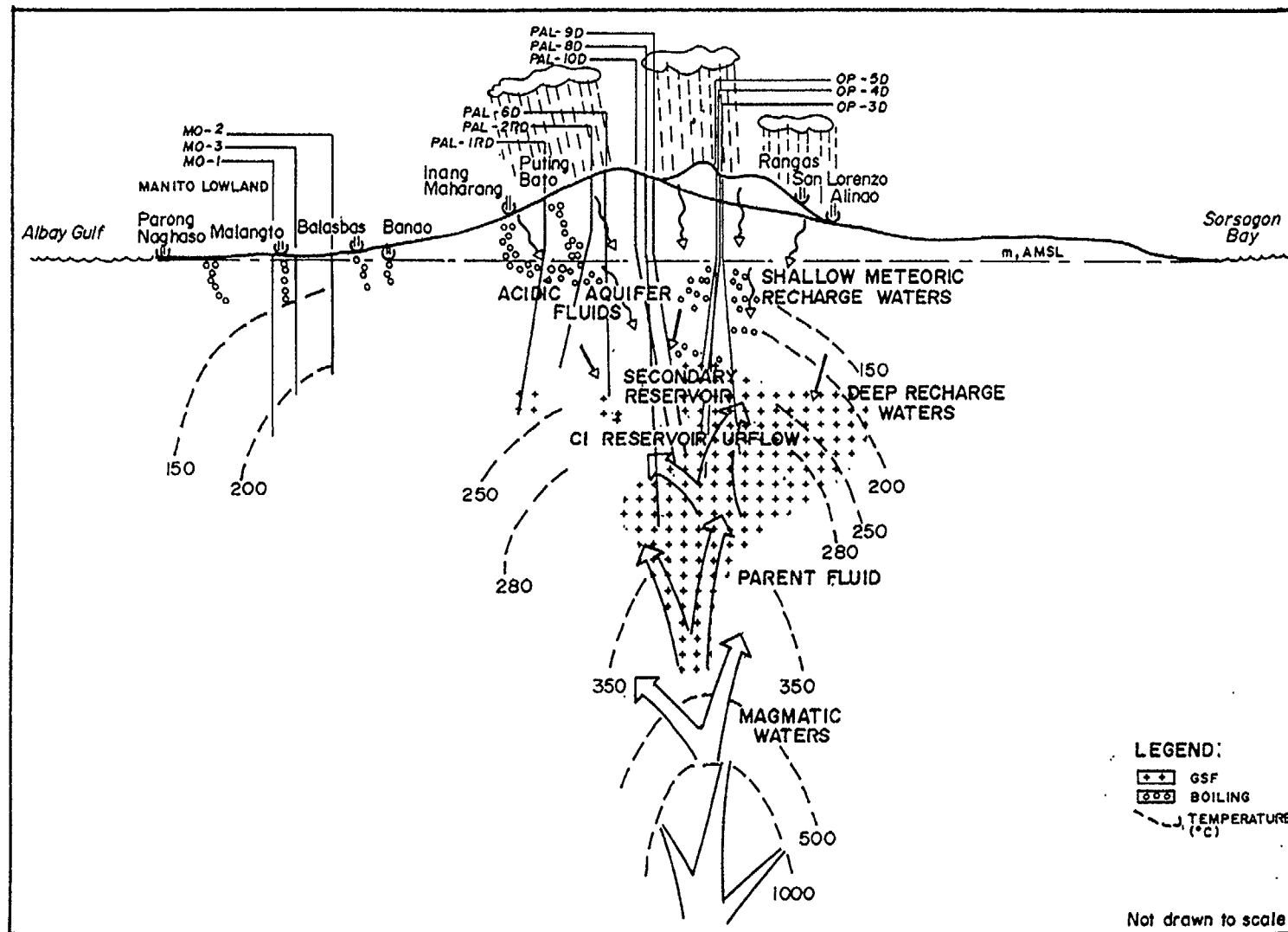


FIG. 12. A conceptual geochemical model of the field. Big arrows pointing upwards represent upflowing geothermal waters. Temperature contours below 350 °C are based on well data, while higher values are purely hypothetical. Downward pointing smaller arrows represent meteoric waters.

temperature,  $^{18}\text{O}$ -shift with  $\text{CaCO}_3$  rather than with  $\text{H}_2\text{O}$  and subsequent steam addition upon entering the wellbore. Pending additional data, it is well OP-3D which is likely to be tapping deep reservoir fluids which have encountered similar high temperatures and undergone prolonged interaction with both  $\text{CaCO}_3$  in the GSF and silicates in the CIC and PV. This could explain its higher Cl, gas and  $^{18}\text{O}$  shift relative to OP-4D.

An alternative explanation is mixing with magmatic water. Recently, Giggenbach [19] has shown that waters from geothermal and volcanic systems along convergent plate boundaries, of which Bacon-Manito is an example, are mostly mixtures of the local meteoric water and waters associated with andesitic magmatism. All Philippine volcanic [14, 19, 20] and geothermal systems [5, 6, 19, 21] studied so far have the above characteristics which makes the Bacon-Manito field unlikely to be an exception.

Extending the regression line to more positive values would, within errors, intersect the postulated location of the "andesitic" water of Giggenbach [19]. OP-3D and OP-4D, could then represent possible mixing combinations between these two end-members. With the slightly greater  $^{18}\text{O}$ -shift from OP-4D to OP-3D, the possible magmatic water contribution to the deep reservoir fluids increases from about 38% to 50%. Based on the chloride values of the isotope samples there is a corresponding increase in Cl from 6500 to about 9000 mg/kg. Based on these values, the end-member magmatic water has a Cl concentration ranging from 15000 to 18000 mg/kg. These values are close to the magmatic Cl value of 15000 mg/kg postulated for the andesitic White Island volcano and Mt. Ruapehu in New Zealand [12].

To verify the actual processes involved, chloride is plotted against  $\delta^{18}\text{O}$  (Figure 11). The trends are similar to that of the Cl-enthalpy plot, thus, confirming that OP-3D and OP-4D are nearest to the upflowing reservoir fluids. Thus, the deep reservoir fluid is estimated to have Cl concentration of 7500-8500 mg/kg Cl.

## 9. A GEOCHEMICAL MODEL

All the available geochemical data can now be synthesized to form a coherent geochemical model of the system as shown in Fig. 12. Remnant heat from the cooling intrusives and hot convective fluids coming ultimately from the subduction zone created the hydrothermal system when deep circulating meteoric water interacts with these heat sources at great depths. The hottest fluid which is essentially single phase, upflows near wells OP-3D and OP-4D at about 325 °C and an initial salinity of up to 8500 mg/kg in chloride. This deep reservoir fluid encounters less permeable horizons southeast of OP-4D. Owing to loss in pressure, steam separates and most of the dissolved gases, predominantly  $\text{CO}_2$  (> 95%), with lesser but detectable amounts of  $\text{H}_2\text{S}$ ,  $\text{NH}_3$ ,  $\text{N}_2$ ,  $\text{H}_2$ ,  $\text{CH}_4$  and Ar are exsolved. A significant portion of this separated steam and exsolved gas enters the wellbore of OP-6D, diluting the highly  $^{18}\text{O}$ -shifted waters that feeds the well and causing it to be gas-enriched.

The degassed liquid phase travels outward along natural hydraulic gradients and geologic structures channel the bulk of the liquid to the west and northwest towards CAW and the lowlands (Manito), some 10-15 kms away. Part of this fluid emerges as dilute alkali chloride springs at PAW, NAG and PAR. A probable further major outflow is towards the southeast, beyond OP-3D.

At the margins of the reservoir, steam condenses due to cooler surrounding temperatures and mixes with meteoric water. Owing to the gases present, the condensed steam forms

the extensive argillic alteration, steam and gas seepages, and the secondary bicarbonate to bicarbonate-sulfate springs at the surface (e.g. DAM, CAW, PUT and INA). Part of the condensed steam percolates back into the reservoir through fractures.

**Acknowledgement** - *The present investigation was carried within the framework of the IAEA Coordinated Research Programme for Asia, Africa and the Middle East on the applications of isotopes and geochemical techniques in geothermal development. The stable isotope portion of the study was made possible under Research Contract No. PHI-6/019/RI/RB between the IAEA and PNOC. The PNOC management is thanked for allowing us to publish proprietary data. Geological and reservoir engineering data are taken fully from internal reports, and are duly acknowledged. Dr. W.F. Giggenbach reviewed the manuscript and his contributions are acknowledged.*

## References

- [1] ROBINSON, B.W., VILLASEÑOR, L.B., CLEMENTE, V.C., "Preliminary stable isotope investigations of acid fluids in geothermal systems of the Philippines" (Proc. 9th New Zealand Geothermal Workshop) (1987) 73-78.
- [2] RUAYA, J.R., PANEM, C.C., Mt. Natib, Philippines: A geochemical model of a caldera-hosted geothermal system, J. Volcanol. Geotherm. Res. **45** (1991) 255-265.
- [3] D'AMORE, F., BUENVIAJE, M.M., SOLIS, R.P., "An evaluation of the deep reservoir conditions of the Bacon-Manito geothermal field, Philippines, using well gas chemistry", (Proc. 18th Annual Geothermal Reservoir Engineering Workshop, Stanford University, USA) (1993).
- [4] GIGGENBACH, W.F., Geothermal solute equilibria. Derivation of Na-K-Mg-Ca geothermometers, Geochim. Cosmochim. Acta **52** (1988) 2749-2765.
- [5] ALVIS-ISIDRO, R.R., SOLAÑA, R.R., D'AMORE, F., NUTI, S., GONFIANTINI, R., Hydrology of the Greater Tongonan geothermal system, Philippines, as deduced from geochemical and isotopic data, Geothermics **22** (1993) 435-449.
- [6] GERARDO, J.Y., NUTI, S., D'AMORE, F., SEASTRES, J.S., GONFIANTINI, R., Isotopic evidence for magmatic and meteoric water recharge and the processes affecting reservoir fluids in the Palinpinon geothermal system, Philippines, Geothermics **22** (1993) 521-533.
- [7] FERRARA, G.C., GONFIANTINI, R., PANICHI, C., Composizione isotopica del vapore di alcuni soffioni Larderello e dell' acqua di alcune sorgenti e mofete della Toscana. Atti della Società Toscana di Scienze Naturali, Serie A, **72** (1965) 570-588.
- [8] CIEZKOWSKI, W., Studium hydrogeochemii wód leczniczych Sudelowów polskich, Pr. Nauk. Inst. Geotech. Politech. Wrocław., **60** (1990) 133 pp.
- [9] VUATAZ, F.D., GOFF, F., Isotope geochemistry of thermal and nonthermal waters in the Valles Caldera, Jemez Mountains, Northern New Mexico, J. Geophys. Res. **91** (1986) 1835-1853.

- [10] HEDENQUIST, J.W., BROWNE, P.R.L., The evolution of the Waiotapu geothermal system, New Zealand, based on the chemical and isotopic composition of its fluids, minerals and rocks, *Geochim. Cosmochim. Acta* **53** (1989) 2235-2257.
- [11] KIYOSU, Y., Variations in N<sub>2</sub>/Ar and He/Ar ratios of gases from some volcanic areas in Northeastern Japan, *Geochem. J.* **19** (1985) 275-281.
- [12] GIGGENBACH, W.F., Redox processes governing the chemistry of fumarolic gas discharges from White Island, New Zealand, *Appl. Geochem.*, **2** (1987) 143-161.
- [13] RUAYA, J.R., RAMOS, M.N., GONFIANTINI, R., Assessment of magmatic components of the fluids at Mt. Pinatubo volcanic-geothermal system, Philippines, from chemical and isotopic data, *Geol. Survey Japan Bull.* **29** (1992) 141-151.
- [14] KIYOSU, Y., YOSHIDA, Y., Origin of some gases from the Takinoue geothermal area in Japan, *Geochem. J.* **22** (1988) 183-193.
- [15] GIGGENBACH, W.F., Geothermal gas equilibria, *Geochim. Cosmochim. Acta*, **44** (1980) 2021-2032.
- [16] RUAYA, J.R., SOLIS, R.P., SOLAÑA, R.R., SEASTRES, J.S., Simple interpretations of chemical transients in multifeed two-phase geothermal wells: Examples from Philippine fields, *Geothermics* **20** (1991) 135-145.
- [17] LOVELOCK, B.G., COPE, D.M., BALTASAR, A.J., A hydrogeochemical model of the Tongonan geothermal field, (Proc. Pacific Geothermal Conference and 4th Geothermal Workshop, University of Auckland) (1982) 259-264.
- [18] CRAIG, H., The isotopic geochemistry of water and carbon in geothermal areas, (Nuclear Geology on Geothermal Areas, CNR, Pisa), (1963) 17-53.
- [19] GIGGENBACH, W.F., Isotopic shifts in waters from geothermal and volcanic systems along convergent plate boundaries and their origin, *Earth Planet. Sci. Lett.* **113** (1992) 495-510.
- [20] REYES, A.G., GIGGENBACH, W.F., Petrology and fluid chemistry of magmatic-hydrothermal systems in the Philippines (Proc. 7th Int. Symp. Water-Rock Interaction, Park City, Utah), (1992) 1341-1344.
- [21] HULSTON, J.R., STEWART, M.K., GLOVER, R.B., CAMALES, R.A., BOGIE, I.M., BARNETT, P. R., Stable isotope geochemistry of the Tongonan geothermal system, Leyte, Philippines, (Proc. New Zealand Geothermal Workshop, Auckland, New Zealand), **4** (1982) 265-270.

# ISOTOPIC AND CHEMICAL COMPOSITION OF WATERS AND GASES FROM THE EAST COAST ACCRETIONARY PRISM, NEW ZEALAND

W.F. GIGGENBACH\*, M.K. STEWART\*, Y. SANO\*\*,  
R.L. GOGUEL\*\*\*, G.L. LYON\*

\* Institute of Geological and Nuclear Sciences,  
Lower Hutt, New Zealand

\*\* Department of Earth and Planetary Science,  
Hiroshima University,  
Kagamiyama, Higashi Hiroshima, Japan

\*\*\* Industrial Research Ltd,  
Lower Hutt, New Zealand

**Abstract** - Gases and saline waters discharged from springs and mud volcanoes along the east coast of the North Island of New Zealand provide a unique opportunity to study the evolution of fluids within an active accretionary prism. The waters show intermediate (5000 mg Cl/kg) to high (26 000 mg Cl/kg) salinities and are enriched in both deuterium ( $\delta^2\text{H}$  from -20 to -2‰) and oxygen-18 ( $\delta^{18}\text{O}$  from +3 to 7‰) with respect to local groundwater. Cl/Br ratios are with  $250 \pm 50$  close to those of seawater (285), B/Cl ratios are higher than those of seawater (0.0003) and range from 0.003 to 0.03 at comparatively uniform Li/B ratios of  $0.05 \pm 0.03$ . Relative Na, K and Mg contents suggest close attainment of water-rock equilibrium at temperatures of  $85 \pm 25^\circ\text{C}$ . Gas geothermometers ( $\text{CO}_2$ ,  $\text{CH}_4$ , Ar) indicate equilibration in the liquid phase at somewhat higher temperatures of  $100 \pm 20^\circ\text{C}$ . Ratios of  $^3\text{He}/^4\text{He}$  in gases from the central sector reach values of  $3.35 R_A$  indicating the presence of about 40% of mantle He. Significant amounts of  $\text{N}_2$  appear to be added from other than atmospheric sources. Formation of the highest Cl water (26 000 mg Cl/kg) is explained in terms of the hydration of basalt of a subducted seamount to form chlorite or serpentine. The isotopic and chemical compositions of the waters in the subducting sediments are compatible with the assumption that they form the main source for the magmatic components of waters discharged from andesitic volcanoes and associated geothermal systems.

## 1. INTRODUCTION

Evidence is mounting that fluids associated with andesitic magmatism are to a considerable degree derived from marine sediments and seawater subducted along convergent plate margins. According to an estimate by Giggenbach (1992a), more than 95% of the magmatic component of water discharged from andesitic volcanoes and associated geothermal systems may be of such origin. The seawater is subducted essentially in two forms, as porewater and as water of hydration in marine clays. The  $^2\text{H}$  isotopic composition of the total amount of water reaching the zones of arc magma generation was thought to be in the range  $-30 \pm 10\text{‰}$ . Waters and gases discharged from an accretionary prism can be expected to provide some information on the isotopic and chemical composition of the fluids involved during, at least, the early stages of the subduction processes. At most subduction zones these fluids are discharged largely below sea level and sampling of representative samples is difficult (Kastner et al., 1991; Moore and Vrolijk, 1992). The waters and gases discharged along the east coast of the North Island of New Zealand provide an excellent opportunity to collect these fluids on dry land.

A detailed description of the structure of this growing accretionary prism is given by Davey et al. (1986). On the basis of seismic reflection profiles, the decollement is found to dip initially at a very shallow angle of 3° from the Hikurangi Trough, some 140 km to the east, to reach the coast at a depth of about 14 km. On land, the top of the subducting Pacific plate is marked by a zone of high seismicity (Reyners, 1980). Several seamounts and volcanic knolls, of Cretaceous age, appear in the seismic reflection profiles attesting to their probably quite common occurrence over the Pacific ocean floor to the east of New Zealand. Convergence rates over the east coast part of New Zealand are of the order of 50 mm/a (Walcott, 1978).

## 2. ISOTOPIC COMPOSITION OF WATERS

The chemical and isotopic compositions of some 23 water samples collected from cold to warm mineral springs over the NE part of the North Island of New Zealand are given in Table 1. Sample locations are shown in Fig.1. The samples are divided into four groups. The first (01 to 08) encompasses waters discharged from the North Island Shear Belt (Cole, 1990), the remainder from northern, central and southern sectors of the east coast of the North Island.

An initial classification of the waters, on the basis of their isotopic compositions, is carried out in Fig. 2. Most of the samples from the Shear Belt lie close to the meteoric water line at positions typical of North Island groundwaters (Stewart and Taylor, 1981). Data points for the samples from the east coast generally show considerable enrichments, by >10‰, in both <sup>2</sup>H and <sup>18</sup>O with respect to meteoric waters. Together with the less enriched samples, a mixing trend is defined linking the very dilute sample (35), close to the meteoric water line, to the most enriched sample (10). There appear to be no obvious isotopic correlations between the generally very dilute waters from the North Island Shear Belt and the much more saline east coast discharges.

The generally accepted explanations for isotopic enrichments in thermal or mineral waters are isotopic exchange with rock (Craig, 1963) or evaporation (Giggenbach and Stewart, 1982). As will be shown later, deep temperatures for any of the waters are about 120°C; neither process, therefore, is likely to have brought about the large observed shifts.

A more likely possibility is mixing with an isotopically enriched water, such as seawater. In Fig. 2, however, the data point for seawater lies well off the observed trend. As discussed earlier (Giggenbach, 1992a), another possible candidate is the isotopically heavily enriched water of hydration of sedimentary marine clays. Because of the uncertainty in the nature of the minerals formed, the temperatures of hydration and dehydration of the minerals, the magnitude of corresponding mineral-water fractionation factors and the degree of attainment of isotopic equilibrium, the isotopic composition of this water can only be estimated within wide limits. Based on data reported by Savin and Epstein (1970), Taylor (1974), O'Neil and Kharaka (1976), James and Baker (1976), Yeh and Epstein (1978), Yeh (1980), Liu and Epstein (1984), and Capuano (1992), effective clay-water fractionation factors for deuterium are likely to lie within the range from -50 to -30‰, with a mean of -40‰, those for oxygen-18 within the range from 14 to 22‰, with a mean of 18‰. The corresponding compositional field of water of hydration in marine clays is shown in Fig. 2.

Attainment of isotopic equilibrium between water and a hydrous mineral through direct "exchange" of isotopic species under sedimentary conditions was found to be very slow (James and Baker, 1976), close approach to equilibrium is usually only achieved upon



Table 1.- Chemical and isotopic composition of waters, in mg/kg and ‰SMOW, of waters discharged over the NE part of the North Island of New Zealand, together with sampling dates and temperatures.

Location	date	°C	pH	Li	Na	K	Rb	Cs	Mg	Ca	B	HCO <sub>3</sub>	SiO <sub>2</sub>	SO <sub>4</sub>	Cl	Br	δ <sup>2</sup> H	δ <sup>18</sup> O
Shear Belt																		
01 Awakeri	870423	67	8.5	0.2	111	2	.005	.001	.20	5	3	151	58	32	46	2.5	-38	-5.4
02 Matahina	870109	19	8.2	0.1	29	5	.022	.001	4.0	14	1	108	93	10	18	0.2	-33	-5.5
03 Pukehinau	970109	45	8.1	0.4	147	1	.005	.001	.03	2	5	113	40	8	155	2.3	-32	-6.4
05 Tarawera	870113	50	8.3	1.7	494	4	.021	.001	.18	10	103	98	32	11	705	4.5	-48	-6.3
06 Mangatainoka	870114	58	8.2	0.5	210	2	.010	<.001	.20	4	12	82	54	7	200	2.8	-53	-8.0
07 Mangatutu	870114	55	8.4	0.1	102	1	.010	.001	.02	1	6	133	54	18	30	0.1	-55	-8.4
08 Waipiropiro	880102	40	8.1	2.4	1010	8	.030	.004	.90	137	62	37	25	1	1766	2.6	-48	-5.0
East Coast, North																		
10 Otopotehetehe	840126	22	7.7	12.9	6020	57	.050	.010	17	289	157	155	19	<1	9250	28.0	-14	+7.1
11 Rotokautuku	840126	16	7.3	0.7	1605	16	<.010	<.010	16	94	14	254	19	17	2570	7.9	-24	-1.9
12 Te Puia	871205	66	6.4	2.8	4840	42	.110	.018	12	745	77	85	46	75	8725	32.0	-18	+4.2
13 Waitangi Oil	840126	17	7.9	1.8	3225	16	<.010	<.010	8	10	20	1660	5	22	3350	14.0	-23	+3.1
14 Waimata	880103	16	8.2	1.7	3880	26	.028	.004	28	137	65	314	12	202	6065	27.0	-21	+3.5
East Coast, Center																		
23 Morere	860101	47	7.0	4.6	6700	84	.100	.004	80	2760	44	30	27	2	15800	83.0	-15	+3.9
24 Kopuawhara	860102	21	7.3	2.7	6040	59	.075	.011	60	2360	30	-	25	41	13700	69.0	-21	+4.8
25 Gisborne #1	920206	15	-	2.2	7140	24	.020	.006	97	624	61	-	11	5	12310	58.0	-11	+4.5
26 Gisborne #2	921203	20	-	2.0	3360	15	.010	.003	26	105	24	-	17	2	5295	22.0	-24	-0.2
28 Mahia	930126	16	-	4.9	11550	78	.030	.020	287	3820	66	-	10	2	25720	140.0	-2	+3.9
East Coast, South																		
31 Tukituki	890324	16	6.8	0.3	1820	21	.030	.003	14	490	50	61	11	<5	3705	13.0	-22	-1.4
33 Kaikopu	890324	18	8.1	1.7	2749	26	.010	<.001	28	95	29	810	19	<5	4020	16.0	-16	+2.1
35 Wairakau	860103	21	8.0	0.1	75	11	-	.003	10	167	-	-	16	19	155	-	-28	-4.6
36 Marapua	870115	17	8.2	0.5	1880	18	.010	<.001	3	30	61	245	10	139	2580	8.8	-18	+3.1
37 Waikokino	911130	14	-	0.4	2050	15	.010	.001	3	24	20	-	11	52	3040	14.0	-17	+4.7
WK Wairakei-66	853012	260	-	10.7	1170	167	2.2	2.0	.006	20	26	4	590	35	1970	5.5	-43	-5.7
BR Broadlands-45	870923	280	-	10.8	930	160	1.7	1.6	.002	1	49	270	820	<10	1370	3.3	-40	-4.5
SW Seawater	-	-	-	0.2	10760	390	0.1	<.001	1290	410	5	140	5	2710	19400	65.0	0	0.0

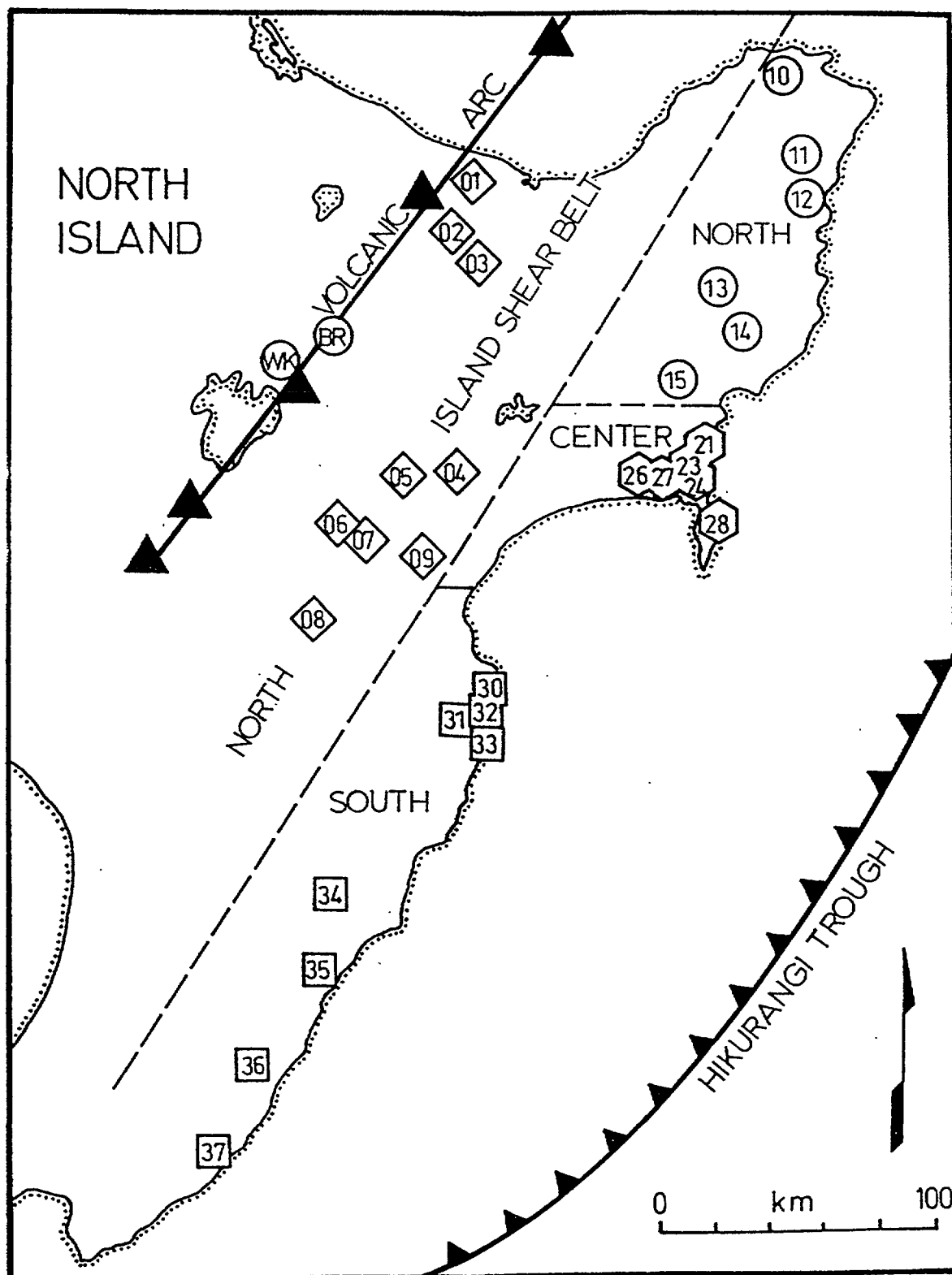


Fig. 1 - Sketch map of the NE part of the North Island of New Zealand. Filled triangles along "volcanic arc" represent Recent andesitic to dacitic volcanoes. For symbols see Tables 1 and 2.

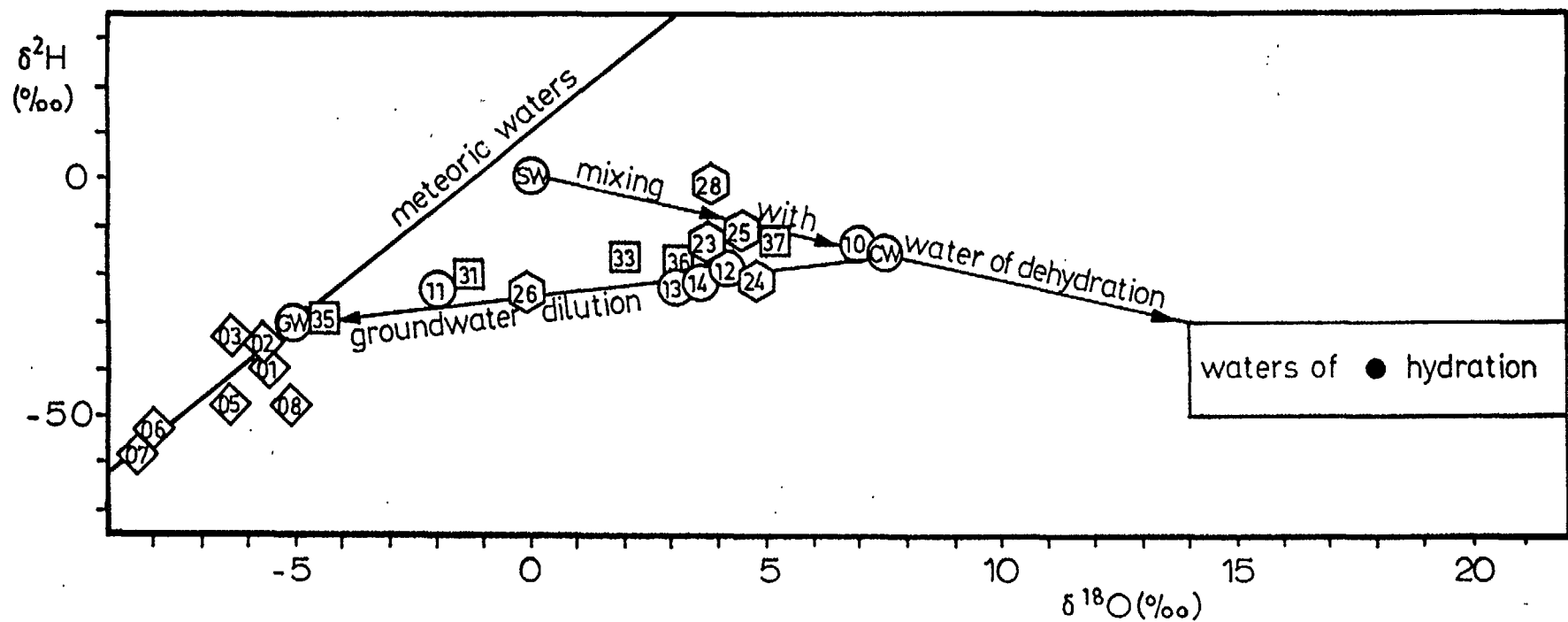


Fig. 2- Isotopic composition of waters from the NE part of the North Island of New Zealand.

GW: east coast groundwater, SW: seawater, CW: water formed from subducted sediments. For symbols see Fig. 1.

virtually complete recrystallisation of a mineral. Under sedimentary conditions, attainment of water-clay isotopic equilibrium can therefore be assumed to be limited to the early formation stages of a mineral and possibly later recrystallisation accompanying dehydration during burial diagenesis.

The most likely process facilitating dehydration and water-clay isotopic equilibration during burial diagenesis was suggested to be the conversion of smectites to illite (Yeh, 1980; Kastner et al., 1991). The fractionation factors for  $^2\text{H}$  and  $^{18}\text{O}$  typical of this process, at somewhat elevated temperatures, may initially be assumed to be not much different from those governing the formation of the marine clays and dehydration can, to a first approximation, be considered to be simply the reversal of the clay hydration process. In this case, the isotopic composition of the early fraction of water released should have a composition close to that of the original seawater, albeit much less saline. At higher degrees of dehydration, the composition of the water released would approach that of the clays.

In Fig. 2, waters of intermediate stages of dehydration would occupy positions along a line connecting seawater to water in clays. Its composition may be obtained by extrapolating the dilution trend line of the east coast samples in Fig. 2 to the clay dehydration line. They intersect at point (CW), near the data point for sample (10). Because the water released during dehydration is obviously very low in Cl, the waters discharged should also have very low salinities. A look at Table 1, however, clearly shows that Cl contents are generally very high, but below that of seawater, suggesting that the waters may contain the low salinity water resulting from the dehydration of clays, but mixed with seawater. Before discussing this aspect further, an attempt will be made to identify more closely the origin of the Cl and to derive likely temperatures of formation on the basis of the chemical composition of the waters and associated gases.

### 3. CHEMICAL COMPOSITION OF WATERS

The most likely source of the generally high salinities of the east coast waters, is seawater. This assumption is checked in Fig. 3 on the basis of relative Cl, Br and B contents. Except for sample (08), data points for the Shear Belt and east coast samples follow entirely different trends confirming the above finding of independent formation of the two types of water. The trend for the former corresponds to very low Cl/Br ratios of about 20 to 100, that of the latter, with Cl/Br ratios of 200 to 300, approaches closely the ratio for seawater of 286, in agreement with the assumption of a seawater origin of the Cl. It is interesting to note that the two data points representing the Wairakei and Broadlands (Ohaaki) geothermal areas fall on the same trend line supporting an earlier suggestion (Giggenbach, 1992) that much of the Cl in New Zealand geothermal water discharges is ultimately also of seawater origin.

While Cl/Br ratios are comparatively uniform, B/Cl ratios for the waters show wide variability from 0.0026, ten times that of seawater (.00025), to those typical of waters discharged over the Taupo Volcanic Zone of 0.01 to 0.03 (Ellis and Sewell, 1963; Giggenbach, 1989), some 80 times that of seawater. Because of the low B/Cl ratio of seawater, and taking into account the geological setting of these water discharges, the excess B can only be of marine sedimentary origin, accreted or subducted. The observed variations in B/Cl ratios then are likely to reflect different degrees of involvement of seawater and sedimentary material in the formation of the rising waters.

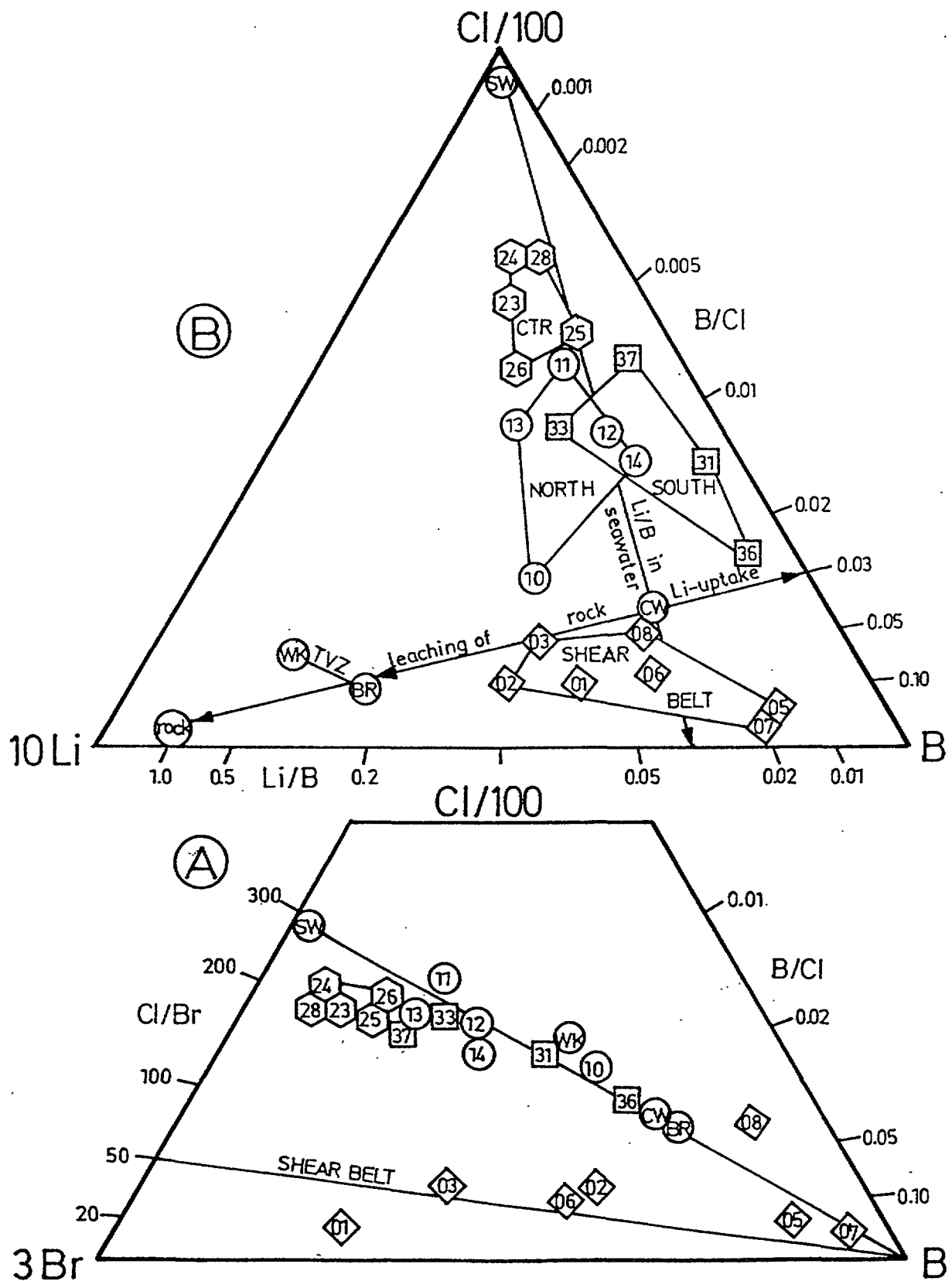


Fig. 3- Relative Cl, Br and B (A) and Cl, Li and B (B) contents in waters from the NE part of the North Island, in mg/kg. For symbols see Fig. 1.

According to Moran et al. (1992) and Bebout et al. (1993), much of the B is lost from subducted sediments, the degree of loss increasing strongly with progressive heating during subduction and virtually all B is removed by the time the sediments reach a temperature of 700°C. The most likely B removal process is transfer from the rock to subducted fluids or fluids generated by devolatilisation of subducted sediments. The highly increased B/Cl ratios, over that of seawater, of the waters discharged along the east coast of the North Island strongly suggests that they represent, to varying degrees, these fluids.

Boron is most likely transported by the subducted sediments absorbed onto clay particles. Confirmation of this assumption may possibly be obtained by comparing its behavior with that of another conservative species derived from the rock, Li. Transfer of Li from rock to water generally requires intense water-rock interaction at high temperatures (Goguel, 1983), while B, if only absorbed onto clays, should be removed much more easily. As shown in Fig. 3B, the samples from the various sectors of the east coast occupy quite distinct positions to either side of the line representing the Li/B ratio of seawater of 0.035. Those from the central sector plot closest to the high-Cl, seawater corner, followed with comparatively lower relative Cl contents by waters from the northern and southern parts of the east coast. Samples from the Shear Belt show a similar range of Li/B ratios, suggesting a similar mechanism for the removal of B, the much lower B/Cl ratios correspond to much lower involvement of seawater. As expected, waters from the two geothermal areas Wairakei and Broadlands have considerably increased Li/B ratios, but at B/Cl ratios similar to those of some of the east coast and Shear Belt samples.

Generally speaking, B and Li appear to be released from the sedimentary rocks, prevailing over the eastern parts of the North Island, in proportions close to those of seawater. On the other hand, the trend observed may also be explained in terms of mixing of two endmember waters, seawater (SW) and a water resulting from the dehydration of clays (CW). This latter water is probably most purely represented by the lower B/Cl samples from the east coast and the Shear Belt samples. The variations in Li/B ratios within all groups are likely to reflect the effects of secondary processes, such as leaching of Li from terrigenous detrital material, including perhaps volcanic ash, shifting compositions towards the composition of average crustal rock, or removal of Li by incorporation into secondary minerals, such as quartz (Goguel, 1983), having the opposite effect.

The B/Cl ratios of the lower Cl samples are very similar to those of  $0.03 \pm 0.015$  of geothermal systems of the Taupo Volcanic Zone (Giggenbach, 1989), with ratios approaching 0.015 being typical of the "rift-type" systems (Wairakei), ratios approaching 0.045, of the "arc-type" systems (Broadlands). On the basis of Fig. 3B, Cl and B in waters of the Broadlands type could be thought to be derived simply through leaching of sedimentary rocks similar to those of the Shear Belt with B/Cl of 0.05. A look at Fig. 3A, however, clearly shows that relative Br contents there, except for samples (5) and (8), are much too low to be compatible with this process. According to Fig. 3A and B, relative Cl, Br and B contents of the geothermal discharges resemble much more closely those of the medium to high Cl waters (8), (10) and (36) at the periphery of the study area (Fig. 1). In spite of their extreme geographic positions, however, these three samples may be most representative of the mixture of waters produced from the subducted seawater and clays, the mixture possibly reaching the zones of arc magma generation.

Summing up findings based on relative Cl, Br, B and Li contents, waters discharged from the east coast of the North Island are likely to represent mixtures of seawater and water of dehydration of clays. Their B/Cl ratios overlap with the range of waters discharged from

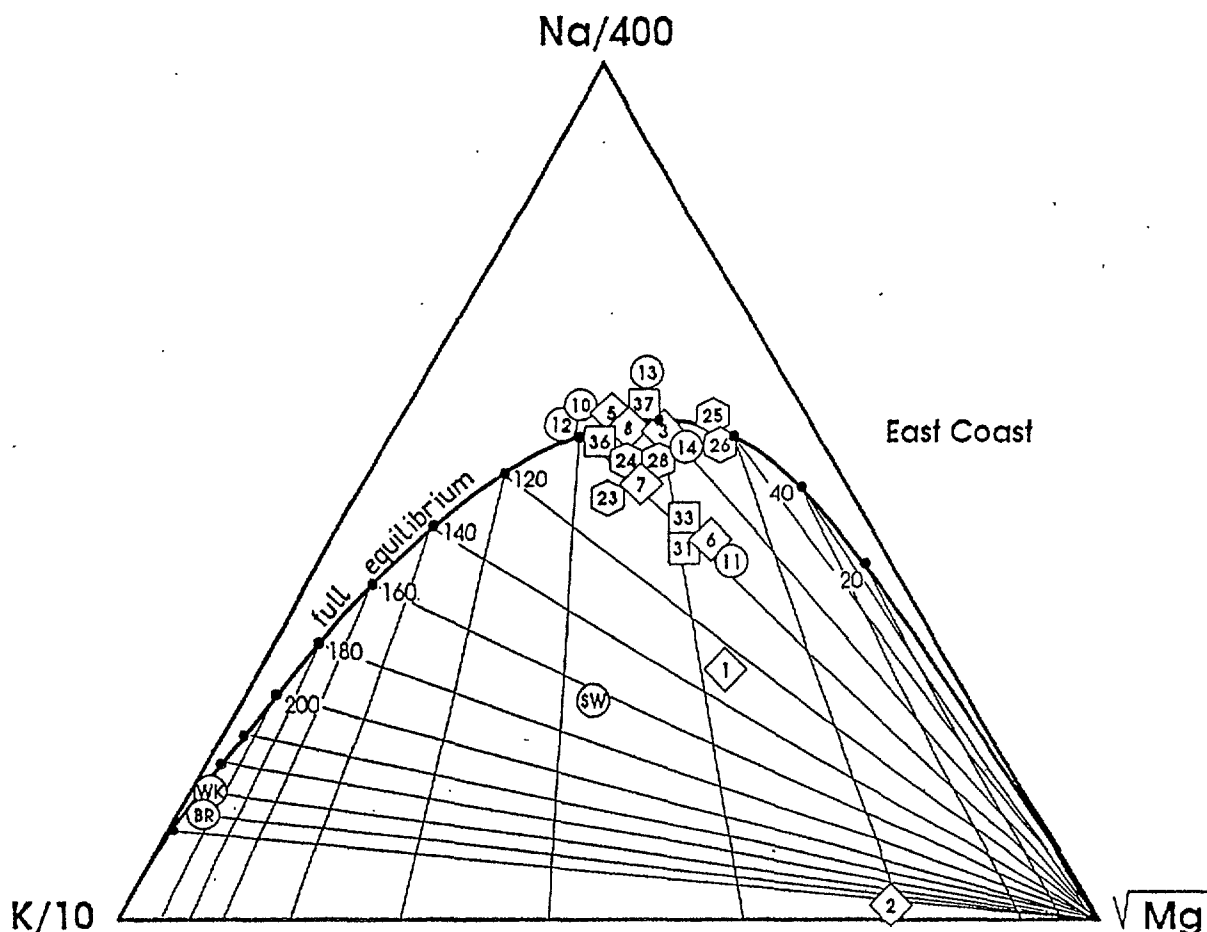


Fig. 4- Evaluation Na, K, Mg equilibration temperatures for waters discharged over the NE part of the North Island of New Zealand. For symbols see Fig. 1.

geothermal systems over the Taupo Volcanic Zone suggesting that B/Cl ratios are largely preserved during the entire cycle from subduction over arc magma generation to sub-solidus degassing of the magmas beneath arc-type hydrothermal systems. Increased relative Li contents in the east coast waters are likely to reflect hydrothermal alteration of detrital material in the sediments during subduction, those in the geothermal waters alteration of crustal rocks during the release and rise of the waters.

An indication of the temperatures experienced by the waters during their travel underground can be obtained by use of the more reactive species. A convenient way to extract water-rock equilibration temperatures is based on the triangular diagram of Fig. 4 based on relative Na, K and Mg contents (Giggenbach, 1988). Data points for most of the east coast and Shear Belt samples lie close to the full equilibrium line at temperatures between 60 and 110°C. Some of the deviations may be explained in terms of the presence of only partially equilibrated seawater (23, 31, 33) or groundwater (1, 2, 6). The position of most of the waters, however, suggests attainment of equilibrium with feldspars probably present in the terrigenous clastic component of the sediments. Equilibration at low temperatures is likely to be facilitated by the fine-grained nature of this material.

Table 2.- Chemical (mmol/mol) and isotopic (‰) composition of gases from the NE part of the North Island of New Zealand, together with sampling dates and temperatures.  $R/R_A$  is  $^3\text{He}/^4\text{He}$  ratio with respect to air.

Locality	date	°C	CO <sub>2</sub>	He	Ne	Ar	H <sub>2</sub>	O <sub>2</sub>	N <sub>2</sub>	CH <sub>4</sub>	R/R <sub>A</sub>	$\delta^{13}\text{C}_{\text{CO}_2}$	$\delta^{13}\text{C}_{\text{CH}_4}$	$\delta^2\text{H}_{\text{CH}_4}$
<b>Shear Belt</b>														
01 Awakeri	870110	47	40	.150	.0120	9.70	0.180	2.4	740	210	0.21	-	-38	-158
04 Te Hoe	900713	15	4	.068	.0010	0.60	0.007	5.6	36	955	0.11	-	-39	-152
06 Mangatainoka	870114	51	45	.363	.0050	4.30	0.050	0.1	322	625	0.10	-	-37	-160
09 Te Pohue	901220	15	15	.002	.0027	1.55	<.005	0.6	61	920	0.74	-	-51	-162
<b>East Coast, North</b>														
10 Otopotehetehe	840126	22	85	.150	.0007	0.29	0.008	2.8	10	900	1.00	-	-34	-138
11 Rotokautuku	840126	16	20	.042	.0004	0.22	<.020	1.3	7	975	0.30	-	-36	-116
12 Te Puia	871205	62	92	.065	.0004	0.32	0.060	1.9	33	877	1.89	-12.0	-42	-145
13 Waitangi Oil	840126	17	40	.090	.0006	0.73	0.009	2.2	25	930	0.08	-12.7	-36	-155
14 Waimata	880103	16	20	.075	.0005	0.15	0.015	0.3	12	960	1.84	-	-41	-175
15 Waikura	920813	12	<1	.110	.0010	0.71	0.017	12.5	37	950	0.21	-	-	-
<b>East Coast, Center</b>														
21 Wilson's Farm	771115		3	.400	-	0.60	0.070	0.3	47	949	-	-	-49	-178
22 Tiromoana	790617		70	.354	-	0.56	0.015	0.7	42	882	-	-14.9	-49	-183
23 Morere	860101	47	4	.065	.0005	0.55	0.025	0.6	14	970	2.71	-13.8	-53	-176
24 Kopuawhara	860102	21	8	.182	.0008	0.62	0.008	0.4	52	960	2.49	-	-57	-177
25 Gisborne #1	921205	15	1	.261	.0010	0.67	0.015	0.6	45	952	3.35	-	-	-
26 Gisborne #2	921203	20	12	.166	.0070	4.50	<.006	34.0	292	658	-	-	-	-
27 Makaretu	921204	15	21	.136	.0160	13.40	<.009	3.2	653	309	-	-	-	-
28 Mahia	931126	16	30	.500	.0020	1.47	0.014	<.2	120	850	0.53	-	-	-
<b>East Coast, South</b>														
30 Pohukio	920810	15	17	.117	.0102	5.18	0.011	48.0	319	610	-	-	-	-
31 Tukituki	890324	16	1	.155	.0002	0.19	0.023	1.6	31	965	0.38	-	-38	-172
32 Waipuka	921106	15	18	.178	.0100	6.20	<.012	<.5	390	585	-	-	-	-
33 Kaikopu	890324	18	20	.150	.0007	0.56	0.008	<.2	60	910	0.33	-	-47	-175
34 Weber	901202	15	23	.052	.0016	0.30	<.005	3.5	38	940	0.38	-	-43	-164
35 Wairakau	860103	21	1	.148	.0003	0.27	0.008	5.3	43	951	0.34	-	-38	-158
36 Marapua	870115	17	85	.157	.0007	0.19	0.020	<.1	19	894	0.83	-5.0	-36	-145
37 Waikekino	911130	14	5	.430	.0006	0.80	0.010	<.2	87	910	1.36	-	-	-
AR Air			0.33	.005	.0182	9.34	-	210	781	-	1.00	-7.1	-	-
AS Air sat. water		20	14.9	.002	.0098	16.40	-	336	633	-	1.00	-	-	-



#### 4. CHEMICAL AND ISOTOPIC COMPOSITION OF THE GASES

The chemical compositions of the gases associated with the water discharges, are listed in Table 2. With the exception of samples (01) and (27), the predominant gas is  $\text{CH}_4$ , generally followed by  $\text{N}_2$  and  $\text{CO}_2$ . Low  $\text{H}_2$  contents point again to quite low temperatures of fluid-rock interaction. A method to obtain gas equilibration temperatures involving the major species  $\text{CH}_4$ ,  $\text{CO}_2$  and Ar, based on techniques discussed by Giggenbach (1991), is used in Fig. 5. The very fact that  $\text{CH}_4/\text{CO}_2$  ratios are  $>1$  already suggests that gas equilibration temperatures are below  $170^\circ\text{C}$ .

Together with the  $\text{CO}_2/\text{Ar}$  geothermometer, the samples are found to plot close to the line representing equilibration of the gases at temperatures of between  $70^\circ\text{C}$  and possibly  $150^\circ\text{C}$ , with the gases dissolved in the liquid phase. Some of the shifts away from the liquid phase equilibration line may reflect actual equilibration in a two-phase environment or the

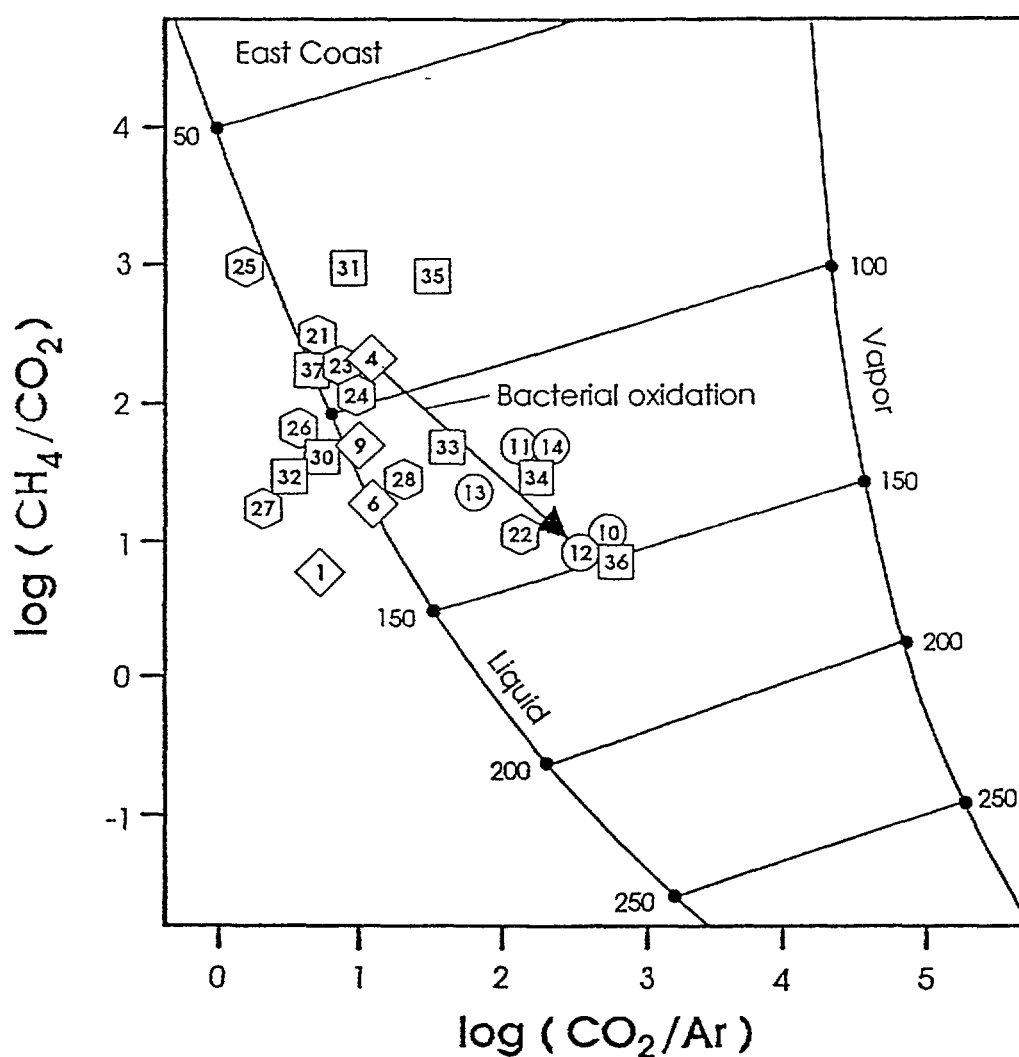


Fig. 5- Evaluation of  $\text{CO}_2$ ,  $\text{CH}_4$ , Ar equilibration temperatures. The arrowed line represent likely shifts in composition due to bacterial oxidation of  $\text{CH}_4$ . For symbols see Fig. 1.

Table 3.- Chemical composition of hydrocarbon gases, in mmol/mol of total hydrocarbons.

Locality	date	°C	methane	ethane	propane	i-butane	n-butane	i-pentane	n-pentane
<b>Shear Belt</b>									
01 Awakeri	870110	47	998	1.87	0.032	0.004	<.001	-	-
04 Te Hoe	900713	15	999	0.12	<.001	<.001	<.001	-	-
06 Mangatainoka	870114	51	999	0.18	0.001	<.001	<.001	-	-
09 Te Pohue	901220	15	999	0.20	<.001	<.001	<.001	-	-
<b>East Coast, North</b>									
10 Otopotehetehe	840126	22	998	1.60	0.050	0.020	0.004	<.001	<.001
11 Rotokautuku	840126	16	966	19.50	7.200	1.570	2.270	0.950	0.690
12 Te Puia	871205	62	972	21.90	4.950	0.910	0.320	0.098	<.001
13 Waitangi Oil	840126	17	886	55.40	29.700	6.650	10.700	3.730	2.960
14 Waimata	880103	16	992	8.10	0.028	0.003	<.001	<.001	<.001
15 Waikura	920813	12	999	0.13	<.001	<.001	<.001	-	-
<b>East Coast, Center</b>									
22 Tiromoana	790617	-	999	0.57	0.004	<.001	<.001	-	-
23 Morere	860101	47	998	2.24	0.138	0.043	0.002	0.004	0.0006
24 Kopuawhara	860102	21	998	1.19	0.013	0.003	0.001	<.001	<.001
25 Gisborne #1	921205	15	999	0.85	<.001	<.001	<.001	-	-
26 Gisborne #2	921203	20	999	0.08	<.001	<.001	<.001	-	-
27 Makaretu	921204	15	999	0.06	<.001	<.001	<.001	-	-
28 Mahia	931126	16	999	0.17	0.002	<.001	<.001	-	-
<b>East Coast, South</b>									
30 Pohukio	920810	15	998	1.51	0.003	<.001	<.001	-	-
31 Tukituki	890324	16	999	0.24	0.002	<.001	<.001	-	-
32 Waipuka	921106	15	989	9.80	0.700	0.060	0.005	<.001	-
33 Kaikopu	890324	18	975	24.10	0.860	0.130	0.025	0.005	0.0007
34 Weber	901202	15	961	30.40	5.040	1.400	0.940	0.430	0.2000
35 Wairakau	860103	21	926	54.80	14.000	2.600	1.830	0.500	0.1500
36 Marapua	870115	17	992	6.80	0.930	0.040	0.016	0.006	0.0003
37 Waikokino	911130	14	994	5.90	<.001	<.001	<.001	-	-

effects of secondary processes, such as formation of CO<sub>2</sub> through bacterial oxidation of CH<sub>4</sub> at shallow levels, as indicated in Fig. 5 by the arrow. Generally speaking, however, the gas data confirm the temperatures suggested by Fig. 4.

According to Fig. 5, CO<sub>2</sub> and CH<sub>4</sub> appear to be in chemical equilibrium, their relative proportions, therefore, may differ greatly from those in any source components. In this case, their isotopic compositions, especially that of the minor species CO<sub>2</sub>, cannot be used anymore either as indicator of their origin. By use of the few data available for the isotopic composition of both CO<sub>2</sub> and CH<sub>4</sub>, <sup>13</sup>C-equilibration temperatures for Morere (23) are about 160°C, rising to 200 and 240°C for Tiromoana (22), Marapua (36) and Te Puia (12), with the highest of just over 300°C for Waitangi Oil (13). Taking into account the extreme slowness in the rates of <sup>13</sup>C-equilibration at these low temperatures (Giggenbach, 1982), the gases appear nevertheless to be quite advanced on their way to isotopic equilibrium. As discussed in more detail by Lyon et al. (1992), <sup>13</sup>C and <sup>2</sup>H of the CH<sub>4</sub> suggest thermogenic production from mature source rocks.

The average δ<sup>13</sup>C value of the east coast carbon, as represented by that of methane, of -42±8‰ is far from that of the carbon discharged from the geothermal systems over the Taupo Volcanic Zone of -6±3‰, or even that of CH<sub>4</sub> of -27±3‰ (Lyon and Hulston, 1984). The finding suggests that the isotopic composition of the CH<sub>4</sub> discharged from the accretionary wedge is not representative of that of the carbon involved in the formation of the gases produced from the volcanic and geothermal systems to the west. As discussed earlier (Giggenbach, 1992a), much of the subducted C is likely to be present in the form of carbonates. Assuming that CH<sub>4</sub> has formed in equilibrium with marine carbonates with δ<sup>13</sup>C

values close to 0‰, the  $\delta^{13}\text{C}$  values of the  $\text{CH}_4$  would correspond to apparent isotopic equilibration temperatures of between 80 and 200°C (Bottinga, 1969). Equilibrium of  $\text{CO}_2$  with calcite at temperatures of about 100°C is supported by the high  $\delta^{13}\text{C}$  value of the  $\text{CO}_2$  of sample (36). For the others, the comparatively low values of -15 to -12‰ may reflect the effects of kinetic processes during chemical equilibration of the  $\text{CO}_2$  with  $\text{CH}_4$ , or of bacterial oxidation of  $\text{CH}_4$  (Coleman et al., 1981).

The contents of higher hydrocarbons, as given in Table 3, are generally very low, an observation compatible with essentially "inorganic" formation of the  $\text{CH}_4$ , possibly through reduction of carbonate. According to Schoell (1983) such gases may, however, also be formed thermogenically from organic sedimentary material by a number of processes and no definite answer as to the origin and history of the hydrocarbons is possible.

Another check on the possible origin of  $\text{CH}_4$  is carried out in Fig. 6 on the basis of relative  $\text{CH}_4$ ,  $^3\text{He}$  and  $^4\text{He}$  contents. For purely crustal origin of the He, data points should lie along the right margin of the diagram in an area marked "crustal", at values of  $R/R_A < 0.1$ ; the composition of very low  $\text{CH}_4$  mantle gases is also given. As shown in Table 2, virtually all the gases have higher values of  $R/R_A$ , some reaching values of  $3.35 R_A$  indicating the

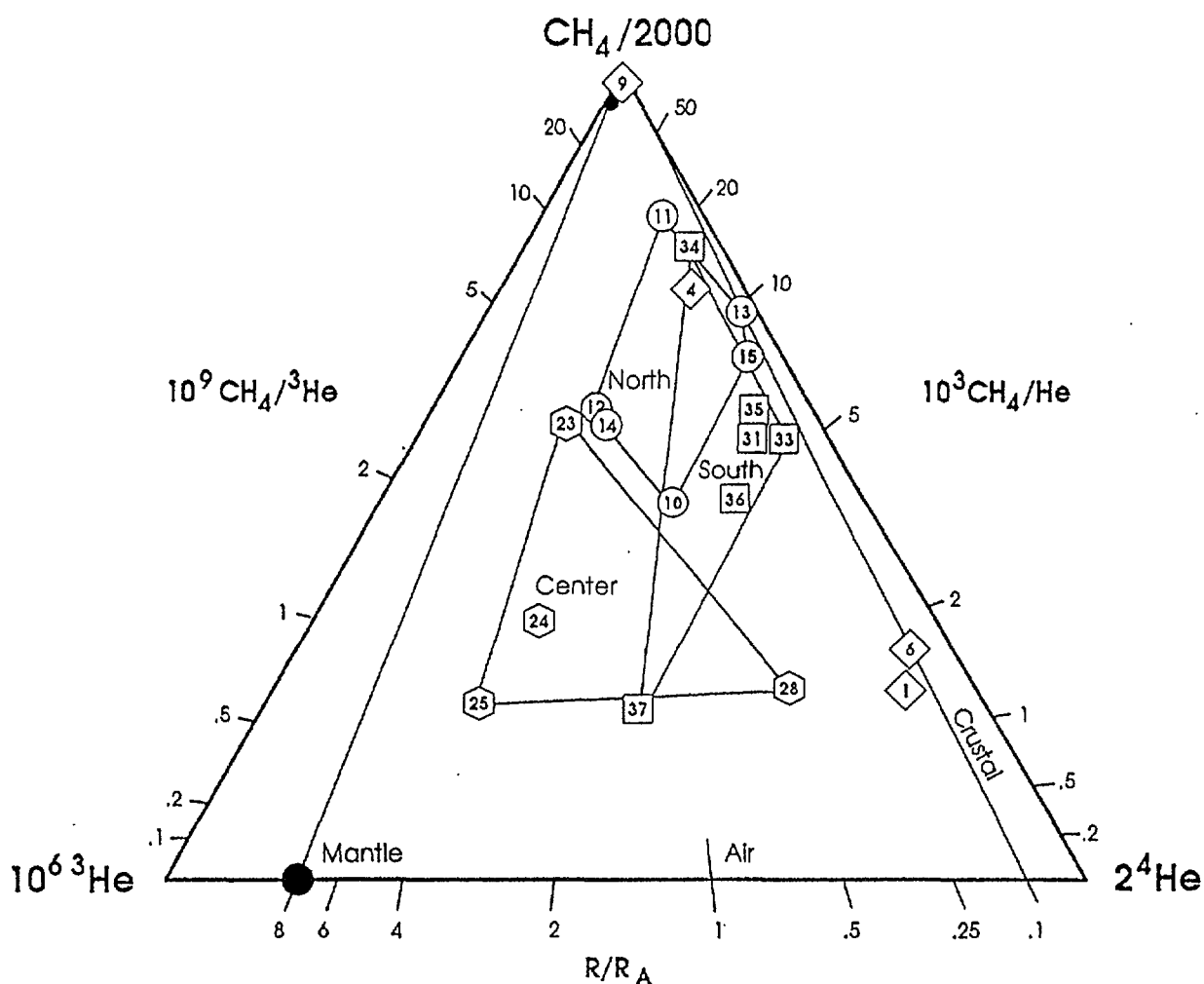


Fig. 6- Relative  $\text{CH}_4$ ,  $^3\text{He}$ ,  $^4\text{He}$  contents of gases from the NE part of the North Islands. For symbols see Fig. 1.

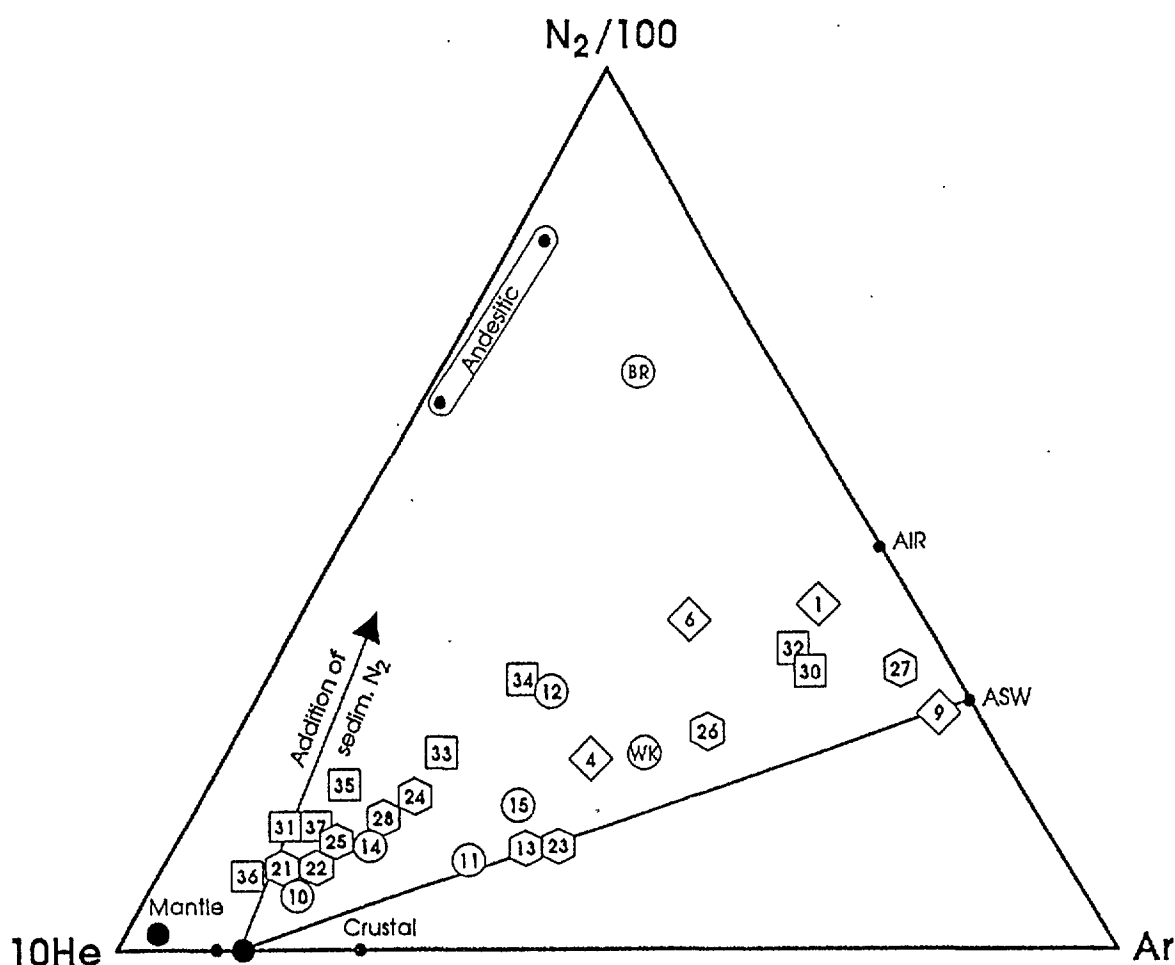


Fig. 7- Relative  $N_2$ , He and Ar contents of gases from the NE part of the North Island.

presence of considerable proportions of mantle He. As discussed earlier (Giggenbach et al., 1993), the most likely path for this mantle He to reach the obviously quite shallow levels of generation of the bulk of the east coast gases, is along the fracture zone separating the overriding from the subducting plate.

Gases from the central sector of the east coast show the highest enrichment in  $^3\text{He}$ . At the same time they were found to contain the highest proportions of seawater (Fig. 3) suggesting this sector to be most "open" to the transport of both seawater from above and mantle gases from below. Conversely, the gases from the southern sector appear to be least affected by the addition of mantle volatiles. There are, in Fig. 6, no obvious trend lines pointing to the existence of well defined endmember components with distinct  $^3\text{He}/\text{CH}_4$  or  $^4\text{He}/\text{CH}_4$  ratios suggesting that production and transport of the He species are entirely decoupled from the formation of  $\text{CH}_4$ .

After  $\text{CH}_4$ ,  $N_2$  is frequently the next most important constituent of the gases listed in Table 2. Its possible origins may be evaluated by use of Fig. 7 in terms of relative  $N_2$ , He and Ar contents. Five potential endmember components are shown: air and air saturated waters (asw, at  $10^\circ\text{C}$ ) along the  $N_2$ -Ar axis, "andesitic" and "mantle" gases as defined by Giggenbach (1992b), and a "crustal" gas with a He/Ar ratio corresponding to the  $^4\text{He}/^{40}\text{Ar}$  production ratio of  $0.6 \pm 0.3$  typical of New Zealand crustal rocks (Giggenbach et al., 1993).

Most of the data points lie within, or close to the triangle outlined by the two atmospheric components and the He corner. The set of gases with highest relative He contents includes samples with both high and low  $^3\text{He}/^4\text{He}$  ratios. This is not too surprising taking into account the  $^3\text{He}/^4\text{He}$  ratio of 8.0 of the likely mantle endmember component. Even sample (25) with the highest value of  $R/R_A$  of 3.35 would only contain about 42% of mantle He. For the remainder of the samples, the crustal component is even more predominant and mixing relationships may be discussed in terms of the two endmember components asw and New Zealand crustal gases.

Accepting that these two components supply most of the He and Ar, the distribution of data points in Fig. 7 suggests addition of significant amounts of  $\text{N}_2$ . Part of this may be due to contamination by air itself. Even allowing for this, most of the high He samples have  $\text{N}_2/\text{Ar}$  ratios  $>50$  or exceeding 100, not enough to raise  $\text{N}_2/\text{Ar}$  ratios to those of the "andesitic" gases, but well above those of mantle gases of 30 (Giggenbach, 1992b). The probably sedimentary source of this excess  $\text{N}_2$ , if surviving subduction, may be the source of the increased  $\text{N}_2$  in "andesitic" gases.

Summing up findings based on the chemical composition of the water and gas samples, relative Cl, Br, B and Li contents of the waters are compatible with the assumption that they represent mixtures of seawater and water of dehydration of marine clays. Seawater contributions and relative Cl contents are highest ( $\text{B}/\text{Cl} < 0.005$ ) over the central sector of the east coast. The  $\text{B}/\text{Cl}$  ratios of the other samples approach those of waters discharged over the Taupo Volcanic Zone of  $0.03 \pm 0.015$ . Na, K and Mg contents suggest close attainment of water-rock equilibrium at temperatures between 60 to  $110^\circ\text{C}$ .  $\text{CO}_2/\text{CH}_4$  and  $\text{CO}_2/\text{Ar}$  ratios are close to those expected for equilibrium of these gases with rock at somewhat higher temperatures of  $120 \pm 20^\circ\text{C}$ . The isotopic composition of the C-species suggests a thermogenic origin. The He isotopic composition with  $R/R_A$  values up to 3.35 indicate addition of up to 42% of mantle He. At present, this He is assumed to have moved up from the mantle along the fracture plane separating the overriding from the downgoing plate. The highest  $^3\text{He}$  contents are observed over the central sector. Relative  $\text{N}_2$ , He, Ar contents suggest that the gases represent mixtures of crustal and meteoric gases and excess  $\text{N}_2$ , probably derived from the subducted sediments.

## 5. GENERAL DISCUSSION

The conclusions based on the chemical composition of the discharges generally agree with those obtained by use of the isotopic composition of the waters (Fig. 2). A more detailed check on the findings is carried out in Fig. 8 on the basis of variations in  $\delta^{18}\text{O}$  and  $\delta^2\text{H}$  with Cl contents. Again samples from the northern, central and southern sectors form distinct groups. In the  $\delta^2\text{H}$  versus Cl plot of Fig. 8A, most data points follow closely a line linking local groundwater (GW,  $\delta^2\text{H} = -30\text{‰}$ ) to seawater (SW). One sample deviating greatly from this trend is that representing water discharges from springs on Mahia Peninsula. Its Cl content is with 25720 mg/kg well above that of 19400 mg/kg of seawater, its formation can, therefore, in no way be explained in terms of mixing of seawater with waters of dehydration of clays.

The processes usually invoked to explain increases in salinity are boiling and evaporation. Both can be excluded to be of any relevance in the low temperature systems discussed here. Another process giving rise to increased salinities is mixing with more saline brines or leaching of evaporitic material. In both cases formation of these, within the

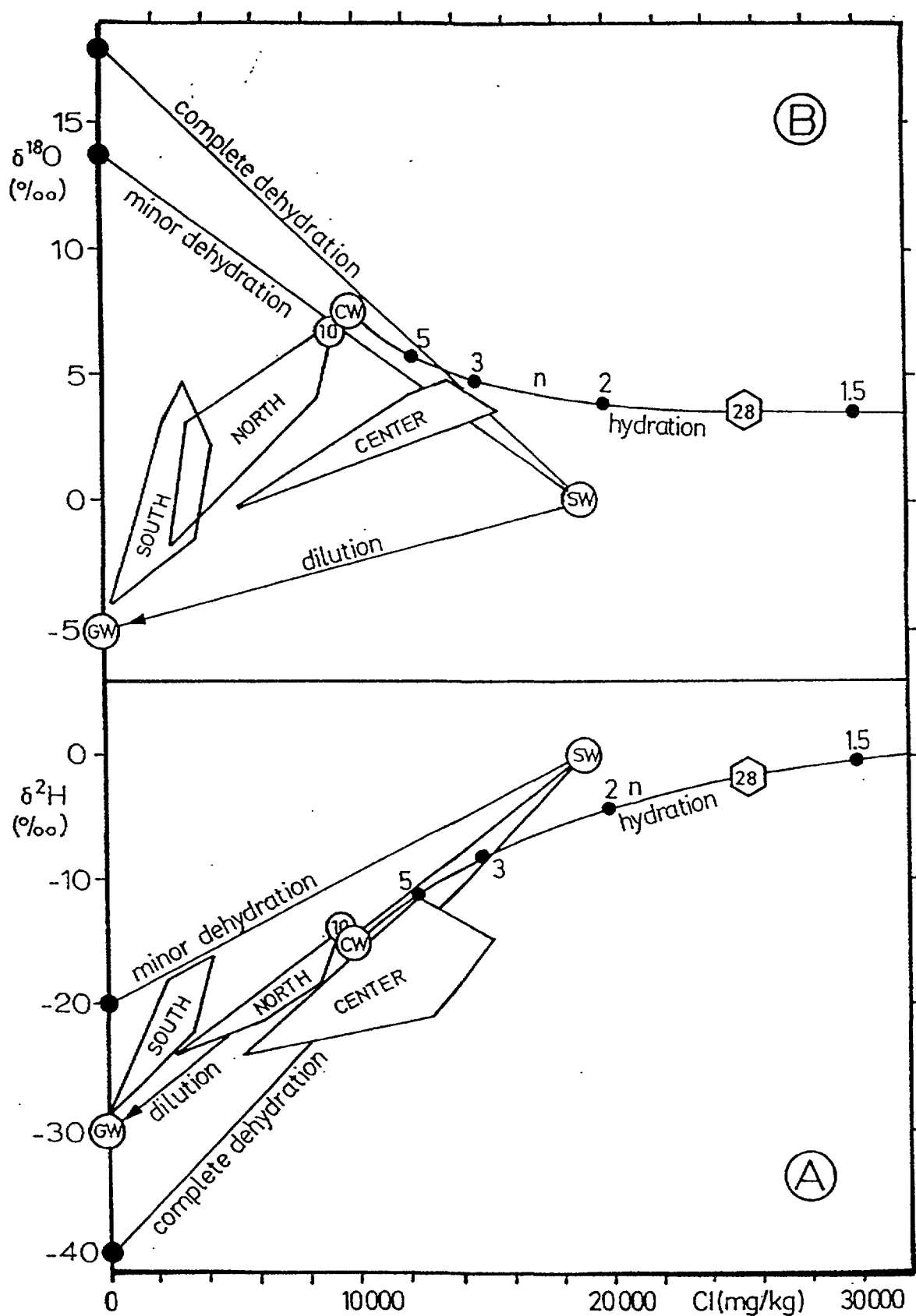


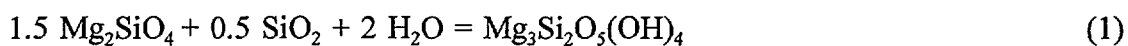
Fig. 8- Plots of  $\delta^2\text{H}$  (A) and  $\delta^{18}\text{O}$  (B), in ‰ SMOW, versus Cl contents, in mg/kg. The curved lines represent variations in the composition of residual waters remaining after hydration of basalt as a function of  $n$ , the ratio of water present to that required to complete the hydration reaction.

geological environment considered here, would have to be explained first. In addition, any suitable process would have to lead to increases in both  $\delta^2\text{H}$  and  $\text{Cl}$ , at a decrease in  $\delta^{18}\text{O}$ .

The most likely process to achieve an increase in salinity and the observed changes in isotopic compositions is the one representing the reverse of the dehydration process, the hydration of anhydrous minerals. The marine sediments, having formed in contact with seawater are unlikely to represent a significant sink for water. The most likely supply of anhydrous material are oceanic basalts generated along mid-ocean ridges or hot spot tracks.

Recently, Glover and Hunt (1994) discussed the possibility that major positive magnetic anomalies observed at several locations along the east coast of the North Island are caused by Cretaceous seamounts being subducted beneath the accretionary prism. The positions of the two major anomalies coincide with the two areas of increased water temperatures and  $^3\text{He}/^4\text{He}$  ratios centered on Te Puia (12) and Morere (23). Glover and Hunt (1994) are able to model the observed magnetic anomalies in terms of a body resembling a seamount with its top at a depth of some 15 to 20 km, 65 km wide and 5 km thick. The disturbances caused by the subduction of such a body on the nature and distribution of fluids over the affected zones can be expected to be considerable. On the one side, mechanical separation of the two plates to accommodate the bulk of the dragged-down seamount is likely to lead to highly increased local permeabilities facilitating both the inflow of fluids from above and below. Extensive fracturing and comminution of the extra material to be subducted will also provide highly reactive mineral surfaces for increased water-rock interaction.

Interaction of seawater, or any other water present, with finely ground basalt, at the temperatures suggested by the geothermometers, is likely to lead to highly hydrated phases such as chlorite or serpentine as symbolised by the reaction



Assuming this reaction to be representative of the hydration process, the changes in the isotopic composition of the residual water may be evaluated by use of the isotopic balances

$$7\delta^{18}\text{O}_{\text{rp}} + 2n\delta^{18}\text{O}_{\text{wi}} = 9\delta^{18}\text{O}_{\text{rs}} + 2(n - 1)\delta^{18}\text{O}_{\text{wf}} \quad (2)$$

and

$$0\delta^2\text{H}_{\text{rp}} + 4n\delta^2\text{H}_{\text{wi}} = 4\delta^2\text{H}_{\text{rs}} + 4(n - 1)\delta^2\text{H}_{\text{wf}} \quad (3)$$

where the subscripts rp and rs refer to the isotopic compositions of primary and secondary rock, and wi and wf to the initial and final composition of the waters, n represents the ratio of the amount of water present in the equilibration zone, to that required to complete reaction (1) (Giggenbach, 1993). Together with  $\varepsilon = \delta_{\text{rs}} - \delta_{\text{wf}}$ , the final compositions of the waters, as a function of n, become

$$\delta^{18}\text{O}_{\text{wf}} = (7\delta^{18}\text{O}_{\text{rp}} + 2n\delta^{18}\text{O}_{\text{wi}} - 9\varepsilon_{18\text{O}})/(7 + 2n) \quad (4)$$

and

$$\delta^2\text{H}_{\text{wf}} = \delta^2\text{H}_{\text{wi}} - \varepsilon_{2\text{H}}/n \quad (5)$$

Values of n may be obtained simply by use of the relationship

$$n = \text{Cl}_f / (\text{Cl}_f - \text{Cl}_i) \quad (6)$$

where the subscripts f and i refer to final and initial Cl contents. In the case of the Mahia sample (28),  $\text{Cl}_f$  corresponds to 25720 mg/kg. A reasonable value of  $\text{Cl}_i$  may be obtained by

assuming the deep water available for hydration of the basalt to represent the least groundwater-diluted mixture of seawater and water of dehydration of clays. By use of Fig. 2, the composition of this water (CW) was obtained by extrapolating the dilution trend onto the seawater-clay water mixing line. The corresponding value for  $\delta^{18}\text{O}$  is +7.5‰, for  $\delta^2\text{H}$  it is -15‰. Point (CW) lies just beyond that of sample (10) with a Cl content of 9250 mk/kg. To a first approximation, the Cl content of the deep mixture was taken to be 10 000 mg/kg. Inserted into eqn (6), the value of  $n$  becomes 1.64 implying that the original water content of the reaction environment contained only 64% more water than the amount used up in the hydration of the basalt.

In the application of eqns (4) and (5), major problems arise from the correct choice of fractionation factors  $\epsilon_{18\text{O}}$  and  $\epsilon_{2\text{H}}$  which are both functions of the actual minerals involved and temperature. Rather than trying to evaluate a series of final water compositions as a function of highly uncertain values of  $\epsilon$ , eqns (4) and (5) were rearranged to yield values of the fractionation factors compatible with the formation of water (28) from water CW. They were found to be -21.3‰ for  $^2\text{H}$  and +3.7‰ for  $^{18}\text{O}$ . Based on the experimental values reported by Taylor (1974), they would correspond to temperatures of interaction with hydrous minerals (chlorite, serpentine, montmorillonite or kaolinite) of between 100 and 200°C, a range compatible with the temperatures derived above. Fig. 8 shows curves representing variations in  $\delta_{\text{wf}}$  as a function of  $n$ . According to the trend in Fig. 8B, the higher Cl waters from the central sector, apart from (28) may well have been affected by the basalt hydration process too, albeit at higher values of  $n$  of about 3.

Assuming the fractionation factors accompanying basalt hydration, as derived above, to be valid for water-rock interaction in this environment generally, lines were drawn in Fig. 8 representing mixing of seawater with waters resulting from complete to minor degrees of dehydration of clays. In the first case, the composition of the water corresponds to that of the parent mineral; in the second case, the water released can be expected to be close to equilibrium with the parent clay and, therefore, to be enriched in  $^2\text{H}$ , but depleted in  $^{18}\text{O}$ . The resulting compositional ranges are delineated in Fig. 8 by lines marked complete and minor dehydration. The point representing CW lies half-way between these lines in both Fig. 8A and B.

According to Fig. 8A, the waters discharged from the southern sector are likely to represent variably diluted mixtures of waters resulting from minor dehydration of clays with minor proportions of seawater, possibly reflecting the young age and low permeability to seawater of the sedimentary environment there. Low permeabilities to fluids generally is also supported by the low  $^3\text{He}/^4\text{He}$  ratios of the gases there (Fig. 6). The opposite is suggested for the waters from the central sector where the position of data points corresponds to high degrees of dehydration of subducted sediments and of mixing with seawater. In part, the high salinities may be due to hydration of basalt as discussed above. Waters from the northern sector occupy intermediate positions.

The above findings on the isotopic evolution of the waters are summarised in Fig. 9. Most of the data points fall within an area outlined by a dilution line linking local groundwater to the endmember component CW, itself a mixture of seawater and water of dehydration of subducted clays, and the curved line representing the composition of waters remaining after hydration of subducted basalt. The composition of the water in the minerals (chlorite, serpentine) formed through hydration of basalt, as a function of  $n$ , is given by the line "hydrated basalt". The hydrous mineral formed in equilibrium with water (28) has a  $\delta^2\text{H}$  value of -28‰, close to that of -30‰ required for the subducted material acting as the source



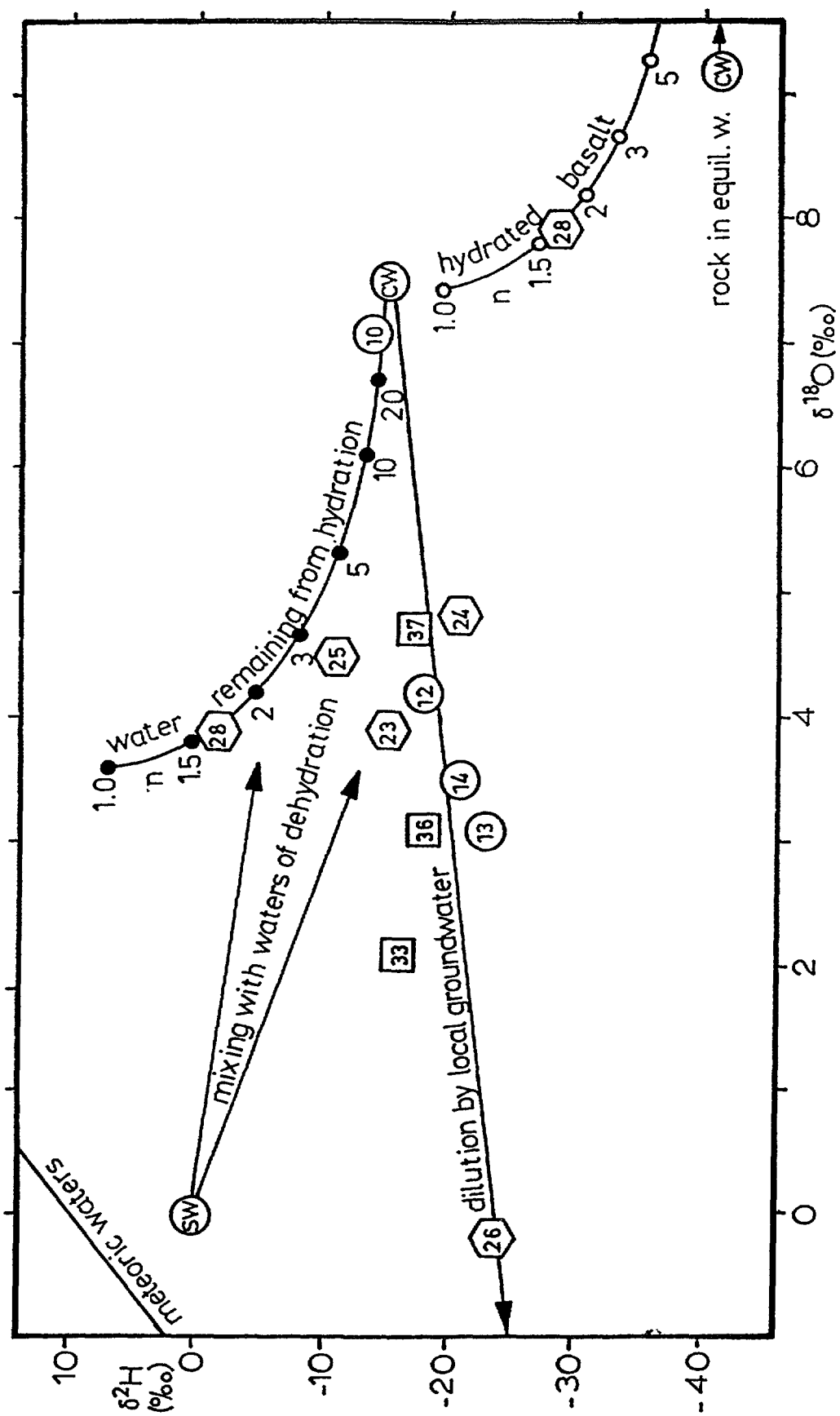


Fig. 9- Plot of  $\delta^2\text{H}$  versus  $\delta^{18}\text{O}$ , in ‰ SMOW, for waters from the NE part of the North Island. See text.

for "andesitic" waters (Giggenbach, 1992a). The clays in isotopic equilibrium with CW, should have a  $\delta^2\text{H}$  value of -41‰. Assuming that not all the intermediate endmember water CW is expelled, but is at least in part subducted together with the clays, the  $\delta^2\text{H}$  values of the total amount of water reaching the zones of arc magma generation should be somewhere within  $-28\pm 12\text{‰}$ , a range again agreeing with that postulated by Giggenbach (1992a).

There appear to be no obvious limits on the concentrations of Cl in these fluids. The value of 10 000 mg/kg for CW cannot be considered representative as a number of feasible processes may conspire to increase or decrease Cl concentrations during the conversion of subducted material to magmatic, volcanic and geothermal volatiles. The actual processes, however, appear to affect relative Cl, Br and B contents, as derived for CW, only little. The above discussion is based on the implicit assumption that the waters and gases discharged along the east coast of the North Island reflect to some degree the composition of subducted fluids and minerals. There are, however, no unequivocal indications that the fluids sampled are actually derived from the subducting, rather than the accreting sediments.

According to Davey et al. (1986), the depth to the top of the subducting plate beneath the study area is some 14 km. Accepting the temperatures of 100 to 200°C, as indicated by the chemical and isotopic compositions, to be representative of fluid-rock interaction at this depth, the area should be characterised by a very low geothermal gradient of only about 10°/km. According to a numerical simulation by Peacock (1991), such low temperatures, at these depths, are well possible. The temperatures in subduction zones are mainly a function of the amount of oceanic crust subducted, its age and the rate of convergence. The high rate of convergence for the Hikurangi margin is with 50 mm/a almost twice that used by Peacock (1991) of 30 mm/a, thus favoring even lower temperatures. In this case, derivation of the fluids through dewatering of sediments subducted beneath the east coast is not inconceivable. Formation of the high Cl waters, as discharged at Mahia, through interaction with subducted basalt, may be taken as evidence that at least these waters are derived from subduction zone depths. Locally increased heatflows (Pandey, 1981) may be explained in terms of the rise of warm fluids expelled at great depths.

**Acknowledgement** - *The authors want to thank D Francis, consultant, for the collection of some of the water and gas samples.*

## References

- Bebout G E, Ryan J G and Leeman W P (1993) B-Be systematics in subduction- related metamorphic rocks: Characterisation of the subducted component. *Geochim. Cosmochim. Acta* **57**, 2227-2237.
- Bottinga Y (1996) Calculated fractionation factors for carbon and hydrogen-exchange in the system calcite-graphite-carbon dioxide-methane-hydrogen and water vapor. *Geochim. Cosmochim. Acta* **33**, 49-64.
- Capuano R M (1992) The temperature dependence of hydrogen fractionation between clay minerals and water: Evidence from a geopressured system. *Geochim. Cosmochim. Acta* **56**, 2547-2554.

- Cole J W (1990) Structural control and origin of volcanism in the Taupo Volcanic Zone, New Zealand. *Bull. Volcanol.* **52**, 445-459.
- Coleman D D, Risatti J B and Schoell M (1981) Fractionation of carbon and hydrogen isotopes by methane-oxidising bacteria. *Geochim. Cosmochim. Acta* **45**, 1033-1037.
- Craig H (1963) The isotopic geochemistry of water and carbon in geothermal areas. *In: Nuclear Geology on Geothermal Areas*, CNR, Pisa 17-53.
- Davey F J, Hampton M, Childs J, Fisher M A, Lewis K and Pettinga J R (1986) Structure of a growing accretionary prism, Hikurangi margin, New Zealand. *Geology* **14**, 663-666.
- Ellis A J and Sewell J R (1963) Boron in waters and rocks of New Zealand hydrothermal areas. *NZ J Sci.* **6**, 589-606.
- Giggenbach W F (1982) Carbon-13 exchange between CO<sub>2</sub> and CH<sub>4</sub> under geothermal conditions. *Geochim. Cosmochim. Acta* **46**, 159-165.
- Giggenbach W F (1988) Geothermal solute equilibria. Derivation of Na-K-Mg-Ca-geoindicators. *Geochim. Cosmochim. Acta* **52**, 2749-2765.
- Giggenbach W F (1989) The chemical and isotopic position of the Ohaaki Field within the Taupo Volcanic Zone. *Proc. NZ Geothermal Workshop* **11**, 81-88.
- Giggenbach W F (1991) Chemical techniques in geothermal exploration. *In Application of Geochemistry in Geothermal Reservoir Development*. F D'Amore ed.. UNITAR-UNDP 119-144.
- Giggenbach W F (1992a) Isotopic shifts in waters from geothermal and volcanic systems along convergent plate boundaries and their origin. *Earth Planet. Sci. Lett.* **113**, 495-510.
- Giggenbach W F (1992b) The composition of gases in geothermal and volcanic systems as a function of tectonic setting. *Proc. Water-Rock Interaction* **7**, 873-878.
- Giggenbach W F (1993) Reply to comment by P Blattner: "Andesitic water": a phantom of the isotopic evolution of water-silicate systems. *Earth Planet. Sci. Lett.* **120**, 519-522.
- Giggenbach W F and Stewart M K (1982) Processes controlling the isotopic composition of steam and water discharges from steam vents and steam-heated pools in geothermal areas. *Geothermics* **11**, 71-80.
- Giggenbach W F, Sano Y and Wakita H (1993) Isotopic composition of helium, and CO<sub>2</sub> and CH<sub>4</sub> contents in gases produced along the New Zealand part of a convergent plate boundary. *Geochim. Cosmochim. Acta* **57**, 4327-4355.
- Glover R B and Hunt T M (1994) Chemistry and origin of strongly mineralised waters from a Cenozoic accretionary prism on the east coast, North Island, New Zealand. *Geology* (in prep.).

- Goguel R L (1983) The rare alkalies in hydrothermal alteration at Wairakei and Broadlands geothermal fields, New Zealand. *Geochim. Cosmochim. Acta* **47**, 429-437.
- James A T and Baker D R (1976) Oxygen isotope exchange between illite and water at 22°C. *Geochim. Cosmochim. Acta* **40**, 235-239.
- Kastner M, Elderfield H and Martin J B (1991) Fluids in convergent margins: what do we know about their composition, origin, role in diagenesis and importance for oceanic chemical fluxes? *Phil. Trans. R. Soc. Lon. A* **335**, 243-259.
- Liu K and Epstein S (1984) The hydrogen isotope fractionation between kaolinite and water. *Isotope Geoscience* **2**, 335-350.
- Lyon G J, Giggenbach W F and Francis D (1992) The stable isotopic composition of some east coast natural gases. *Proc. 1991 NZ Oil Exploration Conf.* 310-319.
- Lyon G L and Hulston J R (1984) Carbon and oxygen isotopic composition of New Zealand geothermal gases. *Geochim. Cosmochim. Acta* **48**, 1161-1171.
- Moore J C and Vrolijk P (1992) Fluids in accretionary prisms. *Rev. Geophys.* **30**, 113-135.
- Moran A E, Sisson V B and Leeman W P (92) Boron depletion during progressive metamorphism: implications for subduction processes. *Earth Planet. Sci. Lett.* **111**, 331-349.
- O'Neil J R and Kharaka Y K (1976) Hydrogen and oxygen isotope exchange reactions between clay minerals and water. *Geochim. Cosmochim. Acta* **40**, 241-246.
- Pandey O P (1981) Terrestrial heat flow in New Zealand. PhD Thesis, Victoria University, Wellington
- Peacock S M (1991) Numerical simulation of subduction zone pressure-temperature-time paths: constraints on fluid production and arc magmatism. *Phil. Trans. Roy. Soc. Lon.* **335**, 341-353.
- Reyners M (1980) A microearthquake study of the plate boundary, North Island, New Zealand. *Royal Astron. Soc. Geophys. J.* **63**, 1-22.
- Savin S M and Epstein S (1970) The oxygen and hydrogen isotope geochemistry of clay minerals. *Geochim. Cosmochim. Acta* **34**, 25-42.
- Schoell M (1983) Genetic characterisation of natural gases. *Amer. Assoc. Petrol. Geol. Bull.* **67**, 2225-2238.
- Stewart M K and Taylor C B (1981) Environmental isotopes in New Zealand hydrology. Part I, Introduction: The role of oxygen-18, deuterium and tritium in hydrology. *NZ J Science* **24**, 295-311.
- Taylor H P (1974) The application of oxygen and hydrogen isotope studies to problems of hydrothermal alteration and ore deposition. *Econ. Geol.* **69**, 843-883.

- Walcott R J (1978) Present tectonics and late Cenozoic evolution of New Zealand. Royal Astronom. Soc. Geophys. J. **52**, 137-164.
- Yeh H-W (1980) D/H ratios and late-stage dehydration of shales during burial. Geochim. Cosmochim. Acta **44**, 341-352.
- Yeh H-W and Epstein S (1978) Hydrogen isotope exchange between clay minerals and seawater. Geochim. Cosmochim. Acta **42**, 140-143.

# ISOTOPE AND GEOCHEMICAL SURVEY OF GEOTHERMAL SYSTEMS OF YOZGAT PROVINCE IN CENTRAL ANATOLIA, TURKEY

Ş. ŞİMŞEK

International Research and Application Center for  
Karst Water Resources (UKAM),  
Hacettepe University,  
Ankara, Turkey

**Abstract** - *In Central Anatolia, which is subject to this project area, there are many geothermal fields. Turkish State Planning Organization (DPT) gives priority and encouragement to the investments of tourism and energy production. Our studies, in Central Anatolia are planned to focus on mainly Yozgat- Nevşehir region. But only Yozgat province results will be given in this paper.*

*Detailed hydrogeological and hydrogeochemical studies have been carried out and periodic hydrogeochemical analyses made in Hacettepe University International Research and Application Center For Karst Water Resources (UKAM) Laboratories. Analyses of samples ( $^2\text{H}$ ,  $^{18}\text{O}$ ,  $^3\text{H}$ ) which were periodically collected from thermal and cold water spots in the project area have been made in IAEA.*

*Hydrogeologic models for important geothermal fields in Yozgat region have been realized as a result of this study. Following are the results obtained from the isotopic evaluations of the geothermal fields;*

- *According to the  $\delta^{18}\text{O}$  vs.  $\delta^2\text{H}$  relation of rain and snow water samples, the project area represents a climatic transition zone between the East Mediterranean and Central Anatolia Climatic - Geographic Regions by the local meteoric line equation of  $\delta^2\text{H}=8*\delta^{18}\text{O}+14$ .*
- *According to the tritium analyses, thermal waters have deep and long groundwater flow paths and these waters are generally older than 50 years.*
- *According to the  $\delta^{18}\text{O}$  vs.  $\delta^2\text{H}$  relation, there are  $^{18}\text{O}$  shift in Yozgat-Saraykent, Boğazliyan and Sorgun.*
- *Yozgat-Saraykent, Sorgun and Boğazliyan geothermal fields are important for geothermal applications as mainly central heating and balneological utilization possibilities.*

## 1. INTRODUCTION

Türkiye has a high potential in terms of geothermal energy as a result of its suitable geological situation for the occurrence of geothermal energy resources; the presence of active volcanism, horst-graben systems and hydrothermally altered areas. There are a total of 900 thermal and mineral water spring groups in Türkiye .

The first important project was conducted by UNDP-MTA at Denizli-Kızıldere Area in 1968. As a result of this project, a geothermal field (212°C) was discovered and first 20 MW pilot power plant installed in 1984 by Turkish Electric Authority. Also many fields such as Aydın-Germencik (232°C), Çanakkale-Tuzla (174°C), Kütahya-Simav (162°C) fields have been discovered at present. Approximately 12000

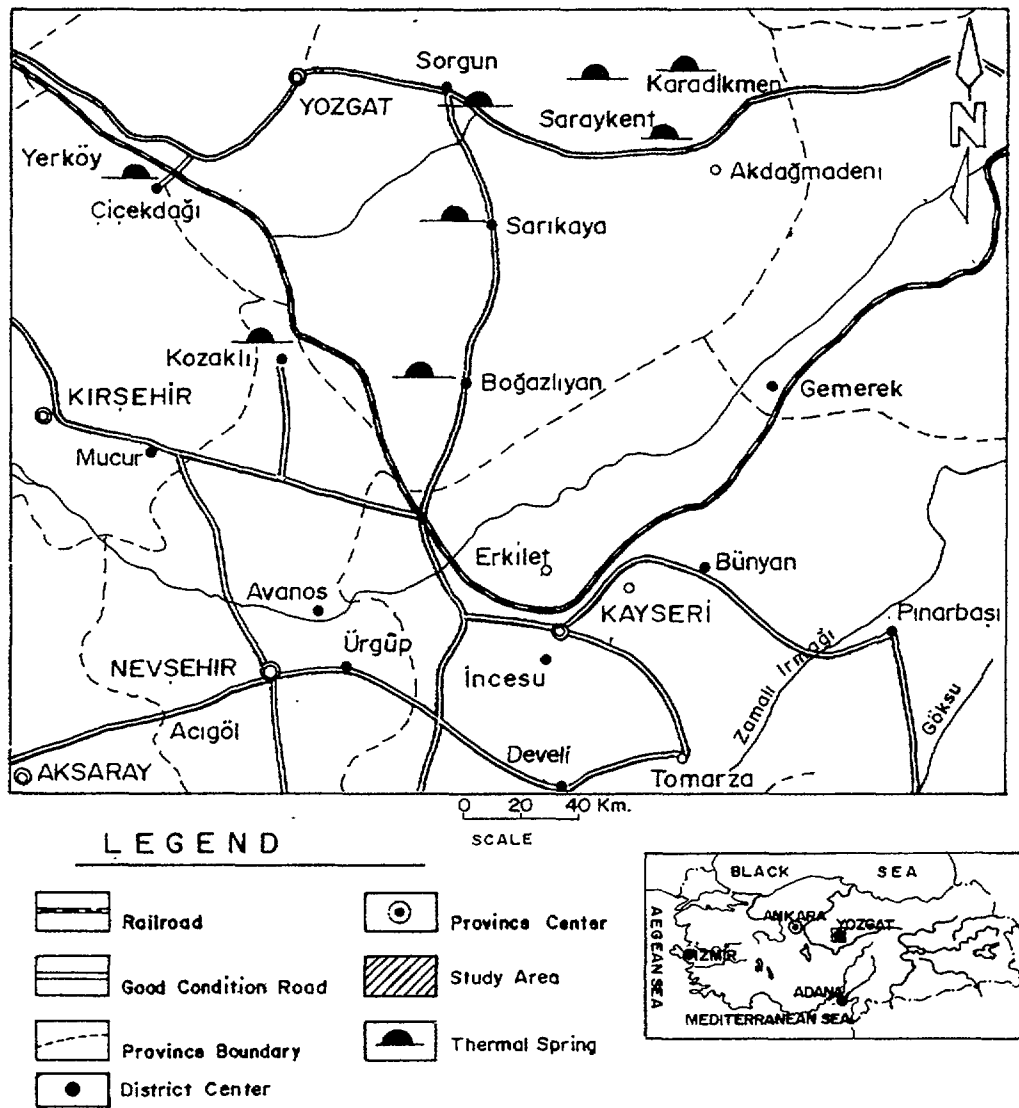


FIG. 1. Location of the study area.

residences and 110000 m<sup>2</sup> greenhouses are heated by geothermal energy (140 MWt). On the other hand, an installation for the production of CO<sub>2</sub> with a capacity of 40000 tons/year established in 1986 [17,18].

The participation of international organizations to Türkiye's geothermal energy investigations have always been encouraged and sought. With such a cooperation utilizing the expertise and newly developed investigation techniques of related international organizations will to help determine the geothermal energy resources potential of a given region.

New developments on exploration methods enhanced hydrogeochemical applications [1, 7, 10, 14 and 19, 21]. Especially by overcoming the problems due to chemical composition of geothermal fluids, new progresses have been recorded such as more precise estimation of reservoir temperature and applications of geothermometer and solution of scaling problem. However isotope techniques which provides a better investigation and usage in hydrochemical methods are not being widely used now a days. By using these methods, it will be easier to establish a precise hydrogeologic-geothermal model and therefore a modern exploration will be provided. Isotopic studies have been made some of the areas in Türkiye [4, 5, 13].

As a part of the IAEA's "Isotope and Geochemistry in Geothermal Exploration in Africa, Asia and Pacific and the Middle East" coordinated project program, the Isotope Survey of Geothermal systems of Central Anatolia sub project started. Yozgat province was selected for pilot study area (Figure 1). Selection criteria of project areas are given below;

- a- The occurrence of thermal springs with the highest temperatures in the region;
- b- The presence of varying magmatic (intrusive and volcanic) metamorphic and sedimentary reservoir and cap rock in the region;
- c- The presence of varying thermal springs in temperature (low-high) at the same field;
- d- The presence of geothermal fields in which the hydrogeological conditions are disturbed by mining activities;
- e- The presence of geothermal fields where investment plans for geothermal energy use are considered by government and/or private enterprises;

This project was commenced in July in 1992. The program includes :

- Detailed hydrogeological investigations of thermal resources of the pilot area,
- Isotopic surveys.

## 2. RESULTS OF THE HYDROGEOLOGICAL-GEOCHEMICAL AND ISOTOPE SURVEY OF THE PROJECT AREA

Yozgat province is located in the Central Anatolia and situated 200 km east of Ankara . Total 8 fields are situated in Project area (Yozgat-7, Nevşehir 1). These fields are, Sorgun, Saraykent, Boğazlıyan, Sarıkaya, Yerköy, Karadikmen in Yozgat and Kozaklı area in Nevşehir. But as a result of this study important potential have been determined in Yozgat Sorgun, Saraykent and Boğazlıyan Geothermal Areas (Figure 1). Climate of the area is a typical continental condition as semi-arid climate. Spring time is the mainly rainy season. The lithology types of reservoir and cap rock of the geothermal fields in project area are listed in Table I. Result of chemical analyses and isotopic data for the project area listed in Table II and III.

### 2.1. Sorgun Geothermal Area

Sorgun Geothermal Area is located 40 km east of Yozgat City and of Sorgun Town. This field is situated on Yozgat-Sivas highway. Average precipitation is 428.3 mm/year during 1960-1990 period.

TABLE I. THE LITHOLOGY TYPES OF RESERVOIR AND CAP ROCK IN THE YOZGAT GEOTHERMAL FIELDS

FIELDS	RESERVOIR ROCK		CAP ROCK	
	LITHOLOGY	AGE	LITHOLOGY	AGE
SORGUN	GRANITE	Paleocene	S.D.	Eocene
SARAYKENT	RHYOLITE	Paleogene ?	RHYOLITE, TUFF	Paleogene ?
BOGAZLIYAN	KARSTIC LMS	Eocene	S.D	Eocene

S.D. : Sedimentary deposits (mainly clay, sandstone, marl, conglomerate alternation)



TABLE II. ISOTOPIC ANALYSES RESULT FOR GEOTHERMAL FIELDS IN THE YOZGAT REGION

NO	DATE	OXYGEN-18	DEUTERIUM	TRITIUM	EXPLANATIONS
Y1-3	APR.-92	-10.86	-82.80	2.30 ± 0.30	SORGUN (Hot Water)
Y2-5	AUG.-92	-10.90	-84.30	2.70 ± 0.30	SORGUN (Hot Water)
Y5-2	MAR.-93	-11.23	-85.10	1.30 ± 0.30	SORGUN (Hot Water)
Y1-5	APR.-92	-10.08	-76.80	9.90 ± 0.50	SORGUN (Hot Spring Water)
Y1-4	APR.-92	-9.47	-69.90	17.70 ± 0.70	SORGUN (Cold Water)
Y2-4	AUG.-92	-9.27	-70.50	20.70 ± 0.90	SORGUN (Stream Water)
Y5-2K	MAR.-93	-9.91	-59.00	9.90 ± 0.40	SORGUN (Snow Water)
R5	NOV.-92	-12.91	-97.50		SORGUN (Rain Water)
R4	NOV.-92	-19.06	-137.70		EYMIR (Rain Water)
Y1-6	APR.-92	-9.43	-85.10	0.00 ± 0.30	SARAYKENT (Hot Water)
Y2-7	AUG.-92	-9.50	-88.80	0.30 ± 0.20	SARAYKENT (Hot Water)
Y5-3	MAR.-93	-9.35	-85.60	0.00 ± 0.20	SARAYKENT (Hot Water)
Y1-7	APR.-92	-11.00	-79.00	14.40 ± 0.60	SARAYKENT (Cold Water)
Y2-8	AUG.-92	-10.44	-76.90	16.00 ± 0.70	SARAYKENT (Stream Water)
Y5-3D	MAR.-93	-11.35	-82.10	15.40 ± 0.50	SARAYKENT (Stream Water)
Y2-6	AUG.-92	-10.03	-89.10		KARADIKMEN (Hot Water)
Y2-10	AUG.-92	-11.77	-80.00	22.20 ± 0.90	TEPEDOGAN (Metamorphic Cold Water)
Y2-11	AUG.-92	-9.85	-72.00		TEPEDOGAN (Cold Water)
Y1-11	APR.-92	-11.07	-78.90	0.20 ± 0.30	BOGAZLIYAN BB-2 (Hot Water)
Y2-14	AUG.-92	-10.88	-80.20	0.40 ± 0.20	BOGAZLIYAN BB-2 (Hot Water)
Y5-5	MAR.-93	-10.87	-80.90	0.10 ± 0.20	BOGAZLIYAN BB-2 (Hot Water)
Y1-12	APR.-92	-10.74	-76.80	0.50 ± 0.30	BOGAZLIYAN BB-1 (Hot Water)
Y2-15	AUG.-92	-10.68	-79.10		BOGAZLIYAN BB-1 (Hot Water)
R2	NOV.-92	-0.95	2.60		BOGAZLIYAN (Rain Water)

TABLE III. CHEMICAL ANALYSIS RESULTS FOR GEOTHERMAL FIELDS IN THE YOZGAT REGION

NO	LOCATION AND DATE	T (°C)	pH	Conduc. (µS/cm)	Na	K	Ca	Mg	HCO <sub>3</sub>	CO <sub>3</sub>	SO <sub>4</sub>	Cl	ANIONS CATIONS
Y1-3	SORGUN HOT WATER APRIL-1992	75	7.62	4650	* 297.5	97.5	165	12.5	42.7	12	228.6	670	Cl>SO <sub>4</sub> >HCO <sub>3</sub> >CO <sub>3</sub>
				**	12.94	2.494	8.233	1.029	0.699	0.399	4.759	19.90	Na>Ca>K>Mg
Y1-5	SORGUN HOT SPRING WATER APRIL-1992	42.8	6.62	2950	* 197	60	318	32	427	12	554	372	SO <sub>4</sub> >Cl>HCO <sub>3</sub> >CO <sub>3</sub>
				**	8.57	1.54	15.87	2.63	6.99	0.399	11.53	10.49	Ca>Na>Mg>K
Y1-4	SORGUN COLD WATER APRIL-1992	18.4	7.21	1380	* 73	22	268	47	475.8	18	253.7	246.4	HCO <sub>3</sub> >Cl>SO <sub>4</sub> >CO <sub>3</sub>
				**	3.176	0.562	13.37	3.868	7.798	0.599	5.282	6.951	Ca>Mg>Na>K
Y1-6	SARAYKENT HOT WATER APRIL-1992	75	7.34	5000	* 385	47.5	187.5	17.5	213.5	24	427.1	542.4	Cl>SO <sub>4</sub> >HCO <sub>3</sub> >CO <sub>3</sub>
				**	16.75	1.215	9.356	1.440	3.499	0.799	8.892	15.30	Na>Ca>Mg>K
Y2-7	SARAYKENT HOT WATER AUGUST-1992	69	7.10	5200	* 515	345	370	27.5	298.9	-	298.7	1287	Cl>SO <sub>4</sub> >HCO <sub>3</sub>
				**	22.40	8.82	18.4	2.26	4.9	-	6.22	36.3	Na>Ca>K>Mg
Y1-7	SARAYKENT COLD WATER APRIL-1992	15.3	7.83	550	* 28	23	103	18	256.2	30	92.21	42.54	HCO <sub>3</sub> >SO <sub>4</sub> >Cl>CO <sub>3</sub>
				**	1.218	0.588	5.139	1.481	4.199	0.999	1.919	1.200	Ca>Mg>Na>K
Y1-11	BOGAZLIYAN-BB2 HOT WATER APRIL-1992	45	6.14	3600	* 265	80.01	317.5	72.5	872.3	-	228.6	565.4	HCO <sub>3</sub> >Cl>SO <sub>4</sub>
				**	10.22	2.046	15.84	5.966	14.29	-	4.759	15.94	Ca>Na>Mg>K
Y2-14	BOGAZLIYAN-BB2 HOT WATER AUGUST-1992	44.5	6.44	3700	* 189	60	856	98	353.8	120	249.6	659.4	Cl>HCO <sub>3</sub> >SO <sub>4</sub> >CO <sub>3</sub>
				**	8.22	1.53	17.76	8.06	5.8	4	5.19	18.6	Ca>Na>Mg>K
Y5-5	BOGAZLIYAN-BB2 HOT WATER MARCH-1992	45	6.45	3250	* 207.5	90	365	50	945.5	-	236.1	514	HCO <sub>3</sub> >Cl>SO <sub>4</sub>
				**	9.03	2.3	18.21	4.11	15.5	-	4.92	14.5	Ca>Na>Mg>K
Y1-12	BOGAZLIYAN-BB1 HOT WATER APRIL-1992	32	6.40	1700	* 60	24	286	59	927.2	-	144.7	134.7	HCO <sub>3</sub> >Cl>SO <sub>4</sub>
				**	2.61	0.613	14.27	4.855	15.19	-	3.012	3.799	Ca>Mg>Na>K
Y2-15	BOGAZLIYAN-BB1 HOT WATER AUGUST-1992	32	6.52	1800	* 46	13	95	58	506.3	12	115.4	44.31	HCO <sub>3</sub> >SO <sub>4</sub> >Cl>CO <sub>3</sub>
				**	2	0.33	4.74	4.77	8.3	0.4	2.4	1.25	Mg>Ca>Na>K

\* : ppm

\*\* : meq/l

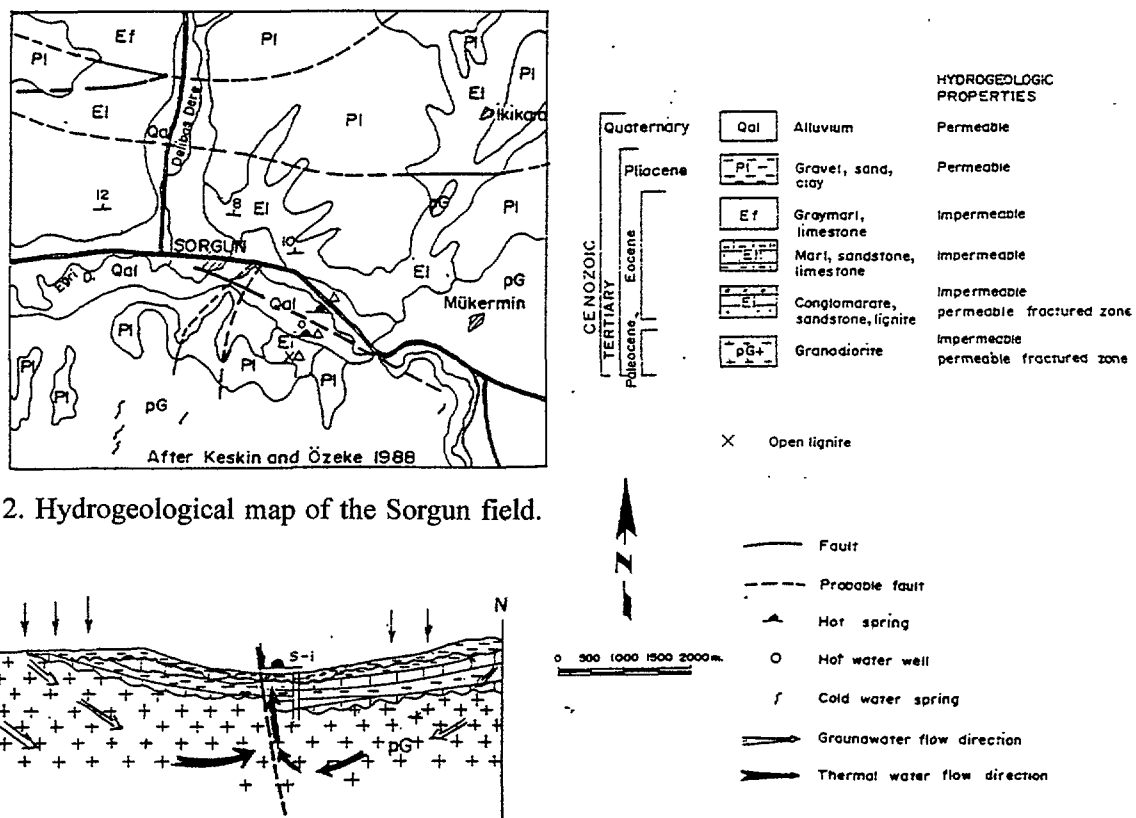


FIG. 2. Hydrogeological map of the Sorgun field.

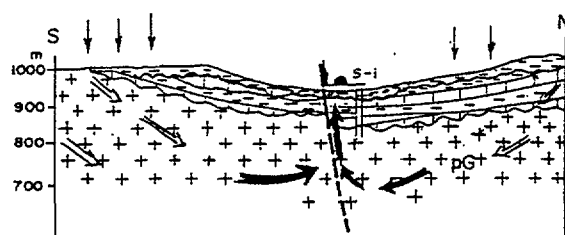


FIG. 3. Schematic cross-section of the Sorgun geothermal area.

The hydrogeological map of Sorgun Field is shown in Figure 2. The basement rocks in the field are granite-granodiorite (Paleocene). The secondary porosity and permeability have been formed at the fracture zones and approximately 40 m from paleotopographic surface in the basement rock. Basement rocks are overlain by Eocene lagoonal conglomerate, sandstone, clay and marl alternations. In this unit, some lignite layers are determined. The Pliocene consist of loose cemented conglomerate, sandstone and clay units.

Thermal water have been produced from five shallow wells in this field. In one of these wells, the production rate which was 30 L/s at the beginning has been reduced to 15 L/s because of the lignite mining activity carried out the close by the well. Schematic cross section of Sorgun Geothermal Field is shown in Figure 3. The conglomerate, sandstone, clay, marl alternations and lignite units of Eocene form the caprock and granite-granodiorite units form the reservoir rock in the Sorgun Area. There is a secondary reservoir in the alluvium formation (Table I).

A hot spring was occurred when the coal mining galleries were opened at the same place of previous spring site. A hot spring with a temperature 40°C and flow rate 7 L/s was determined. After that, spring's piezometric level and discharge rates was decreased so that, it was ceased. Because of this condition in the region, shallow wells were drilled and geothermal fluid has a temperature of 75°C was produced [11].

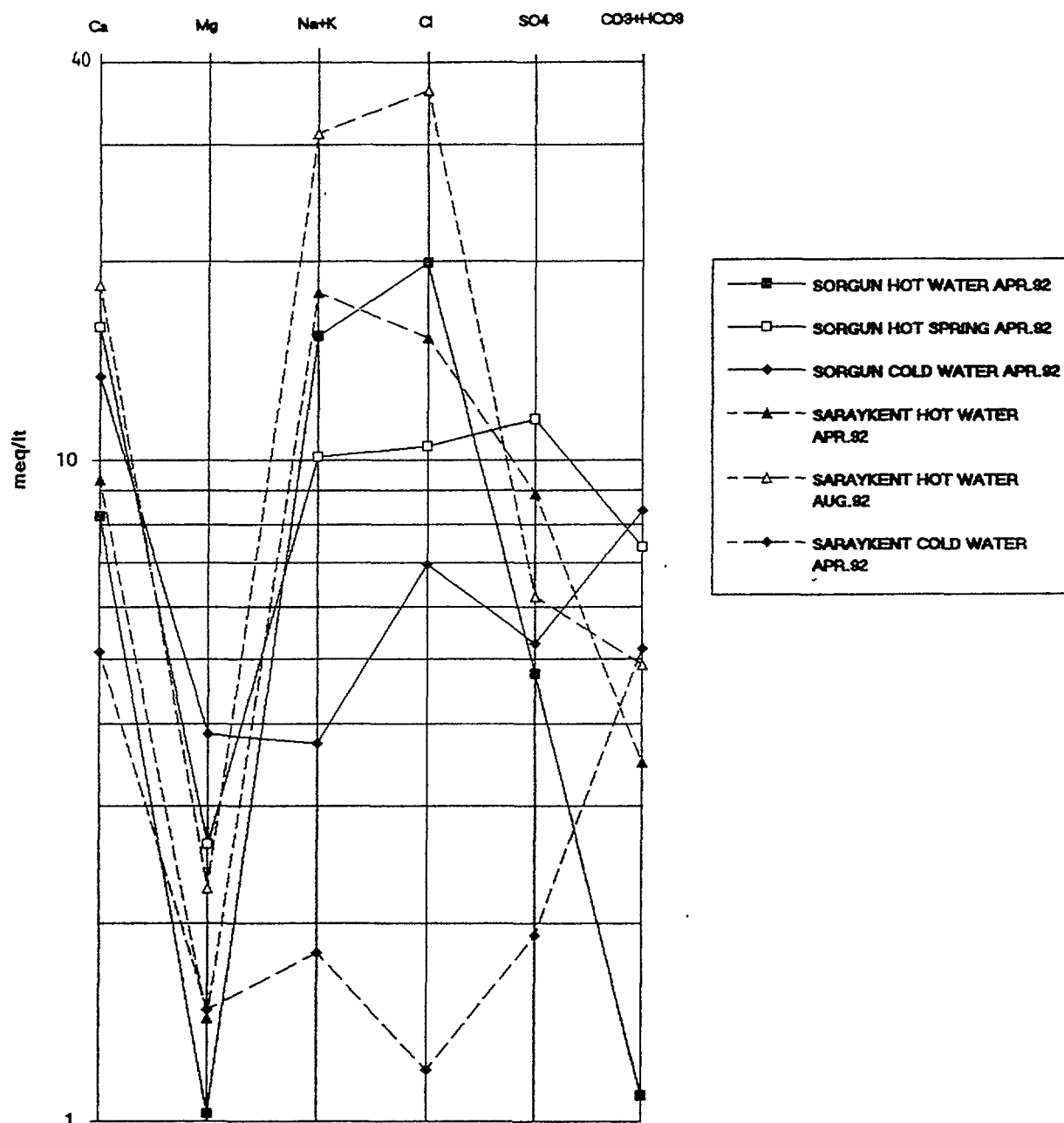


FIG. 4. Schoeller diagram for Sorgun and Saraykent geothermal fields.

Semi-log diagram of the cold and hot water samples collected from the Sorgun at different periods are shown in Figure 4. The cold waters differ remarkably from the hot waters by chemical composition. For example, while the cold water sample has the composition of  $\text{Ca} > \text{Mg} > \text{Na} + \text{K}$  and  $\text{CO}_3 + \text{HCO}_3 > \text{Cl} > \text{SO}_4$ , the hot water samples have the chemical composition of  $\text{Ca} > \text{Na} + \text{K} > \text{Mg}$  and  $\text{Cl} > \text{SO}_4 > \text{CO}_3 + \text{HCO}_3$ . Cold waters are classified as complex waters in which any ionic constituent is less than 50%. Hot waters are of Ca,  $\text{Cl} + \text{SO}_4$  and  $\text{Na} + \text{K}$ ,  $\text{Cl} + \text{SO}_4$  type.

According to the hydrogeologic investigation; thermal water supplied from the granite in the well contains lower amount of Ca,  $\text{HCO}_3$ ,  $\text{SO}_4$ , Mg and TDS than those of other springs. Spring water upraised through the granite and cap rock (marl-clay formation of Eocene age), so that water is enriched by Ca, Mg,  $\text{HCO}_3$ ,

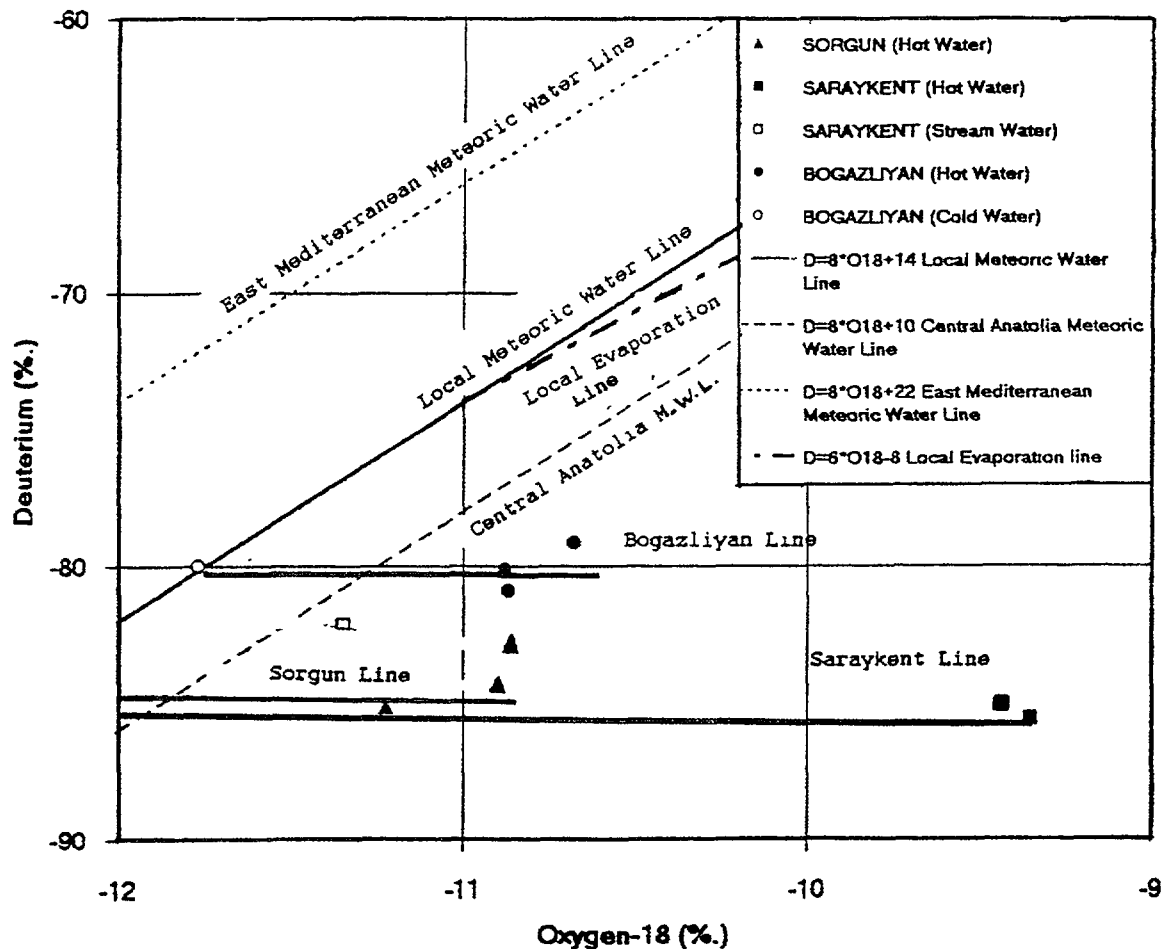


FIG. 5. Oxygen-18–deuterium relationship for the Yozgat region.

TDS but on the other hand become poor in Na, K, Cl. Some geothermometers as Na-K and Na-K-Ca were applied to thermal spring and well in Sorgun Geothermal Area. Temperatures were calculated 130-187°C [1, 10, 20] and 82-129°C [7, 10, 12, 19] for spring and well respectively. According to the geothermometers applications 82-100°C estimated temperatures are more convenient.

Isotopic evaluation of hot waters points out that indicating a clear  $\delta^{18}\text{O}$  shift from the local meteoric line. This suggest that rock-water interaction is an important process for most of hot water samples. Meanwhile, some cold water samples also deviate from the local meteoric line, indicating that, they are under the effect of evaporation. These constitute the shallow circulating part of the local ground water flow system (Figure 5).

The high Cl and low  $^3\text{H}$  content of hot waters suggest that they have longer and deeper groundwater flow paths as compared to those of cold water which belong to relatively shallow circulation system.

## 2.2. Saraykent (Karamağara) Geothermal Area

Saraykent field is located in the 70 km east of Yozgat City and 30 km Sorgun Town respectively. Thermal springs are situated 8 km north of Saraykent Town in the Ilica valley. Average precipitation is 405.8 mm/year during 1960-1990 period.

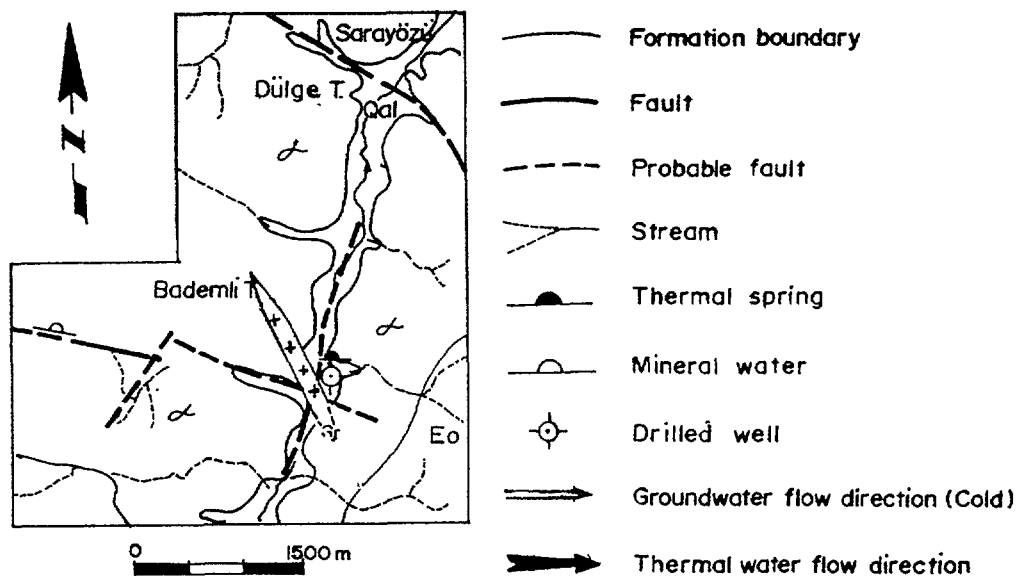


FIG. 6. Hydrogeological map of the Saraykent geothermal field.

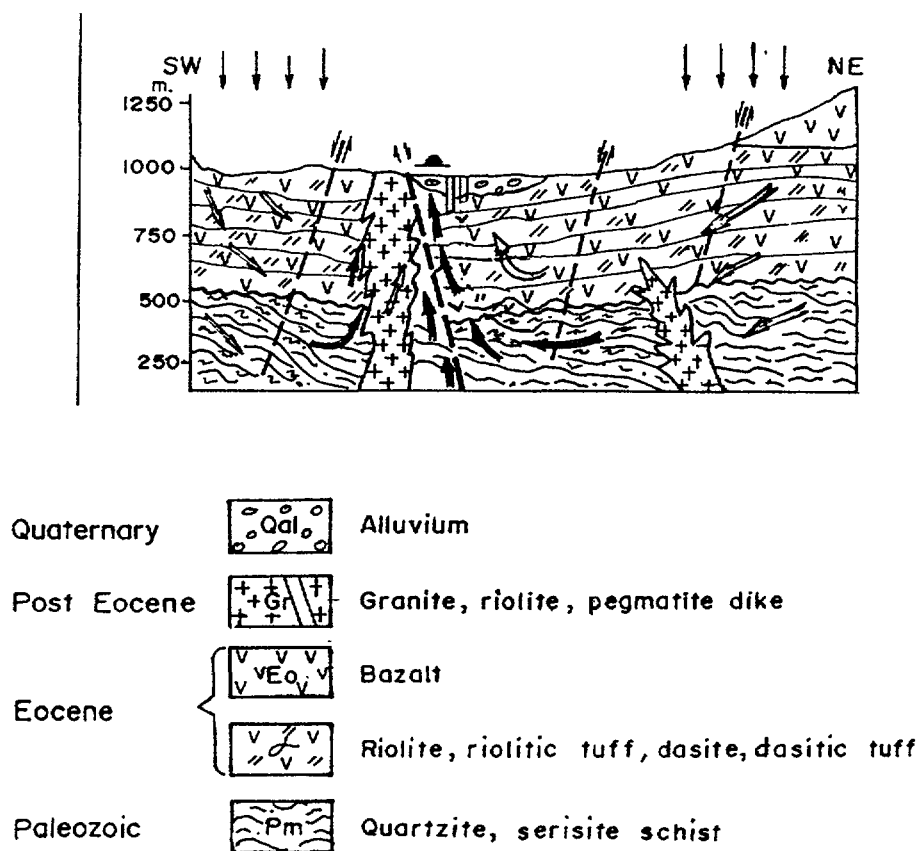


FIG. 7. Schematic cross-section of the Saraykent geothermal field.

The geological map of Saraykent Field is shown in Figure 6. The rhyolitic lava and acidic tuffs are widespread outcrops in the area. Some granite dikes can also be seen in the geothermal area.

Thermal waters are rising from the alluvium (app. 30 m thick) to the surface. The thermal waters have been used for health and touristic purposes since Roman times. Because of the thermal water shortage, State Water Works (DSİ) drilled 2 shallow wells with depths of 30 m and 66 m in recent years. According to the testing results of these wells, total 24 L/s efficient flow rate is obtained at the temperature of 70-74°C [21] Schematic cross section of Saraykent Geothermal Field is shown in Figure 7.

For more utilization of hot water new thermal foundation and greenhouse have been constructed in Saraykent Geothermal Field. Because of inadequate water, two shallow wells were drilled and geothermal fluid with a temperature of 75°C and 10-24 L/s of discharge were produced hot springs flow rates were decreasing during the well production.

Semi-log diagram of the cold and hot water samples collected from the Saraykent Geothermal Field at different periods. The cold water samples have the composition of  $\text{Ca} > \text{Na} + \text{K} > \text{Mg}$  and  $\text{CO}_3 + \text{HCO}_3 > \text{SO}_4 > \text{Cl}$  and hot water samples have the chemical composition of  $\text{Na} + \text{K} > \text{Ca} > \text{Mg}$  and  $\text{Cl} > \text{SO}_4 > \text{CO}_3 + \text{HCO}_3$  Figure 4. Cold waters are of  $\text{Ca}$ ,  $\text{CO}_3 + \text{HCO}_3 + \text{SO}_4$  and  $\text{Na} + \text{K}$ ,  $\text{CO}_3 + \text{HCO}_3 + \text{SO}_4$  type waters and carbonate hardness for these waters are greater than 50%. Hot waters are of  $\text{Na} + \text{K}$ ,  $\text{Cl} + \text{SO}_4$  and  $\text{Ca}$ ,  $\text{Cl} + \text{SO}_4$  type (Table III).

Generally dominant formations are acidic volcanic rocks in the area. Geothermometers were applied to thermal water and temperature 133-174°C [1, 19, 20] calculated for Saraykent Geothermal Area.

Isotopic evaluation of hot waters points out that, there is a clear  $\delta^{18}\text{O}$  shift from the local meteoric line (Figure 5). This suggests that, rock-water interaction is an important process for most of hot water samples. Meanwhile, some cold water samples also deviate from the local meteoric line, suggesting that they are under the effect of evaporation. These constitute the shallow circulating part of the local ground water flow system. The high Cl and low  $^3\text{H}$  content of hot waters suggest that they have longer and deeper groundwater flow paths as compared to those of cold water which belongs to relatively shallow circulation system.

### 2.3. Boğazlıyan Geothermal Area

Boğazlıyan field is located 110 km south east of Yozgat City. Average precipitation is 382.1 mm/year during 1960-1990 period. The geological map of Boğazlıyan Field is shown in Figure 8. The widespread limestone (Eocene) and detritic (Oligocene) outcrops are seen in the area. The Pliocene loose cemented deposits as conglomerate, clay, sandstone and clayey limestone units overlie the Eocene-Oligocene formations. The Quaternary is characterized with alluvium along the rivers.

The flow rate of thermal water is 320 L/s and temperature range is 30-34°C. After drilling flow rate and temperature of the wells is given below [2, 15]:

Well No	Depth(m)	Temp(°C)	Flow rate L/s
B B-1	132	33	125
B B-2	177	46	100

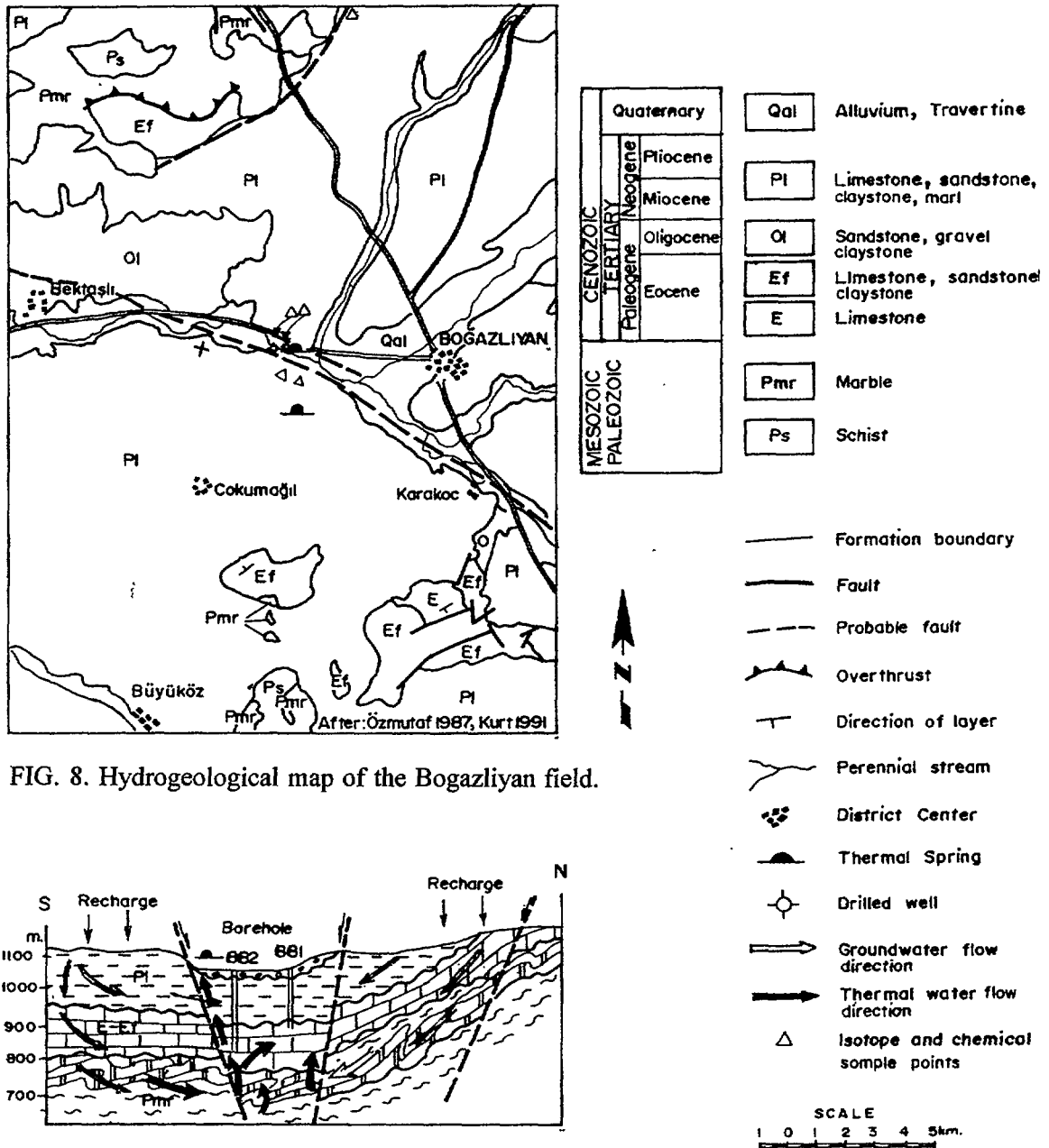


FIG. 9. Schematic cross-section.

As a result of shallow well, log interpretations the Eocene limestone is defined as reservoir, and Oligocene and Pliocene clayey deposits are defined as caprock. Schematic cross section of Boğazlıyan Geothermal Field is shown in Figure 9.

Ponds were occurred around the springs because of large amount of discharge (320 L/s) of thermal water (30°C) spring in Boğazlıyan Field. The wells were drilled and thermal water which has discharge of 125-100 L/s, temperature of 33-47°C were produced.

Semi-log diagram of the cold and hot water samples collected from the Boğazlıyan Geothermal Field at different periods are shown in Figure 10. The cold water samples have the compositions of  $\text{Ca} > \text{Mg} > \text{Na} + \text{K}$ ,  $\text{CO}_3 + \text{HCO}_3 > \text{SO}_4 > \text{Cl}$  and  $\text{Ca} > \text{Na} + \text{K} > \text{Mg}$ ,  $\text{Cl} > \text{HCO}_3 + \text{CO}_3 > \text{SO}_4$ . Hot water samples have the chemical compositions of

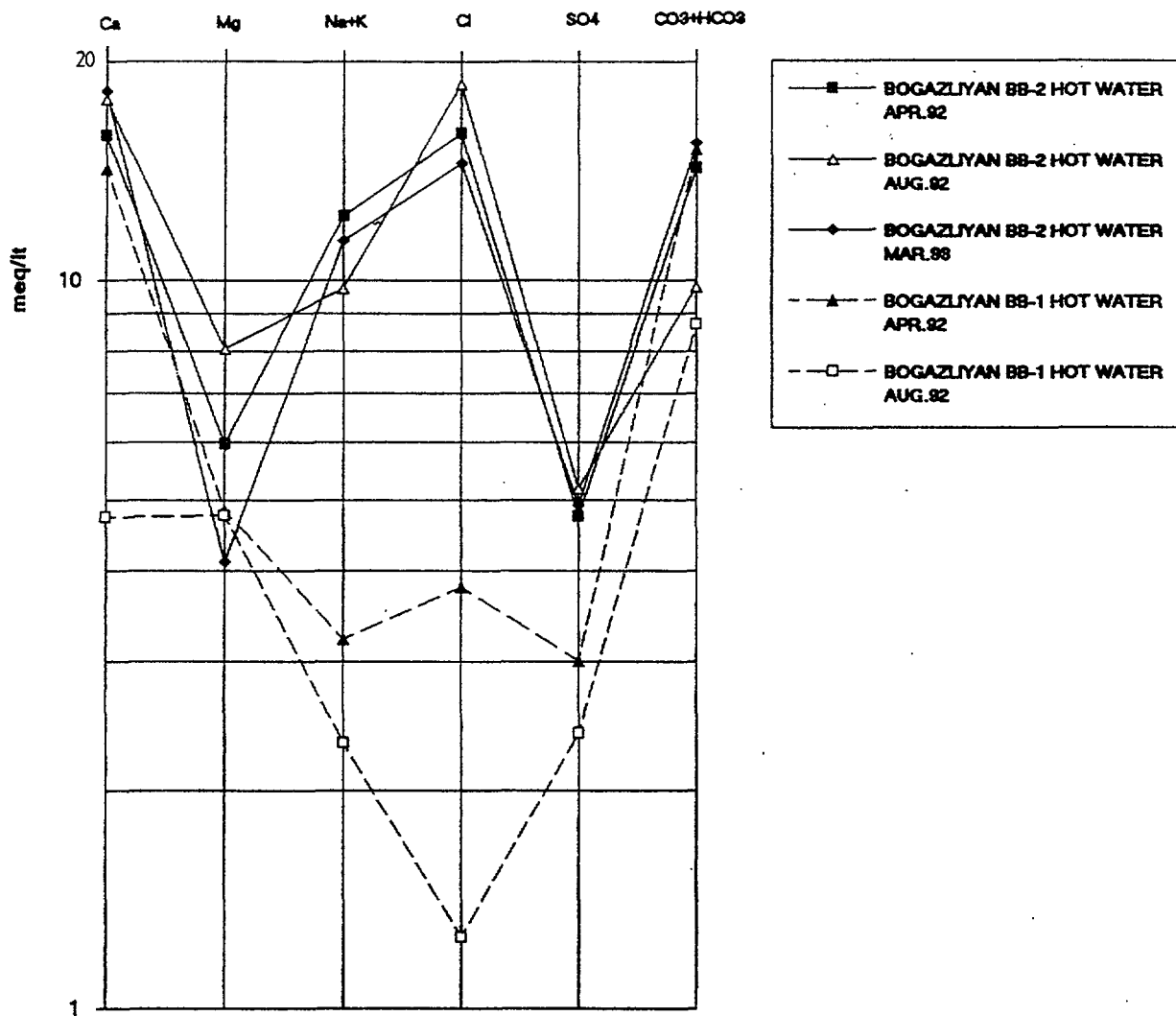


FIG. 10. Schoeller diagram for the Bogazliyan geothermal field.

Ca>Mg>Na+K, CO<sub>3</sub>+HCO<sub>3</sub>>Cl>SO<sub>4</sub> and Ca>Na+K>Mg, Cl>CO<sub>3</sub>+HCO<sub>3</sub>>SO<sub>4</sub> in BB1 and BB2 hot water wells respectively. Cold waters are of Ca, CO<sub>3</sub>+SO<sub>4</sub> and Mg, CO<sub>3</sub>+SO<sub>4</sub> type waters and carbonate hardness of these waters are generally greater than 50%. Hot waters (BB1-BB2 wells) are of CaCO<sub>3</sub> type and have high carbonate hardness.

Water, supplied from the well is in contact with karstic limestone aquifer (reservoir) of Eocene cap rock contains continental-lagoonal claystone, marl, sandstone and conglomerate. Consequently, source of thermal water has karstic character in the region.

Some geothermometers were applied to thermal water and temperature 76-87°C [1, 20] calculated for Boğazlıyan Geothermal Area. But, the because of karstic reservoir, high flow rate of the springs and well; the temperature of main reservoir is around 50-60°C.

Isotopic evaluation of water samples that the cold waters are partially scattered along local meteoric line. Deviations from the line shows that, there is an effect of evaporation on cold waters and they have shallow circulation system. Due to the



water-rock interaction and mixing of meteoric water caused the less deviation from local meteoric line relative to the other fields for hot waters. The high Cl and low  $^3\text{H}$  content of hot waters suggest that they have longer and deeper groundwater flow paths as compared to those of cold water which belong to relatively fresh and shallow circulation system.

### 3. OVERALL EVALUATION OF WATER CHEMISTRY AND ENVIRONMENTAL ISOTOPIC DATA

Hot water samples from Sorgun and Saraykent fields seem to be more mature water than Boğazlıyan Field. The analyses of thermal waters show that any of samples reach complete equilibrium at high temperature [10]. Thermal waters differ from the cold waters. The waters are dominated by Cl ion in solution, the latter from  $\text{HCO}_3$  ion. No water is dominated by  $\text{SO}_4$  (Figure 11).

Water from Sorgun and Saraykent show an evolutive trend from local cold water to the thermal waters. No samples reaches complete equilibrium conditions, as aspected from Figure 11. The extrapolated temperatures seem to indicate exceptionally high values for Saraykent and Sorgun Geothermal Fields (Figure 12).

In order to determine the local meteoric line for the project area, precipitation samples (snow and rain) have been collected from proper locations. The  $\delta^{18}\text{O}/\delta^2\text{H}$  data of the samples collected give the meteoric line equation of  $\delta^2\text{H}=8*\delta^{18}\text{O}+14$ .

Relation of cold waters to local meteoric line ( $\delta^2\text{H}=8*\delta^{18}\text{O}+14$ ) is shown in Figure 5. It is noticed that the cold waters are generally scattered along local the meteoric line. However, because some of the cold water samples are under the effect of evaporation, they are plotted along and evaporation line of  $\delta^2\text{H}=6*\delta^{18}\text{O}-8$ .

Previous isotopic surveys carried out around the study area gave the meteoric line equations of  $\delta^2\text{H}=8*\delta^{18}\text{O}+22$  and  $\delta^2\text{H}=8*\delta^{18}\text{O}+10$  for the East Mediterranean and the Central Anatolia regions, respectively [13]. The meteoric line obtained in this study is located in between these lines this indicates that, the project area represents a climatic transition zone between the East Mediterranean and the Central Anatolia regions.  $\delta^{18}\text{O}/\delta^2\text{H}$  relation of the all samples (cold and hot) from the all geothermal fields are shown in Figure 5. Some of the hot waters shift to the right of local meteoric line, indicating that there is an apparent water rock interaction through geothermal aquifer.

Cl vs.  $\delta^{18}\text{O}$  and Cl vs.  $\delta^2\text{H}$  relations of all samples are as follows;

For cold waters parameters range between; For hot waters parameters range between;

$$\delta^2\text{H} = (-70) - (-90) \text{ (SMOW)}$$

$$\delta^{18}\text{O} = (-9) - (-12) \text{ (SMOW)}$$

$$\text{Cl} = 0-15 \text{ meq/L}$$

$$\delta^2\text{H} = (-70) - (-90) \text{ (SMOW)}$$

$$\delta^{18}\text{O} = (-9) - (-12) \text{ (SMOW)}$$

$$\text{Cl} = \text{Approximately } 15-120 \text{ meq/L}$$

The Cl vs.  $^3\text{H}$  graph suggests that:

-Cold waters have low Cl (0-15 meq/L) and high  $^3\text{H}$  (5-25 TU) and these waters are generally fresh waters and have shallow circulation system.

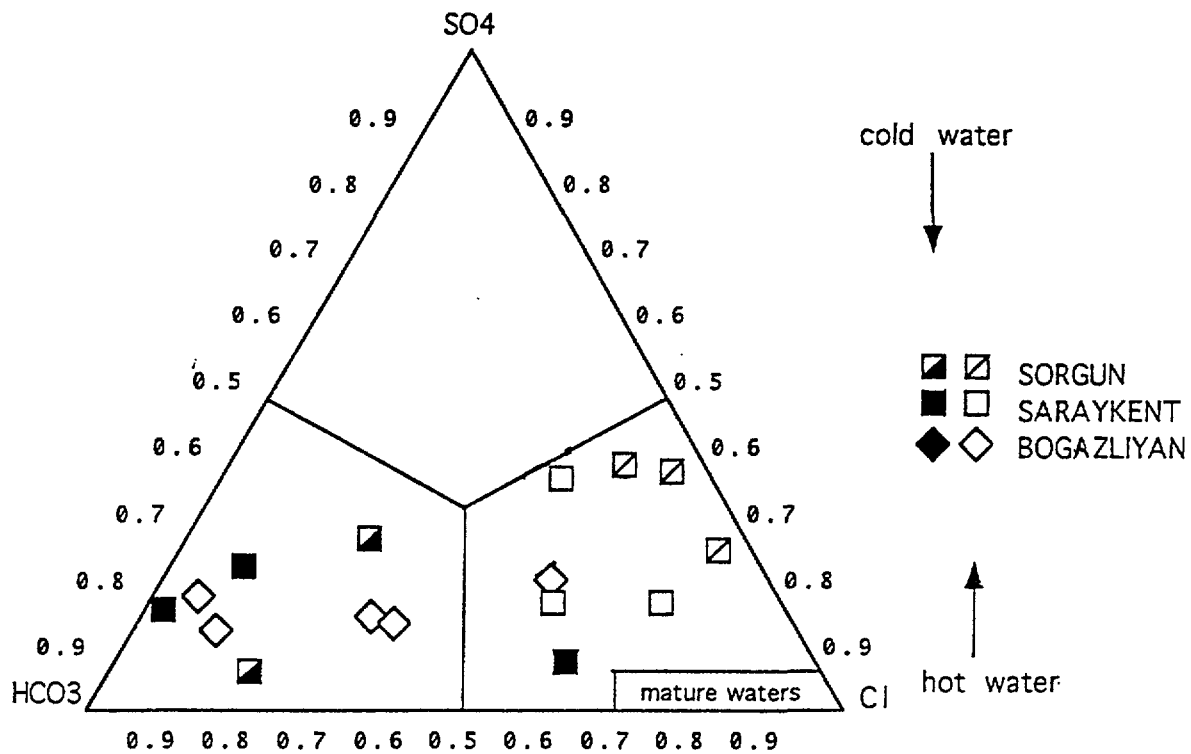


FIG. 11. Triangular diagram (for anions).

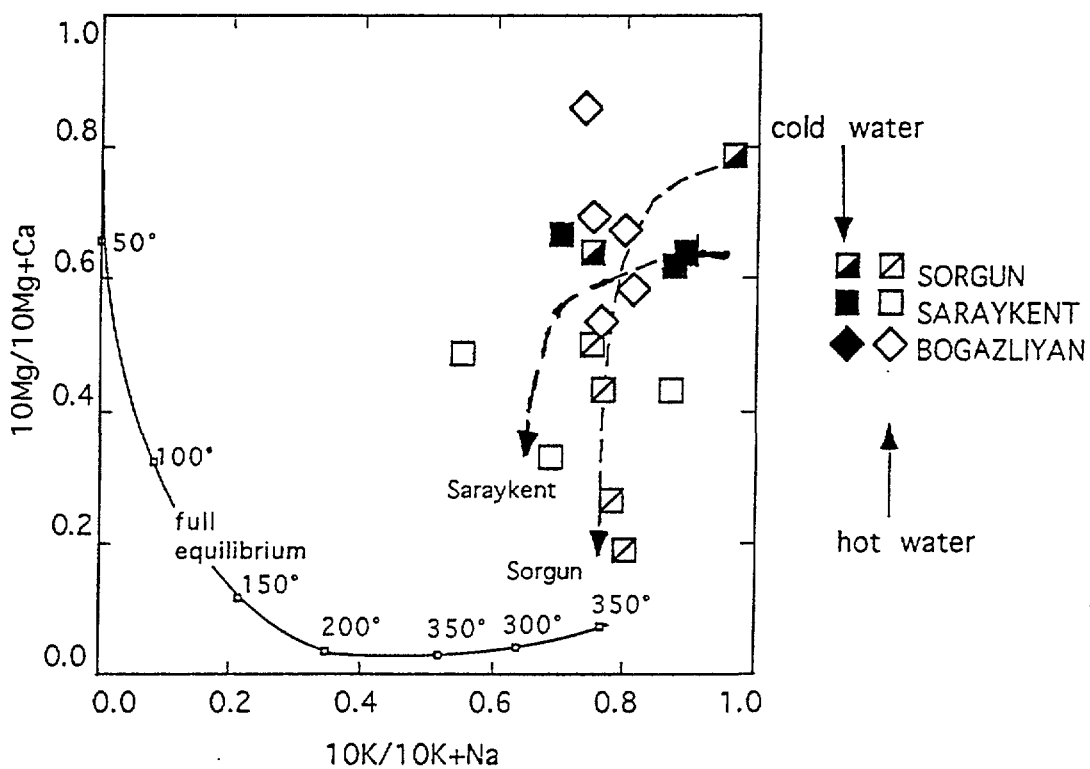


FIG. 12. Square diagram (for cations).

TABLE IV. GENERAL CHARACTERISTICS OF GEOTHERMAL FIELDS IN THE PROJECT AREA

LOCATION	TEMPERATURE °C			FLOW RATES lt/sec	PRESENT CAPACITY MWt	SHALLOW WELLS m	UTILIZATION POSSIBILITIES					
	Hs	SW	Est				DIS.	GRE.	IND.	CL.	BALN.	TOURISM
SORGUN	50 - 61	75	74-101	17	2.63	104	++	+	+	+	++●	+●
SARAYKENT	40	75	103-154	24	3.92	30 - 66	+	+●	-	-	+●	+
BOGAZLIYAN	30 - 42	33 - 46	49 - 57	225	4.6	132-177	++	+	-	-	++	+

++ : important application possibility  
+ : application possibility  
● : application at present

Baln : Balneology  
Gre : Greenhouse  
Est : Estimated reservoir temperature  
Hs : Hot spring

SW :Shallow well  
Ind. : Industrial app.  
Cl : Cooling  
Dis. : District Heating

-Hot waters have high Cl (approximately 15-120 meq/L) and low  $3H$  (0-5 TU) and these waters are generally old and have deep circulation system.

#### 4. GEOTHERMAL ENERGY UTILIZATION POSSIBILITIES OF PROJECT AREA

At the result of the detail hydrogeological and hydrochemical investigation in Yozgat Province Geothermal Fields, there is important geothermal potential have been determined. Especially, there is important fields as in the case of district heating, greenhouse heating and balneological usage (Table IV).

The thermal water has the temperature of 75°C and 15 L/s discharge which is obtained from Sorgun Geothermal field can be utilize for district heating and process heating for sugar factory which is close to the field. Also Boğazlıyan field is 5 km east from the Town center. A well has discharge rate of 100 L/s and temperature of 46°C can be used in different types of heating (i.e. district heating, greenhouse heating). In addition to balneological usage and fish farming utilization can be possible. There is some thermal establishments and greenhouse foundations which has 1700 m<sup>2</sup> area Saraykent. In this field if we obtain high discharge rate geothermal fluid from deep reservoir it can be used for heating purposes in Saraykent Town.

Other thermal waters which is located Sarkaya, Yerköy, Karadikmen and Uzunlu fields in Yozgat province can be evaluated mainly balneological and touristic usage.

#### 5. CONCLUSIONS

-Hydrogeological and hydrogeochemical survey have been completed in Yozgat Province. Periodical samples have been collected from thermal and cold water points (including rain and snow waters) for isotopic and chemical analyses.

-The analyses of thermal, cold and meteoric waters, hydrogeochemical interpretations as diagrams and geothermometers have been evaluated.

-According to the hydrogeological survey, reservoir and caprocks are formed by rocks of different origin.

-According to the tritium analyses, thermal waters have deep and long groundwater flow paths and these waters are generally older than 50 years.

-The project area represents a climatic transition zone between the East Mediterranean and Central Anatolia Regions by the local meteoric line equation of  $\delta^2\text{H}=8*\delta^{18}\text{O}+14$ .

-According to the  $\delta^{18}\text{O}$  vs.  $\delta^2\text{H}$  relation, there is a  $\delta^{18}\text{O}$  shift and these are suggest that different reservoir depth and water-rock interaction in Yozgat-Saraykent, Boğazlıyan and Sorgun geothermal fields.

-According to results, the fields are important for geothermal utilization possibilities in Yozgat-Saraykent, Sorgun and Boğazlıyan geothermal fields in Yozgat Province for central heating and balneological point of view .

-Using isotope technology methods in the geothermal fields of Central Anatolia provided a very useful tool in developing the hydrogeological model of the area. Improvement of the laboratories of the agency as to be able to analyze other isotope contents of both water and gas would contribute to much to the research project that will be implemented in the future.

## ACKNOWLEDGMENT

I would like to express my great thanks to Professor Gültekin GÜNAY (Director - Hacettepe University International Research and Application Center for Karst Water Resources UKAM) for providing scientific and logistic support both in the field and laboratory works. I also thank to Dr.PANICHI from International Institute for Geothermal Researches Pisa-Italy for support of hydrogeochemical evaluation for this paper. I express my appreciation to M.Ş.DOĞDU, H.ÇELİK, Dr.H.ELHATİP and N.AKKUŞ who performed the hydrochemical analysis and assisted with the field work. I also gratefully acknowledge Dr.Levent TEZCAN and Dr. Serdar BAYARI's review comments that encouraged as to improve this manuscript.

## REFERENCES

- [1] Arnorsson, S, Chemical Equilibria in Icelandic Geothermal Systems Implications For Chemical Geothermometry Investigations:Geothermics, 12, (1983),119-128.
- [2] Çağlar, K.Ö. , Türkiye Maden Suları ve Kaplıcaları, MTA yayını Ankara (1961).
- [3] Çelenk, S, Yozgat-Boğazlıyan Havzası Hidrojeolojik Etüt Raporu DSI Raporu, Ankara (1985).
- [4] Filiz, Ş, Investigation Of The Important Geothermal Areas By Using C, H, O Isotopes, Seminar On Utilization Of Geothermal Energy For Electric Power Production and Space Heating, UN Economic Commission for Europe, EP/SEM-14/R34, Ankara, Türkiye (1984).
- [5] Filiz, Ş, Isotopic Analyses Of CO<sub>2</sub> And Travertines In The Denizli Geothermal Province (West Anatolia), Seminar On Utilization Of Geothermal Energy For Electric Power Production And Space Heating, UN Economic Commission For Europe, EP/SEM-14/R34, Ankara, Türkiye (1989).

- [6] Fournier, O. R., A Revised Equation For The Na/K Geothermometer: Geothermal Resources Council Transactions, 3, (1979) 221-224.
- [7] Fournier, O. R., and Potter, R.W., II, Magnesium Correction To The Na-K-Ca Chemical Geothermometer: Geochim Cosmochim Acta, 43,(1979) 1543-1550.
- [8] Fournier, O. R. and Truesdell, A.H., An Empirical Na-K-Ca Geothermometer For Natural Waters: Geochim Cosmochim Acta, 37, (1973) 515-525.
- [9] Fournier, O. R., Lectures on Geochemical Interpretation of Hydrothermal Waters UN Geothermal Training Programme, Report on, Reykjavik-ICELAND (1989), p. 1-20.
- [10] Giggenbach, WF, Geothermal Solute Equilibria Derivation Of Na-K-Mg-Ca Geoindicators: Geochim Cosmochim Acta, 52, (1988) 2749-2765.
- [11] Keskin, B, Akpınar, K, Engin, Ç, Yozgat-Sorgun YS-1 Sıcaksu Sondajı Bitirme Raporu MTA Rapor No: 8485 Ankara (1988).
- [12] Nieva, D. and Nieva, R, Developments In Geothermal Energy In Mexico, Part 12-A Cationic Composition Geothermometer For Prospection Of Geothermal Resources: Heat Recovery Systems And Chp, 7, (1987) 243-258.
- [13] Onhon, E, Ertan, I, Güler, S, Ağacık, G, Determination of Groundwater Characteristics and Groundwater Budget in Edremit Plain by means of isotopes, IAEA 2234/RR/RB Final Report, Ankara (1983).
- [14] Özbek, T, Interpretation of Nevşehir-Kozaklı Geothermal Area UN Seminar on New Developments in Geothermal Energy Ankara (1989).
- [15] Özmutaf, M, Yüce, G, Yozgat-Boğazlıyan-Bahariye (Cavlak) Kaplıcası Sıcaksu Sondajları (B B-1, BB-2) Kuyu Bitirme ve Koruma Alanları Etüdü Raporu MTA Rapor No: 8216 Ankara (1987).
- [16] Özmutaf, M, Yozgat-Sarıkaya Kaplıcası Hidrojeoloji Etüdü, MTA Rapor No: 2715 Ankara (1988).
- [17] Şimşek, Ş., and Okandan E, Geothermal Energy Development in Türkiye Geothermal Energy Council Transactions Vol. 14, part 1 Hawaii-USA (1990) 257-266.
- [18] Şimşek, Ş., and Demir A, Reservoir and Caprock Characteristics of Some Geothermal Fields in Türkiye and Encountered Problems Based on Lithology Journal of Geothermal Research Society of Japan Vol. 13 No:3 , Japan (1990) p.191-204.
- [19] Tonani, F, Some Remarks On The Application Of Geochemical Techniques In Exploration, In Proc. Adv. Eur. Geothermal Resources, Second Symposium, Strasbourg, (1980) 428-443.

- [20] Truesdell, AH, Summary Of Section III Geochemical Techniques In Exploration, In Proceedings Of Second United Nations Symposium On The Development And Use Of Geothermal Resources, San Francisco, 1975, VI: Washington, Dc, Us Government Printing Office, P 1iii-1xxxix (1976).
- [21] Yurdagül, M ,Yozgat-Akdağmadeni-Saraykent (Karamağara Roma Hamamı Hidrojeoloji Etüdü DSİ Raporu Ankara (1986), p. 1-20.

# PRELIMINARY GEOCHEMICAL AND ISOTOPIC STUDY OF THE SOUTH TRUNGBO GEOTHERMAL AREA IN CENTRAL VIET NAM

NGUYEN TRAC VIET, NGUYEN KIEN CHINH, HUYNH LONG,  
NGUYEN DIEU MINH, PHAN THANH TONG

Center of Nuclear Techniques,  
Ho Chi Minh City, Viet Nam

**Abstract** - Stable isotopes (deuterium and oxygen-18) as well as geochemical data from South Trungbo geothermal area have been studied in order to deal with the chemistry classification, recharge area of hot waters and reservoir temperature. From geological and geomorphological point of view, hot waters are divided into two groups, corresponding to two zones: Coastal Strip and Northern Highland. According to stable isotopes, the recharge area of hot waters occur at about 500-600m a.s.l and 700-900m a.s.l for two above zones respectively. Moreover, there is no evidence for isotopic exchange between hot waters and host rock. Several classical geothermometers such as chalcedony, quartz, Na-K, Na-K-Ca as well as the mixing model given by Fournier and Truesdell have been applied to estimate the reservoir temperature. The results obtained are less than 150-180°C. Both geochemical and isotopic data indicate that the South Trungbo is a low-enthalpy geothermal system.

## 1. INTRODUCTION

### 1.1 Location

South Trungbo geothermal area (Fig. 1) is a large mountainous country located in the Central Part of Vietnam extending almost 700km from North to South and covering an area of about 80,000km<sup>2</sup>. The whole area can be divided in to two zones. First is a narrow plain extending along the sea coast to the East and the second one is South Truongson Ridge with many large highland to the West. Elevations rage from 2m in the plain to 2598m in the Ngoclinh Mountain (Fig. 2).

The climate in the area is tropical with two clear distinct seasons: west season from May to October and dry one from November to April. Mean annual temperature affected by elevation changes as follow:

< 500m	:	25 - 26°C
500 - 800m	:	21 - 23°C
800 - 1000m	:	19 - 21°C
> 1500m	:	18°C

The average yearly precipitation varies from zones to zones. On the South it is about 3200-3500mm where in Cheoreo valley it is 1200mm only.

The relief of South Trungbo is dissected by drainage system consisting of three main river systems in the region: Ba, Poko and Dongnai. These originate from the above mentioned highlands and fed by local precipitation.

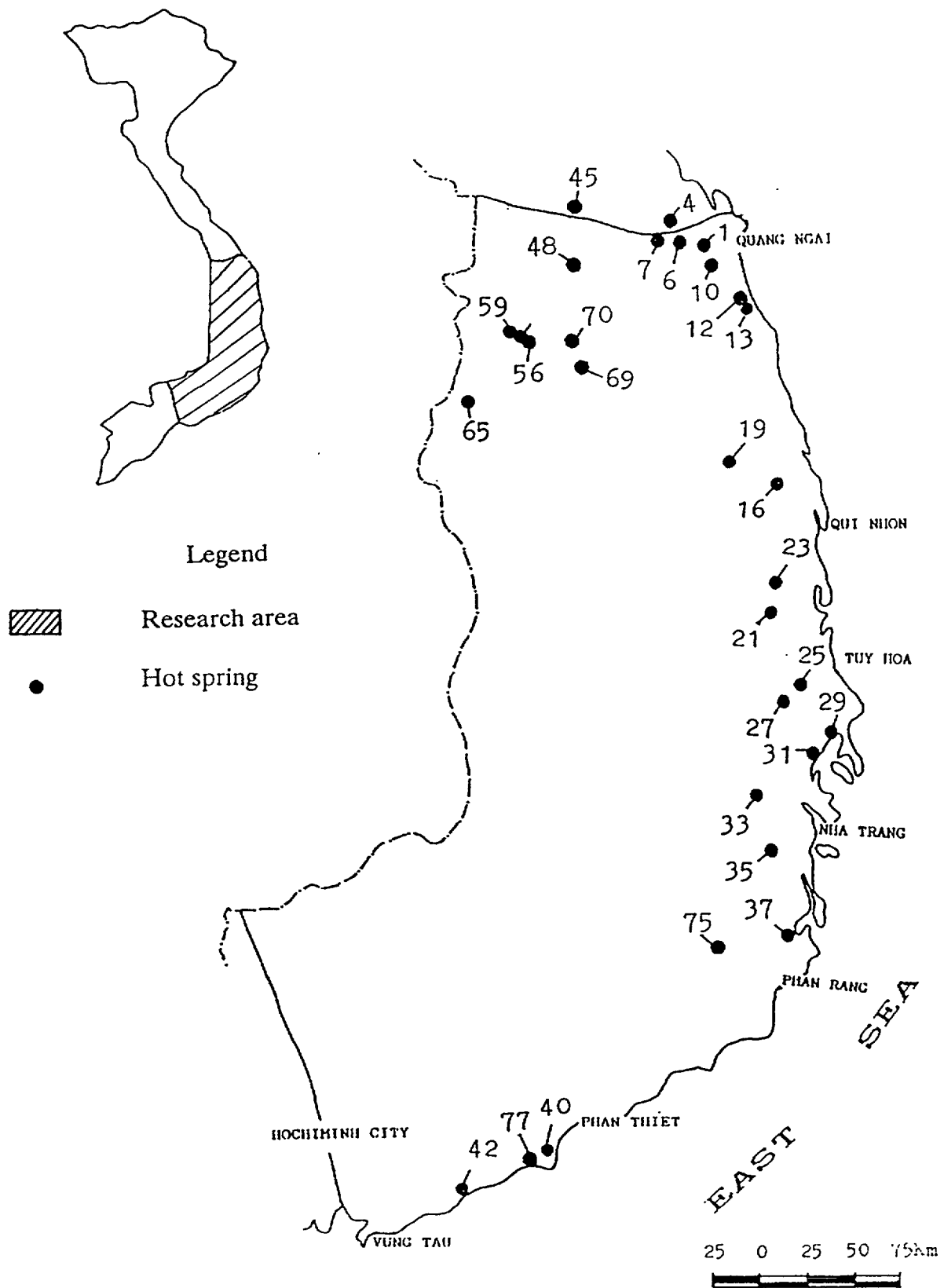


FIG. 1. South Trung Bo geothermal area.



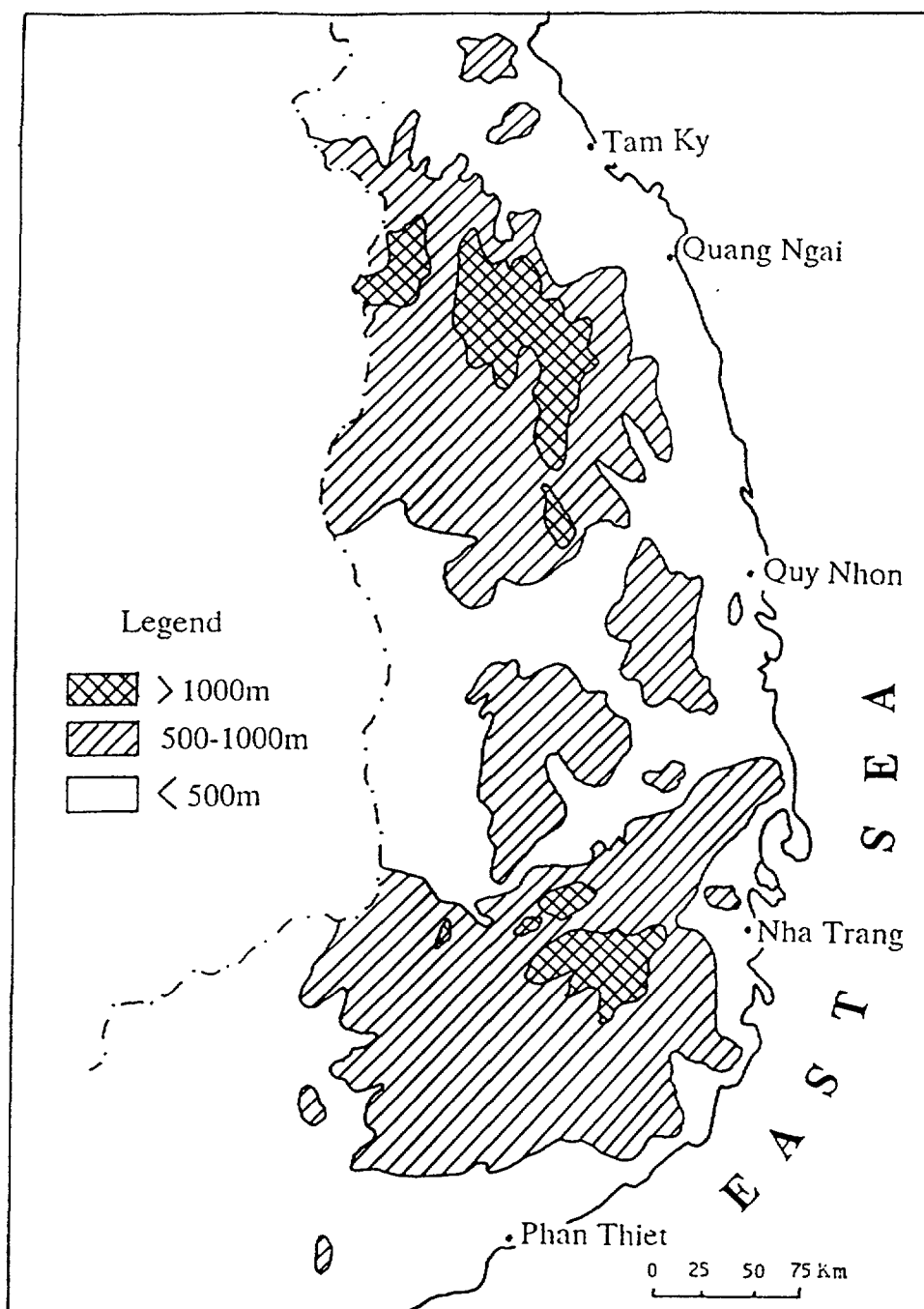


FIG. 2. Elevation map of south Trung Bo area.

## 1.2 Geological Features

South Trungbo is a complex region from structural geological point of view. It is bounded by deep seated Tamky - Queson fault to the North and Vungtau - Locninh fault to the South. In this region, two tectonic units can be identified, namely Kontum mesoblock and South Vietnam one.

Kontum mesoblock is an uplifted massif of crystalline basement consisting of strongly metamorphic rocks (gneiss, mafic granulite, amphibolite, marble and quartzite) of Archeozoic - Proterozoic ages. Paleozoic and Mezozoic sediments outcrop in a wide

Table 1. Chemical composition of the waters (In pm)

Sample	Location	T(°C)	pH	Cond. (µS/cm)	Cl	HCO <sub>3</sub>	CO <sub>3</sub>	SO <sub>4</sub>	F	Na	K	Ca	Mg	Rb	Li	Mn	SiO <sub>2</sub>
1	NGHIAKY	67.0	8.0	590	167.5	133.3	0.0	44.0	6.50	175.5	6.0	12.0	0.05	0.60	0.33	0.00	100.6
3		30.0	7.0	72	3.5	29.3	0.0	4.2		6.9	2.5	4.7	0.70				18.8
4	BINH HOA	65.0	7.0	520	105.0	36.1	0.0	48.0	7.20	122.6	4.6	6.0	0.07	0.00	0.10	0.02	90.5
5		31.0	7.0	53	2.0	27.1	0.0	1.4	0.25	3.3	1.6	6.0	0.60				17.4
6	PHUOCTHO	68.0	8.2	446	35.2	160.0	0.0	52.0	7.10	110.1	3.4	8.0	0.01	0.00	0.17	0.00	84.4
7	XADIEU	62.0	8.2	431	56.0	135.0	0.0	51.7	8.30	112.5	3.8	3.0	0.03	0.00	0.22	0.00	69.6
8		32.0	7.0	46	3.4	22.5	0.0	1.0	0.15	3.7	1.6	4.0	0.50				13.7
9		30.0	6.9	63	3.4	28.4	0.0	0.0	0.25	4.1	2.1	6.4	0.80	0.00	0.30	0.00	15.3
10	HANH DUNG	56.0	7.8	442	13.4	207.8	0.0	20.2	7.00	102.5	4.2	4.0	0.05	0.00			69.6
11		31.0	5.6	49	13.0	67.8	0.0	0.0	0.27	4.5	1.6	19.2	3.00				21.4
12	TUSON	52.0	6.0	4550	2979.0	72.2	0.0	112.0	1.35	1320.0	94.0	561.2	5.10	19.60	3.70	0.10	120.6
13	MODUC	76.0	6.6	5800	2425.0	45.2	0.0	128.0	1.30	1160.0	69.7	401.6	4.67	13.95	2.80	0.00	104.5
14		28.0	6.0	470	120.6	13.5	0.0	11.5	0.45	62.9	9.2	12.8	1.00				12.5
15		31.0	5.6	60	10.1	40.6	0.0	3.8	0.24	5.7	2.3	8.0	0.80	0.22	0.00	0.00	26.8
16	HOVAN	84.0	8.0	757	141.0	137.8	0.6	34.6	14.50	159.9	5.8	4.0	0.01				86.6
17		74.0	8.2	722	157.1	149.1	0.0	50.0	1.30	175.5	5.8	4.8	0.01				71.6
18		28.0	7.0	382	80.4	36.1	0.0	19.2	0.15	60.1	3.0	8.0	0.30				26.3
19	VINH THINH	71.0	8.4	593	52.0	155.9	26.0	72.0	1.45	143.4	3.8	4.8	0.01	0.17	0.00	0.00	88.5
20		32.0	7.8	67	1.3	36.1	0.0	1.5	0.26	3.7	1.7	6.4	0.80				20.1
21	TRIEM DUC	76.0	8.2	594	154.1	74.5	0.0	23.0	2.00	126.2	3.6	12.8	0.01	0.00	0.06	0.02	88.4
22		30.0	7.4	92	6.7	37.8	0.0	1.0	0.20	6.9	2.3	7.6	0.40				19.6
23	PHUOCLONG	52.5	8.4	512	48.6	157.5	0.0	36.5	14.70	126.2	3.4	2.4	0.01	0.00	0.00	0.00	70.4
24		32.0	6.6	124	56.5	17.0	0.0	0.0	0.35	12.4	2.1	8.0	0.90				24.1
25	PHUSEN	63.0	7.6	833	132.0	173.9	0.0	84.0	1.30	170.0	5.8	15.2	0.50	0.00	0.01	0.00	70.4
26		31.0	6.9	84	6.7	42.9	0.0	2.0	0.00	6.9	2.5	9.6	1.30				15.3
27	LAC XANH	58.0	7.7	230	18.0	119.7	0.0	40.8	1.40	75.9	2.1	4.0	0.13	0.00	0.00	0.00	48.2
28		28.0	6.3	46	3.7	13.5	0.0	0.8	0.10	4.1	1.6	2.4	0.20				16.1
29	TUBONG	55.0	8.0	1290	350.0	65.5	0.0	57.6	1.30	251.0	9.2	16.0	4.28	0.00	0.08	0.00	108.6
30		30.0	8.0		22607	140.0	0.0	820.0	1.20	12980	367.0	561.5	655.00				9.9
31	VANGIA	58.0	7.8	622	77.5	227.5	6.6	34.6	5.00	161.9	3.4	12.8	0.05	0.00	0.05	0.00	69.6
32		26.0	7.1	45	5.0	18.1	0.0	0.0	0.00	4.1	1.9	2.0	0.20				22.8
33	NINH HOA	66.0	8.9	362	25.0	106.2	13.2	31.1	1.40	76.0	2.3	5.6	0.02	0.00	0.00	0.02	64.3
34		30.0	8.2	114	6.0	51.5	0.0	4.8	1.47	11.2	2.7	10.0	1.40				22.0
35	DANH THANH	70.0	8.8	278	11.0	128.8	13.0	5.0	1.20	69.5	2.3	4.0	0.01	0.00	0.00	0.00	96.5
36		30.0	6.9	90	14.0	62.3	0.0	5.0	0.15	10.0	2.7	20.0	1.20				6.7

Sample	Location	T(°C)	pH	Cond. (µS/cm)	Cl	HCO <sub>3</sub>	CO <sub>3</sub>	SO <sub>4</sub>	F	Na	K	Ca	Mg	Rb	Li	Mn	SiO <sub>2</sub>
37	BANGOI	54.0	7.6	850	197.5	99.4	0.0	31.0	8.30	175.3	5.4	12.02	0.14	0.00	0.00	0.00	50.2
38		32.0	7.5	77	16.8	38.4	0.0	1.6	0.00	8.1	2.8	12.00	0.70				23.6
39		31.0	7.9		22115	261.6	0.0	820.0	1.30	10420	381.0	440.80	633.00				3.2
40	TAKOU	50.0	6.4	4410	1633.0	101.6	0.0	38.4	1.20	769.0	45.3	300.60	1.44	7.50	1.34	0.10	70.3
41		30.0	6.9	47	6.5	0.0	0.0	11.5	0.00	4.9	1.0	0.56	0.40				8.0
42	BINHCHAU	70.0	6.6	5340	1882.0	79.1	0.0	38.4	4.40	1000.0	38.0	360.20	1.51	9.73	3.70	0.01	111.6
43		28.0	7.4	320	18.1	73.0	0.0	19.2	0.10	43.7	9.7	12.83	1.10				13.7
45	TAVI	63.0	7.6	275	3.4	145.2	0.0	9.6	7.50	62.1	3.0	5.10	0.07	0.00	0.00	0.00	71.4
46		28.0	6.6	59	4.0	30.5	0.0	6.4		7.2	1.5	4.50	1.30				11.5
47		23.0	6.6	46	1.3	15.9	0.0	0.0		3.4	2.1	1.40	0.60				2.4
48	TACTO	67.0	8.8	246	1.6	97.0	13.2	19.2	10.00	66.3	2.5	1.80	0.14	0.00	0.00	0.10	80.4
55			7.4		17671	207.0	3.6	1784.0		10551	453.0	365.00	684.00				0.0
56	KONDU	60.0	8.5	430	3.3	97.0	16.8	63.0	12.17	99.4	3.4	3.20	0.01	0.00	0.00	0.20	82.3
57		31.0	6.5	76	2.3	40.3	0.0	13.7		7.0	5.3	5.10	1.80				14.8
58		25.0	5.7	67	10.4	20.1	0.0	11.0		1.4	2.7	7.40	0.88				6.6
59	RANGRIA	63.0	6.9	970	13.4	515.5	0.0	64.0	8.33	177.1	9.2	63.00	3.58	0.00	0.90	0.00	123.6
60		22.0	6.5	40	3.3	24.4	0.0	0.0		4.0	2.4	2.00	1.40				21.4
61		28.0	6.9	19	0.8	11.6	0.0	0.0		3.2	1.4	0.70	0.08				21.6
62	DAKROMAN	46.0	7.4	364	6.7	201.3	0.0	21.9	7.50	65.1	3.0	21.50	0.06	0.30	0.50	0.20	63.8
63		30.0	6.7	66	2.4	40.3	0.0	0.0		6.5	2.5	5.10	1.50				9.2
64		25.0	6.9	27	8.0	16.5	0.0	0.0		6.7	0.7	1.00	1.00				6.1
65	MORAY	53.0	7.8	685	117.2	148.3	0.0	0.0	16.67	181.0	5.2	7.20	0.02	0.00	0.00	0.00	63.8
66		28.0	6.8	67	5.4	26.2	0.0	0.0		3.7	3.2	6.30	1.53				22.3
67		28.0	7.8	51	6.7	31.7	0.0	0.0		3.2	2.5	5.50	1.56				14.3
68		22.0	7.8	95	7.3	54.9	0.0	0.0		5.0	5.0	9.40	1.60				22.3
69	DAKRUONG	53.0	8.0	523	88.7	125.1	0.0	65.0	20.83	138.8	5.3	17.50	0.06	0.40	0.00	0.30	95.6
70	KONBRAH	60.0	7.9	557	34.7	144.0	0.0	55.1	20.00	118.8	5.5	7.10	0.06	0.00	0.00	0.00	148.8
71		27.0	7.8	41	2.7	24.4	0.0	0.0		4.4	2.2	2.40	0.80				17.8
72		23.0	6.6	44	2.7	24.4	0.0	0.0		3.7	2.2	2.60	0.84				14.3
73		25.0	6.9	54	3.3	13.4	0.0	0.0		6.1	2.3	1.75	0.40				11.6
74		23.0	6.4	82	5.4	12.5	0.0	8.2		9.3	2.1	2.64	0.83				14.3
75	TANMY	48.0	8.0	668	28.4	508.2	0.0	0.0	8.75	181.4	9.1	16.40	0.73	0.00	0.00	0.30	59.5
76		24.0			2.0	17.1	0.0	0.0		2.3	1.6	3.00	0.60				7.1
77	PHONGDIEN	53.0	8.0	5170	1192.0	610.0	0.0	87.8	6.67	962.0	38.0	142.30	9.86	1.15	0.00	0.10	44.6

area while the young eruptive basalts of Cenozoic age develop very strongly, forming broad plateaus. As for the other tectonic unit, Kontum mesoblock is dissected and broken by faults into smaller massifs.

South Vietnam mesoblock is a relatively depressed mesoblock and overlain by Late Paleozoic - Mesozoic platformal cover. According to some geologists, it is a tectonic reactivated area with violent tectonic - magmatic activities began from Early Mesozoic. The depression in Early Jurassic formed a rather thick sedimentary formation, consisting of sandstone, conglomerate, argillite, schists. Basalts widely develop in Pliocene - Pleistocene forming big basalt massifs such as Daknong, Baoloc, Xuanloc.

The intrusive magmatism is widely and non-uniformly developed in South Trungbo region. It is divided into four main megacycles as follows:

- Archeozoic - Early Proterozoic (AR-PR<sub>1</sub> )
- Late Proterozoic (PR<sub>2</sub> )
- Paleozoic - Early Mesozoic (PZ-MZ<sub>1</sub> )
- Late Mesozoic - Cenozoic (MZ<sub>2</sub>-KZ).

The main products are different magmatic rocks such as norite, gabbro-norite, granite, granodiorite, diorite, etc. In Late Cenozoic, the intrusive magmatic activities waned, and were replaced by basaltic eruptive activities.

### 1.3 Hydrological Features

Information on hydrogeological condition of South Trungbo area is limited. Aside from the manifestations discharging from the bedrock, there are some boreholes reaching 100m deep in basalts which are used for water supply.

Based on the data available, hydrogeological condition of the area can be summarized follows:

Ancient magmatic and metamorphic formations of Archeozoic to Mesozoic are not so much fractured. In general, they are impermeable. However, in the fractured zones, low TDS waters of Na-HCO<sub>3</sub>-Cl type exist. Values of TDS range between 100-200mg/l. Discharges of the springs vary from 0.1 to 0.3l/s.

The basement is overlain by Neogene formation and basalts of Neogene and Quaternary ages, those were formed in Cenozoic depression grabens. Neogene formations consist of sand, sandstone, alleurolite, argillite. Discharge of the springs from these formations ranges from 0.1 to 0.3l/s. The type of waters is Na-Ca-Mg-HCO<sub>3</sub>, sometime Ca-Na-SO<sub>4</sub> with TDS ranging from 100 to 1000mg/l.

Water-bearing complex in N-Q basalts is very complicated due to many stages of eruption. In this area, several wells were drilled to depths of 100-120m. The thickness of water-bearing formation is about 30-50m. The type of waters is Ca-Mg-HCO<sub>3</sub> or Mg-Ca-HCO<sub>3</sub> with low TDS (100-200mg/l).

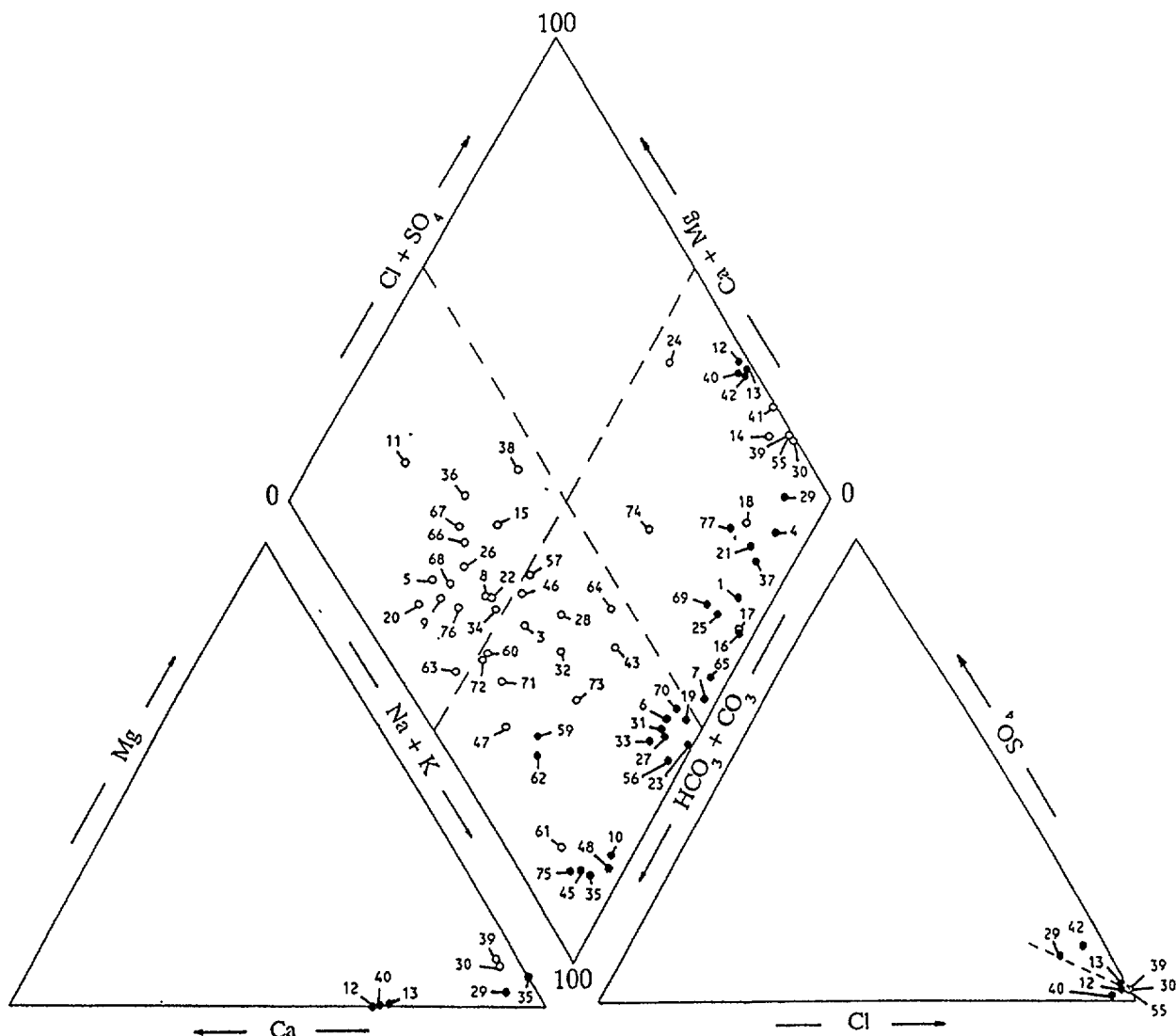


FIG. 3. Hydrogeological families of the waters.

## 2. METHODOLOGY

From geological and geomorphological point of view, the area of study can be divided into two zones: the Coastal Strip and the Northern Highland.

In 1990 and 1991, two field trips were undertaken to the above mentioned zones respectively. During these trips, geochemical and isotopic samples of hot waters and local cold waters were collected for major (Na, K, Ca, Mg,  $\text{HCO}_3$ ,  $\text{CO}_3$ ,  $\text{SO}_4$ ), trace elements (Rb, Li, Mn, F) and stable isotopes (D, O-18).

The obtained information from field and laboratory works allowed the chemical classification of waters, liquid phase thermometry, and the study of origin and recharge area of the hot springs.

### 3. RESULTS AND DISCUSSION

#### 3.1 Chemical Composition of the Waters

Chemical composition of the hot and local cold waters is presented in Table 1. Generally speaking, these waters are dilute, except for some of them. The conductivity ranges from 40-50mS/cm to 5800mS/cm. They represent three main hydrogeochemical water types, namely Na-Cl, Na-HCO<sub>3</sub> and Ca-HCO<sub>3</sub> (Fig. 3).

##### 3.1.1 Local cold water

There were 30 samples of cold waters collected during 1990 - 1991 investigations including 3 samples of sea water. Three main groups can be defined: Na-Cl, Na-HCO<sub>3</sub> and Ca-HCO<sub>3</sub>. They are more dilute than are hot waters with conductivity usually less than 100mS/cm. In Coastal Strip, waters are of three types mentioned above while in the Northern Highland, the cold waters belong to Na-HCO<sub>3</sub> and Ca-HCO<sub>3</sub> types. The silica content is about 15-20ppm.

##### 3.1.2 Hot water

Thermal waters in South Trungbo area are mainly of Na-Cl and Na-HCO<sub>3</sub> types as shown on the Piper diagram (Fig. 3). But some samples (7, 16, 23, 25, 31, 65, 69) belong to subgroup Na-HCO<sub>3</sub>-Cl or Na-Cl-HCO<sub>3</sub> due to their considerable content of Cl or HCO<sub>3</sub>.

Among major species present in hot water, Na is predominant. Its concentration ranges from 62 to 1320ppm and takes up more than 90% in meq. Cl is the principal anionic component. Its concentration varies in a wide range, from 1.6ppm (sample 48) to 2979ppm in high salinity water (sample 12). Furthermore, this water together with other hot water (13, 29, 40 and 42) joint to sea water (30, 39, 55), establishing a linear correlation in the Piper diagram, lower right triangle (Fig. 3). This can be explained by two mechanisms: mixing with sea water and dissolution of sodium chloride.

Studying Na/Cl ratio shows that, most of hot waters have this value more than 1 (Table 2). This means that they are geologically young, circulate in the zone of active exchange and the well related with modern waters. Exceptions are 4 high salinity waters with Na/Cl ratio ranging between 0.65 and 0.85 (12, 13, 40, 42). This may indicate the metamorphic nature of these waters.

HCO<sub>3</sub> is one of the main component in hot water. Because of the relatively high concentration of HCO<sub>3</sub> (ranging from 101.6 to 515.5ppm), possible rock leaching by water with high CO<sub>2</sub> content resulting in Na-HCO<sub>3</sub> or Na-Cl-HCO<sub>3</sub> waters is suggested.

In general, K is directly proportional to Na content. It ranges from few ppm to 94ppm in high salinity water. Unlike K, concentration of Ca varies in a wide range, from few ppm to more than 500ppm. But frequent values are less than 20ppm, except for Rangria (63ppm) and Phongdien (142.2ppm). In contrast to Ca, concentration of Mg is very low, usually below 0.1ppm, except for some high conductivity waters reaching the values of 4-5ppm (12, 13, 29, 40, 42). It is noted that, for some geothermal areas, the more altered waters show the more increased Ca and Mg concentrations.

**Table 2. Na/Cl ratio for geothermal waters**

Location	Sample	Na (meq)	Cl (meq)	Na/Cl	Cond. ( $\mu$ S/cm)	Type of water
NGHIAKY	1	7.63	4.72	1.62	590	Na-Cl
BINH HOA	4	5.33	2.96	1.80	520	Na-Cl
PHUOCTHO	6	4.79	1.00	4.79	446	Na-HCO <sub>3</sub>
XADIEU	7	4.89	1.58	3.09	431	Na-HCO <sub>3</sub> -Cl
HANH DUNG	10	4.59	0.38	12.08	442	Na-HCO <sub>3</sub>
TUSON	12	57.39	83.90	0.68	4550	Na-Cl
MODUC	13	50.43	68.30	0.74	5800	Na-Cl
HOVAN	16	6.95	3.98	1.77	757	Na-Cl-HCO <sub>3</sub>
VINH THINH	19	6.23	1.46	4.27	593	Na-HCO <sub>3</sub>
TRIE MDUC	21	5.48	4.35	1.29	594	Na-Cl
PHUOCLONG	23	5.48	1.37	4.00	512	Na-HCO <sub>3</sub> -Cl
PHUSEN	25	7.39	3.72	1.99	833	Na-Cl-HCO <sub>3</sub>
LACXANH	27	3.30	0.51	6.47	230	Na-HCO <sub>3</sub>
TUBONG	29	10.91	9.87	1.11	1290	Na-Cl
VANGIA	31	7.04	2.19	3.21	622	Na-HCO <sub>3</sub> -Cl
NINH HOA	33	3.30	0.71	4.65	362	Na-HCO <sub>3</sub>
DANH THANH	35	3.02	0.31	9.74	278	Na-HCO <sub>3</sub>
BANGOI	37	7.62	5.57	1.37	850	Na-Cl
TAKOU	40	33.43	46.00	0.73	4410	Na-Cl
BINH CHAU	42	43.48	53.07	0.82	5340	Na-Cl
TAVI	45	2.70	0.10	27.00	275	Na-HCO <sub>3</sub>
TACTO	48	2.88	0.05	57.60	246	Na-HCO <sub>3</sub>
KON DU	56	4.32	0.09	48.00	430	Na-HCO <sub>3</sub> -SO <sub>4</sub>
RANGRIA	59	7.70	0.38	20.26	970	Na-HCO <sub>3</sub>
DAKROMAN	62	2.83	0.19	14.89	364	Na-HCO <sub>3</sub>
MORAY	65	2.87	3.31	2.38	685	Na-Cl-HCO <sub>3</sub>
DAKRUONG	69	6.03	2.50	2.41	523	Na-Cl-HCO <sub>3</sub>
KONBRAIH	70	5.17	0.98	5.28	557	Na-HCO <sub>3</sub>
TANMY	75	7.89	0.80	9.86	668	Na-HCO <sub>3</sub>
PHONGDIEN	77	41.83	33.62	1.24	5170	Na-Cl

Elements F, Rb, Li often regarded as magmatic contribution to hydrothermal systems, resulting from the reaction between water and rock. Their concentration in hot waters is very different. For F, it ranges from 1.2ppm (Danhthanh) to 20.83ppm (Dakruong) and usually show a value of 5-8ppm. Rb and Li usually are present in very small quantity (less than 0.5-0.6ppm). But 4 high salinity waters (12, 13, 40, 42) have relatively high concentration for both Rb and Li (up to 19.6ppm for Rb and 3.7ppm for Li ).

**Table 3. Geothermometers used in the report** (Henley et al., 1984)

Geothermometers	Equation (Dissolved component in mg/l)	Restrictions
a. Chalcedony	$t(^{\circ}\text{C}) = \frac{1032}{4.69 - \log(\text{SiO}_2)} - 273$	$t = 0 - 250$
b. Quartz (no steam loss)	$t(^{\circ}\text{C}) = \frac{1309}{5.19 - \log(\text{SiO}_2)} - 273$	$t = 0 - 250$
c. Na/K (Fournier)	$t(^{\circ}\text{C}) = \frac{1217}{\log(\text{Na} / \text{K}) + 1.483} - 273$	$t > 150$
d. Na-K-Ca	$t(^{\circ}\text{C}) = \frac{1647}{\log(\text{Na} / \text{K}) + \beta [\log(\sqrt{\text{Ca}} / \text{Na}) + 2.06] + 2.47} - 273$	$t < 100, \beta = 4/3$ $t > 100, \beta = 1/3$

### 3.2 Liquid Phase Thermometry

One of the geochemical methods widely applied in geothermal exploration, is the application of geothermometers to estimate the reservoir temperature. Apart from silica and cation geothermometers, the mixing model given by Fournier and Truesdell [3] and Na-K-Mg diagram given by Giggenbach [4] have been used to calculate the reservoir temperature. Table 3 presents the geothermometers used in this report. All calculated results are given in Table 4.

#### 3.2.1 *SiO<sub>2</sub> geothermometer*

The concentration of silica in the thermal waters ranges from 44.6 to 148.8ppm while in the local cold waters is varies from few ppm to 27ppm. Because of unknown solid phase which controls the concentration of dissolved silica, both chalcedony and quartz (no steam loss) geothermometers are used. The results obtained by chalcedony geothermometer show relatively low compared with those obtained by quartz with difference of about 30°C. The maximum value given by quartz geothermometer is 160.4°C (sample 70). Maybe quartz governs the silica solubility at depth rather than chalcedony does.

#### 3.2.2 *Na-K and Na-K-Ca geothermometers*

Na-K geothermometer is less affected than the silica one. But the application of this geothermometer, especially for diluted waters or low enthalpy systems often results in an overestimated temperature [2]. In the meantime, Na-K-Ca geothermometer can be affected by Mg and flux of CO<sub>2</sub> as noted by Giggenbach [4] and Paces et al. [7].

From obtained results, it is noted that the calculated values cluster around 150°C, except for some waters with very high salinity (samples 12, 13).



Table 4. Geothermometry results

Location	Sample	T(in °C)					Note
		Chalcedony	Quartz no steam loss	Na/K	Na-K-Ca	Mix model	
NGHIAKY	1	111.0	137.7	139.2	132.8	*	Well Spring
BINH HOA	4	104.5	131.8	145.0	136.8	244	
PHUOCTHO	6	100.4	128.1	133.8	125.2	206	
XADIEU	7	89.5	118.0	133.8	136.1	202	
HANHDUNG	10	89.5	118.0	150.7	141.2	242	
TUSON	12	122.6	148.1	189.7	169.5	*	
MODUC	13	113.4	139.8	177.0	161.5	218	
HOIVAN	16	102.0	129.4	143.1	142.5	132	
HOIVAN	17	91.0	119.5	137.4	138.3	122	
VINH THINH	19	103.2	130.6	124.6	125.9	200	
TRIEMDUC	21	103.2	130.6	128.3	120.0	172	
PHUOCLONG	23	90.1	118.7	125.8	129.9	258	
PHUSEN	25	90.1	118.7	139.3	130.8	194	
LACXANH	27	70.2	100.3	126.4	119.6	118	
TUBONG	29	115.8	142.0	144.2	139.6	*	
VANGIA	31	89.5	118.0	112.2	111.7	176	
NINH HOA	33	85.1	114.0	132.4	121.6	136	
DANH THANH	35	108.4	135.4	137.4	126.3	214	
BANGOI	37	72.2	102.1	133.1	128.5	140	
TAKOU	40	90.0	118.6	175.6	156.2	*	
BINH CHAU	42	117.6	143.6	146.2	138.4	266	
TAVI	45	90.4	118.9	161.8	139.5	193	
TACTO	48	98.2	126.1	145.7	137.1	200	
KONDU	56	99.6	127.3	139.7	134.6	263	
RANGRIA	59	123.9	149.2	166.8	139.6	297	
DAKROMAN	62	84.1	113.1	158.6	127.7	272	
MORAY	65	84.1	113.1	129.4	129.8	195	
DAKRUONG	69	107.8	134.8	146.5	131.9	*	
KONBRAIH	70	136.5	160.4	159.0	144.9	*	
TANMY	75	80.4	109.7	164.4	148.7	250	
PHONGDIEN	77	66.5	96.8	148.6	146.7	174	

\* no interception

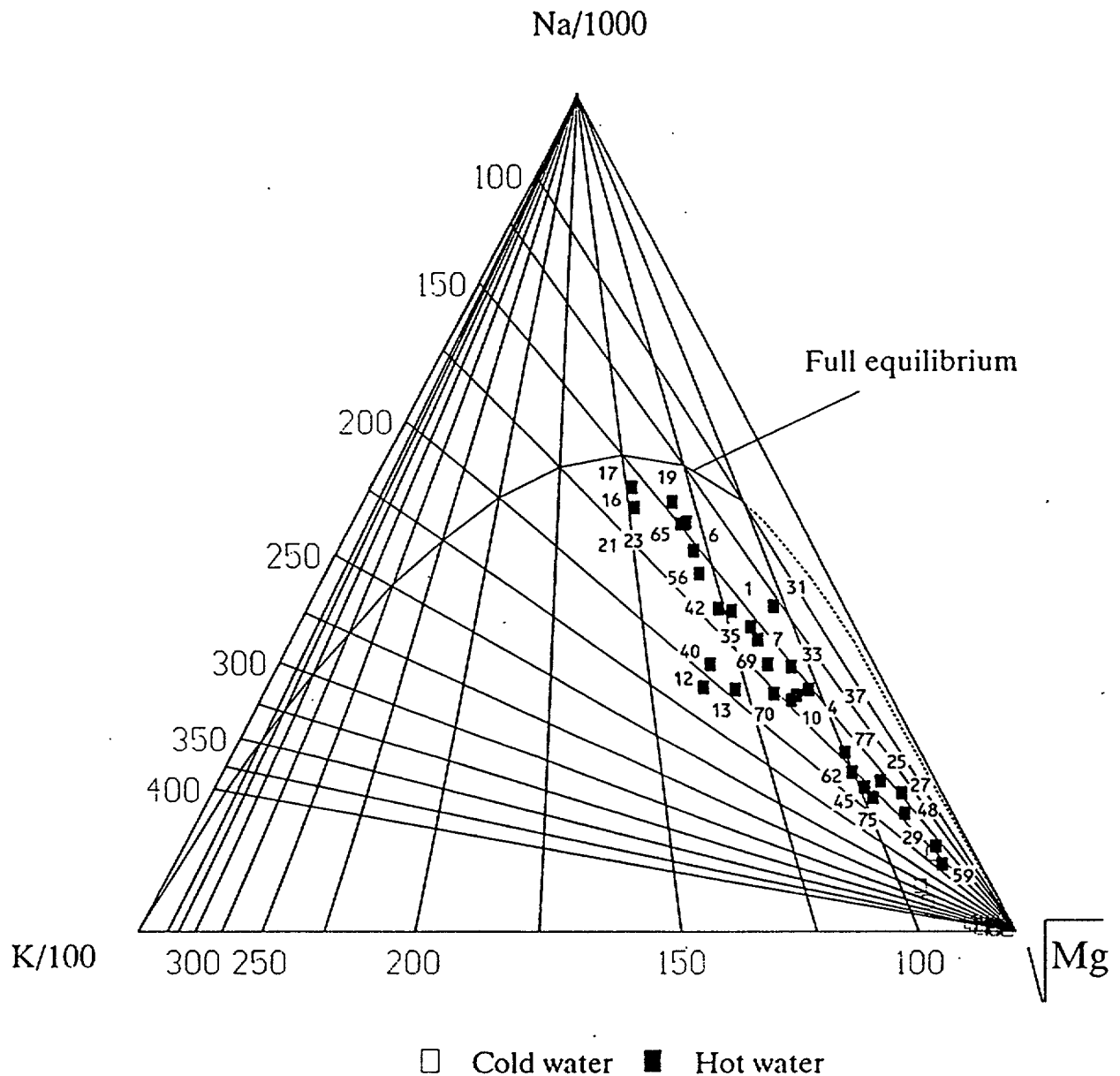


FIG. 4. Na-K-Mg diagram.

### 3.2.3 Na-K-Mg geothermometer

Evaluation of the K-Na-Mg geothermometer is best carried out by using the diagram of Giggenbach [4]. As shown in the constructed diagram for waters collected (Fig. 4), cold waters occupy the low position in the Mg corner as expected while hot waters generally distribute between 150-180°C indicating the homogeneity of samples although the research area is large. Moreover, their position between full equilibrium curve and cold waters shows that hot waters are partially equilibrated or reequilibrated, or mixed with shallow groundwater [5].

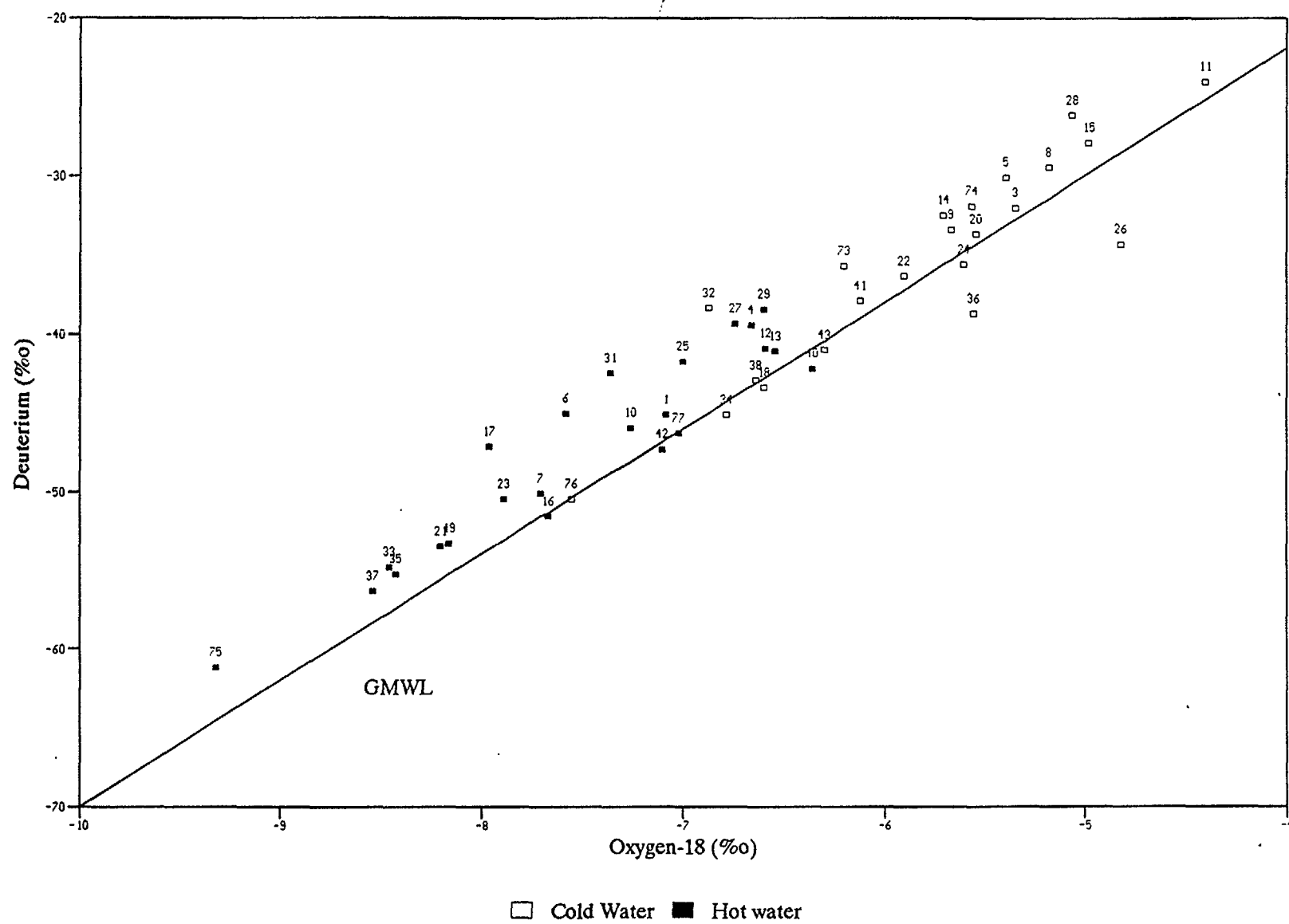


FIG. 5. Deuterium vs oxygen-18 coastal strip.

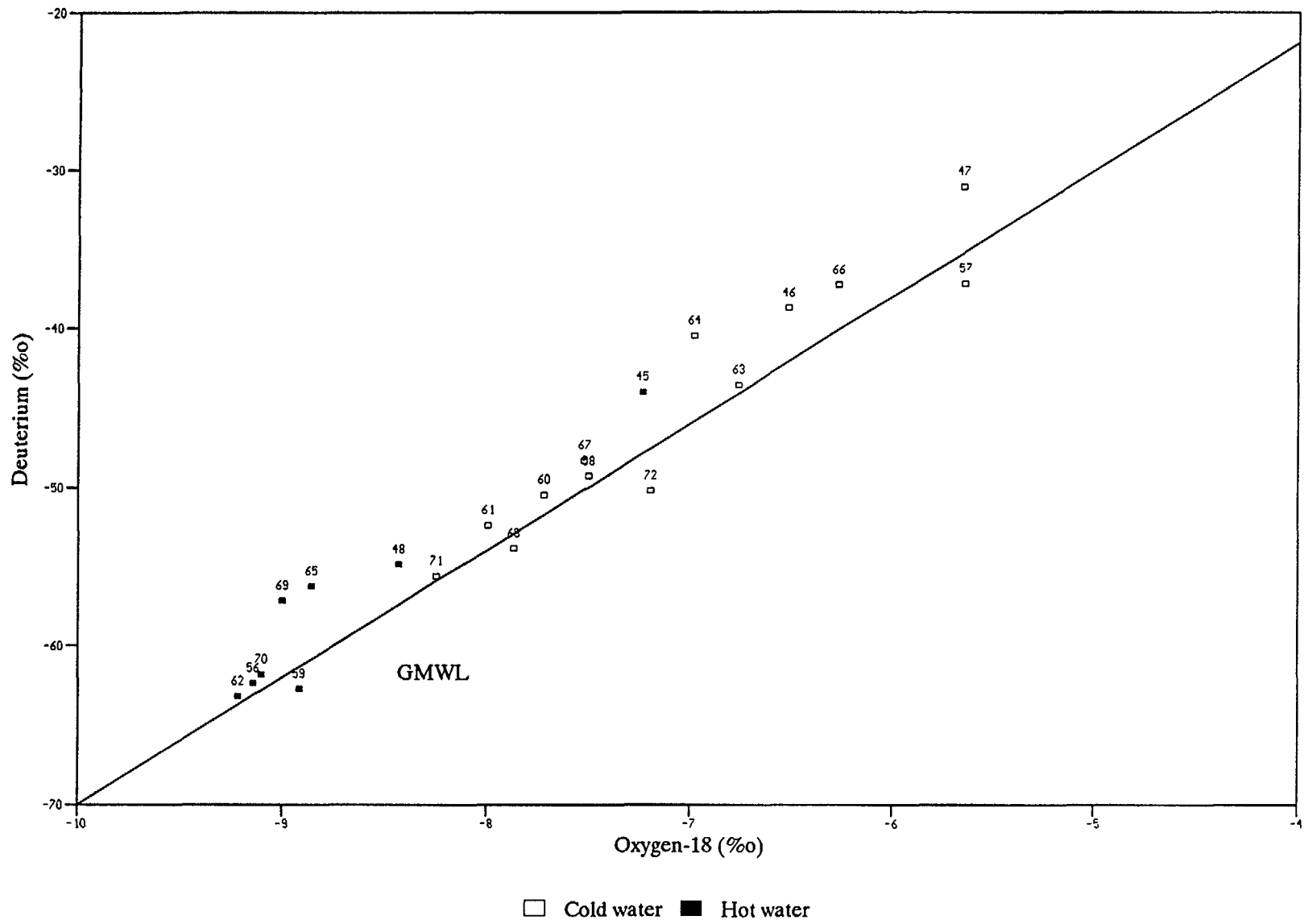
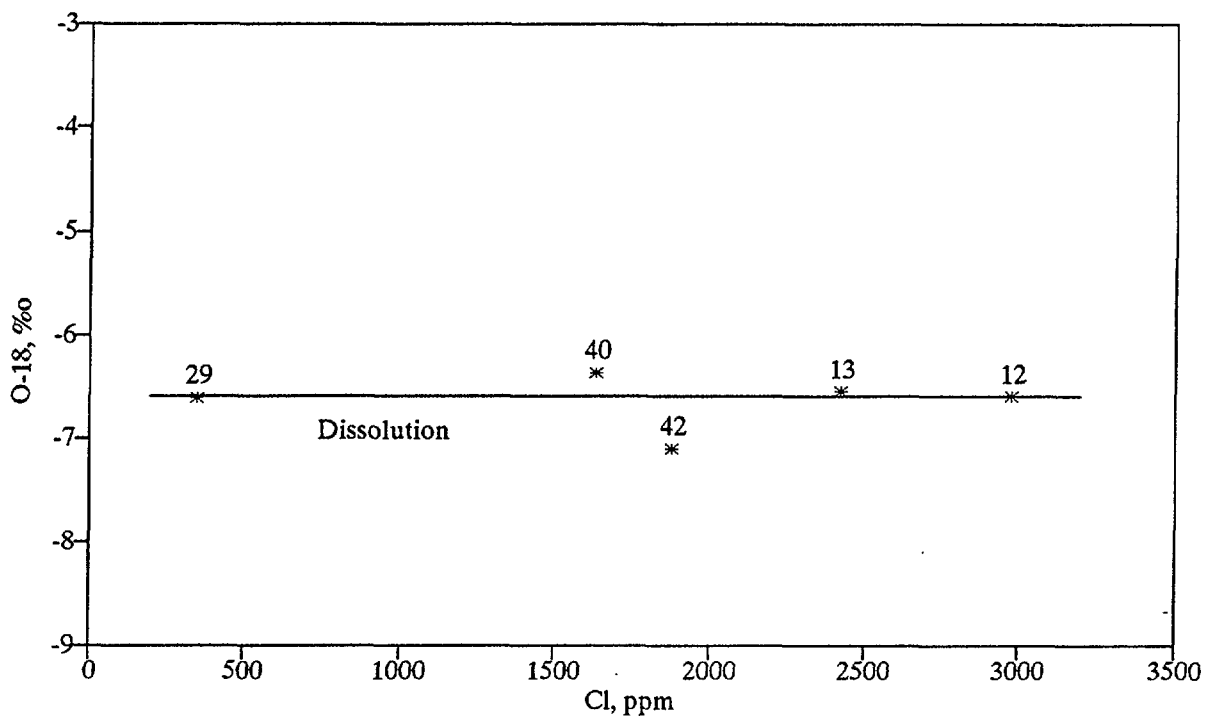


FIG. 6. Deuterium vs oxygen-18 northern highland.

**Table 5. Mean stable isotopic values**

Location	Type of water	$^{18}\text{O}$ (‰)	$\sigma$	D (‰)	$\sigma$	d	$\sigma$	Equation
Coastal Strip	Cold	-5.81	0.74	-35.50	6.29	10.95	2.63	$D = 7.69 \text{ }^{18}\text{O} + 9.14$
	Hot	-7.49	0.77	-47.33	6.20	12.58	2.08	$D = 7.61 \text{ }^{18}\text{O} + 9.65$
Northern	Cold	-7.06	0.82	-45.24	7.41	11.28	2.26	$D = 8.60 \text{ }^{18}\text{O} + 15.50$
Highland	Hot	-8.74	0.61	-57.80	6.04	12.10	2.06	$D = 9.35 \text{ }^{18}\text{O} + 23.88$



**FIG. 7. Oxygen-18 vs chloride for high salinity waters, coastal strip.**

### 3.2.4 Mixing calculation

From data of hot and cold waters (the silica content and temperature), the fraction of cold water in the mixture can be calculated, based on silica and enthalpy considerations. Then, by graphical method, the intersection of the silica and enthalpy curves is found, which indicates the reservoir temperature and cold water fraction in the hot waters.

This methodology has been used for all hot waters (31 samples) but only 25 results were obtained. Table 4 presents all calculated results that show, in general, higher values compared with those obtained by the other geothermometers.

Table 6. Isotopic results

Sample	Location	T(°C)	Date	Cond. ( $\mu\text{S/cm}$ )	O-18 ‰	D ‰	D exc. ‰
1	NGHIAKY	67.0	03/90	590	-7.08	-45.1	11.54
3		30.0	03/90	72	-5.34	-32.0	10.72
4	BINH HOA	65.0	03/90	520	-6.66	-39.4	13.88
5		31.0	03/90	53	-5.39	-30.1	13.02
6	PHUOCTHO	68.0	03/90	446	-7.58	-45.0	15.64
7	XADIEU	62.0	03/90	431	-7.70	-50.1	11.50
8		32.0	03/90	46	-5.18	-29.5	11.94
9		30.0	03/90	63	-5.66	-33.4	11.88
10	HANH DUNG	56.0	03/90	442	-7.26	-45.9	12.18
11		31.0	03/90	49	-4.40	-24.1	11.10
12	TUSON	52.0	03/90	4550	-6.59	-40.9	11.82
13	MODUC	76.0	03/90	5800	-6.54	-41.1	11.22
14		28.0	03/90	470	-5.70	-32.5	13.10
15		31.0	03/90	60	-4.98	-27.9	11.94
16	HOIVAN	84.0	03/90	757	-7.67	-51.6	9.76
17		74.0	03/90	722	-7.96	-47.1	16.58
18		28.0	03/90	382	-6.60	-43.4	9.40
19	VINH THINH	71.0	03/90	593	-8.16	-53.3	11.98
20		32.0	03/90	67	-5.54	-33.7	10.62
21	TRIEM DUC	76.0	03/90	594	-8.20	-53.5	12.10
22		30.0	03/90	92	-5.90	-36.3	10.90
23	PHUOCLONG	52.5	03/90	512	-7.89	-50.5	12.62
24		32.0	03/90	124	-5.60	-35.6	9.20
25	PHUSEN	63.0	03/90	833	-7.00	-41.7	14.30
26		31.0	03/90	84	-4.82	-34.3	4.26
27	LAC XANH	58.0	04/90	230	-6.74	-39.3	14.62
28		28.0	04/90	46	-5.06	-26.2	14.28
29	TUBONG	55.0	04/90	1290	-6.60	-38.4	14.40
30		30.0	04/90	-	0.74	1.6	-4.32
31	VANGIA	58.0	04/90	622	-7.36	-42.4	16.48
32		26.0	04/90	45	-6.87	-38.3	16.66
33	NINH HOA	66.0	04/90	362	-8.46	-54.8	12.88
34		30.0	04/90	114	-6.78	-45.1	9.14
35	DANH THANH	70.0	04/90	278	-8.43	-55.2	12.24
36		30.0	04/90	90	-5.55	-38.7	5.70

Sample	Location	T(°C)	Date	Cond. (μS/cm)	O-18 ‰	D ‰	D exc. ‰
37	BANGOI	54.0	04/90	850	-8.54	-56.3	12.02
38		32.0	04/90	77	-6.64	-42.9	10.22
39		31.0	04/90	-	-0.14	0.6	1.72
40	TAKOU	50.0	04/90	4410	-6.36	-42.2	8.68
41		30.0	04/90	47	-6.12	-37.9	11.06
42	BINHCHAU	70.0	04/90	5340	-7.10	-47.3	9.50
43		28.0	04/90	320	-6.30	-41.0	9.40
45	TAVI	63.0	04/91	275	-7.23	-44.0	13.80
46		28.0	04/91	59	-6.51	-38.7	13.40
47		23.0	04/91	46	-5.65	-31.0	14.20
48	TACTO	67.0	04/91	246	-8.43	-54.9	12.50
56	KONDU	60.0	04/91	430	-9.14	-62.4	10.70
57		31.0	04/91	76	-5.64	-37.1	8.00
58		25.0	04/91	67	-7.50	-49.3	10.70
59	RANGRIA	63.0	04/91	970	-8.92	-62.7	8.70
60		22.0	04/91	40	-7.72	-50.5	11.30
61			04/91	19	-7.99	-52.4	11.50
62	DAKROMAN	46.0	04/91	364	-9.22	-63.2	10.60
63		30.0	04/91	66	-6.76	-43.5	10.60
64		25.0	04/91	27	-6.98	-40.4	15.40
65	MORAY	53.0	04/91	685	-8.86	-56.2	14.70
66		28.0	04/91	67	-6.26	-37.2	12.90
67		28.0	04/91	51	-7.52	-48.3	11.90
68		22.0	04/91	95	-7.87	-53.9	9.10
69	DAKRUONG	53.0	04/91	523	-9.00	-57.2	14.80
70	KONBRAIH	60.0	04/91	557	-9.10	-61.8	11.00
71		27.0	04/91	41	-8.24	-55.6	10.30
72		23.0	04/91	44	-7.19	-50.2	7.30
73		25.0	04/91	54	-6.20	-35.7	13.90
74		23.0	04/91	82	-5.56	-31.9	12.60
75	TANMY	48.0	04/91	668	-9.32	-61.2	13.40
76		24.0	04/91		-7.55	-50.5	9.90
77	PHONGDIEN	53.0	04/91	1190	-7.02	-46.3	9.90

### 3.3 Stable Isotopes

During 1990-1991 investigations, 69 water samples were collected for deuterium and oxygen-18 analysis (31 geothermal waters and 38 adjacent to them surface and shallow underground waters). All these waters are plotted in the deuterium vs oxygen-18 diagram and they lie on or close to the meteoric water line (Fig. 5,6). This may be an evidence for meteoric origin of geothermal waters in the region. Moreover, geothermal waters tend to be more depleted in stable isotopes than cold waters. This is explained by the altitude difference of recharge area, where waters originated.

In the above figures, no oxygen-18 shift is observed. This means that there is no isotopic exchange between hot waters and host rock in condition of low enthalpy system where the maximum reservoir temperature reaches as high as 150-180°C.

From geological and geomorphological point of view, these samples are grouped into two, corresponding to two zones. For each zone, each hot and cold water type, deuterium, oxygen-18 and deuterium excess as well as the linear regression equation D vs O-18 were calculated separately. The results obtained are presented in Table 5. Taking the isotopic gradient for O-18 as -0.3‰ and for D as -2.5‰ per 100m, the recharge area for hot water is at elevation as high as about 500-600m relatively to local meteoric waters for both zones. In addition, the recharge area of hot waters in the Northern Highland is located at elevation of about 700-900m a.s.l., considering their isotope composition relatively to that of cold waters in the Coastal Strip.

Fig. 7 shows the relation between oxygen-18 value and chloride content for some high salinity hot waters of the Coastal Strip (12, 13, 29, 40, 42). They have more or less constant oxygen-18 value but different chloride. The horizontal correlation line indicates that these waters originate from meteoric water at not very high elevation to that of local water and gain high salinity due to the dissolution of salt but not due to mixing with sea water. This confirms one of two hypotheses above mentioned in the Piper diagram. Moreover, these springs are located on or close to the seashore, that makes this hypothesis more plausible. Table 6 presents all isotope data of the samples.

## 4. CONCLUSIONS

Geothermal waters of South Trungbo region are of different types, from Na-HCO<sub>3</sub> to Na-Cl, with the conductivity varying in a wide range from 246 to 5800 mS/cm.

The difference in stable isotope contents of hot and cold water is caused by elevation changes. Considering the altitude effect of -0.3‰ for oxygen-18 and -2.5‰ for deuterium per 100m, the recharge areas of hot waters in Coastal Strip and Northern Highland occur at about 500-600m and 700-900m a.s.l. respectively.

Although located near the sea, chemical composition of hot waters in Coastal Strip (especially high salinity waters) are affected by leaching rather than mixing with sea water.

Different geothermometers show large diversity of the calculated reservoir temperatures. Mixing with local groundwater may be responsible for this discrepancy.



From geothermometry, the South Trungbo geothermal area is a low-enthalpy system with maximum reservoir temperature less than 150-180°C.

*Acknowledgments - The present investigation was carried out within the framework of the IAEA Coordinated Research Programme for Africa, Asia and the Middle East on the Application of Isotope and Geochemical Techniques in Geothermal Exploration. (Research Contract N°. 5840/RB)*

## References

- [1] D'Amore, F., and Panichi, C. "Geochemistry in Geothermal Exploration". Energy Research, Vol. 9, 1985, p. 277-298.
- [2] D'Amore, F., Fancelli, R., Caboi, R. "Observations on the Application of Chemical Geothermometers to some Hydrothermal Systems in Sardinia". Geothermics, Vol. 16, No. 3, 1987, p. 271-282.
- [3] Fournier, R.O., and Truesdell, A.H. "Geochemical Indicators of Subsurface Temperature-Part 2, Estimation of Temperature and Fraction of Hot Water Mixed With Cold Water". Jour. Research U.S. Geol. Survey, Vol. 2, No. 3, 1974, p. 263-270.
- [4] Giggenbach, W.F., Goguel, R.L. "Collection and Analysis of Geothermal and Volcanic Water and Gas Discharges". 1989.
- [5] Gonfiantini, R. "Note on Isotope and Geochemistry in Geothermal Investigations". Group Training in Isotope Hydrology, IAEA, Vienna, Austria, 1991.
- [6] Henley, R.W., Truesdell, A.H., and Barton, P.B., with a contribution by Whitney, J.A. "Fluid-Mineral Equilibria in Hydrothermal Systems". Reviews in Economic Geology, Vol. 1, 1984.
- [7] Paces, T., "Notes on Geochemistry Applied to Geothermal Exploration". (a handout). Course in Geothermal Exploration 1987-1988, International School of Geothermics, Pisa, Italy, 1988.

## PARTICIPANTS DIRECTLY INVOLVED IN THE CO-ORDINATED RESEARCH PROGRAMME

### *Research Contracts:*

Wang Ji-Yang	Institute of Geology Academia Sinica, P.O. Box 634 Beijing, China
Navada, S.	Isotope Division Bhabha Atomic Research Centre, Trombay Bombay 400 085, India
Wandowo	Center for Application of Isotopes and Radiation Jl. Cinere, P.O. Box 2, Kebayoran Lama Jakarta, Indonesia
Hussain, S.D.	Pakistan Institute of Nuclear Science and Technology Islamabad, Pakistan
Gerardo, J.Y.	Geothermal Division Philippine National Oil Co.- Energy Development Corporation Makati, Philippines
Simsek, S.	International Research and Applications Centre for Karst Water Resources Hacettepe University, Beytepe-Ankara Turkey
Nguyen Trac Viet	Isotope Hydrology Section Center of Nuclear Techniques Ho Chi Minh City, Viet Nam

### *Research Agreements:*

Arnorsson, S.	University of Iceland Dunhagi 3, 107 Reykjavik, Iceland
Panichi, P.	Istituto Internazionale per le Ricerche Geotermiche Piazza Solferino 2, 56135 Pisa, Italy
Ahn, Jong Sung	Hydrology Department Korea Atomic Energy Research Institute P.O. Box 7, Daeduk-Danji Taejon, Republic of Korea
Giggenbach, W.	Institute of Geological and Nuclear Sciences P.O. Box 30 368, Lower Hutt, New Zealand
Gonfiantini, R. <i>Project Officer</i>	Isotope Hydrology Section International Atomic Energy Agency P.O. Box 100, Wagramerstrasse 5 A-1400 Vienna, Austria

95-00165